

Hans-Georg Kempfert

Berhane Gebreselassie

Excavations and Foundations in Soft Soils

@Seismicisolation

Hans-Georg Kempfert
Berhane Gebreselassie

Excavations and Foundations in Soft Soils

With 421 Figures



Springer

@Seismicisolation

Herrn
Prof.Dr. Hans-Georg Kempfert
Universität Kassel
FG Geotechnik
Mönchebergstr. 7
34125 Kassel
Germany

Dr. Berhane Gebreselassie
Universität Kassel
FG Geotechnik
Mönchebergstr. 7
34125 Kassel
Germany

e-mail: geotech@uni-kassel.de

Library of Congress Control Number: 2006921905

ISBN-10 540-32894-7 Springer Berlin Heidelberg New York
ISBN-13 978-3-540-32894-0 Springer Berlin Heidelberg New York

This work is subject to copyright. All rights are reserved, whether the whole or part of the material is concerned, specifically the rights of translation, reprinting, reuse of illustrations, recitation, broadcasting, reproduction on microfilm or in any other way, and storage in data banks. Duplication of this publication or parts thereof is permitted only under the provisions of the German Copyright Law of September 9, 1965, in its current version, and permission for use must always be obtained from Springer-Verlag. Violations are liable to prosecution under the German Copyright Law.

Springer is a part of Springer Science+Business Media
springer.com
© Springer-Verlag Berlin Heidelberg 2006
Printed in The Netherlands

The use of general descriptive names, registered names, trademarks, etc. in this publication does not imply, even in the absence of a specific statement, that such names are exempt from the relevant protective laws and regulations and therefore free for general use.

Cover design: E. Kirchner, Heidelberg
Production: Almas Schimmel
Printing: Krips bv, Meppel
Binding: Stürtz AG, Würzburg

Printed on acid-free paper 30/3141/as 5 4 3 2 1 0

@Seismicisolation

Preface

The book is about soft soil engineering and is intended to serve the practicing as well as the research engineers. The planning, design and construction of excavations and foundations in soft to very soft soils is always a difficult and challenging assignment to engineers. The authors have tried to address some of these problems and challenges in this book.

Beside the state of the art of soft soils, authors own research results and experiences from practical projects are presented in the book. Special emphasis is also given among others on the presentation of several case studies corresponding to each topic treated in the book as well as a summary of the experiences in the determination of soil parameters for finite element analysis of geotechnical problems. The book is illustrated by a wealth of photographs and diagrams. The reader is referred to chapter 1 for a general introduction to the content of the book, the motives and backgrounds of the book.

The aim of the authors is to give the readers an overview of the state of the art of material properties of soft soils and their application in excavations, different types of foundations and stabilization methods. The authors emphasize, however, that the presence of soft soil in connection with construction measure should not a priori be classified as extremely difficult and strong cost intensive for the project. By making use of an advance knowledge in soft soil engineering so far available in the field of geotechnical engineering, it is possible to reach at a technically safe and economically justifiable solution for a particular construction project. The book is expected to contribute much in this regard.

The authors are gratefully to their colleagues U. Berner, P. Becker, F. Böhm, D. Fischer, M. Raithel, B. Soumaya and M. Witzel for letting us to use research results, geotechnical documents and measurement data. Special thanks also go to Springer Verlag, the publisher, for meeting and complying with the author's wishes.

Hans-Georg Kempfert

Berhane Gebreselassie

Table of contents

Preface	v
Table of contents	vii
Symbols and abbreviations	xiii
1 Introduction	1
1.1 General	1
1.2 Safety regulations in geotechnical engineering	5
1.2.1 The ultimate and serviceability limit states	5
1.2.2 Total safety concept.....	5
1.2.3 Partial safety concept and the German Code	5
1.2.4 European code of standard	7
1.2.5 Comparison between Eurocode EC 7-1 and German Code DIN 1054...8	
2 Material properties of soft soils	11
2.1 General	11
2.2 Sampling.....	11
2.3 Basic index properties	15
2.4 Compression properties	17
2.4.1 General	17
2.4.2 One-dimensional compression.....	19
2.4.3 Two and three-dimensional compression	27
2.5 Strength properties.....	29
2.5.1 General	29
2.5.2 Total and effective stress analysis	33
2.5.3 Undrained strength	41
2.5.4 Drained strength	50
2.6 Deformation properties.....	51
2.6.1 General	51
2.6.2 Drained and undrained behaviour.....	52
2.6.3 Effect of depth on modulus of elasticity	53

2.6.4 Effect of anisotropy on modulus of elasticity	54
2.6.5 Constrained Modulus from one-dimensional compression	55
2.6.6 Unloading/reloading modulus of elasticity.....	55
3 Constitutive soil models and soil parameters.....	57
3.1 Constitutive soil models	57
3.1.1 Introduction	57
3.1.2 Linear elastic stress-strain law.....	57
3.1.3 Non-linear elastic stress-strain law.....	58
3.1.4 Variable elastic stress-strain law	58
3.1.5 Elasto-plastic stress-strain law	59
3.1.6 Elasto-visco-plasticity	64
3.1.7 Hypoplasticity	65
3.1.8 Cap models	67
3.1.9 The constitutive soil models used in PLAXIS FE-program	68
3.1.10 Requirement for constitutive soil models - example excavation	70
3.1.10 Constitutive relations for interface elements	71
3.2 Derivation of soil parameters for numerical analysis	71
3.2.1 General	71
3.2.2 Determination of compression parameters	71
3.2.3 Determination of strength parameters	78
3.2.4 Deformation parameters under deviatoric loading condition	89
3.2.5 Contact behaviour between wall material and soft soil	99
3.3 Calibration of soil parameters	103
3.3.1 Drained test behaviour.....	103
3.3.2 Undrained test behaviour.....	111
4 Supported excavations in soft soil deposits	117
4.1 General	117
4.2 Unsupported excavations	118
4.3 Excavation retaining systems in soft soils.....	120
4.3.1 Type of wall	120
4.3.2 Type of wall support.....	121
4.3.3 Recommendations for retaining structures according to EAB	122
4.4 Behaviour of excavations	126
4.4.1 General	126
4.4.2 Earth pressure, reaction and section forces.....	128
4.4.3 Movements in and around an excavation	134
4.4.4 Excavation stability in soft soils.....	141
4.5 Execution of excavations.....	144

4.6 Safety factor in design of retaining structures	149
4.7. Drained/undrained analysis of excavation.....	152
4.7.1 General	152
4.7.2 Is drained or undrained behaviour most critical for design of supported excavations?.....	153
4.7.3 The time limit for undrained and drained condition	155
4.7.4 Determination of the earth pressure in short term using the effective strength and the pore pressure parameters	156
4.7.5 Earth pressure in short term using the undrained strength.....	158
4.7.6 Comparison of the different approaches.....	160
4.8 Stress paths in excavations	164
4.9 Some reviews of FE-analysis of excavations	169
4.9.1 General	169
4.9.2 Factors affecting the performance of excavations	170
4.10 Parameter study	173
4.10.1 General	173
4.10.2 System geometry	174
4.10.3 Sensitivity study of the hardening soil model parameters	177
4.10.4 Effect of berms on deformation of excavations.....	185
4.10.5 Effect of the bottom support.....	187
4.10.6 Comparison of drained and undrained analysis.....	188
4.10.7 Mobilization of the passive resistance of a cohesive soil	191
4.11 German recommendation for excavation in soft soils	197
4.11.1 General	197
4.11.2 The shear strength and the coefficient of earth pressure at rest	197
4.11.3 Earth pressures and reactions.....	200
4.11.4 Water pressure	204
4.11.5 Embedment depth and section forces	206
4.11.6 Basal failure.....	207
4.11.7 Drainage measures in excavation	211
4.12 Case histories.....	211
4.12.1 General	211
4.12.2 Project-I: Damgasse - Constance	212
4.12.3 Project-II: Markgrafenstrasse - Constance	239
4.12.4 Project-III: Seeuferhaus – Constance	255
4.12.5 Project-IV: Seekaden Starnberg	262
4.12.6 Project-V: Karstadt building in Rosenheim.....	267
5 Shallow foundations on soft soils.....	275
5.1 General	275
5.2 Historical foundation on soft soil deposits	275

5.3 Type of shallow foundations	278
5.4 Settlement calculations – the serviceability limit state	280
5.4.1 Soft soils deformation behaviour and calculation methods	280
5.4.2 Stresses and settlements due to external load	280
5.4.3 Time settlement behaviour, magnitude and components of settlements of shallow foundations.....	286
5.4.4 Allowable settlements, tilts and angular distortions	297
5.5 Case histories of buildings on raft foundations	310
5.5.1 General	310
5.5.2 Soil condition	310
5.5.3 Review of settlement observations	311
5.5.4 Summary of the back analyses results	321
5.5.5 Effect of load increment and rate on settlement prediction	323
5.6 Two case histories with excessive settlements	326
5.6.1 General	326
5.6.2 Case A: office building.....	327
5.6.3 Case B: Storage tanks.....	329
5.6.4 Numerical analysis	330
5.7 Case history of an embankment	331
5.8 Case history of settlement due to shrinkage	333
5.9 Safety of shallow foundations	336
5.10 Design of raft foundation.....	337
5.10.1 General	337
5.10.2 Parameter study	338
5.10.3 Numerical analysis using the FEM.....	340
5.10.4 Verification of the modified subgrade reaction method on selective projects	342
5.10.5 Effect of creep of the soil on flexural stress of a plate.....	346
5.11 Summary and recommendations	346
6 Pile foundation.....	349
6.1 Introduction	349
6.2 Pile types and construction methods	350
6.2.1 Selection of appropriate pile type.....	350
6.2.2 Displacement piles	352
6.2.3 Bored piles.....	367
6.2.4 Micropiles.....	378
6.3 Pile bearing behaviour	381
6.4 Axial pile resistance	385

6.4.1 General	385
6.4.2 Pile resistance from static Load Tests.....	385
6.4.3 Dynamic pile testing.....	393
6.4.4 Pile resistance against horizontal loadings	395
6.4.5 Determination of pile resistance	395
6.4.6 Change of the bearing capacity of piles with time.....	410
6.5 Negative skin friction	412
6.5.1 General	412
6.5.2 Neutral point.....	414
6.5.3 Actions arising from negative skin friction	415
6.6 Lateral loads and settlement bending	419
6.8 Special pile foundations in deep soft soil deposits	422
6.9 Raft foundation on floating injection piles (RFIP)	424
6.10 Case histories on RFIP-foundation system.....	427
6.10.1 General	427
6.10.2 Project I (RFIP-foundation system).....	428
6.10.3 Project II (RFIP)	432
6.10.4 Project III (Floating displacement piles)	449
6.10.5 Project IV (excavation and old building stabilisation with RFIP)	453
6.10.6 Summary.....	459
7 Soil stabilisation with column-like elements.....	461
7.1 General	461
7.2 Reinforced embankments on pile-like elements	461
7.2.1 General	461
7.2.2 Load transfer mechanism.....	463
7.3 Stone columns and sand compaction piles	467
7.3.1 General	467
7.3.2 Principles of design and analysis	468
7.4 Geotextile encased sand/gravel columns (GEC)	474
7.4.1 General	474
7.4.2 Installation method	474
7.4.2 The bearing system of the GEC.....	476
7.4.3 The analytical calculation approach	477
7.5 CSV Method.....	481
7.5.1 General	481
7.5.2 The method of installation	482
7.5.3 The bearing system.....	483
7.5.4 Design and analysis	484
7.6 Deep mixing method (DMM).....	487

7.6.1 Introduction	487
7.6.2 Dry deep mixing method	488
7.6.3 Wet deep mixing method.....	493
7.6.4 Jet pile method.....	500
7.7 Unreinforced pile like elements.....	501
7.7.1 Grouted stone/gravel column	501
7.7.2 Ready-mixed mortar columns	502
7.7.3 Unreinforced concrete columns.....	502
7.8 Displacement and bored piles.....	503
7.9 Case histories.....	503
7.9.1 Muehlenberger loch - geotextile-encased sand columns (GEC).....	503
7.9.2 Hamburg–Berlin railway line: reinforced embankment on pile like elements	508
7.9.3 City road Trasa Zielona in Lublin-Polen: wet deep soil mixing.....	515
7.9.4 A multistory building on wet deep mixing columns.....	515
7.9.5 Pad and strip foundations on wet deep mixing columns	517
7.9.6 Highway bridges supported on wet deep mixing columns	518
7.9.7 Restoration of an offshore retaining wall with CSV-columns.....	518
7.9.8 Stabilisation of 5-storey building foundation and underground parking with CSV-columns	521
References	525
Index.....	551

Symbols and abbreviations

Here are the most frequently used symbols, abbreviations and expressions. Actually, most of the symbols has already been locally defined in the text. Some symbols may also have one or more definitions.

Geometrical symbols

Symbol	Description
A	pile spacing within a pile group
A_b	nominal value of pile base area
A_e, A_c	cross sectional area of a column, cross sectional area of an influence zone
A_Q	cross sectional area of pile
A_s	nominal value of pile shaft area
a_s	width of a pile with a square cross section
$A_{\varepsilon}, A_{\rho}, A_{\mu}$	surface area at edge, at corner and in middle of a plate
b	width of an excavation
b, b_E, D_s, a_s	width or diameter of a single pile
d	distance behind a wall, thickness, diameter of a column
D	drainage path
D_b	pile base diameter
d_e	equivalent diameter
D_{eq}	equivalent pile diameter
D_s	pile shaft diameter
h	depth of excavation, height of soil specimen
Δh	thickness of a layer
h_0	reference height, initial height
h_B	depth to passive force from bottom of excavation
h_E	depth to active force from surface
L	pile length
L^*	elastic length of pile
l_d	drainage path
r_0	initial radius
r_c	equivalent radius of an influence zone of a single pile
R_c	column radius
S	settlement at pile head
s_d	column spacing
T	embedment into the bearing strata
Z	depth from ground surface, vertical deflection
z_c	depth to tension crack from surface

z_p	depth from bottom of excavation
z_p, z_w	vertical deflection of a pile and a soft layer

Material parameters

Symbol	Description
A, B	coefficient of pore pressure
A_f, B_f	coefficient of pore pressure at failure
$A_{f,s}$	coefficient of pore pressure at failure in standard triaxial compression test
C	composition
c	cohesion
c	wave propagation velocity
c_a	adhesion
C_B	Buisman factor
C_c	compression index
c_h	coefficient of consolidation in horizontal direction
C_p, C_w	subgrade reactions (spring constants) of pile and soft layer
C_s	swelling index
c_u	undrained shear strength
$c_{u,av}$	average shear strength along an assumed rupture surface
$c_{u,col}$	maximum value of undrained strength of a stabilising column
c_{uc}, c_{ut}	undrained shear strength in compression and in tension
c_{uv}, c_{uh}	undrained shear strength in vertical and horizontal directions
c_v	coefficient of compressibility
c_v	coefficient of consolidation in vertical direction
C_α	coefficient of secondary compression
\underline{D}^e	elastic material stiffness matrix
$\underline{\underline{D}}^{ep}$	elasto - plastic stiffness matrix
$\underline{\underline{D}}$	tangential stiffness tensor of the material
E	drained modulus of elasticity
e	void ratio
\overline{E}	weighted average of the elasticity modulus of a column material and soil
e_0, e_p	initial void ratio
E_{50}	secant modulus of elasticity at 50% of deviator stress at failure (drained)
$E_{50(u)}$	secant modulus of elasticity at 50% of deviator stress at failure (undrained)
E_b	dynamic modulus of elasticity of pile material
E_h, E_v	modulus of elasticity in horizontal and vertical directions
E_i	initial tangent modulus of elasticity
e_L	void ratio at liquid limit
E_m	compressibility modulus
$E_{m,ur}$	compressibility modulus for un-/reloading
E_{oed}	constrained modulus of elasticity
$E_{oed,0}$	initial constrained modulus
$E_{oed,s}$	constrained modulus of the soft soil layer
$E_{oed,ur}$	constrained modulus of elasticity for un-/reloading
E^{ref}	reference drained modulus of elasticity

E_{sec}	secant modulus of elasticity
E_t	tangent modulus of elasticity
E_u	undrained modulus of elasticity
$E_{u,i}$	initial undrained modulus of elasticity
$E_{u,ur}$	undrained modulus of elasticity for un-/reloading
E_{ur}	modulus of elasticity for un/reloading
f_{bt}	tensile strength of a masonry wall
G	shear modulus
G^{ref}	reference shear stiffness at reference stress p^{ref}
G_s	specific gravity of a soil
G_s	shear modulus of unstabilised soil
G_{si}	undrained shear stiffness
G_u	undrained shear modulus
I_c	consistency index
I_D	relative density
I_L	liquidity index
I_p	plasticity index
I_v	viscosity index
$I_{v\alpha}$	coefficient of viscosity
J	stiffness of geosynthetic membrane
k	influence factor, dimensionless modulus number
k	coefficient of permeability of soil
K'	drained bulk modulus of elasticity
K_0	coefficient of earth pressure at rest
$K_{0(NC)}$	coefficient of earth pressure at rest for normally consolidated and overconsolidated soils
$K_{0(OC)}$	coefficient of active earth pressure
K_a	coefficient of active earth pressure of a column material in Rankin's special case
\underline{K}^p	elasto - plastic material stiffness in the finite element formulation
K_p	coefficient of passive earth pressure at limit state
K_a^T	ratio of total horizontal and vertical stresses in active state
K_p^T	ratio of total horizontal and vertical stresses in passive state
$K_{p,c}$	coefficient of passive earth pressure of a column material in Rankin's special case
K^{ref}	reference bulk modulus of elasticity
k_s	subgrade modulus on pile axis
K_u	bulk undrained modulus of elasticity
K_w	bulk modulus of water
LL	liquid limit
M	slope of critical state line in p - q diagram
m	stiffness exponent
M_c	compressibility modulus of columns
M_s	compressibility modulus of unstabilised soil
m_v	coefficient of compressibility for one-dimensional compression
OCR	overconsolidation ratio
PL	plastic limit
U	shape-factor
U_c	degree of consolidation

ΔV	volume change
w	water content of soil
\bar{w}	average water content of soil
W	total amount of slurry
w/c	water-cement ratio
W_p	amount of injected slurry
w_s	water content at shrinkage limit
Δw	water content difference
α_b	base resistance coefficient
α_k	shear coefficient
α_s	adhesion coefficient
β_s	settlement reduction factor
δ	wall friction
γ	unit weight of soil
γ'	buoyant unit weight of soil
γ_d	dry unit weight of soil
γ_D	unit weight of soil above the foundation level
γ_r, γ_{sat}	saturated unit weight of soil
γ_w	unit weight of water
φ	angel of internal friction
φ'_s	angel of overall shear strength
φ_u	undrained angel of internal friction
$eqv. \varphi_{cu}$	equivalent angel of total friction
φ'_c, φ'_t	effective angel of internal friction in compression and in tension
$\varphi'_{s,c}, \varphi'_{s,t}$	angle of overall shear strength in compression and extension
κ	slope of un/reloading line
κ^*	modified swelling index
λ	slope of normal consolidation line
λ^*	modified compression index
λ_{cu}	normalised undrained shear strength
$\lambda_{cu,s}$	normalised undrained shear strength in standard triaxial compression test
μ^*	modified creep index
ν	Poisson's ratio
ν'	drained Poisson's ratio
ν_u	undrained Poisson's ratio
ν_{ur}	Poisson's ratio for un/reloading
ν_v, ν_h	Poisson's ratio in vertical and horizontal direction
ρ	density of material
ρ_w	density of water dependent on temperature
τ	shear strength of soil
τ_{av}	average shear stress
τ_f	field vane shear strength
τ_m	mobilised shear strength
τ_n	negative skin friction
τ_{uv}, τ_{uh}	vane shear strength in vertical and horizontal directions
v	specific volume

v_c , v_q , v_γ	shape factors for cohesion
v_{0t} , v_{kt}	specific volume corresponding to $p'=1$ kN/m ²
ψ	angle of dilatancy

Deformations, forces and stresses

Symbol	Description
B	strain matrix
c_{ve}	equivalent coefficient of consolidation
D	strain rate
de_e	recoverable elastic compression under constant effective stress
de_{ir}	irrecoverable compression under constant effective stress
de_v	irrecoverable viscous compression under constant effective stress
dp	incremental mean principal stress
dq	incremental shear stress
$d\varepsilon$	incremental strain
$d\varepsilon_t$	incremental total strain tensor
$d\varepsilon_1$, $d\varepsilon_2$, $d\varepsilon_3$	incremental principal strains
$d\varepsilon^e$	incremental elastic strain tensor
$d\varepsilon^p$	incremental plastic strain tensor
$d\varepsilon_q$	incremental shear strain
$d\varepsilon_v$	incremental volumetric strain
$d\varepsilon^{vp}$	incremental visco - plastic strain tensor
$d\sigma$	incremental stress tensor
$d\sigma$	incremental stress
E	actions, effect of actions
e_{0h} , e_{0v}	earth pressure at rest in horizontal and vertical directions
e_{ah} , e_{av}	active earth pressure in horizontal and vertical directions
e_c	stress dependant critical void ratio
e_{c0} , e_{i0} , e_{d0}	limiting void ratios
E_h	characteristic horizontal load on a single pile
e_h , e_v	earth pressure in horizontal and vertical direction
e_i , e_d	stress dependant limiting void ratio
e_{ph} , e_{pv}	passive earth pressure in horizontal and vertical directions
F	force on pile head, stabilising actions
f	settlement coefficient
$F(\sigma), F(\sigma.h)$	yield function
F_I	impact force
F_2	measured force of wave reflected at the base
f_c	skin friction of cone penetration test (CPT)
F_n	additional downdrag force on piles
ΔF_r	hoop tensile force in the geotextile coating
f_s	relative stress level, local skin friction
G	stabilising actions
G_{si}	initial shear stiffness

H	horizontal component of reaction forces
$h(d\mathcal{E}^p)$	hardening function
h_s	granular hardening
I_1	the first invariant of the stress tensor
J_2	the second invariant of the deviatoric stress tensor
J_3	the third invariant of the deviatoric stress tensor
$k_{s,e}, k_{s,r}, k_{s,m}$	modulus of the subgrade reaction at the edge, at the corner and in the middle of the plate
p	surcharge load
p^*	existing stress level
p, p'	total and effective mean principal stresses
p_1, p_2^*	stresses before and after load change
p_f	characteristic flow-pressure
p_f, p'_f	total and effective mean principal stresses at failure
p'_m	previous maximum mean effective stress in which a soil was subjected
p'_t	mean stress at time t
p_{max}	absolute stress in surrounding soil at limit state
p_p^{ref}	isotropic pre-consolidation stress
p^{ref}	reference pressure
q	deviatoric stress, total applied pressure (q_1+q_2)
$Q, Q(\sigma)$	potential function
q_1	pressure on columns
q_2	pressure on unstabilised soil
q_b	base resistance, point resistance, end bearing
$q_{b,l}$	ultimate base resistance
q_c	cone resistance
q_c	point resistance of cone penetration test (CPT)
Q^{col}	ultimate bearing capacity of a single column
q_f	deviatoric stress
q_s	shaft resistance
Q_S	shaft resistance for displacement piles
$q_{s,l}$	ultimate shaft resistance
$q_{s,l,t}$	ultimate shaft resistance in tension
$q_{s,t}$	shaft resistance in tension
q_t	deviatoric stress at time t
Q_T	total pile resistance for displacement piles
q_u	unconfined compressive strength
q_{ult}	ultimate asymptotic value of a deviatoric stress
Q_{ult}^{group}	total bearing capacity of a group of columns
R	resistance, aspect ratio of a cap
R_b	base resistance of a single pile
R_{cp}	resistance of end B2-columns
R_{dyn}	dynamic resistance
R_g	expected ultimate pile resistance
R_s	skin resistance of a single pile
R_{stat}	available static resistance
R_{tot}	total dynamic resistance
s	shear displacement

S	resultant tensile force in reinforcement membrane
s_0	immediate settlement
s_{ult}	settlement in ultimate limit state (ULS)
s_2	settlement of unstabilised soil
s_c	settlement of stabilising column, settlement of a foundation at a characteristic point
s_{cal}	calculated settlement
s_g	limit settlement
s_G	settlement due to group effect
s_p	consolidation settlement
s_s	settlement of the soil
s_{sg}	limit settlement for the settlement-dependent characteristic pile shaft resistance
s_∞	final settlement
s_z^{ES}	compression of an invalid column
s_B^{ES}	settlement of an invalid column
Δs	differential settlement
\mathbf{T}	stress tensor
$\dot{\mathbf{T}}$	Jaumann stress rate as a function of stress level
u	pore water pressure
u_0	pore water pressure at steady state (hydrostatic), initial pore pressure
Δu	excess pore water pressure
Δu_f	excess pore water pressure at failure
W	strain energy density function
α	maximum angular rotation between two column rows
δ_v, δ_v	horizontal and vertical deflection of a wall
ε	strain
ε_f	strain at failure
ε_h	strain in horizontal direction
ε_{krit}	critical strain
ε_v	strain in vertical direction, volumetric strain
$\Delta \varepsilon$	change in strain
$\Delta \varepsilon_{vol}$	change in volumetric strain
$\dot{\varepsilon}$	rate of strain
$\dot{\varepsilon}_v$	porosity of a soil
$\dot{\varepsilon}_o$	strain rate at reference time t_0
$\dot{\varepsilon}_i$	strain rate at reference time t_i
λ	positive scalar of proportionality dependant on state of stress and load history
μ	fluidity parameter
$\underline{\sigma}$	stress tensor
σ_{10}, σ_{30}	initial major and minor principal normal stress
σ_c, σ_s	pressures on column and soil
σ_{max}	ultimate load
σ_N	normal stress
$\sigma_{v,0,c}$	initial vertical stress in column
$\sigma_{v,0,s}$	initial vertical stress in soil

σ_x, σ_y	stresses in x- and y-directions
σ_{zo}	effective stress on top of soft soil layer
σ_ϕ	tangential stress
σ'_{vc}	effective consolidation stress
σ'_h	effective horizontal stress
σ'_c	effective cell pressure
σ'_1	effective major principal stress
σ'_2	effective intermediate principal stress
σ'_3	effective minor principal stress
σ'_e	effective Hvorslev's equivalent stress
σ'_p	effective pre-consolidation pressure
σ'_0	effective net pressure on footing, contact pressure
σ'_b	effective stresses due dead and live loads from buildings
σ'_u	uplift pressure
σ'_A	constant effective stress
σ'_B	effective apparent pre-consolidation stress
$\sigma'_{v,max}$	maximum vertical effective pressure on column
$\sigma'_{h,max}$	maximum horizontal effective pressure on surrounding soil
$\sigma'_{h,0}$	effective initial horizontal stress in soil before column installation
σ'_m	effective mobilised stress
σ'_f	effective failure stress
σ'_r	effective radial stress
$\Delta\sigma'$	additional effective stress
$\dot{\sigma}_w$	rate of excess pore water pressure
σ'_{vm}	previous maximum vertical effective stress in which a soil was subjected
$(\sigma'_1 - \sigma'_3)_f$	deviator stress at failure in triaxial test
σ', σ'_x	effective normal stress
$\sigma_{v0}, \sigma'_{v0}$	total and effective overburden pressures respectively
σ'_z, σ'_v	effective vertical stress
$\sigma'_{3,0}, \sigma'_{1,0}$	effective consolidation pressure in triaxial test
$\Delta\sigma_1, \Delta\sigma_3$	principal stress increments
τ_{xy}	shear stress

Miscellaneous

Symbol	Description
a	factor to represent the calibration of the model on the Matsuoka-Nakai yield function
a_c	area displacement ratio
C_1, C_2, C_3	constants
CAD	anisotropically consolidated drained
CAU	anisotropically consolidated undrained
CID	isotropically consolidated drained
CIU	isotropically consolidated undrained
C_r	shape factor
CPT	Cone penetration test
DSS	direct simple shear
EQU	loss of equilibrium of structures or ground
$F.S$	factor of safety against basal heave
F_d	factor of safety on the depth of penetration
f_a, f_e, f_b	factors to simulate the barotropy and pycnentropy effects
F_{np}	factor of safety on the moment of the net active forces
f_g, f_{wa}	safety factors on action forces and water pressure on the active side
F_r	factor of safety on the moment of activating forces
f_r, f_{wp}	safety factors on passive forces and water pressure
F_{sp}	factor of safety on the soil parameters for passive earth pressure
F_ϕ, F_c, F_{cu}	partial safety factors on friction ϕ , cohesion c and undrained strength c_{cu}
GEO	loss of failure of the ground (geotechnical failure)
GZ	limit state for German word "Grenzzustand"
HYD	hydraulic heave, internal erosion and piping in the ground caused by hydraulic gradient
i_p, i_c	influence factor for the calculation of σ_z
index d	design value
index k	characteristic value
K	principal stress ratio
m	proportion of load carried by stabilising column
M	slope of the failure line in critical soil mechanics
N	number of load tests
n	proportionality constant, viscosity exponent, stress concentration factor, rate of the volumetric strain
N, N_b, N_c	stability number
N_{30}	number of blows for 30 cm penetration test
N_k	empirical cone factor
N_q, N_c, N_γ	bearing capacity factors
R^2	coefficient of correlation
R_f	failure stress ratio
R_{int}	interface element parameter (parameter reduction factor to account the wall friction and adhesion)
R_{inter}	interface factor
R_p, R_w	rotational speed of the mixing pool during penetration and withdrawal
SLS	serviceability limit state
SPT	Standard penetration test

STR	loss of structures or structural elements
T	blade rotation number
T^*	time from which viscosity starts to act
T, t	time
T_0	reference time
TC	triaxial compression
t_c	time required for primary consolidation
TE	triaxial extension
t_f	time to failure
t_i	time
t_p	primary consolidation time
tr	tensor
T_v	time factor
ULS	ultimate limit state
UPL	loss of equilibrium of structures, of elements of structures or ground due to uplift
UU	unconsolidated undrained
V	velocity
V_I	velocity of impact
V_2	velocity of wave reflected at the base
V_p, V_w	penetration and withdrawal velocity respectively
Z	impedance
$Z(t)$	time factor
ΣM	total number of mixing blades
α_k	shear coefficient
β	reciprocal of the gradient of the stress path
γ_{3D}	partial safety factor for passive resistance
γ_c	partial safety factor for cohesion
γ_{cp}	partial safety factor for load tests
$\gamma_{dst}, \gamma_{stb}$	partial safety factors for destabilising/stabilising actions
γ_F, γ_q	partial safety factor for actions or effect actions
γ_R, γ_r	partial safety factor for resistance
γ_{wa}	partial safety factor for water pressure
γ_ϕ	partial safety factor for angle internal friction
η_p	total safety factor on passive pressure
λ_{3D}	factor for three dimensional case
$\lambda_b, \lambda_b, \lambda_c$	bearing capacity coefficients
μ	empirical correction factor
μ_l, μ_2	the effect of the width of excavation
μ_A	anisotropic correction factor to the vane shear strength
μ_R	anisotropic and the rate of shearing correction factor to the vane shear strength
$\omega_b, \omega_{s,q}, \omega_{s,f}$	empirical reduction factors
$\omega_{s,s}$	factor of anisotropy, correlation factor for evaluation of pile load tests
ξ	

1 Introduction

1.1 General

Geotechnical design and execution of civil engineering structures on/in soft to very soft soils are usually associated with substantial difficulties. Since this type of soils are sensitive to deformations and possesses very small shear strength, they may lead to structural damages during the execution as well as throughout the life of the projects specially in urban areas. This can be due to:

- excessive settlements or tilting of newly constructed building structures,
- entrainment settlement of old structures near newly erected structures,
- an adverse effect of excavations on nearby structures, etc.

Also highways and railways as well as other infrastructure projects on soft soils are frequently associated with construction problems and damages or requires a special and substantial construction measures to completely avoid or limit the damage to certain extent.

Geologically young, normal consolidated cohesive soft soils are distributed world wide along coastal areas and around lakes and rivers. For example:

- Southeast Asia, Japan, India,
- North and central America (e.g. Mexico Clay, Cancagua or lacustrine sediments; Eastern Canada),
- South America and Africa (e.g. along the Nile delta, around the Victoria and Tana lakes),
- Europe (e.g. in Germany along the marshy area of the river Elbe in North, and around the Bavarian Lakes and Lake Constance in South; in Switzerland around Lake Zurich, etc.)
- Southern Norway, etc.

Independent from the geological definitions and terms, soft soils are defined in the following as normal consolidated or under consolidated or light overconsolidated fine grain soils with very soft to soft consistency (see also section 2.1).

Soft soil layers are extended to a depth of more than 30 m. Most often several silt and sand seams may be encountered in nature in post glacial deposits such as lacustrine clays in which initial excess pore pressure may still exist. This initial excess pore pressure may contribute to the instability of the soft soil layer specially during excavation.

According to the working group „excavation“ EAB of the German Geotechnical Society, the following criteria should be fulfilled in order to define the soil as a

soft soil in terms of constructional purposes. All the criteria should not however simultaneously be fulfilled.

- very soft to soft consistence with a consistency index $I_c < 0.75$,
- fully or nearly fully saturated,
- the undrained shear strength $c_u \leq 40 \text{ kN/m}^2$,
- inclined to flow,
- light to middle plastic property,
- very sensitive to vibrations (sensitivity is defined here as the ratio between the undrained strength at failure and the residual strength in field vane shear test),
- thixotropic property, etc.

The “state of the art” of material properties and classifications of soft soils can be found in Chapter 2.

The book also treats the main foundation systems on soft soils and their geotechnical requirements. These include:

- excavations,
- shallow foundations,
- pile foundations,
- raft foundation on floating piles,
- soil improvement techniques with column like elements.

Moreover, special emphasis is given to case histories, which are collected together predominantly from the authors own experience in Europe and in particular in southern Germany.

With the advent of advanced computer technology in the past few decades, numerical modelling of foundations and excavations using Finite Element Method (FEM) of analysis has become increasingly popular and powerful analytical tool. Nowadays some FEM codes specially written for geotechnical problems are available on market. Major progress has also been shown in understanding the strength and deformation behaviour of soft soils. Various constitutive models, from simple elastic models to mathematically complex non-linear elasto-plastic models have been developed. However, there is still problem e.g. in prediction of movements in and around an excavation with the numerical method. Even for a given real excavation problem with known soil and structural parameters, a large discrepancy of the finite element calculation results submitted by different individuals was reported by Schweiger 2000, let alone the discrepancies in the measured and computed results. Kempfert and Gebreselassie 2000 also reported a large discrepancy among the numerical and analytical comparative results carried out by different groups. Similar experiences is also available in numerical calculations of shallow foundations, pile foundations and soils stabilisation.

The results of numerical analysis may be influenced significantly by the constitutive relationship chosen to model the behaviour of soils. Therefore, the choice of one or a group of soil models for one particular problem that addresses the constitutive relations of stress and strain of soil is very important. Even for a particular soil model, the selection of soil strength and deformation parameters may affect the results. Besides many other factors, the deformation of soils is found to be

stress path dependent. It is therefore necessary to consider whether the state of a stress at a point involves primary loading, unloading, reloading or any other possible stress path. For that matter a summary the historical development of constitutive soil models followed is briefly presented in chapter 3. The merits and demerits as well as the limitations of the various soil models are discussed in relation to geotechnical problems in soft soils. This chapter also includes the measurement of soil parameters for numerical modelling of foundations and excavations in soft soils. The evaluation of the results of series of triaxial tests; both isotropic and anisotropic consolidation, standard and stress path dependent tests, and one-dimensional, isotropic and anisotropic (K_0) compression tests can be found in this chapter which also consists a data bank of different soil parameters for lacustrine soft soil. Finally, a result of parameter study of the stress-strain behaviour of soft soils using the FEM is presented and the degree of influence of each parameters have been identified.

The numerical investigations of the theoretical and practical examples in this book are carried out using the Finite Element Code PLAXIS. The most important elements in numerical calculation of excavation and foundation problems, such as wall element, anchor system, interaction between soil and wall, the construction steps followed at the construction site, etc., can be successfully modelled with this code. Furthermore, the program offers a variety of constitutive soil models that are capable of simulating the linear and non linear behaviour, elastic and elasto-plastic behaviour, shear hardening and compression hardening, time dependent behaviour (creep effect), and stress dependent stiffness of soils (Brinkgreve 2002). Different options of analysis methods are also available in the program. These are plastic calculations (drained and undrained), consolidation analysis and update mesh analysis.

Starting with a review of design and construction principles of excavations in soft soil deposits, safety factor in the design of retaining structures, stress paths in an excavation as well as review of FE-analysis of excavations, chapter 4 discusses the total and effective stress analyses methods in design of excavations. Most of the previous works in the literature for prediction or to back analysis of the performance of excavations in soft soil by means of the FEM (for example, Clough and Mana 1976; Clough and Tsui 1974; Mana 1978; Palmer and Kenny 1972; Brooks and Spence 1993; Burland and Hancock 1977; Burland and Simpson 1979; Wong and Broms 1994; etc.) are based on the undrained strength of the soil. They assumed that the excavation is usually constructed quickly enough so that undrained soil behaviour governs. However, in an excavation problem, both drained and undrained strength of soil may be equally important depending on the duration of the excavation, the rate of pore water dissipation and the stress path it follows at different location of the excavation. Unlike other geotechnical problems such as embankment or foundation design, undrained analysis in an excavation problem may not always lead to the unfavourable condition. The choice of the effective or the total stress analysis methods in the analytical design and analysis of an excavation is also addressed in chapter 4.

A parameter study is a powerful tool to investigate the extent of the influence of model parameters on the performance of excavations. Chapter 4 presents a re-

sult of parameter studies of the hardening soil model parameters using the FEM based on an idealised excavation. After introducing briefly the new recommendation on excavations in soft ground by the German working group on “excavations” EAB, chapter 4 is concluded with case histories of five excavation projects. All the projects are constructed in soft soil deposits.

Shallow foundations on soft underground require an intensive geotechnical investigations and planning. In chapter 5 special features of shallow foundations on soft soil are summarised and research results on selection of parameters as well as own experiences from practical projects are presented.

A review of pile foundation in general followed by pile bearing behaviour are presented in chapter 6. Negative skin friction due to settlement of soft layers arising from consolidation due to own weight or additional external surcharge is a common feature of pile in soft underground. This topic is also treated in this chapter.

Pile foundations in very deep soft layer may not be feasible and economical. A combination of floating pile and raft foundation, the so called combined piled raft foundation are in practice nowadays. The book presents a special form of the combined piled raft foundation which is called raft on floating injection piles (RFIP) . The RFIP foundation system is relatively new and it have been successfully applied on projects on soft lacustrine soils in southern Germany. The injection piles are micro-piles with a steel rode on the middle and filled with cement suspension under high pressure. Experiences on such foundations system are compiled at the end of chapter 6 in form of case studies.

Construction of engineering and geotechnical structures on soft soils usually involves with excessive settlements, deformations and stability problems. Soil improvement and stabilisation is one geotechnical measures used to avoid or reduce such problems. The final chapter in this book presents construction and design aspect of stabilisation methods using pile/column like elements. Moreover, case studies of practical projects are compiled at the end of chapter 7.

Safety factors play a major role in design of geotechnical structures. Many countries adopt different safety concepts. The European countries are trying at present to introduce a common safety concept based on partial safety factor. The following section introduces the new European code “Eurocode EC 7-1” together with the German code DIN 1054 and experiences.

The aim of the authors is to give the readers an overview of the state of the art of material properties of soft soils and their application in excavations, different types of foundations and stabilisation methods. We would like to emphasize, however, that the presence of soft soil in connection with construction measure should not a priori be classified as extremely difficult and strong cost intensive. By making use of an advance knowledge in soft soil engineering so far available in the field of geotechnical engineering, it is possible to reach at a technically safe and economically justifiable solution for a particular construction project. The book is expected to contribute much in this regard.

1.2 Safety regulations in geotechnical engineering

1.2.1 The ultimate and serviceability limit states

In the ultimate limit state design (ULS) of foundations, the bearing capacity of the foundation is compared to the actions from the various loading conditions. By introducing partial safety factors both on the actions (by multiplication) and on the bearing resistance (by division), it can be verified that the foundation is sufficiently far away from the failure conditions. In a similarl way the foundation can be verified against structural failure.

In the serviceability limit state (SLS) design of foundations one must prove that settlements and deformations of shallow foundations and piles due to the characteristic loads are compatible with the building.

1.2.2 Total safety concept

In many countries, up till now, the bearing capacity has been determined on the basis of a total safety concept. The allowable bearing capacity of a shallow and pile foundation is determined by dividing the ultimate bearing capacity by a total factor of safety (F.S.), for e.g. F.S. = 2.0 is used in Germany.

1.2.3 Partial safety concept and the German Code

The new generation of norms and standards (see also section 1.2.4) in Europe are developed based on the partial safety concept. The original concept for the safety requirement was based on probability theory. In contrast, the new generation of norms separates pragmatically the total safety factors which has been used till now into partial safety factors for actions or effect of actions and resistance.

The basis for stability calculations are the characteristic values of actions or effect of actions and resistance. The characteristic value denoted by subscript k is that value which can be assumed that it will never fall below or above this value for a given probability during the life of the structure. The selection of the characteristic values for geotechnical parameters are based on derived values resulting from laboratory and field tests, complemented by well-established experience.

If, for example, the verification of the internal or external bearing capacity of piles is required, the following effects of actions are needed at the pile head or at any section in the pile:

- section forces, e.g., axial force, shear force and bending moment,
- stresses, e.g., compression, tension, shear, bending stresses and others.

Moreover, the following effects of actions may also occur as:

- dynamic and cyclic forces
- a change in part of the structure, e.g., extension, deformation or cracks,

- a change of position of a single pile or pile group, e.g., displacement, settlement, rotation, etc.

To obtain the design values of actions or effects of actions and resistance, the characteristic values of actions or effect of actions are multiplied and the resistance divided by partial safety factors. The design values are denoted by subscript d. In the safety verifications, a distinction has to be made between different limit states. Thereby, the term limit state is used in two different definitions:

- a) The limit state is defined in soil mechanics as plastic flow, in which the displacement of each soil grain in a soil mass or at least in the region of a failure surface is very large relative to each other and hence the shear strength reaches its maximum value. The shear strength cannot be increased beyond the maximum value when the soil movement increases further, but a fall of the shear strength to a lower rest value is possible in some cases. The active and passive states, the bearing failure conditions, the external pile failure, the slope failure and global failure surface are categorised as limit state of a plastic flow.
- b) In sense of the new partial safety concept, the term limit state is a state of a structure, in which it fails to fulfil the requirements given in the design.

The partial safety concept is first applied in the German standard DIN 1054 "Ground–Verification of the safety of earthworks and foundations" in 2003. In terms of the partial safety concept, distinction has to be made between the following limit states, whereby the terms are adopted from DIN 1054: 2005:

- a) The ultimate limit state is a limit state of the bearing capacity or strength and it is denoted by GZ 1 in DIN 1054. The ultimate limit state GZ 1 is again divided into three cases: GZ 1A, GZ 1B and GZ 1C.
- b) The serviceability limit state is a limit state in which a structure fails to fulfil a functional requirement and it is denoted by GZ 2 in DIN 1054.

The verification of the loss of static equilibrium of structural elements and ground categorised in the ultimate limit state GZ 1A include:

- safety against uplift,
- safety against hydraulic heave
- safety against overturning

In GZ 1A, there are only actions and no resistances are expected to exist. A verification of this limit state requires the fulfilment of the following inequality:

$$F_d = F_k \cdot \gamma_{dst} \leq G_k \cdot \gamma_{stb} = G_d \quad (1.1)$$

That is, the destabilising design value of actions should not exceed the design value of the stabilising actions, where $\gamma_{dst} \geq 1$ and $\gamma_{stb} < 1$ are partial safety factors for destabilising and stabilising actions respectively.

The ultimate limit state GZ 1B describes the failure condition of a structure or element of a structure as well as the underground. This includes:

- a) The verification of the ultimate limit state of structures and elements of a structure which are subjected to a load from the underground or they are supported by the underground.

- b) The verification of the ultimate limit state of the underground, e.g., in form of passive, bearing, pile or slid resistances.

The following inequality must be satisfied in the verification of the ultimate limit state GZ 1B:

$$E_d = E_k \cdot \gamma_F \leq R_k / \gamma_R = R_d \quad (1.2)$$

That is, the design value of actions should not exceed the design value of resistance, where $\gamma_F \geq 1$ and $\gamma_R > 1$ are partial safety factors for actions and resistance respectively.

The ultimate limit state GZ 1C is a special feature in geotechnical engineering which describes the loss of the overall stability. This include:

- a) The verification of safety against slope failure, and
- b) The verification of safety against global failure.

The inequality to be satisfied in GZ 1C is,

$$E_d \leq R_d \quad (1.3)$$

That is, the design value of actions should not exceed the design value of resistances, where the design values are calculated from the beginning using the reduced (design) shear parameters according to the equations:

$$\tan \varphi'_d = \frac{\tan \varphi'_k}{\gamma_\varphi} \quad \text{and} \quad c'_d = \frac{c'_k}{\gamma_c} \quad (1.4a)$$

$$\tan \varphi'_{u,d} = \frac{\tan \varphi'_{u,k}}{\gamma_\varphi} \quad \text{and} \quad c'_{u,d} = \frac{c'_{u,k}}{\gamma_c} \quad (1.4b)$$

where γ_φ and γ_c are partial safety factors for shear parameters with value > 1 .

In the serviceability limit GZ 2, the expected displacements and deformations should be consistent with the function of the structure.

1.2.4 European code of standard

The analysis and design of geotechnical structures are regulated in EN 1997-1-2004: Eurocode 7 “Geotechnical design – Part 1: general rules”. However, the application of this code requires a common agreement in Europe and an additional preparation of a national document for application in each European country.

According to the commission of the European union, the Eurocode EC 7 will come to effect starting from 2007 and is binding for application in all the European countries. However, the national codes will remain valid parallel to Eurocode till 2010.

The Eurocode EC 7 is briefly presented in the following. The partial safety factors are grouped in three different sets depending on the various views of the different European countries. The sets are denoted by A for actions or effects of actions, M for soil parameters and R for resistances. Again there are three design

approaches recommended by EC 7-1 which include different combination of set of the partial safety factors. These are:

Design approach 1 is developed based on experiences in Great Britain and the Scandinavian countries and suggests the evaluation of the following combinations of sets of partial factors:

Combination 1: A1 + M1 + R1

Combination 2: A2 + (M1 or M2) + R4

It is obvious that one of these combinations governs the design. It is therefore not necessary to evaluate other combinations. The partial safety factors for the soil parameters in combination 2 are selected depending on the type of loading. M1 is used for calculating resistances of piles or anchors and M2 for unfavourable actions on piles owing e.g. to negative skin friction or transverse loading.

Design approach 2 follows the experiences in most of the European countries and considers the following combination of sets of the partial factors:

Combination: A1 + M1 + R2

All the partial factors for soil parameters in set M1 are normally set to 1.0. The partial safety factors are therefore come into play in this design approach for actions and resistances only.

A special German application form of the design approach 2 denoted by design approach 2* suggests to perform the calculations using the characteristic values first and to factor them with partial safety factors at the end.

Design approach 3 requires the verification of the limit state using the following combination of sets of the partial factors:

Combination: (A1 or A2) + M2 + R3

The partial factor set A1 and A2 are used in the case of structural and geotechnical actions respectively.

1.2.5 Comparison between Eurocode EC 7-1 and German Code DIN 1054

The definitions of the different limit states according to Eurocode EC 7-1 are as follows:

- a) EQU: loss of equilibrium of the structure or the ground, considered as a rigid body, in which the strengths of structural materials and the ground are significant in providing resistance
- b) STR: internal failure or excessive deformation of the structure or structural elements, including e.g. footings, piles or basement walls, in which the strength of the structural material is significant in providing resistance.
- c) GEO: failure or excessive deformation of the ground, in which the strength of soil or rock is significant in providing resistance.
- d) UPL: loss of equilibrium of the structure or the ground due to uplift by water pressure (buoyancy) or other vertical actions.
- e) HYP: hydraulic heave, internal erosion and piping in the ground caused by hydraulic gradient.

To compare the ultimate limit state GZ 1B in DIN 1054 with the limit states terminology of the Eurocode EC 7-1, the ultimate limit state GEO must be divided into GEO B and GEO C.

- a) GEO B: failure or excessive deformation of the ground in relation to the determination of section forces and dimensions of a structural element, i.e. the calculation of passive resistance, slide resistance, bearing resistance, pile base and shaft resistance and in verification of safety against slip of the ground behind a returning structures together with the ground anchors or tension piles, or on slip surfaces that intersect a number of anchor elements with the use of the shear strength.
- b) GEO C: failure or excessive deformation of the ground in relation to the verification of the overall stability, i.e. in verification of safety against slope failure, global failure as well as the structural slope stabilisation, e.g. slope doweling, rock anchors, soil nails, element walls, geotextile-reinforced slopes and geotextile-reinforced constructions, as well as reinforced earth structures with the use of the shear strength.

The definitions of limit states in DIN 1054 and Eurocode EC 7-1 can be matched as follows:

- The ultimate limit state GZ 1A in DIN 1054 corresponds to the ultimate limit state EQU, UPL and HYP in EC 7-1.
- The ultimate limit state GZ 1B in DIN 1054 corresponds to the ultimate limit state STR in EC 7-1. Moreover, GEO B matches with GZ 1B in relation with the design of foundation elements, e.g. external pile resistance and bearing resistance.
- The ultimate limit state GZ 1C in DIN 1054 corresponds to the ultimate limit state GEO C in relation with the verification of safety of the overall stability, i.e. the verification of the safety against slope and global failure with the use of the shear parameters.

2 Material properties of soft soils

2.1 General

Since there is such a wide variety of soil types, it is necessary to describe and classify soils in terms which convey their characteristics clearly and concisely, and which are generally accepted and understood by geotechnical engineers and researchers. Bjerrum 1973 classify soft clays based on their engineering geological history and emphasising the change in properties which have occurred since their deposition as normally consolidated young clays, normally consolidated aged clays, overconsolidated clays, weathered clays in upper crust, quick clay deposits and cemented clays. In this book, however, the term "soft soil" is defined as clay or silty clay soil which is geologically young, and come to an equilibrium under its own weight but has not undergone significant secondary or delayed consolidation since its formation. It is characterised by the fact that it is just capable of carrying the overburden weight of the soil, and any additional load will result in relatively large deformation. Soils which have not completed the consolidation under their own weight are also included in this group.

The study of soil behaviour may be approached in four main characteristic groups; index properties, compression properties, strength properties and deformation properties under deviatoric loading condition. In the following sections these four main characteristic groups will be discussed.

2.2 Sampling

The determination of soil properties of soft soils requires undisturbed samples of high quality. The quality of the samples depends on the sampling, storage and preparation techniques. All the apparatus so far developed for sampling from the surface are based on the same principle, which is to push a tube in the soft soil layer. Lefebvre and Poulin 1979 reviewed several studies (e.g. Rochelle and Lefebvre 1970; Bozozuk 1970; Eden 1970; Raymond et al. 1971) on the effect of sample disturbance on strength and compression properties of sensitive soils. All the studies agree that tube sampling damages the structure of the soil. Tube sampling is the simplest and economical way of sampling, although it is associated with sample disturbance. The main causes of sample disturbance in tube sampling are (Rochelle et al. 1981):

- Disturbance of the soil to be sampled before the beginning of sampling, ei-

ther as a result of poor drilling operation or direct pushing of a piston sampler,

- Mechanical distortion during the penetration of the sampling tube into the soil,
- Mechanical distortion and suction effects during the retrieval of the sampling tube,
- Release of the total in-situ stresses.

The first cause can be eliminated by sampling within properly cleaned bore-holes advanced by using bentonite slurry. The second and third causes are directly associated with the sampler design and can be controlled to certain extent. The forth cause is unavoidable even though its effect may be quite variable depending on the depth of sampling and soil properties.

The change of volume resulting from the intrusion of sampling tube into a soil mass is known to produce appreciable distortions in the soil sample. Several improvements on the sampling tool and sampling techniques has been done in order to improve the quality of the sample. Such new development include the stationary-piston thin-wall tube sampler, which has for many years been considered to give satisfactory results in sensitive soils. However, several studies have shown that even such samplers can produce enough mechanical distortion that a large part of the soil sample is remoulded and its mechanical properties are altered (e.g. Fig 2.1) (see also Eden 1970; La Rochelle and Lefebvre 1971; Raymond et al. 1971; La Rochelle et al. 1981). During the intrusion of the sampling tube and its subsequent extraction from the ground, large changes in total stresses are taking place which result in substantial variations of pore pressures in the sample (Schjetne 1971).

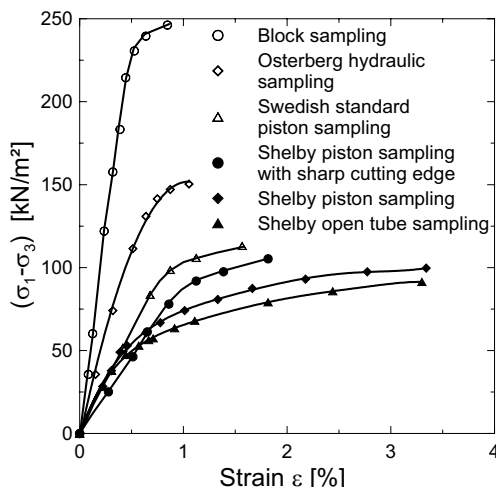


Fig. 2.1. Comparison of typical stress-strain curves for different types of samples (after Raymond et al. 1971)

As mentioned above the other cause of disturbance is the release of the in-situ stress. The change in the total stress and pore pressure produces reorganisation of interparticle contacts and it can change the stress-strain behaviour of soil samples (Graham et al. 1987; Ladd and Azzouz 1983), even though the sampling technique is otherwise perfect, which implies that no mechanical distortion should result from the sampling operation. It is a common engineering practice to improve the test performance of a soil by first consolidating the sample prior to undrained testing.

Scherzinger 1991 introduced a new technique for handling soft soil (lacustrine soil in Constance, Germany) samples from the thin tube sampler to avoid sample disturbance as a result of release of in-situ stresses during extracting, transporting and storage (see also Goldscheider and Scherzinger 1991). The samples are extracted from test pits and boreholes by thin and smooth steel tubes inserted into a sampler with a slender cutting ring. After the device is pushed into the soft soil and reached the required depth, a partial vacuum can be applied through a thin pipe in the space above the sample in order to retain the sample in the tube during pulling. The suction pressure at the lower part of the sample resulting from the piston effect during pulling can be compensated through a furrow which is cut by a tooth attached to the cutting ring. Immediately after the sample is extracted from the borehole or test pit its both open ends are trimmed and sealed watertight using a rubber disc and a perforated aluminium plates. The sealed sample with its original tube is then inserted into a pressure cell. The cell pressure is filled with water and pressurised with compressed air which is equivalent to the vertical in-situ total stress. In this way the sample is believed to retain its in-situ vertical stress until it is ready for the laboratory test.

There is a general understanding that the larger the samples are, the better the quality is. That is why nowadays a 100 mm tube samples are a common engineering practice. A comparative study between a 54, 75 and 100 mm tube samplers using unconfined compression and oedometer tests by Sarrailh 1975 shows that the specimens performed better as the size of the specimens increase. Depending on the importance of the project samples up to 200 mm diameters are also possible (e.g. see La Rochelle et al. 1981). It should be realised, however, that there are not only economical but also technical limitations to the increase of the diameters of piston sampler because the size of the zone influenced by the suction and piston effect will increase as the diameter is increased. This implies that the length of the sampling tube should also be increased proportionally in order to ensure that the middle third of the sample is of good quality. The increase of the length of the tube may lead to a massive sample with little efficiency and a higher cost. To avoid such excessive long samples and at the same time disturbance of the samples due to suction or negative stresses during sampling, La Rochelle et al. 1981 suggested a technique of overcoring and to keep the borehole filled with bentonite slurry at all times. Samples from 200 tube sampler had proven to supply a comparable strength, deformation and compression parameters as compared with block samples (La Rochelle et al. 1981).

As the discussion above shows, block sampling seems to provide a high quality samples which are used as a reference for studying the effect of disturbance of

tube samples on the strength and deformation characteristics of soft soils. Block samples are usually extracted from a bottom of a test pit or a trench, which in soft soils has to be braced to prevent accidents. Due to the cost and difficulties related to deep braced excavation, block sampling is often limited to a shallow depth of about 3 to 4 m. On large projects where money and equipment are available for deeper braced excavation, the depth of the trench could be limited by the ability of the clay to resist bottom heave. For example, in a soil with an undrained shear strength of 15 kN/m², the depth of the trench will be limited to about 4 m, if a total factor of safety of 2.0 is to be maintained against bottom heave (Lefebvre and Poulin 1979).

Lefebvre and Poulin 1979 and later Lefebvre et al. 1984 reported about a new block sampling method from the surface by allowing a hole to be kept full of water or bentonite slurry. The idea is to have a cylinder of soil about 250 mm in diameter carved in the deposit by three cutting tools arranged at every 120° and having annular motion permitting the opening of a slot about 50 mm wide around the clay cylinder. Fig. 2.2 illustrates schematically the technique of the sampler. It has been proven that block samples can be retrieved at depth of up to 9.5 m from the surface with the new technique.

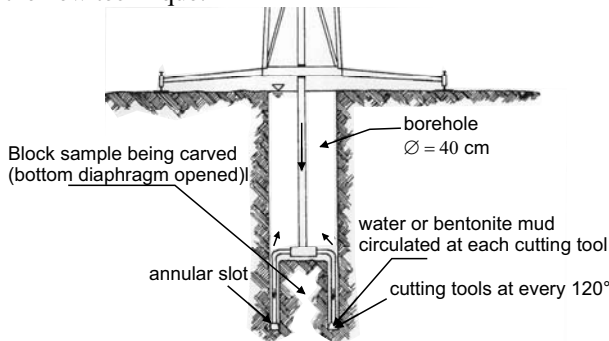


Fig. 2.2. Schematic view of deep block sampling (from Lefebvre and Poulin 1979)

A detailed presentation of sampling technique in geotechnical engineering can be found in foundation text and hand books, e.g. Joyace 1982; Hvorslev 1949; Fang 1991; Smoltczyk 2002; etc. The aim of this section is to make the reader aware of possible influence of the type and size of the samples on the strength and deformation properties of soft soils. Sample disturbance can often be responsible for large errors in the prediction of settlement of structures and deformation of retaining walls in open excavations. The engineer have to decide on the type of the techniques and the size of samples according to the importance of a particular project. It should, however, emphasised that an expensive but good quality samples might be in the end economical than a cheap and less quality samples as regard to overall cost of a project.

2.3 Basic index properties

The index parameters are a measure of the physical properties and behaviour of a soil. They are generally governed to a large extent by its geological history, mineralogical composition, the amount of clay fraction, the structure and distribution of the grains, texture of the grains. Index parameters are mainly used for the purpose of identification, description and classification of soils. Moreover, since their determination in laboratory is relatively simple, and they share the same factors that influence the strength (Table 2.1) and compression properties, they are usually employed in empirical correlation to predict compression, strength and other parameters. For example, the compression index can be estimated from liquid limit (Table 2.4), the undrained shear strength of clay from liquidity index or plasticity index (Table 2.11). The characteristic groups of the index properties and the corresponding index parameters are listed in (Table 2.1).

The principal minerals in a clay deposit tend to influence its engineering behaviour. For example, the plasticity of a clay soil is influenced by the amount of its clay fraction and the type of clay minerals present, since clay minerals greatly influence the amount of attracted water held in a soil. The undrained shear strength is related to the amount and type of clay minerals present in a clay deposit together with the presence of cementing agents. In particular, strength reduces with increasing content of mixed-layer clay and montmorillonite in the clay fraction (Fig. 2.3). The increasing presence of cementing agents, especially calcite enhances the strength of the clay. The principal clay minerals are: kaolinite, halloysite, illite, montmorillonite and chlorite. According to Scherzinger 1991, the lacustrine soft clays in southern Germany are mainly composed of non-clay minerals such as carbonate (5-25%), quartz (20-30%), and clay minerals such as chlorite (5-20%), illite (5-10%) and montmorillonite (10-20%).

Table 2.1. Characteristics and factors hypothesized to have relation with soil strength

Characteristics	Factors considered to have a relation with soil strength
Grain size	Grain size distribution, maximum grain size, mean grain size, coefficient of uniformity, shape of particles, content of fine fraction.
Density	Void ratio, relative density, dry density, specific gravity.
Plasticity	Liquid limit, plastic limit, shrinkage limit, plasticity index, consistency index, liquidity index.
Moisture	Natural moisture content and degree of saturation.
Texture	Type, proportion and structure of minerals and organic matter
Stress history	Age of deposition, number and magnitude of stress change experience, weathering, and physio-chemical effects

Geological age has also an influence on the engineering behaviour of a clay deposit. The porosity, water content and plasticity normally decrease in value with increasing depth, whereas the strength and elastic modulus increase.

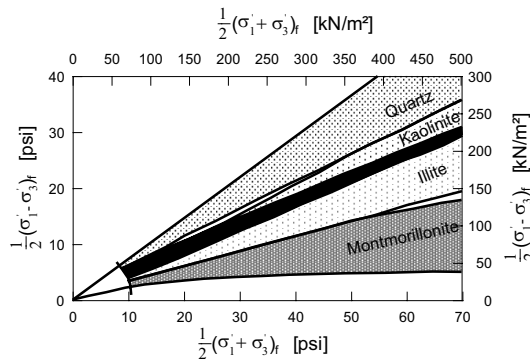


Fig. 2.3. Ranges in effective stress failure envelopes for pure clay minerals and quartz (originally from Olson 1974, reprinted from Mitchell 1993)

The engineering performance of clay deposits is also affected by the total moisture content and by the energy with which this moisture is held. For instance, the moisture content influences their consistency and strength, and the energy with which moisture is held influences their volume change characteristics. The Atterberg limits reflect both the type and amount of clay in a soil. Both liquid and plastic limits are easily determined quantities, and their correlation with soil composition and physical properties have been quite established. The liquid limit and the plastic limit are in effect indicators of the strength of clay at two different water contents of clay. The strength of clay at plastic limit is about 70 - 100 times that at liquid limit. It is generally believed that soils will have almost the same undrained shear strength (1.7-2.5 kPa) at the liquid limit, and different but again constant shear strength at the plastic limit (Wroth and Wood 1978; Atkinson and Bransby 1978; Mitchell 1993; Powrie 1997).

A plot of the plasticity index as a function of liquid limit, known as plasticity chart (Fig. 2.4a), divides the soils into different groups, and it is an essential part of soil classification system. The data for lacustrine soft soils in south Germany shown in Fig. 2.4a, obtained from Scherzinger 1991, author's own investigation and other sources show that the lacustrine soil lie in the zone of inorganic clay of low to high plasticity except the samples from one location (FHK), where they lie in the zone of inorganic silts of medium to high compressibility and organic clays and silts (DIN 18 196 (1998)). The activity of this soil is also shown in Fig. 2.4b. The activity chart is an indication of the influence of the amount of the clay fraction in the behaviour of the soil. The best fit line (Fig. 2.4b) for lacustrine soft soils in southern Germany gives an activity value of 0.41, which indicates that the soil is less active. Its consistency varies from very soft to stiff.

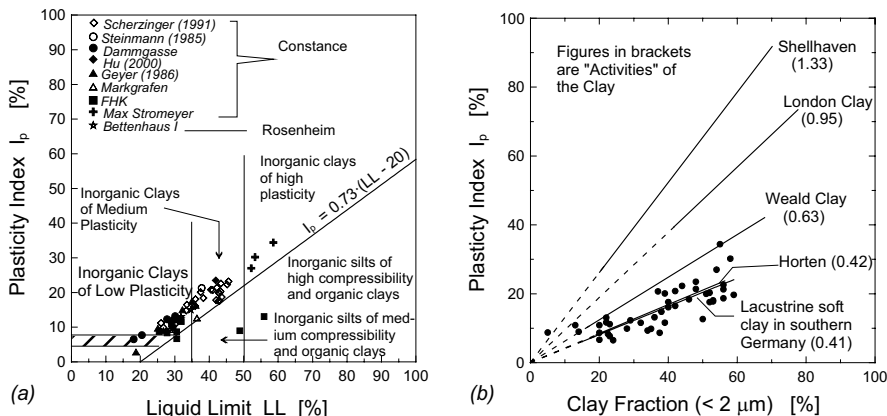


Fig. 2.4. a) Plasticity chart (DIN 18 196 (1998)), and b) Activity chart (after Mitchell 1993)

2.4 Compression properties

2.4.1 General

Volume changes in clays may occur:

1) Due to swelling or shrinkage independent of loading. Differences in the period and magnitude of precipitation and evapotransportation are the major factors influencing the swell-shrinkage response of a clay. Generally, kaolinite has the smallest swelling capacity of the clay minerals. Illite may swell by up to 15% but intermixed illite and montmorillonite may swell 60 - 100%. Swelling in Ca montmorillonite is very much less than in the Na variety; it ranges from about 50 to 100%. Swelling in Na montmorillonite occasionally can amount to 2000% of the original volume. One of the most widely used soil properties to predict swell potential is the activity of clay. Fig. 2.5 shows the range of the degree of expansiveness of a clay based on the activity. The lacustrine soft clays in southern Germany fall in the area of low expansion zone.

Retaining structures built in an unsaturated expansive soil that undergoes substantial changes in volume with changes in water content, require additional attention in the calculation of the earth pressures. The calculation must take into account the additional pressure or suction due to swelling or shrinkage of the soil.

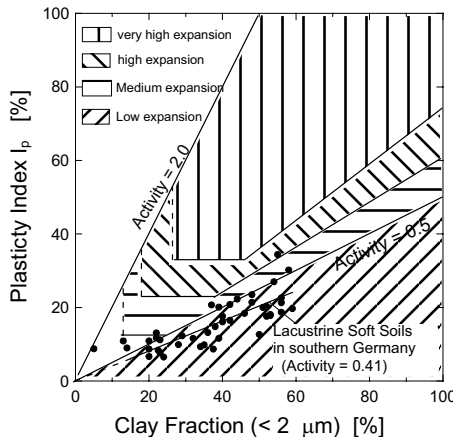


Fig. 2.5. Estimation of the degree of expansiveness of clay soil (after Bell 1993)

2) As a result of loading and unloading which bring about consolidation and heave respectively. When a load is applied to a clay soil its volume will be reduced, this being principally due to a reduction in the void ratio. If the soil is saturated, the load is initially carried by the pore water which causes an excess pore pressure to develop. The excess pore pressure dissipates at a rate which depends on the permeability of the soil mass and the length of the maximum drainage path, and then the load is eventually transferred to the soil structure (Fig. 2.6). The primary consolidation is brought about by reduction in the void ratio due to slippage of the soil particles as the soil skeleton rearranges itself to accommodate higher load. The component of such deformation is described as irrecoverable or plastic.

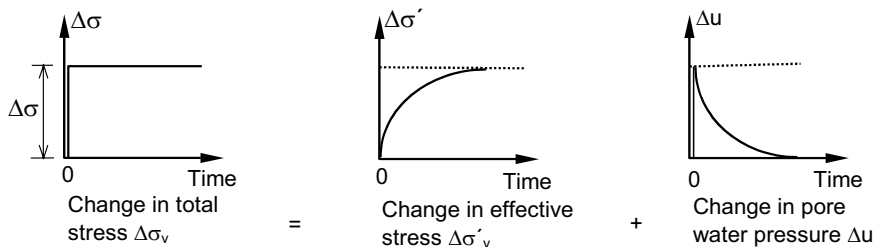


Fig. 2.6. Change of vertical effective stress excess pore pressure

The heave potential arising from stress release depends upon the nature of the diagenetic bonds within the soil. For example, when an excavation is made in a clay with weak diagenetic bonds, elastic rebound causes immediate dissipation of some stored strain energy in the soil, thus being manifested in certain amount of heave. The component of deformation due to heave (unloading) and reloading is

considered as recoverable or elastic, because changes in stress can be accommodated without the need for the rearrangement of the soil skeleton.

Further consolidation may occur due to rearrangement of soil particles or in another word due to the soil creep. Such process is often known as secondary compression. Though in many cases creep deformations are small compared to those due to changes of effective stress, it is necessary to recognize that small time-dependent deformations that are not exclusively due to changes of effective stress. The creep deformation is estimated as large as 5% (Mitchel 1993) of the deformation due to changes of effective stress for normally consolidated soft soils.

2.4.2 One-dimensional compression

Primary compression

Soils are compressed by the weight of successive layers of sediments during deposition. During deposition as well as subsequent compression, it is believed that no horizontal strain develop in any element because of symmetry. Therefore, in its natural state, the state of stress of a soil correspond to the state of one-dimensional compression. One-dimensional compression can be simulated in laboratory using oedometer, in which the boundary conditions are shown in Fig. 2.7.

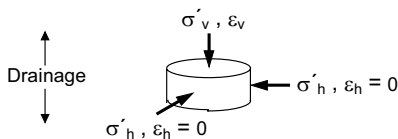


Fig. 2.7. Boundary conditions for one dimensional compression

The ratio of the horizontal effective stress to the vertical effective stress known as the coefficient of earth pressure at rest K_0 , is given by:

$$K_0 = \frac{\sigma'_h}{\sigma'_v} \quad (2.1)$$

$$\sigma'_v = \sigma_v - u \text{ and } \sigma'_h = \sigma_h - u \quad (2.2)$$

where σ'_h and σ'_v are the effective horizontal and vertical stresses respectively, σ_h and σ_v are the total horizontal and vertical stresses respectively, the corresponding strains ϵ_v in vertical direction and $\epsilon_h = 0$ in horizontal direction, and u is the pore water pressure. K_0 can be obtained either from laboratory test carried out on undisturbed sample or field tests. It may also be readily estimated from the well known Jaky 1944 empirical equation:

$$K_0 = 1 - \sin \varphi' \quad (2.3)$$

where φ' is the effective angle of internal friction. K_0 may also reasonably correlate with plasticity index and liquid limit. Some correlation for normally consolidated soft soils are given in Kempfert and Stadel 1997 and are re-produced in Table 2.2.

There is no enough available data to correlate the K_0 with plasticity index or liquid limit or others for the lacustrine soft clays in southern Germany. However, in order to identify an empirical equation that best approximates the K_0 for these soils, the few data from Scherzinger 1991 together with the empirical equations in Table 2.2 have been plotted in Fig. 2.8. From these figures, it can be seen that Jaky 1944 (Fig. 2.8c) and Alpan 1967 (Fig. 2.8a) equations do not fit the data. It is disappointing that the Jaky's equation, which is the most popular and widely used empirical equation among engineers and researchers, underestimate the K_0 value for this type of soil. On the other hand, the Lee and Jin 1979 (Fig. 2.8a) and Sherif and Koch 1970 (Fig. 2.8b) empirical equations seem to fit the data reasonably. In particular, the Sherif and Koch 1970 empirical equation is recommended to predict the K_0 value for the lacustrine soft clays in southern Germany.

Table 2.2. Empirical equations to estimate the earth pressure coefficient at rest, K_0 (after Kempfert and Stadel 1997)

Equation	Reference	Regions of Applicability
$K_0 = 0.19 + 0.233 \cdot \log I_p (\%)$	Alpan 1967	Soft clays
$K_0 = 0.24 + 0.31 \cdot \log I_p (\%)$	Lee and Jin 1979	Soft clays
$K_0 = 10^{(0.00275 \cdot (LL - 20\%)) - 0.2676}$	Sherif and Koch 1970	Soft clays

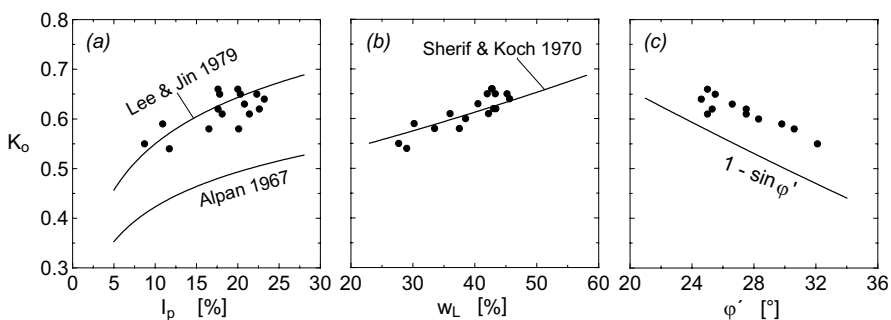


Fig. 2.8. Empirical equations to estimate K_0 from **a**) plasticity index I_p , **b**) liquidity limit LL and **c**) effective angle of friction φ' (data from Scherzinger 1991)

Schmidt 1966 developed an empirical equation to approximate the K_0 value from overconsolidation ratio (OCR) as follows:

$$\frac{K_{0(OC)}}{K_{0(NC)}} = OCR^m \quad (2.4)$$

where $K_{0(OC)}$ and $K_{0(NC)}$ are K_0 values for overconsolidated and normally consolidated cases respectively and m is a constant which depend on type of soil. After correlating m with plasticity index of several soils, Ladd et al. 1977 showed that the value of m varies from about 0.42 for low plasticity clays to about 0.32 to high plasticity clays (Wroth and Houlsby 1985). They emphasised that Eq. 2.4 should be taken only to estimate the value of K_0 during primary unloading, but K_0 will not be uniquely related to OCR for soil deposits that have been subjected to more than one cycle of deposition and erosion. Schmidt 1966 and Schmertmann 1975 also suggested $m = 0.41$, where as Meyerhof 1976 suggested $m = 0.50$. Recently, Parry 1995 proposed $m = \varphi'$ (where φ' in radian), and Alpan 1967 recommended:

$$m = 0.54 \cdot e^{(-I_p / 281)} \quad (2.5)$$

where I_p is the plasticity index of the soil. K_0 can also be roughly estimated from cone penetration test results (Kulhawy and Mayne 1990)

$$K_0 = 0.10 \cdot \left(\frac{q_c - \sigma'_{vo}}{\sigma'_{vo}} \right) \quad (2.6)$$

where q_c is the cone resistance, σ_{vo} and σ'_{vo} are the total and effective overburden pressures respectively.

Bishop 1958 stated that if the granular structure of the soil behave as an ideal elastic material, it can readily be shown that K_0 would be a function of Poisson's ratio v and would thus be a constant for a given material:

$$K_0 = \frac{v}{1-v} \quad (2.7)$$

Although the stress-strain characteristics of soil depart from those of an ideal elastic material even at small strains, it is found experimentally (Bishop 1958) that, K_0 on first loading, is sensibly constant over a wide range of stress. On unloading and reloading, however, hysteresis is evident (Fig. 2.9).

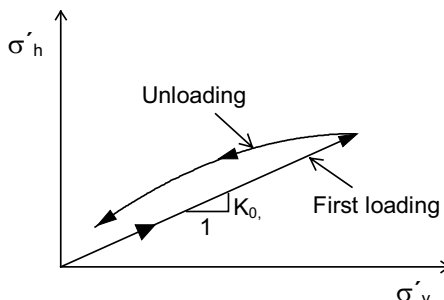


Fig. 2.9. Variation of horizontal effective stress with vertical effective stress for primary loading and unloading

One-dimensional compression behaviour is usually used for determination of settlement of structures. This requires however due consideration of the different deformation parts of the soil (see also section 5.4.3)

A typical oedometer test result on normally consolidated soil is shown in Fig. 2.10. Generally, the result of one-dimensional compression is represented in terms of the effective stress and the corresponding void ratio. The vertical effective stress is plotted either to the natural scale (Fig. 2.10a) or to logarithmic scale (Fig. 2.10b). The sample is loaded one dimensionally along A-B, unloaded to D, reloaded to B then to C, and finally unloaded to F. The line A-B-C is known as normal consolidation line, where as line B-D and C-E are called the swelling lines. A soil which is on the normal compression line has never before been subjected to a vertical effective stress higher than the current value, and it is described as normally consolidated. However, a soil which is on the swelling line has previously been subjected to higher vertical effective stress than that which currently acts, and it is called overconsolidated. The overconsolidation ratio is defined as:

$$OCR = \frac{\sigma'_{vm}}{\sigma'_{vc}} \quad (2.8)$$

where σ'_{vm} is the maximum vertical effective stress in which the soil is subjected and σ'_{vc} is the current vertical effective stress. The various equations necessary to define the settlement-stress curve of one-dimensional compression are listed in Table 2.3.

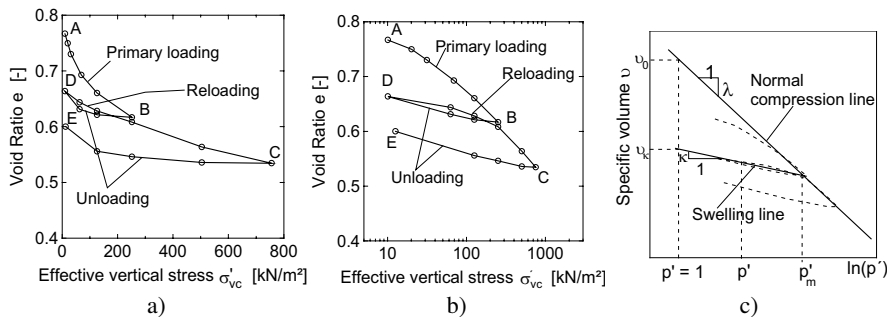


Fig. 2.10. One-dimensional compression for normally consolidated lacustrine soft soil; **a)** natural scale, **b)** semi-logarithmic scale, and **c)** idealization of one-dimensional compression

If the values of σ'_v , σ'_h and the specific volume v are known throughout a one dimensional compression test, the result may also be plotted on v versus $\ln(p')$ as shown in Fig. 2.10c. In this diagram, the one-dimensional compression behaviour of normally consolidated soft soil is idealised by straight lines, in which the slopes and the positions of the lines depend on the particular type of soil. The equations of the normal compression line and the swelling line are given by Eqs. 2.16 and 2.17 respectively. However, it should be noted that the position of the swelling line is not uniquely defined, but it depends on the maximum previous stress, p'_m .

Since $d(\log_{10} \sigma'_v) = 0.434 \cdot d(\ln \sigma'_v)$, $de = dv$ and K_0 is assumed constant in normal compression line ($d\sigma'_v / \sigma'_v = dp' / p'$ ($d\sigma'_v / \sigma'_v = dp' / p'$)), λ can be related to C_c as shown in Eq. 2.18. In one-dimensional swelling, K_0 is not constant (Fig.2.9), and hence there is no simple relationship between C_s and κ . However, if K_0 is approximately assumed constant, κ may also be approximated from Eq. 2.19.

Table 2.3. List of equations defining the one-dimensional compression behaviour of soils

Equation	Equation no.	Remark
$-C_c = \frac{de}{d\log_{10} \sigma'_v}$	(2.9)	Slope of the primary load line (compression index) (Fig. 2.10b)
$-C_s = \frac{de}{d\log_{10} \sigma'_v}$	(2.10)	Slope of the reloading/unloading line (swelling index) (Fig. 2.10b)
$p' = \frac{\sigma'_v + 2 \cdot \sigma'_h}{3}$	(2.11)	Mean principal stress (the intermediate principal stress is equal to the minor principal stress)
$v = I + e$	(2.12)	Specific volume
$v = I + w \cdot G_s$	(2.13)	Specific volume for fully saturated soils
$-\lambda = \frac{dv}{d(\ln p')}$	(2.14)	Slope of normal compression line (Fig. 2.10c)
$-\kappa = \frac{dv}{d(\ln p')}$	(2.15)	Slope of swelling line (Fig. 2.10c)
$v = v_0 - \lambda \cdot \ln p'$	(2.16)	Equation of the normal compression line (Fig. 2.10c)
$v = v_\kappa - \kappa \cdot \ln p'$	(2.17)	Equation of the swelling line (Fig. 2.10c)
$\lambda = 0.434 \cdot C_c$	(2.18)	Relationship between the compression index and the slope of idealised normal compression line
$\kappa \approx 0.434 \cdot C_s$	(2.19)	Relationship between the swelling index and the slope of idealised swelling line
$-C_\alpha = \frac{de}{d(\log_{10} t)}$	(2.20)	Coefficient of secondary compression (Fig. 2.13)

where e = void ratio, σ'_v , σ'_h = the effective vertical and horizontal stresses respectively, w = moisture content, G_s = specific gravity, v_0 , v_κ = the specific volumes of corresponding to $p' = 1 \text{ kN/m}^2$ for normal compression line and swelling line respectively, t = time.

Empirical equations to predict compression parameters

In the absence of enough data, the compression parameters can be estimated from simple index parameters using empirical equations. Some empirical equations used to estimate the values of C_c , C_s , λ , and κ are listed in Table 2.4. It is produced from Bowles 1984, Nagaraj 1983 and other sources as indicated in the list. Fig.

2.11 also shows the relationship between the plasticity index versus the compression index and swelling index. The C_c and C_s values of the soft soils in southern Germany, are also correlated with natural moisture content and liquid limit as shown in Fig. 2.12. It was found that C_c and C_s correlate fairly well with these parameters. The correlation are given by:

$$C_c = 0.00454 \cdot (w - 10) \quad (2.21)$$

$$C_c = 2.88 \times 10^{-4} \cdot LL^{1.6352} \quad (2.22)$$

$$C_s = 16.433 \times 10^{-6} \cdot w^{2.015} \quad (2.23)$$

$$C_s = 6.89 \times 10^{-6} \cdot w^{2.215} \quad (2.24)$$

where w is the moisture content and LL is the liquid limit. The ratio of C_c/C_s is a constant value and varies between 2.5 and 5. For the lacustrine soft clays in southern Germany, Scherzinger 1991 found that the ratio C_c/C_s is on average 5.

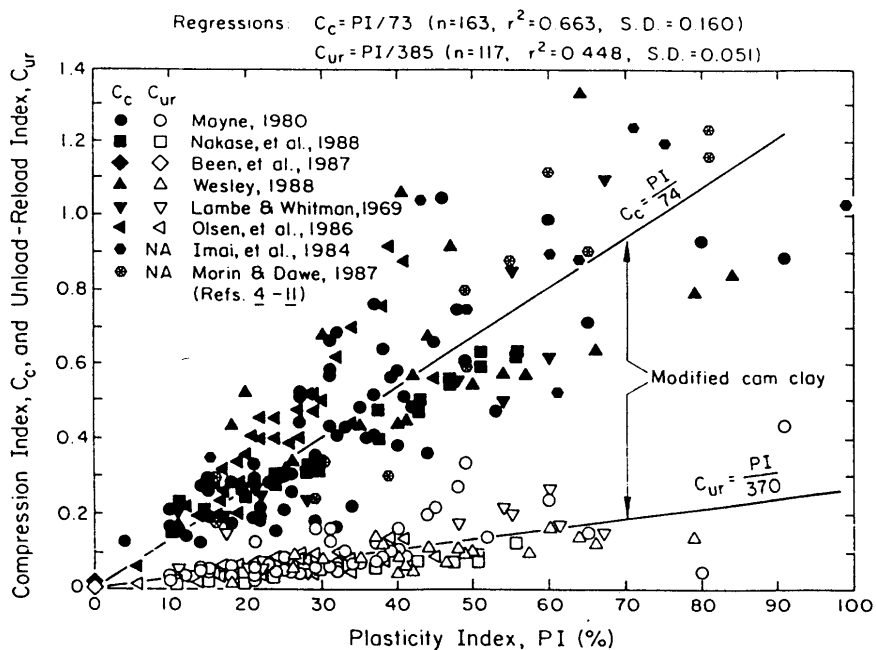


Fig. 2.11. Compression and unload-reload indices as a function of plasticity index (originally from Kulhawy and Mayne 1990, adopted from Mitchell 1993)

Table 2.4. Empirical equations to predict, C_c , C_s , λ and κ

Equation	Reference	Regions of Applicability	
$C_c = 0.007 \cdot (LL - 10)$	Skempton 1944	Remoulded clays	
$C_c = 0.009 \cdot (LL - 10)$	Terzaghi and Peck 1967	Normally consolidated , moderately sensitive	
$C_c = 0.007 \cdot (LL - 7)$	Bowles 1984	Remoulded clays	
$C_c = 0.01 \cdot w$	Koppula 1981, Bowles 1984	Chicago clays and Alberta Province in Canada	
$C_c = 0.0115 \cdot w$	Bowles 1984	Organic silts and clays	
$C_c = 0.75 \cdot (e - 0.50)$	Bowles 1984	Soils with low plasticity	
$C_c = 0.0046 \cdot (LL - 9)$	Bowles 1984	Brazilian clays	
$C_c = 1.21 + 1.055 \cdot (e_0 - 1.87)$	Bowles 1984	Motley clays from Sao Paulo city	
$\lambda = 0.208 \cdot (e_0 + 0.0083)$	Bowles 1984	Chicago clays	
$\lambda = 0.156 \cdot e_0 + 0.0107$	Bowles 1984	All clays	
$C_c = 1.15 \cdot (e - e_0)$	Nishida 1956	All clays	
$C_c = 1.15 \cdot (e - 0.35)$	Nishida 1956	Natural soils	
$C_c = 0.54 \cdot (e - 0.35)$	Nishida 1956	Inorganic silty sand -silty clay	
$C_c = 0.30 \cdot (e_0 - 0.27)$	Hough 1957	Remoulded clays, $25 \leq w_L \leq 60$ (soils above the A-line) or $0.6 \leq e_L \leq 4.5$	
$C_c = 0.256 \cdot e_L - 0.04$	Burland 1990	Natural soils in their normally consolidated uncemented state, for pressure range between 25 to 800kPa.	
$C_c = 0.543 \cdot e_L \cdot 10^{(-0.168 \cdot \log_{10} p)}$	Nagaraj 1983	All clays	
$C_c = 0.141 \cdot G_s^{1.2} \cdot [(1+e_0)/G_s]^{2.38}$	Herrero 1983	Soil system of all complexities and all types	
$C_c = 0.5 \cdot (\gamma_w/\gamma_d)^{2.4}$	Oswald 1980	Wroth and Wood 1978, Wood 1983	All remolded normally consolidated clays
$C_c = 0.5 \cdot I_p \cdot G_s$	Kulhawy and Mayne 1990	Data from different soils	
$C_s = I_p/370$	Kulhawy and Mayne 1990	Data from different soils	
$\lambda = 0.217 \cdot G_s \cdot I_p$	Yudhbir and Wood 1989, Atkinson and Bransby 1978	Based on critical soil mechanics	
$\kappa = 0.048 \cdot G_s \cdot I_p$	Yudhbir and Wood 1989	Based on critical soil mechanics	
$\lambda = 0.235 \cdot G_s \cdot I_p$	Powrie 1997	Based on critical soil mechanics	
$C_c = 0.24 \cdot e_0 + 0.03$	Ruppert 1980	Lauenberger clay	

w = moisture content (%), LL = liquid limit (%), e = void ratio, e_0 = initial void ratio, e_L = void ratio at liquid limit, I_p = plasticity index (%), G_s = specific gravity, γ_w = unit weight of water, γ_d = dry unit weight of the soil.

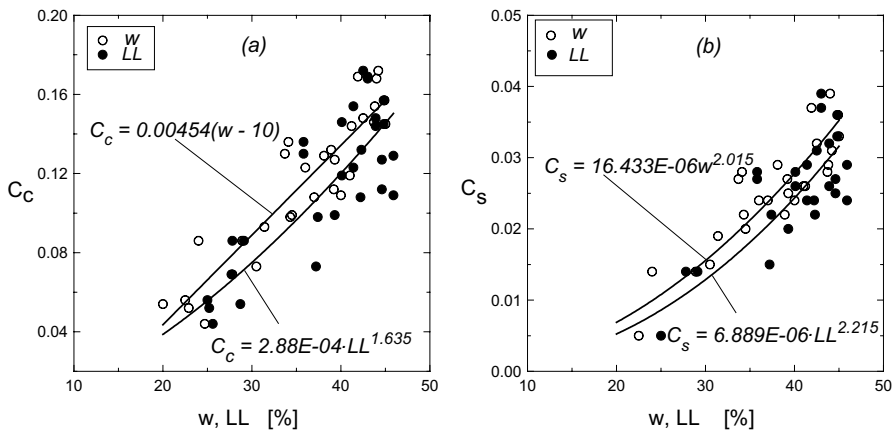


Fig. 2.12. Correlation of (a) compression index C_c and (b) the swelling index C_s , with the natural moisture content w and liquid limit LL for lacustrine soft clay soils in southern Germany (data are partially obtained from Scherzinger 1991)

Secondary compression

The relationship between void ratio and logarithm of time during secondary compression is usually linear (Fig. 2.13) for most soils over the time ranges of interest after the completion of primary consolidation. Thus, the coefficient of secondary compression may be defined by Eq. 2.20. in Table 2.3. The value of C_α is usually rather uniquely related to the compression index C_c as shown in Table 2.5. Tsukada and Yasuhara 1995 had also correlated C_α with initial void ratio for soft soils as:

$$C_\alpha = 0.0145 \cdot e_0^{1.555} \quad (2.25)$$

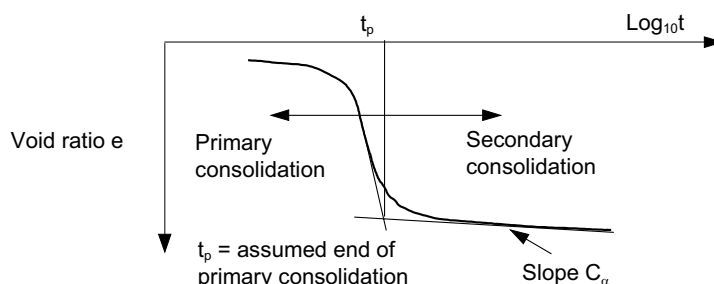


Fig. 2.13. Secondary one-dimensional consolidation

Table 2.5. Values of the ratio of C_α/C_c for natural soils (partially after Mitchell 1993)

C_α/C_c	Reference	Regions of Applicability
0.03 - 0.04	Mesri and Godlewski 1977	Whangamarino clay
0.025 - 0.06	Mesri and Godlewski 1977	Leda clay
0.026	Mesri and Godlewski 1977	Soft blue clay
0.025 - 0.055	Mesri and Godlewski 1977	Portland sensitive clay
0.04 - 0.06	Mesri and Godlewski 1977	San Francisco bay mud
0.03 - 0.06	Mesri and Godlewski 1977	New Liskeard varved clay
0.032	Mesri and Godlewski 1977	Silty clay
0.055 - 0.075	Mesri and Godlewski 1977	Nearshore clays and silts
0.03 - 0.035	Mesri and Godlewski 1977	Mexico city clay
0.05 - 0.07	Mesri and Godlewski 1977	Post glacial organic clay
0.04 - 0.06	Mesri and Godlewski 1977	Organic clays and silts
0.04 - 0.075	Mesri and Godlewski 1977	New Haven organic clay silt
0.03	Mesri et al. 1995	Batiscan and St Hiaire soft clays
0.02 - 0.04	Scherzinger 1991	Lacustrine soft clays in Constance
0.025 - 0.032	Klobe 1992	Lacustrine soft clays in Constance

2.4.3 Two and three-dimensional compression

Ladd et al. 1977 reported that the two and three-dimensional loading of a saturated clay results in several important differences from the simple one-dimensional loading condition, because:

1. An initial settlement, due to undrained shear deformations, occurs upon application of the load and some regions of the foundation clay may undergo local yielding (contained plastic flow).
2. The initial excess pore pressure beneath the loaded area does not equal the vertical stress increment and strain during consolidation are no longer one-dimensional.
3. Lateral drainage increases the rate of consolidation compared to the one-dimensional case, particularly with soils having high anisotropic permeability ratio.
4. Creep movements may become more significant both as a result of “undrained” deformations occurring during the consolidation process and due to drained creep after dissipation of excess pore pressure.

The above comments should only be understood in connection with the general stress-strain behaviour and rate of consolidation conditions, otherwise, as far as the simple compression parameters C_c , C_s , C_α , λ and κ are concerned, the effect of the two and three-dimensional loading is very minimum. Atkinson and Bransby 1978 pointed out that both normal consolidation lines for one-dimensional and isotropic compression are almost parallel with slopes $-\lambda$, and similarly the swelling lines with slopes $-\kappa$ (Fig. 2.15). Mesri et al. 1995 indicated that the ratio C_c/C_α has the same magnitude for both one-dimensional and three-dimensional compression.

Critical soil mechanics assumes that the soil undergo isotropic compression, before the application of the deviatoric stress. The boundary condition for isotropic compression in a triaxial test is given in Fig. 2.14, where an all round cell pressure σ'_c is applied to the specimen, i.e., $\sigma'_c = \sigma'_v = \sigma'_h$. The horizontal strain, however, is different from zero unlike to the one-dimensional case.

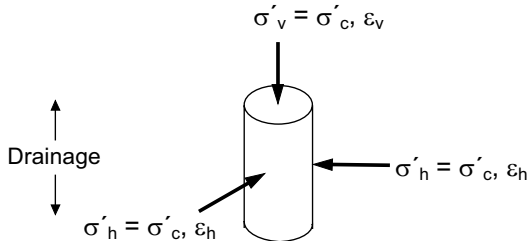


Fig. 2.14. Boundary conditions for isotropic compression

Similar to one-dimensional compression, the isotropic compression may also be idealised by straight lines as shown in Fig. 2.15. Equation of the normal compression line for isotropic compression is given by,

$$v_i = v_{0i} - \lambda \cdot \ln p' \quad (2.26)$$

and for swelling line,

$$v_i = v_{ki} - \kappa \cdot \ln p' \quad (2.27)$$

where v_{0i} , v_{ki} are the specific volumes corresponding to $p' = 1 \text{ kN/m}^2$ for normal compression line and an overconsolidated soil respectively.

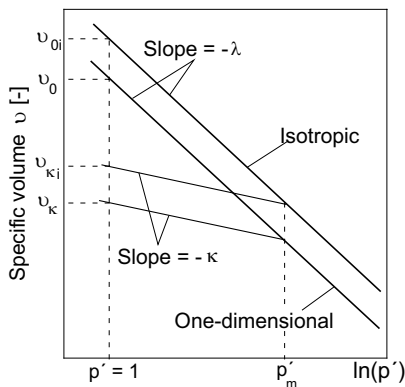


Fig. 2.15. Isotropic and one-dimensional compression of normally consolidated soil

The location of the normal compression line and swelling line for isotropic compression to the right of the corresponding one-dimensional case as shown in

Fig. 2.15, implies that for a given value of the specific volume v , the effective vertical stress carried by the soil under isotropic compression is higher than that of soil under one-dimensional compression.

2.5 Strength properties

2.5.1 General

The shearing resistance of a soil depends on many factors, and a complete equation might be of the form (Mitchel 1993):

$$\text{Shearing resistance} = F(e, \varphi, C, \sigma', c, H, T, \varepsilon, \dot{\varepsilon}, S) \quad (2.28)$$

where e is the void ratio, φ is the angle of internal friction, C is the composition, σ is the effective normal stress, c is the cohesion, H is the stress history, T is the temperature, ε is the strain, $\dot{\varepsilon}$ is the strain rate, and S is the structure. All these parameters may not be independent to each other, however, a functional forms all the factors are not yet known. The Mohr-Coulomb equation, which is a simplified form of Eq. 2.28, is by far the most widely used equation for shearing resistance. It is given by:

$$\tau = c + \sigma \cdot \tan \varphi \quad (2.29)$$

where τ is the shearing resistance of the soil. Eq. 2.29 may also be rewritten in terms effective soil parameters as:

$$\tau' = c' + \sigma' \cdot \tan \varphi' \quad (2.30)$$

For practical purposes, the validity of Eqs. 2.29 and 2.30 are widely accepted, but parameters c' and φ' may take many different values, depending on stress path, stress level and drainage condition. Values of c' and φ' are determined using specified test type such as; direct shear, simple shear, triaxial compression/tension, or other plane strain tests, with due consideration to the drainage conditions, rate of loading, range of confining pressure, and stress history. In many cases it may be possible to take account of the factors in Eq. 2.28 by properly selecting soil specimens and testing conditions which simulate the corresponding field situation.

The general state of a stress in a true triaxial test may be expressed in terms of three principal stresses σ_1 , σ_2 , and σ_3 , where σ_1 is the major principal stress, σ_2 is the intermediate principal stress and σ_3 is the minor principal stress, and $\sigma_1 > \sigma_2 > \sigma_3$. The principal stresses can also be written in the form of the mean principal stress:

$$p = \frac{(\sigma_1 + \sigma_2 + \sigma_3)}{3} \quad \text{or} \quad p' = \frac{(\sigma'_1 + \sigma'_2 + \sigma'_3)}{3} \quad (2.31)$$

and the deviatoric stress may be written as

$$q = q' = \frac{1}{\sqrt{2}} [(\sigma_1 - \sigma_2)^2 + (\sigma_2 - \sigma_3)^2 + (\sigma_3 - \sigma_1)^2]^{1/2} \quad (2.32)$$

where $\sigma' = \sigma - u$, σ' is the effective stress, σ is the total stress and u is the pore water pressure. In a standard triaxial test, the intermediate principal stress is assumed equal to the minor principal stress, i.e., $\sigma_2 = \sigma_3$, and hence the Eqs. 2.31 and 2.32 reduce to

$$p = \frac{(\sigma_1 + 2\sigma_3)}{3} \quad \text{or} \quad p' = \frac{(\sigma'_1 + 2\sigma'_3)}{3} \quad (2.33)$$

$$q = q' = (\sigma_1 - \sigma_3) \quad (2.34)$$

While p or p' and q , usually known as Cambridge composite parameters, are important parameters in critical soil mechanics, the intermediate principal stress is usually ignored in presentation of the triaxial test result and determination of shear strength parameters. Thus, p , p' and q ' may be rewritten as

$$p = \frac{(\sigma_1 + \sigma_3)}{2} \quad \text{or} \quad p' = \frac{(\sigma'_1 + \sigma'_3)}{2} \quad (2.35)$$

$$q = q' = \frac{(\sigma_1 - \sigma_3)}{2} \quad (2.36)$$

At failure the Mohr-Coulomb effective stress envelope is tangential to the effective stress circle, with slope ϕ' and intercept c' as shown in Fig. 2.16. A failure line can also be drawn through the maximum shear stress at A in Fig. 2.16 which represents the stress envelope for p - q stress paths. This line is called the K_f -line and has a slope of α' and intercept b' . It is easy to show that $\tan \alpha' = \sin \phi'$ and $b' = c' \cdot \cos \phi'$.

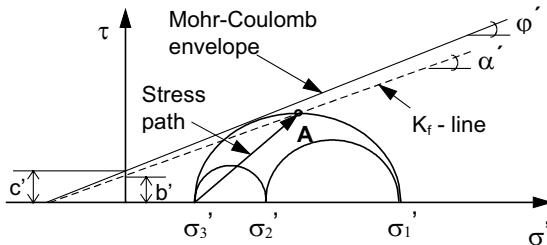


Fig. 2.16. Mohr-Coulomb envelope and K_f -line

It is possible to take the specimen in a triaxial cell to failure either in axial compression or axial extension. The specimen can be compressed axially either by increasing the axial compressive stress (path OA in Fig. 2.17) or decreasing the

lateral stress (path OB) or varying the stresses in both direction (path OC). Similarly, axial extension can be achieved either by decreasing the vertical stress (path OD) or increasing the lateral stress (path OE) or varying the stresses in both direction (path OF).

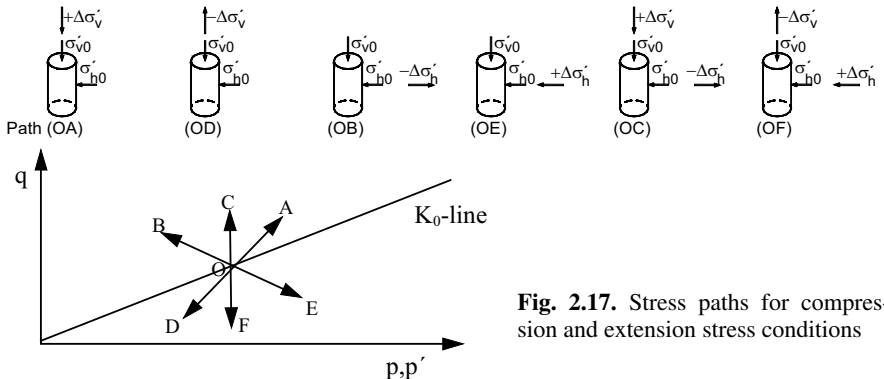


Fig. 2.17. Stress paths for compression and extension stress conditions

A finite element calculation result of the response of the hardening soil model (refer to Table 3.2) parameters to different stress paths for the case of isotropic (left) and K_0 -consolidation (right) are shown in Fig. 2.18 for a triaxial state of stress. The model parameters are the same as those given in Table 3.15. In the case of isotropic consolidation, the specimen was first consolidated under a confining pressure of $\sigma_{30} = \sigma_{10} = 100 \text{ kN/m}^2$, before it had undergone to different stress paths. Similarly, the specimen was consolidated first at a confining pressure of $\sigma_{30} = \sigma_{10} = 100 \text{ kN/m}^2$ and $\sigma_{10} = 175 \text{ kN/m}^2$, i.e., $K_0 = 1 - \sin \varphi' = 0.573$ in the case of the K_0 -consolidation.

As shown in the Fig. 2.18a & b, the effective stress path for all total stress paths above the isotropic stress line or above the K_0 -line (compression), i.e., the stress paths A, B and C, is unique. That is also true for those total stress paths (D, E and F) below the isotropic stress line or below the K_0 -line (extension). This is an approval of the test results in section 3.2.3. The unique effective stress paths in compression as well as in extension also leads to a unique deviatoric stress at failure (Fig. 2.18c & d). It is not only the deviatoric stress at failure, but also the courses of the deviatoric stress vs axial strain for the total stress paths A, B, and C in compression, and D, E, and F in extension respectively are exactly the same.

However, The deviatoric stresses at failure in compression and extension are different. This leads to differences in the undrained shear strength c_u and the angle of overall shear strength φ'_s in compression and in extension. The ratios of the respective values are calculated to be:

$$\frac{c_{uc}}{c_{ut}} = \begin{cases} 1.41, & \text{isotropic consolidation} \\ 1.33, & K_0\text{-consolidation} \end{cases} \quad (2.37)$$

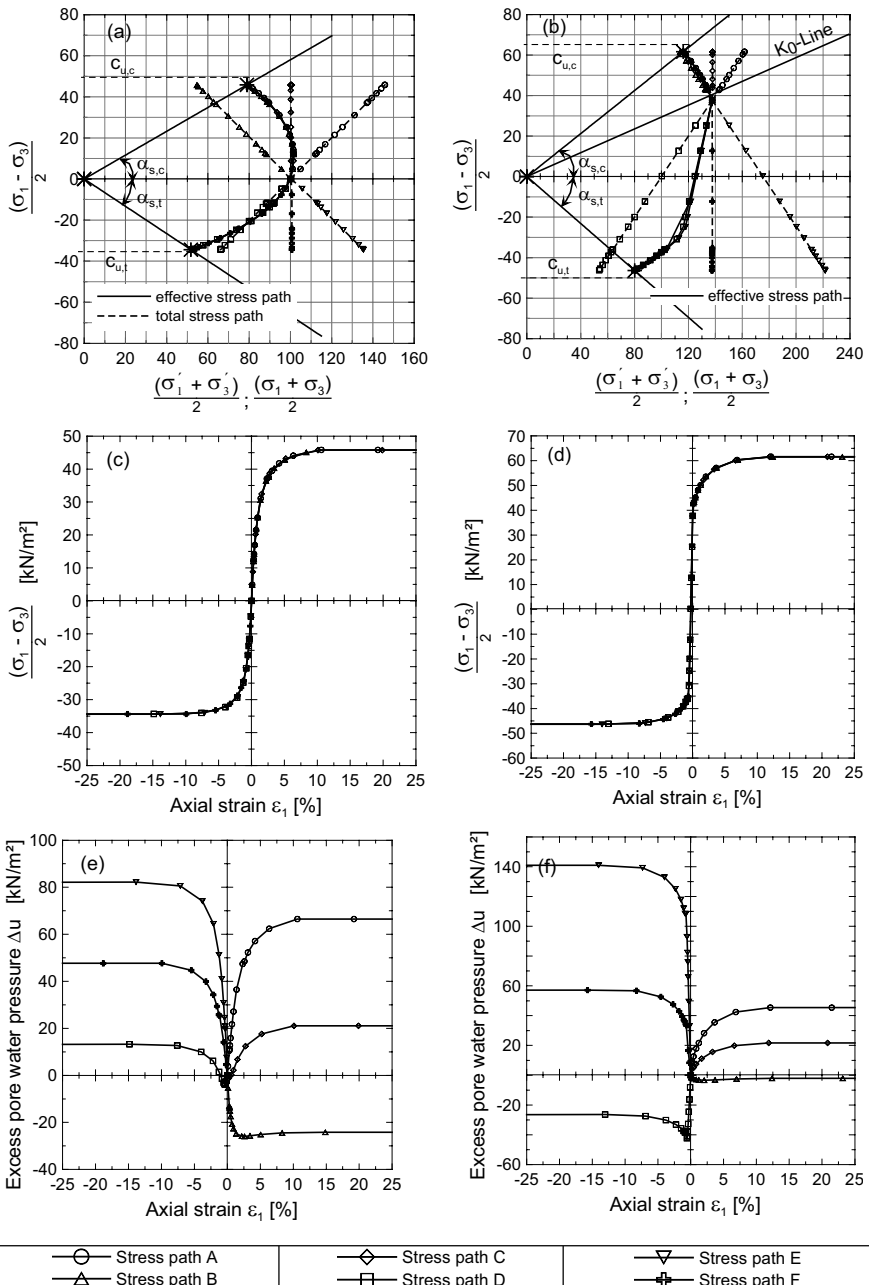


Fig. 2.18. Response of the hardening soil model to different stress paths using FEM under triaxial state of stress: a) & b) stress paths, c) & d) deviatoric stress, and e) & f) excess pore water pressure, for the case of isotropic consolidation (left) and K_0 -consolidation (right)

and

$$\frac{\tan \alpha_{sc}}{\tan \alpha_{st}} = \frac{\sin \varphi_{sc}}{\sin \varphi_{st}} = \begin{cases} 0.87, & \text{isotropic consolidation} \\ 0.92, & K_0\text{-consolidation} \end{cases} \quad (2.38)$$

Eq. 2.37 is comparable with Eq. 2.62, but not to all values listed in Table 2.9. This is because the c_{uc}/c_{ut} is not a constant value, rather it depends on the plasticity of the material (see Fig. 2.28). Eq. 2.38 is also fairly comparable with most of the values listed in Table 2.12.

Comparing the isotropic consolidation with K_0 -consolidation, the later reacts stronger than the earlier one. The deviatoric stress at failure in the case of K_0 -consolidation is higher by a factor of 1.4 than the case of isotropic consolidation for the given specimen.

Unlike to the effective stress path and the deviatoric stress, the development of the excess pore water pressures for the different stress paths are quite different (Fig. 2.18e & f). The excess pore water pressure at failure (or approaching failure) for stress paths A and B is lower and for the stress paths D, E and F higher in the case of K_0 -consolidation than in the case of isotropic consolidation, while the stress path C remains unaffected by the type of consolidation.

From the above discussion it would appear that there is no need to reduce the undrained strength to account for stress induced anisotropy in FEM - computations under undrained condition. However, the inherent anisotropy remains ignored in the FEM - computation.

2.5.2 Total and effective stress analysis

General

The choice of total or effective stress analysis is of importance in the design and analysis of excavations in soft deposits. The shear strength of a soil in terms of the effective shear parameter is given in Eq. 2.30 and rewritten here as:

$$\tau = c' + \sigma' \cdot \tan \varphi' \quad (2.30)$$

where $\sigma' = \sigma - u$, $u = u_0 - \Delta u$, u_0 = steady pore pressure, Δu = excess pore pressure, and in terms of the total stress it is given by

$$\tau = c_u \quad (2.39)$$

In Germany, it is a common practice to include the effect of cohesion in the angle of internal friction for soft soils, and hence Eq. 2.30 may be redefined as

$$\tau = \sigma'_e \cdot \tan \varphi'_s \quad (2.40)$$

where φ'_s is defined as the angle of the overall shear strength and σ'_e is the Hvorslev's equivalent stress (see DIN 18 137: 1990 or Scherzinger 1991). In this the term φ'_s will be used instead of φ' through out the text.

The flow chart below (Fig. 2.19) shows schematically the type of analyses in geotechnical engineering and the preconditions for each type of analysis.

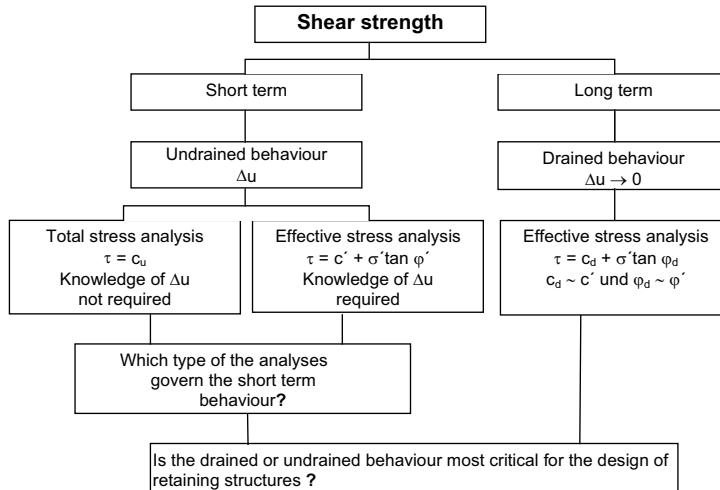


Fig. 2.19. Schematic presentation of the type of analysis in geotechnical engineering

Which type of the analyses govern the short term behaviour?

It is a well known fact that the behaviour of soils is primarily governed by the effective stresses independent of the drainage condition. Referring to the works of Hvorslev 1937; Rendulic 1937; Brinch-Hansen and Gibson 1949; Schmertmann 1975 and his own experiences on open excavations in soft soils, Janbu 1977 tried to verify the above statement, and he came to the conclusion that the short term undrained behaviour of saturated clays are governed by the effective stresses. The main reason for using the total stress approach for short term undrained conditions in clay is to avoid predicting the excess pore pressure and hence the effective stresses. If the excess pore pressure Δu is known or can reasonably be predicted, the short term undrained behavior of soils may be written in terms of the effective strength parameters c' and φ' (Eq. 2.30). Δu may be estimated from the commonly used Skempton and Bishop equation,

$$\Delta u = B \cdot [\Delta \sigma'_3 + A \cdot (\Delta \sigma'_1 - \Delta \sigma'_3)] \quad (2.41)$$

Eq. 2.41 assumes a triaxial stress condition $\sigma_3 = \sigma_2$. For saturated normally consolidated clays $B \approx 1$, hence, Eq. 2.41 may be rewritten as,

$$\Delta u = [\Delta \sigma'_3 + A \cdot (\Delta \sigma'_1 - \Delta \sigma'_3)] \quad (2.42)$$

However, the prediction of Δu is much more complicated than it is given by Eqs. 2.41 and 2.42 (see for example Franke 1980). The pore pressure parameter A is not a unique value for a given soil, rather it is dependent on the direction of the principal stresses, the initial stress state and the plastic volumetric strain (see also Schweiger 2002).

Estimating the effective strength parameter from c_u value

As mentioned above, even the short term undrained behaviour of saturated clays are governed by the effective stresses. This implies that there exists a relationship between the total and effective strength parameters. The question is how can one benefit from the huge experiences in and the data available on the undrained strength parameter c_u in order to estimate the effective strength parameter φ' .

Janbu 1977 derived a relationship between the vane undrained strength τ_f and the effective shear parameters as follows

$$\tau_f = \alpha_v \cdot (\sigma'_{vc} + a) \quad (2.43)$$

where

$$\alpha_v = \frac{K_0 \cdot \tan \varphi'}{I + 2 \cdot A_f \cdot \tan \varphi'} = \alpha_v \cdot (\sigma'_{vc} + a) \quad (2.44)$$

and

$$a = c' \cdot \cot \varphi' \quad (2.45)$$

Brinch-Hansen and Gibson 1949 also developed theoretical expression for the variation in undrained strength with mode of failure for normally consolidated clay as follows,

$$\begin{aligned} \frac{c_u}{\sigma'_{vc}} &= \frac{c'}{\sigma'_{vc}} \cdot \cos \varphi' + (1 + K_0) \cdot \sin \varphi' - \sin \varphi' \cdot (2 \cdot A_f - 1) \\ &\times \left[\left(\frac{c_u}{\sigma'_{vc}} \right)^2 - \frac{c_u}{\sigma'_{vc}} \cdot (1 - K_0) \cdot \cos^2 \left(45 + \frac{\varphi'}{2} - \alpha \right) + \left(\frac{1 - K_0}{2} \right)^2 \right]^{1/2} \end{aligned} \quad (2.46)$$

where α is the inclination of the failure plane to the horizontal.

Based on the above principles and a standard triaxial condition, a simplified relationships for different stress paths have been developed. Fig. 2.15 shows a schematic plot of a typical standard isotropically and anisotropically consolidated undrained triaxial test in a p - q plane.

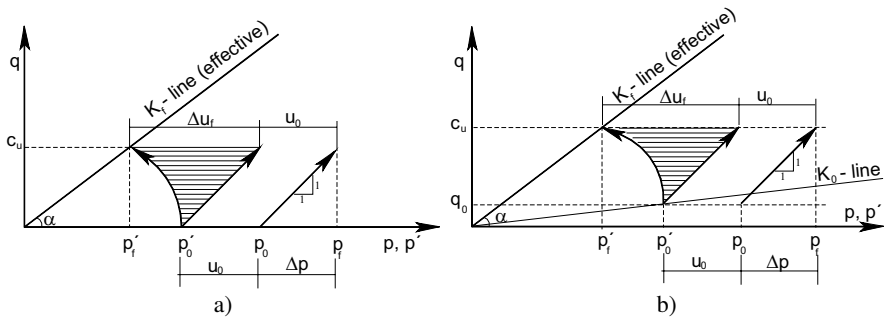


Fig. 2.20. Effective and total stress paths for standard a) isotropically and b) anisotropically consolidated undrained triaxial compression test

From Fig. 2.20a,

$$\tan \alpha = \frac{c_u}{p'_f} = \sin \varphi'_s \quad (2.47)$$

$$p'_f = p_f - (u_0 + \Delta u_f) = p_0 + \Delta p - u_0 - \Delta u_f = p'_0 + \Delta p - \Delta u_f \quad (2.48)$$

and $\Delta p = p_f - p_0 = c_u$. Hence,

$$p'_f = p'_0 + c_u - \Delta u_f \quad (2.49)$$

For normally consolidated saturated cohesive soils, the pore pressure at failure Δu_f can be approximated from Eq. 2.42. Since $\Delta \sigma_3 = 0$ for standard triaxial compression test, Eq. 2.42 becomes,

$$\Delta u_f = A_f \cdot \Delta \sigma_I \quad (2.50)$$

but $\Delta \sigma_I = 2 \cdot \Delta p = 2 \cdot c_u$ (Fig. 2.20a), hence,

$$\Delta u_f = 2 \cdot A_f \cdot c_u \quad (2.51)$$

Substituting Eqs. 2.50 & 2.49 into Eq. 2.47,

$$\sin \varphi'_s = \frac{c_u}{p'_0 + c_u + -2 \cdot A_f \cdot c_u} = \frac{\frac{c_u}{p'_0}}{1 + \frac{c_u}{p'_0} \cdot (1 - 2 \cdot A_f)} \quad (2.52)$$

Taking the normalised undrained strength parameter $\lambda_{cu} = \frac{c_u}{p'_0}$

$$\sin \varphi'_s = \frac{\lambda_{cu}}{I + \lambda_{cu} \cdot (1 - 2 \cdot A_f)} \quad (2.52)$$

Eq. 2.53 can also be rewritten as,

$$\sin \varphi'_s = \frac{I}{\frac{I}{\lambda_{cu}} - 2 \cdot A_f + I} \quad (2.54)$$

Eq. 2.54 shows that with the knowledge of the pore pressure parameter at failure A_f and the normalised undrained strength parameter λ_{cu} , the effective strength parameter φ'_s may be estimated. Following the same procedure, the relationship between the total and effective strength parameter for K_0 -consolidated undrained triaxial compression test (Fig. 2.20b) may be given by,

$$\sin \varphi'_s = \frac{I}{\frac{I}{\lambda_{cu}} - (K_0 + (1 - K_0) \cdot A_f) - 2 \cdot A_f + I} \quad (2.55)$$

Fig. 2.21 shows a plot of Eq. 2.55 with an assumption of a constant value of $K_0 = 0.577$. It should be noted that Eq. 2.55 also depends on the K_0 -value, therefore, the final value of the calculated φ'_s should be obtained by iteration.

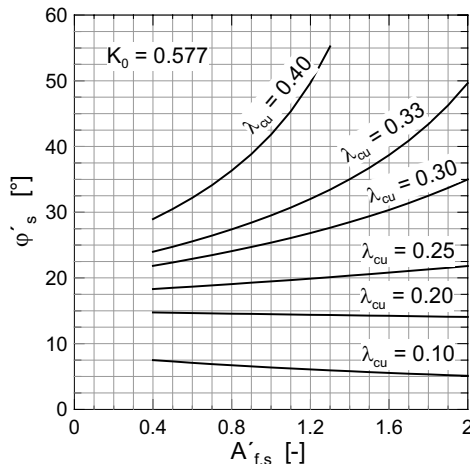


Fig. 2.21. A typical plot of the φ'_s against $A'_{f,s}$ according to Eq. 2.55 and for $K_0 = 0.577$

For the other stress path directions shown in Fig. 2.22 such as the active stress path B ($\Delta\sigma_3$ decreasing and $\Delta\sigma_I = 0$), the so called passive stress path E ($\Delta\sigma_3$ increasing and $\Delta\sigma_I = 0$) and extension stress path D ($\Delta\sigma_3 = 0$ and $\Delta\sigma_I$ decreasing),

the relationships between the total and effective strength parameters are given in Table 2.6. The stress path on the passive side of an excavation for example can neither be represented by stress path E nor by the stress path D during the excavation, because there is a change of the total stress in the vertical direction due to the excavation as well as a change of the total horizontal stress due to the wall displacement below the bottom of the excavation. The exact proportion of the change of the stresses in the vertical and the horizontal directions is not known. It depends on the type of soil, the rate of excavation and the type of retaining structure. However, assuming a proportionality constant of $-n$ between the vertical and the horizontal total stress increments, i.e., $\Delta\sigma_1 = n \cdot \Delta\sigma_3$, and

$$\beta = \frac{n-1}{n+1} \quad (2.56)$$

where β is the reciprocal of the gradient of the stress paths below the K_0 -line. For example, $\beta = 1$ for stress path D and $\beta = -1$ for stress path E.

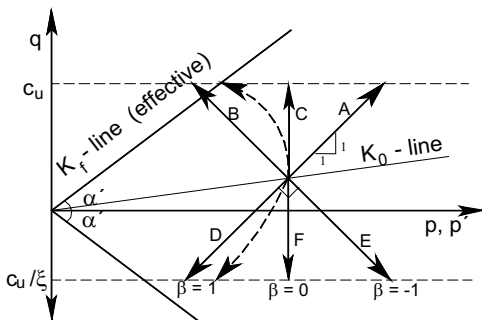


Fig. 2.22. Common stress paths

If one assumes that the effective strength parameters are independent of the direction of the total stress path, all the above equations must yield the same $\sin\phi'_s$. The only parameter that make difference is the pore pressure parameter A_f , which is dependent on the direction of the principal stresses, K_0 and the plastic volumetric strain.

Most often the undrained shear strength c_u is determined in-situ using the field vane shear test. This test is more or less similar to the K_0 -consolidated undrained triaxial test except that the rate of shear in vane test is faster than in the triaxial test. The insertion and rotation of the vane lead to change of total horizontal stresses which resembles the passive stress path case in triaxial test, and hence one may use the corresponding equation to estimate the effective parameter from the vane shear test with due consideration of the time and inherent anisotropy effect.

Table 2.6. Estimating the effective shear parameter φ'_s from c_u

Stress paths	Isotropic consolidated	K_0 - consolidated
$\Delta\sigma_3$ decreasing and $\Delta\sigma_l = 0$ (B)	$\sin\varphi'_s = \frac{I}{\frac{I}{\lambda_{cu}} - 2 \cdot A_f - 1}$	$\sin\varphi'_s = \frac{I}{\frac{I}{\lambda_{cu}}(1 + A_f \cdot (1 - K_0)) - 2 \cdot A_f - 1}$
$\Delta\sigma_3$ increasing and $\Delta\sigma_l = 0$ (E)	$\sin\varphi'_s = \frac{I}{\frac{I}{\lambda_{cu}} + 2 \cdot A_f + 1}$	$\sin\varphi'_s = \frac{I}{\frac{I}{\lambda_{cu}}(1 + A_f \cdot (1 - K_0)) + 2 \cdot A_f + 1}$
$\Delta\sigma_3 = 0$ and $\Delta\sigma_l$ decreasing (D)	$\sin\varphi'_s = \frac{I}{\frac{I}{\lambda_{cu}} + 2 \cdot A_f - 1}$	$\sin\varphi'_s = \frac{I}{\frac{I}{\lambda_{cu}}(K_0 + A_f \cdot (1 - K_0)) + 2 \cdot A_f - 1}$
$\Delta\sigma_3$ increasing and $\Delta\sigma_l$ de- creasing with $\Delta\sigma_l = -n \cdot \Delta\sigma_3$ $\beta = (n-1)/(n+1)$	$\sin\varphi'_s = \frac{I}{\frac{I}{\lambda_{cu}} + 2 \cdot A_f - \beta}$	$\sin\varphi'_s = \frac{I}{[\frac{I}{2 \cdot \lambda_{cu}}(1 + K_0 + \beta \cdot (K_0 - 1)) - A_f \cdot (1 - K_0)) + 2 \cdot A_f - \beta]}$

The coefficient of pore pressure at failure A_f

The pore pressure parameter at failure A_f is not a unique value for a given soil, rather it is dependent on the direction of the principal stresses, the initial state of the stresses and the plastic volumetric strain (Fig. 2.23). On the other hand, if the effective shear parameters are assumed to be independent from the stress path directions, it would be worthwhile to find a relationship between the $A_{f,s}$ values for standard compression test and the other stress paths, since the value of $A_{f,s}$ for common soil types in standard undrained triaxial compression test is usually known (see for example Table 2.7) and it can readily be determined from standard triaxial compression test. Therefore, equating Eqs. 2.54 and 2.55 with the equations of the other stress paths in Table 2.6 and taking into account the effect of anisotropy ξ , one may arrive at the relationship of the A_f value for different stress path directions based on the $A_{f,s}$ value as shown in Table 2.8. This assumption may be enough for practical purposes, however, if one assumes different φ'_s values for compression and extension case of loading (section 2.5.3), the equations in Table 2.8 should be corrected according to the ratio,

$$\zeta = \frac{\sin\varphi'_{s,t}}{\sin\varphi'_{s,c}} \quad (2.57)$$

where $\varphi'_{s,c}$ and $\varphi'_{s,t}$ are the angle of the overall shear strength in compression and extension respectively.

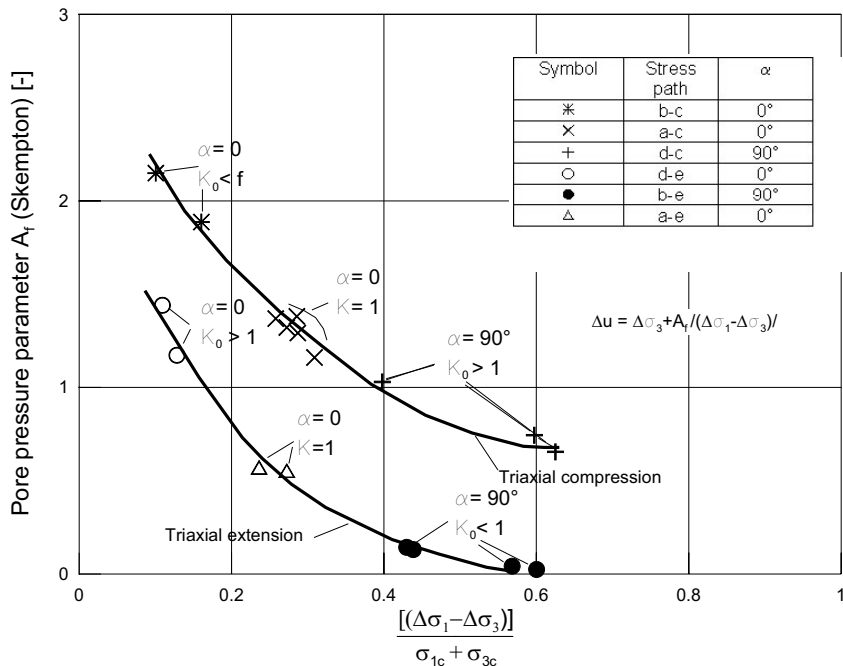


Fig. 2.23. The dependency of the pore pressure parameter A_f at failure on the principal stress directions and the initial state of stress (from Franke 1980).

Table 2.7. Values of the pore pressure parameter at failure (after Skempton 1954, source: Bowles 1984)

Soil	A_f
Loose, fine sand	2 - 3
Sensitive clay	1.5 - 2.5
Normally consolidated clay	0.7 - 1.3
Lightly overconsolidated clay	0.3 - 0.7
Heavily overconsolidated clay	-0.5 - 0.0
Compacted sandy clay	0.25 - 0.75

Table 2.8. Relationship between the values of A_f for different stress path directions (see Fig. 2.22)

Stress paths	A_f
$\Delta\sigma_3 = 0$ and $\Delta\sigma_1$ increasing (A)	$A_f = A_{fs}$
$\Delta\sigma_3$ decreasing and $\Delta\sigma_1 = 0$ (B)	$A_f = A_{fs} - I$
$\Delta\sigma_3$ increasing and $\Delta\sigma_1 = 0$ (E)	$A_f = \frac{K_0 - \xi + A_{fs} \cdot (I - K_0 - 2 \cdot \lambda_{cu,s})}{(\xi \cdot (I - K_0) + 2 \cdot \lambda_{cu,s})}$
$\Delta\sigma_3 = 0$ and $\Delta\sigma_1$ decreasing (D)	$A_f = \frac{K_0 \cdot (I - \xi) + 2 \cdot \lambda_{cu,s} + A_{fs} \cdot (I - K_0 - 2 \cdot \lambda_{cu,s})}{(\xi \cdot (I - K_0) + 2 \cdot \lambda_{cu,s})}$
$\Delta\sigma_3$ increasing and $\Delta\sigma_1$ decreasing with $\Delta\sigma_1 = -n \cdot \Delta\sigma_3$	$A_f = \frac{\beta}{2} + \frac{\lambda_{cu,s} - \xi / 2 + A_{fs} \cdot (I - K_0 - 2 \cdot \lambda_{cu,s}) + K_0 \cdot (1 - \xi / 2)}{(2 \cdot \lambda_{cu,s} - \xi \cdot (K_0 - 1))}$

A_{fs} and $\lambda_{cu,s}$ are the pore pressure parameter at failure and the normalised undrained strength respectively in standard triaxial compression test, and $\beta = (n - 1)/(n + 1)$

2.5.3 Undrained strength

Undrained strength plays an important role in geotechnical engineering, both as an essential input to calculate the short term stability and bearing capacity, and also as an indicator of soil behaviour to correlation with other engineering properties, such as index parameters. The undrained shear strength of a soil is usually determined in laboratory from unconfined compression test or unconsolidated undrained (UU) triaxial test or consolidated undrained (CU) or laboratory shear vane. In the field it can be readily obtained from field shear vane test, pressuremeter, cone penetrometer, etc. The major factors that influence the undrained strength of normally consolidated soils are the water content (void ratio), the stress history (anisotropy) and time.

Effect of water Content on undrained strength

The undrained strength of clay at plastic limit is about 70 times (Powrie 1997) or 100 times (Wroth and Wood 1978) than at liquid limit. It is generally believed that soils will have almost the same undrained shear strength (0.7 - 2.5 kPa) (Casagrande 1932; Russel and Mickle 1970; Wroth and Wood 1978; Whyte 1982; Skempton and Northe 1953; Norman 1958; Skopek and Ter-Stepanian 1975; Youssef et al. 1965) at the liquid limit, and different but again constant shear strength at the plastic limit (Atkinson 1978).

Effect of anisotropy on undrained strength

Anisotropy is one of the most important property of soils which affects their behaviour. Two types of anisotropy are recognised in soil mechanics. These are the inherent anisotropy and the stress induced anisotropy. Anisotropy as a result of preferred particle orientation during one-dimensional compression is called inherent anisotropy. Macroscopic variations in fabric can also produce inherent anisotropy. Examples are stiff fissured clays and varved glacial lake deposits containing alternating layers of ‘silt’ and ‘clay’ (Ladd et al. 1977). Inherent anisotropy will lead to anisotropy of mechanical properties governing elastic, plastic and failure behaviour. By comparing strengths of the specimens at various angles, a measured of inherent anisotropy can be obtained. This method has been used by a number of researchers such as Duncan and Seed 1966; Lo and Milligan 1967; DeLory and Lai 1971; Lo and Morin 1972; Eden and Law 1980.

Table 2.9 shows the effect of anisotropy on undrained shear strength of normally consolidated soft soils. The undrained strength in the vertical and horizontal direction may differ by as much as 40% (Mitchell 1993) as a result of fabric anisotropy. However, the information in Table 2.9 shows that the difference can be as high as 65%. These differences in undrained strength result from differences in pore water pressures developed during shear (Duncan and Seed 1966; Bishop 1966).

Soil can also exhibit a stress induced anisotropy whenever K_0 is not equal to unity. This results from the fact that different increments of shear stress are required to produce failure as the major principal stress at failure varies between the vertical an horizontal direction (Ladd et al. 1977).

The anisotropy possessed by a soil element existing in-situ under a set of applied stresses, after being subjected to a particular stress history, is a combination of both the inherent and induced anisotropy and is called the initial anisotropy (Zdravkovic and Potts 1999).

The behaviour of the undrained strength in compression and extension may be determined using the critical soil mechanics concept. The slope of the critical state line (Fig. 2.24) in compression is given by:

$$M = \frac{6 \cdot \sin \phi_c'}{3 - \sin \phi_c'} \quad (2.58)$$

and for extension,

$$M = \frac{6 \cdot \sin \phi_t'}{3 + \sin \phi_t'} \quad (2.59)$$

where ϕ_c' , and ϕ_t' are the effective internal friction in compression and extension respectively. At critical state the undrained strength is also given by:

$$c_u = \frac{q}{2} = \frac{M \cdot p'}{2} \quad (2.60)$$

Table 2.9. Effect of anisotropy on undrained shear strength

Equation	Reference	Regions of Applicability
$c_{uc}/c_{ut} \approx 3.0$	Larsson 1980	Inorganic low plastic clays
$c_{uc}/c_{ut} \approx 1.0$	Larsson 1980	Inorganic high plastic clays
$c_{uc}/c_{ut} = 2.5$	Bjerrum et al. 1972	Normally consolidated soil
$c_{uc}/c_{ut} = 1.75$	Eden and Law 1980	Canada South Gloucester soft soil
$\tau_{uv}/\tau_{uh} = 1.25 - 1.54$	Eden and Law 1980	Canada South Gloucester soft soil
$c_{uc}/c_{ut} = 2.0$	Scherzinger 1991	Constance lacustrine soft clays
$c_{uv}/c_{uh} = 1.3$	Lo 1965	Welland clay
$c_{uv}/c_{uh} = 1.43$	De Lory and Lai 1971	Welland Clay
$c_{uv}/c_{uh} = 1.28 - 1.56$	Wesley 1975	Mucking Flata clay
$c_{uv}/c_{uh} = 1.25$	Duncan and Seed 1966	San Francisco Bay mud
$c_{uv}/c_{uh} = 1.20$	Parry and Nadarajah 1975b	Fulford clay
$c_{uc}/c_{ut} = 1.60$	Vaid and Campanella 1974	Undisturbed Haney sensitive clay
$c_{uc}/c_{ut} = 2.13$	Ladd et al. 1971	Resedimented Boston blue clay
$c_{uc}/c_{ut} = 1.75$	Bjerrum 1973	Bangkok clay
$c_{uc}/c_{ut} = 1.36$	Bjerrum 1973	Matagami clay, Canada
$c_{uc}/c_{ut} = 2.67$	Bjerrum 1973	Drammen plastic clay
$c_{uc}/c_{ut} = 3.56$	Bjerrum 1973	Vater land clay
$c_{uc}/c_{ut} = 3.78$	Bjerrum 1973	Drammen lean clay
$c_{uc}/c_{ut} = 2.67 - 3.75$	Aas 1976(see Janbu 1977)	Norwegian clay, $10 < I_p < 20$
$c_{uc}/c_{ut} = 2.0 - 2.33$	Aas 1976(see Janbu 1977)	Norwegian clay, $I_p = 40$
$c_{uc}/c_{ut} = 1.63$	Aas 1976(see Janbu 1977)	Norwegian clay, $40 < I_p < 100$
$c_{uc}/c_{ut} = 1.72$	Jamiolkowski et al. 1985	Lean sensitive normally consolidated clay ($K_0 = 0.5$)
$c_{uc}/c_{ut} = 1.12$	Jamiolkowski et al. 1985	Plastic insensitive normally consolidated clay ($K_0 = 0.75$)

c_{uv} = undrained shear strength in vertical direction, c_{uh} = undrained shear strength in horizontal direction, c_{uc} = undrained shear strength in compression, c_{ut} = undrained shear strength in extension. τ_{uv} = shear vane strength in vertical direction, τ_{uh} = shear vane strength in horizontal direction

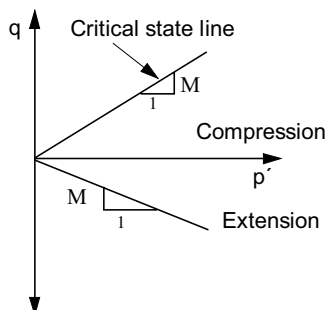


Fig. 2.24. Comparison of triaxial compression and extension at critical state strengths

Substituting the value of M from Eqs. 2.58 and 2.59 into Eq. 2.60, the ratio of undrained strength in compression and extension becomes

$$\frac{c_{uc}}{c_{ut}} = \frac{3 + \sin \varphi'_t}{3 - \sin \varphi'_c} \quad (2.61)$$

Taking the average values of $\varphi'_c = 29^\circ$ and $\varphi'_t = 26^\circ$ for the lacustrine soft soil in Constance (Scherzinger 1991), the ratio $c_{uc}/c_{ut} = 1.38$ may be obtained. For normally consolidated clays, Ladd et al. 1977 compared the undrained strength from triaxial and plane strain tests as follows

$$\frac{c_{u(\text{triaxial})}}{c_{u(\text{plain strain})}} \begin{cases} = 0.92 + 0.05 \Rightarrow \text{Compression} \\ = 0.82 + 0.02 \Rightarrow \text{Extension} \end{cases} \quad (2.62)$$

For practical purposes, however, the combined effect of both components of anisotropy can be considered collectively using K_0 - consolidated undrained test corresponding to the stress system and sample orientation that will exist in-situ (Ladd 1974). This will be in particular very important in an excavation, where the stress system and orientation behind the wall, in front of the wall and around the bottom of the wall are different.

Bjerrum et al. 1972 introduced a correction factor μ_A to account for the effect of anisotropy in undrained strength of normally consolidated soils obtained from field vane shear test as follows:

$$c_u = \mu_A \cdot \tau_f \quad (2.63)$$

For normally consolidated soft soils with plasticity index $I_p < 50\%$, Kempfert and Stadel 1997 suggested that $\mu_A = 1.5$ for triaxial compression and $\mu_A = 0.5$ for triaxial extension. However, these values must be justified by more data before applying to lacustrine soft soil in southern Germany.

Influence of time on undrained strength

Time is a factor of such an importance that it should be considered and taken into account in any stability analysis in which soft clays are involved. It is a factor associated with the cohesive component of the shear strength and that the frictional component of the shear strength is to a greater extent independent of time (Bjerrum 1973). The effect of time can be seen in four different ways: thixotropy, ageing, rate of strain, and creep. It is beyond the scope of this book to discuss these four factors. An extensive coverage of this topic can be found in the “state of the art” reports by Bjerrum 1973, Ladd et al. 1977, Jamiolkowski et al. 1985 and other text books such as Mitchell 1993.

The effect of the rate of strain on undrained shear strength can be considered in laboratory tests by proper selecting the time to failure and strain at the time of failure. On the other hand it may not be easy to control the strain rate in the field vane shear apparatus, though a rate of $1^\circ/\text{sec}$ (Ladd et al. 1977) is usually recom-

mended. Even then the vane shear strength overestimates the undrained strength of normally consolidated soils. After analysing embankment failures on clay foundations and unsupported excavations, Bjerrum et al. 1972 introduced a correction factor μ_R which depends on plasticity index of the soil. Thus

$$c_u = \mu_R \cdot \tau_f \quad (2.64)$$

where c_u is the undrained strength of the soil and τ_f is the field shear vane strength of the soil. Ladd et al. 1977 supported by different data, had studied the Bjerrum's curve and confirmed that the relationship between the correction factor μ_R and the plasticity index of the soil is quite sound (Fig. 2.25a).

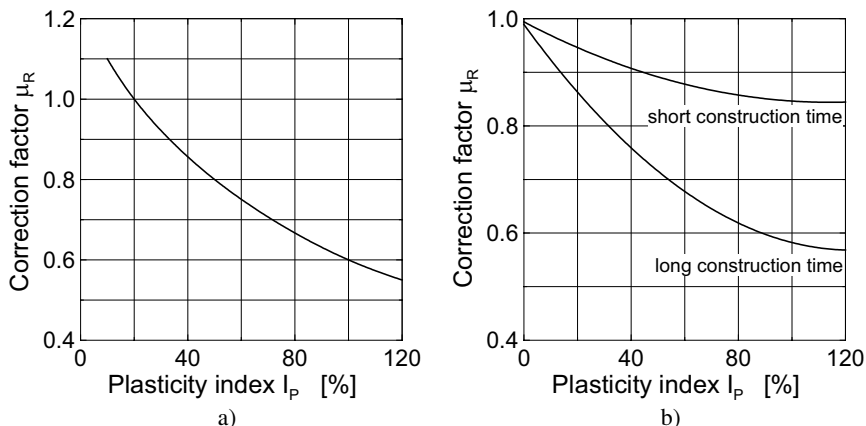


Fig. 2.25. Field vane correction factor versus plasticity index a) after Bjerrum et al. 1972; b) after Hettler et al. 2002

Fig. 2.25a considers only the different rate of mobilisation of the shear strength from several seconds or minutes by field vane test and several weeks or months by slope problems. Hence, the Bjerrum factor definitely underestimates the strength, if the mobilisation of the strength takes only few hours. Hettler et al. 2002 complemented the Bjerrum correction factor by including an additional curve (Fig. 2.25b) for the estimation of the undrained strength in case of fast mobilisation of the strength. This may be the case, for example, when an excavation is executed very fast within few hours. They derived the correction factor based on the equation suggested by Leinenkugel 1976 for estimation of the influence of the rate of strain on the undrained strength, i.e., the undrained strength c_u at any rate of strain $\dot{\epsilon}$ can be estimated from undrained strength $c_{u\alpha}$ at a reference rate of strain $\dot{\epsilon}_\alpha$ provided that the coefficient of viscosity $I_{v\alpha}$ is also known, for example from test results.

$$c_u = c_{u\alpha} \cdot \left[1 + I_{v\alpha} \cdot \ln \left(\frac{\dot{\epsilon}}{\dot{\epsilon}_a} \right) \right] \quad (2.65)$$

For the determination of the coefficient of viscosity in laboratory refer to Leinenkugel 1978.

Estimation of undrained shear strength from penetration results

The undrained shear strength c_u can also be estimated from the cone penetration field test using the equation:

$$c_u = \frac{(q_c - \sigma_{vo})}{N_k} \quad (2.66)$$

where q_c is the measured cone resistance, σ_{vo} is the total in-situ vertical stress, and N_k is the empirical cone factor. The value of N_k should be selected according to the experience in a particular soil type. Various attempts to determine the N_k values or to correlate it with plasticity index can be found in Lunne et al. 1997. In general, the value of N_k varies between 10 and 20. Jörß 1998 recommends $N_k = 20$ for marine clay and $N_k = 15$ for boulder clays in northern Germany.

Gebreselassie et al. 2003 compiled data from various regions in Germany and suggested the value of N_k for different type of soils as shown in Table 2.10.

Table 2.10. N_k values for different type of soils in Germany (Gebreselassie et al. 2003)

Soil type	N_k
Sludge	7.6
Marine young clay	14.1
Lacustrine soft soil	18.8
Quaternary clay and clay stone	89.3
Tertiary clay	28.4

Though a standard rate of penetration of the cone 20 mm/s is usually recommended, there are evidences which show that q_c increases with the increasing rate of penetration, and there is a minimum value of cone resistance at a rate of penetration 1 - 2.5 mm/s for slightly overconsolidated soft clays (see Lunne et al. 1997).

The undrained strength can also be estimated from the standard penetration (SPT) results. According to Stroud 1975, compressibility modulus E_{oed} and undrained strength c_u can be estimated from the following equations:

$$c_u = f_1 \cdot N_{30} \quad [kN / m^2] \quad (2.67)$$

$$E_{oed} = \frac{I}{m_v} = f_2 \cdot N_{30} \quad [MN / m^2] \quad (2.68)$$

where f_1 and f_2 are factors which are dependant on the plasticity index as shown in Fig. 2.26 and N_{30} is the number of blows for 30 cm penetration in SPT-test.

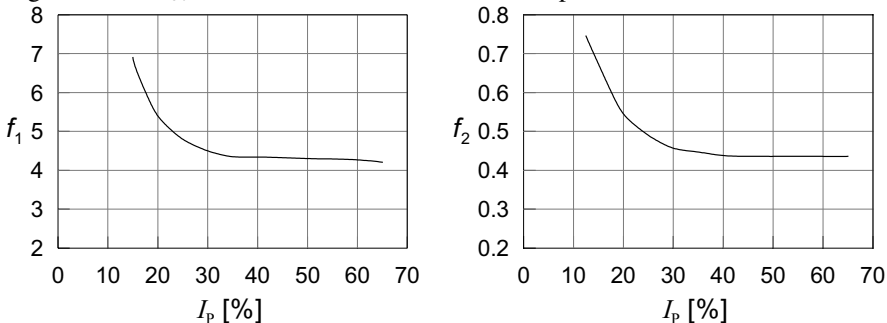


Fig. 2.26. The factors f_1 and f_2 dependent on the plasticity index (after Stroud 1975)

Estimation of the undrained shear strength from empirical equations

There have been continuous attempts, right from the early stages of the development of soil mechanics, to develop simple methods to predict the undrained strength of soils from simple soil index parameters, such as consistency limits. Although the literature in this respect is very rich, only few of them have been selected and listed in Table 2.11. These simple correlation are used to estimate the undrained strength of soils. However, attention should be given to the conditions in which the correlation had been made and the statistical accuracy of the equations, before choosing a single empirical equation for a particular type of soil.

Some of the empirical equations and data from Constance lacustrine soft soil (Scherzinger 1991) are also plotted in Fig. 2.27. It can clearly be observed that neither of the equations would satisfy the Constance soft soil for the given range of data, rather most of the data points lie between $c_u/\sigma'_{vc} = 0.22$ (Mesri 1975) and $c_u/\sigma'_{vc} = 0.33$ (Larsson 1980) lines. After analysing a large number of data from Eastern Canada and Scanadivean soils, Windisch and Yong 1990, also showed that non of the empirical equations would apply to eastern Canadian clays. Instead, they recommend a mean value of $c_u/\sigma'_{vc} = 0.27$. Burland 1990 also showed that for remoulded clays the normalised undrained strength remains constant, $c_u/\sigma'_{vc} = 0.30$. Therefore, the normalised undrained shear strength of normally consolidated clay can be fairly assumed to be constant for a particular soil, provided that the groundwater is located at relatively shallow depth. Kempfert and Stadel 1997 introduced a constant λ , where

$$\frac{c_u}{\sigma'_{vc}} = \lambda_{cu} = \text{constant} \quad (2.69)$$

and they used λ_{cu} to calculate the earth pressure at the end of construction stage (initial condition). The value of λ_{cu} varies from soil to soil. For the lacustrine soft clays in Constance, Scherzinger 1991 approximated $\lambda_{cu} = 0.26$. For similar lacustrine soils in this region, Heil et al. 1997 reported that $\lambda_{cu} = 0.30$ for triaxial test and $\lambda_{cu} = 0.20$ for vane tests.

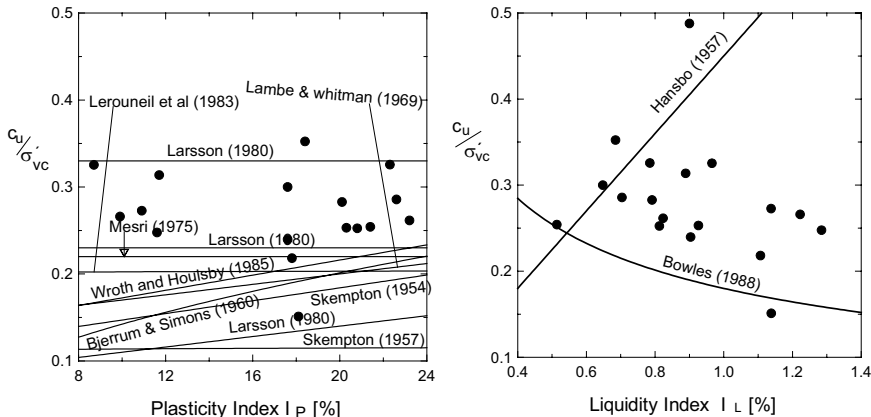


Fig. 2.27. Relations between normalized undrained strength and a) plasticity index, b) liquidity index (Data from Scherzinger 1991)

The effect of stress system induced anisotropy can also be seen from correlation of the normalised undrained strength with plasticity index of the soil as shown in Fig. 2.28. It would appear from Fig. 2.28 that less plastic and often more sensitive clays tend to have higher anisotropy than more plastic clays.

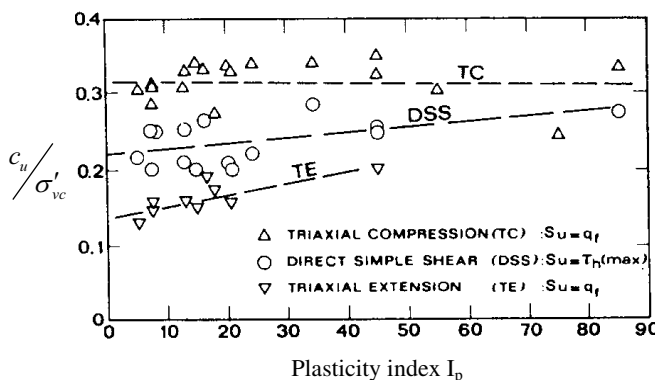


Fig. 2.28. Undrained strength anisotropy from CK_0U tests performed on normally consolidated clays (from Jamiolkowski et al. 1985)

Table 2.11. Empirical equations to estimate undrained shear strength

Equation	Reference	Regions of Applicability
$c_u = 170 \cdot \exp(-4.6 \cdot I_L)$	[kPa] Wroth and Wood 1978	Remoulded clays
$c_u = 1/(I_L - 0.21)^2$	[kPa] Mitchell 1993	From several clays (remoulded strength)
$c_u/\sigma'_{vc} = 0.11 + 0.0037 \cdot I_p$	Skempton 1954, Bowles 1984	Normally consolidated soils, $I_p > 10\%$
$c_u/\sigma'_{vc} = 0.11 + 0.0037 \cdot \log I_p$	Skempton 1957 (see Kempfert and stadel 1997)	Normally consolidated soil, $I_p < 60\%$
$\tau_f/\sigma'_{vc} = 0.2 + 0.0024 \cdot I_p$	Lerouneil et al. 1983	Clays from eastern Canada, $I_p < 60\%$
$\tau_f/\sigma'_{vc} = 0.22$	Mesri 1975	Soft clays
$c_u/\sigma'_{vc} = 0.08 + 0.55 \cdot I_p$	Larsson 1977	Scandinavian clays
$c_u/\sigma'_{vc} = 0.23 \pm 0.04$	Larsson 1980	Soft sedimentary clays, $I_p < 60\%$
$c_u/\sigma'_{vc} = 0.33$	Larsson 1980	Inorganic clays
$c_u/\sigma'_{vc} = (0.23 \pm 0.04) \cdot (OCR)^{0.8}$	Jamiolkowski et al. 1985	All clays
$c_u/\sigma'_{vc} \approx 0.26$	Scherzinger 1991	Constance lacustrine soft clays
$c_u/\sigma'_{vc} = 0.45 \cdot w_L$	Hansbo 1957	Scandinavian clays
$c_u/\sigma'_{vc} \approx 0.30$	Burland 1990	Natural sensitive clays
$c_u/\sigma'_{vc} = 0.14 + 0.003 \cdot I_p$	Lambe and Whitman 1969	All clays
$c_u/\sigma'_{vc} = 0.45 \cdot (I_p/100)^{1/2}$	Bjerrum and Simons 1960	Normally consolidated clays
$c_u/\sigma'_{vc} = 0.18 \cdot (I_L)^{-1/2}$	Bjerrum and Simons 1960	Normally consolidated clays
$c_u/\sigma'_{vc} = 0.45 \cdot w_L$	Bowles 1984	Normally consolidated soils, $w_L > 40\%$
$c_u = 11.4 + 0.169 \cdot \sigma'_{vc}$	[kPa] Windisch and Yong 1990	Barlow-Ojibway Lacustrine clays
$c_u = 2.32 + 0.260 \cdot \sigma'_{vc}$	[kPa] Windisch and Yong 1990	East Canadian marine clays
$c_u = 3.05 + 0.260 \cdot \sigma'_{vc}$	[kPa] Windisch and Yong 1990	Champlane sea clays
$c_u = 7.69 + 0.117 \cdot \sigma'_{vc}$	[kPa] Windisch and Yong 1990	Scandinavian clays
$c_u/\sigma'_{vc} = -0.09 + 0.0092 \cdot I_p$ [kPa]	Windisch and Yong 1990	Scandinavian clays
$c_u/\sigma'_{vc} = -0.18 + 0.0072 \cdot w_L$ kPa]	Windisch and Yong 1990	Scandinavian clays
$c_u/\sigma'_{vc} = 0.129 + 0.00435 \cdot I_p$	Wroth and Houlsby 1985	Normally consolidated clays
$\frac{c_u}{\sigma'_{vc}} = 0.5743 \cdot \frac{3 \cdot \sin \varphi'}{(3 - \sin \varphi')}$	Wroth and Houlsby, 1985	Normally consolidated soils

c_u = undrained shear strength, τ_f = undrained vane shear strength, σ'_{vc} = effective consolidation pressure, w_L = liquid limit, I_p = plasticity index (%), I_L = Liquidity index, OCR = over consolidation ratio, φ' = angle of internal friction

2.5.4 Drained strength

The drained strength of a soil is represented by the parameters c' and φ' and used for long-term analysis. Values of c' and φ' can be obtained from drained tests or undrained tests with measurements of pore water pressure during shear. The drained strength of a normally consolidated soils is also influenced by the same factors as those that affect the undrained strength, except the magnitude of the influence may be less in drained strength.

Duncan and Seed 1966; Morgenstern and Tchlenko 1967b stated that the drained strength is independent of the stress orientation relative to fabric orientation. Mitchell 1993 also added that the effective stress strength parameters are independent of sample orientation. He showed that the effective parameters for two samples of the same soil but tested in different direction; one in vertical and the other in horizontal direction, are the same though the stress paths followed different direction.

There is a conflicting evidence on the influence of initial stress and structure anisotropy on φ' at failure, but the bulk of presently available evidence suggests that inherent anisotropy has very little influence on φ' measured in triaxial compression tests. Compression and extension tests on soft Fulford clay at different sample orientation carried out by Parry and Nadarajah 1975b show that the influence of initial anisotropy to be much less than the influence of stress direction in producing failure (Table 2.12). The difference in c' values may not be significant, as this parameter is very sensitive to slight changes in test data.

Fig. 2.29 illustrates a fall in the angle of internal friction with increasing plasticity of the soil, which in turn is dependant on the mineralogy of the soil.

Like in undrained strength the combined effect of both components of anisotropy can be considered collectively using K_0 -consolidated undrained test or drained test (triaxial compression or extension or plane strain test) corresponding to the stress system and sample orientation that exist in situ. This will be in particular very important for excavations, where stress system and orientation behind the wall, in front of the wall and around the bottom of the wall are different.

Table 2.12. Influence of anisotropy on effective stress parameter φ'

Soil type	$\varphi'_{(comp)} / \varphi'_{(ext)}$		Reference
	Vertical	Horiz.	
Soft Fulford clay	0.76	0.83	Parry and Nadarajah 1975b
Koalin (Isotropic)	1.095		Parry and Nadarajah 1974a
Koalin (K_0)	0.75		Parry and Nadarajah 1975b
Speswhite kaolin (1-dimensional, then K_0 consolidated)	0.75		Atkinson, et al. 1987
Speswhite kaolin (Isotropic, then K_0 consolidated)	0.89		Atkinson, et al. 1987
Undisturbed Haney sensitive clay	0.73		Vaid and Campanella 1974
Constance soft soil	1.12		Scherzinger 1991
Undisturbed San Francisco Bay mud	1.08		Duncan and Seed 1966

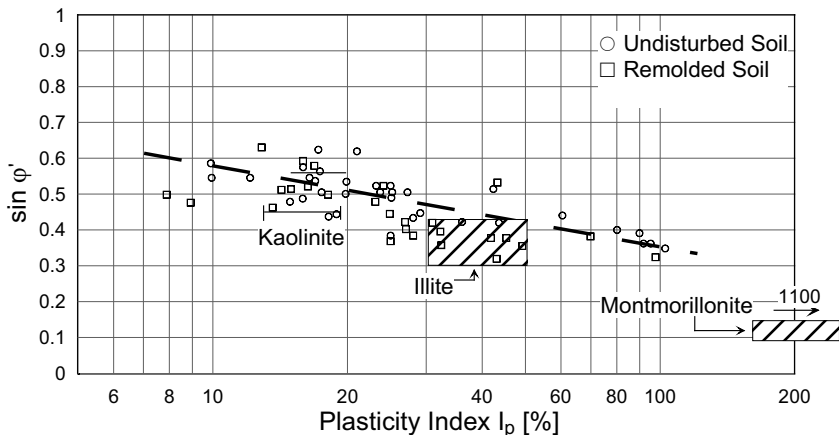


Fig. 2.29. Relationship between $\sin \varphi'$ and plasticity index for normally consolidated soils (from Mitchell 1993)

2.6 Deformation properties

2.6.1 General

Deformation of a soil is one of the most important physical aspect in geotechnical problems. Many investigators have revealed that the soil deformation modulus was found to have the greatest influence on deformation behaviour of geotechnical structures e.g. excavations, shallow foundations, etc. The material properties required for deformation analysis are conventionally those four constants used in the theory of elasticity, namely, the Young's modulus E , the Poisson's ratio ν , the shear modulus G and the bulk modulus K . In reality, however, the shear modulus G and bulk modulus K can be written in terms of the Young's modulus E and Poisson's ratio ν as

$$G = \frac{E}{2(1+\nu)} \quad (2.70)$$

$$K = \frac{E}{3(1-2\nu)} \quad (2.71)$$

There are two alternative definitions of the modulus of elasticity, namely, the secant modulus E_{sec} , and tangent modulus E_t (Fig. 2.30).

In most stress-strain curves from triaxial test on normally consolidated soil samples, the slope of the curve at a lower strains is not uniquely defined, and the correct estimation of the initial tangent modulus of elasticity is not simple. Moreover, in an elastic calculations the strain depends on both the stress and modulus. If the soil depends on strain, an iterative procedure must be adopted, in which the calculations are repeated until the strain is consistent. For this purpose, it is easier to use the secant, rather than the tangent modulus (Powrie 1997). The PLAXIS FE-program uses the secant modulus at 50% of the maximum deviatoric stress ($\sigma'_1 - \sigma'_3$)_f denoted as E_{50} as initial modulus (Fig. 2.27). For further details refer to section 3.2.4.

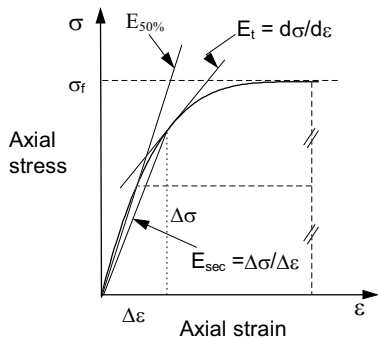


Fig. 2.30. Schematic diagram of stress strain behavior of soils

2.6.2 Drained and undrained behaviour

Like strength behaviour, it is essential to distinguish between undrained and drained behaviour of the deformation of soils. The relevant elastic properties are either E_u , v_u or E , v for undrained and drained conditions respectively.

For perfectly elastic soil, the value of the shear modulus is unaffected by the drainage condition, since the water within the soil skeleton has zero shear stiffness. Hence

$$\frac{E_u}{2 \cdot (1 + v_u)} = G_u = G = \frac{E}{2 \cdot (1 + v)} \quad (2.72)$$

Since the bulk undrained modulus is defined as

$$K_u = \frac{\Delta\sigma}{\Delta\varepsilon_{vol}} = \frac{E_u}{3 \cdot (1 - 2 \cdot v_u)} \quad (2.73)$$

and for undrained condition, the volumetric strain $\Delta\varepsilon_{vol} = 0$, K_u becomes infinite. This requires that the undrained Poisson's ratio $v_u = 0.5$. Hence

$$\frac{E_u}{E} = \frac{3}{2 \cdot (1 + \nu)} \quad (2.74)$$

For most soils, the effective Poisson's ratio ranges between 0.12 and 0.35 (Wroth and Housby, 1985). Therefore,

$$\frac{E_u}{E} \approx 1.11 \text{ to } 1.34 \quad (2.75)$$

2.6.3 Effect of depth on modulus of elasticity

It is necessary to take account of the fact that soil stiffness is likely to increase with increasing effective stress. This effect is often modelled by assuming that the soil stiffness is proportional to the depth. According to Ohde 1939,

$$E_t = k \cdot p_{ref} \cdot \left(\frac{\sigma'_{vc}}{p_{ref}} \right)^m \quad (2.76)$$

where k is a dimensionless modulus number, m is an exponent, and p_{ref} is reference pressure usually taken as atmospheric pressure. The values of k and m can be determined from a plot of the effective consolidation stress against the tangent modulus for a series of test data. In practice, however, it is common to assume the undrained modulus of elasticity to vary linearly with undrained shear strength (Table 2.13), because the undrained shear strength is also assumed to vary proportional with depth.

Table 2.13. Variations of undrained modulus of elasticity with undrained strength

Equation	Reference	Regions of Applicability
$E_{u,i} = 200 \cdot c_u$	Clough and Mana 1976	San Francisco clay
$E_{u,i} = (600 \text{ to } 1200) \cdot c_u$	Clough and Mana 1976	San Francisco clay (obtained from back analysis of excavation)
$E_{u,i} = 280 \cdot c_u$ *	Ladd and Edgers 1972	Atchafalya CH Clay
$E_{u,i} = 420 \cdot c_u$ *	Dames and Moore 1975	AGS CH Clay
$E_{u,i} = 600 \cdot c_u$ *	Ladd and Edgers 1972	Maine organic CH-OH clay
$E_{u,i} = 670 \cdot c_u$ *	Ladd and Edgers 1972	Bangkok CH clay
$E_{u,i} = 820 \cdot c_u$ *	Ladd and Edgers 1972	Boston CL clay
$E_{u,i} = 280 \cdot c_u$	Ladd 1964	Not known
$E_{u,i} = (250 \text{ to } 500) \cdot c_u$	Bjerrum 1964	Normally consolidated Norwegian clays
$E_{u,i} = 275 \cdot \sigma$ *	Ladd 1964	Laqunillas normally consolidated clay
$E_{u,i} = 175 \cdot \sigma$ *	Ladd 1964	Kawasaki normally consolidated clay

* Values are for stress level $(c_u/c_{u(max)}) = 1/3$, $E_{u,i}$ = initial tangent undrained modulus

2.6.4 Effect of anisotropy on modulus of elasticity

Soils in the field are consolidated under anisotropic stress conditions giving them different stiffness in the vertical and horizontal directions. Normally consolidated soft soils will usually be stiffer in the vertical direction than in the horizontal direction (Parry 1995). For soft recently deposited clays, Parry and Wroth 1981 showed that the ratio n between the vertical E_v and horizontal E_h modulus of elasticity is of the order,

$$\frac{E_h}{E_v} = n \cong 0.5 \quad (2.77)$$

However, they also indicated that the value of n varies with different stress paths and sample orientation as shown in Fig. 2.31. The combined effect of the stiffness in vertical and horizontal direction may be taken as the average of the two (Parry 1995).

Likewise, the Poisson's ratio in vertical direction differs from that in horizontal direction. If ν_v and ν_h are assumed the Poisson's ratio in vertical and horizontal directions respectively, the combined effect may be estimated from (Henkel 1971):

$$\nu = \frac{1}{2} \cdot \nu_v \cdot (1 + n) \quad (2.78)$$

Orientation	Compression			Extension			
	n	Stress Path	Gradient	Orientation	n	Stress Path	Gradient
Vertical	0.5	OA	1.4	Vertical	0.5	OE	1.4
Vertical	1.0	OB	3.0	Vertical	0.25	OF	1.1
Horizontal	1.5	OC	∞	Horizontal	1.5	OG	∞
Horizontal	3.0	OD	-2.4	Horizontal	0.75	OH	-2.0

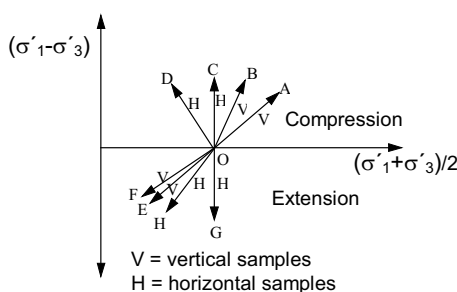


Fig. 2.31. Influence of sample orientation on modulus of elasticity (after Parry, 1995)

2.6.5 Constrained Modulus from one-dimensional compression

The constrained modulus from one-dimensional compression oedometer E_{oed} can be related with the modulus of elasticity using the elasticity theory as:

$$E = E_{oed} \cdot \frac{(1+\nu) \cdot (1-2\cdot\nu)}{(1-\nu)} \quad (2.79)$$

For most soils, ν ranges between 0.12 to 0.35. Hence,

$$\frac{E}{E_{oed}} \cong 0.623 \text{ to } 0.967 \quad (2.80)$$

However, since soils are known as elasto-plastic material, the above relationship might not always holds true. Vermeer and Meier 1998 asserted that $E_{50} < E_{oed}$ for stiff overconsolidated clay, $E_{50} > E_{oed}$ for soft soils, and $E_{50} \approx E_{oed}$ for sands, specifically for analysis with the FE-code PLAXIS.

2.6.6 Unloading/reloading modulus of elasticity.

The behavior of soils during unloading/reloading is assumed elastic, because changes in stress can be accommodated without the need for a rearrangement of the soil skeleton, i.e., deformation is primarily due to distortion of the soil particle which is recoverable. Hence, soils are stiffer in unloading/reloading than in the first loading, even over the same stress range. The unloading/reloading stress-strain curves are fairly approximated by straight lines, where the modulus of elasticity in unloading and reloading are assumed to be same, and they are denoted by a single symbol E_{ur} . Due to the fact that soil behaves elastically during unloading/reloading, E_{ur} is a true elasticity modulus unlike E_{50} , which determines the magnitude of both the elastic and plastic strains. Hence, using Eq. 2.79, E_{ur} can be related with the constrained unloading/reloading modulus $E_{u, oed}$

$$E_{ur} = E_{ur, oed} \cdot \frac{(1+\nu_{ur}) \cdot (1-2\cdot\nu_{ur})}{(1-\nu_{ur})} \quad (2.81)$$

where ν_{ur} is the Poisson's ratio for unloading/reloading. The un/reloading modulus is also to some extent dependent on the previous stress level before the unloading has taken place.

3 Constitutive soil models and soil parameters

3.1 Constitutive soil models

3.1.1 Introduction

The essential features of soil behaviour include: soil acts as a multi-phase material, soil response is non-linear and path-dependent, soil deformation include irrecoverable (plastic) strains, soils may dilate or compact, soil response is influenced by its load history, natural soils are anisotropic, and soils exhibit time-dependent behaviour. Ideally a perfect soil model would be able to predict these soil behaviour under all type of loading condition.

An increasing number of stress-strain relations have been formulated to model the behaviour of soils. These models can be grouped into linear elastic, non-linear elastic (hyperelasticity, hypoelasticity), variable moduli, elasto-plastic, elasto-visco-plastic, cap models and hypoplasticity. Several references can be cited in connection with the formulation of constitutive soil models: Duncan and Chang 1970; Naylor and Pande 1981; Evgin and Eisenstein 1985; Britto and Grun 1987; Mizuno and Chen 1986; Chen and McCarron 1986; McCarron and Chen 1987; Hayashi and Yamanouchi 1986; Gudehus 2002; Chen and Mizuno 1990; Kirkgaard and Lade 1993; Brinkgreve 2002; etc. The development of the models have been briefly reviewed in the following sub-sections.

All the numerical analysis of practical projects and parameter studies in this book are conducted using the finite element program “PLAXIS”. Therefore, the constitutive soil models included in this program, their advantages and limitations in connection with excavation in soft normally consolidated soil, the soil parameters required and their evaluation is briefly assessed in this chapter.

3.1.2 Linear elastic stress-strain law

A linear elastic model is the simplest one and it is based on the Hook's law of linear stress-strain relation. The law relates the total stress or the effective stress to strains, depending on the type of analysis selected. The stress-strain law can be expressed in terms of two soil parameters, namely modulus of elasticity E (or the bulk modulus K , or the shear modulus G) and Poisson's ratio ν . In incremental form, the stress-strain relation can be written as:

$$d\underline{\sigma} = \underline{\underline{D}}^e \cdot d\underline{\varepsilon}^e \quad (3.1)$$

where $d\underline{\sigma}$ is the incremental stress tensor, $d\underline{\varepsilon}^e$ is the incremental elastic strain tensor, and $\underline{\underline{D}}^e$ is the elastic material stiffness matrix that includes G and v . The linear elastic models are usually inappropriate to model the highly non-linear behaviour of soils. However, there are piecewise linear elastic models that overcome the non linearity problem by representing the stress-strain curve with piecewise linear relations.

3.1.3 Non-linear elastic stress-strain law

A non-linear elastic model is regarded as an extension of the piecewise linear elastic model using infinitesimal linear intervals. The material constants are assumed to be a function of stress, strain or their invariants. This model has the shortcomings that the direction of strain increment coincides with that of the stress increments, and that dilatancy can not be taken into consideration. To overcome some of these shortcomings, advanced non-linear elastic soil models such as the hyperelastic and hypoelastic models have been developed. The hyperelastic model has the general form:

$$\underline{\sigma} = \frac{\partial W}{\partial \underline{\varepsilon}} \quad (3.2)$$

where W is the strain energy density function. The model is developed based on the first law of thermodynamics and law of kinetic energy and it is stress path independent (i.e. the stresses are only expressed in terms of strains). On the other hand, hypoelastic models, which include terms of stress increments and strain increments as well as the stresses and strains, can predict behaviour of soils with stress path dependence. The hypoelastic model is generally written in incremental linear form as:

$$d\underline{\sigma} = \underline{\underline{D}}(\underline{\sigma}) \cdot d\underline{\varepsilon} \quad (3.3)$$

where $\underline{\underline{D}}$ is the tangential stiffness tensor of the material which in turn is a function of the stress tensor $\underline{\sigma}$.

3.1.4 Variable elastic stress-strain law

In this model, the bulk and shear moduli are both taken as non-linear function of the stress and/or strain tensor invariants. Thus, unlike the non-linear elastic models, different function are used for initial loading, unloading, and reloading to

reflect the irreversible characteristics of the inelastic deformations. In the simplest form the variable moduli model can be written as:

$$dp = K \cdot d\varepsilon_v \quad (3.4a)$$

$$dq = 3 \cdot G \cdot d\varepsilon_q \quad (3.4b)$$

where $d\varepsilon_v = d\varepsilon_1 + d\varepsilon_2 + d\varepsilon_3$ and

$$d\varepsilon_q = [\frac{2}{3} \cdot (d\varepsilon_1 - d\varepsilon_2)^2 + (d\varepsilon_2 - d\varepsilon_3)^2 + (d\varepsilon_3 - d\varepsilon_1)^2]^{\frac{1}{2}}$$

are strain invariants.

3.1.5 Elasto-plastic stress-strain law

Elasto-plastic soil models based on incremental plasticity theory can overcome the shortcomings in the above mentioned soil models. Existing elasto-plastic models, such as hardening soil and the soft soil models in PLAXIS, have gained popularity because they are defined by few material parameters which can be determined from standard tests and yet represent important material characteristics such as dilatancy, stress path dependency, non-linear behaviour, etc. There are three ingredients to the elasto-plastic stress-strain laws:

1. A yield function which signals if the material is yielding plastically or not and symbolically written as:

$$F(\underline{\sigma}) = 0 \quad (3.5)$$

2. A hardening function which indicates the manner in which the yield function changes due to plastic straining $h = h(\underline{\varepsilon}^p)$, in which case the yield function (Eq. 3.5) may be re-written as:

$$F(\underline{\sigma}, h) = 0 \quad (3.6)$$

3. A flow rule which determines the direction of plastic straining and it is given by:

$$d\underline{\varepsilon}^p = d\lambda \cdot \frac{\partial Q}{\partial \underline{\sigma}} \quad (3.7)$$

where F is the yield function, $\underline{\sigma}$ is stress tensor, h is the hardening parameter, $d\underline{\varepsilon}^p$ is the incremental plastic strain, Q is a plastic potential function, and λ is a positive scalar of proportionality dependent on the state of stress and the load history. As shown in Fig. 3.1, $F(\underline{\sigma}) < 0$ implies elastic behaviour and $F(\underline{\sigma}) > 0$ is an impossible stress situation. The most common yield surfaces in soil mechanics, their advantages and limitations according to Chen and McCarron 1986; and Chen

and Mizuno 1990 are presented in Table 3.1. Von-Mises and Drucker-Prager yield criteria are used in geotechnical analysis as a simplification of Tresca and Mohr-Coulomb yield criteria. All these four models are perfect plasticity models and they are formulated based on the assumption of the associated flow rule. On the other hand, the Lade-Duncan model is a work hardening constitutive law. It was first developed for cohesionless soils only. However, Kirkgrad and Lade 1993 showed that the Lade-Duncan failure criteria fits reasonably well for the failure points of specimens of normally consolidated clay, which are tested under cubical triaxial test, in particular for the values of θ in the range of 0 to 90°. θ is the angle between the projection of the σ_x axis on the octahedral plane and any stress point ($\sigma_x \sigma_y \sigma_z$) measured in clockwise direction. An excellent, a complete description and derivation of these different yield functions can be found in Chen and Mizuno 1990.

Eq. 3.6 implies the direction of the plastic strain incremental vector is normal to the plastic potential surface (Fig. 3.1) at the current stress point. However, if an associated flow rule is assumed, i.e., $Q = F$, the normality is also associated with the yield surface. This assumption is an essential framework for most elasto-plastic soil models in order to simplify the formulation, although, in reality soil exhibits a non associated behaviour. Wong and Mitchell 1975 showed that most soils appear not to conform precisely to the associated flow rule. Tests results on normally consolidated soft clay in Winnipeg, Canada (Graham et al. 1983) and San Francisco (Kirkgrad and Lade 1993) also showed that the plastic increment vectors are not precisely normal to the yield surface. Nowadays, with the advent of high speed and large capacity computer technology, it becomes possible to implement highly sophisticated material models. Some of the set backs in the mathematically complex material models are the difficulties to obtain the required soil parameters from the conventional soil tests.

The elasto-plastic stress-strain law can now be formulated as follows. In theory of incremental plasticity, the increments of stress and increments of strain can be related by the relationship:

$$d\sigma = \underline{D}^{ep} \cdot d\varepsilon \quad (3.8)$$

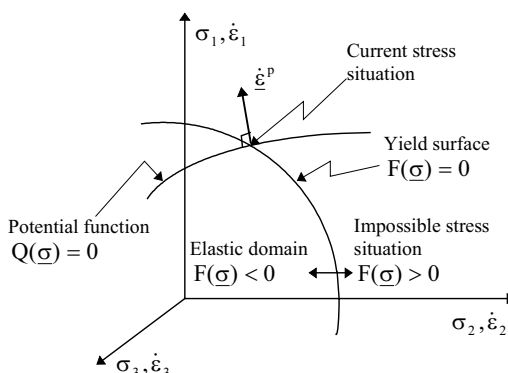
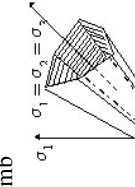
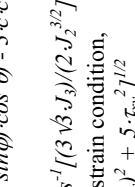


Fig. 3.1. Schematic representation of the yield surface, the potential function, and the flow rule

Table 3.1. Different failure models, their advantages and limitations (after Chen and Mizuno 1990; Chen and McCarron 1986)

Soil Model	
von Mises	 <p>$F = \sqrt{J_2} - c_u = 0$ for plane strain, $F = J(\sigma_z - \sigma_y)^2 + 5 \cdot \tau_{xy}^2 J^{1/2} - 2 \cdot c_u$</p>
Tresca	 <p>$\sigma_1 = \sigma_2 = \sigma_3$</p> <p>$F = [(\sigma_x - \sigma_y)^2 - 5c_u^2]^{1/2} / (\sigma_x - \sigma_y)^2 - 5c_u^2 = 0$ for plane strain, $F = [(\sigma_x - \sigma_y)^2 + 5 \cdot \tau_{xy}^2]^{1/2} - 2 \cdot c_u = 0$</p> <ul style="list-style-type: none"> • simple • smooth

Table 3.1. (cont.)

Lade-Duncan	Drucker-Prager	Mohr-Coulomb
 $F = J_3 - (I/3) \cdot J_I \cdot J_2 + (1/27 - I/\kappa_I) \cdot J_I^3 = 0$ <p>where $\kappa_I = I_I^3/I_3$</p>	 $F = \alpha \cdot I_I + \sqrt{J_2} \cdot J_2^{1/2} (1 - \sin\varphi) \cdot \sin\theta$ <p>where $\alpha = (2 \cdot \sin\varphi) / (\sqrt{3} \cdot (3 - \sin\varphi))$</p> $k = (6 \cdot c \cdot \cos\varphi) / (\sqrt{3} \cdot (3 + \sin\varphi))$	 $F = I_I \cdot \sin\varphi + \sqrt{J_2} / 2 \cdot J_2^{1/2} (1 - \sin\varphi) \cdot \sin\theta$ <p>where</p> $\theta = (I/3) \cdot \cos^{-1} [(3 \cdot \sqrt{3} \cdot J_3) / (2 \cdot J_2^{3/2})] = 0$ <p>or for plane strain condition,</p> $F = [(\sigma_x - \sigma_y)^2 + 5 \cdot \tau_{xy}^2]^{1/2}$ $- (\sigma_x + \sigma_y) \cdot \sin\varphi - 2 \cdot c \cdot \cos\varphi = 0$

where $\underline{\underline{D}}^{ep}$ is the elasto plastic matrix and $d\underline{\underline{\varepsilon}}$ is the total strain increment tensor and assumed to be the sum of the elastic strain increment tensor $d\underline{\underline{\varepsilon}}^e$ and plastic strain increment tensor $d\underline{\underline{\varepsilon}}^p$, i.e.

$$d\underline{\underline{\varepsilon}} = d\underline{\underline{\varepsilon}}^e + d\underline{\underline{\varepsilon}}^p \quad (3.9)$$

Recalling that the stress increments are also related to the elastic components of strains using the Hook's law (Eq. 3.1) and substituting Eq. 3.1 into 3.9, it becomes:

$$d\underline{\sigma} = \underline{\underline{D}}^e \cdot [d\underline{\underline{\varepsilon}} - d\underline{\underline{\varepsilon}}^p] \quad (3.10)$$

The consistency condition requires that $dF = 0$, i.e., during the plastic yield the stress remains on the yield surface. Expanding $dF = 0$ using the chain rule, we obtain:

$$dF = \frac{\partial F}{\partial \underline{\sigma}} \cdot d\underline{\sigma} + \frac{\partial F}{\partial h} \cdot \frac{\partial h}{\partial \underline{\underline{\varepsilon}}^p} \cdot d\underline{\underline{\varepsilon}}^p = 0 \quad (3.11)$$

Substituting Eq. 3.7 into Eq. 3.11, rearranging, simplifying, and defining new parameters, the elasto-plastic matrix can be obtained from:

$$\underline{\underline{D}}^{ep} = \underline{\underline{D}}^e - \frac{I}{\beta} \cdot \underline{b}_q \cdot \underline{b}_f^T \quad (3.12)$$

where $\underline{b}_q = \underline{\underline{D}}^e \cdot \underline{a}_q$; $\underline{b}_f = \underline{\underline{D}}^e \cdot \underline{a}_f$; $\underline{a}_q = \partial Q / \partial \underline{\sigma}$; $\underline{a}_f = \partial F / \partial \underline{\sigma}$;

$\beta = H + \underline{a}_f^T \cdot \underline{\underline{D}}^e \cdot d\underline{\underline{\varepsilon}}$, and finally $H = -\frac{\partial F}{\partial h} \cdot \left(\frac{\partial h}{\partial \underline{\underline{\varepsilon}}^p} \right)^T \cdot \underline{a}_q$. For ideal plasticity,

such as Mohr-Coulomb model, the yield function is independent of hardening parameter, i.e., $\partial F / \partial h = 0$, hence, $H = 0$ and $\beta = \underline{a}_f^T \cdot \underline{b}_q$.

The choice of the hardening rule depends on the type of the material and on the ease with which it can be applied. Three types of hardening rules are commonly used to describe the behaviour of soils. These are isotropic, kinematic, and mixed hardening. Isotropic hardening represents a uniform expansion of the yield surface in all direction, whereas kinematic hardening represents a simple means of accounting plastic anisotropy, i.e., during plastic flow, the yield surface is assumed to translate as a rigid body, maintaining its size, shape and orientation. Mixed hardening represents a combination of the isotropic and kinematic hardening. As far as this work is concerned, however, it is limited to an isotropic hardening only, because the soil models in the available finite element code (PLAXIS) for this study is based on this type of hardening.

Eq. 3.12 is an important part of the element stiffness matrix $\underline{\underline{K}}^{ep}$ for elasto-plastic material in the finite element formulation, i.e.,

$$\underline{\underline{K}}^{ep} = \int_v \underline{\underline{B}}^T \cdot \underline{\underline{D}}^{ep} \cdot \underline{\underline{B}} \cdot dv \quad (3.13)$$

where $\underline{\underline{B}}$ is a matrix that relates the strains inside the element with the nodal displacements and usually referred as the B-matrix or strain matrix. $\underline{\underline{K}}^{ep}$ is a non-symmetric matrix because $\underline{\underline{D}}^{ep}$ is a non-symmetric matrix due to the terms $\underline{b}_q \cdot \underline{b}_f^T$ in Eq. 3.12. However, if an associated flow rule ($Q = F$) is assumed, the elasto-plastic matrix becomes symmetric.

3.1.6 Elasto-visco-plasticity

In contrast to the elasto-plasticity, the elasto-visco-plasticity theory assumes that all plastic strains in the material are time dependent and further postulated that the stress trajectories can cross the yield surface so that stress situation outside the yield surface are admissible, i.e., $F > 0$. Other-wise, the concept of yield function, flow law and hardening law developed in the contest of elasto-plasticity are also applied to elasto-visco-plasticity. In incremental form the total strain may be written as:

$$d\underline{\varepsilon} = d\underline{\varepsilon}^e + d\underline{\varepsilon}^{vp} \quad (3.14)$$

where $d\underline{\varepsilon}^{vp}$ represents the visco-plastic strain. The flow equation is given by the rate of visco-plastic strains as:

$$\dot{\underline{\varepsilon}}^{vp} = \mu \cdot \langle F \rangle \cdot \frac{\partial Q}{\partial \underline{\sigma}} \quad (3.15)$$

where μ is the fluidity parameter. The brackets $\langle \rangle$ denotes that the quantity in this brackets is zero if $F \leq 0$, i.e. $\dot{\underline{\varepsilon}}^{vp} = 0$, but if $F > 0$, the flow Eq. 3.15 applies as it is. The plastic strain increment is given by:

$$d\underline{\varepsilon}^p = \dot{\underline{\varepsilon}}^{vp} \cdot dt \quad (3.16)$$

where dt represents an infinitesimal time step. Using Eqs. 3.14, 3.15 and 3.16 and keeping in mind that stresses can be related to elastic strains, one can arrive at the following relationship:

$$d\underline{\sigma} = \underline{\underline{D}}^e \cdot \left(d\underline{\varepsilon} - \mu \cdot \langle F \rangle \cdot \frac{\partial Q}{\partial \underline{\sigma}} \cdot dt \right) \quad (3.17)$$

3.1.7 Hypoplasticity

Hypoplasticity describes stress change in soil grain particles by means of tensors. Contrary to the elasto-plastic constitutive models, the hypoplastic model does not divide deformations into elastic and plastic components and hence explicit definitions of yield function, flow rule, hardening, softening, etc. are not necessary. The terminology in this sections are adopted directly from the original papers and they may differ from those used in the rest of the chapter, however, they are defined locally whenever necessary.

The mechanical property is described with the stress rate $\overset{o}{T}$ (Jaumann stress rate) as a function of the stress level and strain rate D as well one more state variable, i.e. the void ratio e . There exist a non-linear relationship between the stress rate and the strain rate. The hypoplastic model is stress dependant and therefore cannot be integrated, i.e. there exist normally no relationship of the form $T = F(E)$, where T is stress tensor and E is strain tensor.

The hypoplastic model for granular materials with only four material parameters was first introduced by Kolymbas 1988, whereby the term hypoplasticity was first given by Wu 1992 following the term hypoelasticity. The material matrix $\partial \overset{o}{T}_{ij} / \partial D_{kl}$ of the hypoplastic model is not symmetric. The general equation of the hypoplastic model can be written in a tensor form as:

$$\overset{o}{T} = F(T, D, e) \quad (3.18)$$

where F is a tensor valid function with two state variables T and e . The rate of the void ratio is also given by the equation:

$$\dot{e} = (1 + e) \cdot \text{tr}D \quad (3.19)$$

Different authors have tried to modify and extend the equation with regard to the stress dependency of the material property (barotropy) and the influence of density on the material property (pycnotropy) (Wu 1992; Bauer 1992). Wu et al. 1993 showed different concepts to describe viscosity in hypoplastic constitutive model. Kolymbas et al. 1995 introduced the hypoplastic with an additional state variable, the so called structural tensor. Gudehus 1996; Bauer 1996; von Wolfersdorff 1996 have developed a hypoplastic model, which covers a wide range of stresses, void ratios and deformation directions. For that purpose, a factorial decomposition of the material equation is used, which allows a separate determination of parameters that corresponds to a particular material property.

On the mean time, there are several version of the hypoplastic model just much versions as hypoelastic models. They are dependant on the governing material property of each given problem.

The version by Wu 1992 ignores the barotropy and pycnotropy and it can be expressed by

$$\overset{o}{\dot{\mathbf{T}}} = C_1(\text{tr } \mathbf{T}) \mathbf{D} + C_2 \frac{\text{tr}(\mathbf{T}\mathbf{D})}{\text{tr } \mathbf{T}} + C_3 \frac{\mathbf{T}^2}{\text{tr } \mathbf{T}} \sqrt{\text{tr } \mathbf{D}^2} + C_4 \frac{\mathbf{T}^{*2}}{\text{tr } \mathbf{T}} \sqrt{\text{tr } \mathbf{D}^2} \quad (3.20)$$

where C1, C2 and C3 are constants to be determined experimentally.

The further development of this version by von Wolffersdorff 1996 considers the missing barotropy and pycnotropy effects and gives a very good results, however, its application cyclic loading condition is very limited. However, this problem had been removed in the model version by Niemunis and Herle 1997.

For description of the rate dependant behaviour (Agrotropy) of viscous cohesive soils, Niemunis (1996) developed the so called visco-hypoplasticity formulation, which adopts some elasto-plastic principles from the Cam Clay Model families. With this model, creep and relaxation processes can be described.

The recent version of the hypoplastic model (see von Wolffersdorff 1996; Kolymbas 2000) is given by:

$$\overset{o}{\dot{\mathbf{T}}} = f_b \cdot f_e \frac{1}{\text{tr}(\hat{\mathbf{T}}^2)} \cdot \left[F^2 \mathbf{D} + a^2 \hat{\mathbf{T}} \text{tr}(\hat{\mathbf{T}} \cdot \mathbf{D}) + f_d \cdot a \cdot F(\hat{\mathbf{T}} + \hat{\mathbf{T}}^*) \|\mathbf{D}\| \right] \quad (3.21)$$

with

$$\begin{aligned} \hat{\mathbf{T}} &= \frac{\mathbf{T}}{\text{tr } \mathbf{T}}; \quad \hat{\mathbf{T}}^* = \hat{\mathbf{T}} - \frac{1}{3} \cdot \mathbf{I} \\ F &= \sqrt{\frac{1}{8} \tan^2 \psi + \frac{2 - \tan^2 \psi}{2 + \sqrt{2} \tan \psi \cos 3\vartheta} - \frac{1}{2\sqrt{2}} \tan \psi} \\ \tan \psi &= \sqrt{3 \text{tr} \hat{\mathbf{T}}^{*2}}; \quad \cos 3\vartheta = -\sqrt{6} \frac{\text{tr} \hat{\mathbf{T}}^{*3}}{[\text{tr} \hat{\mathbf{T}}^{*2}]^{\frac{3}{2}}} \end{aligned} \quad (3.22)$$

and the factor a represents the calibration of the model on the Matsuoka-Nakai-yield function and depends on critical friction angle φ_c .

$$a = \frac{\sqrt{3}(3 - \sin \varphi_c)}{2\sqrt{2} \sin \varphi_c} \quad (3.23)$$

The factors f_d, f_e and f_b are used to simulate the barotropy and Pycnotropy effects and they are given by:

$$f_d = \left(\frac{e - e_d}{e_c - e_d} \right)^\alpha \quad (3.24)$$

$$f_e = \left(\frac{e_c}{e} \right)^\beta \quad (3.25)$$

$$f_b = \frac{h_s}{n} \left(\frac{e_{i0}}{e_{c0}} \right)^\beta \frac{1+e_i}{e_i} \left(\frac{-tr \mathbf{T}}{h_s} \right)^{l-n} \times \left[3 + \alpha^2 - \alpha \sqrt{3} \left(\frac{e_{i0}-e_{d0}}{e_{c0}-e_{d0}} \right)^\alpha \right]^{-l} \quad (3.26)$$

where e_i and e_d are stress dependant limiting void ratios and e_c is again a stress dependant critical void ratio. There exist a relationships between the different form of the void ratio in the form of:

$$\frac{e_i}{e_{i0}} = \frac{e_c}{e_{c0}} = \frac{e_d}{e_{d0}} = \exp \left[- \left(\frac{-tr \mathbf{T}}{h_s} \right)^n \right] \quad (3.27)$$

As it can be witness from the above equations, the hypoplastic model requires 8 material parameters. These are the critical friction angle φ_c , the granular hardening h_s , the limiting void ratios e_{i0} , e_{c0} and e_{d0} , as well as the exponents n , α and β . According to Herle 1997, these constants can be determined from simple index and element tests in laboratory.

3.1.8 Cap models

Historically, Drucker et al. 1957 were the first to introduce the concept of work hardening plasticity cap models. They introduced a spherical end cap to the Drucker-Prager model in order to control the plastic volumetric change of soil. The Cambridge group also developed a family of models for normally consolidated or lightly overconsolidated clay known as Cam-Clay models based on critical state concept (Schofield and Wroth 1968; Rosco and Burland 1968). Since then several attempts have been made to use various version of these models in the numerical solution of boundary value problems and prediction of soil behaviour in the field. A more general cap models for the application of a wide range of soils are in use nowadays. The loading surface for cap model consists of two parts: a failure surface for perfectly plastic material response F (Drucker-Prager or Mohr-Coulomb or other curved surface failure criteria) as discussed in section 3.1.4 above and an elliptical work-hardening cap F_c of the form (Chen and Mizuno 1990):

$$F_c = (I_1 - l)^2 + R^2 \cdot J_2 - (x - l)^2 \quad (3.28)$$

where l is the position of the center of the ellipse and R is the aspect ratio of the cap (Fig. 3.2). The movement of the cap is controlled by the increase or decrease of the plastic volumetric strain through the hardening parameter x , which is given by:

$$x = x(\underline{\varepsilon}_v^p) \quad (3.29)$$

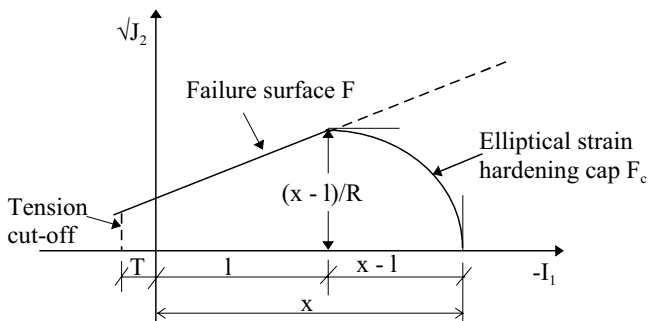


Fig. 3.2. Cap model with elliptic hardening surface

3.1.9 The constitutive soil models used in PLAXIS FE-program

The finite element code PLAXIS professional version is used for back analysis the practical projects and for performing parametric studies in this book. The PLAXIS program contains constitutive soil models from simple linear elasticity to advanced elasto-plastic cap soil models. The details of each soil model can be found in PLAXIS users manual (Vermeer and Brinkgreve 1995; Brinkgreve and Vermeer 1998; Brinkgreve 2002). A summary of the basic features, the failure criteria, the required soil parameters, range of application, etc. of the three main soil models available in PLAXIS are given in Table 3.2. In the earlier version of PLAXIS, up to version 6.0, the hard soil model (HSM) and the soft soil model (SSM) are primarily used for hard soils such as gravels, sands and heavily overconsolidated cohesive soils, and for normally consolidated and lightly overconsolidated clays respectively. This is mainly because the HSM was developed on the assumption that plastic straining is dominated by shearing and associated volumetric strains are relatively small and cause dilation rather than compaction which is a property of non-cohesive and heavily consolidated cohesive soils. On the other hand the SSM was developed based on the assumption of compression hardening, which is mainly a property of soft clays. In contrast to this basic formulation of the models, (Freiseder (1998)) believed that the HSM give more realistic results on deformation of the wall and settlement of ground behind the wall in an excavation in normally consolidated clay than the other models.

In the PLAXIS version 7 and above, the SSM was superseded by the HSM, and the HSM comes out as advanced double hardening model applied for all types of soils, i.e., it is now based on shear as well as compression hardening, a property of both hard soils and soft soils. In these versions, the name hard soil model is replaced by the hardening soil model. The HSM assumes a uniform expansion of the yield surface in all direction, i.e., it is based on isotropic hardening. The soft soil model is also modified to include time dependent behaviour of soft soils and it is called the soft soil creep model (SSCM). The Mohr-Coulomb model (MCM), which is an elastic-perfect plastic model, can be applied for all types of soils.

Table 3.2. Summary of the main constitutive soil models in PLAXIS FE-program.

	Hardening Soil Model (HSM)	Soft Soil Creep Model (SSCM)	Mohr-Coulomb Model (MCM)
Type of model	• elasto-plastic strain hardening cap model	• elasto-plastic work hardening cap model	• elastic perfect plastic
Basic features	<ul style="list-style-type: none"> stress dependent stiffness according to power law $E = E^{ref} \left(\frac{c' \cdot \cos \varphi - \sigma_3 \cdot \sin \varphi}{c' \cdot \cos \varphi + p^{ref} \cdot \sin \varphi} \right)^m$ plastic straining due to primary deviatoric loading Plastic straining due to primary compression Elastic unloading/ reloading Hyperbolic stress-strain relation and soil dilatancy 	<ul style="list-style-type: none"> stress-dependent stiffness (logarithmic compression behaviour) distinction between primary loading and unloading/reloading Secondary (time-dependant) compression memory of pre-consolidation stress 	<ul style="list-style-type: none"> offers a special option for the input of a stiffness increasing with soil dilatancy
Failure criterion	• Mohr-coulomb	• Mohr-coulomb	• Mohr-Coulomb
Cap yield surface	$F_c = \frac{\tilde{q}^2}{\alpha^2} + p^2 - p_p^2$; $\tilde{q} = \sigma_i + (\delta - I) \cdot \sigma_2 - \delta \cdot \sigma_3$; $\delta = \frac{3 + \sin \varphi}{3 - \sin \varphi}$	$F_g = \frac{q^2}{M^4 \cdot (p + c \cdot \cot \varphi)} + p - p_p$	<ul style="list-style-type: none"> • none
Flow rule	<ul style="list-style-type: none"> non-associated in shear hardening associated in compression hardening (cap) 	• associated	• non-associated
State of stress	• Isotropic	• Isotropic	• Isotropic
Hardening	• Isotropic; shear and compaction	• Isotropic; compression	<ul style="list-style-type: none"> • None
Soil parameters	• $c', \varphi', \psi, E_{sg}^{ref}, E_{ur}^{ref}, E_{oed}^{ref}, m, K_0^{nc}, \nu_{ur}$	• $c', \varphi', \psi, \lambda^*, \kappa^*, \mu^*, \nu_{in}, M, K_b$	<ul style="list-style-type: none"> • $c', \varphi', \psi, E, \nu$
Range of application	• All types of soils	• Normally consolidated or lightly overconsolidated clay or clavay soils	<ul style="list-style-type: none"> • All types of soil

3.1.10 Requirement for constitutive soil models - example excavation

Ideally a soil model would be able to predict the stress-strain and time dependent behaviour under all types of loading. However, such models are mathematically complex and difficult to use. Therefore, a solution to practical problems requires that some simplifying idealization are made regarding the behaviour of soils. The elasto-plastic cap models have the advantage that they address the important behaviour of soils, such as non-linearity, stress-path dependency, plasticity, dilatancy and compaction, etc. However, there is still a need at least to partially evaluate the response of each constitutive model to some typical stress-strain paths associated with laboratory or field conditions. For example, Gudehus 1985 suggests that any constitutive law for an excavation analysis in saturated overconsolidated clay should respond to the stress and strain path shown in Fig. 3.3 with an adequate accuracy. Fig. 3.3 represents the behaviour of undrained earth pressure problem. It consists of soil sedimentation (path 0-1), erosion (path 1-2), and active or passive loading/unloading/reloading (2-3-4-5). It shows only one case where the wall rotates about its foot. Other arts of wall rotation may lead to different stress and strain paths. The stress and strain paths at different positions with in the excavation are also different.

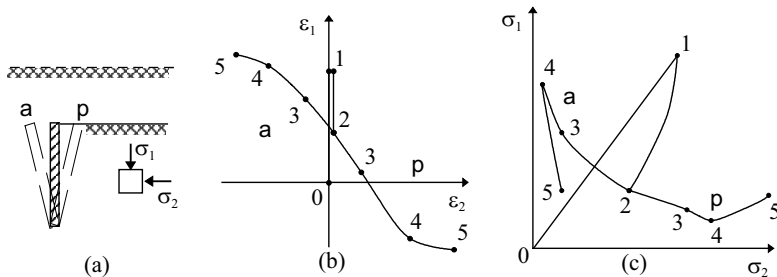


Fig. 3.3. Strain (b) and stress (c) paths in active and passive earth pressure in saturated clay (a) (after Gudehus 1985)

Chen and McCarron 1986; Chen and Mizuno 1990 proved that the cap models are capable of responding to the stress-strain paths and the history dependent behaviour. Freiseder 1998 had compared the three soil models (HSM, SSM and MCM, see Table 3.2) available in PLAXIS using an idealized excavation in normally consolidated lacustrine clay which is supported by diaphragm wall. He concluded that the HSM provides a realistic result as far as the horizontal deflection of the wall and settlement of the surface behind the wall are concerned, though it was first developed to model the behaviour of non-cohesive soils and overconsolidated clays. He further commented that the response of the HSM to stress path at some points with in the excavation is more realistic than the other models. It should be noted that the HSM in this version was without a cap. Therefore, there

should be no doubt that the introduction of the cap in to the HSM in PLAXIS version 7 and 8 will increase its performance and its range of application.

The response of the latest version of the HSM to different stress-strain paths has been evaluated in section 3.3.

3.1.10 Constitutive relations for interface elements

Clough and Duncan 1971 studied the interaction between the wall and the backfill material with the help of shear box test and showed that the stress-displacement behaviour of the interface is similar to the stress-strain behaviour of soils. In order to implement the interface behaviour in the finite element analysis of retaining walls, Clough and Duncan 1971 developed a non-linear, stress dependent stiffness, hyperbolic stress-strain constitutive relation to represent interface behaviour similar to those developed by Duncan and Chang 1970 to model the stress-strain behaviour of soils.

Like the behaviour of soils, interface behaviour may also be represented by complex advanced models. However, Gens et al. 1989 underlined the use of less complex models. They used an elastic-perfectly plastic model with out dilatancy effect in their finite element study of the soil-reinforcement interaction. In PLAXIS the MCM is used to represent the interface behaviour, whatever model is applied to represent the soil behaviour.

3.2 Derivation of soil parameters for numerical analysis

3.2.1 General

In the planning, design and construction of excavations in normally consolidated soft clays in urban areas, careful consideration of the magnitude and distribution of the ground movement is required. The prediction of the complete ground movement pattern involves three processes: the choice of an appropriate analytical or numerical model, the choice of the appropriate analysis method, and the selection of appropriate soil parameters. Different constitutive soil models require different soil parameters, but they also share the same parameters. In this section, the determination of deformation and strength parameters is presented based on the author's experience on lacustrine soil deposit.

3.2.2 Determination of compression parameters

One-dimensional consolidation

The stress-strain relationships of normally consolidated soft clays in one-dimensional consolidation can be investigated using the conventional oedometer apparatus with daily increment of vertical load to a submerged specimen contained in a rigid ring. Drainage may be permitted through porous stone at the top

and bottom. The ratio of the load increment to existing load is usually taken as 1, i.e. the load is doubled each day assuming that the time required for primary consolidation is 24 h. A classic behaviour of normally consolidated clay in one-dimensional consolidation is shown in Fig. 3.4 in which the results have been plotted as axial strain ε_l or void ratio e against the effective consolidation stress σ'_{vc} . The axial strain and the void ratio are plotted on the vertical axis on an arithmetic scale and the stress on a logarithmic scale.

The compression and swelling indexes. The plots of void ratio versus $\log(\sigma'_{vc})$ can be idealised by straight line and give rise to the conventional definition of the compression index C_c and the swelling index C_s . The slope of the normal consolidation line and the swelling lines when the void ratio is plotted against pressure in natural logarithmic scale is given by the symbol λ and κ respectively. These parameters are important for the cam-clay model families. Similarly, when the strain is plotted against pressure in natural logarithmic scale, they are denoted by λ^* and κ^* respectively. The relationship between conventional C_c , λ and λ^* is given by:

$$\lambda^* = \frac{\lambda}{1+e_0} = \frac{C_c}{2.3 \cdot (1+e_0)} \quad (3.30)$$

The relationship between C_s , κ and κ^* is also given by Brinkgreve 2002 as:

$$\kappa^* = \frac{\kappa}{1+e_0} = \frac{2 \cdot C_s}{2.3 \cdot (1+e_0)} \quad (3.31)$$

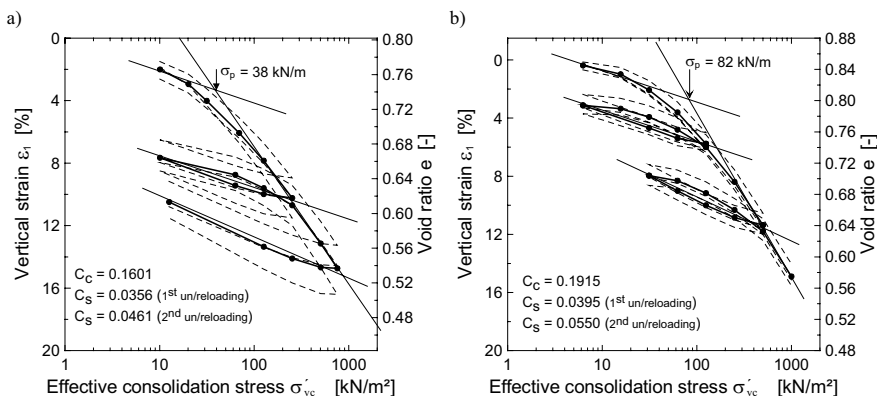


Fig. 3.4. Typical one-dimensional test results for lacustrine soil in southern Germany

Eq. 3.21 is derived based on the assumption that the vertical and horizontal stresses during one dimensional unloading are equal. According to Brinkgreve 2002 one can use the average void ratio that occurred during the test or just the

initial void ratio e_0 for e . If the un/re-loading can be approximated by a straight line, then $C_s \approx 2.3 \cdot \kappa$ (Wroth and Housby 1985; Atkinson and Bransby 1978).

Compression parameters from one-dimensional compression tests for lacustrine soils in southern Germany are given Table 3.3 and Table 3.4 for primary loading and un/reloading condition respectively. From Table 3.4, it can be seen that the swelling index is not a unique value for a particular soil, rather it depends on the maximum previous stress σ'_{vm} at which the sample was subjected before it starts to swell. The void ratio in Table 3.4 is the value just before the unloading starts. The values of κ in Table 3.4 are read directly from the diagram assuming that the swelling lines can be fairly approximated by straight lines. These values of κ match very well with those values estimated from the relationship $C_s \approx 2.3 \cdot \kappa$. Obviously, the values of κ calculated from Eq. 3.31 are twice higher than that approximated or read directly from the plot.

Table 3.3. One-dimensional compression parameters under primary loading for a lacustrine soil in southern Germany

Test description	w [%]	e_0 [-]	C_c [-]	λ [-]	λ^* [-]
Damcon2	31.8	0.803	0.1601	0.0696	0.0386
Damcon3	33.6	0.881	0.2001	0.0870	0.0462
Maxcon1	30.9	0.815	0.2210	0.0961	0.0529
Maxcon3	31.1	0.849	0.1915	0.0833	0.0450
Fhkcon2	70.9	1.881	0.4624	0.2010	0.0697

Table 3.4. One-dimensional compression parameters under un/reloading for a lacustrine soil in southern Germany

Test description	w [%]	e [-]	σ'_{vm} [kN/m ²]	C_s [-]	κ (read) [-]	$\kappa = C_s/2.3$ [-]	$\kappa^* = \kappa/(1+e)$ [-]
Damcon2	31.8	0.618	252	0.0356	0.0150	0.0154	0.0093
		0.537	756	0.0461	0.0200	0.0200	0.0130
Damcon3	33.6	0.649	202	0.0406	0.0171	0.0177	0.0104
		0.526	806	0.0568	0.0244	0.0247	0.0160
Maxcon1	30.9	0.657	278	0.0406	0.0187	0.0177	0.0113
Maxcon3	31.1	0.743	125	0.0395	0.0169	0.0172	0.0097
		0.639	500	0.0550	0.0233	0.0239	0.0142
Fhkcon2	70.9	1.660	103	0.0225	0.0109	0.0098	0.0041
		1.374	403	0.0361	0.0143	0.0157	0.0060

The constrained modulus. The stress - strain relationships in compression is generally non - linear. As the stress increases, the strain increases but at a decreasing rate. The slope of the load-deformation curve at any point is called constrained modulus E_{oed} and by definition, it is

$$E_{oed} = \Delta\sigma'_{vc} / \Delta\varepsilon \quad (3.32)$$

However, since the field virgin compression curve is usually approximated by straight lines with a slope of C_c in a logarithmic plot, the constrained modulus can also be approximated from (Scherzinger 1991; Gudehus 1981),

$$E_{oed} = \frac{1 + e_0}{C_c} \cdot \sigma^* \quad (3.33)$$

where $\sigma^* = (\sigma' - \sigma'_0) / \ln(\sigma' / \sigma'_0)$ (Fig. 3.5) is the average pressure.

Similarly the un/re-loading soil stiffness $E_{ur,oed}$ may be approximated from,

$$E_{ur,oed} \approx \frac{1 + e_{vm}}{C_s} \cdot \sigma^* \quad (3.34)$$

where $\sigma^* = (\sigma' - \sigma'_{vm}) / \ln(\sigma' / \sigma'_{vm})$ (Fig. 3.5). It should be noted that the $E_{ur,oed}$ is not a unique value for a given soil, even at the same consolidation pressure. It is dependent on the maximum pressure (σ'_{vm}) that the soil was subjected before it swells.

For the same situation, the constrained modulus at a reference pressure of p^{ref} may be estimated from (Brinkgreve 2002),

$$E_{oed}^{ref} = \frac{P^{ref}}{\lambda^*} \quad (3.35)$$

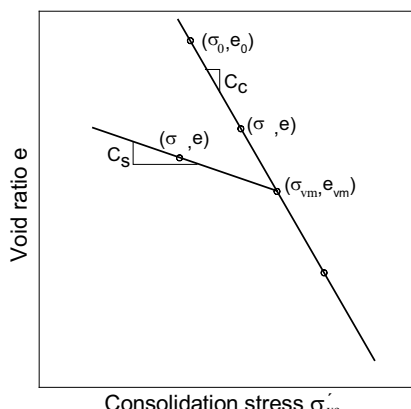


Fig. 3.5. Idealized plot of one-dimensional compression

and

$$E_{ur,oed}^{ref} = \frac{3 \cdot p^{ref} (1 - 2 \cdot v_{ur})}{\kappa^*} \quad (3.36)$$

assuming a plastic soil with a stress exponent $m = 1$ in Ohde 1939 expression for the stress dependency of the constrained modulus (Eq. 2.76). A modification of the Ohde equation is available in PLAXIS manual (Brinkgreve 2002), which includes a term to account the stiffness of the soils at the ground surface. The modified power law is given by,

$$E_{oed} = E_{oed}^{ref} \cdot \left(\frac{c' \cdot \cot \varphi' - \sigma'_{vc} \cdot \sin \varphi'}{c' \cdot \cot \varphi' + p^{ref} \cdot \sin \varphi'} \right)^m \quad (3.37)$$

where $E_{oed}^{ref} = k \cdot p^{ref}$ and k is the dimensionless modulus number (Eq. 2.76). This modified power law will also apply for the un/reloading condition, i.e., the un/reloading constrained modulus is also stress dependant.

A typical plot of the variation of the constrained modulus with the consolidation pressure is given in Fig. 3.6 From this figure and Table 3.5, it would appear that the stress exponent m for the investigated soil is not exactly 1. It varies rather from 0.70 to 0.85 with a mean value of 0.81 for the loading condition. For the un/reloading condition, m varies between 0.58 and 1.0. The un/reloading modulus is not unique, it depends on the maximum previous pressure at which the soil was subjected before it starts to swell.

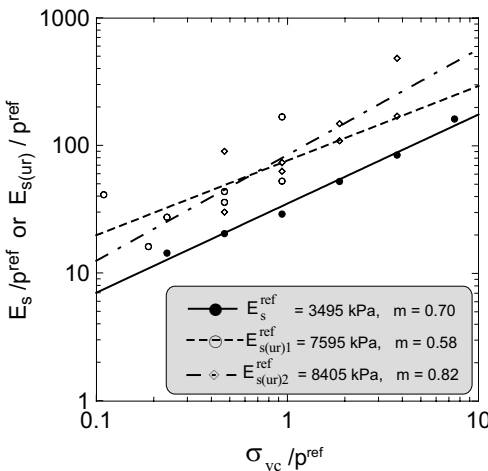


Fig. 3.6. The variation of the constrained modulus with consolidation pressure in one-dimensional compression for lacustrine soil in southern Germany

Table 3.5. Reference constrained modulus at a reference pressure $p^{ref} = 100 \text{ kPa}$

Test	E_{oed}^{ref} [kPa]	m [-]	1 st un/reload		2 nd un/reload		E_{oed}^{ref} (Eq. 3.35)	$E_{ur,oed}^{ref}$ (Eq. 3.36)*
			$E_{ur,oed}^{ref}$ [kPa]	m [-]	$E_{ur,oed}^{ref}$ [kPa]	m [-]		
Damcon2	3263	0.85	8411	0.73	6700	1.42	2591	19355
Damcon3	2633	0.82	10092	0.76	8541	1.20	2165	17308
Maxcon1	2512	0.84	14146	0.69			1890	15929
Maxcon3	3495	0.70	7595	0.58	8405	0.82	2222	18556
Fhkcon2	1763	0.78	11729	0.58	22353	0.82	1435	43902

* für $\nu_{ur} = 0.2$

The reference constrained modulus as estimated from Eqs 3.35 and 3.36 (assuming $m = 1$ and $\nu_{ur} = 0.2$) are also given in Table 3.5. It appears that the reference stiffness of the soil during the primary loading is underestimated by 19 to 28%, if one assumes $m = 1$ and applies Eq. 3.35. On the other hand, the un/reloading reference stiffness from Eq. 3.36 are higher than that derived from test result. This is mainly due to the selection of the value of κ^* . It is already mentioned above that the modified swelling index κ^* derived from Eq. 3.31 is twice higher than that estimated from the assumption $C_s \approx 2.3 \cdot \kappa$ or directly read from the plot assuming a linear relationship. It seems that there is an external factor of 2 in Eq. 3.36. Hence, if Eq. 3.36 is going to be used to estimate the reference un/reloading stiffness, κ should be calculated from Eq. 3.31.

The pre-consolidation pressure. Another very important characteristics of clays is the pre-consolidation pressure σ'_p . It is the vertical effective stress beyond which large strains occur and controls the overall behaviour of clays, particularly the sensitive clays. Previously, it was believed that the pre-consolidation pressure estimated with Casagrande method was primarily due to previous loading, usually of geologic nature. However, it has become evident in recent years that the profile of the pre-consolidation stress observed in some deposits is greater than the maximum past pressure that could have existed during its geologic history. This discrepancy was attributed to a number of factors, including desiccation, long-term secondary compression, thixotropy, weathering and cementation (Fang 1991; Jamiolkowski et al. 1985; Leroueil et al. 1983; Scherzinger 1991). Since the exact origin of the pre-consolidation pressure is difficult to establish, the term has been extended to define the break of the $e - \log \sigma'_p$ curve (Leroueil et al. 1983; Scherzinger 1991). From practical point of view engineers are interested in this threshold point beyond which important plastic deformation take place, particularly in sensitive clays where the normally consolidated branch of the compression curve is very steep. The pre-consolidation pressure serves as basis for normalising the strength and stiffness characteristics of cohesive deposits. For young normally consolidated soft clays, the effective pre-consolidation pressure is equal to the effective overburden pressure, where the soil deposit is not subjected to previous external load such as building loads.

Several methods have been proposed in literature for determining σ'_p . The Casagrande method is one of the most popular method so far. Another common method is to simply draw tangents to the virgin compression curve and the re-compression curve; the intersection is called the pre-consolidation stress. Scherzinger 1991 compared the two methods for normally consolidated clays in southern Germany using conventional oedometer test result and found out an average ratio of 1.21 between the pre-consolidation pressures determined by Casagrande method and by the secant method. Leroueil et al. 1983 showed that the in-situ pre-consolidation pressure $\sigma'_{p(in-situ)} = \alpha \cdot \sigma'_{p(laboratory)}$, where $\alpha = 1.1$ for normally consolidated clays ($OCR < 1.2$), $\alpha = 1.0$ for slightly overconsolidated clays ($1.2 < OCR < 2.5$), and $\alpha = 0.9$ for overconsolidated clays ($2.5 < OCR < 4.5$). A rough estimation of the pre-consolidation pressure found out in this study for the three locations are given in Table 3.6. The values were estimated by the tangent method and corrected to the Casagrande method and in-situ condition.

Table 3.6. preconsolidation pressure

Test description	σ'_{v0} [kN/m ²]	$\sigma'_{p(tan)}$ [kN/m ²]	$\sigma'_{p(corrected)}$ [kN/m ²]	OCR
Damcon2	34.4	38.0	46.0	1.34
Damcon3	22.4	25.0	30.3	1.40
Maxcon1	39.0	91.0	99.1	2.54
Maxcon3	39.0	82.0	98.4	2.52
Fhkcon2	50.7	36.0	47.9	0.95

Isotropic and anisotropic (K_0) compression

A soil specimen can also be tested under isotropic or anisotropic compression condition in a triaxial cell, where an all-round cell pressure ($\sigma'_1 = \sigma'_3$) in the case of isotropic and a separate application of the horizontal and vertical pressure ($\sigma'_3 = k_0 \cdot \sigma'_1$) in case of anisotropic can be applied to the specimen. Unlike the one-dimensional compression test, the specimen is allowed to deform in all directions in these type of compression test. The drainage can be permitted at both ends and radial through vertical filter paper strips on the side of the sample. The stresses are applied in equal increments, each having a duration of 24 h. Volume changes can be measured either by calibrated burette or by means of volume change transducer. The result of an isotropic consolidation is usually presented as specific volume v ($v = 1 + e$) against the effective mean stress p' in natural logarithmic scale. The slope of the normal compression line is denoted by λ and the slope of the swelling line by κ . Similar to one-dimensional compression, if instead of the specific volume, the volumetric strain ε_v is plotted against $\ln(p')$, the slopes of the normal compression and the swelling lines become λ^* and κ^* respectively. A typical plot of the isotropic and anisotropic compression test is shown in Fig.

3.7 and the comparison of the results with one-dimensional compression is given in Table 3.7.

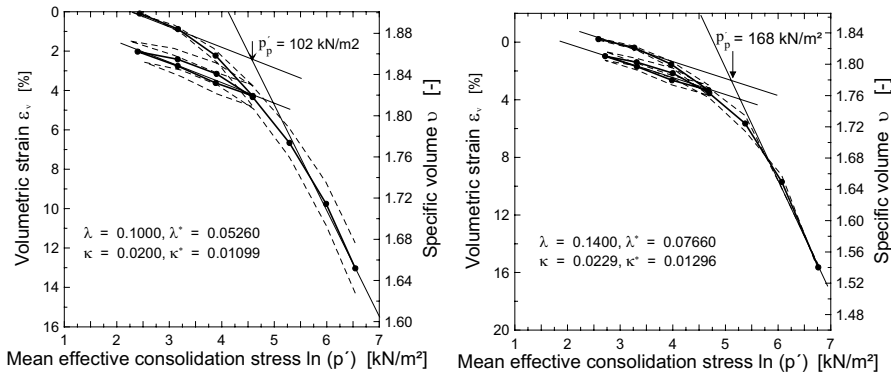


Fig. 3.7. a) Isotropic compression ($K_0 = 1$) and b) Anisotropic compression ($K_0 \neq 1$)

Table 3.7. Comparative values of the compression parameters

Test type	w [%]	e_0 [-]	λ [-]	λ^* [-]	e [-]	κ [-]	κ^* [-]
One-dimensional	31.1	0.743	0.1915	0.0833	0.7430	0.0169	0.00970
Isotropic($K_0 = 1.0$)		0.901	0.1000	0.0526	0.8196	0.0200	0.01099
Anisotropic ($K_0 = 0.8$)		0.828	0.1400	0.0766	0.7665	0.0229	0.01296

3.2.3 Determination of strength parameters

General

The determination of the strength and deformation parameters for numerical analysis of foundations in general and excavations in particular are demonstrated by means of a series of standard triaxial test; drained/undrained, isotropic/anisotropic, and controlled stress path tests conducted on lacustrine soil samples from three locations in Constance city, southern Germany.

The rate of strain is one of the important factors that influence the strength and deformation properties of soils. The maximum rate of strain to be applied in a strain control triaxial tests can be approximated from,

$$\dot{\varepsilon} = \frac{\varepsilon_f \cdot h}{100 \cdot t_f} \quad (3.38)$$

where $\dot{\varepsilon}$ is the rate of strain of the load application in mm/min, ε_f is the strain at failure in percentage (%), h is the height of the specimen in mm, and t_f is the time

required to failure in min. For undrained test with side drains and height to diameter ratio of 1:1, the time to failure given by Head 1986 is $t_f = 0.201 t_{100}$ and $t_f = 1.418 \cdot t_{100}$ for drained test with similar conditions. The graph of volume change against square - root time is used to derive the time intercept t_{100} (Fig. 3.8).

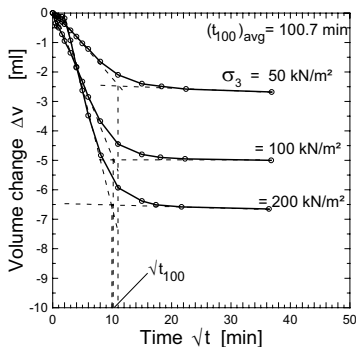


Fig. 3.8. Volume change-time graph

There are different failure criteria for determining the shear strength of a specimen. These are peak deviatoric stress, maximum principal stress ratio, limiting strain, critical state, and residual state. Most often, the stress-strain diagram for normally consolidated cohesive soils does not show a distinct peak value, rather the stress increases gradually as deformation of the soil sample increases. Hence, the maximum principal stress ratio and the maximum deviatoric stress at predefined strain can be taken as failure criteria for undrained tests. On the other hand, since the effective stress changes in drained tests are equal to the total stress changes, the principal stress ratio curve has the same shape as the deviatoric stress plot. Hence, the limiting strain failure criteria may be used for drained tests. According to Head 1986, the strain at failure for normally consolidated cohesive soils may be assumed between 15 and 20% for both drained and undrained tests. DIN 18137 1990 recommends 20% strain at failure where there is no distinct peak point in the deviatoric stress - strain plot.

There is a general argument that the triaxial tests are not reliable type of tests for determining the shear parameters of a normally consolidated soft soils, because such soils are sensitive to sample disturbance and the restraining effect of the rubber membrane enclosing a triaxial specimen, which contributes to resistance offered against compression. Head 1986 suggested a membrane correction for samples undergoing a barrelling type of distortion as shown in Fig. 3.9. The barrelling mode of distortion is typical in specimens of normally consolidated soft soils. The correction is developed based on the axial strain in the sample, the compression modulus of the membrane and the initial diameter of the specimen. The solid line in Fig. 3.9 is the original curve from Head 1986 and it is based on 38 mm diameter samples fitted with a membrane 0.20 mm thick. For specimens of any other diameter (D in mm) with any other membrane thickness (t in mm), the correction is multiplied by $[(38/D) \cdot (t/0.2)]$. The dashed line in Fig. 3.9 is the corrected membrane correction for specimens of 50 mm diameter.

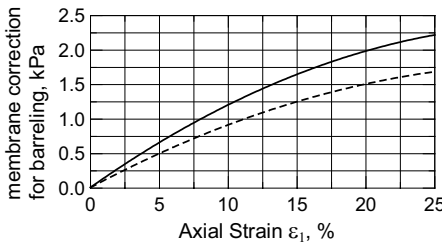


Fig. 3.9. Membrane correction curves for barreling type of distortion for 38 mm diameter samples (solid line) and for 50 mm diameter samples (dashed line), and membrane thickness $t = 0.2$ mm (after Head 1986)

Isotropically consolidated standard triaxial test

The standard type of triaxial test for the determination of the effective shear parameters of a soil are the isotropically consolidated drained (CID) and undrained (CIU) tests. Typical stress-strain relationships, volume change characteristics and the stress paths followed in a CID tests are shown in Fig.3.10. The stress-strain curves are usually non-linear from the beginning and they show no extreme value, rather they deform continuously to a large strain, but they appear to level off and eventually approach a constant value at axial strain greater than 20%. The stresses at 20% strain may be defined as the failure stresses. The un/reloading curves show approximately a linear behaviour. The volumetric strains primarily contraction in the case of soft soils (Figure 3.10b) vary almost linearly up to an axial strain of approximately 10% and they appear to increase further linearly with the axial strain.

Table 3.8. Strength parameters from CID tests

Test	Cell pressure [kN/m ²]	w [%]	γ/γ_d [kN/m ³]	e_0 [-]	c' [kN/m ²]	φ' [°]	v [-]
site1							
damcid05	50, 100, 200	30.7	19.5/15.0	0.79	17.7	24.4	0.420
damcid07	50,100,200	28.3	19.7/15.4	0.74	10.7	24.3	0.460
damcid15	50,100,230	34.2	18.7/14.1	0.90	16.5	25.8	0.374
site2							
maxcid01	50,100,200	31.0	19.5/14.9	0.82	20.3	24.8	0.470
maxcid05	50,100,200	34.9	19.1/14.1	0.93	17.7	24.4	0.374
maxcid15/16	50,100,200,300, 400,500	32.8	19.1/14.2	0.89	22.2	20.5	0.413
maxcid ♠	50,100,200	27.5	19.5/15.3	0.78	11.1	22.5	0.395
maxcid13 *	50,100,200	25.6	20.2/16.1	0.69	25.6	28.6	0.466
site3							
fhkcid34	50,100,200	75.1	15.3/8.71	2.16	17.4	25.9	0.154
fhkcid36	25,50,100,200	74.5	15.3/8.77	2.13	17.1	29.3	0.206
fhkcid389 *	50,100,200	74.0	15.2/8.76	2.14	17.3	31.4	0.294

* = horizontal samples, ♠ = remoulded sample

In Fig. 3.10c the lateral strains calculated from the measurement of the water drained out of the sample are plotted against axial strain. The ratio of the lateral to axial strains without distinguishing between the elastic and plastic part of the strains are also plotted against the axial strain in Fig. 3.10c. This is not, however, the Poisson's ratio, because the Poisson's ratio is purely an elastic constant, which is defined as the ratio of the lateral to the axial elastic strain. The deformations in a triaxial tests, however, contains both elastic and plastic strains. It seems that the ratio of the lateral and axial strains is not a unique value for one type of soil, rather it increases almost linearly with the axial strain. Fig. 3.10c shows that this ratio varies from an average value of 0.35 at low strain to about 0.45 at about 20% strain.

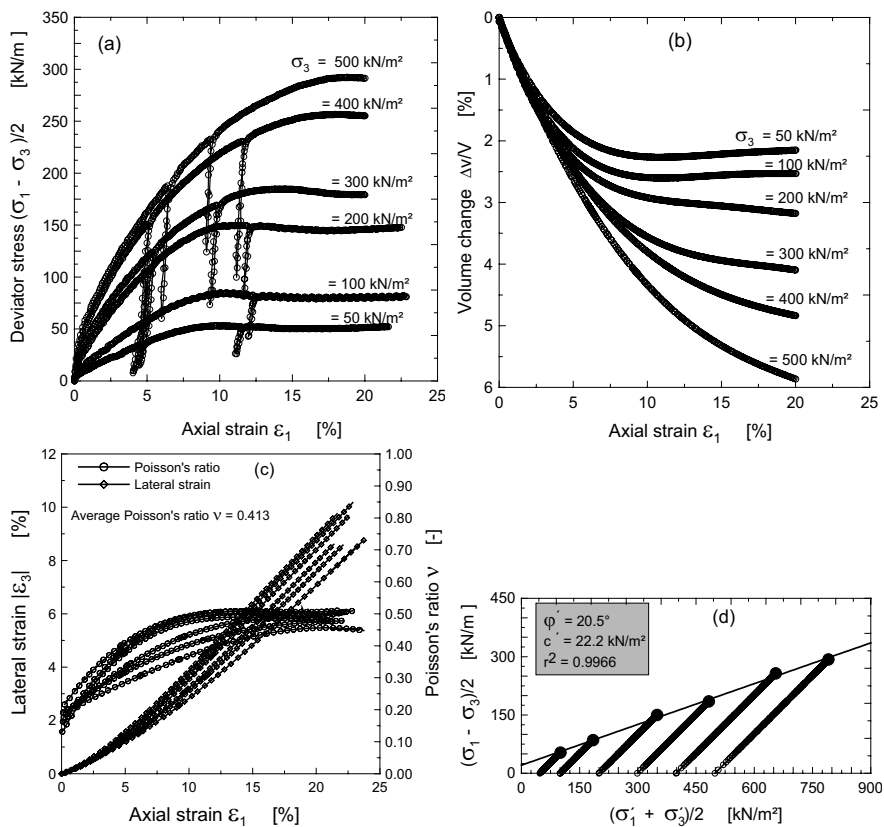


Fig. 3.10. a) Stress-strain relationship, b) volume change - strain relationship, c) lateral strain and Poisson's ratio vs axial strain plot, and d) plot of the stress path of CID tests on vertically oriented samples

The stress paths followed during drained test are shown in Fig. 3.10d. Whether it is a normal loading or unloading or reloading, the drained stress path in com-

pression test ($\sigma_3 = \text{constant}$) followed a straight line at 45° degree from the horizontal in anti-clockwise direction. The strength parameters from CID triaxial tests for three different sites in the southern Germany around the city Constance are summarised in Table 3.8.

Typical undrained stress-strain response, the excess pore water pressure during loading, unloading and reloading, and the stress path it followed during shearing are shown in Fig. 3.11. The stress - strain curves (Fig. 3.11a) are non-linear even at low stresses and show no peak values, rather they continue to deform at large strain, but they appear to level off and eventually approach a constant value at a larger axial strain similar to the drained tests. The effective principal stress ratio diagrams (Fig. 3.11c) also show no peak values except for local peaks that had been resulted from the response of the pore water pressure during un/reloading. This is why the strength parameters shown in Fig. 3.11d derived using both failure criterion $((\sigma'_1/\sigma'_3)_{\max} / (\sigma_1 - \sigma_3)_{\max \text{ or } 20\%})$ are almost the same. As shown in Fig. 3.11b, the excess pore water pressure drops down very quickly to certain minimum value during unloading and starts to build up slowly even before the reloading process is started. During reloading the excess pore water pressure build up quickly beyond the initial point and it starts to stabilise slowly to its normal position.

Table 3.9. Strength parameters from CIU tests

Test description	Cell pressure [kPa]	w [%]	γ/γ_d [kN/m ³]	e_0 [-]	τ_f^* [kN/m ²]	$c'*$ [kN/m ²]	$\phi'*$ [°]
site1							
damciu4/30	50, 100, 200, 300, 400, 500	30.3	19.5/15.0	0.80	350	14.1/14.1	26.5/26.5
damciu6	50, 100, 200	28.3	19.8/15.4	0.74	50	11.1/15.4	27.0/25.0
damciu10	50, 100, 200	26.5	19.4/15.4	0.75		6.10/5.80	30.6/30.6
damciu14	88, 112, 200	33.2	19.1/14.3	0.87	17.8	2.60/3.70	32.7/31.8
site2							
maxciu2	50, 100, 200	30.6	19.5/15.0	0.82	40	10.5/17.3	26.0/21.7
maxciu *	50, 100, 200, 300, 400	25.6	19.7/15.7	0.73		17.1/18.4	21.6/21
maxciu3 *	50, 100, 200	30.4	19.3/14.8	0.84	19	11.3/13.5	27.7/26.1
site3							
fhkciu35	50, 100, 200	75.8	15.7/9.02	2.09	13	3.40/3.40	39.5/39.5
Others							
Jaegerkaserne	100, 200, 300	20.4	20.6/17.1	0.58		9.1/-	25.5/-
Schwandorf	100, 200, 300	16.0	21.3/18.4	0.47		24.4/18.8	26.3/26.4
Fhk	100, 200, 300	72,8	15.8/9		12	3.0	27.3
Stromeyersdorf	100, 200, 300	24.0	20.3/16.4	0.65		16.3/-	21.1/-

* = According to the two failure criterion $(\sigma'_1/\sigma'_3)_{\max} / (\sigma_1 - \sigma_3)_{\max \text{ or } 20\%}$; * = Field shear vane strength (uncorrected); * = Horizontal sample; * = reconstituted samples

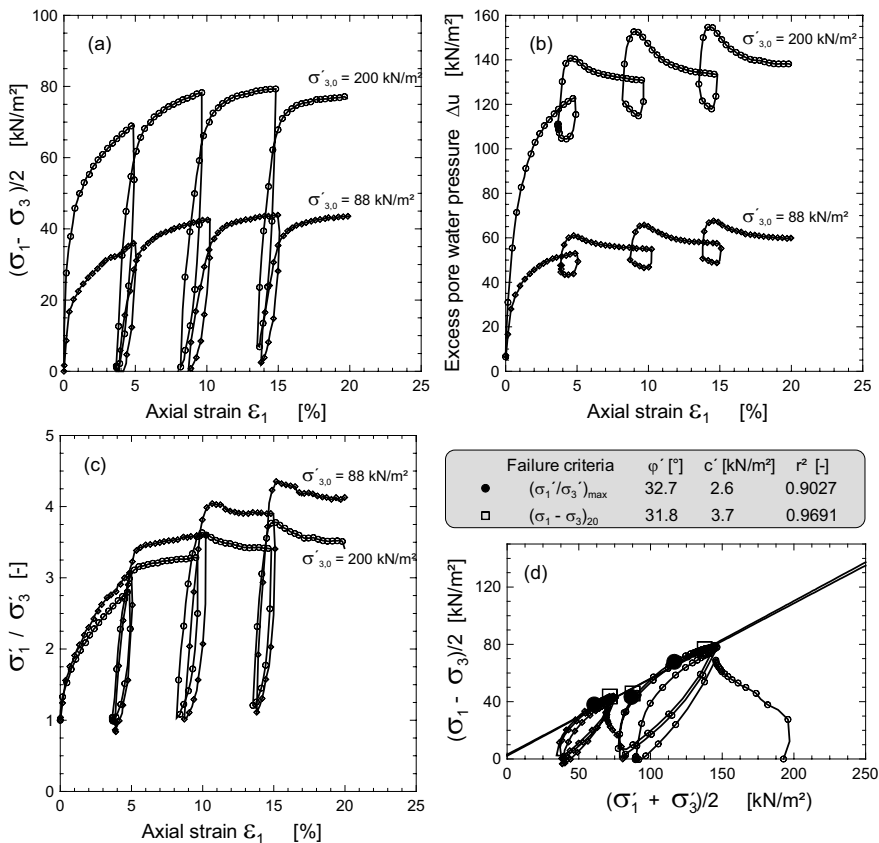


Fig. 3.11. a) Stress - strain relationship, b) excess pore water pressure, c) effective principal stress ratio, d) plot of the stress path of *CIU* test on vertically oriented samples

The effective stress paths during normal loading shown in Fig. 3.11d are typical for undisturbed normally consolidated clays and the hysteresis during un/reloading cycles are typical for overconsolidated clays. A summary of the strength parameters from the CIU triaxial tests from different sites around the city of Constance in the southern of Germany are given in Table 3.9

Anisotropically consolidated triaxial compression test

These type of tests can be performed in a triaxial cell with special arrangements for the application of additional vertical stress independent of the axial load and cell pressure during the K_0 consolidation. An example of a special arrangement for the additional vertical pressure by means of a pneumatic cylinder positioned at the top of the triaxial cell and below the motorised load cylinder is shown in Fig. 3.12. The specimens is first subjected to all round cell pressure and the vertical

stress is simultaneously increased through the pneumatic cylinder to maintain the K_0 condition. After the specimen is fully consolidated under the K_0 condition, it can be sheared drained or undrained depending on the drainage condition by applying an axial load by means of the motorised load cylinder.

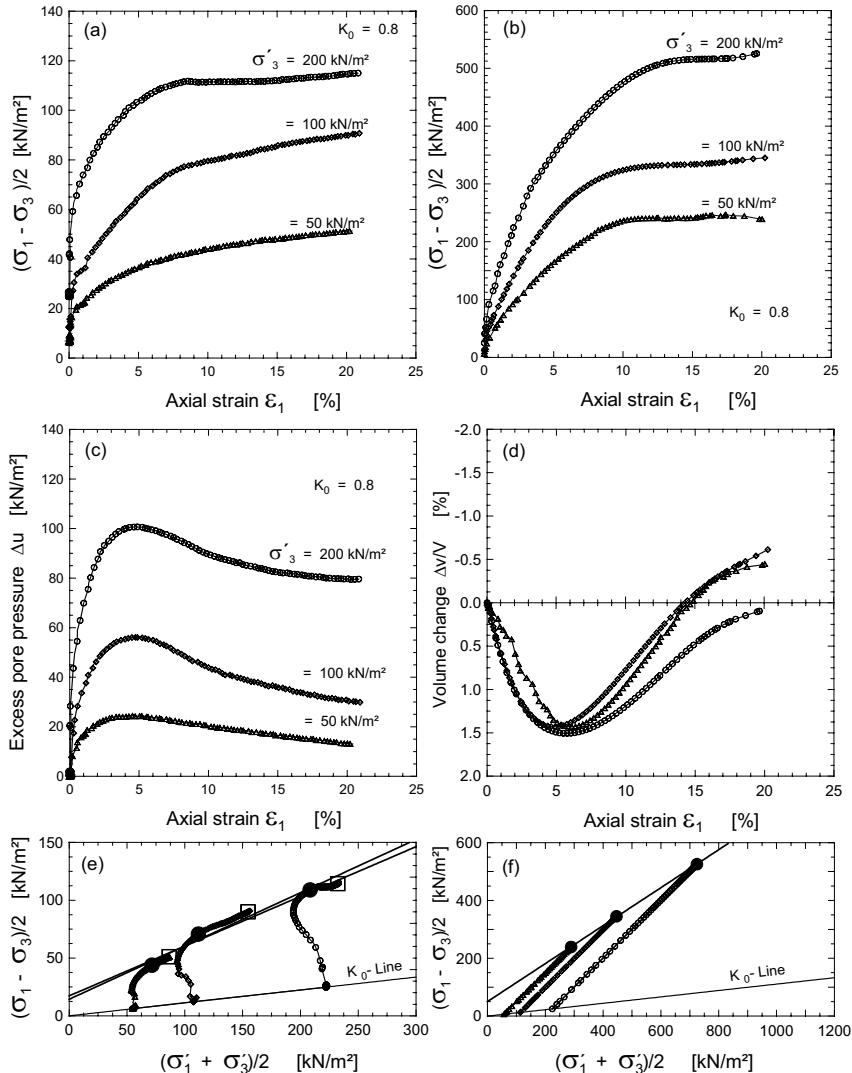


Fig. 3.12. Results of CAU (a, c and e) and CAD (b, d and f) triaxial tests on lacustrine soft soils in southern Germany (from Gebreselassie 2003)

The stress-strain relationship, excess pore water pressure and the stress path from the CAU tests are shown in Fig. 3.12a, c, and e. The stress-strain curves from

the CAU test (Fig. 3.12a) seems to have higher initial stiffness, and larger stresses at failure than the corresponding stress-strain curves from CIU tests (Fig. 3.11a) on similar samples. The excess pore water pressure in the CAU test (Fig. 3.12c) reaches its peak value at relatively lower axial strain (about 3 to 4%) than that in the CIU test (5 to 6.5%) (Figure 3.11). The rate of drop of the pore water pressure after it reaches the peak value is higher in CAU tests than in CIU tests. The strength parameters from CAU tests (Fig. 3.12e) are higher in cohesion and lower in friction than the corresponding CIU tests.

The stress-strain relationship, volumetric strain, and the stress paths in the CAD tests are shown in Fig. 3.12b, d & f. The course of the stress-strain curves (Fig. 3.12b) are similar to that from CID tests. However, the stress-strain curves show a higher initial stiffness than from CID tests, and the stresses at failure in the CAD tests are almost 2 to 3 times higher than the failure stresses in the CID tests. It can also be observed that the stress - strain curves appear to level off and approach a constant value at lower strain than in the CID tests. The volume change curves in Fig. 3.12d show a decrease in volume up to a strain of 5% and an increase in volume afterwards unlike that observed in CID tests. The stress path diagram (Fig. 3.12f) also shows exceptionally high value of the strength parameter.

Controlled stress path triaxial tests

It is generally believed that the strength and deformation behaviour of a soil at a particular point in the field depends on the stress path it follows. The possible stress paths assuming an initial anisotropic state of stress at point O are already shown in Fig. 2.17 (see also Fig. 4.29). Here the stress paths A, B and C are illustrated for isotropic and anisotropic initial stress state condition. The path A is the total stress path followed during standard triaxial compression test ($\Delta\sigma_3 = 0$, $\Delta\sigma_3 > 0$), and it had already been presented in the previous section.

The apparatus for controlled stress path test is the same as that of the anisotropically consolidated standard triaxial apparatus. The controlled stress path tests are effected by varying the stresses incrementally according to the postulated stress paths. Both the increment and decrement of the vertical and horizontal stresses has been controlled by computer program. It is possible to apply the pressures in up to 15 pressure increments. In each step, the stress increments or decrements are applied at a stress state of 0.4 - 0.5 kN/m². First the all round cell pressure was adjusted followed by adjustments of the vertical stress through the pneumatic cylinder every minute. The stress rate can be approximated from the time required to failure and the stress at failure from strain controlled CIU tests in order to compare the results with the strain controlled tests. All the stress paths are performed under undrained condition.

The postulated total stress path B at 1:1 slope is effected by decreasing the horizontal stress and maintaining the vertical stress constant. The horizontal stress is decreased by decreasing the cell pressure incrementally. The decrease of the cell pressure would decrease the vertical stress too. Therefore, to maintain the vertical stress constant, a vertical pressure increment which is equal to the cell pressure decrement is applied through the pneumatic cylinder. Similarly, the postulated to-

tal stress path C at a slope of infinity is effected by increasing the vertical stress and decreasing the horizontal stress. The decrease of the horizontal stress is effected by decreasing the cell pressure, while the increase of the vertical stress is effected by additional vertical pressure, which was twice higher than the cell pressure.

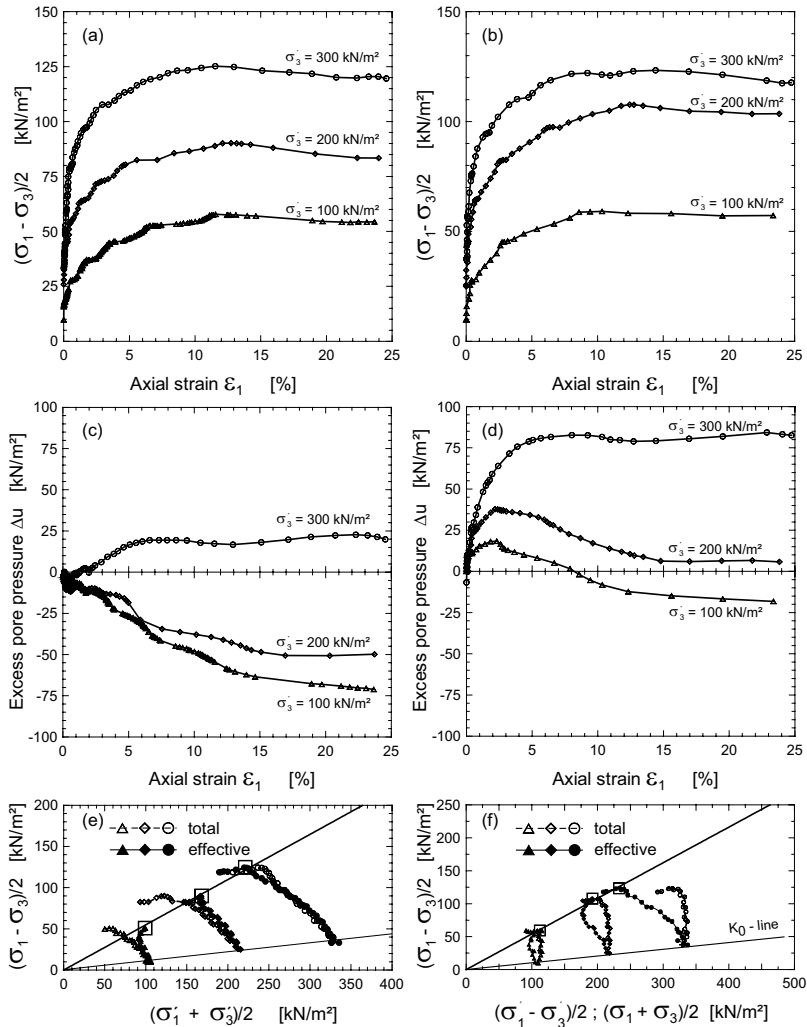


Fig. 3.13. Stress path dependent triaxial test result for the idealized stress path B (a, c, and e) and for the idealized stress path C (b, d, and f)

Fig. 3.13 shows the results of controlled stress CAU triaxial tests on undisturbed samples at 100, 200, and 300 kPa cell pressure for the postulated stress path B and C. The course of the stress-strain curves is similar, even so they are similar

to the other standard stress paths, except that they show a gradual small decrease in the deviator stress after they reach 10 - 15% axial strain. The excess pressure in stress path B (Fig. 3.13c) is negative for the cell pressure of 100 and 200 kPa, and it is positive for cell pressure of 300, but very small (< 25 kPa). The excess water pressure in stress path C (Fig. 3.13d), with cell pressure 100 and 200 kPa reached their maximum value at an axial strain of 2.5% before they dropped gradually to minimum value at large axial strain, while the pore pressure with 300 kPa cell pressure reaches its maximum value at 7.5 % axial strain and remains almost constant through out the test. Actually this curve would have to follow the same course as the other two curves.

The stress paths in controlled stress path - CAU triaxial tests for the postulated stress path B and C are shown in Fig. 3.13e and f respectively. The test paths in all the specimens are very similar to the postulated stress paths until they approximately reach $(\sigma_1 - \sigma_3)_{max}$, after which the paths begins to deviate from the postulated paths. Since the horizontal stresses and vertical stresses has been changed in a stepwise, the actual stress path reproduced in the laboratory have a stair case pattern. However, the general trend of the stress condition are faithfully reproduced. The effective stress path in both stress path B and C appear to be almost the same, independent from the direction of the total stress paths.

Comparison of the strength parameters

A comparison of the test results e.g. the two failure criteria in undrained test, drained/undrained tests, vertical/horizontal oriented specimens, isotropic/anisotropic consolidated tests, different controlled stress path tests, and standard/stress path tests, will follow in this section.

It would appear from the p-q diagrams (e.g. Fig. 3.11d) and Table 3.9 that the effective strength parameters obtained using the failure criterion $(\sigma'_1/\sigma'_3)_{max}$ and $(\sigma_1 - \sigma_3)_{at\ 20\%}$ do not differ much, even some times the strength envelopes overlaps one over the other. One may observe, however, that there is a general trend of increasing the effective friction and decreasing effective cohesion using $(\sigma'_1/\sigma'_3)_{max}$ failure criteria and vice versa by the $(\sigma_1 - \sigma_3)_{at\ 20\%}$ failure criteria. If one is interested in the effective angle of overall shear strength φ'_s , one may arrive at the same value from both failure criterion. According to DIN 18 137, 1990,

$$\tan \varphi'_s = \tan \varphi + \lambda_c \quad (3.39)$$

where λ_c is the normalized cohesion and it is given by $\lambda_c = c' / \max \sigma'_e$, and σ'_e is the equivalent pressure.

Theoretically, the effective cohesion in a drained analysis is assumed to be zero, however, the drained and undrained tests show a cohesion values ranging from 10 - 20 kN/m².

Regarding the drained and undrained isotropically consolidated tests, the average effective friction in undrained tests appear to be higher and the effective cohesion lower than the corresponding parameters in drained tests. It seems again that

there is a compensation effect between effective friction and effective cohesion. At site2, however, the average friction angles are more or less comparable, but the average effective cohesion values are higher in drained test than in undrained test. Fig. 3.14 shows the mean strength envelope from both drained and undrained tests at all sites. From Fig. 3.14, it would appear that the failure stress from drained and undrained tests lie on and closed to the mean strength envelope, particularly for $p' \leq 400 \text{ kN/m}^2$.

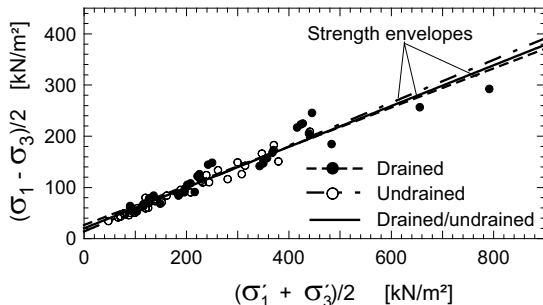


Fig. 3.14. Strength envelopes from drained and undrained triaxial test

The effective strength parameters from undrained tests on horizontally oriented specimens at site2 are comparable with those obtained from vertically oriented specimens. On the other hand, the drained tests on horizontally oriented specimens at site2 and site3 seem to produce relatively higher effective friction than those on vertically oriented specimens, but the effective cohesion is comparable. Taking into account the variation of the effective strength parameters that would exist even with in the same group of vertically oriented samples, the small difference between the effective parameters of vertically and horizontally oriented specimens may be neglected. This assumption lead us to a generalized conclusion that the effective strength parameters for practical purposes remain fairly the same irrespective of the sample orientation.

As far as the effective strength parameters of a soil element are concerned, they appear to be independent of the stress path, to which the soil was subjected during the triaxial test. Both the controlled stress path - CAU tests (postulated paths B and C, Fig. 3.13) on undisturbed samples and other controlled stress path - CIU tests (Postulated Path A, B and C) on reconstituted specimens show that the strength parameters are stress path independent. NG and Lo 1985 had also arrived at the same conclusion that the strength envelope is insensitive to test type and stress path, and the absolute magnitude of the effective stress parameter c' and φ' are the same for compression and extension. Comparing the effective strength parameters from controlled stress path - CAU tests with standard strain controlled CAU tests, however, it may be shown that the effective friction from the stress path test is higher, and the effective cohesion is lower than that obtained from strain controlled CAU tests. Similarly, the effective friction is higher in controlled stress path - CIU tests than that from strain controlled CIU tests. The effective cohesion, however, remains more or less the same in both tests.

3.2.4 Deformation parameters under deviatoric loading condition

General

The stress-strain relationship of specimens from triaxial tests are illustrated in section 3.2.3. From these strain stress curves, the basic deformation parameters, namely the modulus of elasticity E , the secant modulus at 50% failure stress E_{50} , the un/reloading modulus of elasticity E_{ur} , and the exponent m (Eq. 2.76) can be derived.

The relationship between axial strain ε and deviator stress $(\sigma_1 - \sigma_3)$ in a conventional triaxial compression test of a soil may mathematically be expressed by the hyperbolic function according to Kondner 1963 as follows,

$$(\sigma_1 - \sigma_3) = \frac{\varepsilon}{a + b \cdot \varepsilon} \quad (3.40)$$

where a and b are constants. If the stress-strain data (Fig. 3.15a) are plotted on the transformed axes (Fig. 3.15b), the value of the constants a and b may be determined readily, where Eq. 3.40 is rewritten in the following form,

$$\frac{\varepsilon}{(\sigma_1 - \sigma_3)} = a + b \cdot \varepsilon \quad (3.41)$$

It may be noted that a and b are the intercept and the slope of the resulting straight line (Fig. 3.15b). It can also be seen readily that $1/a = E_i$, i.e., the initial tangent modulus, and $1/b = q_{ult}$, i.e., the ultimate asymptotic value of the deviatoric stress. Duncan and Chang 1970 introduced a failure stress ratio $R_f = (\sigma_1 - \sigma_3)/(\sigma_1 - \sigma_3)_{ult}$, because the $(\sigma_1 - \sigma_3)_{ult}$ usually exceeds $(\sigma_1 - \sigma_3)_f$. Eq. 3.40 can now be re-written as

$$(\sigma_1 - \sigma_3) = \frac{\varepsilon}{\frac{1}{E_i} + \frac{R_f \cdot \varepsilon}{(\sigma_1 - \sigma_3)_f}} \quad (3.42)$$

For an anisotropically consolidated clay, a state of zero strain is associated with a non zero end of consolidation deviator stress $(\sigma_1 - \sigma_3)_0 = \sigma_3 \cdot (1-K)/K$, where $K = \sigma'_3 / \sigma'_1$ is the consolidation stress ratio. As in the case of conventional isotropically consolidated clay, a state of zero stress associated with a state of zero strain is required in hyperbolic stress-strain relations. This requires an introduction of a new definition of deviatoric stress after consolidation, i.e., $(\sigma_1 - \sigma_3)_m = (\sigma_1 - \sigma_3) - (\sigma_1 - \sigma_3)_0$, and it is zero at the end of the consolidation. Eq. 3.42 could be re-written by analogy as follows:

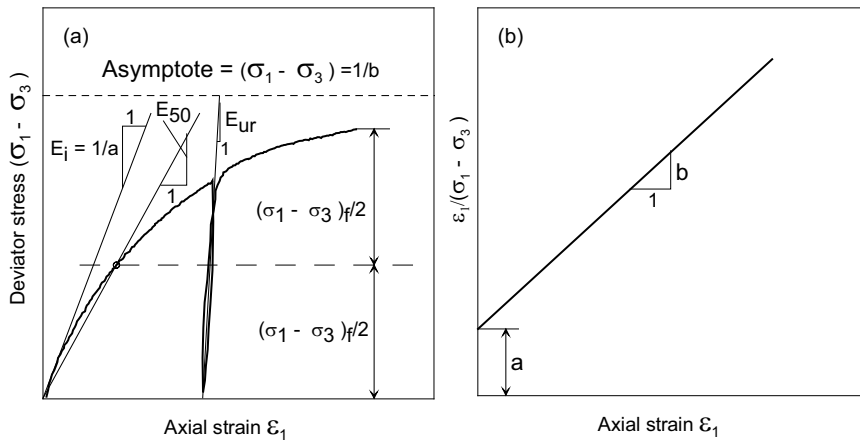


Fig. 3.15. a) Hyperbolic stress-strain curve, b) transformed hyperbolic stress strain curve

$$(\sigma_1 - \sigma_3)_m = \frac{\varepsilon}{\frac{1}{E_i} + \frac{R_f \cdot \varepsilon}{(\sigma_1 - \sigma_3)_{m,f}}} \quad (3.43)$$

Except in the case of unconsolidated-undrained tests on saturated soils, the tangent modulus and compressive strength of soils are believed to vary with the confining pressure (Duncan and Chang 1970) according to Eq. 2.76. A modified Ohde equation is also available in PLAXIS manual (Brinkgreve and Vermeer 1998; Brinkgreve 2002), which accounts the stiffness of the soil at the surface. The modified power law is given by,

$$E_i = E_i^{ref} \cdot \left(\frac{c' \cdot \cot \varphi' - \sigma'_3 \cdot \sin \varphi'}{c' \cdot \cot \varphi' + p^{ref} \cdot \sin \varphi'} \right)^m \quad (3.44)$$

where σ'_3 is the effective confining pressure in triaxial test, E_i^{ref} is the reference initial tangent modulus at a reference pressure of p^{ref} , and m is the exponent. $E_i^{ref} = k \cdot p^{ref}$, where k is the dimensionless modulus number in Eq. 2.76.

The secant modulus at 50% of the failure stress E_{50} is used in PLAXIS as main input stiffness property, because the exact determination of the initial tangent modulus for soft and sensitive soils is difficult. Another important form of the modulus of elasticity is the modulus of elasticity during unloading and reloading, denoted by E_{ur} . It is believed that E_{ur} is much higher than E_i and E_{50} . Like E_{i0} , E_{50} and E_{ur} also vary with the confining pressure according to Eqs. 2.76 & 3.44, the only thing to do is to substitute E_{50} or E_{ur} instead of E_i , and E_{50}^{ref} or E_{ur}^{ref} instead of E_i^{ref} .

Drained deformation parameters

The initial tangent modulus E_i and the failure factor R_f from the CID tests have been determined using the hyperbola relationship (Eq. 3.42) for all range of confining pressure, while E_{50} and E_{ur} are read directly from the stress - strain curves by drawing a tangent through the corresponding points (Fig. 3.15). A typical transformed hyperbolic stress-strain diagrams (CID) from three different sites in southern Germany in the city of Constance are given in Fig. 3.16. It may be noted that the transformed test data in Fig. 3.16 a fairly approximates a linear relationship, indicating that the stress-strain curve for this particular test is fairly hyperbolic in shape, in spite of the small divergent from the linear relationships at very low strains. On the other hand, the transformed lines in Fig. 3.16b and c respectively diverge from a linear relationship, indicating that the stress-strain curve for these tests may not be exactly hyperbolic in shape. The transformed data seem to follow a non-linear wave like curve in (Fig. 3.16b) and a non-linear hyperbolic curve in (Fig. 3.16c), particularly at lower confining pressure, instead of a straight line as it would be expected. However, the transformed data are approximated by the best fit lines. The deviation of the transformed data from the straight line at a very low strains are reported in the literature.

In most CID tests, it may be observed that the data in the transformed-stress-strain curves is non-linear at low strains (sometimes up to 5% axial strain). If the test data are approximated by a best fit line or by a line passing through the points where 70% and 95% of the strength are mobilized according to Duncan and Chang 1970, it will underestimate the initial stiffness of the soil particularly at lower strains. Amann et al. 1975 suggested a two line piecewise approach, where one line approximate the test data at low strain and the other line the rest of the data. With this approach, they attained a better hyperbolic approximation of the stress-strain curves of the test data on sands. This suggestion have, however, its practical limitations due to the fact that it is difficult to apply it in the already available computers codes.

Another observation from the transformed stress-strain curves include the divergence of the data from a linear relation is more prominent in specimens with low confining pressure.

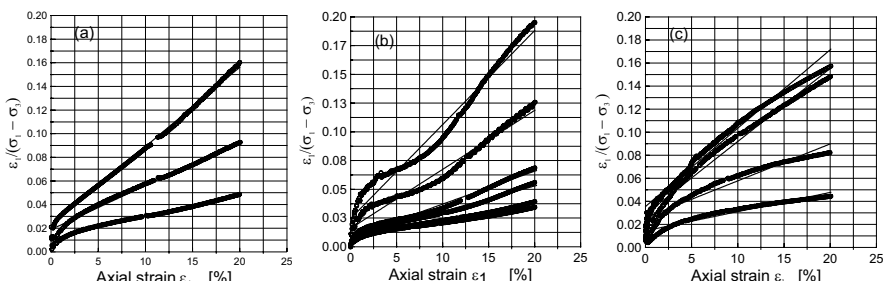


Fig. 3.16. A typical transformed hyperbolic stress-strain curves of samples from sites

The reference values of the parameters E_i , E_{50} , E_{ur} and the corresponding exponent m at a reference pressure $p^{ref} = 100 \text{ kPa}$ can be determined using Eq. 2.76 by plotting the different values of them at a different confining pressures in double logarithmic as shown in Fig. 3.17. These values for all specimens under CID test conditions are summarized in Table 3.10. From this table, it would appear that $m_{tangent} < m_{secant} < m_{un/reloading}$ with an average value of 0.53, 0.57, and 0.78 respectively. The ratio E_i^{ref} / E_{50}^{ref} varies between 1.9 to 2.2 with an average value of 2.1, the ratio E_{ur}^{ref} / E_i^{ref} varies between 2.9 to 6.53 with an average value of 4.2, the ratio $E_{ur}^{ref} / E_{50}^{ref}$ varies between 5.9 to 12.7 with an average value of 8.6, and R_f varies between 0.73 to 0.88 with a mean value of 0.82. Due to the limited number of tests performed on horizontal oriented samples (in this case only two series of tests), it is not easy to draw a general trend, however, they appear to be 1.1 to 2.2 stiffer than the vertical oriented samples, which opposes to what usually would be expected.

A plot of all the data from all CID tests shown in Fig. 3.17 seems to verify the arithmetic mean values obtained from Table 3.10. In spite of the scattering of the data, it would appear from Fig. 3.17 that E_{ur}^{ref} remains unaffected from the relative stress level at which the unloading started. The relative stress level denoted as f_s in the diagram is defined as the ratio between the stress at which the unloading starts and the stress at failure.

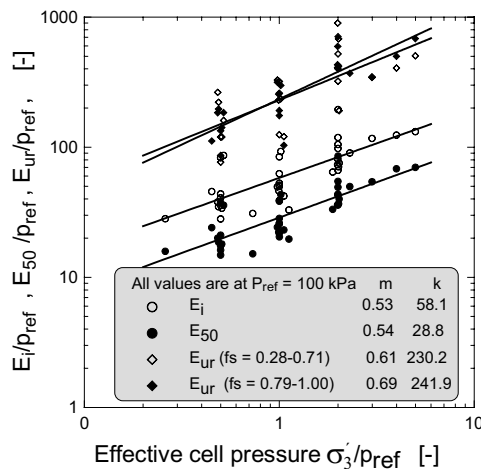


Fig. 3.17. The variation of the modulus of elasticity with confining pressure under CID test condition

Table 3.10. Deformation parameters from CID tests

Test	Tangent modulus		Secant modulus		Un/re-loading modulus			R_f [-]
	p'^{ref} [kN/m ²]	m [-]	$E_i'^{ref}$ [kN/m ²]	m [-]	E_{50}^{ref} [kN/m ²]	m [-]	E_{ur}^{ref} [kN/m ²]	
	site1							
damcid05	100	0.30	5300	0.39	2700			0.81
damcid07	100	0.31	8430	0.51	3830			0.88
damcid15	100	0.42	5990	0.45	3230	0.74	19170	0.80
site2								
maxcid01	100	0.72	5600	0.66	2550			0.82
maxcid05	100	0.70	4400	0.71	2360	0.61	11860	0.80
maxcid16/15	100	0.52	6400	0.66	2660	0.67	16710	0.83
maxcid	100	0.79	3600	0.84	1910			0.73
maxcid13 *	100	0.60	11480	0.65	5040	0.94	30000	0.86
site3								
fhkcid34	100	0.56	4870	0.51	2430	0.89	22400	0.84
fhkcid36	100	0.42	4680	0.38	2480	0.79	36500	0.82
fhkcid389 *	100	0.54	5400	0.54	2780	0.85	38470	0.79

* = horizontal samples

The stress-strain curves for the anisotropically consolidated drained tests are given, for example in Fig. 3.12b, and they appear to be initially stiffer than those from CID tests. Similar to what was observed in the CID tests on similar specimen, it may be noted from Fig. 3.18 that the transformed hyperbolic lines data also diverge from a linear relationship, indicating again that the stress-strain curve for these particular specimens is not precisely hyperbolic in shape, however, they may be approximated by the best fit lines. From Fig. 3.18b, the reference modulus of $E_i'^{ref} = 22840 \text{ kPa}$, $E_{50}^{ref} = 11110 \text{ kPa}$ and the corresponding $m = 0.55$ and 0.61 respectively can be determined.

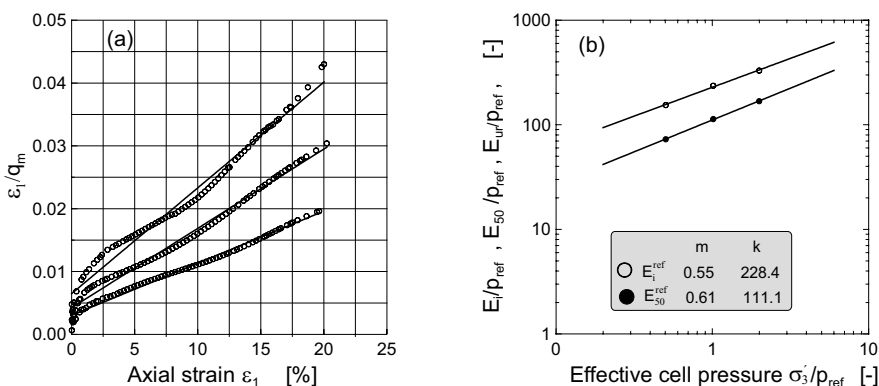


Fig. 3.18. a) Transformed stress-strain relationship, and b) the variation of the modulus of elasticity with confining pressure under CAD test condition

Undrained deformation parameters

Similar to the drained tests, the undrained deformation parameters can be determined from the strain-stress diagrams, for example in Fig. 3.11, assuming that the curves may be represented by hyperbolic relationship. Typical transformed hyperbolic stress-strain curves under CIU test condition are given in Fig. 3.19. The transformed stress-strain curves are fairly linear, except that the curves in Fig. 3.19a and b show non-linear relationship at low axial strains (< 2.5%). A plot of the variation of the modulus of elasticity with the confining pressure under CIU test condition also shown in Fig. 3.20.

As far as the strength of normally consolidated soils is concerned, we have seen in section 3.2.3 that the strength parameters obtained by applying both failure criterion are almost the same. However, this is not the case when it comes to deformation parameters. The choice of the failure criteria has a considerable influence on the value of the secant modulus $E_{50(u)}$ and the corresponding k , m and R_f values. In general, $E_{50(u)}$ and k obtained applying the $(\sigma'_1 / \sigma'_3)_{max}$ failure criteria are 1 to 2 and 1 to 1.5 times higher than those obtained using $(\sigma_1 - \sigma_3)_{max}$ or 20% failure criteria respectively. Therefore, in order to get a consistent deformation parameters, one has to decide which of the limiting state to use. Though it not easy to answer the question, which of the limiting state governs the failure mechanism of normally consolidated soils, the authors suggest to use the maximum (or 20%) deviator stress failure criteria, because 1) there is hypothesis that the normally consolidated soils require larger deformation to reach their limiting state, and 2) the constitutive soil model (the Hardening Soil Model) selected for numerical analysis of excavations in soft soil later in this book is based on the deviator stress failure mechanism.

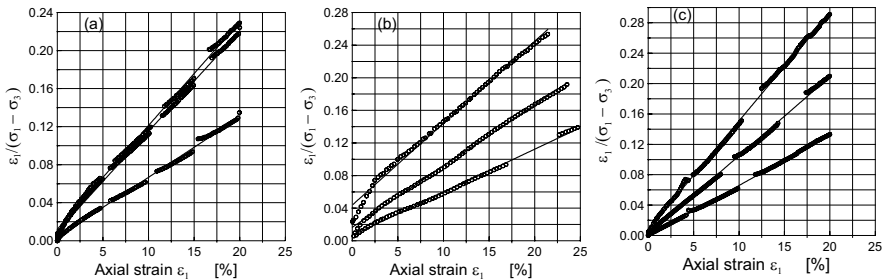


Fig. 3.19. A typical transformed hyperbolic stress - strain curves under CIU test condition

The effective confining stress σ'_3 in undrained triaxial test is not constant throughout the test due to the development of excess pore pressure. Hence, A constant total confining pressure σ_3 is assumed in the analysis of the stress dependency behaviour of the elasticity modulus under undrained condition.

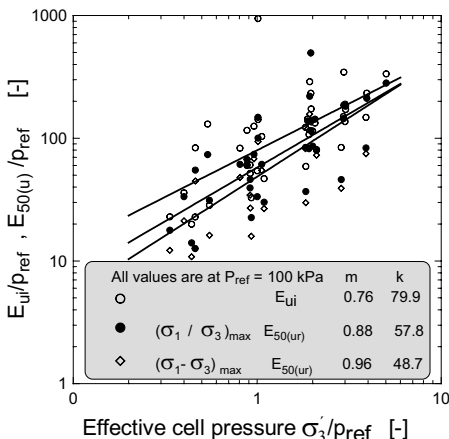


Fig. 3.20. The variation of the modulus of elasticity with the confining pressure under CIU test condition

The deformation parameters corresponding to the maximum deviator stress failure criteria for a reference pressure of 100 kPa are given in Table 3.11. From this table, it can be seen that E_{ui}^{ref} varies between 2990 to 51560 kPa. The higher stiffness was recorded at site 3. The soil at this location is very soft and sensitive, contains organic substances such as grass roots and mussels, and has a water content above 70% and an initial void ratio of 2. The values of m corresponding to E_{ui}^{ref} ranges from 0.72 to 1.73. The $E_{50(u)}^{ref}$ varies between 1907 to 17050 kPa, and the corresponding value of m varies between 0.64 to 1.48 with, and R_f varies between 0.70 to 0.96. The exponent m is believed to vary between 0 and 1 for a drained condition. To the knowledge of the Author, there are no comparable data available in the literature regarding the exponent m in undrained condition. Hence, until further studies, the value of the exponent greater than 1 should be set to one for practical applications. The ratios $E_{ui}^{ref} / E_{50(u)}^{ref}$ varies between 1.29 to 3.02 with an average value of 1.9. Although only one series of CIU test on 3 horizontally oriented specimens was conducted, it appears that these specimens are stiffer than those similar vertically oriented specimens. From Table 3.11, it appears that E_{ui}^{ref} and $E_{50(u)}^{ref}$ from horizontally oriented specimens are 2.1 and 1.8 times higher than those similar vertically oriented specimens respectively.

The stress - strain curves of the anisotropically consolidated undrained tests are already shown, for instance in Fig. 3.12a, and they appear to be initially stiffer than those from CIU tests. The transformed stress-strain relations and the variation of the modulus of elasticity are shown in Fig. 3.21. Similar to what was observed in the CIU tests on similar specimens, the transformed lines (Fig. 3.21a) are fairly linear except at low axial strain (< 2.5%), indicating again that the stress-strain curves for this particular test are fairly hyperbolic in shape. From Fig. 3.21b, the reference modulus $E_{ui}^{ref} = 8420$ kPa and $E_{50(u)}^{ref} = 6530$ kPa can be determined.

Table 3.11. Deformation parameters from CIU tests

Test	p^{ref} [kN/m ²]	m [-]	E_{ui}^{ref} [kN/m ²]	m [-]	$E_{50(u)}^{ref}$ [kN/m ²]	R_f [kN/m ²]
site1						
damciu04	100	0.83	4360	1.14	2850	0.88
damciu06	100	0.90	9550	1.12	6450	0.91
damciu10	100	1.06	5470	1.32	3360	0.90
damciu14	100	1.48	10600	1.43	5880	0.96
damciu30	100	1.50	2990	1.25	3780	0.94
site2						
maxciu02	100	0.99	6710	1.11	4040	0.86
maxciu	100	0.88	3720	0.84	1907	0.83
maxciu03 *	100	0.71	13930	0.64	7230	0.96
site3						
fhkciu35	100	1.73	51560	1.48	17050	0.99
Others						
Jaegerk.	100	0.86	6860	0.92	6890	0.70
Schwand	100	0.78	12930	0.62	9220	0.93
Stromey.	100	0.87	5610	0.98	3570	0.77

* = horizontal sample

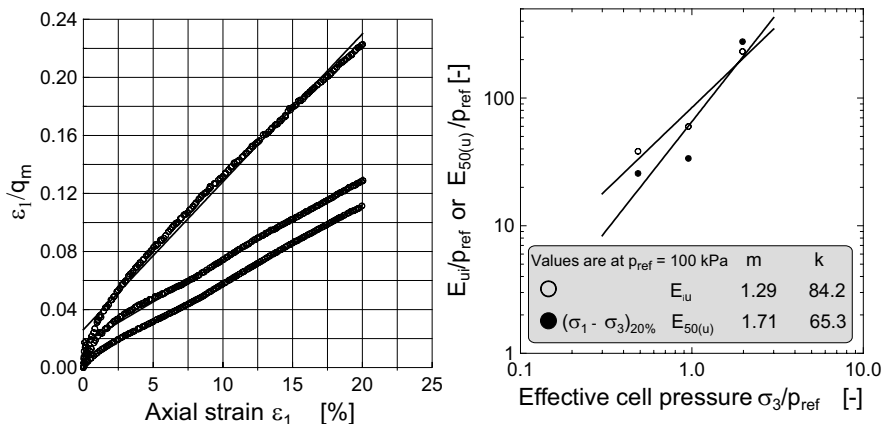


Fig. 3.21. a) Transformed stress-strain relationship, and b) the variation of the modulus of elasticity with confining pressure under CAU test condition

Some stress-strain curves under controlled stress path anisotropically consolidated undrained tests on undisturbed specimens for the postulated stress paths B and C are already shown in Fig. 3.13 a&b. A typical transformed stress-strain relationship and the variation of the modulus of elasticity with the confining pressure for the postulated paths B are shown in Fig. 3.22 It can be seen from Fig. 3.22a

that the transformed data may fairly be approximated by a straight lines, though non-linearity to some degree may exist, in particular in those curves with confining pressure of 100 kPa. The values of the deformation parameters at a reference pressure of 100 kPa are given in Table 3.12. The result of three more stress path - CIU tests on reconstituted specimens for the postulated stress paths A, B and C are also given in Table 3.12. It appears from this table that no general conclusion can be made regarding the dependency of the stiffness of the soil sample on the direction of the total stress paths. For example, the stress path C appear to be stiffer than stress path B in the CAU test on undisturbed samples, whereas the opposite can be observed from the CIU test on reconstituted samples. This shows a need for further investigation on a number of samples in order to have a general picture of the relationship between the stiffness of the soil and the stress paths.

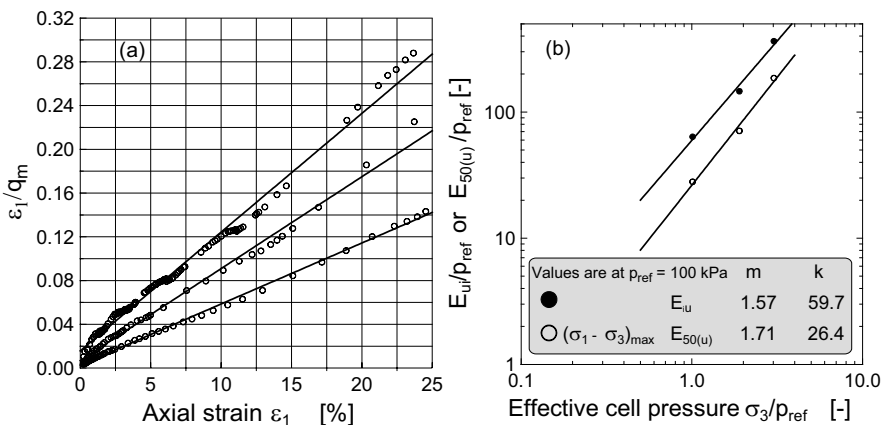


Fig. 3.22. a) transformed stress-strain relationships, b) variation of the modulus of elasticity with confining pressure, under controlled stress path B - CAU test condition

Table 3.12. Deformation parameters from controlled stress path

Stress path	Tangent modulus			Secant Modulus		
	p^{ref}	E_{ui}^{ref}	m	$E_{50(u)}^{ref}$	m	R_f
	[kPa]	[kPa]	[-]	[kPa]	[-]	[-]
Controlled stress path - CAU tests on undisturbed samples						
B	100	5970	1.57	2640	1.71	1.00
C	100	9310	1.2	3400	1.4	1.00
Controlled stress path - CIU tests on reconstituted samples						
A	100	6340	0.75	4000	0.69	0.843
B	100	6094	0.64	3890	0.59	0.805
C	100	5560	0.58	3210	0.87	0.842

Comparison of deformation parameters

In the foregoing sections, the deformation parameters obtained from different type of tests have been presented and discussed. In this section, the different deformation parameters are compared to each other. The comparisons are between the deformation parameters from oedometer and triaxial tests, from the drained and undrained tests, from isotropic and anisotropic consolidation tests, from the standard and stress path tests, from different stress paths, from vertically and horizontally oriented specimens, from first loading and unloading (reloading) conditions, etc.

The average ratio of $E_i^{\text{ref}} / E_{\text{oed}}^{\text{ref}}$ is found to be 2.08, 1.63 and 2.82 at the three sites respectively. Comparing the reference constrained modulus with the reference secant modulus in drained test, the ratio $E_{50}^{\text{ref}} / E_{\text{oed}}^{\text{ref}}$ is found to be 1.03, 0.77 and 1.45 at the three sites respectively. The range of the ratio $E_{ur}^{\text{ref}} / E_{ur,\text{oed}}^{\text{ref}}$ is 2.33 to 2.52, 1.29 to 2.09 and 1.32 to 2.51 at the three sites respectively.

The relationships between drained and undrained modulus of elasticity is given by Eqs. 2.72 to 2.75. The ratio E_u / E approximately varies between 1.11 to 1.34 for range of Poisson's ratio between 0.12 to 0.35. The average ratio $E_{ui}^{\text{ref}} / E_i^{\text{ref}}$ is found to be 1.08, 1.29 and 10.3 at the three sites respectively. Taking into account the high value of the Poisson's ratio found in the drained test, the ratio of the undrained to drained modulus at site1 & 2 seems to fall in the range of Eq. 2.76, whereas site3 is exceptionally high and unacceptable. In general, the stress exponent m is found to be higher in undrained tests than in drained tests.

The modulus of elasticity from CAD tests is found to be 3.6 to 5.2 (on average 4.4) times higher than that from CID tests. The m values are lower in CAD test than those in CID tests. The undrained modulus of elasticity in CAU tests are 1.3 to 1.6 higher than the corresponding values from CIU tests. The m values are higher in CAU test than those in CIU tests.

The stiffness of the soil in the horizontal direction appears to be 1.8 to 2.0 and 1.1 times higher than the stiffness of the soil in vertical direction at site2 and site3 respectively. This seems to contradict with that given in section 2.6.4, where it is stated that normally consolidated soils are stiffer in vertical direction than in horizontal direction and hence it requires further investigation.

No general conclusion can be made regarding the dependency of the stiffness of the soil sample on the direction of the total stress paths. For example, the stress path C appear to be stiffer than stress path B in the CAU test on undisturbed samples, whereas the opposite can be observed from the CIU test on reconstituted samples. The general understanding is that the soil behaves stiffer as the stress path direction changes from right to left. This shows a need for further investigation on a number of samples in order to have a general picture of the relationship between the stiffness of the soil and stress paths.

The undrained stiffness of the soil specimens under controlled stress path - CIU test appears to be higher than the stiffness of the specimen under standard undrained tests. This is not, however, because of the stress paths that the speci-

mens were subjected to follow, but it is most probably because of the type of the application of the load. The postulated stress path A is the same as the standard total stress path in drained/undrained triaxial compression test ($\Delta\sigma_3 = 0$, $\Delta\sigma_1 > 0$), however, it shows higher stiffness in stress controlled tests than in strain controlled tests.

An average failure ratio $R_f = 0.82$, 0.89 , 0.90 , is found from drained, undrained and controlled stress path tests respectively. The value of m is different for tangent modulus, secant modulus and un/reloading modulus. An average values of 0.53 , 0.57 and 0.78 respectively are found out from drained tests. Similarly, average $m = 1.05$ and 1.1 was found out from the undrained tests for tangent modulus and secant modulus respectively.

The range of the ratios between the different forms of the modulus of elasticity are given in Table 3.13.

Table 3.13. The proportion of the different forms of modulus of elasticity

site	Test condition	E_i^{ref} / E_{50}^{ref}	E_{ur}^{ref} / E_i^{ref}	$E_{ur}^{ref} / E_{50}^{ref}$	$E_{oed,ur}^{ref} / E_{oed}^{ref}$
site1	Drained	2.02	3.20	5.93	2.60
	Undrained	1.48			
site2	Drained	2.17	3.10	6.72	3.63
	Undrained	1.84			
site3	Drained	1.94	6.55	12.66	6.65
	Undrained	3.02			
Average	Drained	2.04	4.28	8.43	4.29
	Undrained	2.11			

3.2.5 Contact behaviour between wall material and soft soil

General

The contact behaviour between the retaining wall and the soil plays an important role in numerical simulations of retaining structures. Most standards recommend a wall friction value of zero for soft soils, which results in unrealistic deformations of the wall and the soil in numerical analysis. Terzaghi was the first to study the influence of wall friction on earth pressures in early 1930's. After him a number of studies had been conducted to study the frictional characteristics of interfaces between soils and structural elements (see for example Potyondy 1961; Clough and Duncun 1971).

Beside the wall friction, the stiffness of the interface is equally important to simulate the contact behaviour. Some FE-programs, for example PLAXIS, requires an input parameter R_{inter} (an interface factor, which is taken as the ratio of the wall friction to friction of the soil) for the interface elements. The interface elements take the material property from nearby soil cluster after reducing the val-

ues of all parameters by a factor R_{inter} , even the shear modulus which is a key parameter as regard to the deformation of the soil should be reduced by factor $(R_{inter})^2$ (see Freiseder 1998; Brinkgreve and Vermeer 1998; Brinkgreve 2002). This results in unrealistic deformations. Though the PLAXIS version 7 and 8 allows a separate material input of the interface elements, the exact values of the input parameters (wall friction and stiffness) for soft deposits is still open.

Description of the interface test

To determine the friction and stiffness behaviour of the contact elements, a strain controlled large size (365 x 550 mm) direct shear boxes (LSB) is used. Rusted steel and rough concrete plates are used as construction material. The specimens are prepared from disturbed lacustrine soil at an average dry density of 14.72 kN/m³ and corresponding water content of 32%. The soil specimens had an average liquid limit of 56% and plasticity index of 31%. The soil is compacted in the lower part of the shear box, and the concrete or the steel plate is placed on the top of the soil in the upper box. The specimen is first consolidated at normal stress of 50, 75, 100, 150, 200, and 300 kN/m² and then sheared at an average constant rate of strain of 0.025 mm/min. At the end of the test a drop in water content (on average $w = 27.9\%$) and an increase in the dry density (on average $\gamma_d = 16.01 \text{ kN/m}^3$) are measured. A total of 18 tests are conducted, among which 10 tests are on concrete soil contact and the rest on steel soil contact.

Moreover, 30 interface tests has been conducted at 32% and 40% water content in a medium (100 x 100 mm) and small (63 x 63 mm) scale shear boxes (SSB) for the purpose of comparison. The normal stresses applied are 50, 75, 100, 150, 200 and 300 kN/m². The contact between the soil and concrete/steel is subjected to shear stress at a constant strain rate of 0.02 mm/min.

Wall friction

Typical results of the interface tests are shown in Fig. 3.23 b & c. For comparison purpose a soil to soil shear tests were also performed in a medium size and small size direct shear box (SSB) with normal stresses of 25, 50, 75, 100, 150, 200 and 300 kPa at water content of 32% and 40%. Fig. 3.23a also shows the shear strength diagram of the soil. The results of the tests are summarized in Table 3.14.

As shown in Table 3.14, the angle of wall friction δ obtained from small shear box (SSB) is in general higher than that determined from large scale shear box (LSB) for the same water content. The minimum ratio of δ/φ for soil-concrete plate contact is found to be 0.462 and for that soil-steel contact $\delta/\varphi = 0.458$. The adhesion c_a seems, however, larger than the cohesion c for both construction materials. This is theoretically unacceptable because the adhesion should not be larger than the minimum of the cohesion of the elements in contact. On the other hand, one may assume a ratio of 1 taking into account the sensibility of the determination of the adhesion or cohesion in shear tests. The influence of the water content on the wall friction is evident from the SSB interface tests.

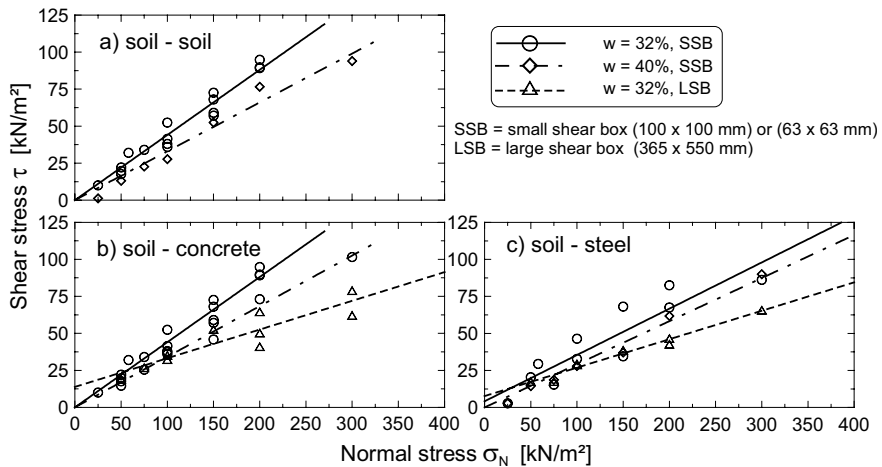


Fig. 3.23. Wall friction: a) soil to soil, b) soil to concrete contact, and c) soil to steel contact

Table 3.14. Relative values of friction and adhesion of the contact surfaces

	Soil - Soil		Soil – Concrete		Soil – Steel		
	SSB	SSB	SSB	SSB	LSB	SSB	SSB
w = 32% w = 40%	w = 32% w = 32% w = 40% w = 32% W = 32% W = 40% w = 32%	0	0	3.1	0	13.8	4.2
c or c _a [kPa]	c or c _a [kPa]	c or c _a [kPa]	c or c _a [kPa]	c or c _a [kPa]	c or c _a [kPa]	c or c _a [kPa]	c or c _a [kPa]
φ or δ [°]	23.8	18.3	20.2	18.9	11	17.4	16.2
c _a /c [-]	0	0	0	0	0	0	0
δ/φ [-]	1.000	0.769	0.849	0.794	0.462	0.731	0.681
tanδ/tanφ [-]	1.000	0.750	0.834	0.776	0.441	0.710	0.659
							7.7
							10.9
							0.458
							0.437

Stiffness property of the interface

Fig. 3.24 show the non-linear stress-displacement relations of the soil and the interfaces. It would appear from this figure observe that the interfaces seem to react initially stiffer than the soil.

The stress-displacement behaviour of the interface up to the point of assumed failure shear stress may be conveniently represented by means of equations similar to those developed by Duncan and Chang 1970 used to model the stress-strain behaviour of soils (section 3.2.4). The transformed curves are shown in Fig.3.25. It should be noted that in the transformed data, only those data points up to the assumed failure shear stress has been considered. From Fig.3.26, one can easily read the initial shear stiffness, here denoted as G_{si} . The variation of the initial shear stiffness with the normal stress may be expressed analogue to the Ohde 1939 equation as,

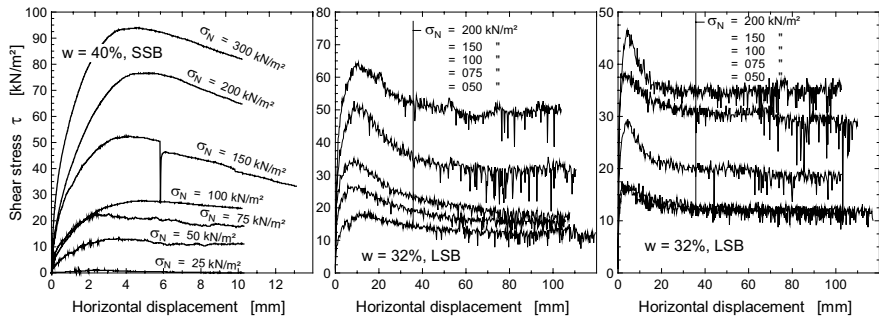


Fig. 3.24. Shear stress-displacement behaviour of the soil and interface: a) soil to soil, b) soil to concrete, and c) soil to steel

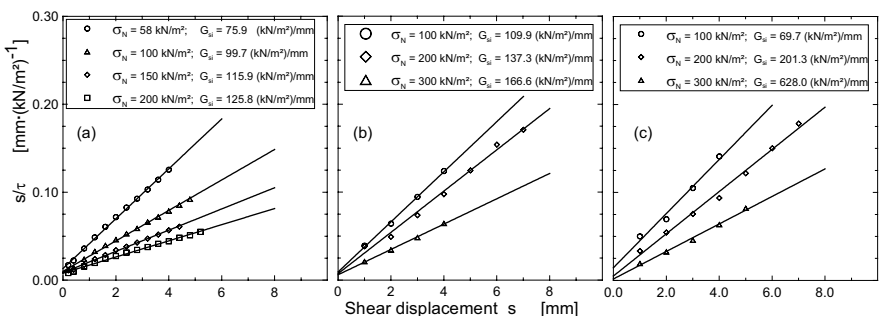


Fig. 3.25. Transformed stress-displacement curves for a) soil to soil, b) concrete to soil, and c) steel to soil contacts

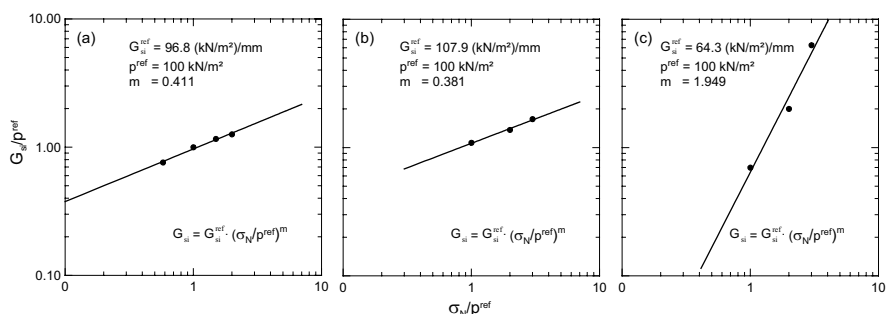


Fig. 3.26. The initial reference shear stiffness: a) soil to soil, b) concrete to soil, and c) steel to soil contacts

$$G_{si} = G_{si}^{ref} \cdot \left(\frac{\sigma_N}{p^{ref}} \right)^m \quad (3.45)$$

where G_{si}^{ref} is the reference initial shear stiffness at reference stress of p^{ref} , σ_N is the normal stress and m is the stiffness component. The double logarithmic plot of Eq. 3.45 is shown in Fig. 3.26. For the results shown in Fig. 3.26, the initial shear stiffness has the value 96.8, 107.9 and 64.3 kN/m²/mm for soil-soil, soil-concrete and soil-steel contact respectively. This shows that the stiffness of the contact surface is not as low as usually being assumed. Hence, adopting the stiffness of the soil fully to the interface element might help in reducing the excessive and unrealistic deformations of the wall in an excavation in soft deposits during finite element calculations.

3.3 Calibration of soil parameters

In this section the soil parameters obtained from triaxial tests and compression tests in section 3.2 are calibrated for the hardening soil model using the PLAXIS finite element program. The aim of the calibration is to see whether the finite element simulation of the tests lead to the same result as the tests, if not to find out the possible factors that lead to such variations

3.3.1 Drained test behaviour

The average reference soil parameters for the hardening soil model are given in Table 3.15 below. These parameters are obtained from one of the triaxial and one-dimensional compression tests results in section 3.2.

Table 3.15. Reference soil parameters for hardening soil model

γ [kN/m ³]	φ' [°]	ψ' [°]	c' [kN/m ²]	E_{50}^{ref} [kN/m ²]	E_{oed}^{ref} [kN/m ²]	E_{ur}^{ref} [kN/m ²]	p^{ref} [kN/m ²]	m [-]	R_f [-]	K_0^{nc} [-]	v_{ur} [-]
19.5	25.3	0	13.2	3253	2948	19170	100	0.63	0.83	0.573	0.20

The triaxial test and the oedometer test were simulated by means of an axisymmetric geometry, with the real dimension of the test set-up, that represent half of the soil sample (0.025 x 0.05 m in case of the triaxial test and 0.035 x 0.02 m in case of oedometer test). In the triaxial model, the displacements normal to the boundaries are fixed and the tangential displacements are kept free to allow for smooth movements along the axis of symmetry (the left hand side) and the bottom boundaries. The top and the right side boundaries are fully free to move. Similarly, the displacements normal to the boundaries are fixed and the tangential displace-

ments are kept free to allow for smooth movements along the axis of symmetry (the left hand side) and the right hand side boundaries in the oedometer model. Both the normal and tangential displacements along the bottom boundary are fixed, whereas the top boundary is fully free to move.

The triaxial test procedure was modeled by means of applying first an all round confining pressure $\sigma'_{3,0} = \sigma'_{1,0} = 50,100, \text{ and } 200 \text{ kN/m}^2$ for three specimens respectively and then by increasing the vertical stress $\Delta\sigma$ up to failure. The choice of the three confining pressure allows the study the influence of the different soil parameters at the reference pressure $p^{ref} = 100 \text{ kN/m}^2$ and at stress level below and above the reference pressure possible. Similar to the test condition, the following load increments were used in the FEM - simulation of the oedometer test: 10.8, 20.1, 30, 69, 126, 252, 126, 69, 10.8, 69, 126, 252, 504, 756, 504, 126, 12.6 kN/m^2 .

In order to study the effect of the different hardening soil model parameters on the stress-strain, the strength and the volume-change behaviour of the soil specimens, several variations of the soil parameters have been considered during the FEM-computations. These variations are listed in Table 3.16.

Table 3.16. Variations of the soil parameters under drained condition

Cases	Parameter
FEM-1	Reference parameters (Tabel 3.15)
FEM-2	same as FEM-1, but E_{50}^{ref} increased by a factor of 1.25
FEM-4	same as FEM-1, but E_{50}^{ref} increased by a factor of 2.0
FEM-6	same as FEM-1, but $m = 0.83$ (m from oedometer test result, see Table 6.6)
FEM-8	same as FEM-1, but $E_{oed}^{ref} = E_{50}^{ref} = 253 \text{ kN/m}^2$
FEM-9	same as FEM-1, but E_{oed}^{ref} reduced by a factor of 0.75
FEM-10	same as FEM-1, but E_{oed}^{ref} increased by a factor of 1.25
FEM-11	same as FEM-1, but $E_{ur}^{ref} = 3 \cdot E_{50}^{ref} = 9759 \text{ kN/m}^2$
FEM-12	same as FEM-1, but K_0^{nc} increased to 0.71
FEM-13	same as FEM-1, but K_0^{nc} reduced to 0.48
FEM-14	same as FEM-1, but $\nu_{ur} = 0.10$
FEM-15	same as FEM-1, but $\nu_{ur} = 0.30$
FEM-16	same as FEM-1, but $R_f = 0.97$
FEM-17	same as FEM-1, but $R_f = 0.67$
FEM-18	MCM with $E_{oed} = 2948 \text{ kN/m}^2$ at a confining pressure of $\sigma'_{3,0} = 100 \text{ kN/m}^2$ and $\nu = 0.35$
FEM-19	MCM with $E_{50} = 3253 \text{ kN/m}^2$ at a confining pressure of $\sigma'_{3,0} = 100 \text{ kN/m}^2$ and $\nu = 0.35$
FEM-23	same as FEM-1, but E_{50}^{ref} increased by a factor of 1.1, E_{oed}^{ref} reduced by a factor of 0.90, $m = 0.73$, $K_0^{nc} = 0.59$, and $\nu_{ur} = 0.05$

Stress-strain behaviour of a soil specimen in triaxial and one-dimensional compression test

The stress-strain relationship of the soil specimen from the FEM computation and test results are presented in Fig. 3.27. The test results are indicated with dashed lines and the shaded regions show the range of the variation of the test results. Note that Fig. 3.27a shares the same legend as Fig. 3.27b. Since the hardening soil model requires soil parameters both from the triaxial test and one-dimensional compression test, the comparison of the FEM- results are presented parallel, for example, Fig. 3.27a for the triaxial loading system and Fig. 3.27b for oedometer loading condition.

It would appear from Fig. 3.27a that the FEM-results of the triaxial model (FEM-1) underestimate the stiffness of the soil specimen at an axial strain less than 5 - 6 % for all cases of confining pressures. This might be happen due to the fact that the hardening soil model use the secant modulus E_{50} instead of the initial tangent modulus E_i ($E_i \approx 2 \cdot E_{50}$, see section 3.2.4). The FEM-simulation of the triaxial test, however, lies reasonably within the range of variations of the test results for an axial strain greater than 5 - 6%.

Contrary to the triaxial simulation, the FEM-simulation of the oedometer (FEM-1) overestimates the stiffness of the specimen up to a vertical strain of 7% , and thereafter it joins the region of the range of the test results (Fig. 3.27b).

The FEM simulates very well the un/reloading stiffness of the specimen in the triaxial loading condition, whereas it overestimates it in the oedometer loading condition. Lowering the un/reloading modulus to $E_{ur}^{ref} = 3 \cdot E_{50}^{ref}$ (FEM-11), which is given in PLAXIS as a default value, would result in underestimation of the un/reloading stiffness of the triaxial test, whereas it still overestimates it in the oedometer test for the 1st un/reloading at about a vertical pressure of 200 kN/m², but much closer to the test result than the reference case (FEM-1). For the 2nd un/reloading case at higher stress level in the oedometer test, the FEM simulation underestimates the un/reloading stiffness. If one wants to keep the triaxial un/reloading stiffness unchanged, since it match very well to the test results, and on the other hand to adjust it to the test results in the oedometer simulation, the only possibility available is to vary the value of the Poisson's ratio for un/reloading ν_{ur} . This parameter is the only parameter that influence the un/reloading behaviour of the one-dimensional compression without affecting much the un/reloading behaviour in the deviatoric state of stress.

Apart from its influence on the un/reloading behaviour of both test conditions, the E_{ur}^{ref} has no significant influence on the stress-strain behaviour of the specimen during the 1st loading.

Taking the value of the exponent $m = 0.83$ (FEM-6) from oedometer test result (Table 3.5) instead of $m = 0.63$ from triaxial test increases the stiffness of the soil specimen for a stress level above the reference pressure and decreases the stiffness for a stress level below the reference pressure in both loading conditions (Fig. 3.27) as it would expected. The optimal solution seems to lay between these two values.

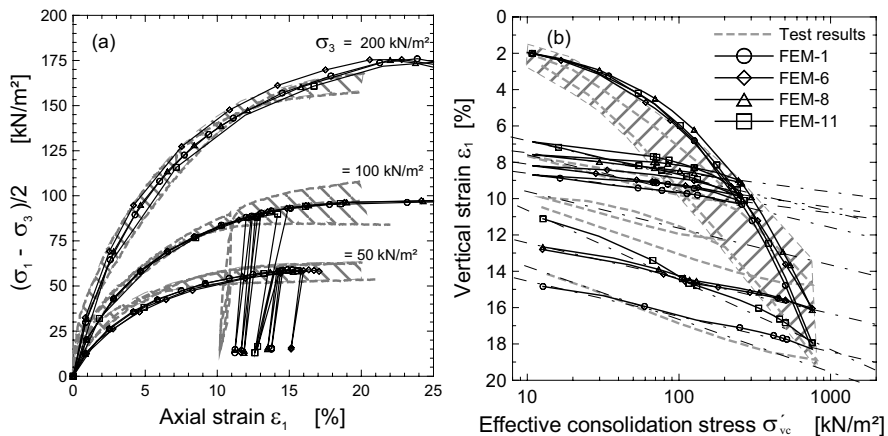


Fig. 3.27. Calibration of the HSM parameters based on drained triaxial and oedometer test results

The assumption $E_{oed}^{ref} = E_{50}^{ref}$ (FEM-8), which is recommended in PLAXIS as a default value, has no significant influence on the deviatoric stress-strain behaviour, whereas it reacts stiffer in one-dimensional compression (Fig. 3.27). This approves that the E_{oed}^{ref} is largely a compression hardening parameter (cap parameter). In both loading systems, the assumption $E_{oed}^{ref} = E_{50}^{ref}$ has no effect on the un/reloading stress-strain behaviour.

It would appear from Fig. 3.27 that the deviatoric stress at failure remains unaffected from the variations of the parameters m , E_{oed}^{ref} and E_{ur}^{ref} , although the strain at which the failure occur might be different. This is because the failure stress is mainly controlled by the shear parameters c' and φ' in drained analysis.

Stress-strain at a lower axial strain. Fig. 3.28a shows a zoomed out stress-strain diagram at lower axial strain (< 4%) for specimen with a confining pressure of 100 kN/m^2 . From the figure, it can be seen that the FEM-computational result (FEM-1) remains below the test result for the reference case. This is probably due to the use of the secant modulus of elasticity E_{50} instead of the initial tangent modulus E_i . Doubling the stiffness of the soil (FEM-4) may narrow the gab between the measured and computed lines at a lower strain, but it exaggerates the stiffness thereafter (Fig. 3.28b). Such problem may be overcome by introducing two hyperbola with two different stiffness lines (Amann et al. 1975), and loading the specimen piece wise in two steps each with different material sets (see also section 3.2.4). The first loading step may run up to a known limit stress with a higher stiffness. Then the second loading step may follows till failure with the corresponding relatively smaller stiffness. The stress level dependent limit stress (the transition stress) can be estimated from the test results using the power law. This kind of load and stiffness arrangement is not implemented in the hardening soil model and it may violate the hyperbolic assumption of the model.

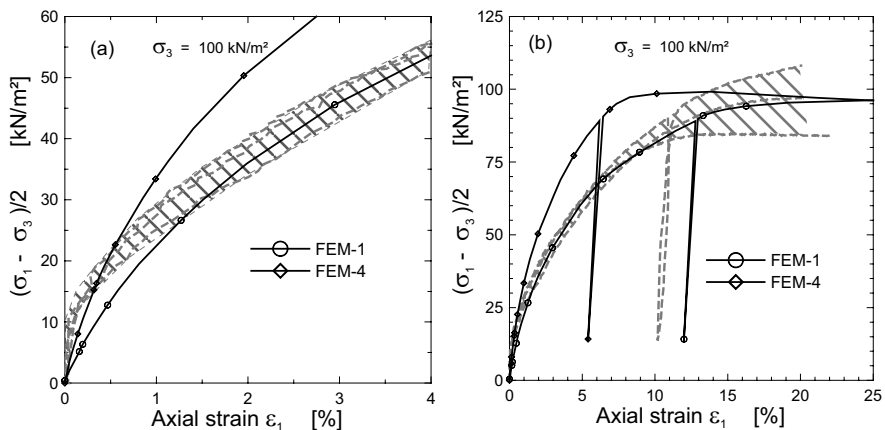


Fig. 3.28. The deviation of the FEM-computational results from the test results at lower axial strain, a) at a lower strain, and b) till failure

Influence of the stiffness parameters E_{50} , E_{oed} and E_{ur} on stress-strain behaviour. In order to study the influence of the different hardening soil model parameters on the stress-strain behaviour of the soil specimen, various FEM - computations are conducted according to the cases listed in Table 2. The first group of variations are the stiffness parameters E_{50} , E_{oed} and E_{ur} . Increasing the value of the E_{50}^{ref} by 25% (FEM-2) shifts the reference curve upwards and partly lies above the range of the measured values, but it joins the reference curve as failure approaches (Fig. 3.29a). E_{50} has no effect at all on the one-dimensional compression as shown in Fig. 3.29b. On the other hand, changing the value of E_{oed}^{ref} by $\pm 25\%$ (FEM-9 & 10) has no significant influence on the deviatoric stress, whereas it affects the stress-strain characteristics of the one-dimensional compression accordingly. This is a clear proof of the fact that the parameter E_{50} is purely shear hardening parameter (shear yield surface), whereas the parameter E_{oed} is purely a compression hardening parameter (cap yield surface).

Although lowering the value of the parameter E_{ur}^{ref} as much as 50% of the reference value (FEM-11) has no significant influence on the stress-strain curves of both loading systems during the first loading, it affects both loading systems equally during un/reloading. Hence, E_{ur} is a parameter common to both yield surfaces.

For a purpose of comparison, the respond of the Mohr-Coulomb Model (MCM) to the triaxial test condition for two different cases are presented in Fig. 3.29a. It would appear from the figure that taking the constrained stiffness modulus as a reference value (FEM-18) underestimates the stiffness of the specimen considerably. Although the use of the E_{50} as a reference parameters (FEM-19) partly underestimates and partly overestimates the stiffness of the soil specimen, however, it is more closer to the test result than the case of the FEM-18.

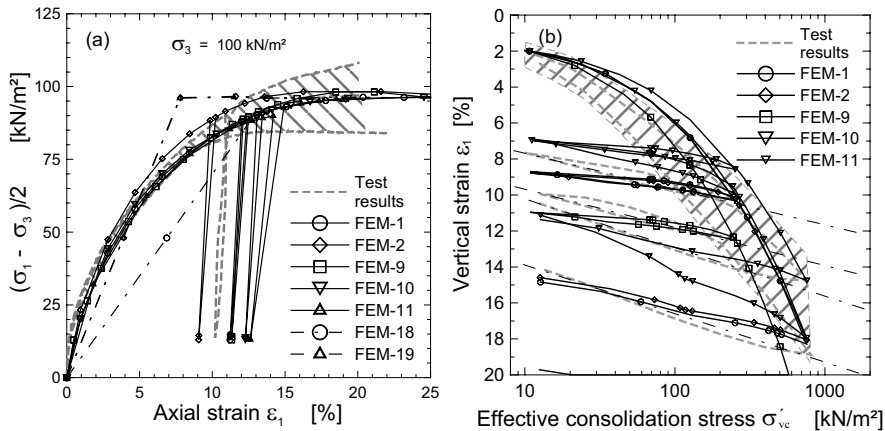


Fig. 3.29. The influence of the stiffness parameters E_{50}^{ref} , $E_{\text{oed}}^{\text{ref}}$ and $E_{\text{ur}}^{\text{ref}}$ on the stress-strain characteristics of a soil specimen a) triaxial case ($\sigma_{3,0} = 100 \text{ kN/m}^2$), and b) oedometer case

Comparing the MCM with the HSM, one would expect relatively a higher deformation from the MCM up to a stress approximately equal to half of the stress at failure and vice versa thereafter. Once the soil reaches the failure stress, the deformation in MCM depends mainly on how long the soil can be allowed to plasticify. Since both soil models are based on the Mohr-Coulomb failure criteria, the deviatoric stress at failure remains the same independent of the variation of the stiffness parameters, except that the strain at which the failure may occur might be different.

Influence of the parameters v_{ur} , K_0^{nc} and R_f on stress-strain behaviour. In the second group of variation belong the parameters v_{ur} , K_0^{nc} and R_f . Varying the value of v_{ur} to 0.1 (FEM-14) and to 0.3 (FEM-15) has no significant influence on the deviatoric primary loading and un/reloading state of stress (Fig. 3.30a), whereas it has a considerable effect on the un/reloading stiffness of one-dimensional compression (Fig. 3.30b). While lowering v_{ur} to 0.1 decreases the un/reloading stiffness and fairly approaches the test result, increasing v_{ur} to 0.3 tends to increase the un/reloading stiffness and diverges further from the test results. v_{ur} is the single parameter that affects the un/reloading stiffness of the one-dimensional compression without affecting the corresponding un/reloading stiffness of the deviatoric loading system. If a match of the computation and the test results during the un/reloading state is desired, this is the suitable parameter for a variation to deal with.

The HSM distinguishes between the model parameter K_0^{nc} and the K_0 which defines the initial state of stresses. Since the initial stresses in the very small triax-

ial model will have no as such an influence on the stress-strain behaviour, it is assumed that $K_0^{nc} = K_0$. Increasing the value of K_0^{nc} by 25% (FEM-13) results in a divergence of the stress-strain curve below the reference curve whereas decreasing its value by the same amount (FEM-12) leads to an increase of the stiffness of the soil above the reference value in both triaxial (Fig. 3.30a) and oedometer(Fig. 3.30b) loading systems. However, the effect of varying K_0^{nc} seems to be stronger for the triaxial loading system than for the one-dimensional loading system. In both cases, K_0^{nc} seems to have no significant influence on the un/reloading state of stress.

The lines of the FEM-simulation of the variation of the influence of the failure factor R_f above (FEM-16) and below (FEM-17) the reference value in Fig. 3.30a, follows the course of the reference curve up to approximately an axial strain of 5% from which they start to diverge upwards (FEM-17) and downwards (FEM-16). Its final effect is to retard the failure in the case of increasing its value and to accelerate it in the case of lowering its value. However, the influence of increasing R_f value above the reference value seems to be larger than the opposite one.

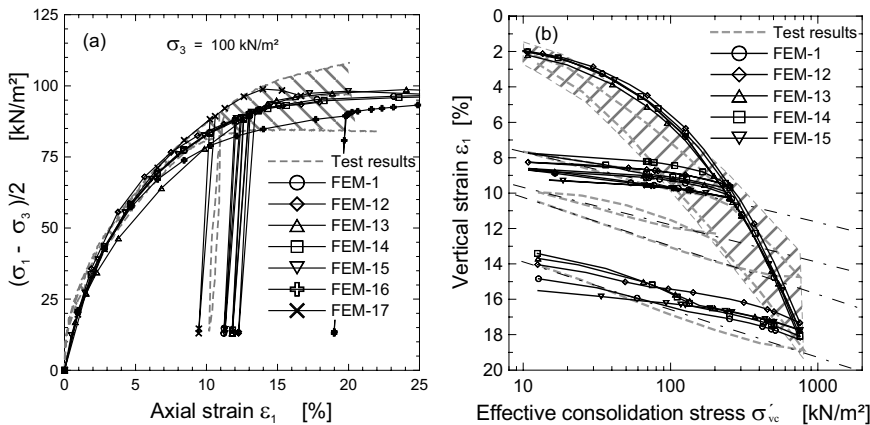


Fig. 3.30. The influence of the parameters v_{ur} , K_0^{nc} and R_f on the stress-strain characteristics of a soil specimen: a) triaxial case ($\sigma_{3,0} = 100 \text{ kN/m}^2$), b) oedometer case

Volume change behaviour. The volume change behaviour of the specimen under drained triaxial test condition has also been studied by means of varying the soil parameters of the hardening soil model. The results of the element study against the test results for a specimen with a confining pressure of 100 kN/m^2 are shown in Fig. 3.31. It can be seen from this figure that the range of the test results is very wide and it is difficult to compare the computational result with the test result directly. However, one can see the general tendency of the volume change behaviour from the test results and the influence of each parameter from the sensitivity study. From Fig. 3.31, it would appear that all the parameters in one way or the

other way may affect the volume change behaviour of the specimen. The most sensitive parameters with regard to the volume change behaviour, however, are K_0^{nc} and E_{50} (FEM-8, 9 & 10) and (FEM-12 & 13), and the least sensitive parameter is the ν_{ur} (FEM-14 & 15). It is interesting to see that increasing the E_{50} value above the reference value increases the volumetric strain, when one expects the opposite result.

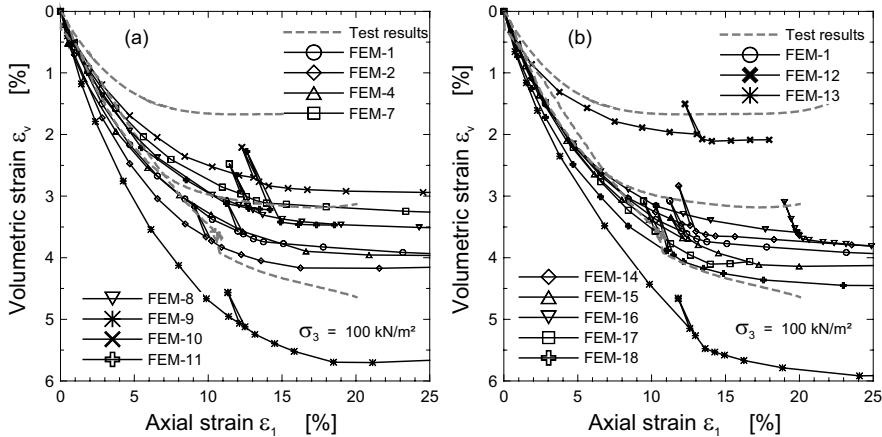


Fig. 3.31. The influence of the HSM parameters on the volume change behaviour of a soil specimen at confining pressure of 100 kN/m^2 : a) stiffness parameters: E_{50} , E_{oed} , E_{ur} and m , b) other parameters: ν_{ur} , K_0^{nc} and R_f .

Adjusted parameters. The computational result after a slight adjustment of the parameters (FEM-23) according to the foregoing parameter studies are shown in Fig. 3.32.

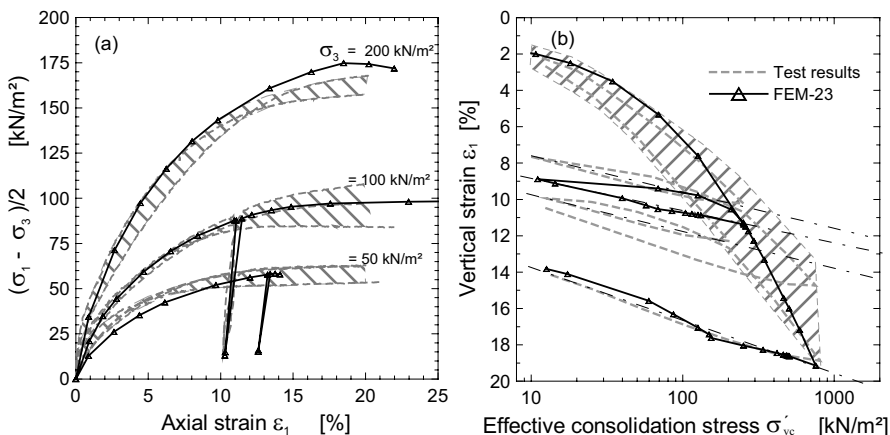


Fig. 3.32. Adjusted soil parameters for the case of drained condition

3.3.2 Undrained test behaviour

In PLAXIS FE-program it is possible to perform undrained analysis using the effective shear and stiffness parameters. The program calculates the rate of the excess pore water pressure from the volumetric strain rate according to:

$$\dot{\sigma}_w = \frac{K_w}{n} \cdot \dot{\varepsilon}_v \quad (3.46)$$

where $\dot{\sigma}_w$ is the rate of the excess pore water pressure, K_w is the bulk modulus of water, $\dot{\varepsilon}_v$ is the porosity of the soil, and n is the rate of the volumetric strain. The ratio in Eq. 3.46 is calculated from:

$$\frac{K_{w,ref}}{n} = K_u - K' \quad (3.47)$$

where,

$$K_u = \frac{2 \cdot G(1 + v_u)}{3(1 - 2 \cdot v_u)} \text{ and } K' = \frac{E'}{3(1 - 2 \cdot v')} \quad (3.48)$$

K_u , v_u (≤ 0.495), K' and v' are the undrained and drained bulk modulus and Poisson's ratio respectively. G and E' are the shear modulus and the effective modulus of elasticity of the soil. For detail derivations and relations regarding the calculation of the rate of the excess pore water pressure, refer to Brinkgreve and Vermeer 1998; Brinkgreve 2002.

The program accepts the effective model parameters v' , c' , φ' and E' , and calculates automatically the undrained bulk modulus using the Hook's law of elasticity according to the Eq. 3.48. Theoretically, the effective shear parameters obtained from drained and undrained tests should be the same. The test results from both test type in Fig. 3.14 may serve as a proof of this postulate taking into account the usual scatter of data expected in geotechnical tests. Hence, one has the choice to determine effective shear parameters from either of the two. It is obvious, however, that the modulus of elasticity in undrained test E_u is higher than the drained modulus of elasticity E' . Assuming a linear elastic behaviour, the two parameters can be related using Eqs. 2.70 to 2.75. To be consistent with the previous section, however, the effective parameters in Table 3.16 are adopted as a reference parameters for the FEM-simulation of the undrained triaxial test using the hardening soil model.

Similar to the drained test, the various variations of the soil parameters for the parameter study are listed Table 3.17. This is first to see whether the FEM-results match with the test results, and second to study the influence of each parameter on the behaviour of the strain-stress and excess pore pressure of the soil specimen.

Table 3.17. Variations of soil parameters under undrained loading condition.

Cases	Parameter
FEM-UD1	reference parameters (Table 3.15)
FEM-UD2	same as FEM-UD1, but $E_{oed}^{ref} = E_{50}^{ref} = 3253 \text{ kN/m}^2$
FEM-UD3	same as FEM-UD1, but $E_{oed}^{ref} = E_{50}^{ref} = 2948 \text{ kN/m}^2$
FEM-UD4	same as FEM-UD1, but $E_{ur}^{ref} = 3 \cdot E_{50}^{ref} = 9759 \text{ kN/m}^2$
FEM-UD5	same as FEM-UD1, but E_{oed}^{ref} reduced by a factor of 0.75
FEM-UD6	same as FEM-UD1, but E_{oed}^{ref} increased by a factor of 1.25
FEM-UD7	same as FEM-UD1, but $\nu_{ur} = 0.10$
FEM-UD8	same as FEM-UD1, but $\nu_{ur} = 0.30$
FEM-UD9	same as FEM-UD1, but K_0^{nc} reduced to 0.44
FEM-UD10	same as FEM-UD1, but K_0^{nc} increased to 0.71
FEM-UD11	same as FEM-UD1, but $R_f = 0.70$
FEM-UD12	same as FEM-UD1, but with an assumed dilatancy $\psi = 5^\circ$
FEM-UD13	same as FEM-UD1, but with un/reloading phases (Table 3.15)
FEM-UD14	same as FEM-UD13, but $\nu_{ur} = 0.05$
FEM-UD15	same as FEM-UD13, but $E_{ur}^{ref} = 3 \cdot E_{50}^{ref} = 6506 \text{ kN/m}^2$
FEM-UD16	same as FEM-UD1, but E_{50}^{ref} increased by a factor of 1.25

Comparison of the undrained computational results with the test results. The comparison of the FEM-computation results of the triaxial test model under undrained loading condition with the test results of the specimens from site 1 for a range of confining pressure from 50 to 500 kN/m² are shown in Figure 7.10. To compare the respond of the FEM-simulation to the deviatoric stress and the development of the excess pore pressure in the specimen, they are presented side by side in Fig. 3.33a & b respectively. The stress paths are also shown in Fig. 3.33c.

It would appear from Fig. 3.33 that the FEM-results match badly with the test results. If we look at the result of the FEM with the reference parameters (FEM-UD1), they deviate from the test result both at the beginning of the curve and while approaching failure. The deviation of the FEM-result at the beginning of the curve may be corrected mainly by adjusting the stiffness parameters, while the main reason for the deviation of the FEM-results approaching failure is accounted to the gradual falling of the excess pore water pressure in the test after it has reached a maximum value at lower axial strain (around 5%) (Fig. 3.33b). This is a typical behaviour of a dilatant material, although the material in question is not known as dilatant material. The volume change behaviour of similar specimens in the drained tests show no dilatant behaviour. However, if one considers the angle of overall shear strength ϕ'_s , i.e. the sum of the effect of effective cohesion c' and effective friction angel ϕ' , one may come to the result $\phi'_s = 36.7^\circ, 32.2^\circ, 29.8^\circ, 28.9^\circ, 28.5^\circ, 28.2^\circ$ for confining pressure of 50, 100, 200, 300, 400, and 500 kN/m² respectively. From this result one can see that the effect of the cohesion on the overall shear strength ceases as the confining pressure increases from 50 to

500 kN/m². This in turn will have an effect on the development of the excess pore pressure, which can clearly be seen from the test results in Fig. 3.33b, where the rate of the drop of excess pore pressure ceases gradually as the confining pressure increases from 50 to 500 kN/m². The HSM in its current stand cannot simulate the drop of the pore pressure as can be seen in Fig. 3.33b.

For the matter of completeness, the effect of the assumptions $E_{oed}^{ref} = E_{50}^{ref}$ (FEM-UD2), $E_{50}^{ref} = E_{oed}^{ref}$ (FEM-UD3), and $E_{ur}^{ref} = 3 \cdot E_{50}^{ref}$ (FEM-UD4) on the FE-simulation are also presented in Fig. 3.33. The 1st assumption has no significant influence on the initial stiffness up to approximately 5% axial strain, and deviates slightly from the reference curve while approaching failure. However, it affects the excess pore water pressure right from the beginning. Obviously, the 2nd assumption has a significant influence right from the beginning, but tends to converge to the reference line while approaching failure. The 3rd assumption has considerable influence on the deviatoric stress and excess pore water pressure. In all cases of the assumptions, their influence on the deviatoric stress and excess pore water pressure increases with the confining pressure.

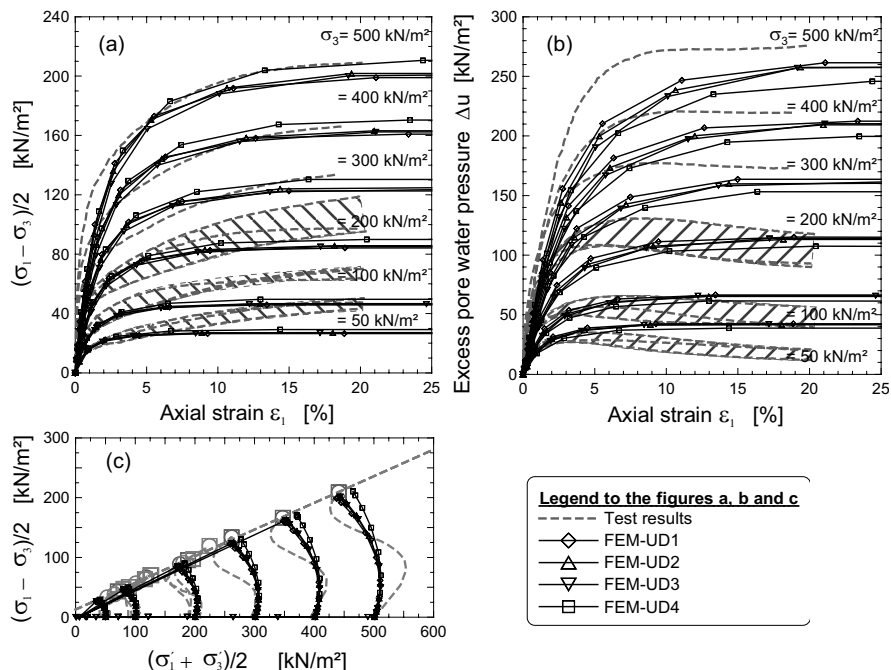


Fig. 3.33. The respond of a triaxial FEM- Model to undrained loading condition as compare to the test results: a) deviatoric stress vs. axial strain, b) excess pore water pressure vs. axial strain, and c) the stress path

The stress path diagram (Fig. 3.33c) shows that the strength parameters of the specimen remain unaffected by the various assumptions, although the deviatoric stress at failure changes. The stress at failure in the p-q diagram changes accordingly, but it remains on the failure line by shifting itself to a new position. Unlike the drained condition the deviatoric stress at failure is not only dependent on the effective shear parameters, but also on those parameters which affect the excess pore pressure. These parameters are discussed in the following section.

Sensitivity study of the model parameters under undrained loading conditions. The influence of the hardening soil model parameters under undrained loading condition has been studied by varying the parameters in the FEM-computations according to the Table 3.17 for a selected specimen with confining pressure of 100 kN/m^2 . The results of the sensitivity study are shown in Fig. 3.34. As it would appear from the figure that all the parameters in question have an effect on the deviatoric stress and excess pore pressure. The most sensitive parameter, however, is the K_0^{nc} . Varying K_0^{nc} from the default value of $K_0^{nc} = 1 - \sin \varphi' = 0.573$ to a lower value of 0.44 (FEM-UD9) and a higher value of 0.71 (FEM-UD10) results in considerable decrease/increase of the deviatoric stress and increase/decreases of the excess pore water pressure respectively, specially while approaching failure stress. The effect of the E_{s0} is more noticeable on the first part of the curve, say up to 5 to 6% axial strain for this particular test, whereas the effect of the E_{oed} , E_{ur} and K_0^{nc} is at later stage of the curve while approaching failure. It is obvious that the decrease in E_{oed} results in more compressibility of the soil, which give rise to more excess pore water pressure, in particular while the soil approaches failure as shown in Fig. 3.34 (see also Schweiger 2002).

Although the soil in question is not known to posses a dilatancy behaviour, an introduction of the dialatancy angle $\psi' = 5^\circ$ (FEM-UD12) into the FEM-computation at least shows the general tendency of the drop of the excess pore water pressure and increase of the deviatoric stress with the axial strain. However, even the introduction of ψ' did not help to follow the course of the deviatoric stress curve exactly.

Similar to what it has been discussed above in section 3.3.1, the deviatoric stress at failure remains on the failure line independent of the variation of the parameters (Fig. 3.34c). However, it shifts its position to the right or left of the reference point according to the variation of the various parameters.

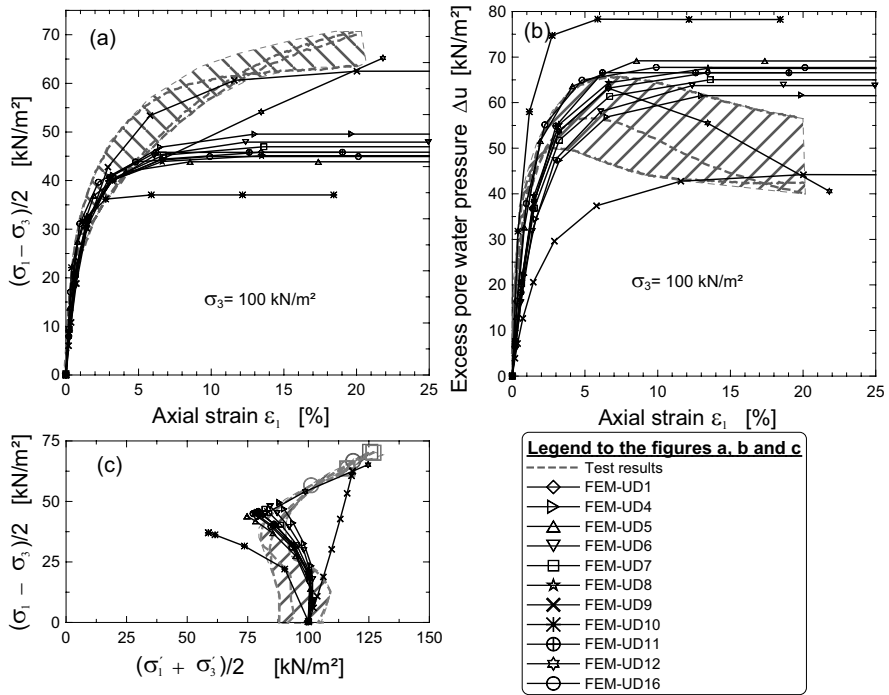


Fig. 3.34. Sensitivity study of the influence of the hardening soil parameters on the a) strain-stress behaviour, b) development of excess pore water pressure, and c) stress path of a specimen with a confining pressure of 100 kN/m²

Response of the FE-Model to un/reloading state of stress under undrained condition. A FEM-simulation of the un/reloading under undrained condition was carried out using the HSM parameters in Table 3.16. The FEM-simulation with the reference parameters (FEM-UD13) fails to respond correctly to undrained loading condition as shown in Fig. 3.35. Firstly, the un/reloading phases occur earlier than it was expected. It was assumed that the 1st, 2nd, and the 3rd un/reloading phase would occur at around an axial strain of 5, 10 and 15% respectively according to the test result. This shows that for a given stress level, the FEM-model reacts stronger than the test, which is not usually the case in the drained simulations. Secondly, the un/reloading stiffness is much higher in the FEM-result than the measured value. Since the un/reloading modulus E_{ur} is an elastic parameter, it can be approximated from the undrained un/reloading modulus $E_{u,ur}$ according to the elasticity theory using Eqs. 2.72 to 2.75.

For $E_{ur}^{ref} = 19.2 \text{ MN/m}^2$ from the drained test and $\nu_{ur} = 0.2$ one may obtain $E_{u,ur} = 24.0 \text{ MN/m}^2$, which is much higher than the measured undrained modulus (4.5 MN/m^2). If $E_{u,ur}$ from the test result will be used as a basis for the FEM-

computation by converting it to E_{ur} according to Eq. 2.74, one may obtain $E_{u,ur} = 3.6 \text{ MN/m}^2$. This value is much lower than the minimum un/reloading modulus allowed in PLAXIS, i.e., $E_{ur}^{\text{ref}} \geq 2 \cdot E_{50}^{\text{ref}}$. Obviously, the use of $E_{ur}^{\text{ref}} = 2 \cdot E_{50}^{\text{ref}}$ (FEM-UD15) will narrow the difference in the slope of the un/reloading lines between the FEM and test results (Fig. 3.35a), but on the other hand it has the effect of lowering the excess pore pressure and increasing the deviatoric stress (Fig. 3.35a & b). The considerable deviation of the FEM-computation result from the test result can also be seen from the stress path diagram (Fig. 3.35c).

The other parameters such as v_{ur} (FEM-UD14), E_{oed} (FEM-UD6), E_{50} (FEM-UD16) and K_0^{nc} (FEM-UD10) have shown no effect on the un/reloading behaviour of the soil specimen (Fig. 3.35).

The smooth reaction of the excess pore water pressure to the unloading, its stable position at $\Delta\sigma \approx 0$, its sudden rise on reloading beyond its value before unloading, and gradual drop of the excess pore water pressure observed during the test is not to see from the FEM-computation. In general, one may conclude that the simulation of the undrained test both during the primary loading, unloading or reloading using the hardening soil model is not as satisfactory as the drained test.

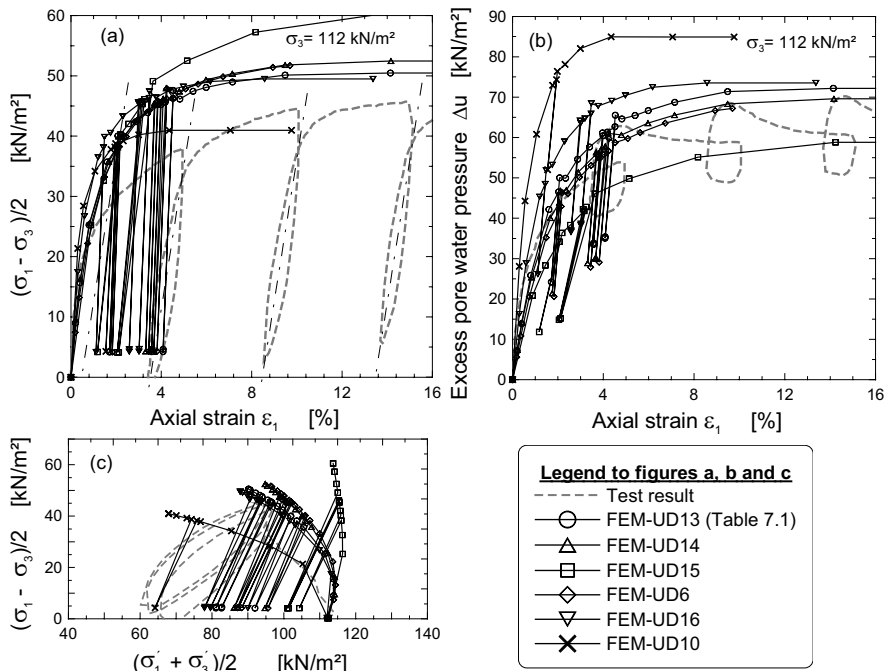


Fig. 3.35. Response of the FEM-simulation under undrained un/reloading condition: a) deviatoric stress, b) excess pore water pressure, and c) stress path

4 Supported excavations in soft soil deposits

4.1 General

The state of the knowledge regarding the excavation behaviour in soft clays has expanded substantially over the last few decades. Several excellent state of the art reports on this subject have been published (Peck 1969; Lambe 1970; Bijerrum et al. 1972; Clough and Schmidt 1977; Clough and O'Rourke 1990). Moreover excellent handbooks and textbooks, that explain the construction and design principles of excavation in more detail, such as Smoltczyk 1996; Clayton et al. 1993; Weißenbach 1985; Fang 1991; etc. are also available. The aim of this chapter is therefore not to repeat the previous works, rather to review and point out some problems of design and construction of supported excavation.

Peck 1969 summarised the experiences with performance of deep excavation support system, and the factors that are most important in controlling the performance. These factors include the type and strength of the soil around and beneath the excavation, the excavation and supporting procedure, and workmanship. Beside the above factors, the groundwater condition, the flexibility or rigidity of the components used for construction, the time taken for construction are also important factors that influence the performance of excavations. Mana 1978 classified the factors into: parameters under designer control, parameters partially under designer control, and fixed parameters not subject to designer control (Table 4.1).

Table 4.1. Factors affecting the performance of supported excavations (after Mana 1978)

Parameters under designer control	Parameters partially under designer control	Fixed parameters not subject to designer control
1. Type of support system	1. Method of support system construction	1. Subsoil conditions and properties
2. Stiffness of support system	2. Construction period	2. Surrounding structures
3. Degree of wall embedment	3. Method of construction of structures within excavation	3. Excavation shape and depth
4. Degree of pre-loading	4. Size of surcharge loads 5. Weather	

The magnitude and extent of ground movement around an excavation depends as much on the method of construction as on any of the above factor. Although the designer may specify a particular form or method of construction, the precise details of support, their sequence and timing can not be controlled accurately since

they depend on a large factor which vary from day to day on a construction site. These make the exact simulation of the construction process in numerical analysis complex and difficult. This may be one of the reasons for the discrepancy in the FE-computational results and the field measured data.

The topic of excavation and its support system is very broad. Thus, this chapter limits itself only to temporary or permanently supported excavations in urban areas and its influence on nearby structures. The term excavation is used throughout of the text to represent the supported excavation.

4.2 Unsupported excavations

An unsupported cut with free slopes in soft cohesive soils are limited to very shallow depths (max. 3 m). Independent from the depth, however, unsupported excavations require protection using different techniques, such as:

- slope protection against erosion using geotextile membrane (e.g. Fig. 4.1),
- providing a filter layer made of gravel or single-grained concrete (e.g. Fig. 4.2), whereby the filter stability requires additional attention. Geotextile filter mat, for example, may help to insure the filter stability, and
- stabilising the slope by means of vacuum drainage (e.g. Fig. 4.3)



Fig. 4.1. Sloped excavation with surface protection



Fig. 4.2. Slope protection using single-grained concrete

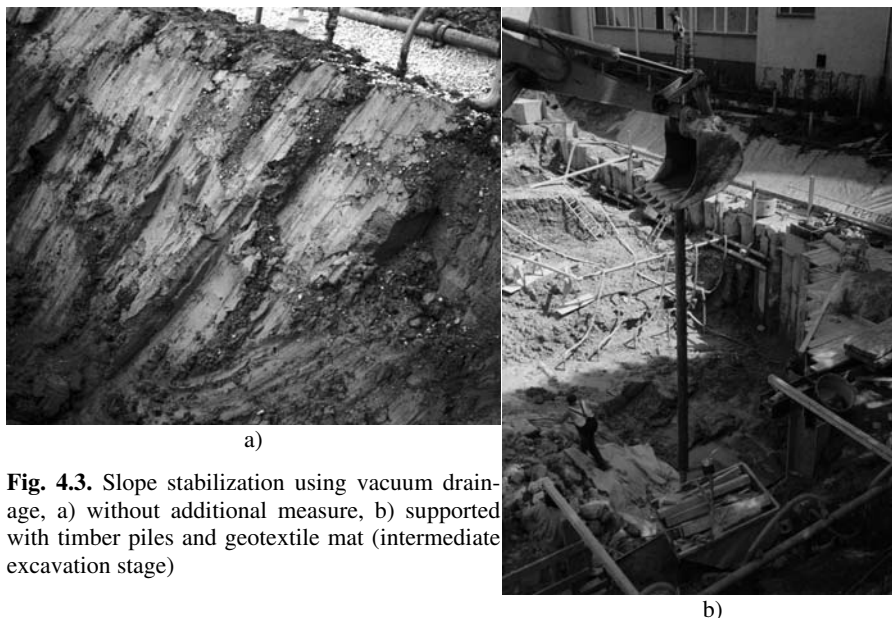


Fig. 4.3. Slope stabilization using vacuum drainage, a) without additional measure, b) supported with timber piles and geotextile mat (intermediate excavation stage)

If berms and sloped excavations remain unprotected or unstabilised, delayed slides and mass flow can occur as shown in Fig. 4.4.



Fig. 4.4. Slope slide and collapse of unprotected slope in soft soil: a) in lacustrine soils; b) in alternate peat and clay layer

The depth of excavation of unprotected excavation in soft soils should not normally exceed 3 m. A slope up to 45° (1:1) can be used for temporary slopes without a need for further verification of its safety, provided that slope is located above the groundwater. The height of a safe and long-term stable slope is also dependant on the plasticity and the undrained strength of the soft soil. Soils with low plasticity are usually prone to flow, specially when they contain a fine sand and silt seems filled with water.

By large excavation works under groundwater, a verification of the safety of the sloped excavation is necessary. Thereby, the standard safety factors or the mobilisation of the shear strength can be used, provided that the expected deformation of the soil will affect neither buildings nor pipe lines, other structures or streets.

In all other cases and deep excavations in soft soils, providing support to the excavation using wall systems, struts, anchors, raking props, bottom slab, etc. is necessary and cannot be ignored.

4.3 Excavation retaining systems in soft soils

4.3.1 Type of wall

The components making up a retaining structure can be broadly classified into: facings and supports. The common type of facings include: Kingposts and planking (braced excavation), bored piles, diaphragms, and steel sheeting. Kingpost and planking include: steel H-sections (solder piles) with timber sheeting and bored piles with gunnite and mesh facings, and the contiguous, secant and tangent piles belong to the bored piles group. The main differences between the different types of walls are: the construction technology, the material in which they are made of, and the flexibility and rigidity of the wall. The feasibility of any construction method depends to a great extent upon the ground and groundwater conditions at the site, and upon locally available skill, equipment and experience. For excava-

tions in normally consolidated soft clays, stiffer walls such as diaphragms and bored pile walls are usually recommended. However, even with stiffer walls, it is practically impossible to completely eliminate the ground movements in and around an excavation in soft soils (Palmer and Kenny 1972; Burland et al. 1979; Fujita 1994).

After statistically analysing the data from literature about construction and performance of deep excavation support systems since 1962, Duncan and Bentler 1998 reported that the percentage of excavations supported by sheet piles have decreased over time, while the percentage of excavations supported by diaphragm walls and other walls (mainly secant, tangent and contiguous pile walls) has increased steadily. They also found that settlements and horizontal movements due to excavation are tending to decrease with time. This improvement in performance is likely related to more frequent use of stiffer walls, such as concrete diaphragm walls and greater care in construction. The introduction of bentonite technology to a new area of the world, the rapid change in boring and excavation techniques and the fact that they can deal satisfactorily with difficult soil conditions, greatly contribute to the frequent use of the diaphragm and bored pile walls.

4.3.2 Type of wall support

Tie back anchors, ground anchors, struts, props or rakers, berms, basement floors (in top down construction), and soilcrete-slab (jet grouting) are the most common types of support systems. These support systems are schematised in Fig. 4.5. The relative rigidity of these components and the facings, and their interconnection and packing, is important in determining the amount of ground movement, and thus the reduction in ground pressure, and the forces and stresses applied to a wall.

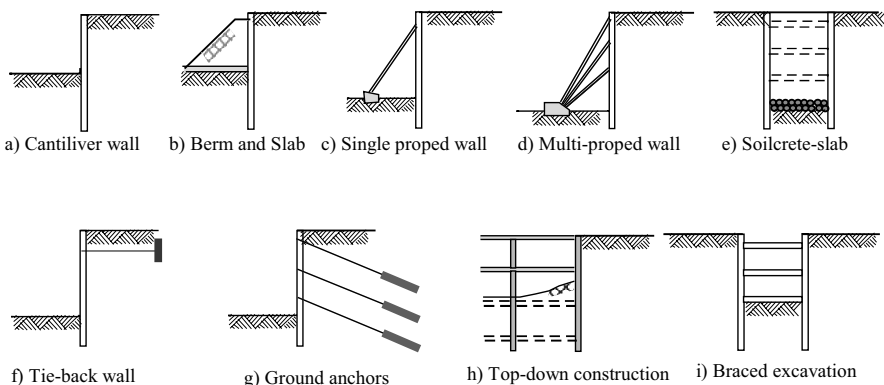


Fig. 4.5. Common types of wall support schemes

Duncan and Bentler 1998 indicated that there is a tendency to use struts more frequently than tie back anchors. This is mainly due to the problem associated with the installation of the tie back anchors, i.e., the installation of anchors might lead to settlement or heaving of the ground in built up area. Some times it may also be difficult to install tied back anchors in built up areas due to land ownership problem. The use of the top-down construction method has also increased, but still represents a small number. Though the top-down method of construction is widely known in preventing the ground movements effectively, the construction method is relative complicated and there is very limited experience available in practice.

4.3.3 Recommendations for retaining structures according to EAB

Some parts of the German recommendations for excavations in soft underground are introduced in section 4.11 (EAB 2006). One more recommendation regarding retaining structures in excavations in soft soils, namely EAB EB 92, is presented briefly in the following. It provides guidelines for selection of the appropriate support system for excavations in soft soils.

If there is a limited space due to existing buildings, pipe lines, other structures or other reasons and the excavation cannot be executed with sloped excavation according to section 4.2, the excavation has to be supported by appropriate retaining structure braced by struts or tied back by anchors. A wall system appropriate for excavations in soft soils is the one whose installation process does neither result a significant deformations in the surrounding soil nor in the nearby structures. Basically, the following wall systems are appropriate for excavations in soft soils: sheet pile wall (e.g. see Fig. 4.6), bored pile wall (tangent or secant) (e.g. see Fig. 4.7) and diaphragm wall. Normally, soldier pile walls with timber, concrete or gunite (shot-crete) sheeting between the piles placed in the course of the excavation are not suitable as support system for excavations in soft soils (Fig. 4.8).



Fig. 4.6. Braced sheet pile wall



Fig. 4.7. Protection of existing building near an excavation using tangent pile wall



Fig. 4.8. Problems with soldier piles in excavation in soft lacustrine soil

During sheet pile installation special attention is required, so that the effect of vibration on the nearby building shall be kept minimum as much as possible. The old buildings on soft underground are usually founded on shallow foundation and they may already been suffered from settlements, which is related to a higher strain in the underground hence posses very limited deformation reserve. The risk of soil flow and hence settlement problems in neighboring buildings is higher by vibration type of installation than by driving type. In specific cases, the following requirements have to be satisfied:

a) When installing sheet pile wall using impact hammers, the impact energy per blow and the frequency shall be selected based on test driving as described. In general, a gentle installation of sheet piles in soft soils can be achieved, when the vibrations as result of an impact ceases before the next impact (no overlapping of vibrations).

b) Vibratory installation methods are not at all suitable, when the underground is found to be sensible to vibrations, possesses thixotropy character or some sand and silt seems filled with water are present in the layer. In soft soils with a higher

plasticity or lightly sensitive to vibrations, sheet piles can be installed using the vibratory method, however, the oscillatory speed should be reduced to its minimum value as much as possible. For this purpose, a test vibratory driving is necessary. Experiences show that nearby buildings may suffer least from the vibration, when the sheet pile is driven with a frequency of more than 2000/min. Moreover, a large vibration effect on the nearby structures during turning on/off of the motor should be avoided by using a vibrator with variable out-of-balance masses.

c) Sheet pile installation by pressing is particularly suitable in homogenous soft soils without any obstacles. Top soils with high pressing resistance such as fill material composed of building rubble shall be removed first by means of boring, trench excavation or soil exchange before pressing the sheet pile.

Guidelines for installation of pile walls can be found in DIN EN 1536. Following are additional information in regard to pile wall installation in soft soils.

a) For the installation of single piles of a bored pile wall, a vibration free boring method has to be adopted. Moreover, a loss of material and softening of the soil surrounding the borehole due to the boring process must be avoided, e.g. by means of:

- advancing the casing below the drill pit with an offset higher than that requirement in DIN EN 1536,
- avoiding a drill pit that has a size in excess of the diameter of the casing,
- using drill pit with sharp cutting edge but no chopper end,
- using boring tools that exercise no or minimum suction effect on borehole base.

Moreover, it is necessary to keep a constant water pressure in the borehole according to the recommendation of DIN EN 1536.

b) Basically, the following construction arts come to question for pile walls in soft soils:

- bored pile walls with secant piles,
- bored pile walls with intermittent piles where the interpile gaps will be filled with small diameters usually unreinforced piles on back side,
- bored piles with tangent piles, where the space between the piles can be filled in the course of the excavation.

The unreinforced secondary piles have to be extended deep enough until the necessary safety can be achieved against basal or hydraulic failures.

c) In selecting the type of construction, the following points require attention:

- The cutting of the primary piles in secant type of pile wall is only possible so long the concrete is not fully set. Moreover, an extra offset for the casing below the borehole base is not possible,
- Though the squeezing of the soft soil between unavoidable interpile gaps in tangent piles can be prevented by pushing timber wedges, the lowering of the groundwater to certain extent cannot be fully avoided. Moreover, there will be a risk of a hard impact and vibrations, when the drill pit encounters an outgrowth of the already installed neighboring pile. Furthermore, this type of construction method assumes a soft soil above the bottom of excavation only.

d) Piles can also be installed using uncased borings supported by suspension slurry similar to diaphragm wall. However, auger boring is not suitable for pile walls due to the danger of loosing the surrounding soil.

e) Provided that the undrained shear strength $c_u \leq 15 \text{ kN/m}^2$ and the consistency index $I_c \leq 0.25$, concreting the soil immediately is not allowable according to DIN EN 1536. However, this can be ignored for the part of the pile wall above the excavation bottom, provided that the wall will be carefully examined for possible failure spots while exposing during excavation.

Guidelines for construction and design of diaphragm walls in general can be found in DIN 4126 and DIN EN 1538. Here are some more information in connection with soft soils.

a) The minimum distance to the neighboring building, specially by highly loaded gable foundations, should be more than half of the depth of the diaphragm wall or at least 5 m or the wall should remain outer the rupture surface of the nearby foundation.

b) No arching effect has to be considered in the verification of the stability of the trench filled with suspension in soft soil. Therefore, the suspension pressure in the soft layer

$$\sigma_s = \gamma_F \cdot z \quad (4.1)$$

at any depth z should be at least 10% higher than the total horizontal pressure

$$\sigma_h = e_a + w \quad (4.2)$$

where e_a is active earth pressure according to Eqs. 4.4 and 4.6 and w is the water pressure.

When necessary the suspension pressure can be increased, for example, by providing a guide wall or by using a suspension with a higher density.

c) The safety of the trench filled with suspension against sliding of single soil grains into the slurry and the sliding of the active wedge into the trench as well as the composition of the slurry should be examination by means of a test pilot.

d) Furthermore, the succession of the trench, the pressure of the fresh concrete and the concreting technics will have an influence on the performance of the soft soil (Schäfer and Triantafyllids 2004)

The wall installation shall begin at location far away from the nearby structures but within the premises of the project on trial base and has to be optimized through investigations carried out parallel, e.g. concrete consumption, integrity checking, vibration and settlement measurements.

Basically, struts are less yielding than anchorage (Fig. 4.6). If, however, ground anchors are used, the grout part of the ground anchor shall be located deep in bearing layer. The same precondition will apply for anchors tied back with concrete block. Moreover, the anchor installation should not result a loss of material and softening of the soft soil (Fig. 4.9).



Fig. 4.9. a) Back anchored pile wall for protection of existing building near an excavation (see also Fig. 4.7); b) anchor boring with the help of casing for the part of the anchor hole in the soft soil layer

Independent from the type of support system, the working place for the installation of the walls has to be prepared in such a way that the soft underground will not loose its strength and tends to flow. In the absence of a load bearing fill layer at top, the soft soil has to be protected as much as possible or it has to be exchanged by bearing material. Moreover, construction equipment with minimum effect on the soft underground due to e.g. vibrations and contact pressure has to be adopted for the installation of walls, anchors and bottom slabs. If necessary a rigid mat can be used on the top of the soft soil to distribute the load uniformly from the equipment down to the soft soil.

4.4 Behaviour of excavations

4.4.1 General

In soil mechanics the two common limits occur due to:

- shear failure of the soil, leading to excessive distortion of a structure or a disruption of highways and services;
- excessive displacement of the soil, inducing unacceptably high stresses in a structure as a result of differential movement.

For retaining structures, failure is a performance problem, related to either strength or deformation. A retaining structure can fail to perform in a satisfactory way for a number of reasons, associated with the failure of the structure itself, failure of the soil or because of unacceptable deformation.

Some possible failure situations in retaining structures are shown in Figure 4.10. In general, the design of a retaining structure should consider the following points: moment equilibrium of the system (overturn), horizontal force equilibrium (sliding), vertical equilibrium (bearing capacity), overstress of any part of the structure (bending or shear), and the general stability of the soil around the structure (slope failure, overall stability, basal stability). The stability of the structure

should be satisfactory both in short-term and in the long-term. Because many retaining structures are associated with decreased level of total stress, it is normal to carry out long-term analysis in terms of effective stresses and effective strength parameters. This will normally give the worst conditions (Clayton et al. 1993).

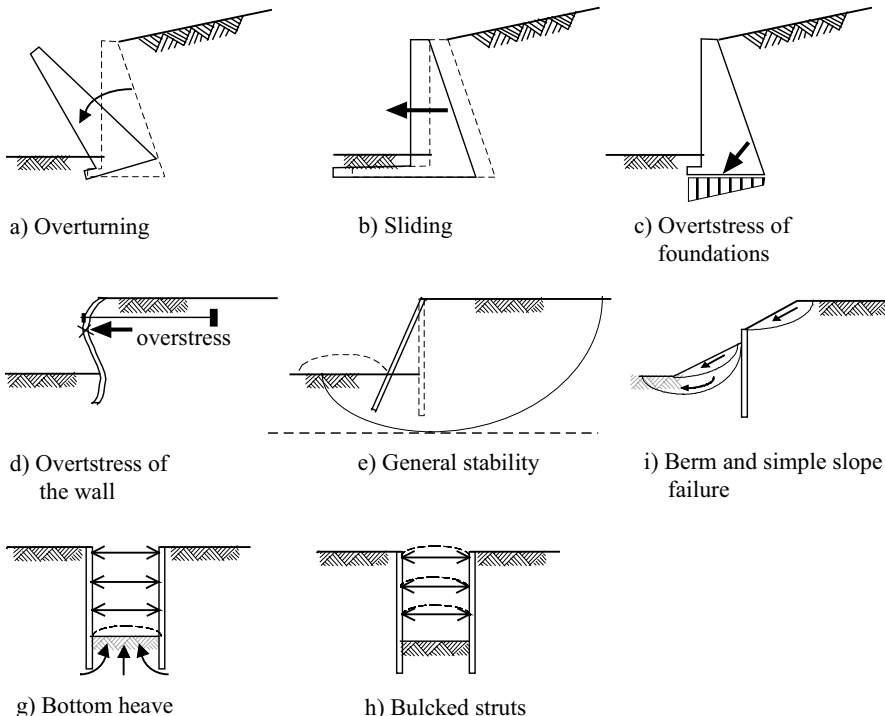


Fig. 4.10. Common types of Failures in supported excavations

On the other hand, a retaining structure may perform unsatisfactorily because of the excessive displacement it undergoes. It is seldom possible to predict such movements of the retained ground with any degree of confidence analytically. To limit the excessive displacement, it is common to apply a large factor of safety against failure to the critical area. For example a total factor of safety of 1.5 to 2.0 (EAB 1994) is applied on the passive resistance to reduce tilt and lateral displacement of the wall in sands and stiff clays.

The design of a retaining wall include the selection of the type of the retaining wall, determination of the depth of penetration of the wall, determination of the section size of the wall, determination of the strut or anchor load, prediction of the deflection of the wall and ground movements, and checking the stability of the excavation. In the following subsequent sections, the most important components of retaining structures design, namely a) earth pressure, strut and anchor load, and bending moment of the wall, b) ground movements in and around an excavation,

c) stability of retaining structures, in particular basal stability, and d) safety factor in the design of retaining structures are presented.

4.4.2 Earth pressure, reaction and section forces

Earth pressure

Pradel 1994 grouped earth pressure computations into three categories:

- a) Methods based on the theory of plasticity determine stresses assuming that plastic failure is fulfilled either in the whole mass or along specific lines or surfaces. They can be divided into slip line (Brinch-Hansen 1953; Sokolovski 1960), lower bound (Rankine 1857; Arai and Junk 1990) and upper bound methods (James and Brandsby 1971; Chen 1975).
- b) Methods based on extreme conditions select a slip surface and then determine the forces acting on the boundaries of the earth mass. The definite slip surface is the one that gives the maximum or minimum earth pressure (Coulomb 1773; Janbu 1957; Bang 1985).
- c) Methods based on constitutive soil models can be used to characterize the stress-strain behaviour of a soil. Using the numerical techniques such as FEM, the values of stresses and deformations can be found throughout the soil mass. This method requires extensive testing to obtain the constants of the constitutive models and access to a sophisticated computer program.

Whatever the method used, the lateral earth pressure on a retaining structure depends on several common factors. These include: the physical properties of the soil, the time-dependent nature of the soil, the imposed loading, the interaction between the soil and retaining structure at the interface, and the general characteristics of the deformation in the soil-structure composite.

Traditionally, the Rankine's method is typically used to compute the earth pressure distribution in normally consolidated cohesive soils. Table 4.2 shows the different formulas (Eqs. 4.3 to 4.7) used to calculate earth pressure at different state condition and type of analysis, where K_0 is the coefficient of earth pressure at rest (see section 2.4.2.), K_a and K_p are the coefficients of active and passive earth pressure respectively and they depend on the effective friction φ' , the wall friction δ , the geometry of the wall and the retained soil and the effective cohesion c' , γ' is the effective unit weight of the soil, z_a is the depth to the point of interest from surface, $z_c = 2 \cdot c' / \gamma' \cdot \sqrt{K_a}$ is the depth to the tension crack from the surface, z_p is the depth from bottom of excavation downward, σ'_z is the vertical effective stress at depth z_a , and c_u is the undrained shear strength of the soil.

Table 4.2. Formulas for lateral earth pressure calculations

Type of analysis	State	Equation	Equation No.
Effective	Rest	$e_{0h} = K_0 \cdot \gamma' \cdot z_a$	(4.3)
Effective	Active	$e_{ah} = K_a \cdot \gamma' \cdot (z_a - z_c)$	(4.4)
Effective	Passive	$e_{ph} = K_p \cdot \gamma' \cdot z_p + 2 \cdot c' \cdot \sqrt{k_p}$	(4.5)
Total	Active/Passive	$e_h(z) = \sigma'_z(z) \mp 2 \cdot c_u$	*
Total	Active/Passive	$e_h(z) = \sigma'_z(z) \mp 2 \cdot \lambda_{cu} \cdot \sigma'_{vc}$	(4.7)

* (-) Active, (+) Passive

The undrained shear strength c_u is usually normalized by the effective consolidation pressure σ'_{vc} to give a dimensionless constant λ_{cu} . Kempfert and Stadel 1997 rewrite Eq. 4.6 by replacing $c_u = \lambda_{cu} \cdot \sigma'_{vc}$ and the new equation is given by Eq. 4.7. λ_{cu} is found to fall within a range of values for normally consolidated cohesive soft soils (see section 2.5.3). The shear strength parameters required to calculate the earth pressures should be obtained from the corresponding laboratory or field tests. If the undrained shear strength is obtained from field vane test, the value should be corrected by a factor to account for the effect of the strain rate and anisotropy on the strength of the soil (see section 2.5.3). The choice which type of analysis to use for a particular type of excavation depends on factors such as the construction time, the drainage conditions, the stress path and soil type.

In order to reduce or increase the earth pressure from “at-rest” condition to an active or passive earth pressure state respectively, a certain amount of wall movement is required. The amount of the movement required to activate the active or the passive earth pressure depends on the type of the wall movement pattern. There are four types of wall movements patterns recognized in the literature. These are: rotation of the wall about the toe, rotation of the wall about the top, deflection of the wall, and lateral translation of the wall. Most often, a combination of the above movement pattern may also takes place. The movement required to reach extreme pressures depends on the type and density of the soil. The movement required to reach the passive state is of the order of ten times as large as the movement required to reach the active state (Clough and Duncan 1991). Much experimental work has not been done on the effect of wall movement on earth pressure in clays in general let alone in soft clay. On the other hand, a lot of experimental works have been conducted on sand. Bjerrum et al. 1972 stated that the movement of the wall required to reduce the lateral pressure in soft to medium clays to its active value is of the same order of magnitude as those observed in sand and amounts to 0.1 - 2% of the depth of excavation. After revising different model studies on sand, Weissenbach 1985 agreed that a minimum average value of wall movement of 0.1% of the depth of excavation is required to reduce the pressure from rest condition to active state. He further asserted that for soft cohesive soils the normal wall movements are sufficient enough to reduce the lateral earth pressure to its active state. Das 1987 indicated that the amount of wall

movement required to reach the passive state in the case of rotation of the wall about toe of the wall in soft clay is about 5% of the depth of penetration.

The type of wall movement pattern will also have an influence on active and passive pressure distributions. Fig. 4.11 shows the distribution of active earth pressure for different wall movements in an excavation supported by sheet pile wall. Except for the case of the fixed end cantilever wall (Fig. 4.11a), the earth pressure distributions deviate from that of Rankine. These differences are mainly caused by the arching effect as a result of non-uniform deformation of the soil mass. In a braced excavations the amount of arching is controlled by the magnitude of deformations in the soil beneath the excavation relative to those of the struts (Bjerrum et al. 1972). For tied back flexible sheet pile walls, the amount of arching is controlled by the deflected shape of the wall and anchor yield. It increases with increasing the deflection of the wall and decreases with an increase in anchor yield. A typical active earth pressure distribution in a tie-back wall is shown in Fig. 4.12. As it can be seen from Figs. 4.11 and 4.12, the total resultant active pressure is approximately equal to the resultant of the Rankine active earth pressure calculated over the entire depth of the wall, provided that the wall movements are large enough to induce active earth pressure state (Bjerrum et al. 1972; Mana 1978).

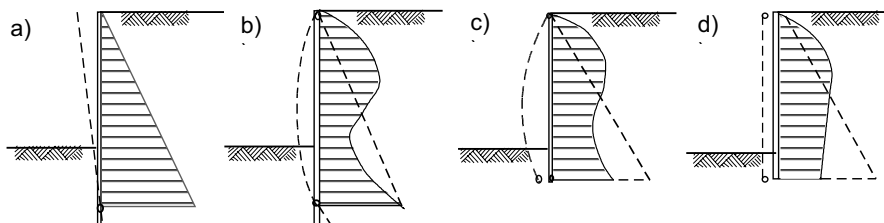


Fig. 4.11. Effect of wall movement on active earth pressure distribution behind a sheet pile wall: a) fixed end cantilever wall, b) fixed end and supported at the top of the wall, c) free end and supported at the top, and d) free end and supported at several positions (after Weisenbach 1985)

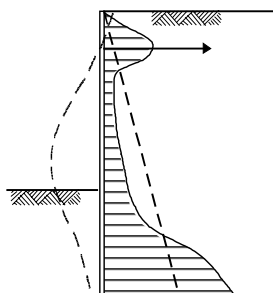


Fig. 4.12. Typical active pressure distribution behind a flexible wall

Collective works of different authors on the effect of wall movement on passive earth pressure distribution in sand can be found in Weissenbach 1985. Most of the works indicate that the passive earth pressure distribution is more or less parabolic; concave downward when the wall rotates about toe of the wall (Fig. 4.13a) and concave upward when the wall rotates about top of the wall (Fig. 4.13b). For the lateral transition of the wall, the passive distribution remains more or less linear (Fig. 4.13c).

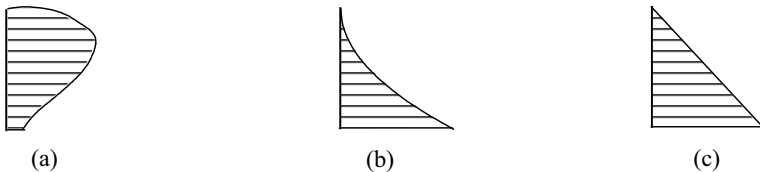


Fig. 4.13. Art of the passive earth pressure distributions dependent on the wall movement patterns: (a) rotation about the bottom, (b) rotation about the top, and (c) lateral translation of the wall

Reaction forces

The pressure exerted against bracing is different from that usually assumed for retaining walls for the reasons explained in the previous section. Most design of braced excavation is made based on empirical methods developed from field tests data. The most widely used load diagram for struts and anchors in soft to medium clay (undrained condition) is that recommended by Terzaghi and Peck 1967 and later modified by Peck 1969 (Fig. 4.14). Although several load diagrams have been developed, all versions are based on the Terzaghi and Peck distributions and are somewhat similar (Mana 1978). The load diagram for rakers, however, follow the classical earth pressure distribution (Fang 1991).

As the excavation depth increases, the stability number of the layer also increases. According to Terzaghi and Peck 1967, a plastic zone begins to form in the clay near the lower corner of the excavation at about N values on the order of 3 to 4, and as N increases the plastic zone enlarges. As a result the wedge behind the cut merges with the plastic zone bounded by a surface of sliding that extends much farther from the edge of the cut and much deeper into the subsoil than normally assumed sliding surface that extends from the ground surface to the lower bottom of the cut. Correspondingly the earth pressure increases. For this reason, Terzaghi and Peck introduced a reduction factor m (Fig. 4.14). As far as N does not exceed 4, m can be taken as unity. However, if N exceeds 4 and the plastic zone could form freely below the bottom of excavation, m can be assumed as less than unity. A value of m as small as 0.4 is possible. Peck 1969 had modified the above as follows: $m = 1$ for $N < 6$ to 8, and $m = 0.4$ for $N > 6$ to 8 provided that the soft clay extends to a great depth below the cut. Omitting the reduction factor m and introducing a new stability number N_b for the soil below the cut, Peck et. al.

1974 recommended that as far as $N_b < 7$ the strut loads can be determined from the conventional diagram in Fig. 4.14 even for values of N as great as 10 to 12, however, the width of the diagram should not be less than $0.4 \cdot \gamma \cdot h$ regardless of the value of N . When N_b exceeds 7 and base failure is imminent, no recommendation is given except that the strut loads could be much larger than those determined from the conventional diagram. After studying the case of the load diagram using the finite element method, Mana 1978 believed that the recommendation by Peck et al. 1974 is reasonable.

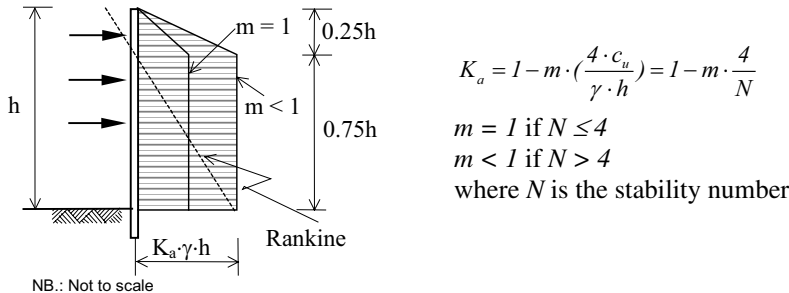


Fig. 4.14. Apparent pressure diagram for calculating strut loads in soft to medium clays (after Terzaghi and Peck 1967)

The apparent pressure diagram by Terzaghi and Peck was developed for flexible structures and does not include the effect of the position of the struts or anchors and number of the struts. On the other hand, the German working group “Excavation” (EAB) recommends apparent pressure diagrams that incorporates the influence of the above factors. The shape of the diagram varies from simple rectangular to trapezoidal distribution according to the position of the struts, the number of the struts, and type of the structure. Table 4.3 summarizes the EAB recommendations for non cohesive and stiff clays. The superposition is based on the assumption that the resultant pressure on the struts is equal to that computed from classical theories.

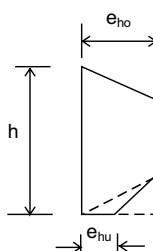
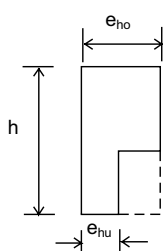
Section forces

According to Simpson 1992, there are two methods of determining the bending moment of the wall. These are:

- The bending moment is calculated by taking the full strength of the soil, i.e., safety factor equal to unity, and multiplying the maximum bending moment by a factor of 1.4 or 1.5 for ultimate design of the wall section; or
- The depth of penetration is determined using the stability requirement, i.e., applying the appropriate factor of safety (see section 4.6) and using the derived bending moment directly for ultimate limit state design. This often gives a higher bending moment than method (a).

Table 4.3. Apparent pressure diagrams for supported excavations in sand and stiff clays according to the recommendation of EAB 1994

Support condition	Location of the support from wall top	Shape of the apparent pressure diagram	Location of the change in the apparent pressure diagram	e_{ho} / e_{hu}	
				Soldier piles	Sheet piles and cast in-situ walls
single support	1) $\leq 0.1 \cdot h$	Rectangle	uniform	1.0	1.0
	2) between $0.1 \cdot h$ and $0.2 \cdot h$	Two rectangles	$0.5 \cdot h$	>1.5	>1.2
	3) between $0.2 \cdot h$ and $0.3 \cdot h$	Two rectangles	$0.5 \cdot h$	>2.0	>1.5
double support	1) when the first support is near the top of the wall and the second support is within the top half of the excavation dept 2) when the first support is near the top of the wall and the second support is about half of the excavation depth 3) when both struts are located at lower position	Trapezoid	at the second support positions at the first and the second support positions	2.0	1.5
three or more supports	equally spaced supports	Rectangle or trapezoid	uniform for soldier piles; at the second support position for sheet pile walls and cast in-situ walls	1.0	1.0
		trapezoid	at the second and the third support positions for walls with three supports; at the second and the forth support positions for walls with more than three supports	∞	2.0



NB: 1) The hidden lines show the possible shapes of the apparent pressure diagram for different loading and/or wall types.

2) The ordinates e_{ho} and e_{hu} are determined in such a way that the resultant force from theoretical pressure distribution will be equal to the resultant force from the apparent pressure diagram.

Due to the fact that the earth pressures on flexible sheet piles are different from those predicted by the classical earth pressure theories, the moments in the wall are smaller than the classical theories would indicate. Rowe 1952, 1957 introduced a reduction factor based on the flexibility of the wall to reduce the maximum bending moment in the wall for excavations in sands, if the bending moment is calculated on the basis of the classical earth pressure distributions. Skempton 1953 suggested that no moment reduction is required for walls in clays. Powrie 1997 also commented that Rowe's moment reduction factor may be unsuitable for walls in clays where the in-situ earth pressure coefficient is high, because of Rowe's analysis assumes an active state in the retained soil. There is no information, however, how to apply the reduction factors for walls in soft clays or the safety factors to determine the bending moment, and thus requires a further study.

Refer also to section 4.11.5 for determination of embedment depth and section forces according to EAB "The Working Group on Excavation" of the German Society of the Geotechnical Engineering (EAB 2006).

4.4.3 Movements in and around an excavation

General

Ground movements in and around excavations are caused by changes in stress field in the surrounding material primarily due to the horizontal and vertical relief of stresses. The horizontal stress relief leads to horizontal movement of the wall and settlement of the ground around an excavation whereas as the vertical stress relief at the base of an excavation can give rise to both heaving of the soil beneath the base of the excavation and lateral movement of the wall. Moreover, driving, drilling and grouting, lowering of groundwater, overexcavation, inadequate support, timing, unpredicted traffic etc. may contribute to the total ground movements.

Ground movements can be categorised as horizontal movement (usually known as the displacement of the wall), vertical ground movement (settlement behind the wall), and heaving of the bottom of excavation.

Horizontal movements

The horizontal movements are very much a function of the mode of deformation of the wall. The mode of deformation of the wall in turn is a function of the support system, the properties of the ground and construction practice. The designer of lateral support can take account of the first two of the above factors in predicting deformations, however, factors related to construction activities tend to be unpredictable as they often arise in response to the conditions encountered on site during the excavation of the work.

The stiffness of the support system may be considered in terms of the lateral (struts, anchors), flexural (wall system) and the vertical (wall system, anchors) stiffness components. Each support system possesses a combination of these com-

ponents which determines both the magnitude and shape of the deflection. Where a system with a high lateral support stiffness is used, much of the deformation at any level within the retained ground occurs prior to installation of the lateral support and is governed by the flexural stiffness of the wall and the ground property. Burland and Hancock 1977 reported that 75 to 85 % of the observed total deformation at any depth of excavation occurred prior to the installation of the prop at that level for diaphragm wall propped by the floors of the permanent structure. Similar phenomenon was reported by Day 1994, in which significant deformations (more than 50%) were observed prior to support installation particularly over the lower half of the face in an excavation supported by soldier piles with anchor system. The movement of the ground after installation of the lateral support is governed by the horizontal stiffness of supports Day 1994. This depends not only on the stiffness of the lateral support elements but also on the point at which the load is transferred to the soil.

A significance difference in performance can also be expected between support systems where the wall is installed prior to commencement of excavation and those where the wall is constructed hand-over-hand as excavation progresses. In the case of hand-over-hand excavation, the ground movement prior to the installation of wall and support highly depends on the stiffness of the soil.

The maximum horizontal deflection of the wall can be related to the depth of excavation as shown in Fig. 4.15. According to Clough and O'Rourke 1990, on average the maximum horizontal deflection of the wall in stiff clays, residual soils and sands is about 0.2% of the depth of excavation, but there are cases where it becomes 0.5% or more. No significant differences are noted between the different type of walls in Fig. 4.15.

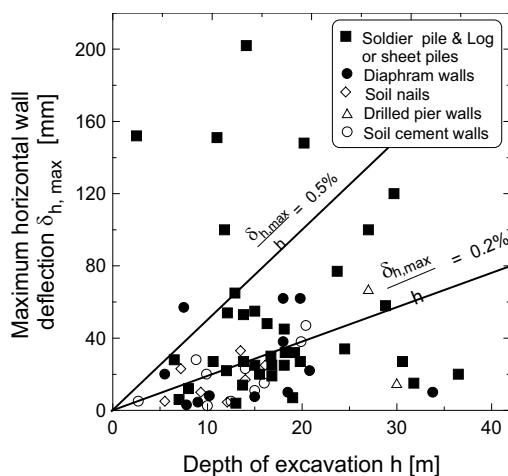


Fig. 4.15. Observed maximum horizontal deflection of wall for various wall types in stiff clays, residual soils and sands (After Clough and O'Rourke 1990)

Ground settlement behind the wall

The prediction of the ground settlement behind the wall is very important as it is directly related to the safety of the nearby structures. The ground settlement behind the wall is generally caused by one of the following:

Ground settlement induced by wall deflection during excavation. During excavation, the relief of horizontal stresses results in inward movement of the ground and the wall. The horizontal movement of wall results in the settlement of the ground behind the wall. The magnitude of the surface settlement in fact depends on the type and stiffness of the support, position of the support, and on the stiffness of the wall. For example, if the wall is permitted to deflect as a cantilever (Fig. 4.16a), the horizontal movement can be greater than the settlements (Burland et al. 1979), and the maximum settlement usually takes place directly behind the wall. On the other hand, if the wall is well propped near the surface (Fig. 4.16b), inward movements will usually take place at a deeper depth. In such cases the horizontal surface movements will be significantly less than the settlements, and the maximum settlement may take place further from the wall. In both cases the settlement profiles can be viewed as nearly parabolic curves joined by tangent lines or inflection points that can be divided into two categories: concave downward (hogging) and concave upward (sagging) (Boone 1996).

Clough and O'Rourke 1990 reported that the maximum horizontal wall movement is considered to be about 0.2% (Fig. 4.15), while the average maximum settlement is about 0.15% (Fig. 4.19) of the depth of excavation. This shows that the maximum settlement is about 75% of the wall maximum horizontal movement in a braced diaphragm or bored pile walls. They also reported that in the case of soldier piles with wood lagging or sheet piles, substantial settlement occurred behind the wall. On the other hand, Duncan and Bentler 1998 showed that there is a wide variation in the ratio between the maximum vertical settlement $\delta_{v,max}$ and maximum horizontal settlement $\delta_{h,max}$. The ratio $\delta_{v,max}/\delta_{h,max}$ varies widely between 0.25 and 4.0. This wide variation is an indication of the importance of construction procedure and construction details. Factors that contribute to large settlements do not necessarily produce large horizontal movements, but the reverse is always valid, i.e., factors that contribute to a large horizontal movement may produce large settlement.

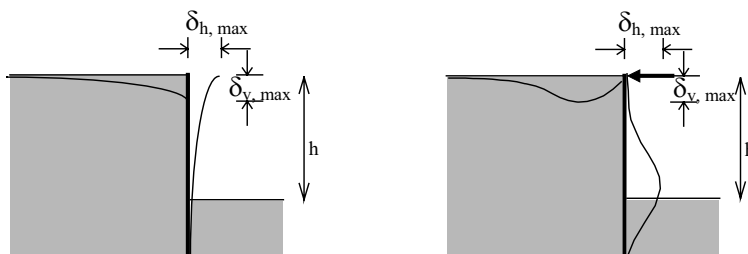


Fig. 4.16. Horizontal deflection and settlement pattern of a retaining wall: a) cantilever wall, and b) propped wall

Ground settlements induced by wall installation. Excavation walls may be of either a displacement or a replacement type. Displacement type walls are typically placed by driving either steel or pre-cast concrete sections into the soil. It is unlikely that the driving of commonly used sheet piles sections will lead to a significance change in in-situ horizontal stress conditions. However, some ground settlements are usually observed during driving or vibrating the sheet piles, and in case of temporary support, during removal of the sheet pile walls after completion of the excavation. Fujita 1994 reported that about 50% of the total settlement of the ground 2.5 m behind the wall in a 14.65 m deep braced excavation was caused during driving and extracting of the sheet piles.

On the other hand, the excavation of diaphragm wall panels or bored piles wall is certain to result in significant total stress relief, because during formation of the wall a hole, unsupported or supported by bentonite slurry, must be excavated in the soil. The total horizontal stresses on the boundary of this hole will reduce from the initial in-situ horizontal total stresses in the undisturbed soil to either zero if the hole is unsupported, or to a value which approximates to pressure exerted by a fluid with the same bulk density as bentonite (Gunn and Clayton 1992). This reduction in the total horizontal initial stresses may result in a ground movement. Moreover, the vibrations produced during boring and excavating the slurry trench may contribute to the ground movements. Burland and Hancock 1977 reported that the vertical and horizontal ground movements out-side the excavation due to the installation of the diaphragm walls and piling amounted to approximately 50% of the total movements recorded on the completion of the main design in London clay. Similarly, Lehar et al. 1993 reported that about 60% of the total settlement at the ground surface was due to the installation of the diaphragm wall constructed in Salzburg lacustrine soft clay. After studying the performance of diaphragm wall at different sites, Clough and O'Rourke 1990 also reported that the ground settlements caused by the installation of diaphragm walls, with the exception of few cases where heaving was observed, ranges from about 5 to 15mm. Fig. 4.17 shows the settlement envelope caused by the installation of diaphragm walls. Poh and Wong 1998 had observed a maximum settlement of 23.5 mm and a maximum lateral movement of 45 mm during trench excavation in a well instrumented 55.5 m deep field trial test diaphragm wall in predominantly soft soil layer.

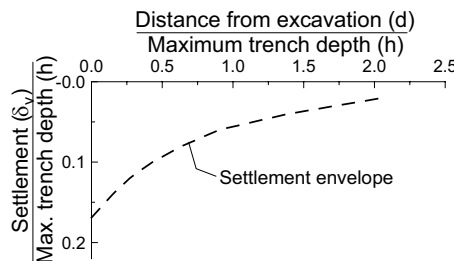


Fig. 4. 17. Ground settlement caused by installation of diaphragm walls (after Clough and O'Rourke 1990)

Ground movements induced by anchor installation. Similar to the wall installation, a hole is required to install the anchor tendons. The amount of ground movements depend on the method of drilling and material used for temporal support of the boring process. The effect can be considerable when anchoring is made in soft cohesive soil under groundwater conditions. More than 70% of the total settlement was recorded during the installation of the anchor in an excavation in lacustrine soft soil in Constance, Germany (see section 4.12.2 of this chapter and Kempfert and Gebreselassie 1999).

Ground movements induced by dewatering. The contribution of dewatering to the settlement of the ground is evident. Normally consolidated clays may settle to a far greater extent in response to dewatering than clays heavily consolidated. Schweiger and Breymann 1994 reported that about 75% of the settlement of the ground at the surface was occurred during the lowering of the groundwater in an excavation supported by diaphragm wall in Salzburg lacustrine soft soil.

Thus, the total ground settlement is the sum of the settlements induced by all of the above factors. The prediction of ground movements may be made using finite element method. With the use of realistic input soil parameters and modelling the detailed construction technique and sequences, a reasonable prediction of the ground movements may be made. Some of the effect of the above factors can be taken into account in the analysis of ground deformations using finite element method. For example, Gunn et al. 1993; De Moor 1994; Ng et al. 1995; Schweiger and Breymann 1994; Gourvenec and Powrie 1999; NG and Yan 1999 showed how to model the effect of wall installation. However, the effect of vibrations, overexcavations, delay and inadequate support, and unpredicted traffic near the excavation is difficult to take into account in the analysis of ground deformations.

Empirical methods can also be employed to estimate ground movements behind an excavation wall from graphical summaries of information from previously instrumented cuts. Peck 1969 was the first to present a summarised study of the observations of vertical movements around a number of braced excavations in various soil types in graphical form (Fig. 4.18). According to this figure, the size of the settlement behind the wall varies according to the three categories of ground. In other words, for average workmanship, the maximum settlement is less than 1% of the depth of the excavation in sand and soft to hard clay, and is more than 2% in case of very soft to soft clay with a significant depth.

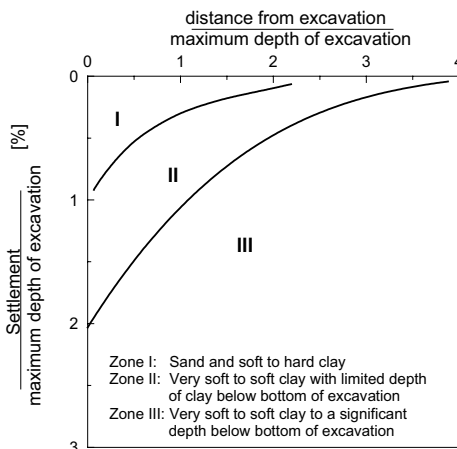


Fig. 4.18. Summary of surface settlements adjacent to braced excavation in various soils (after Peck 1969)

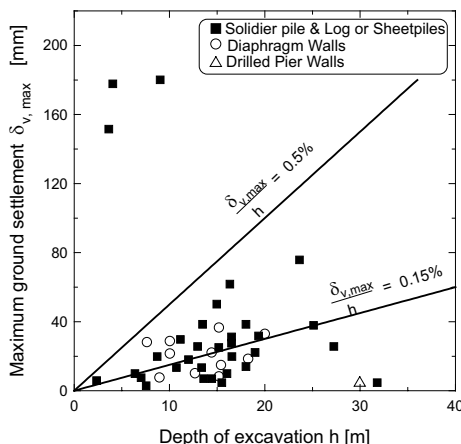


Fig. 4.19. Observed maximum settlements adjacent to excavations (after Clough and O'Bourke 1990)

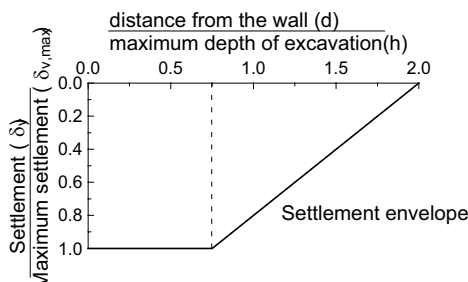


Fig. 4.20. Dimensionless settlement profile recommended for estimating the distribution of settlement adjacent to excavation in soft to medium clays (after Clough and Bourke 1990)

However, with the development of recent design and construction technologies, and frequent usage of more stiff walls such as diaphragm and bored pile walls, the magnitude of ground movement has generally declined. Clough and O'Bourke 1990 showed that on average $\delta_{v,max}/h$ is about 0.15% (Fig. 4.19) and $\delta_{h,max}/h$ is about 0.2% (Fig. 4.15). They produced a dimensionless ground surface settlement

envelope for estimating the distribution of settlement adjacent to an excavation in soft to medium clays as shown in Fig. 4.19. According to this figure, the vertical movement may extend from the edge of an excavation to a distance twice the depth of excavation for soft to medium clays. In Peck's diagram (Fig. 4.18), however, the influence extends as far as 2 to 4 times the depth of excavation in very soft to soft soils. Fujita 1994 also quoted a report from Uchida et al. 1993 that a maximum settlement of 0.08% of the depth of the excavation had occurred in a 36.6 m deep excavation in soft ground in Tokyo. Duncan and Bentler 1998 summarised the performance of excavation in soft to stiff clays since 1960 and showed that the average value of $\delta_{v,max}/h$ is 1.3% for the 1962-1975 time period, where as for the 1990-1998 time period $\delta_{v,max}/h$ is about 0.4%.

Excavation heave

Bottom heave in an excavation in normally consolidated soft soils is primarily caused by the elastic swelling of the bottom of excavation due to the relief of vertical stresses during the excavation process, the deflection of the foot of the wall which pushes the soil inwards, and the plastic deformation of the soil below the excavation level due to the change of the principal stresses. The factors that affect the heave at bottom of the excavation include the depth of excavation, the stiffness (primarily) and strength (secondarily) of the ground, and the depth to the firm layer below bottom of excavation.

The elastic part of the heave δ_{vh} can be predicted analytically from the equations shown in Table 4.4. The main difference between the three equations in Table 4.4 is that Weissenbach 1977 assumes the un/reloading modulus of elasticity instead of the modulus of elasticity for primary loading. Moreover, Eq. 4.9 takes into account the contribution of the horizontal displacement of the wall toe to the heave of the cut. This approach seems more reasonable because the soil below the cut is under unloading condition during excavation.

The stress path method (Lambe 1967; Lambe and Marr 1979) may also give reasonable estimate of the heave of the cut provided that a stress path test can be conducted in laboratory that simulate the possible stress path in the field. This method also requires the stress history of the soil deposit. Of course the best means of prediction the heave in an excavation today is the finite element method, where the heave due to stress relief, plastic deformation of the soil and the wall displacement and deflection at the foot of the wall can be evaluated simultaneously by choosing the appropriate soil behaviour model.

Table 4.4. Prediction of the elastic part of the heave at the center of an excavation

Equation	Equation No.	Reference
$\delta_{vh} = \mu_1 \cdot \mu_2 \cdot \frac{N}{\xi}$	(4.8)	Bjerrum et al. 1972
$\delta_{vh} = \frac{4 \cdot i_{si} \cdot \gamma \cdot h \cdot \Delta z}{E_{ur}} + \frac{3 \cdot s_d \cdot t}{b}$	(4.9)	Weissenbach 1977
$\delta_{vh} = C_r \cdot A_{strip} \cdot \frac{\gamma \cdot h^2}{E_u}$	(4.10)	Fang 1991

where δ_{vh} is the elastic vertical heave at the centre of the excavation; μ_1 and μ_2 in Eq. 4.8, i_{si} in Eq. 4.9, and A_{strip} in Eq. 4.10 represent the effect of the width of excavation, depth of excavation, and depth to a firm strata, though they are referred to different charts or tables according to the corresponding Authors; $N = \gamma h/c_u$ or in the case of a surcharge load p (Clough and Schmidt 1977), $N = (\gamma h + \gamma p)/c_u$ is the stability number; ξ is a constant that relate the undrained shear strength with the undrained modulus of elasticity ($E_u = \xi \cdot c_u$, and ξ usually lies between 200 and 800 (Table 3.12) for normally consolidated soft clays); Δz is the thickness of the soil below the cut; t is the depth of penetration of the wall; s_d is the horizontal displacement of the foot of the wall, C_r is a shape factor, E_u and E_{ur} are the undrained modulus of elasticity for loading and unloading.

4.4.4 Excavation stability in soft soils

The stability failure modes: the failure of berm and slopes surrounding the excavation, deep-seated rotational type failure and basal heave failure are among the possible mode of failure in an excavation in soft clays shown in Fig.4.10. Most often, the stability failure may not show a complete collapse, rather manifests itself in large movements. The stability of berms, slopes surrounding excavations, and deep-seated rotational failure can be checked using the common type of conventional slope stability analysis methods. A revision of the different approaches for stability analysis of braced excavations in soft soils according to total safety concept is given in the following. More information on basal and sliding failure of braced and anchored excavations, in particular based on the partial safety concept can be found in section 4.11.6.

A special procedure is usually adopted to check the stability of an excavation against basal heave failure. Heave failure is caused by the relief of the vertical stress during excavation. Several basal heave analysis methods have been suggested in literature, however, only four of them will be presented here, because most of them are based on similar principles. Terzaghi 1943 was the first to develop a method for bottom heave analysis for shallow or wide excavation ($h/b < 1$) as shown in Fig. 4.21. For $r > b$, the factor of safety against basal heave is given by

$$F.S. = \frac{5.7 \cdot c_u}{h \cdot \left(\gamma - \frac{c_u \cdot \sqrt{2}}{b} \right)} \quad (4.11)$$

and for $r < 0.7b$

$$F.S. = \frac{5.7 \cdot c_u}{h \cdot \left(\gamma - \frac{c_u}{r} \right)} \quad (4.12)$$

where c_u is the undrained shear strength of the soil, γ is the unit weight of the soil, and h , b , and t are the depth of the excavation, the width of the excavation and the depth to firm layer respectively as shown in Fig. 4.21.

Later, Bjerrum and Eide 1956 developed a method for bottom heave analysis for deep braced excavations in soft clays (Fig. 4.22a). It is given by

$$F.S. = \frac{N_c \cdot c_u}{h \cdot \gamma + p} \quad (4.13)$$

where N_c is the bearing capacity coefficient (Fig. 4.22b) and p is the surcharge load. Both methods above are developed based on the principles of bearing capacity failure of the clay below the excavation level while neglecting the effect of support flexibility above the excavation level and the influence of the stiffness and depth of the wall below the excavation.

Based on similar principle as the above methods but assuming different shape of the failure zone (Fig. 4.23), considering the friction force between the moving block above the excavation level and the rest of the retained soil, and taking into account the depth of penetration of the wall, Weissenbach 1985 formulated the safety factor against basal heave failure as:

$$F.S. = \frac{P_G + R_v}{G + P} \quad (4.14)$$

where $G = b_g \cdot (h + t) \cdot \gamma$, $P = p \cdot b_g$, $R_v = E_{av} + K_v$, $E_{av} = E_{ah} / \tan \varphi$, $K_v = c \cdot (h + t)$, $P_G = (\gamma t \cdot \lambda_t + \gamma b_g \cdot \lambda_b + c \cdot \lambda_c) \cdot b_g$, E_{ah} is the horizontal earth pressure force on the right side of the sliding block (Fig 4.23), and λ_t , λ_b and λ_c are the bearing capacity coefficients according to DIN 4017-1.

Since the determination of the values of G , P and P_G require the value of b_g which is unknown, the factor of safety should be calculated for different value of b_g until a minimum safety factor is obtained. According to Weissenbach 1985, the length of the failure surface $l_g \leq b + 0.5 \cdot b_g$ (Fig. 4.23) is the critical situation and $l_g \geq b + 0.5 \cdot b_g$ is impossible.

On the other hand, Kempfert and Stadel 1997 proposed a method based on the principal of virtual work done for analyzing the basal heave failure in wide exca-

vations ($h/b < 1$) in normally consolidated soft clays. The failure mechanism is shown in Fig. 4.24. The safety factor against basal heave is thus given by

$$F.S = \frac{c_{u1} \cdot (3 \cdot t + h) + 6.87 \cdot r \cdot c_{u2}}{r \cdot \sqrt{2} \cdot (h \cdot \gamma_r + p)} \quad (4.15)$$

where c_{u1} and c_{u2} are the undrained shear strength of the soil above and below the excavation level respectively. Kempfert and Stadel 1997 recommended that the value of c_{u1} on the passive side should be reduced by half in order to account for the effect of the inherent anisotropy on the strength of the soil. They further suggested that if the wall is made up of bored piles and the firm strata is at relatively shallow depth below the excavation level, it is recommended to extend some of the piles up to the firm layer in order to reduce the danger of the basal heave failure.

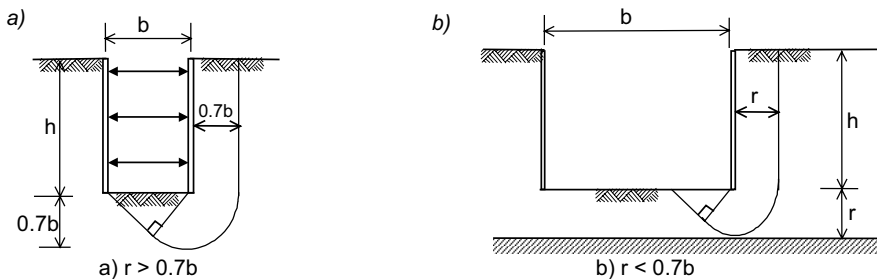


Fig. 4.21. Bottom heave analysis for deep excavations ($h/b < 1$) (after Terzaghi 1943)

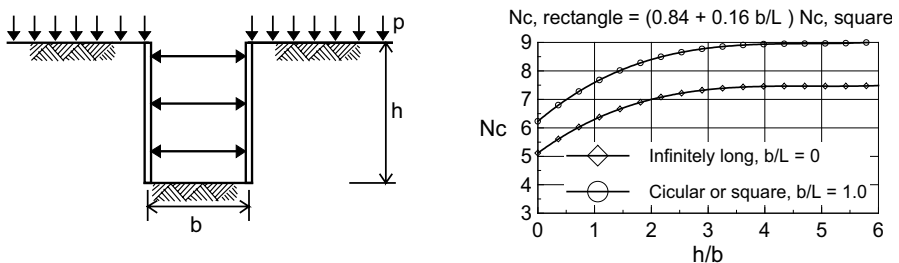


Fig. 4.22. Bottom heave analysis for deep excavations ($h/b > 1$) (after Bjerrum and Eide 1956)

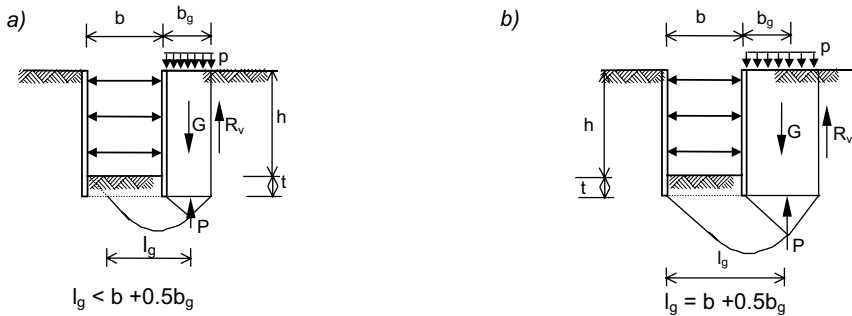


Fig. 4.23. Failure mechanism for basal heave analysis (after Weissenbach 1977)

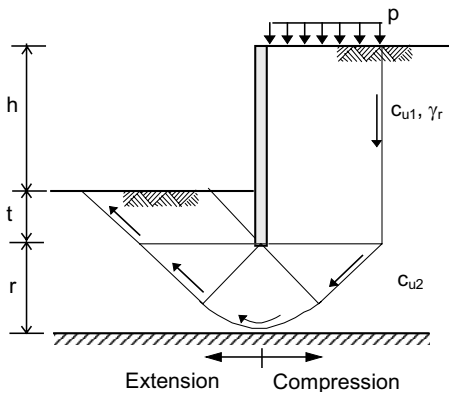


Fig. 4.24. Failure mechanism for basal heave analysis (Kempfert and Stadel 1997)

4.5 Execution of excavations

A selection of construction methods and stages that take into account the underground conditions is of great importance for a successfully execution of a deformation free excavation and will be described briefly in the following.

The installation of the bottom support on the bottom of an excavation that lies in the soft soil immediately after full excavation or partial excavation is also of great importance for the stability of the excavation and settlement behaviour of nearby buildings founded on shallow foundation. Thereby, a distinction has to be made between the following cases:

a) If the soft soil layer is relatively homogeneous, possesses high plasticity, contains no fine sand seems and no groundwater is available, the excavation bottom can be sealed off in sections with base concrete slab immediately after the final excavation.

b) In all other cases, however, a geotextile filter mat, a layer of non-compacted filter material (about 10 cm thick) e.g. split gravel and then a watertight geomem-

brane are laid in respective order on bottom of the excavation before the placement of a sub-base or bottom support concrete slab. Drainage pipes can also be inserted in this layer to provide temporal drainage during the construction period. Refer to Fig. 4.25 and 4.26 for illustrations. Therewith, the excavation can also be protected against possible piping failure.

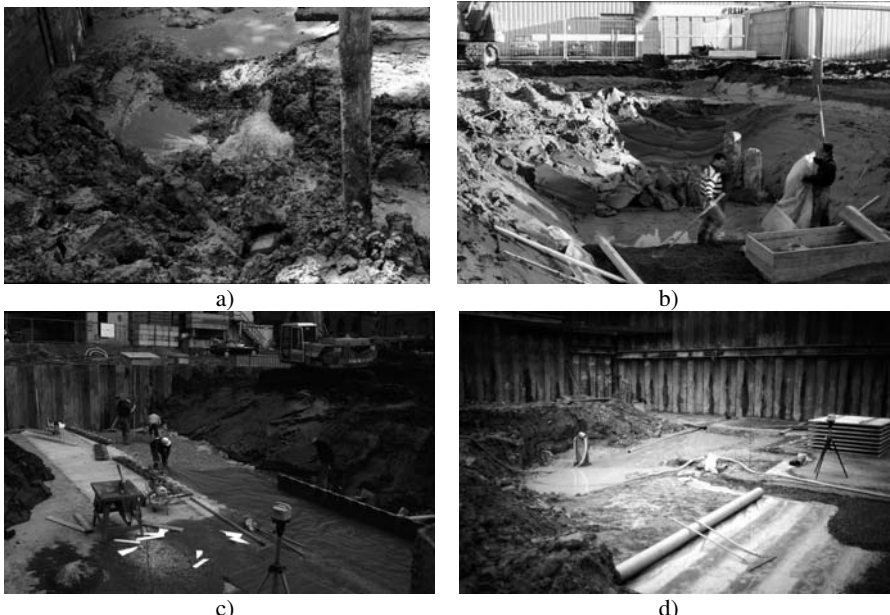


Fig. 4.25. Protection of excavation bottom: a) piping failure, b) to d) overview of construction of drainage layer and bottom slab.



Fig. 4.26. Drainage of excavation bottom: a) work begin at corner, b) temporal drainage duct

Guidelines for the execution of excavations in soft underground are given in EAB EB 93 (EAB 2006) and they are summarised in the following.

Since a fixed or free end support of retaining walls is very limited in excavations in soft soils due to the expected displacements depending on the depth and size of excavation as well as soil and groundwater conditions, the approaches presented in the following are necessary (Weißenbach and Kempfert 1994). It takes into account the unfavourable condition of the underground where the soft soil extends from the ground surface to a depth far enough below the excavation bottom. However, if there exists a favourable underground conditions, the measures has to be corrected.

Independent from the depth of excavation, the top of sheet pile walls will often be capped together by reinforced concrete beam or steel girder to distribute loads arising from already cut portion of an excavation to the untouched part. Moreover, the top beam may serve to limit the displacement of the wall head. In this regard, it will be appropriate to arrange the top beam in such as way that they can also serve as wales for the first row of struts at the top. This also applies for cast-in-place walls provided that no other measure is taken to prevent the isolated movement of single piles or slices of a diaphragm wall.

In an excavation with shallow depth (up to 3 m) and relatively small size, the excavation can be followed in a daily output basis by means of sloped trenches in slices with base width of 2 to 3 m parallel to the smallest side of the excavation and an immediate placement of base concrete slab that may also serve as a bottom support to the wall during the excavation of the next slice. The installation of the base slab in succession (Fig. 4.25 and 4.27a & b) can provide the wall an additional horizontal support at bottom of excavation. At the corner areas of an excavation it can be appropriate to arrange the base slab diagonally (Fig. 4.27c & d)). If these measures are not enough to prevent an impermissible deflection of the wall top it may be appropriate to provide a vertical wall support to the slices or a strut support to the external wall at the top.

Sometimes it may be appropriate to execute the excavation in several strips where each strip is supported by wall. The soil in each strip will the be cut in slices followed by an immediate base slab placement in the same way as described in the previous paragraph (see also section 4.12.2, Fig. 4.85 and 4.87)

To enhance the execution of the excavation and to optimise the daily capacity, a fast hardening cement shall be used for the base slab. The minimum recommended thickness of the base slab is 0.20 m and it can be reinforced if necessary.

Excavations 3 to 5 m deep have to be executed in two or more stages supported by struts or other support mechanism. If the wall is not supported at the top in connection with the top beam, the cutting of the soil up to the first strut level follows stepwise in sloped slices as described above before the strut will be installed. The remaining soil can be dug in the same fashion up to the bottom of excavation and base slab will be placed immediately after the excavation of each slices to provide a bottom support to the wall. If the excavation requires a second strut or more, the procedure repeats itself for each construction stage and strut level. Fig. 4.27b illustrates an excavation stages with one strut level and a base slab.

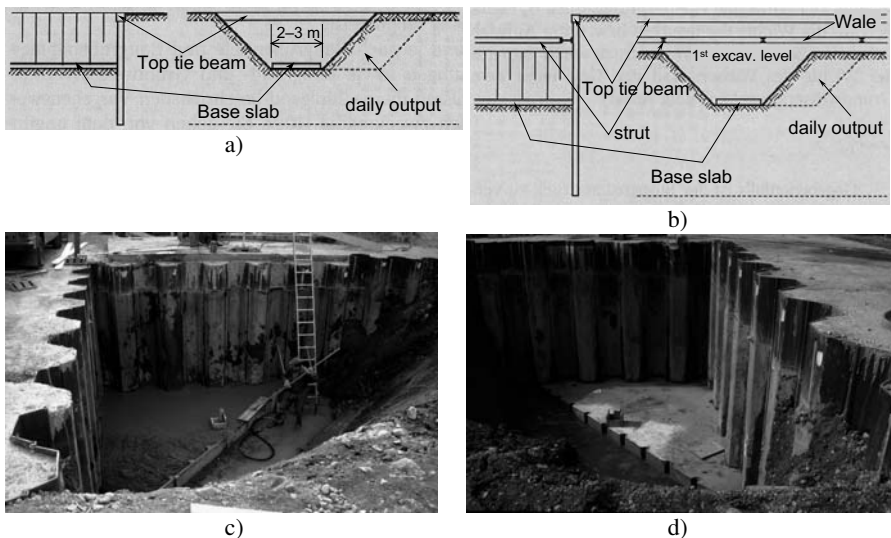


Fig. 4.27. a), b) Illustrations of construction steps in non-braced and braced excavations respectively (EAB 2006); c), d) practical examples of providing bottom support at corners

Sometimes the excavation can be very wide and it becomes difficult to apply the above construction measures for excavations with shallow or middle depths. In such case, the central part of the foundation slab of the future structure can first be placed on a sloped or supported trench. In the second step the wall will be supported with rakers, the remaining berms will be removed stepwise and finally the foundation slab will be extended towards the wall. In this way the wall receives gradually a continuous support at bottom of the excavation. Fig. 4.28 demonstrates principally such type of construction measure.

For deep excavations with a depth more than 5 m in a deep layer of soft soil deposit, it is necessary to provide the retaining wall a bottom support in advance of the excavation work, for example, by means of soilcrete installed by grout jetting from the ground surface (Katzenbach et al. 1992; Ostermayer and Gollub 1996). The soil above the bottom of excavation can be removed in similar way as described above for shallow and middle depth excavations.

Soft soils are particularly sensitive to dynamic loads and change of the primary stress state as a result of the excavation. Hence, in order to avoid the danger of soil flow, the soft soil should not be driven at excavation level. The excavation has to be carried from a higher level. If this is not partly possible, a sufficient thick layer of work space must be prepared on the top of the soft soil.

Soft soils, particularly with fine sand and silt seems under groundwater are usually inclined to flow strongly. Therefore, the safety of slopes and berms in connection to the construction measures described above shall be secured using stabilisation methods such as vacuum wells or vacuum lances (Breymann 1992)(see also section 4.11.7).

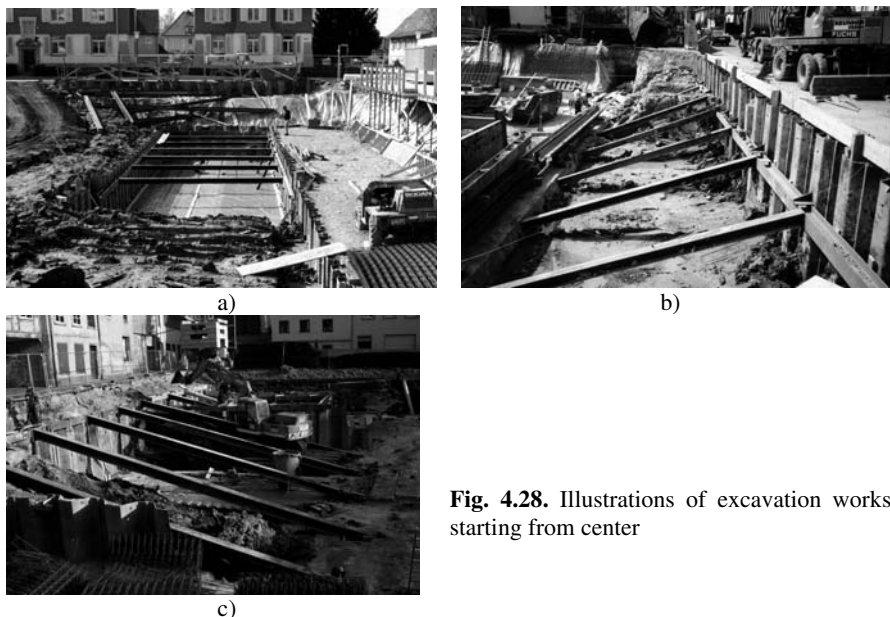


Fig. 4.28. Illustrations of excavation works starting from center

Since a formation of an arching in soft soil is not reliable and the rearrangement of stresses is connected directly with the wall displacements, all support systems has to be installed deformation free using a hydraulic press in small sections.

Excavations in soft soils are prone to basal and hydraulic failures, which may cause a substantial heave of the excavation bottom and settlement behind the wall. The following measures can be used to avoid or limit such danger:

- executing the excavation and the structure in stepwise in sections,
- extending the wall length downwards beyond that required for end support,
- placement of a reinforced or unreinforced base slab stepwise in sections from wall to wall,
- providing anchorage to the base or to the bottom support slab.

Finally, it is indispensable to document the state of the nearby structures before construction starts and install monitoring system on each part of the structural elements, the soil and neighbouring structures, since the performance of an excavation and deformations in soft soils cannot be predicted with absolute reliability. If on the course of the construction inadmissible large movements is observed at neighbouring buildings, pipe lines, streets or other structural facilities, additional constructional measures has to be taken or the construction method has to be completely changed.

4.6 Safety factor in design of retaining structures

In the design of retaining structures safety factors are applied on one hand in order to account for the uncertainty in applied load, soil strength parameters, groundwater conditions and soil geometry, on the other hand to provide a margin of safety against failure, and to keep deformations within acceptable limit. Most designs of retaining walls are based on either working stress method (total factor of safety) or limit state method (partial safety factor). The current development of safety in geotechnical engineering in Europe based on the partial safety concept is illustrated briefly in section 1.2. Therefore, this section will concentrate on the historical development of safety concept in geotechnical engineering and comparison of different approaches.

Fig. 4.29 illustrates the different methods employed in retaining wall design, where the shaded part of the pressure diagram shows those forces contributing to the resisting and mobilising moments after applying the corresponding factor of safety. These methods are:

1. Factor of safety on passive earth pressure: This method is based on Terzaghi's finding that passive pressure requires more movement to be mobilised than active pressure. Hence, the passive pressure used in design is reduced by a factor η_p (Fig. 4.29a). Values of η_p between 1.5 and 2.0 are usually employed (CP2 1951; EAB 1994). For normally consolidated soft soil $\eta_p > 2$ is also possible
2. Factor of safety on net total passive pressure: The design condition in this method is such that the moment of the net active forces should not exceed a fraction of $1/\eta_{np}$ of the moment of the net passive force (Fig. 4.29b). η_{np} is a load factor and a value of 2 is normally adopted (Burland et al. 1981).
3. Factor of safety on all effective strength parameters: The strength of the soil used in the design is reduced by a factor $\gamma_s (\gamma_\phi, \gamma_c, \gamma_u)$. This has the effect of increasing the active pressure and reducing the passive pressure (Fig. 4.29c). Values of γ_ϕ between 1.25 and 1.5 and γ_c between 1.5 and 2.0 are commonly used (Burland et al. 1981; Valsangkar and Schiver 1991; Clayton et al. 1996).
4. Factor of safety on passive effective strength parameters: This is the same as method (3) except that the soil parameters are reduced by a factor of safety γ_{sp} before the passive earth pressure coefficients are calculated (Fig. 4.29d) (GCO 1982). Values γ_{sp} between 1.2 to 1.5 are usually used for clays analyzed in long terms (Clayton et al. 1996).
5. Increased depth of embedment to provide a margin of safety: One of the simplest methods of ensuring stability of a sheet pile wall is to determine the depth of embedment to achieve limiting equilibrium (i.e. a factor of safety of unity) and multiply it by a factor F_d . Values of F_d usually lies between 1.2 and 2.0 (Clayton et al. 1993). This method was suggested by Teng 1962, and Tschebotarios 1973.
6. Revised factor of safety by Burland et al. 1981: This method was developed based on the analogy with a bearing capacity of strip load. The method requires that the moment of activating forces should not exceed a factor $1/\eta_r$ of the

moment of the net available passive resistance of the underlying ground (Fig. 4.29e). The mobilising moments arise due to earth pressure on the wall above the excavation level and due to the surcharge applied by the soil above the excavation level, whereas the resisting moment derives from both the active and passive side of the wall below the excavation level. Values of η_r between 1.5 and 2.0 were recommended by Burland et al. 1981, whereas Valsangkar and Schriver (1991) recommended 1.5.

7. Factor of safety on strength parameter and load: This method is proposed by Meyerhof 1984 and recommended by Canadian Geotechnical Society. It is based on the overload and under-strength factors and thus accounts for the uncertainties in applied loads and shear strength parameters. Load modification factors γ_q and γ_{wa} to active force and water pressure in the active side respectively, resistance modification factors γ_r and γ_{wp} to passive force and water pressure in the passive side respectively, and strength factors γ_ϕ and γ_c for friction and cohesion respectively are employed in the analysis. Common values are: $\gamma_q = 1.25$, $\gamma_r = 0.8$, $\gamma_{wa} = 1.25$, $\gamma_{wp} = 0.85$, $\gamma_\phi = 0.8$ ($\phi'_f = \tan^{-1}(\tan \phi' / \gamma_\phi)$) and $\gamma_c = 0.65$ (Meyerhof 1970, 1982, 1984; Valsangker and Schriver 1991).
8. Factor of safety according to Gudehus and Weissenbach 1996: They commented on the partial safety factors on strength and proposed a partial safety factors γ_F to the action forces and η_R on the resisting force. A retaining structure with strut support, for example, can be treated as vertical beam with two supports A and B (Fig. 4.29g). The support forces A and B are assumed to be the nominal action forces and are obtained from the nominal earth pressure E with two equilibrium conditions. The nominal resistance force of the earth support is the passive earth pressure E_p calculated with characteristic soil parameters. Applying the partial safety factor $\gamma_F \approx 1.4$ to E and $\eta_R \approx 1.4$ to E_p is the same as the familiar total factor $\eta_b = \gamma_F \cdot \eta_R \approx 2.0$. Therefore, according to Gudehus and Weissenbach 1996, the proposed partial factors can be easily related with established total factors without losing the ample experience suddenly with a new format.

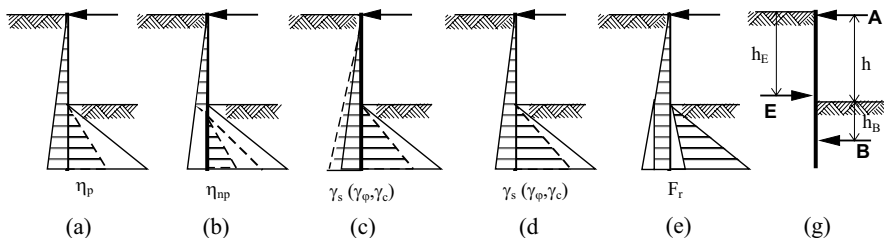


Fig. 4.29. Different methods of applying safety factor in the design of earth retaining structures

It is clear from the above discussion that there is a considerable difference in applying the safety factors. After carrying a parameter study on the different defi-

nitions of the factor of safety in a propped retaining wall, Burland et al. 1981 showed that there appears to be no logical or consistent relationship between η_p (method (a)) and the factor of safety on strength γ_s and its use can lead to very conservative values of wall penetration for drained condition with $\varphi' < 25^\circ$ and for undrained conditions. With regard to η_{np} its use with recommended values of about 2 leads to factor of safety on shear strength generally less than 1.1 for both drained and undrained conditions.

Further, Burland et al. 1981 showed that method (5) maintains a more or less constant factor of safety for drained conditions in uniform ground, though it is unscientific. However, difficulties and inconsistencies arise when F_d is used in undrained condition or where the strength properties of the ground vary significantly with depth. In undrained analysis, $F_d = 2$ is equivalent to the factor of safety on strength $\gamma_s = 1$ (limiting condition) for all values of undrained strength c_u .

The revised safety factor (method (6)) on the other hand has proved to give results that are logical and consistent with the factor of safety on shear strength for soils ranging from purely frictional to cohesive, for both drained and undrained analysis (Burland et al. 1981).

Valsangkar and Schriver 1991 showed that method (7) will lead to very conservative estimates of the depth of penetration, if water pressures are considered on both sides of the wall. However, if net water pressures are used, the estimated depths of penetration is comparable with those estimated in method (1).

Though the concept of the factor of safety with respect to passive failure of the toe of an embedded retaining wall is widely used in design and has the attraction that the overall stability can be expressed by a single factor, the above discussion shows that the most consistent approach is to apply the factor of safety to the soil strength directly (limit state design method); in particular for normally consolidated soft clays, where the effective angle of friction is usually less than 30° and its undrained strength plays its own role. Recently this method is adopted by standard code of practices (Eurocode EC 7-1 DIN EN 1997; BSI BS 8002 1994). A further investigation, however, is required to study the relationships and differences between the different method of applying the factor of safety by considering layered soils, interaction between the retained soil mass and the wall, groundwater flow, and support conditions.

Moreover, the limit state method implicitly assume that displacements will be a secondary problem, related only to minor serviceability limit states. However, in the case of retaining walls displacements may be larger than normally expected in concrete or steel structures. If the retained soil supports other structures or services, ground movements could be large enough to cause severe distress to them even though the retaining wall itself is quite stable. The distress may be sufficiently severe to constitute an ultimate limit state (Simpson 1992). Bolten et al. 1990a, b developed a method of relating displacements to the degree of mobilization of the soil strength, or the strength factor γ_ϕ . Using this method, Simpson 1992 indicated that a strength factor in the range 1.2 - 1.3 will not lead to unacceptable displacements in stiff London clay. A more detailed numerical analysis

would be worthwhile to examine the relationship between partial safety factor on strength and displacement in normally consolidated soft clays.

Beside the above mentioned method of applying the safety factor, it is common practice to increase 0.5 m or 10% of the retained height for the embedded cantilever wall to account for an unplanned excavation in front of the wall (BSI BS 8002 1994), and to add a uniform surcharge of 10 kPa on the retained surface to account for unseen loads from equipment and others (BSI BS 8002 1994; EAB 1994).

Recently, the working group on safety in geotechnical engineering of the German National Institute for standards (DIN) issued a standard norm of safety in geotechnical engineering (DIN 1054: 2005) based on the partial safety factor concept parallel to Eurocode EC 7-1: 1997 (see also section 1.2). The ultimate limit state GZ 1B (STR) governs the design of supported excavations. For deep-seated rotational failure, however, a proof of the safety of the excavation is required based on the ultimate limit state GZ 1C (GEO C). For proof of the safety factor against overturning, uplift and hydraulic failure, the ultimate limit state GZ 1A (EQU, UPL, HYP) governs the situation. Abbreviations in parenthesis are according to EC 7-1 (refer to section 1.2). Serviceability can also be checked using deformations determined at the same time with characteristic section forces.

4.7 Drained/undrained analysis of excavation

4.7.1 General

For a vertical and smooth wall with horizontal ground surface, the effective active and passive earth pressures are usually determined using the classical Rankine equation from,

$$e_a = \gamma' \cdot z \cdot K_a \quad (4.16)$$

$$e_p = \gamma' \cdot z \cdot K_p \quad (4.17)$$

and the undrained active and passive pressures can also be given by

$$e_a = \gamma' \cdot z - 2 \cdot c_u / \xi = \gamma' \cdot z \cdot (1 - 2 \cdot \lambda_{cu} / \xi) = \gamma' \cdot z \cdot K_a \quad (4.18)$$

$$e_p = \gamma' \cdot z + 2 \cdot c_u / \xi = \gamma' \cdot z \cdot (1 + 2 \cdot \lambda_{cu} / \xi) + (\gamma' \cdot H \cdot 2 \lambda_{cu} / \xi) \quad (4.19)$$

where ξ is a factor of anisotropy and it is usually taken as 1 for active case and 2 for passive case, $\lambda_{cu} = c_u / \sigma'_{v0}$ is the normalised undrained strength and it varies between 0.2 and 0.33 for normally consolidated soft clays (see section 2.5.3), H is the excavation depth and z is the depth below the ground surface for the active case and it is the depth below the bottom of excavation for the passive case. Note that the hydrostatic water pressure is not included in Eqs.4.16 to 4.19. They should be calculated separately.

As it is already mentioned in section 3.2.3, it is a well known fact that the behaviour of soils is primarily governed by the effective stresses independent of the drainage condition. Referring to the works of Hvorslev 1937; Rendulic 1937; Brinch-Hansen and Gibson 1949; Schmertmann 1975 and his own experiences on open excavations in soft soils, Janbu 1977 tried to verify the above statement, and he came to the conclusion that the short term undrained behaviour of saturated clays are governed by the effective stresses. The main reason for using the total stress approach for short term undrained conditions in clay is to avoid predicting the excess pore pressure and hence the effective stresses. If the excess pore pressure Δu is known or can reasonably be predicted, the short term undrained behaviour of soils may be written in terms of the effective strength parameters c' and φ' . Δu can be estimated from the commonly used Skempton and Bishop equation (Eqs. 2.41 & 2.42). However, the prediction of Δu is much more complicated than it is given by Eqs. 2.41 & 2.42 (see for example Fig. 2.23). The pore pressure parameter A is not a unique value for a given soil, rather it is dependent on the direction of the principal stresses, the initial stress state and the plastic volumetric strain (Franke 1980; Schweiger 2002).

4.7.2 Is drained or undrained behaviour most critical for design of supported excavations?

The effective stress path $A' \rightarrow B'$ in Fig. 4.30 below corresponds to undrained loading and $B' \rightarrow C'$ corresponds to swelling and reduction in the mean normal effective stress. The pore pressure immediately after construction u_i is less than the final steady state pore pressure u_c and so there is an initial excess pore pressure which is negative. As time passes the total stresses remains approximately unchanged at B but the pore pressure rises. The wall will fail in some way if the states of all elements along the slip surfaces reach the failure line; if B' reaches the failure line the wall fails during the undrained excavation and if C' reaches the line the wall fails some time after construction. The figure demonstrate that unlike footing foundations or embankment foundations or retaining walls loaded by fill, where the foundation becomes stronger with drainage, the factor of safety of a retaining walls supporting an excavation will decrease with time (Atkinson 1993).

Since the un/reloading modulus of elasticity is 5 to 7 times higher than the modulus of elasticity in primary loading, the time required to reach an approximate steady condition after excavation is usually measured in weeks or months, i.e. during the normal construction periods. Freiseder 1998 presented a field pore pressure measurements during the construction of a 6.3 m deep excavation for underground park in Salzburg (Fig. 4.31). It appears from this figure that the excess pore pressure stabilises to a steady state quickly in a time of 10 to 30 days after excavation. Hence, it appears logical to use effective stress stability analysis for open excavations in clays, using a steady seepage condition as basis for the pore pressure.

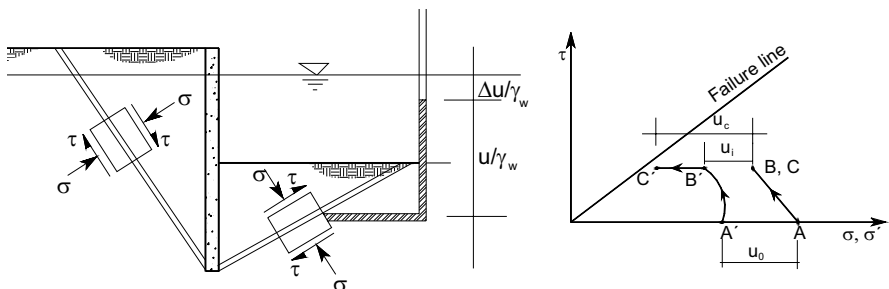


Fig. 4.30. Change of stress and pore pressure for a wall retaining excavation (after Atkinson 1993)

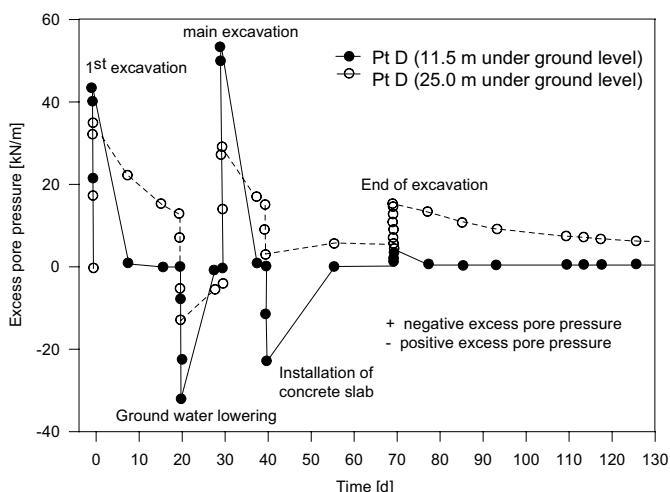


Fig. 4.31. The development and dissipation of pore pressure under excavation (after Freieder 1998)

After reviewing six open excavations (5 to 11m deep) case records in clay, Janbu 1977 concluded that the stability is best expressed in terms of effective stress analysis. He reasoned that the readjustment of stresses and pore water pressures to correspond with a state of steady seepage may often take place in the course of few days or few weeks or at most some months. He further commented that the simple total stress analysis for excavations in clay will frequently lead to erroneous results both for safety factor and shear surface location.

Lafleur et al. 1988 had observed the behaviour of a well instrumented, 8 m deep excavation slope in soft Champlain clay. They reported that the effective stress approach may give a reasonable estimate of the factor of safety. On the

other hand, all the stability analyses using a short term approach overestimated the factor of safety of the failed slopes.

From the above discussions it is clear that there is a possibility of undrained failure in excavation, although the drained (steady state) condition is most critical.

4.7.3 The time limit for undrained and drained condition

According to the flow chart in Fig. 2.19, a drained condition is defined when the excess pore pressure approaches to zero ($t \rightarrow \infty$) and undrained condition when the excess pore pressure is at full ($t = 0$). The behaviour of the excavation between this extreme cases should be dealt with a consolidation analysis. However, for practical purposes, may one allow a certain pore pressure dissipation but still undrained? Similarly, may one let some excess pore pressure to remain but still defined drained? Vermeer and Meier 1998; Vermeer 1998 suggested an approach for the approximation of the time limit for undrained or drained condition for excavation based on the classical consolidation theory,

$$T_v = \frac{c_v}{D^2} \cdot t = \frac{k \cdot E_s}{\gamma_w \cdot D^2} \cdot t \quad (4.20)$$

Where T_v is the dimensionless time factor, c_v is the coefficient of compressibility, t is the time, k is the permeability of the soil, E_s is the constrained modulus, γ_w the unit weight of water and D is the drainage path. According to Vermeer and Meier 1998, the depth of embedment below the bottom of excavation can often be regarded as the drainage length and they assumed that if the dimensionless time factor $T_v < 0.1$, the excavation can be assumed in an undrained state with degree of consolidation only around 10%.

Applying Eq. 4.20 to lacustrine soft soil in southern Germany, a relationship between the drainage depth and the time required for a predefined excess pore pressure dissipation has been developed as shown in Fig. 4.32. The value of c_v is determined from back analysis of measured settlement data of 9 practical projects in and around the city of Constance (Kempfert et al. 2001). It varies from 3.1 to 46.5 m²/year with one exceptionally large value of 103.5 m²/year. In Fig. 4.32, only the average c_v value of 26 m²/year and the minimum recorded value of 3.1 m²/year was considered. The authors assumed undrained condition to prevail, if up to 10% of the excess pore pressure dissipates. Similarly, if more than 90% of the excess pore pressure are already dissipated, a drained condition may be assumed. This is simply a rough estimation to see how much time it would be required for this two conditions.

From Fig. 4.32, it can be observed that the time required for undrained condition, for example for an excavation with 8 m depth of penetration, varies from less than 10 days to a maximum of 80 days. Similarly, the time required for drained condition varies from less than 800 days to maximum of 6000 days. It should be noted that in developing Fig. 4.32 it was assumed that there exist a relative permeable soil layer at depth equal to the depth of penetration below the toe of the wall,

which in reality may not be always true. Fig. 4.32 indicates that one may need more time to assume a fully drained condition. In other words, the situation at field may lay some where between these two extreme cases. Therefore, a decision should be taken based on the information at hand, experience and engineering judgement for a particular project for an analytical analysis of excavations. The best way of handling an excavation problems numerically is to perform a consolidation analysis that considers the exact time of the end of construction activities.

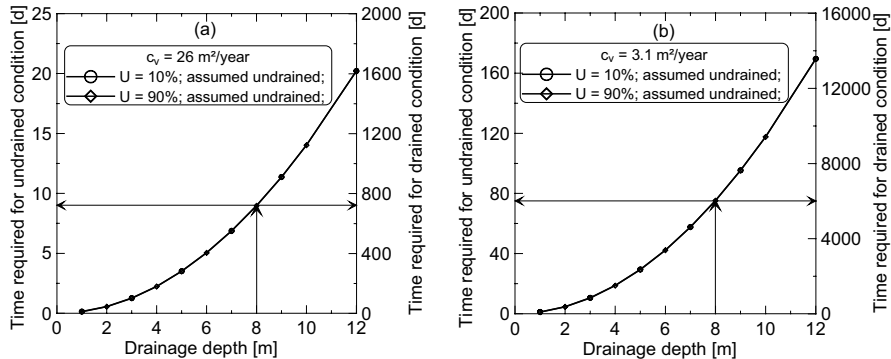


Fig. 4.32. Assumed time required for drained and undrained condition: a) $c_v = 26 \text{ m}^2/\text{year}$, and b) $c_v = 3.1 \text{ m}^2/\text{year}$

4.7.4 Determination of the earth pressure in short term using the effective strength and the pore pressure parameters

If one is in a position to determine the effective strength parameters either in laboratory directly or indirectly as given in section 2.5.2, the earth pressure in short terms may be calculated using the effective strength parameters. The effective stress ratio in the case of active earth pressure is given by

$$\frac{\sigma'_h}{\sigma'_v} = K_a \quad \text{or} \quad \sigma'_h = \sigma'_v \cdot K_a \quad (4.21)$$

but $\sigma'_h = \sigma_h - (u_0 + \Delta u_f)$ and $\sigma'_v = \sigma_v - (u_0 + \Delta u_f)$, thus

$$\sigma_h - (u_0 + \Delta u_f) = [\sigma_v - (u_0 + \Delta u_f)] \cdot K_a$$

$$\begin{aligned} \sigma_h &= [\sigma_v - (u_0 + \Delta u_f)] \cdot K_a + (u_0 + \Delta u_f) \\ &= \sigma_v \cdot K_a + u_0 \cdot (1 - K_a) + \Delta u_f \cdot (1 - K_a) \end{aligned} \quad (4.22)$$

Substituting $\Delta u_f = A_f \cdot (\Delta \sigma_v - \Delta \sigma_h) = -A_f \cdot \Delta \sigma_h = -A_f \cdot (\sigma_h - \sigma'_{vo} \cdot K_0)$ in to Eq. 4.22 and rearranging, the total active pressure may be calculated from,

$$e_a = \sigma_h = \frac{\sigma'_{vo} \cdot [K_a + A_f \cdot K_0 \cdot (1 + K_a)] + u_0}{[1 + A_f \cdot (1 + K_a)]} \quad (4.23)$$

Similarly, in the case of passive pressure,

$$\frac{\sigma'_h}{\sigma'_v} = K_p \quad \text{or} \quad \sigma'_h = \sigma'_v \cdot K_p \quad (4.24)$$

but $\sigma'_h = \sigma_h - (u_0 + \Delta u_f)$ and $\sigma'_v = \sigma_v - (u_0 + \Delta u_f)$, thus

$$\sigma_h = \sigma_v \cdot K_p + u_0 \cdot (1 - K_p) + \Delta u_f \cdot (1 - K_p) \quad (4.25)$$

Substituting $\Delta u_f = A_f \cdot (\Delta \sigma_v - \Delta \sigma_h) = -A_f \cdot \Delta \sigma_h = -A_f \cdot (\sigma_h - \sigma'_{vo} \cdot K_0)$ in to Eq. 4.25 and rearranging, the total passive pressure can be calculated from

$$e_p = \sigma_h = \frac{\sigma'_{vo} \cdot [K_p + A_f \cdot K_0 \cdot (1 - K_p)] + u_0}{[1 + A_f \cdot (1 - K_p)]} \quad (4.26)$$

Eq. 4.26 is valid only for the stress path where the horizontal stress increases while the vertical stress remains constant, which is the standard passive failure case usually assumed in practice. In other words, Eq. 4.26 gives passive pressure which is independent of the depth of excavation. Note that σ'_{vo} and u_0 in Eq. 4.26 are the effective weight of the soil and the weight of the water respectively after full excavation. However, in the case of excavations the vertical stress changes as well during construction (undrained), which leads to a different total stress path than that normally assumed for passive case. If failure during excavation is assumed to occur, the changes in vertical pressure should be taken in to account. The relative rate of change of the vertical stress and horizontal stress during excavation is not known, but it lies somewhat between the two extreme cases: the passive case ($\Delta \sigma_3$ increasing and $\Delta \sigma_I = 0$) and extension case ($\Delta \sigma_3 = 0$ and $\Delta \sigma_I$ decreasing). In such cases the excess pore pressure becomes,

$$\begin{aligned} \Delta u_f &= A_f \cdot (\Delta \sigma_v - \Delta \sigma_h) = A_f \cdot [(\sigma_v - \sigma'_{vo}) - (\sigma_h - \sigma'_{vo})] \\ &= A_f \cdot [(\sigma_v - \sigma_h) + \sigma'_{vo} \cdot (K_0 - 1)] \end{aligned} \quad (4.27)$$

Substituting Δu_f from Eq. 4.27 in to Eq. 4.25 and rearranging, the total passive pressure becomes,

$$e_p = \sigma_h = \frac{\sigma_v \cdot [K_p + A_f \cdot (1 - K_p)] + (1 - K_p) \cdot [A_f \cdot \sigma'_{vo} \cdot (K_0 - 1) + u_0]}{[1 + A_f \cdot (1 - K_p)]} \quad (4.28)$$

Here σ_v is the total weight of the soil after excavation, σ'_{vo} is the effective weight of the soil before excavation and u_o is the weight of the water after excavation. Note that the value of the pore pressure coefficient A_f is different in Eqs. 4.23, 4.26 and 4.28 (see Table 2.8).

4.7.5 Earth pressure in short term using the undrained strength

Based on an analytical parameter study, Hettler et al. 2002 show the uncertainty and difficulty of determination of the embedment depth of retaining structures in soft soil analytically based on undrained strength c_u . For this reason, the working group “Excavation” (EAB) suggests in its draft recommendation for excavation in soft soils to use an equivalent total angle $eqv.\varphi_{cu}$ in calculating the earth pressures instead of c_u . The attempt in this section is to find out a relationship between the undrained strength c_u and the equivalent total angle $eqv.\varphi_{cu}$ based on a consolidated undrained triaxial test, so that to determine the earth pressure in short term. Fig. 4.21 shows a schematic plot of the total and effective stress paths for isotropically and anisotropically consolidated triaxial compression test.

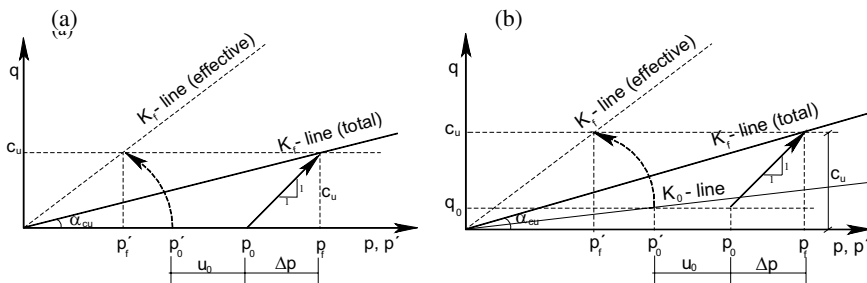


Fig. 4.33. Estimation of the equivalent total angle for the case of a) isotropically and b) anisotropically consolidated triaxial compression tests

From Figure 4.33, the following relationship may be derived,

$$\tan \alpha_{cu} = \frac{c_u}{p_f} = \sin(eqv.\varphi_{cu}) \quad (4.29)$$

but $p_f = p_0 + u_0 + c_u$, hence Eq. 4.29 becomes

$$\begin{aligned} \sin(eqv.\varphi_{cu}) &= \frac{c_u}{p_0' + u_0 + c_u} = \frac{c_u}{p_0' \cdot (1 + \frac{u_0}{p_0'} + \frac{c_u}{p_0'})} = \frac{\lambda_{cu}}{1 + \lambda_{u0} + \lambda_{cu}} \\ &= \frac{1}{\frac{1}{\lambda_{cu}} + \frac{\lambda_{u0}}{\lambda_{cu}} + 1} \end{aligned} \quad (4.30)$$

where λ_{u0} is the normalised initial (steady) pore water pressure.

Similarly, for the case of K_0 -consolidated compression triaxial test,

$$\sin(eqv.\varphi_{cu}) = \frac{1}{\frac{K_0}{\lambda_{cu}} + \frac{\lambda_{u0}}{\lambda_{cu}} + 1} \quad (4.31)$$

For other stress path directions, the equivalent total angle is given in Table 4.5 below.

Table 4.5. Equations to convert the undrained strength c_u to equivalent total angle $eqv.\varphi_{cu}$

Stress paths	Isotropic consolidated	K_0 -consolidated
$\Delta\sigma_3$ decreasing and $\Delta\sigma_1 = 0$ (B)	$\sin(eqv.\varphi_{cu}) = \frac{1}{\frac{1}{\lambda_{cu}} + \frac{\lambda_{u0}}{\lambda_{cu}} - 1}$	$\sin(eqv.\varphi_{cu}) = \frac{1}{\frac{1}{\lambda_{cu}} + \frac{\lambda_{u0}}{\lambda_{cu}} - 1}$
$\Delta\sigma_3$ increasing and $\Delta\sigma_1 = 0$ (E)	$\sin(eqv.\varphi_{cu}) = \frac{1}{\frac{1}{\lambda_{cu}} + \frac{\lambda_{u0}}{\lambda_{cu}} + 1}$	$\sin(eqv.\varphi_{cu}) = \frac{1}{\frac{1}{\lambda_{cu}} + \frac{\lambda_{u0}}{\lambda_{cu}} + 1}$
$\Delta\sigma_3 = 0$ and $\Delta\sigma_1$ decreasing (D)	$\sin(eqv.\varphi_{cu}) = \frac{1}{\frac{1}{\lambda_{cu}} + \frac{\lambda_{u0}}{\lambda_{cu}} - 1}$	$\sin(eqv.\varphi_{cu}) = \frac{1}{\frac{K_0}{\lambda_{cu}} + \frac{\lambda_{u0}}{\lambda_{cu}} - 1}$

The ratio of the horizontal to the vertical stresses can be obtained from Fig. 4.34 as follows,

$$\sin(eqv.\varphi_{cu}) = \frac{(\sigma_{vf} - \sigma_{hf})/2}{(\sigma_{vf} + \sigma_{hf})/2} \quad (4.32)$$

Rearranging and solving Eq. 4.32,

$$K_a^T = \frac{\sigma_{hf}}{\sigma_{vf}} = \frac{1 - \sin(eqv.\varphi_{cu})}{1 + \sin(eqv.\varphi_{cu})} = \tan^2(45 - \frac{eqv.\varphi_{cu}}{2}) \quad (4.33)$$

where K_a^T is the ratio of the total horizontal and vertical stresses in active state. Likewise the ratio of the total horizontal and vertical stresses in passive state K_p^T can be calculated from,

$$K_p^T = \frac{\sigma_{hf}}{\sigma_{vf}} = \frac{1 + \sin(eqv.\varphi_{cu})}{1 - \sin(eqv.\varphi_{cu})} = \tan^2(45 + \frac{(eqv.\varphi_{cu})}{2}) \quad (4.34)$$

Using Eqs. 4.33 & 4.34, one is in a position to calculate the total active and passive pressure based on the total equivalent angle φ_{cu} .

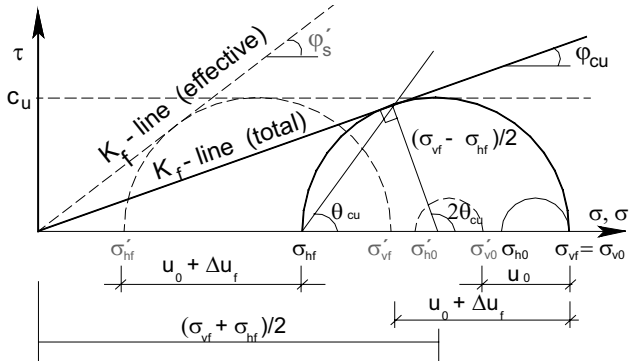


Fig. 4.34. The Mohr-Coulomb stress circle in active state

4.7.6 Comparison of the different approaches

To compare the different approaches discussed in this section, an idealised excavation with groundwater at the surface, $\gamma' = 10 \text{ kN/m}^3$, $\gamma_w = 10 \text{ kN/m}^3$, $\lambda_{cu} = 0.30$ is assumed. The different comparisons are shown in Figs. 4.35 to 4.39.

Fig. 4.35 shows the resultant total passive force calculated using the effective stress analysis. It appears from Fig. 4.35 that for values of $A_f > 0$ the total passive force in undrained condition is greater than that in drained condition and vice versa for $A_f < 0$. The result also shows how the passive force depends on the development of pore pressure and the depth of excavation. The question is which ranges of A_f value should be taken for the passive case. Fig. 4.36 shows variation of the A_f values with the gradient of the total stress path below the K_0 -line and the anisotropy factor x , taking the A_f value for the standard anisotropically consolidated triaxial compression as a reference value. If the value of $\xi = 2$ is taken as it is usually the case in the literature and practice, the A_f values for all the stress paths below the K_0 -line are negative.

However, it is a well known fact that the pore water pressure for the stress path D ($\beta = 1$) (Fig. 2.22) is negative, which gives a positive pore pressure parameter

A_f . Therefore, it seems logical to take $\xi = 1$ for the passive pressure calculation that is recently proposed by the working group “Excavations“ (EAB) of the German Society of Geotechnical Engineers. In such case the value of A_f for normally consolidated clays lies in the positive range of values.

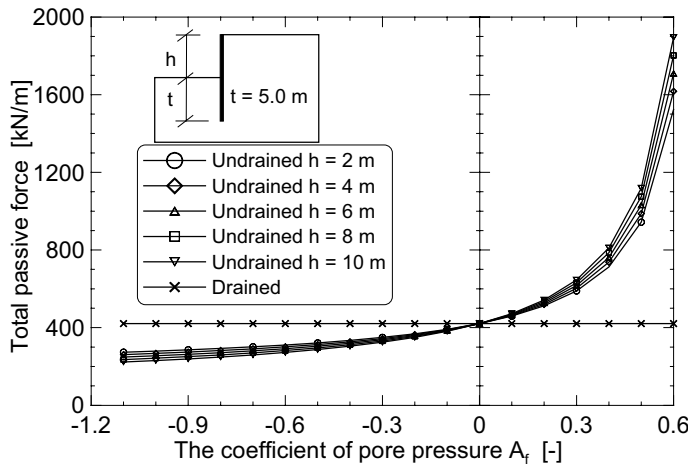


Fig. 4.35. The total passive force calculated using the effective strength parameter and the pore pressure parameter

Similarly, the resultant total active force in undrained condition calculated using the effective stress analysis is shown in Fig. 4.37. It appears from this figure that the total active force in undrained condition is less than that in drained condition for values of $A_f > 0$, and it is greater than in drained condition for values of $A_f < 0$, even greater than the earth pressure at rest. According to Table 2.7 and 3.8, the values of A_f for sensitive clays lay between 0.5 to 1.5 and for normally consolidated soils between -0.3 to 0.3. This indicates that for sensitive soils and partly for normally consolidated soils the drained condition is critical as far as the active earth pressure is concerned.

The other approach to handle the problem of earth pressure calculations in undrained condition is to estimate an equivalent total angle $eqv.\varphi_{cu}$ from the undrained strength c_u . Fig. 4.38 shows that a very good agreement between the resultant active forces calculated assuming drained condition, undrained condition using $eqv.\varphi_{cu}$, and using the classical equation for undrained condition ($e_a = \gamma' z (1 - 2 \cdot \lambda_{cu})$). The classical equation ignores the tensile force.

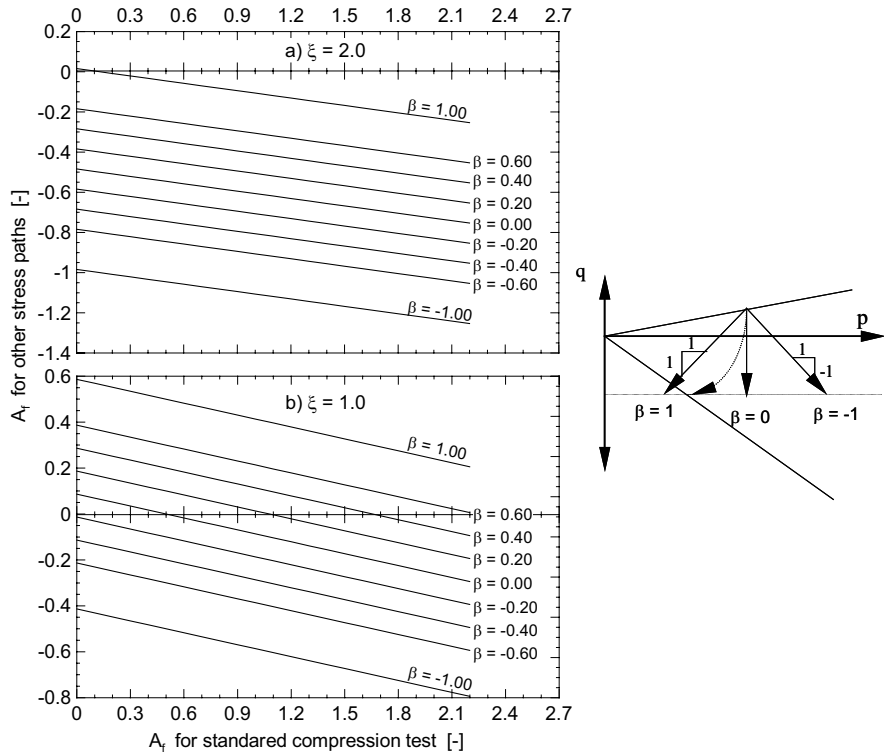


Fig. 4.36. The variation of the pore pressure parameter for different direction of the stress paths below the K_0 -line: a) $\xi = 2.0$, and b) $\xi = 1.0$

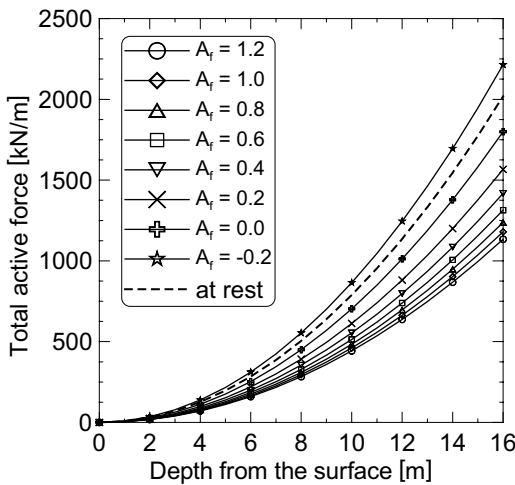


Fig. 4.37. The total active force calculated using the effective strength and pore pressure parameters

The total passive force calculated for $b = 1$ and -1 , and $\xi = 1$ and 2 using the equivalent total angle of internal friction is shown in Fig. 4.39. Besides, the total passive force using the classical earth pressure equation for undrained condition ($e_p = \gamma' z \cdot (1 + 2 \cdot \lambda_{cu}/\xi) + \gamma' \cdot H \cdot 2 \cdot \lambda_{cu} / \xi$) for $H = 5$ m and 10 m, and $\xi = 1$ and 2 is also shown in the diagram. From Fig. 4.39, it can be observed that the total passive force is subjected to different factors. All the lines, however, seem to lay between the drained and at rest condition with one exceptional case ($H = 10$ m and $\xi = 1$). The increase of undrained strength with depth was considered in determining the total passive force using the classical equation.

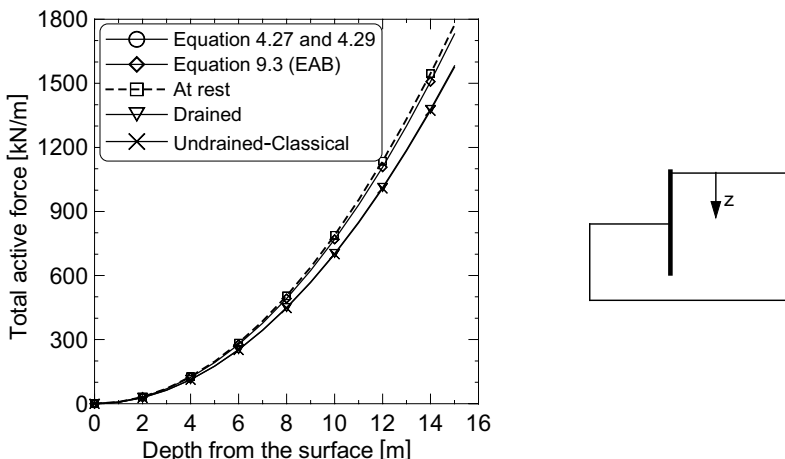


Fig. 4.38. Total active force calculated using the equivalent total angle of friction $eqv. \varphi_{cu}$

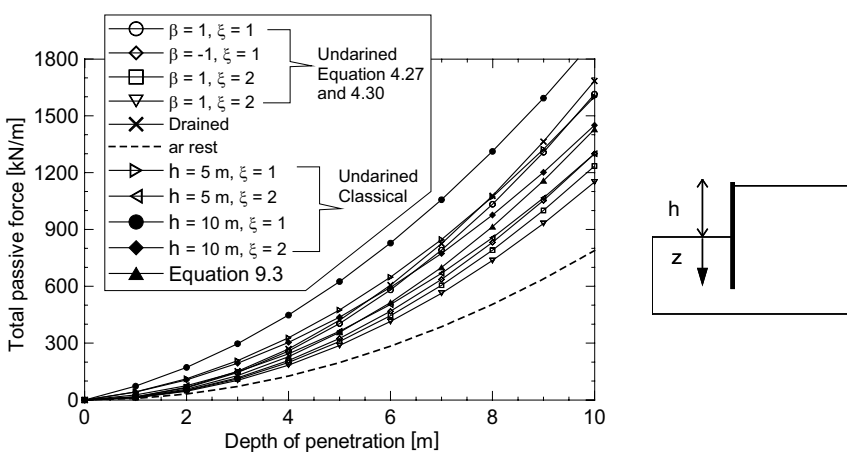


Fig. 4.39. Total passive force calculated using the equivalent total angle of friction $eqv. \varphi_{cu}$ for different depth of excavation

4.8 Stress paths in excavations

As already mentioned in section 2.5.1, it is possible to take the specimen in a triaxial cell to failure either in axial compression or axial extension. For ready reference Fig. 2.17 is reproduced here as Fig. 4.40. The specimen can be compressed axially either by increasing the axial compressive stress (path OA in Fig. 4.40) or decreasing the lateral stress (path OB) or varying the stresses in both direction (path OC). Similarly, axial extension can be achieved either by decreasing the vertical stress (path OD) or increasing the lateral stress (path OE) or varying the stresses in both direction (path OF). Path OA is typical to the state of stress under the axis of an embankment or foundation footing, path OD is typical to the state of stress under the centre of excavation, path OB is typical to the state of stress behind a retaining structure, and path OE is typical to the state of stress in front of the retaining structure and below the excavation level (passive case), where the change of vertical stress due to vertical stress relief is assumed very small. The relief of vertical stress due to excavation and increase of horizontal stress due to the movement of the wall on the passive side may be represented by the path OF, provided that the stress increments in both directions remains the same. Similarly, the increase of vertical stress due to external load at the surface and decrease of the horizontal stress due to wall movement in active side may be represented by path OC.

Rotation of the principal stresses usually occurs around the bottom of the wall and anchor fixing points in an excavation. Although the reversal of the principal stresses on horizontal and vertical principal planes as discussed on the above paragraph may be tested using a modified triaxial apparatus, it is impossible to simulate the rotation of the principal stress on inclined principal planes in a standard triaxial apparatus, unless and otherwise sample are extracted at a specified angel. The rotation of principal stresses, however, can be simulated in a direct simple shear. A true triaxial apparatus where the three principal stresses can vary independent from each other is also available nowadays to simulate the 3-dimensional state of stresses of a soil specimen. Biaxial or plane strain apparatus, where the three principal stresses vary again independently, but the strain in one of the principal stresses direction remains zero, is also widely used for research purpose to simulate a plane strain condition.

Stroh 1974 produced a diagram showing the zones of different stress paths in an excavation in frankfurter overconsolidated clay supported by multiple ground anchors as shown in Fig. 4.41.

Zhu and Liu 1994 divided the excavation in soft soil in four zones of stress path as shown in Fig. 4.42. They used the principal stress ratio $K = \sigma'_1 / \sigma'_3$ to show the variation of the stress paths in the four zones. However, they did not indicate how the σ'_1 and σ'_3 varies in a particular stress path, which is more important than the stress ratio K .

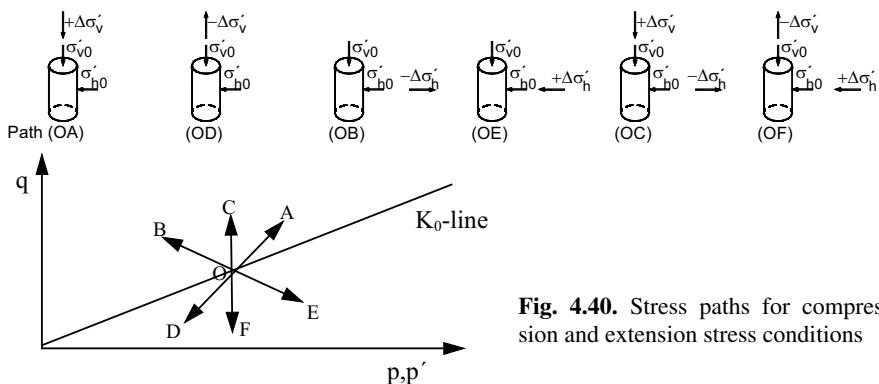


Fig. 4.40. Stress paths for compression and extension stress conditions

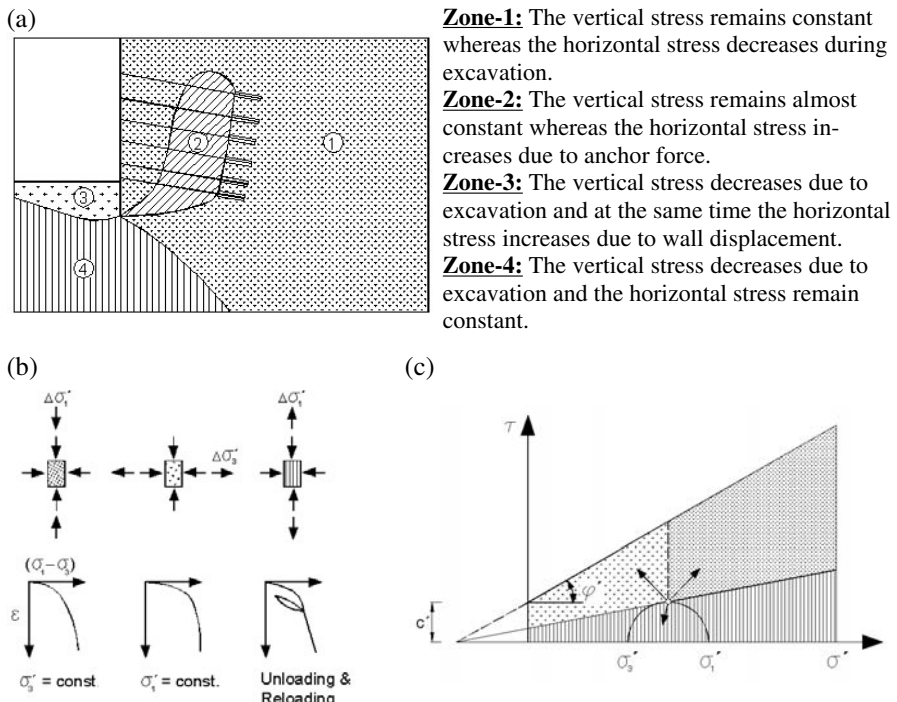


Fig. 4.41. a) Stress paths in an anchored excavation, b) stress - strain relationships, c) criteria for different stress paths (after Stroh 1974)

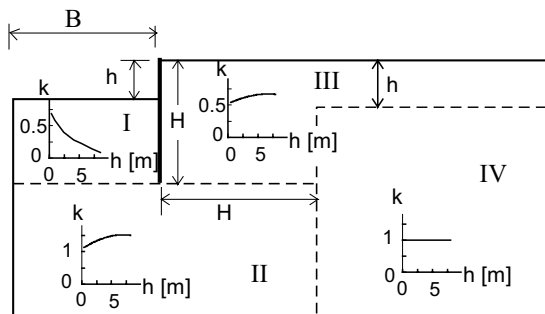


Fig. 4.42. Sub zones of the stress path (after Zhu and Liu 1994)

It would be unwise to generalise the stress path zones as it might differ according to the type of wall system, type of support system, the surcharge load, and groundwater conditions. A finite element parameter study might help to identify the different zones particularly in normally consolidated soft clay soils. For example, a typical stress paths based on the FE-computations at different locations in an excavation (Fig. 4.43) are presented in Fig. 4.44.

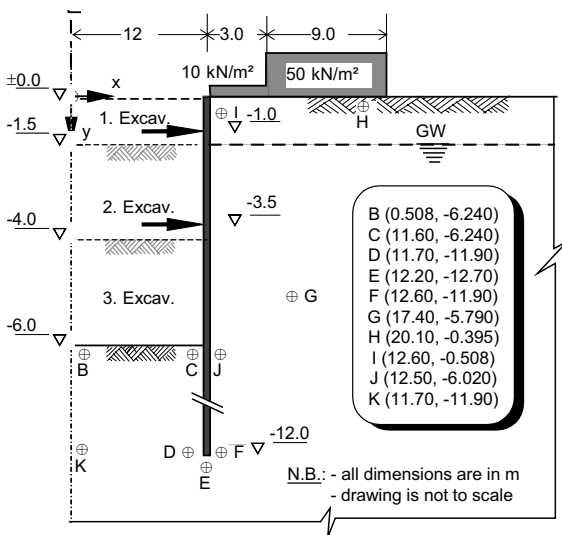


Fig. 4.43. The idealized excavation problem with the location of the stress path points

It is possible to follow some of the idealized stress paths (Fig. 4.40) in laboratory in triaxial test apparatus. The question is, however, whether these stress paths represent the actual stress paths in the field, in particular in the case of excavations.

tions. To investigate the stress paths at different locations of the supported excavation, representative points as shown in Fig. 4.43 are selected. The input parameters for the finite element calculation is the same as that used in the parameter study in section 4.11 as a reference parameter (Table 3.15). The effective and the total stress paths followed at different locations in the excavation are shown in Fig. 4.44. In order to study only the stress paths during the excavation, the stress paths starting from stage 3 (1st excavation) only are presented in the diagram.

Fig. 4.44a shows both the effective and total stress paths at points (B, C, D and K) at the passive side of the wall below the bottom of excavation. As expected all the stress paths at these points lie on the extension zone (below the K_0 -line). The total stresses at locations B and K follow a path downwards towards left, whereas the effective stresses follow a vertically downward path. The total stress path at these points are fairly comparable with the stress path OD in Fig. 4.40, i.e., the vertical decrement of the stress is more dominant than the horizontal increment of the stress due to the wall movement.

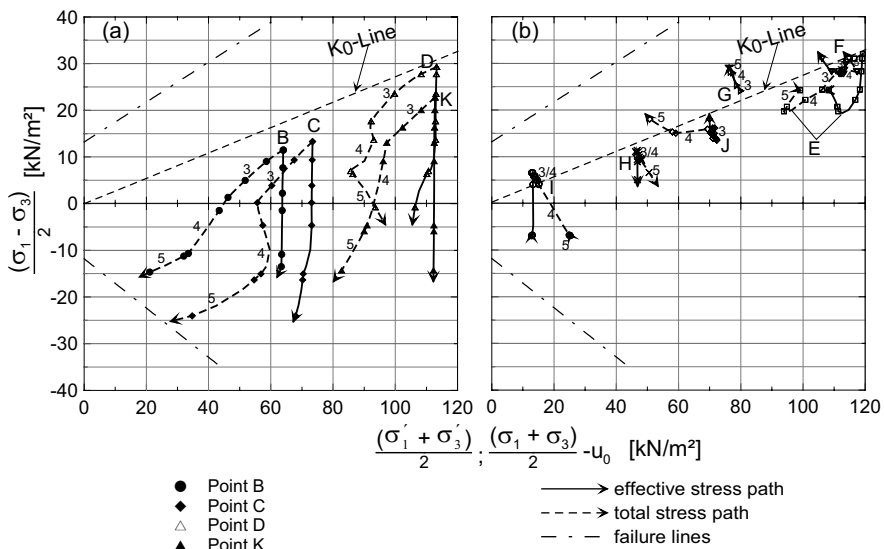


Fig. 4.44. Total and effective stress paths at selective location in an excavation

The total stress path at location C first runs parallel to the stress path at B (stage 3), then changes its direction downward with a slight inclination to the right and then to the left (stage 4), and finally it deflects to the left and follows the path parallel to the stress path at point B (stage 5). There is no single stress path among the idealized stress paths in Fig. 4.40 that can match with this stress path at point C. One can, however, match the total stress path at C stagewise as follows:

- Stress path at point C during the 1st excavation (Stage 3) \Rightarrow Stress path OD (Fig. 4.40),
- Stress path at point C during the 2nd excavation (Stage 4) \Rightarrow Stress path OF (Fig. 4.40),
- Stress path at point C during the 3rd excavation (Stage 5) \Rightarrow Stress path OD (Fig. 4.40),

i.e., both the vertical stress decrement due excavation and the horizontal stress increment due to the wall movement has proportionally played a role during stage 4, whereas the vertical stress decrement due to the excavation has remained dominant during stage 3 and 5.

Similarly, the total stress at point D first follows a parallel path to the stress path at location K (stage 3), then changes its path downwards before it deflects towards left at the end of stage 4, and finally it deflects downward towards the right (stage 5). Again there is no single stress path among the idealized stress paths in Fig. 4.40 that can match with this stress path, but it can be fairly matched stagewise as follows:

- - Stress path at point C during the 1st excavation (Stage 3) P Stress path OD (Fig. 4.40),
- - Stress path at point C during the 2nd excavation (Stage 4) P Stress path OF (Fig. 4.40),
- - Stress path at point C during the 3rd excavation (Stage 5) P Stress path OE (Fig. 4.40),

i.e, the horizontal stress increment due to wall movement was more dominant during stage 5.

Fig. 4.44b also shows the effective and total stress paths at points (F, G, H, I and J) at the active side of the wall and at point E just below the toe of the wall. As can be shown from the figure, the stress paths at the active side of the wall may not necessarily all lie with in the compression zone (above the K_0 - line). The total stress at point I starts with an upward path towards the left during stage 3 (\approx path OB in Fig. 4.40), then it turns its direction by 180° and follows a downward path towards the right during stage 4 (\approx path OE in Fig. 4.40), where it completes its path in the extension zone. During stage 5 the total stresses remained constant with a slight change of its direction upwards. There appears to happen a rotation of the principal total stresses at this point.

The total stress at point H follows similar course as the stress path at point I during stage 3 and 4. During the stage 5 it follows its course further downwards towards the right. The total stress at point J follows first a vertical upward path (stage 3), then it turns its direction towards the left with slight inclination downwards (stage 4), before it finally turns its direction upwards towards the left (stage 5) and completes its path in the compression zone.

The point G lies approximately along the active sliding line behind the wall. The total stress path at this location is the only path that starts and ends in the compression zone. It also shows no significant change of direction of its path during the construction stages 3, 4 and 5 and it can be fairly approximated by idealized stress paths OB in Fig. 4.40. As can be seen from the Fig. 4.44b, the total and effective stress path at point G almost overlap each other, indicating that no significant excess pore pressure was developed during the excavation phases.

The total stress path at F forms a triangular loop, where it starts its path downwards towards the left (stage 3), then changes its course and runs horizontally towards the right (stage 4), and finally it closes up the loop by changing its course once again upwards towards the left (stage 5). The effective stress path does not close in a rectangular loop showing that there was an excess pore water pressure at this point at the end of the excavation.

The point E is located in a zone where maximum rotation of the principal stresses usually occurs. The total stress path at this point (Fig. 4.40b) proves this

fact. It starts downward towards the left (stage 3), runs further downward again towards the left but with a moderate slope (stage 4), and finally it changes its course in the upward direction towards the right (stage 5).

The stress paths in Fig. 4.44 are only valid for the given excavation case supported by a sheet pile. For other excavation cases and support conditions, a different stress paths maybe possible, but the general trend remains the same.

4.9 Some reviews of FE-analysis of excavations

4.9.1 General

The finite element method is one of the powerful numerical methods available to date to predict the ground movement pattern in and around an excavation. In the last 3 to 4 decades several authors used the finite element method to predict or to back analyze the performance of an excavation. Since then there is a lot of progress in understanding the material behaviour of soils, and the application of the finite element method to geotechnical problems. Freiseder 1998 also discussed in his thesis the progress of the finite element analysis of excavations and the corresponding constitutive material models. In the seventies and eighties, the analysis of excavations using the finite element method was mostly made using undrained, linear or non-linear, elastic or elasto-plastic soil behaviours, but nowadays sophisticated programs are available for both drained and undrained analysis. Several finite element programs that are written specifically for geotechnical purposes are also commercially available.

However, the need to obtain realistic input parameters for a complex soil model, and the need to model detailed construction technique and sequences remain the major challenge in using the finite element method. There is also no fast and hard rule on how to specify the extent of the boundary, the type and number of elements. For these and other unknown reasons there is a large discrepancy in the out put of the finite element analysis of the same problem but calculated by different individuals. A good example is the prediction presented by 18 individuals to the test excavation on sand conducted at the University of Karlsruhe (Andreas 1997). According to von Wolfferdorf 1997, there was large discrepancies between the predictions, let alone with the actual field test result. Even those predictions that are calculated using the same finite element program did differ to each other. Another similar example is the comparative finite element analysis of excavation in sand and clay recently made by 7 individuals in request of the German working group “Excavation” (EAB) in which the Author was a participant (Kempfert and Gebreselassie 2000). In these comparative analyses more than 150% deviation from the average value was recorded. The comparative analysis of a 16.8 m deep excavation (Schweiger 2000) made by 14 individuals shows also similar discrepancy among the results. According to Schweiger 2000, the main reasons for the discrepancy of the results were the identification of parameters in particular the stiffness of the soil in working state, the application of the laboratory

results to the in-situ condition, and modeling in general. These leads to the conclusion for an immediate need for standardising the finite element analysis of excavations. At present there is an effort to standardize the calculations methods by the Working Groups on “Excavation” (EAB) and “Numeric in Geotechnics“ (DGGT AK 1.6) of the German Society of Geotechnical Engineers. These efforts should be supported with further investigation, especially for excavations in normally consolidated soft clay.

Most excavation are analyzed assuming plane strain condition. While plane strain analysis can give reasonable results for excavations with relatively long walls in out of plane direction, its result, however, is questionable for short walls. Varzi and Troughton 1992 suggested a wall length in excess of 60 m could be considered to be effectively a plane strain condition. Most often, the size of excavations in built up area for high rise buildings is not greater than 60 m. Moreover, the struts at internal corners, the overlap of anchors at external corners, the arrangements of berm construction, and the excavation and placement of bottom slab in slices demand for a three dimensional analysis in excavations for high rise buildings or underground parks. According to Moormann et al. 2000 the plane strain analysis overestimates the earth pressure and the wall displacements around the middle of the excavation.

In the following section the factors that affect the performance of an excavation in view of parameter study using the finite element method in the literature are presented.

4.9.2 Factors affecting the performance of excavations

1. Effect of wall stiffness:

In general, a change of the stiffness of the wall within practical limits for a given soil has negligible effect on the ground movements. (Palmer and Kenny 1972; Burland et al. 1979; Mana 1978; Zeng et al. 1986; Freiseder 1998). Clough and Tsui 1974 showed that an increase in wall stiffness by a factor of 32 had resulted in the corresponding reduction of the movements by a factor of 2 only. Clough and Tsui 1974; Mana 1978; Zeng et al. 1986; Freiseder 1998 reported increase in the rigidity of the wall results in an increase in the bending moment and support loads. Potts and Fourie 1985; Potts and Bond 1994, however, commented that the effect of wall stiffness is rather a function of the initial stress condition. It is higher for soils with $K_0 = 2$ than for soils with $K_0 = 0.5$. For smaller values of K_0 , for instance $K_0 = 0.5$, the effect is very small on bending moment and almost negligible on support load.

2. Effect of the lateral support stiffness:

A very stiff lateral support system reduces the deflection of the wall at the support levels and increases strut loads and bending moment accordingly (Palmer and Kenny 1972; Clough and Tsui 1974; Burland et al. 1979; Mana 1978; Zeng et al. 1986; Freiseder 1998). However, surface settlement is inevitable, primary because

of the amount of deformation which occurred below the excavation are not affected much by the rigidity of the support.

3. Effect of horizontal support spacing:

The effect of horizontal spacing of support is usually included in the stiffness of the support and separate study is not important.

4. Effect of the vertical distance between the support and bottom of the excavation:

Since most horizontal movement occurs at the embedded portion of the walls between the completion of excavation and the installation of the supports at each level, the magnitude of the load acting on that portion and the type of soil and its properties are closely related to the magnitude of the horizontal movement. In order to reduce the magnitude of the load, it is necessary to reduce the distance between the supports to be installed and bottom of excavation for each level. This should be kept as short as possible whilst allowing the work to proceed (Fujita 1994). On the other hand, Palmer and Kenny 1972 reported that vertical spacing of supports is only of moderate importance.

5. Effect of pre-stressing supports:

While pre-stressing of the struts and anchors is desirable to reduce the ground movements, the pre-stress loads should be limited by the yield properties of the soft clay soil (McRostie et al. 1972). It is suggested that a small amount of pre-stress could be beneficial in ensuring early effectiveness of the supporting system but a large amount of pre-stress may not provide additional benefits (Palmer and Kenny 1972; Clough and Tsui 1974; Mana 1978). This is, according to Palmer and Kenny 1972, a consequence of the fact that a great deal of the wall deflection occurs well below the excavation level and pre-stressing primarily affects the active soil mass which in itself does not greatly influence the overall performance of the excavation.

6. Effect of depth of excavation:

It is evident that the surface settlement, wall deflection and bending moment increase with the depth of excavation. All back analysis results and parametric studies confirm this fact.

7. Effect of depth of penetration of the wall

If the depth of penetration is determined on the basis of the stability of the excavation, further increase of the penetration depth will have a minimum influence on the performance of the excavation (Zeng et al. 1986). Mana 1978 compared the free end and fixed end wall condition for sheet pile and showed that the difference in the ground movement pattern is very slight but the fixed end wall has a slightly larger zone of yielding. He further showed that increasing the depth of embedment slightly increases the bending moment in the embedded portion of the wall where as the earth pressure distribution acting on the expose part of the wall are essentially the same for both free end and fixed end walls.

8. Effect of berms as temporary support

Peck 1969 suggested that the berm size should be as large as possible in order to limit wall and soil movements. Potts et al. 1993 had made a parameter study on the berm size and confirm Peck's statement that the greater the volume of the berm, the smaller will be the wall deflections and the movements of the retained ground surface behind the wall. An efficiency up to 65% can be achieved with berm volume equal to 30% of the total excavation volume. Fig. 4.40 shows the relationship between the efficiency of the berm in reducing the deformation and its total volume.

On the other hand, Clough and Denby 1977 showed that the effect of a berm is not a unique function of the berm size rather it is also influenced by wall stiffness, excavation depth, wall end conditions, and soil shear strength. They reported that at low stability numbers, increase in berm size produce minimal movement reduction, whereas at high stability number, increasing the berm size leads to a large reduction in settlements. However, at high stability number, even with large berms, large movements may occur because deep seated movements may take place beneath the berm. As a result the effectiveness of the berm is diminished.

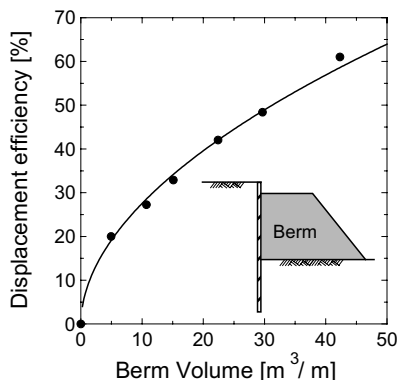


Fig. 4.45. Variation of displacement efficiency with berm volume (Potts et al. 1992)

9. Effect of soil strength and stiffness:

All back analysis results and parametric study reported in the literature show that primarily the stiffness of the soil and then the shear strength of the soil have the greatest influence on the performance of an excavation. Palmer and Kenny 1972, however, reported that the shear strength do not have significant influence on the behaviour of excavation that was studied. They admitted however, that in the case of excavation with flexible wall, or with stiffer soils, or partially penetrating wall, the soil strength might have greater influence.

10. Effect of in-situ stress (K_0):

There are contradicting views on the effect of the initial stress on the performance of excavation. Palmer and Kenny 1972 concluded that K_0 has little influence on the excavation behaviour. On the other hand, by taking a wide range of K_0 (0.5 - 2.0) in the parametric study and in combination with limit state method, Potts and Fourie 1985; Potts and Bond 1994 showed that wall deflection, bending moment

of the wall and support load increase as the value of K_0 increases. Recently, Freiseder 1998 also indicated that the horizontal wall deflection at the top of a diaphragm wall increases linearly with the increase of K_0 , whereas the deflection of the wall is almost independent of the value of K_0 . Further, he showed that the effect of K_0 is more pronounced on bending moment of the wall, support load and earth pressure. These values increase greatly as K_0 increases from 0.3 to 1.0. Gunn and Clayton 1992 also showed that the main reason for the effect of the installation of diaphragm or bored pile wall on the ground movement before soil excavation is the change of the in-situ stresses surrounding the trench or the drill hole. Therefore, the contradicting conclusion of Palmer and Kenny 1972 might come from the fact that they had considered a narrow range of K_0 values (0.5 - 0.7), where the effect is very small.

11. Effect of soil-structure interaction:

Freiseder 1998 showed that the variation of the interface reduction factor has insignificant influence on earth pressure and horizontal wall deflection at the wall toe, whereas it has slight influence on the bending moment of the wall and considerable effect on the horizontal wall deflection and vertical displacement of the top of the wall.

12. Effect of width of excavation:

Mana 1978 investigated the effect of width of excavation and showed that the wider the excavation, the larger are the magnitude of ground movements and the size of the yield zones as expected. He also indicated that the predicted zone of yielding are larger than those assumed by Terzaghi 1943 (Fig. 4.13b), especially on the active side of the wall.

13. Effect of depth to firm layer:

The influence of depth to firm layer is seen to be very important in terms of magnitude and distribution of strut loads (Mana 1978). This is in agreement based on the postulate of Bijerrum et al. 1972 (see also section 4.4.2), where they said that the increase in earth pressures behind the exposed part of the wall and the resulting large strut load are mostly a function of the soil deformations taking place below the bottom of excavation.

4.10 Parameter study

4.10.1 General

A parametric study is a study of the effect on the solution or behaviour of a problem by varying the value of one parameter while keeping all other parameters at a constant or reference value. By doing so, the sensibility of the performance of the problem, in this case excavation, to each model parameter or geometry or others can be identified. The finite element method (FEM) provides the best condition for parametric studies. In this book, the two dimensional FE - program "PLAXIS" version 8.1 is used to perform the parametric studies. Triangular elements with 15

nodes (see Brinkgreve and Vermeer 1998; and Brinkgreve 2002) are used in all the FEM- computations in this section. This element provides a fourth order interpolation for displacements and it involves twelve numerical integration stress points (Gauss points). Basically, the hardening soil model (HSM) is used to simulate the soil behaviour and the Mohr-Coulomb model (MCM) to simulate the interface element. An elastic behaviour is assumed for all structural elements.

The influence of the hardening soil model parameters on the stress - strain, volume change and excess pore pressure behaviour has been discussed in Section 3.3 for a triaxial and one-dimensional compression test condition. Once more, the influence of these parameters on the performance of an idealised excavation are investigated in this section. First, however, the recommendation of the working group "Numerics in Geotechnics" (DGGT AK 1.6) of the German Society of Geotechnical Engineers (Meißner 2002), regarding the size of the finite element model of an excavation has been examined for excavations in soft soils.

Berms provide support to the retaining structures before the strut or anchor or bottom slab or propped support are installed in place. The efficiency of the berms in reducing the movement of the wall and the soil has also been dealt with in this section.

An installation of a support at the bottom of excavation prior to the end of excavation either by means of a column jet pile or soilcrete or bottom concrete slab placed in slices reduces the wall movement at the toe and at the excavation level to some extent. The efficiency of such support system is going to be dealt with in this section.

4.10.2 System geometry

In order to investigate the influence of the size of the FEM - model on the deformation behaviour of an excavation, an idealised excavation shown in Fig. 4.46 has been chosen. The ground is assumed to be a deposit of a homogeneous lacustrine soft soil with the groundwater table located at 1.5 m below the ground surface. The excavation 6.0 m deep is supported by a sheet pile wall of the type Hoech 134 with a total length of 13.0 m, with an embedment depth of 8.1 m and with two levels of struts (IPB 360 St 37). A building load of 50 kN/m² at a distance of 3 m behind the wall and a traffic load of 10 kN/m² is assumed at the ground surface.

A drained type of analysis has been used, because it is believed that this condition is most unfavourable condition for excavations in soft deposits. The reference soil parameters are adopted from Table 3.15 for the HSM. The stiffness of the soil were taken as it is for the interface element, whereas the shear parameter were reduced by a factor of 1/3 in the MCM. The wall and the struts are assumed to behave linear-elastic with the following material properties:

Wall: $EA = 3.591 \times 10^6 \text{ kN/m}$, $EI = 5.355 \times 10^4 \text{ kN-m}^2/\text{m}$, $w. = 1.34 \text{ kN-m/m}$, $\nu = 0.30$

Strut: $EA = 3.801 \times 10^6 \text{ kN}$, $L_{spacing} = 2.0 \text{ m}$

Three excavation width $B = 12, 24$, and 48 m has been considered in the parametric study. For each case of the excavation width, the horizontal distance behind the wall and the vertical depth below the bottom of the excavation up to the right

side and bottom boundaries respectively are varied according to the table in Fig. 4.46. In order to avoid the influence of the size and number of the elements on the results of the comparison, an inner zone which is 12 m behind the wall and below the excavation bottom is defined. The number of elements in this inner zone are held as much as possible constant for all cases of variations, whereas a slight variation in the size of the elements out side this zone are allowed. The program automatically generates the mesh of the model which makes it difficult to control the size of the elements in case of a change of model geometry.

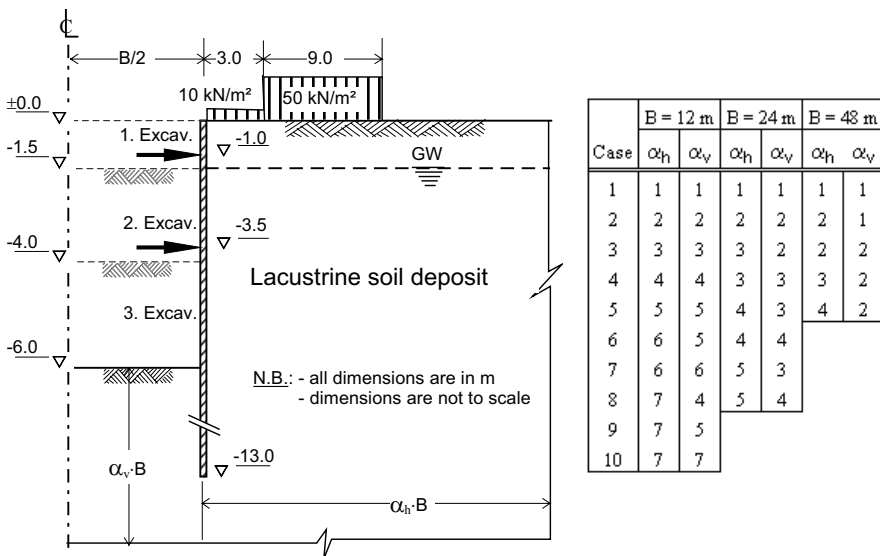


Fig. 4.46. Idealized excavation problem and variation of the geometry of the FE - Mode

The results of the variation of the geometry of the model are shown in Fig. 4.47. It would appear from the Fig. 4.47 that the effect of the FEM - model size on the deflection of the wall is very minimum. The maximum difference in the deflection of the wall from the different size of the geometry lies below 4% for a given width of excavation. However, the deflection of the wall seems to increase as the width of the excavation increases (Fig. 4.47a).

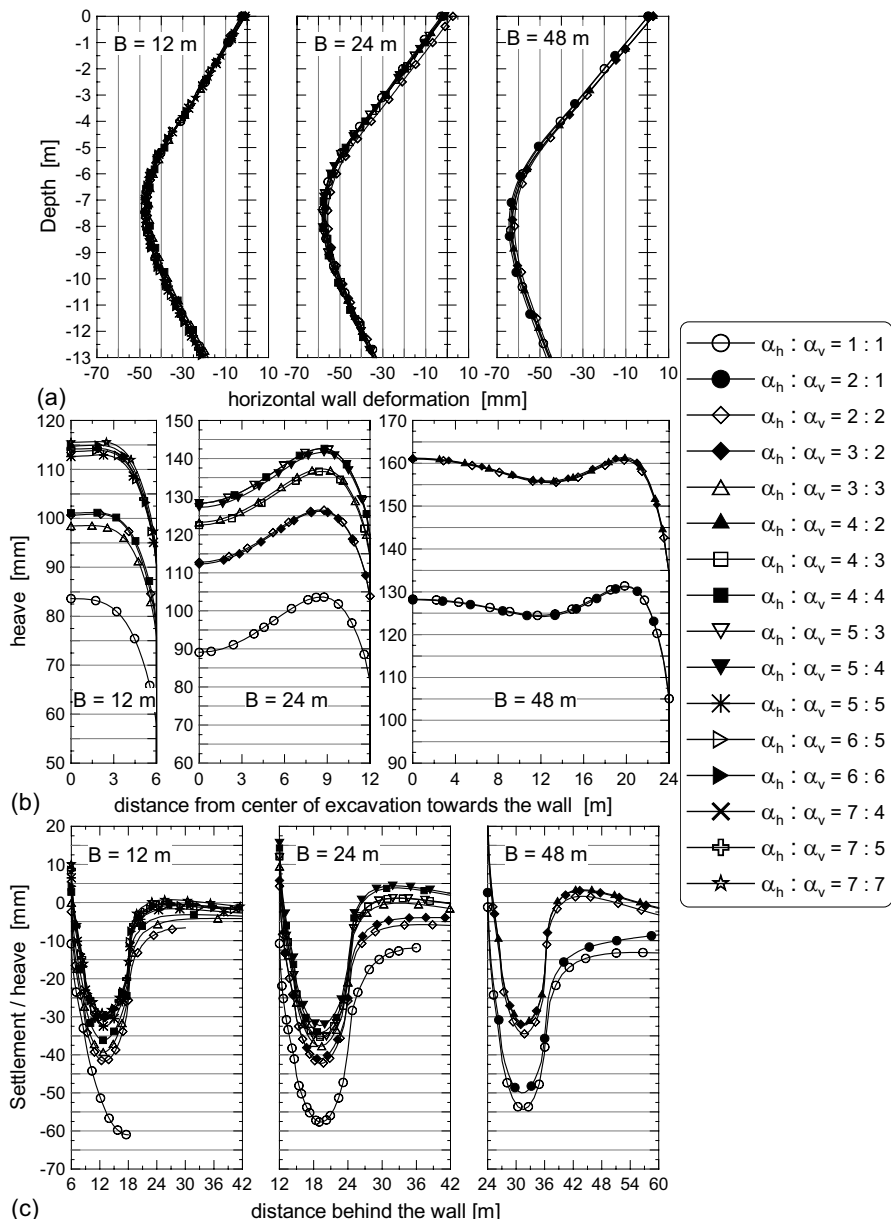


Fig. 4.47. The influence of the size of the FEM-Model on: a) deflection of the wall, b) heave at the bottom of excavation, c) settlement or heave at the surface behind the wall

The effect of the model size may clearly be seen on the heave of the bottom of the excavation (Fig. 4.47b). The heave increases with the increase of the geometry, but its rate of increase ceases with the geometry size. For example, an increase of the geometry size from 84×78 m to 108×102 m for the case of $B = 24$ m results in a 3.8% increase of the maximum heave. On the other hand, it would appear from Fig. 4.47b that the height of the model plays a significant role on the heave property of the excavation than its width. Keeping the height of the model constant and enlarging its width resulted in almost no heave at the bottom of the excavation (Fig. 4.47b). This is very important in regard to the selection of the model size, because the depth of the soft soil is somewhat limited in most cases (for example the lacustrine soft soil deposit in southern Germany is limited to a maximum depth of 60 to 70 m). Underneath the soft soil a bearing layer, for example gravelly sand moraine or boulder clay is usually encountered. In other words, if the depth of the model to the lower boundary can be fixed, there is no need to enlarge the model in the horizontal direction more than twice the excavation width.

In general the following conclusions can be made from the result of the above parameter study. Horizontal wall deflection and displacements do not be affected by the size of the model, however, the deflection increases with the increase of the width of excavation. The main factor that influence the heave at the bottom of the excavation and settlement at the surface is the height of the model rather than the width of the model. Another general observation is that the deflection of the wall, the heave at excavation bottom increase with increase of the width of excavation, whereas the settlement at the surface tends to decrease with increasing width of excavation.

4.10.3 Sensitivity study of the hardening soil model parameters

Problem formulation

The sensitivity study of the hardening soil parameters using the FEM has been presented in Section 3.3 based on triaxial test specimens. In this section a further study of the influence of each HSM parameters on the performance of an idealized excavation problem has been investigated. The FEM-model chosen is similar to that used for the study of the model geometry in Section 4.10.2 (Fig. 4.46), except that the geometry of the FEM-model here is fixed to 48×42 m². The idealized excavation problem is shown in Fig. 4.48 on the left and on the right is the corresponding section of the FEM-model and its mesh. The ground is assumed to consist a homogeneous lacustrine soft soil deposit and the support system is the same as that described in section 4.10.2 (Fig. 4.46).

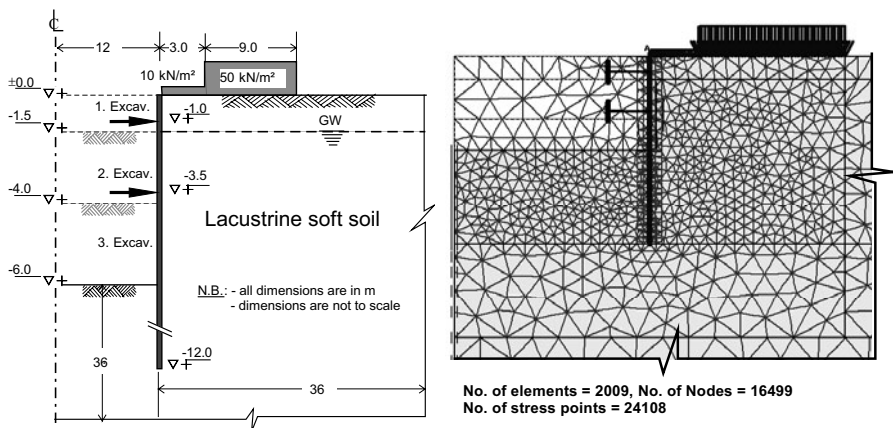


Fig. 4.48. Idealized excavation problem and the corresponding FEM-model with mesh

Drained analysis

For the drained analysis of the idealized excavation problem, the HSM parameters in Table 3.15 is adopted as a reference parameters for the soil body. The shear parameters for the contact surface are adopted from the soil body after reducing the values by a factor of 1/3. The stiffness of the interface elements is assumed to be the same as the soil. The following construction stages are followed in the FEM- calculation:

- Stage 0: generation of the initial stresses (K_0 - method)
- Stage 1: application of the surcharge and traffic loads
- Stage 2: installation of the wall
- Stage 3: first excavation
- Stage 4: installation of the 1st strut and 2nd excavation
- Stage 5: installation of the 2nd strut and 3rd excavation

The results of the sensitivity study for the case of the end of excavation under fully drained condition are shown in Figs. 4.49 to 4.54.

The effect of the Poisson's ratio. As it can be seen from Fig. 4.49, the Poisson's ratio for un/reloading ν_{ur} seems to be a pure deformation parameter. In other words, ν_{ur} may affect the deformation of the wall and soil movements but not the earth pressure and bending moment of the wall. A change of the ν_{ur} from its reference value of 0.2 to a smaller value of 0.05 and a larger value of 0.3 has resulted in a uniform change of the wall deflection by about -7 and 4% respectively. Similarly, a change of the heave by about 15 and -10%, and a change of the surface settlement by about -21 and 15% respectively are calculated.

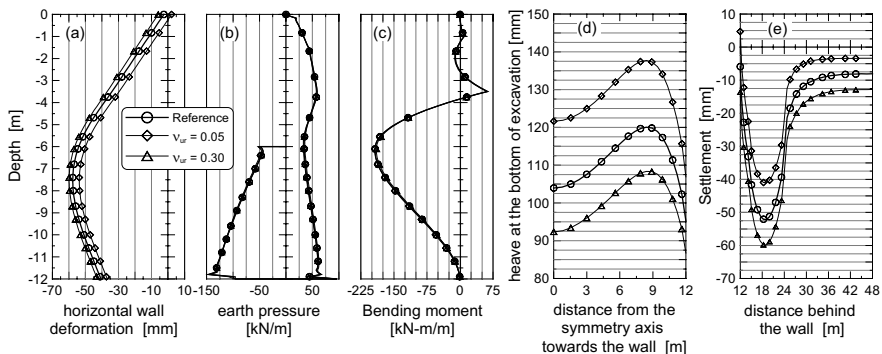


Fig. 4.49. The effect of v_{ur} on a) deformation of the wall, b) earth pressure, c) bending moment of the wall, d) heave of the bottom of excavation, and e) settlement of the surface

The effect of the coefficient of the earth pressure at rest. The HSM treats K_0^{nc} and K_0 separately. While K_0^{nc} is a model parameter which is closely related to the stiffness parameters E_{50} , E_{oed} , E_{ur} and v_{ur} , the K_0 is purely used to define the initial state of the stresses. For normally consolidated soils, however, these values are more or less the same. The value of K_0^{nc} as a model parameter can not be varied indefinitely. For example, for the given reference parameters, the minimum and maximum possible values of K_0^{nc} are 0.437 and 0.71 respectively. Here K_0 is assumed to vary with the K_0^{nc} . As it can be seen from Fig. 4.50, the parameter K_0^{nc} would affect the deformation of the wall, the soil movements, the earth pressure and bending moment of the wall, although the magnitude of its influence is moderate as compare to the triaxial case of loading.

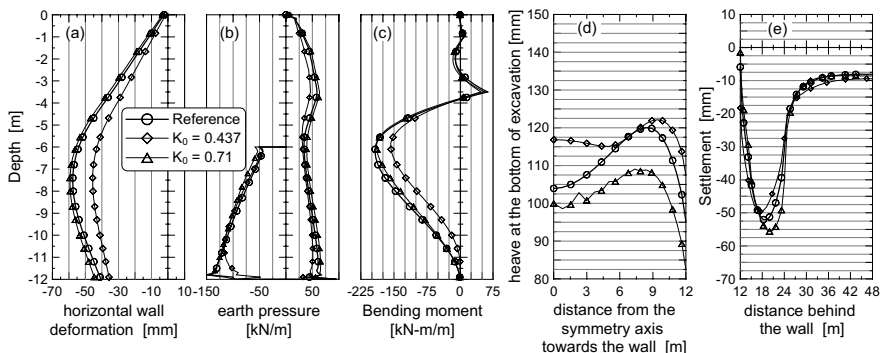


Fig. 4.50. The effect of K_0^{nc} on a) deformation of the wall, b) earth pressure, c) bending moment of the wall, d) heave of the bottom of excavation, and e) settlement of the surface

Varying the value of K_0^{nc} from the reference value of 0.573 to those extreme values has resulted in a change of the maximum wall deformation of about -21 and 3% respectively. Similarly, a change of the heave by about 2 and -9%, a change of the surface settlement by about -5 and 7%, a change of the earth pressure by about -21 and 8%, and a change of the bending moment by about -18 and 2% respectively are calculated. From the above percentage difference presentation and Fig. 4.50, it appears that varying K_0^{nc} value towards the lowest limit is more sensitive than varying its value towards the upper limit, although the difference between the reference value and the extreme values is almost the same.

The effect of the failure factor. In triaxial and oedometer loading conditions, it has been proved that the failure factor R_f plays an important role in enhancing or retarding the failure of the soil body. Its influence on the idealized excavation, however, seems to be minimum, with exception of the settlement behind the wall (Fig. 4.51). Varying the value of R_f from the reference value of 0.83 to 0.67 and 0.97 has resulted in a change of the surface settlement by about -8 and 6% respectively. For all the other cases, the difference remains below $\pm 5\%$.

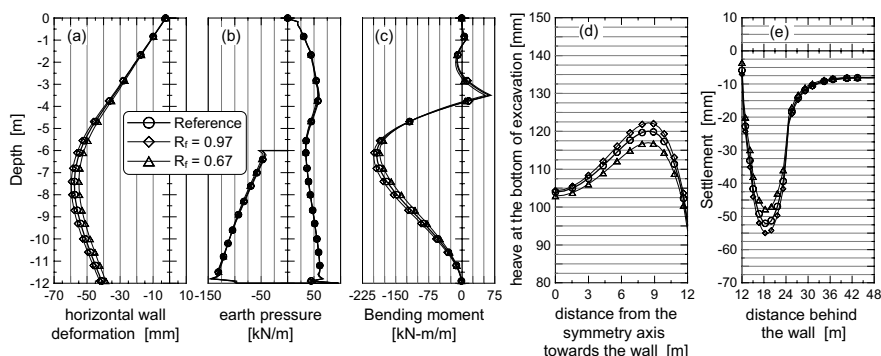


Fig. 4.51. The effect of R_f on a) deformation of the wall, b) earth pressure, c) bending moment of the wall, d) heave of the bottom of excavation, and e) settlement of the surface

The effect of the constrained modulus. As shown in Fig. 4.52, a variation of the constrained modulus E_{oed} by about $\mp 50\%$ its reference value, has resulted in a change of the maximum wall deflection by about -30 and 5% respectively. Similarly, a change of the heave by about -17 and -4%, a change of the surface settlement by about -24 and 2%, a change of the maximum earth pressure above the bottom of excavation by about -17 and 2%, and a change of the bending moment by about -23 and 3% respectively were observed (Fig. 4.52). Hence, the following conclusion may be drawn with regard to the response of the excavation to the change of E_{oed} .

- In all cases E_{oed} is more sensible to a change of value below the reference value than to value greater than the reference. It can be seen from Fig. 4.52 that a re-

duction of the reference value of E_{oed} by 50% has caused a reduction of the wall and soil movements, the active earth pressure and the bending moment by about 17 to 30%, whereas increasing the reference value by same amount (50%) show no significant influence (2 to 5%). It seems that the ratio of the E_{50}/E_{oed} is more important than the absolute value of E_{oed} . For the reference case, this ratio becomes 1.1. If E_{oed} is increased or decreased by about 50%, the ratio becomes 0.73 and 2.20 respectively. The ratio in the case of increasing E_{oed} is more closer to the reference ratio than the other way round. This might be the reason why the change of the E_{oed} is more sensible to a value below the reference than above the reference value.

- b) Contrary to expectation, a reduced value of E_{oed} has resulted in a reduction of wall and soil movements.
- c) Fig. 4.52b shows a reduced active pressure and an increased passive pressure for the case of E_{oed} smaller than the reference value. This again contradicts with the reduced wall movement that is discussed in (b). A reduced wall movement would have resulted a higher active earth pressure and lower passive pressure.
- d) A reduced active pressure on one side and an increased passive pressure on the other side has resulted in a reduced bending moment, which seems logical in respect to the given loading condition but not in a general sense.

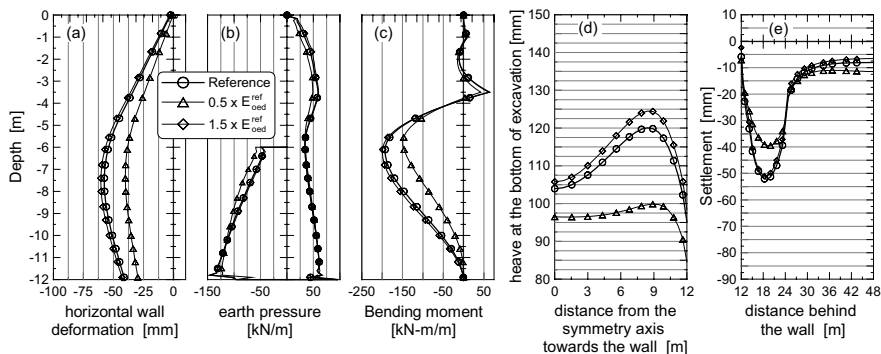


Fig. 4.52. The effect of E_{oed} on a) deformation of the wall, b) earth pressure, c) bending moment of the wall, d) heave of the bottom of excavation, and e) settlement of the surface

The effect of the un/reloading modulus of elasticity. The reference value of the un/reloading modulus of elasticity E_{ur} is directly taken from triaxial test result and it is equal to. Lowering the reference value to $3 \cdot E_{ur}$, which is usually recommended in practice with the absence of a test result, and further lowering the reference value to $2 \cdot E_{ur}$ have resulted in an increase of the displacement of the toe of the wall by about 27 and 63% respectively. Similarly, a change of the heave of the bottom of excavation by about 75 and 150%, a change of the surface settlement by about -15 and 30%, a change of the active pressure above the bottom of excavation by about -16 and 22% respectively, and an insignificant change of the maxi-

mum bending moment (below 2.5) are calculated (Fig. 4.53). The earth pressure below the excavation level on both active and passive side also shows no significant change relative to the reference value. Contrary to the expectation, the settlement at the surface for the reduced values of E_{ur} is less than that from the reference value. This is mainly due to the upward displacement of the wall. The whole soil body seems to heave upwards due to lower values of the E_{ur} .

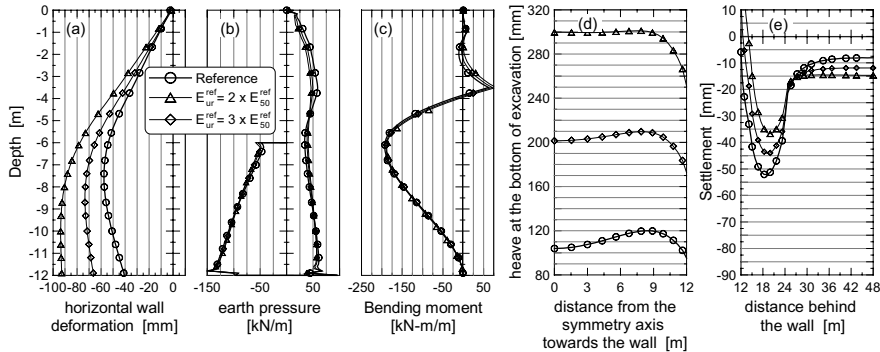


Fig. 4.53. The effect of E_{ur} on a) deformation of the wall, b) earth pressure, c) bending moment of the wall, d) heave of the bottom of excavation, and e) settlement of the surface

The effect of the secant modulus of elasticity. Fig. 4.54 shows the effect of the variation of the secant modulus of elasticity at 50% failure stress E_{50} by $\pm 50\%$ from its reference value. These variations of E_{50} have resulted in a change of the maximum wall deflection by about 45 and -24% respectively. Similar change of the heave by about 21 and 11%, the surface settlement by about 71 and -37%, the maximum earth pressure above the bottom of excavation by about 19 and -15%, and the maximum bending moment by about 27 and 18% respectively are observed.

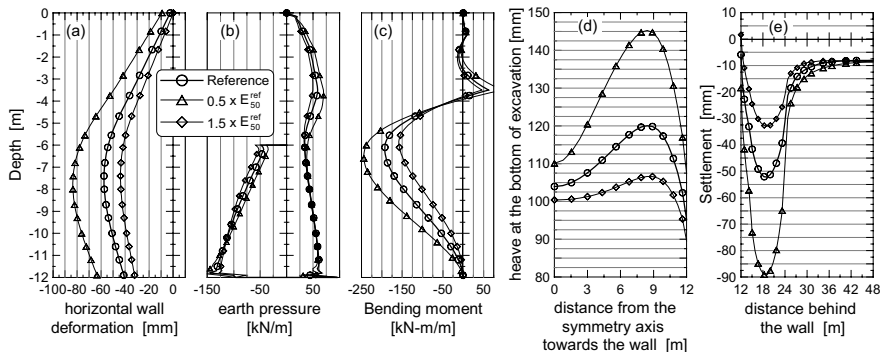


Fig. 4.54. The effect of E_{50} on a) deformation of the wall, b) earth pressure, c) bending moment of the wall, d) heave of the bottom of excavation, and e) settlement of the surface

At first glance, it seems that an increased wall movement should result in higher passive resistance, because the soil is more close to the passive limit state. However, as the numerical study of the mobilization of the passive resistance also shows, the passive resistance is lower for lower values of the modulus for a given displacement of the wall and keeping the shear parameter constant. This is exactly what one can observe in Fig. 4.54. Lower value of E_{50} leads to higher wall movement but a lower passive resistance and vice versa.

Undrained condition

For a reason of comparison, the HSM parameters in Table 3.15 are adopted as a reference parameters for the soil body in the undrained analysis of the idealized excavation problem (Fig. 4.48) similar to the drained analysis. As already mentioned in section 3.3.2, it is possible to perform undrained analysis with the PLAXIS program using the effective shear and stiffness parameters. The parameters for the contact element were the same as the drained analysis except that the analysis was undrained. The construction steps followed in the undrained analysis are also the same as the drained analysis. However, the undrained behaviour was ignored in the first three calculation phases.

The effect of the strength and stiffness parameters on the performance the given excavation under undrained condition is more or less the same as in the drained analysis. All the tendencies and comments in the previous section for the drained condition are valid for the undrained condition except for the case of the influence of v_{ur} on the heave at the bottom of the excavation (Fig. 4.55a) and the influence of v_{ur} and E_{ur} on the settlement at the surface behind the wall (Fig. 4.55 b&c).

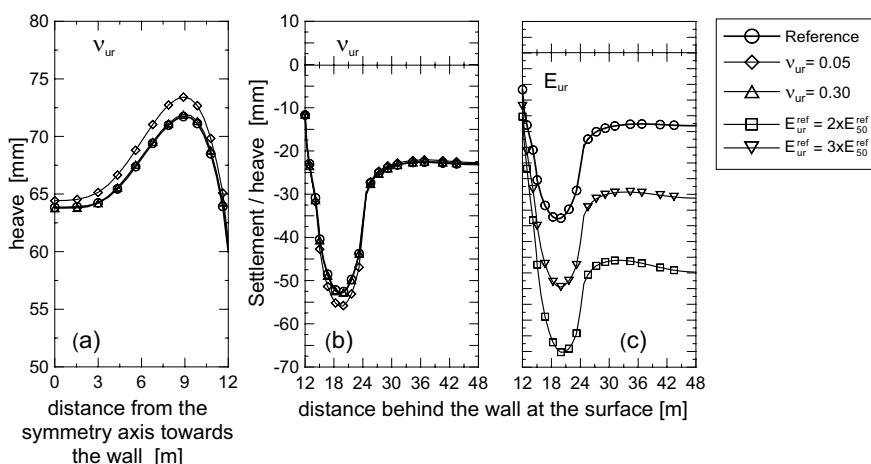


Fig. 4.55. a) The influence of v_{ur} on the heave at the bottom of excavation, b) The influence of v_{ur} on the settlement of the surface behind the wall and c) The influence of E_{ur} , on the settlement of the surface behind the wall under undrained condition

As it can be seen from Fig. 4.55 a&b, the effect of the v_{ur} on the heave at the bottom of the excavation and settlement of the surface behind the wall is marginal as compared to the case of drained analysis. On the other hand, the parameter E_{ur} shows a significant influence on the settlement of the surface contrary to the drained condition (Fig. 4.55c)

The effect of v_{ur} , R_f , K_0^{nc} , E_{oed} , E_{ur} , and E_{50} on excess pore water pressure. The sensibility of the excess pore water pressure to the variation of the HSM parameters is shown in Fig. 4.56. As shown in the figure, three points are selected for the sensibility study: one at the middle of the excavation and just below the bottom of the excavation (Point B), one near the wall and just below the bottom of excavation (Point C), and the other just below the wall toe (Point E). It can be seen from the Fig. 4.56 that the excess pore water pressure is more sensible to the variation of the K_0^{nc} value (Fig. 4.56a) and the parameter E_{ur} (Fig. 4.56b). The influence of these two parameters on the excess pore water pressure is abundantly clear at Point E. At this point the other parameters do also affect the excess pore pressure to some extent.

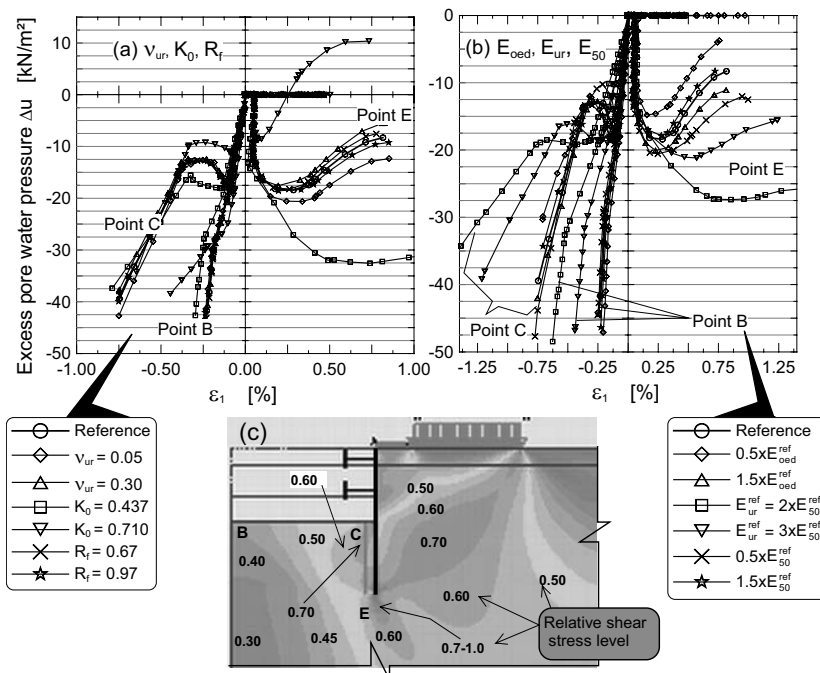


Fig. 4.56. The influence of a) v_{ur} , K_0^{nc} and R_f , and b) E_{oed} , E_{ur} , and E_{50} on the development of the excess pore pressure at selective points, and c) the relative shear stresses contour for the reference case

The relative shear shading (Fig. 4.56c) for the reference case shows that the soil around point E is at failure or near to failure, whereas the point B is far away from failure. Almost 75% of the strength of the soil around point C is already mobilised. Referring back to section 3.3, it is apparent that the influence of some parameters starts first while the soil approaches failure. This can be the reason why the influence of these parameters at point E is abundantly clear.

4.10.4 Effect of berms on deformation of excavations

The FEM-model in Fig. 4.48 is adopted to study the efficiency of berms. The geometry, the material properties of the soil, the contact element and the structural elements remain the same as in section 4.10.3. The construction steps are also the same as that in section 4.10.3, except that the last excavation has been executed stepwise in six additional sub-steps as shown in Fig. 4.57. There are two cases investigated. In case 1, the excavation is assumed to proceed from the middle of the excavation towards the wall (Fig. 4.57 (left)), whereas in case 2 the excavation is assumed to proceed in the opposite direction (Fig. 4.57 (right)). The soil body in front of the wall is not as such a berm, but since it is there to provide support and hence reduce the soil and wall movements, it is considered as a berm in this parametric study.

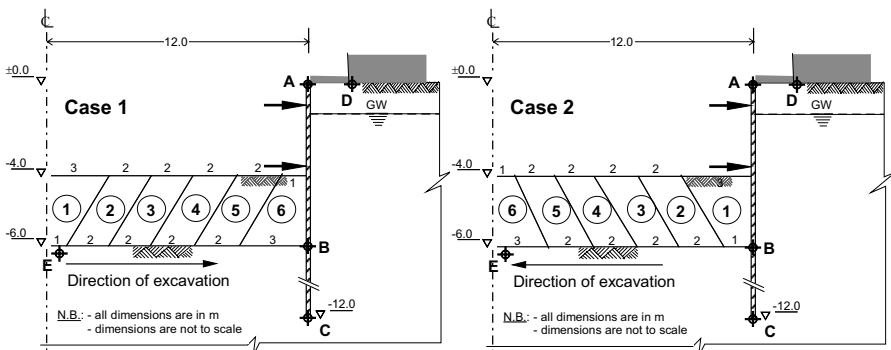


Fig. 4.57. Model for the study of the berm effect

The deformation and displacement of the wall at the locations A, B, and C, the heave of the bottom of excavation at location E, and the settlement at the surface at point D (Fig. 4.57) are considered to evaluate the efficiency of the berms. The efficiency is defined as:

$$\text{Efficiency}[\%] = \left(1 - \frac{\text{deformation / heave / settlement at the end of each stage } x}{\text{deformation / heave / settlement without berm}} \right) \cdot 100$$

The results of the parameter study under fully drained condition are shown in Fig. 4.58. The efficiency at points A, B, C and D drops rapidly at the beginning (100 - 80%) in both cases and continue to fall linearly or non-linearly in a form of

a parabolic curve as the volume of the berm decreases. At point E in case 1, however, the efficiency drops slowly at the beginning and joins the other curves later. The reason for the increase of the efficiency at this point beyond 100% in case 2 is that the soil at this point has settled rather than heaved during the first excavation.

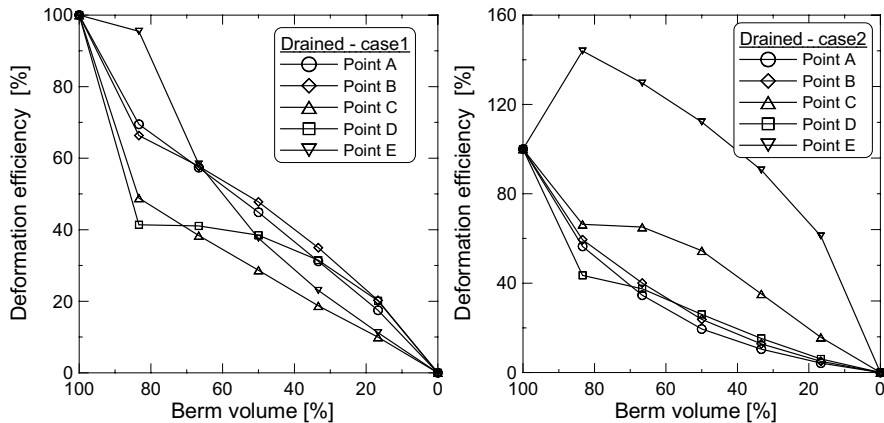


Fig. 4.58. Efficiency of berms under fully drained condition

For the case of undrained condition and case 1, the efficiency lines of all points are almost linear with the exception of point E, which follows an inverted parabolic shape (Fig. 4.59 (left)). On the contrary, the efficiency lines of all points in case 2 are non-linear with the exception of point C, which follows a linear line (Fig. 4.59 (right)). It can be seen from Fig. 4.59 (right) that no support can be expected for a berm volume of $\leq 20\%$.

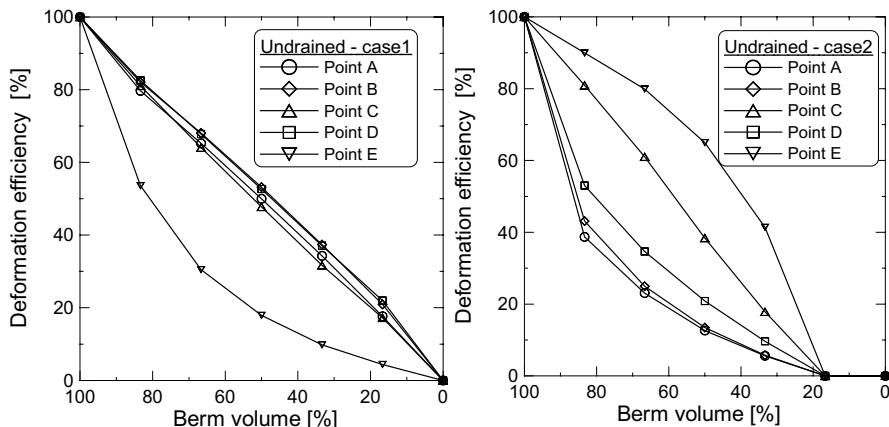


Fig. 4.59. Efficiency of berms under undrained condition

It would appear from Fig. 4.58 that about 40% berm volume may help to reduce the settlement at the surface (point D) by about 35 and 20% for case 1 and case 2 respectively under drained condition. Similarly, for the case of undrained condition (Fig. 4.58) about 43 and 15% reduction of the settlement at the surface (point D) may be achieved with a berm volume of 40% for the case 1 and case 2 respectively. As far as the settlement at the surface and the wall movements are concerned, the second way of handling the excavation (case 2) may not help much to increase the efficiency of the berms.

4.10.5 Effect of the bottom support

Again the same FEM-model as in Fig. 4.48 is used to study the effect of bottom support except that a bottom support is here introduced at different stage of constructions. The geometry, the material properties of the soil, the contact element and the structural elements remain the same as in section 4.10.3. As a bottom support, a 50 cm thick concrete slab with a stiffness $EA = 15 \times 10^6 \text{ kN/m}$ is assumed. The investigated cases include:

- Case 1: Reference situation, i.e., without bottom support*
- Case 2: Bottom support installed before the 1st excavation*
- Case 3: Bottom support installed after the 1st excavation but before the 2nd excavation*
- Case 4: Bottom support installed after the 2nd excavation but before the 3rd excavation*

The locations of the selective points for the evaluation of the deformation efficiency of the bottom support are same as that shown in Fig. 4.57. These include the deformation of the wall at three locations, namely, at the top (point A) at the bottom of the excavation (point B) and at the toe (point C); the settlement at the surface behind the wall (point D) and the heave at the bottom of excavation (point E). The results of the parametric study are shown in Figs. 4.60 and 4.61. Fig. 4.60 shows the effect of the installation of the bottom support at different construction stages on the deformation of the wall at locations A, B and C. The wall at the location A deflects first towards the excavation during the 1st excavation and it deflects back towards the soil during the consequent excavations. As shown in the Fig. 4.48 (top-left), the effect of the bottom support on deflection of the wall at the top is mainly limited to prevent the deflection towards the soil. By installing the bottom support before the 1st excavation (case 2), before the 2nd excavation (case 3) and before the final excavation (case 4), an efficiency of about 97, 92, and 36% respectively may be achieved at point B (Fig. 4.60 (top-right)). Similarly, an efficiency of about 37, 37, and 24% respectively may be achieved at point C (Fig. 4.60 (bottom-left)).

The effect of the installation of the bottom support has a negligible effect on the heave of the bottom of the excavation at point E (Fig. 4.61 (right)). At point D, however, an efficiency of about 76, 72 and 29% can be achieved for the cases 2, 3 and 4 respectively (Fig. 4.61 (right)). Comparing the efficiency achieved at all points for cases 2 and 3, one can observe that the installation of the bottom support

before the 1st excavation would have no significance effect, i.e., a comparable efficiency may be achieved by installing the bottom support before the 2nd excavation.

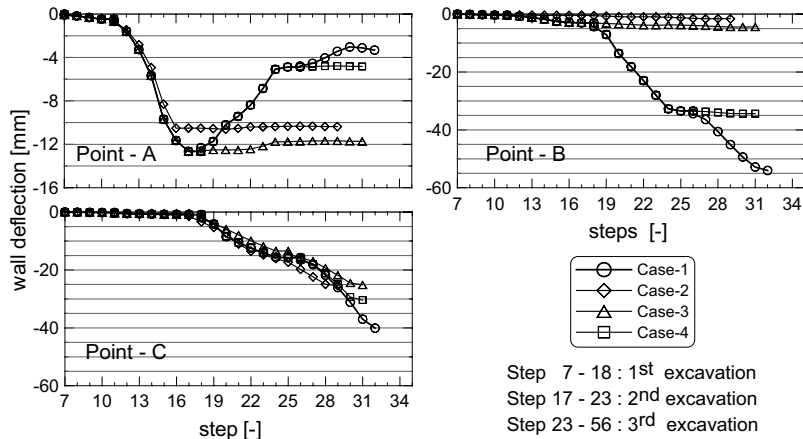


Fig. 4.60. The effect of installation of a bottom support on the deformation of the wall at the top (Point A), at the bottom of excavation (Point B) and at the toe (Point C)

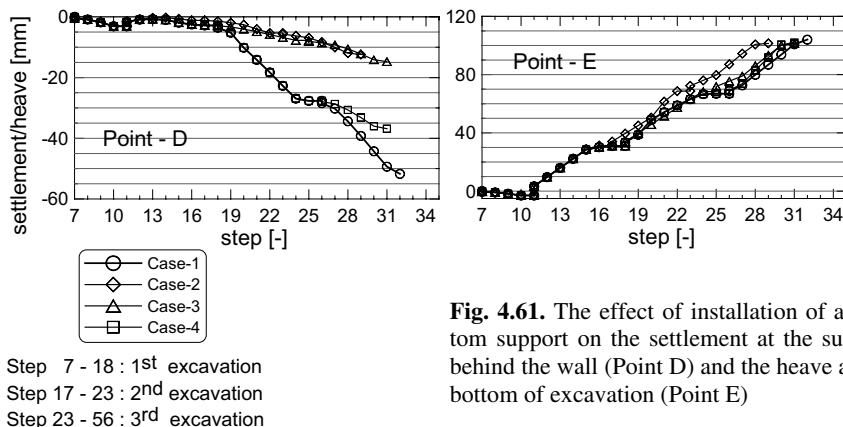


Fig. 4.61. The effect of installation of a bottom support on the settlement at the surface behind the wall (Point D) and the heave at the bottom of excavation (Point E)

4.10.6 Comparison of drained and undrained analysis

One may expect that a drained analysis is nothing other than performing an undrained loading followed by consolidation analysis with an infinite consolidation time (until the excess pore pressure approaches to zero). However, because

the two types of analysis follow different stress paths, the end result of both analysis may not necessarily be the same. In order to see the difference in the result of the two analyses, a numerical comparison between the drained and undrained analyses followed by consolidation has been conducted. The FEM- model used is the same as that shown in Fig. 4.48 except that a 12 m thick sand layer is introduced at the bottom of the model instead of a homogeneous lacustrine soft soil throughout the depth in order to allow drainage downwards. A thick lacustrine soft soil underlain by a moraine (gravely sand) is typical soil profile in southern Germany in the city of Constance and the surroundings. The HSM is used to simulate the behaviour of the sand layer and the corresponding parameters are listed in Table 4.6. The following cases have been investigated:

Drained: drained analysis with reference parameter from Table 3.15

Undrained: undrained analysis followed by consolidation analysis after full excavation (the same parameters as case 1)

For all cases of undrained analysis followed by consolidation, a minimum pore water pressure of 1 kN/m² has been achieved at the end of the consolidation process. The soil is allowed to consolidate first after the full excavation has been reached.

Table 4.6. HSM parameters for the sand layer

γ_{sat} [kN/m ³]	φ' [°]	ψ' [°]	c' [kN/m ²]	E_{50}^{ref} [kN/m ²]	E_{oed}^{ref} [kN/m ²]	E_{ur}^{ref} [kN/m ²]	p^{ref} [kN/m ²]	m [-]	R_f [-]	K_0^{nc} [-]	V_{ur} [-]
21.0	33.0	3.0	1.0	35000	35000	140000	100	0.50	0.90	0.46	0.20

The result of the numerical study is given in Figs. 4.62 and 4.63. The comparison of the deformation of the wall and the soil movements between the two cases listed above have been made at a selective reference points. The location of these reference points are shown in Fig. 4.57. The drained and undrained analysis have shown different wall deformations at point A (Fig. 4.62 - top-left). At locations B (Fig. 4.62 - top-right) and C (Fig. 4.62 - bottom - left) the undrained analysis has reached almost the same deformation as the drained analysis before even consolidation started. After the consolidation phase, the deformation at C remains almost unchanged, whereas at B the deformation increased further slowly.

Similar phenomenon may be observed from Fig. 4.63 - left, where the undrained analysis has resulted almost the same settlement at point D even before the consolidation started. On the other side, the soil at point E (Fig. 4.63 -right) has reacted stiffer under undrained condition. The heave at point E at the end of the undrained analysis followed by the consolidation phase was the same as that at the end of the drained analysis. As can be seen from the Fig. 4.62 and 4.63, no significant difference in the deformation results of the two undrained analysis cases can be observed except at point A.

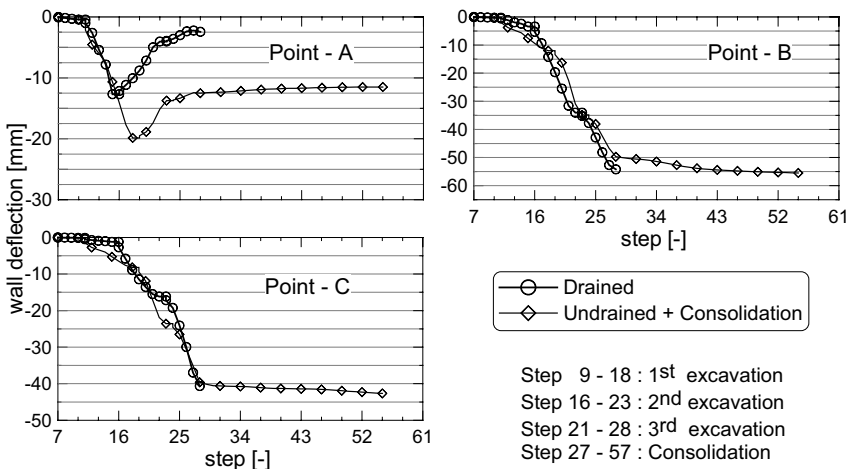


Fig. 4.62. Comparison of the drained and undrained analysis based on the deformation of the wall at locations A, B and C

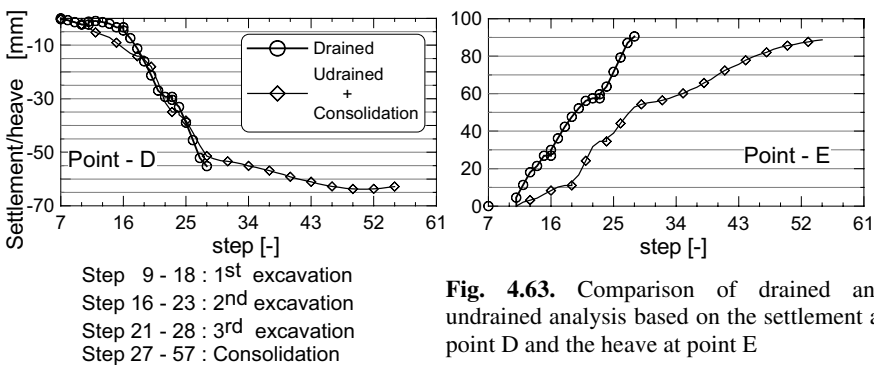


Fig. 4.63. Comparison of drained and undrained analysis based on the settlement at point D and the heave at point E

To summarize, the wall displacement at the toe and at the level of the bottom of excavation and the surface settlement behind the wall seem to be unaffected by the type of the analysis, whereas more heave at the middle bottom of the excavation is computed from undrained analysis followed by consolidation. This shows that the assumption drained = undrained + consolidation should not necessarily be always true as mentioned previously.

4.10.7 Mobilization of the passive resistance of a cohesive soil

General

In order to mobilize the earth pressure fully, active or passive, a certain wall movement is required. The amount of the movement required depends on the type of the wall movement pattern and the soil type. There are four recognized types of wall movements patterns. These are: rotation of the wall about toe, rotation of the wall about top, deflection of the wall and lateral translation of the wall. Most often, a combination of the above movement pattern may also take place. Much experimental work has not been done so far to study the effect of the wall movement on earth pressure in cohesive soils in general let alone in soft cohesive soils. On the other hand, a lot of experimental works have been conducted on sand. Besler 1998 summarized in his dissertation work the model tests so far conducted on sand and the recommended mobilization functions for sand. The attempt on all the model tests on sand was to develop a mobilization function of the passive resistance dependent on the wall displacement.

Based on model tests on sand, Besler 1998 developed a mobilization function of the form:

$$K'_{ph} = A + \frac{B}{C + \xi} \quad (4.35)$$

where K'_{ph} is the mobilised earth resistance; ξ is the ratio between the available wall displacement and the wall displacement at limit state; C is a function of ξ , the earth resistance at limit state K_{ph} and the earth pressure at rest K_0 ; A and B are a function of C , K_{ph} and K_0 .

In the following section is presented an attempt to develop a soil stiffness dependent mobilization function of the earth resistance of normally consolidated soft soils numerically using the FEM. Three types of the wall movement have been investigated. These are: parallel translation of the wall, rotation of the wall about the top and rotation of the wall about the toe (Fig. 4.64).

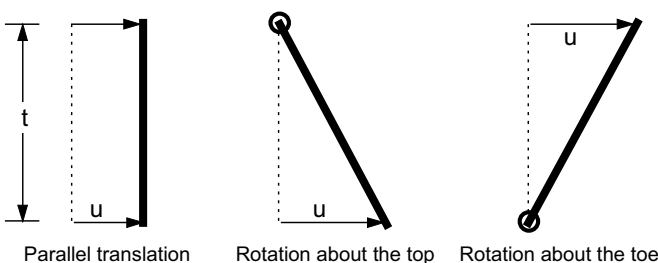


Fig. 4.64. Types of the wall movement

Soil parameters and model geometry

A homogeneous soft soil is assumed, whose behaviour can be simulated using the advanced constitutive soil model known as the Hardening Soil Model (HSM). The soil parameters required for the HSM are given in Table 4.7. The contact between the soil and the wall is simulated by interface elements using the Mohr-Coulomb-Model (MCM) and its properties are given in Table 4.8. The wall is assumed rigid, elastic and weightless with a stiffness of $EA = 7.5 \times 10^6 kN/m$ and $EI = 1.0 \times 10^6 kN/m^2$.

Table 4.7. HSM parameters for the soft soil layer

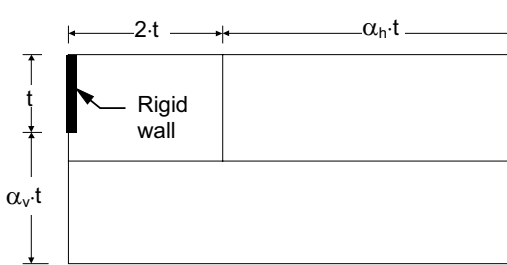
γ_{sat} [kN/m ³]	φ' [°]	c' [kN/m ²]	$E_{50}^{ref} = E_{oed}^{ref}$ [MN/m ²]	E_{ur}^{ref} [MN/m ²]	p^{ref} [kN/m ²]	m [-]	R_f [-]	K_0^{nc} [-]	v_{ur} [-]
19.5	25.0	1.0	0.75 - 10	$5 \cdot E_{50}^{ref}$	100	0.90	0.90	0.58	0.20

Table 4.8. MCM parameters for the interface elements

γ_{sat} [kN/m ³]	$\delta = \frac{1}{3} \cdot \varphi'$ [°]	c' [kN/m ²]	E_{ref} [MN/m ²]	$E_{increment}$ [kN/m ²]	y_{ref} [kN/m ²]	c_{ref} [-]	v [-]
19.5	8.33	0.33	0.75 – 10.0	0.0	0.0	0.0	0.35

Since the main aim of the study is to develop a soil stiffness dependent mobilization function of the earth resistance, the stiffness of the soil, namely the $E_{50}^{ref} = E_{oed}^{ref}$ is varied between $0.75 - 10 MN/m^2$ and the ratio $E_{ur}^{ref} / E_{50}^{ref} = 5$ is kept constant.

In order to limit the influence of the model geometry on the mobilization of the passive resistance, a preliminary analysis is performed by varying the width and height of the model as shown in Fig. 4.65. The smallest soil stiffness in Table 4.7 ($E_{50}^{ref} = E_{oed}^{ref} = 0.75 MN / m^2$) is taken in the preliminary study. The calculation is performed by applying a uniform prescribed displacement on the 8 m long rigid wall in the direction of the soil mass.



Model	α_h	α_v
1	2	1
2	3	1
3	4	1
4	5	1
5	2	2
6	3	2
7	4	2
8	5	2

Fig. 4.65. Model geometry selection

The result of the preliminary FE-computation is presented in Fig. 4.66. The figure shows the passive force as a function of the displacement for the various model sizes, but for $t = 8 \text{ m}$ and $E_{50}^{\text{ref}} = E_{\text{oed}}^{\text{ref}} = 0,75 \text{ MN/m}^2$. As it can be seen from this figure, the passive resistance forces obtained from different model sizes lie in a very narrow band showing a negligible influence of the model size. After closed observation of the principal stress orientations and the displacement vectors near the boundaries and based on Fig. 4.66, the model 8 is chosen for a further numerical study of the mobilization of the earth resistance.

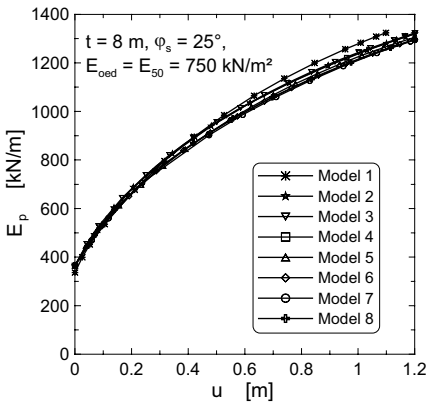


Fig. 4.66. Mobilised passive force for different model sizes

Development of the mobilization function

Once the model geometry had been fixed and the soil model parameters are identified, the FEM-calculations had been started by applying a prescribed displacement either uniformly in the case of parallel translation or in a triangular shape with zero at the top and maximum at the bottom in the case of rotation about toe or again triangular shape but reversed in the case of rotation about head. Two cases of the height of the wall $t = 8 \text{ m}$ and $t = 4 \text{ m}$, seven variations of the stiffness of the soil $E_{50}^{\text{ref}} = E_{\text{oed}}^{\text{ref}} = 0,75, 1,5, 3,0, 4,5, 6,0, 7,5, 10,0 \text{ MN/m}^2$ are investigated.

The results of the parametric studies are shown in Fig. 4.67. A dimensionless presentation is preferred to avoid the effect of the height of the wall on the results and in order to treat the net resistance instead of the total passive force which includes the earth pressure at rest. The dimensionless mobilised net passive resistance is defined as:

$$K_{p(\text{mob})}^* = \frac{(E_{ph} - E_0)}{\left(\frac{1}{2} \cdot \gamma \cdot t^2\right)} \quad (4.36)$$

where E_{ph} is the passive force at limit state and E_0 is the earth pressure at rest. The dimensionless displacement is also defined as u/t . As can be observed from Fig.

4.67, the mobilised resistance for $t = 8 \text{ m}$ and $t = 4 \text{ m}$ almost lie on the same line in all the cases of the wall movement showing the advantage of using the dimensionless parameters.

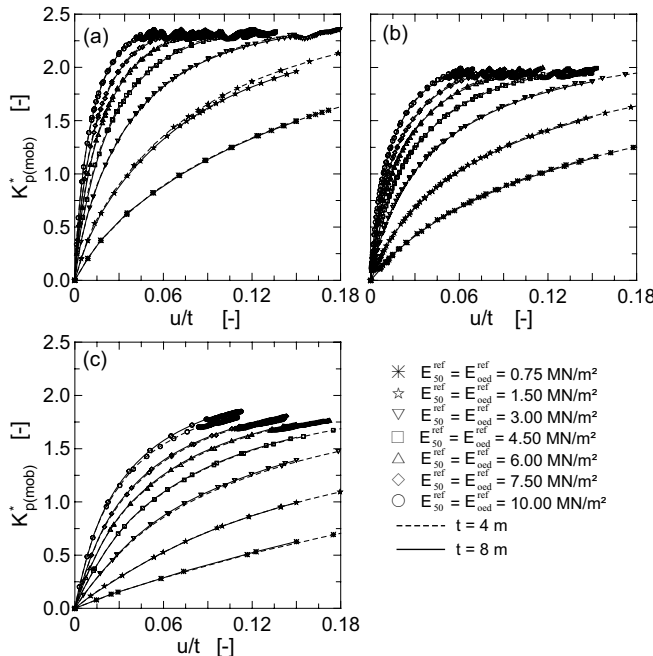


Fig. 4.67. The mobilization of the net passive resistance: a) parallel translation, b) rotation about the head, and c) rotation about the toe

The mobilization curves in Fig. 4.67 may be approximated by a hyperbolic function analogue to the Kondner and Zelasko 1963 hyperbolic equation as follows:

$$K_{p(mob)}^* = \frac{(u/t)}{[a + b \cdot (u/t)]} \quad (4.37)$$

or in a transformed form,

$$\frac{(u/t)}{K_{p(mob)}^*} = [a + b \cdot (u/t)] \quad (4.38)$$

where a and b are the intercept and the slope of the transformed straight lines (see also Fig. 3.15, section 3.2.4). The constants a and b may be obtained from the best fit line of the transformed lines, but the question remains whether there exists a definite relationship between these curve constants and the physical parameters of the soil. Fig. 4.68 shows that the curve parameter a may almost be 100% corre-

lated with the normalized stiffness parameter of the soil using a potential function of the form

$$a = \alpha_1 \cdot \left[\frac{E_{oed}}{\gamma \cdot t} \right]^{\alpha_2} \quad (4.39)$$

The values of the constants α_1 and α_2 are given in Fig. 4.68 for the three cases of wall movement. The slope b is usually related to the deviatoric stress at failure in approximating the stress - strain behaviour of soils with a hyperbolic function according to Duncan and Chang 1970. Analogue to this, b may be related to the passive resistance at limit state, namely the coefficient of the passive earth pressure K_{ph} . That is,

$$b = \frac{\beta}{K_{ph}} \quad (4.40)$$

Reading the value of the slope b from the transformed lines and K_{ph} from standard tables for $\varphi' = 25^\circ$, the value of b may be calculated for different stiffness values of the soil. It appears that the values of b are fairly constant for a given range of stiffness of the soil. Therefore, its value may be fixed as an average value as shown in Table 4.9 for two ranges of the stiffness values.

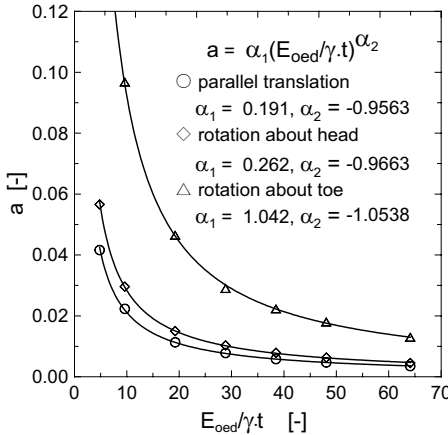


Fig. 4.68. Relationships between the normalized constrained modulus E_{oed} and the curve constant a for $t = 8 \text{ m}$

Hence, substituting a and b from Eqs. 4.39 and 4.40 into Eq. 4.37, one may arrive at the mobilization function of the form:

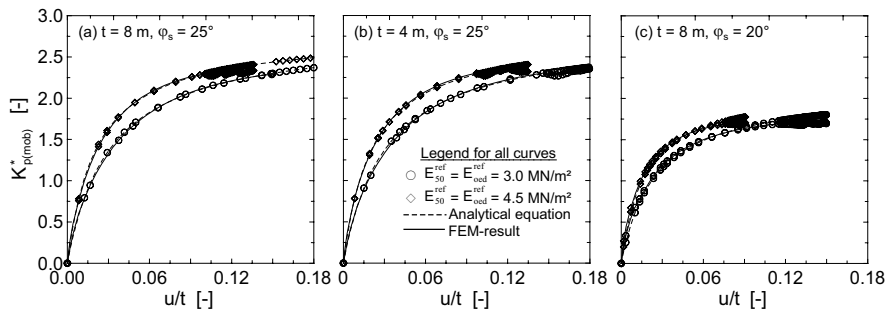
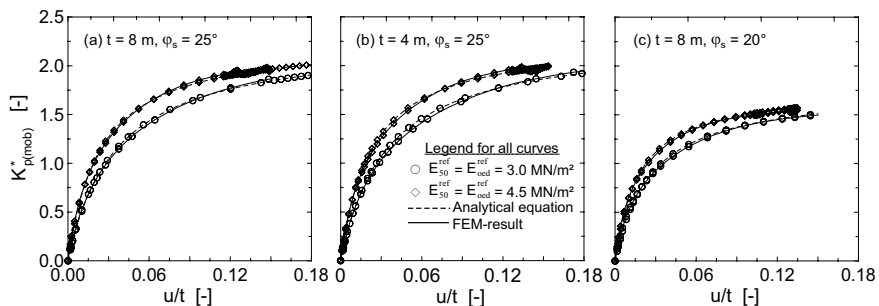
$$K_{p(mob)}^* = \frac{(u/t)}{\left[\alpha_1 \cdot \left(\frac{E_{oed}}{f \cdot \gamma \cdot t} \right)^{\alpha_2} + (u/t) \cdot \frac{\beta}{K_{ph}} \right]} \quad (4.41)$$

Where $f = 8/t$ is a correction factor for the height of the wall.

Table 4.9. Values of the constant b for a range of stiffness of the soil

$E_{so}^{ref} = E_{oed}^{ref}$ [kN/m ²]	Values of β		
	Parallel translation	Rotation about head	Rotation about toe
< 3000	1.1880	1.5268	0.9146
≥ 3000	1.1106	1.3518	1.3355

The comparison of the FEM - results with the analytical results from Eq. 4.42 are given in Figs. 4.69, 4.70 and 4.71 for the cases of parallel translation of the wall, rotation about head and rotation about toe respectively. It appears from these figures that the results of the FEM and the analytical agree very well. Therefore, the mobilisation of the passive resistance may fairly be approximated using Eq. 4.41.

**Fig. 4.69.** Comparison of the analytical (Eq. 4.42) and the FEM-results for the case of parallel translation of the wall**Fig. 4.70.** Comparison of the analytical (Eq. 4.42) and FEM-results for the case of rotation of the wall about head

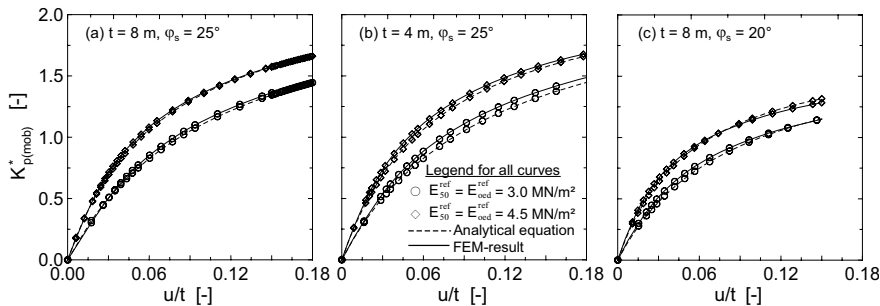


Fig. 4.71. Comparison of the analytical (Eq. 4.42) and FEM-results for the case of rotation of the wall about toe

4.11 German recommendation for excavation in soft soils

4.11.1 General

The working group “Excavations” (EAB) of the German Geotechnical Society (DGGT) have extended the known standard recommendation for excavations to include a new recommendation for excavations in soft soils (EAB 2006). Some information and specification from this new recommendations have been already presented in section 4.3 and 4.5. In the following are some more extracts from the recommendation regarding strength parameters, earth and water pressure calculations, determination of embedment depth and section forces, stability requirements as well as drainage in excavations.

4.11.2 The shear strength and the coefficient of earth pressure at rest

Based on the discussion on the drained and undrained analyses (Kempfert and Gebrselassie 2002) (see also section 4.7) and the analytical parameter study on undrained analysis of excavations in soft soils by Hettler et al. 2002, EAB recommends to use mainly the drained analysis as governing method of the calculation of excavation in soft soils, but leaves room for the geotechnical expert to decide based on the situation at the site. To perform the drained analysis, one requires the effective shear parameters. These can only be determined in triaxial or direct shear tests in laboratory. However, the soft soil is very sensible to such kind of test. The disturbance of the structure of the soil specimen during sampling, the rubber membrane used in triaxial test, and the friction resistance in shear box, etc. might lead to failure in estimating the shear parameters, and hence the laboratory tests are conditionally suitable to determine the effective shear parameters according to the draft recommendation of the EAB. On the other hand there are a huge experiences available in the undrained strength of normally consolidated soft soils.

Therefore, it is worthwhile to make use of these experiences and data bank to estimate the effective shear parameters (see section 2.5.2). The EAB adopts Eq. 2.55 or the equations listed in Table 2.6 to estimate the effective shear parameter φ'_s (the angle of the overall shear strength). Eq. 2.55 is once again displayed here for ready reference:

$$\sin \varphi'_s = \frac{I}{\frac{I}{\lambda_{cu}} \cdot (K_0 + A_f \cdot (1 - K_0)) - 2 \cdot A_f + I} \quad (4.42)$$

On the other hand, dependent on the range of application and on local conditions where a positive excess pore pressure may be expected, the undrained conditions might govern the analysis of the excavation. If this is the case, the EAB recommends to use an equivalent angle of total friction instead of the undrained strength c_u . Based on the stress paths in a triaxial test, the author suggests Eq. 4.31 or the equations listed in Table 4.5 according to the expected stress path to convert the undrained strength c_u into the equivalent angle φ_s written as *eqv.* φ_s hereafter. For a comparison purpose, Eq. 4.31 is once again displayed below.

$$\sin(\text{eqv.} \varphi_{s1}) = \frac{I}{\frac{K_0}{\lambda_{cu}} + \frac{\lambda_{u0}}{\lambda_{cu}} + I} \quad (4.43)$$

Analogue to Eq. 4.43, the EAB recommends a simplified form for practical applications as presented below. For soils above the groundwater table and c_u linearly increases with depth (Fig. 4.72a),

$$\sin(\text{eqv.} \varphi_{s1}) = \frac{c_{u1}}{\sigma'_{v1}} \quad \text{mit} \quad \sigma'_{v1} = \gamma_I \cdot z_I \quad (4.44)$$

Similarly, for soils below the groundwater table and c_u linearly increases with depth (Fig. 4.72a),

$$\sin(\text{eqv.} \varphi_{s2}) = \frac{\Delta c_{u2}}{\sigma'_{v2} - \sigma'_{v1}} \quad \text{mit} \quad \sigma'_{v2} = \gamma_I \cdot z_I + \gamma'_2 \cdot z_2 \quad (4.45)$$

For soils with a constant c_u with depth (Fig. 4.72b), but above the groundwater table,

$$\sin(\text{eqv.} \varphi_{s1}) = \frac{c_{u1}}{\sigma'_{vm1}} \quad \text{mit} \quad \sigma'_{vm1} = \frac{1}{2} \cdot \gamma_I \cdot z_I \quad (4.46)$$

Likewise, for soils below the groundwater table and constant c_u (Fig. 4.72b),

$$\sin(\text{eqv.} \varphi_{s2}) = \frac{c_{u2}}{\sigma'_{vm2}} \quad \text{mit} \quad \sigma'_{vm2} = \gamma_I \cdot z_I + \frac{1}{2} \cdot \gamma'_2 \cdot z_2 \quad (4.47)$$

where σ'_{vm} is the mean effective consolidation stress or the overburden pressure of the layer.

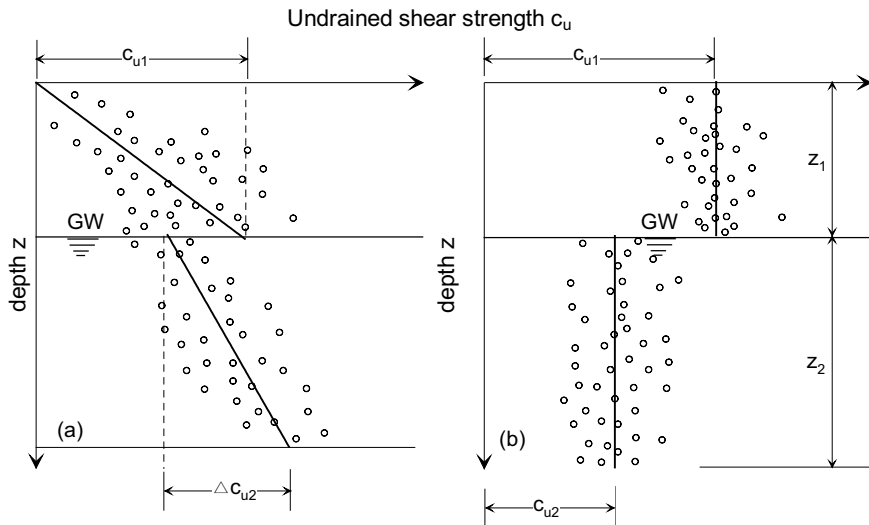


Fig. 4.72. Determination of an equivalent angle of total friction equiv. ϕ_s a) c_u increases linearly with depth, and b) constant c_u with depth

The coefficient of the earth pressure at rest K_0 is usually estimated from the known Jaki's formula,

$$K_0 = I - \sin \phi' \quad (4.48)$$

but there are also empirical equations to estimate the K_0 according to Alphan 1967, Lee and Jin 1979; Sherif and Koch 1970 (see Table 2.2) based on the plasticity index and the liquid limit of the soil. After comparing this empirical equations and Eq. 4.49 with a measured K_0 value from Scherzinger 1991 (Fig. 2.8), the Alphan 1967 equation lies far away from the range of the measured values and gives small values of K_0 and hence will not be recommended for soft soils. A tabular values K_0 calculated from the empirical equations and Jaki's equation are shown in Table 4.10.

Table 4.10. The coefficient of the earth pressure at rest K_0 for normally consolidated soils

Jaki's equation		Lee and Jin 1979		Sherif and Koch 1970	
ϕ' [°]	K_0 [-]	I_p [%]	K_0 [-]	w_L [%]	K_0 [-]
30	0.500	5	0.456	10	0.505

25	0.577	15	0.605	20	0.540
20	0.658	25	0.673	30	0.575
15	0.741	35	0.719	40	0.613
5	0.826	45	0.752	50	0.653

4.11.3 Earth pressures and reactions

Following are extracts from EAB EB 95 and EB 96 regarding the determinations of the pressures on the wall and the earth reactions. All the values shown below are characteristic values unless and otherwise they are specifically written with the indices k and d to indicate that the characteristic and design values respectively.

The acting load on the active side of the wall

a) The earth pressure at rest

The earth pressure at rest for a homogeneous soil layer may be calculated from:

$$e_{og} = \gamma_r (\text{or } \gamma') \cdot K_0 \cdot z_a \quad (4.49)$$

The following conditions should be fulfilled before applying the earth pressure at rest as a governing load on the active side of the wall.

When a minimum or no wall movements at the top of the wall or at the level of the bottom of excavation toward the excavation is expected, an earth pressure at rest can be applied above the bottom of the excavation. This can be the case, for example, when rigid walls are used, or when a bottom support can already be placed before the excavation starts by means of a jet pile column or soilcrete, or when the first support can be installed and pre-stressed before any major excavation starts (Fig. 4.75b).

When a minimum or no wall movements at the wall toe or at the level of the bottom of excavation toward the excavation is expected, an earth pressure at rest can be applied below the bottom of the excavation. This can be the case, for example, when rigid walls are used, or when a bottom support can already be placed before the excavation starts by means of a jet pile column or soilcrete (Fig. 4.75b).

When the earth pressure at rest would be applied in the case of rigid walls for the above mentioned reasons, for the same situation but relatively flexible, an increased active earth pressure (Fig. 4.76a) according to the EB 22 (EAB, 1994) can be applied below and above the bottom of the excavation. Moreover, when the rotation of the wall top toward the soil and the wall toe toward the excavation due to the sum effect of the pre-stressing of the upper strut and a higher load from the building and water pressure is expected, an earth pressure at rest above and an active earth pressure below the bottom of excavation can be applied (Fig. 4.76 b).

b) The active earth pressure

The active earth pressure can be calculated using,

$$e_{ag} = \gamma_r (\text{or } \gamma') \cdot K_a \cdot z_a \quad (4.50)$$

The coefficient of the active earth pressure K_a shall be determined with the assumption of a wall friction $\delta_a = \varphi'/3$.

In order to apply the active earth pressure as a governing load on the wall, the following conditions should be fulfilled:

When the wall movements at the top of the wall or at the level of the bottom of excavation toward the excavation is expected. This may be the case, for example, when the first strut is located relatively deep, or when full mobilization of the passive pressure can be expected, or when the bottom support is installed stepwise in slices.

If on one hand a pre-stressing of the upper strut is required, and on the other hand, a full support of the wall toe may be claimed, the active earth pressure above the bottom of the excavation level may be redistributed to a trapezoidal or rectangular diagram (Fig. 4.73b).

The earth reaction on the passive side of the wall

Dependent on the expected amount and the art of the displacement of the wall, the earth resistance may take the value between the active and the passive earth pressure at limit state as described below.

In the case of an excavation supported by a strut at the top but without a bottom support (Fig. 4.73), the classical passive pressure can be assumed as earth reaction. The passive earth pressure at limit state can be obtained from

$$e_{pgh} = \gamma_r (\text{or } \gamma') \cdot K_{pgh} \cdot z_p \quad (4.51)$$

where K_{pgh} is the coefficient of the passive earth pressure based on wall friction angle $\delta_p = -\varphi'/3$. In this case the following verification of the ultimate and serviceability limit state are required:

The mobilised earth resistance is then given by

$$\sigma_{ph} = e_{pgh} \cdot \eta_p \quad (4.51)$$

where η_p is an adjustment factor.

a) With respect to the effect of anisotropy of the strength of soft soils, the characteristic passive resistance force $E_{ph,k}$ should be reduced by an adjustment factor $\eta_p \leq 0.5$ and the following inequalities must be satisfied:

$$B_{h,k} \leq E_{ph,k} \cdot \eta_p \quad (4.52)$$

where $B_{h,k}$ is the reaction of the wall on the passive side arising from the equilibrium condition of the load on the active side and strut or anchor forces (Fig. 4.73).

b) The design reaction force should be at most equal to the design value of the passive resistance force:

$$B_{h,d} \leq E_{ph,d} \quad (4.53)$$

c) With respect to serviceability to limit the wall displacement, the following condition must be fulfilled:

$$B_{h,k} \leq E_{0g,k} + (E_{ph,k} - E_{0g,k}) \cdot \eta_p \quad (4.54)$$

where $E_{0g,k}$ is the characteristic force resulting from the earth pressure at rest with origin at bottom of excavation and η_p is again an adjustment factor ≤ 0.75 .

In the case of an excavation with bottom slab installed stepwise in slices (Fig. 4.74), the equilibrium condition of the forces is ensured primarily by the reaction from the bottom slab.

If the bottom slab is in place before remarkable displacement of the wall below the excavation had occurred, one can assume the soil to retain the earth pressure at rest that exist before the excavation had started as follows

$$e_{og} = \gamma_r (\text{or } \gamma') \cdot K_0 \cdot (H + z_p) \quad (4.55)$$

Just below the bottom slab, the passive earth pressure at limit state ($e_{pg,h}$) with $\delta_p = 0$ dominates the reaction diagram due to the rotation of the principal stresses in this region. The Eq. 4.55 together with this assumption provides a basic modified reaction system.

If an active earth pressure due soil weight only governs the loading system on the active side, the basic modified earth reaction should be reduced to a level equal to the available active pressure on the other side.

If on the other hand, the sum of the acting pressures below the bottom of excavation is larger than the basic modified earth resistance due to earth pressure from structural loads or water pressures, a subgrade reaction K_s can be introduced below the intersection point of the e_{og} and $e_{pg,h}$ lines to provide an additional earth reaction to the wall. The modulus of the subgrade reaction may be determined from:

$$k_s = \frac{E_{oed}}{t_B} \quad (4.56)$$

where E_{oed} is the constrained modulus of elasticity and t_B is the distance between wall toe and the intersection point of e_{og} and $e_{pg,h}$.

The characteristic earth reaction mobilised by the subgrade reaction $B_{Bh,k}$ must however satisfy the following condition:

$$B_{Bh,k} = (E_{ph,k} - E_{V,k}) \cdot \eta_p \quad (4.57)$$

where $E_{V,k}$ is the characteristic resultant force of the modified reaction system as defined above (Fig. 4.74) and η_p is an adjustment factor which has a value ≤ 0.75 .

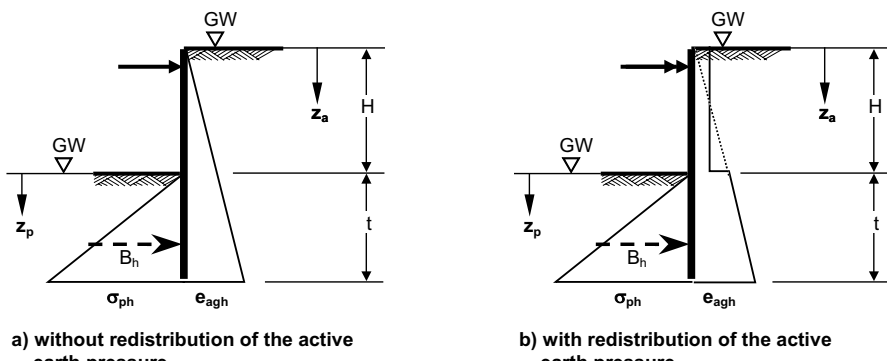


Fig. 4.73. Possible load diagram for a wall supported at the top only

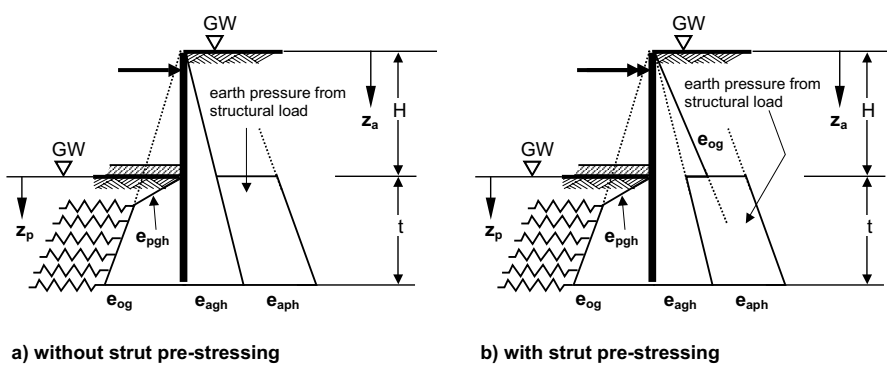


Fig. 4.74. Possible load diagram for a wall supported by a strut at the top and by stepwise installed bottom slab

In the case of an excavation with bottom slab installed by means of column jet pile or soilcrete, the equilibrium condition of the forces is also ensured primarily by the bottom slab.

If the wall is displaced in the direction of the active soil during the installation of the bottom slab, an active earth pressure with due consideration of the weight of the slab can be assumed as earth reaction on the passive side (Figs. 4.75 and 4.76a).

$$e_{ah} = \gamma_r (\text{or } \gamma') \cdot K_{agh} \cdot z_p + p \cdot K_{agh} \quad (4.58)$$

If a flexible wall is used, the struts or anchors are heavily pre-stressed and the sum of the acting forces on the active side due to structural loads and water pressure is too large so that the wall below the bottom of the excavation level can deflect toward the excavation, the modified earth reaction system with or without the

subgrade reaction (Fig. 4.76b) can be used similar to the case with the stepwise installed bottom slab.

Note that the above equations are formulated assuming a homogenous soil layer and groundwater at surface level. For all other cases, e.g. underground with more layers or groundwater at other location, the equation must be modified to take the new condition into account.

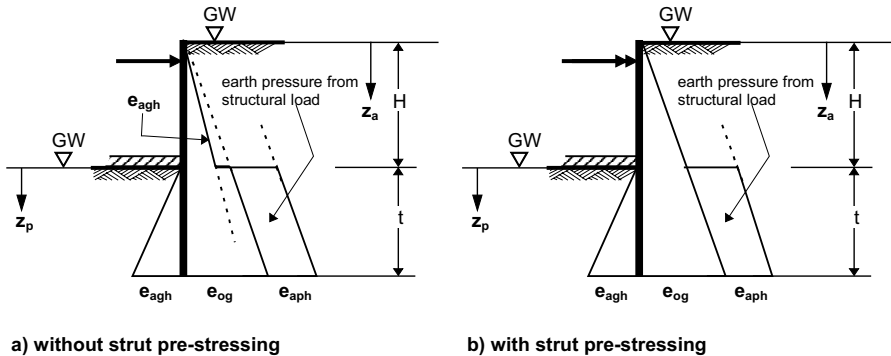


Fig. 4.75. Possible load diagram for a rigid wall supported by a strut at the top and by a bottom slab installed by means of jet pile column or soilcrete

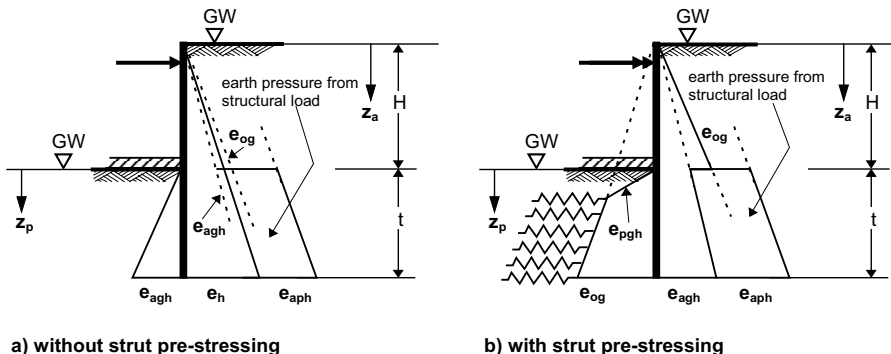


Fig. 4.76. Possible load diagram for a flexible wall supported by a strut at the top and by a bottom slab installed by means of jet pile column or soilcrete

4.11.4 Water pressure

According to EAB 2006 (EB 97) the water pressures on the active and passive sides have to be first determined separately and superimposed later for the calculation of the section forces. The water pressure is determined assuming either a hy-

drostatic pressure or groundwater flow conditions depending on the boundary conditions.

If the wall is embedded in an impermeable layer and no groundwater flow is to be expected or a simplification on calculation of the water pressure is required for some reasons, a hydrostatic water pressure can be assumed as shown in Fig. 4.77a, provided that the water below the excavation bottom is not subjected to water lowering.

On the other hand, if the wall is not embedded into an impermeable layer, the correct way of determining the water pressure is to take into account the seepage forces as shown in Fig. 4.78a .

For example, if the water table is located at the ground surface, the water pressure can be calculated as follows:

$$w_a = (\gamma_w - i_a \cdot \gamma_w) \cdot z_a \text{ on the active side} \quad (4.59)$$

$$w_p = (\gamma_w + i_p \cdot \gamma_w) \cdot z_a \text{ on the passive side}$$

where i is the hydraulic gradient and it can be determined from flow net or for simplification $i = H/(H + 2t)$ can also be taken.

It should be noted that the net water pressure (Figs. 4. 77b and 4.78b) shall be used in verification of stability or determination of section forces and embedment depth, i.e. no water pressure will be used on the passive side.

For the case of a hydrostatic water pressure, the earth pressure is calculated using the buoyant unit weight γ' for the part of the soil under groundwater. On the other hand, if groundwater flow is assumed and seepage forces are taken into account, adjusted unit weights

$$\gamma'_a = \gamma' + i_a \cdot \gamma_w \text{ on the active side} \quad (4.60)$$

$$\gamma'_p = \gamma' - i_p \cdot \gamma_w \text{ on the passive side}$$

will be adopted in the calculation of the earth pressures below the groundwater table.

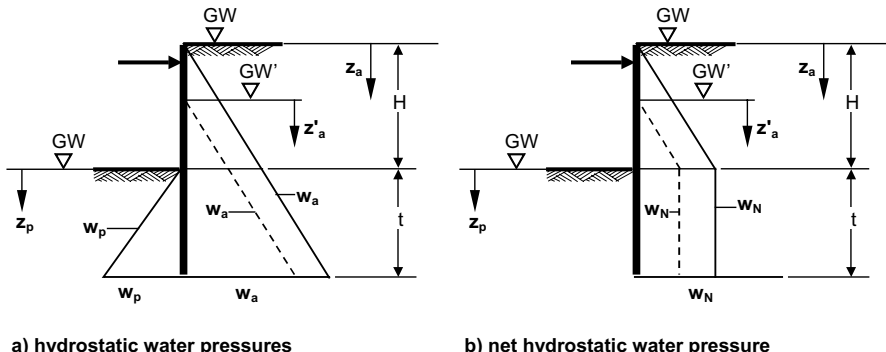
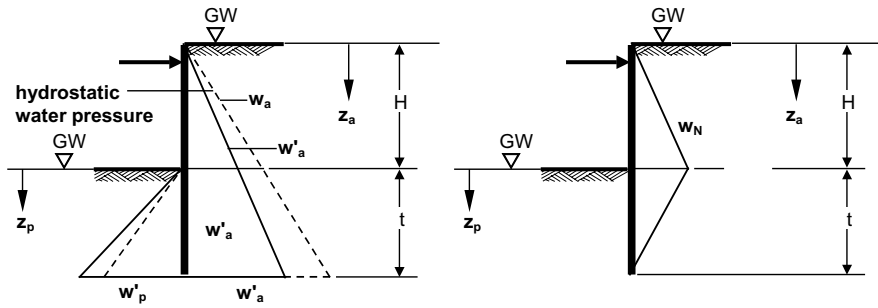


Fig. 4.77. Hydrostatic water pressure assuming wall embedded into impermeable layer (EAB 2006)



a) water pressure considering seepage forces b) net water pressure

Fig. 4.78. Water pressure considering groundwater flow through wall toe (EAB 2006)

In case an excess pore pressure still exist as a result of fill or foundation load near the planned excavation, the water pressure is required to be increased by amount equal to excess pore pressure. Moreover, a natural excess pore pressure may also exist in saturated soft soils with fine sand or silt seems.

4.11.5 Embedment depth and section forces

All the construction phases require to be investigated separately in the determination of the embedment depth and section forces of retaining walls of an excavation in soft underground. Moreover, deflections of the retaining wall in the past construction stages should be taken into account in the determination of the section forces in the current stage in form of displacement of the support point. This is because the shifting of the reaction point will have a substantial influence on the section forces.

For the verification of the state of each construction stage of an excavation executed according to the construction measures in section 4.5, an investigation of the following two cases is required:

- the first trench is cut with slopes on both sides, and
- trench slices are limited on one side by the base slab and they are sloped on the other side.

In the verification, a temporal arching effect in soil, load distribution through the top tie beam and the effect of already installed base slab as bottom support can be assumed. Beside the above investigations, it is always advisable to observe the deflection of the wall during the execution of the excavation.

However, such verification can be ignored, if the following construction and safety conditions are be fulfilled:

- a) The embedment depth of the retaining wall is sufficient enough for safety against:

- failure of an intermediate excavation phase assuming an equivalent bottom level (Fig. 4.79) ,
- against a basal failure (section 4.11.6) without the consideration of the weight of the base slab,
- against hydraulic failure, and
- against global stability of the retaining structure whenever the case be.

b) The excavation of a trench starts at an uncritical location first with a small width. The width can be optimized on the course based on observation and measurement results.

c) During execution of trench works and subsequent placement of base slabs as well as other support systems, a closed control of the deformation of the wall, settlements behind the wall and bottom heave is required.

Independent from that whether a verification of safety of the short term condition of a trench is carried out or not according to the above paragraphs for the first trench excavation, the embedment depth is determined assuming an equivalent excavation level, which is about two thirds of the height from the final bottom of excavation (Fig. 4.79). This is valid, although it is known that final excavation level is reached at the first trench and consequent trenches as well as the well gets support from the soil and partly from the base slab.

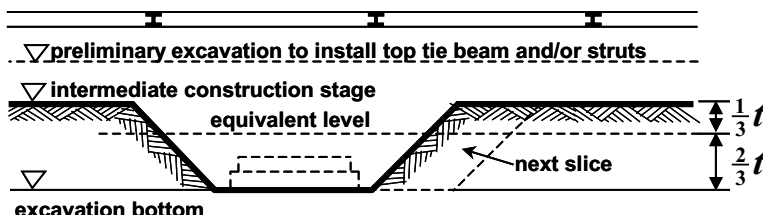


Fig. 4.79. Equivalent excavation level for an intermediate construction phase with slices

For a free end retaining wall supported only once by a strut or other systems, both the classical earth pressure distribution and redistribution pressure according to Fig. 4.73 are valid. If, however, doubts exist, whether approach to apply, i.e. with or without earth pressure redistribution, both cases have to be investigated. Instead of an additional determination of the embedment depth and section forces using the pressure redistribution, the reaction force at the strut or anchor level can be increased by 30%.

4.11.6 Basal failure

The recommendations described in section 4.11.3 to 4.11.5 assume an unfavorable soil condition where a homogeneous soft soil exists from the ground surface to wall toe or deeper (Fig. 4.80a). Relative favorable conditions may exist when a soft soil layer is overlain by a bearing layer (Fig. 4. 80b). Still more favorable

conditions may exist when a soft layer on the top is underlain by a bearing layer (Fig. 4.80c). The change in layer may occur at any depth below or above the bottom of excavation. In some of these cases an additional verification of the safety is required for the following conditions.

Excavations in homogeneous soft soil (Fig. 4.80a) are strongly subjected to a basal failure. Although to relatively lower extent, excavations in layered underground according to Fig. 4.80b are also subjected to basal failure ([Weißenbach 1977/1997]). The verification of the safety of the excavation bottom against basal failure is usually carried out using the undrained shear strength c_u . For an excavation in a homogeneous saturated soft soil layer with a depth H and $B > 0.20 \cdot H$ (Fig. 4.81), the following condition should be fulfilled (Hettler and Stoll 2004):

$$G_d + P_d \leq R_{v,d} + R_{Gr,d} \quad (4.61)$$

where the characteristic weight of the soil G_k and the surcharge load P_k are factored by the partial safety factor for dead and live loads respectively. EAB considers all surcharge pressure $p_k \leq 10 \text{ kN/m}^2$ as dead load.

The design value of the vertical component of the resistance from the cohesion is given by:

$$R_{v,d} = \frac{c_{u,k} \cdot (H + t_g)}{\gamma_{Gr}} \quad (4.62)$$

and the design value the bearing resistance can be determined from:

$$R_{Gr,d} = \frac{b_g \cdot [\gamma \cdot t_g + 5,14 \cdot c_{u,k}]}{\gamma_{Gr}} \quad (4.63)$$

The unit weight γ will be replaced by γ_r when the soil below the excavation bottom is saturated or by γ' when the soil is under buoyancy.

The width b_g is calculated as follows:

- Without any lateral surcharge pressure $b_g = B$, provided that the $c_{u,k}$ is constant with depth,
- With lateral surcharge pressure and with variable $c_{u,k}$ with depth, the width b_g shall be varied till a maximum mobilization of the safety is reached (Hettler and Stoll 2004).

Normally, a risk of basal failure does not exist, if $B \leq 0.20 \cdot H$ (Weißenbach 1996/1997).

The effect of anisotropy of the soil due to sedimentation and rotation of the principal stresses on undrained shear strength c_u can be ignored, because it is assumed that its effect on the active side and passive side will cancel each other, or otherwise the exact determination of the anisotropy factor is not simple (Scheringer 1991; Bjerrum 1973).

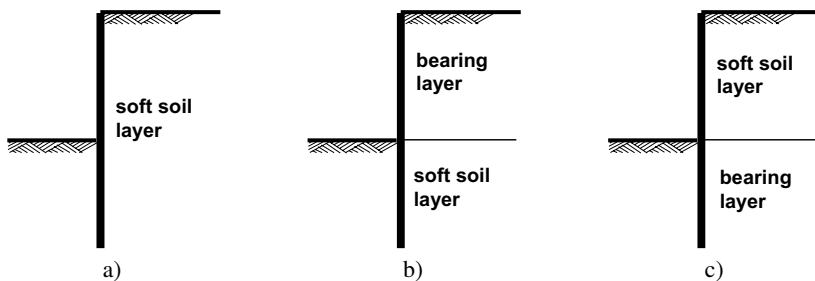


Fig. 4.80. Excavation in layered underground

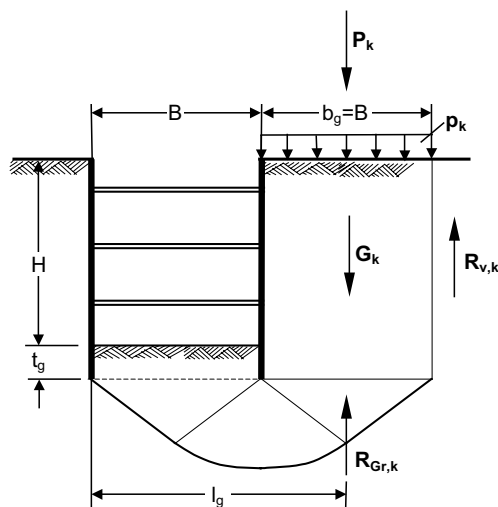


Fig. 4.81. Basal failure

Excavations in layered underground (Fig. 4.80b) and with shallow groundwater level are particularly subjected to hydraulic failure. Similarly, excavations in a homogeneous layer (Fig. 4.80a) may also prone to hydraulic failure but in a smaller degree. The verification of safety against hydraulic failure shall follow the recommendation in EB 61 (EAB 2006).

A verification of the safety against a deep seated stability failure is also required for excavations in a homogeneous or layered underground (Figs. 4.80a & b). The normal forces and shear resistance arising from the base slab can also be considered in the calculation of resisting forces or moments. The verification follows similar to slope stability problems.

In a tied back excavations a check of equilibrium is required for deep rupture failure. This ensures that the free length of the anchor is adequate and the forces are transmitted far enough back from the wall. The equilibrium will be checked for a wedge of soil between the back of the wall and the center of the grout body

of the anchor. The deepest rupture line of the wedge usually passes through the wall toe (for details refer to EB 44 EAB 2006). For a change of layer at the bottom of excavation level as shown in Fig. 4.80b, the excavation must be protected against the movement of the soil block between the wall and the anchor load transmitting point by means of bracing of the wall at a lower position or by installing a base slab stepwise in slices or by introducing a soilcrete layer at the bottom of excavation.

In excavations, where the soft layer is located below the wall toe (Fig. 4.82) and a fixed end support of the wall is possible in the bearing layer, the following points require consideration:

- The active earth pressure is calculated assuming an active wall friction $\delta_a = 0$, because a transfer of the vertical component of the earth pressure to the underground can not be granted.
- In braced excavations and for the condition shown in Fig. 4.82, a proof of a sufficient embedment depth in the bearing layer is necessary. To do so, a passive wall $\delta_p = 0$ shall be assumed in the calculation of the passive pressure so that the a sliding surface on the soft soil will not be developed. Hence, the following condition must be fulfilled:

$$B_{h,d} \leq E_{ph} \quad (4.64)$$

A verification of a sufficient safety against sliding is required for tied back excavation as shown in Fig. 4.82b, i.e.

$$E_{ah,d} + W_{N,d} \leq E_{ph,d} + R_{t,d} \text{ or } K_d \quad (4.65)$$

The passive resistance in the bearing layer shall be calculated assuming $\delta_p = 0$, and the resistance against sliding from

$$R_{t,k} = G_k \cdot \tan\varphi_k \text{ or } K_k = c \cdot L \quad (4.66)$$

The smallest value of resistance will be governing.

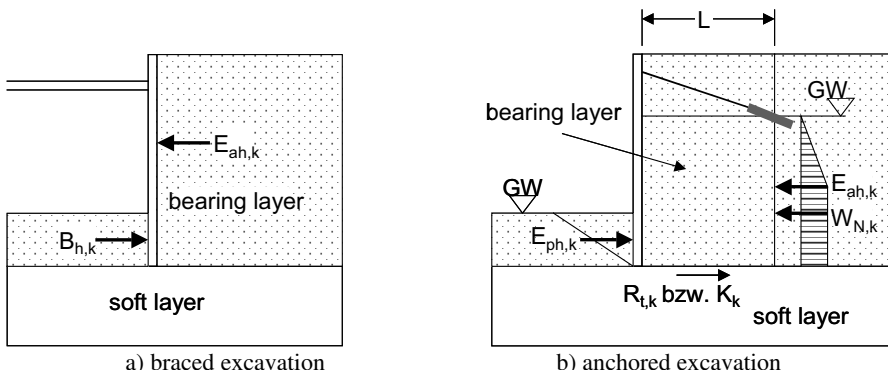


Fig. 4.82. Excavations with soft soil layer below the wall toe

4.11.7 Drainage measures in excavation

Soft soils are prone to a substantial settlement, when they are subjected to groundwater lowering. Therefore, it is highly recommended to conduct the groundwater lowering within a very close distances. Sand seems require special attention during lowering.

Groundwater is usually subjected to seasonal fluctuations. Therefore, it is highly recommended to lower the groundwater table to its lowest known level by means of a ring drainage system, because of the unfavorable influence of the water pressure on the determination of depth of embedment and section forces of the retaining wall.

It may be necessary to drain sand and silt seems or confined groundwater by pumping within the excavation between the retaining walls, provided that the wells remain above the wall toe to keep the effect of the drainage within the excavation only. For that purpose, a vacuum filter well can be used when a gravity drainage is not sufficient or if additional hardening of the soil is required.

The use of local vacuum lances for stabilization of sloped trenches and berms for the purpose of installation of a base slab are usually harmless in respect to the safety of nearby structures. Rest water in layers and surface water can be drained using a filter stable surface drainage system. The pump has to continue working until an uplift of base slab is no more possible.

In all cases, however, a closed supervision of the effects of the dewatering measures is necessary through monitoring systems.

4.12 Case histories

4.12.1 General

The area around the lakes near the foot of the Alps in southern Germany is known to consist a thick layer of post glacial young soft lacustrine deposit. The case histories presented in this section are all located in this region. Excavation on such thick soft soils in urban areas is usually prone to movements of soils which damages the nearby structures. Now a days the possible movement of soil in excavations in urban areas is predicted by means of the Finite Element Method. However, experiences show that predicted deflection of wall and settlement behind the wall does not usually match with the measured values. A back analysis of two of the case histories is also included in this section. It is shown that besides the understanding of the soil and the soil-structure-interaction behaviour, and their simulation using an advanced constitutive soil models, the understanding and simulation of each detail of the construction process is also equally important.

4.12.2 Project-I: Damgasse - Constance

Introduction

A multi-storey building for the purpose of apartments and shopping centre which include two basements for underground park was built in 1997/98 in the old part of the Constance city, southern Germany. The site was fairly level (397.50 MSL), measured about 40 x 60 m and surrounded by old and relatively new 3 - 5 story buildings (Fig. 4.83 & 4.86). The retaining structure used was a sheet pile wall of the type Hoech 134. There were a double row of sheet pile walls on the north and south part of the site. Fig. 4.66 is a section through the site. The walls were temporarily supported by wooden ($\phi = 26\text{ cm}$) strut, propped wooden plumbs ($\phi = 26\text{ cm}$), propped I-Steel beam (IPB 360) and bottom concrete slab ($d = 25\text{ and }30\text{ cm}$). The positions of the supports are shown in Fig. 4.85. The soil exploration, monitoring and construction information are documented in Kempfert + Partner 1994-1998 and are partly reported by Berner 1997.

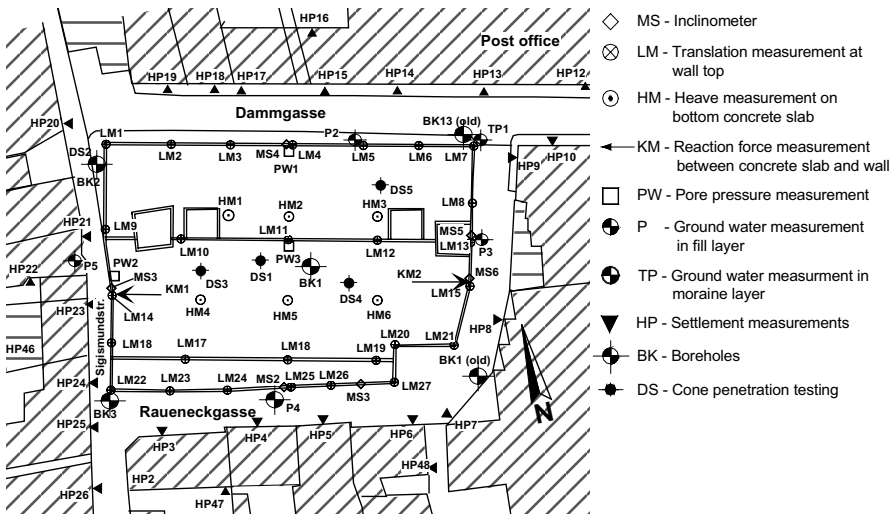


Fig. 4.83. Site plan, locations of bore-holes and instrumentation

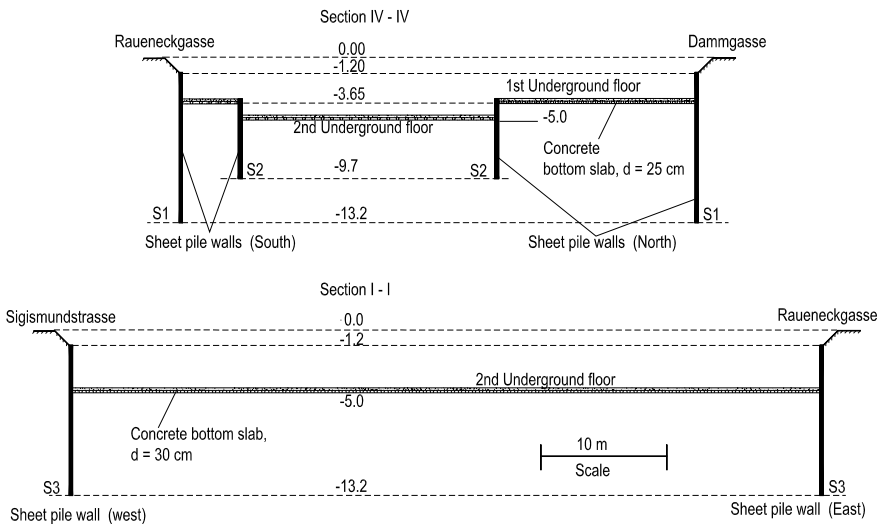


Fig. 4.84. Section through site

Construction stages

The excavation was proceeded in slices in a daily output basis according to the construction phases shown in Fig. 4.85. After each slice was excavated, a fast hardening concrete had been placed providing support to the walls (see Fig. 4.87), before the next slice excavation had begun. The construction stages consists of:

- Excavation to a depth of 1.2 m below the surface (11.11.96 - 20.11.96).
- Cutting a trench for sheet pile wall installation (15.11.96 - 23.11.96).
- Sheet pile wall installation (04.12.96 - 29.01.97).
- Inserting the wooden struts and excavation phase 1a and simultaneously placement of the bottom fast hardening concrete slab on daily output basis, Slices 1.1 - 1.20, South (03.02.97 - 26.02.97).
- Excavation phase 1b and simultaneously placement of the bottom fast hardening concrete slab on daily output basis, Slices 1.1 - 1.7, North (21.02.97 - 27.02.97). The wooden struts in phase 1a removed.
- Excavation phase 2 and simultaneously placement of the bottom fast hardening concrete slab on daily output basis, Slices 2.1 - 2.9, (04.03.97 - 18.03.97).
- Cut away the inner sheet pile walls S2 up to the 1st underground floor level
- Inserting the wooden propped support in trench, excavation phase 3 and simultaneously placement of the bottom fast hardening concrete slab on daily output basis, Slices 3.1 - 3.18, North (03.04.97 - 14.07.97).

- i) Inserting the wooden propped support in trench, excavation phase 4a and simultaneously placement of the bottom fast hardening concrete slab on daily output basis, Slices 4.1 - 4.9, West (09.04.97 - 21.04.97).
- j) Inserting the wooden propped support in trench, excavation phase 4b and simultaneously placement of the bottom fast hardening concrete slab on daily output basis, Slices 4.1 - 4.9, East (30.06.97 - 17.07.97).
- k) Placement of the basement reinforced concrete slab and removal of the propped support.

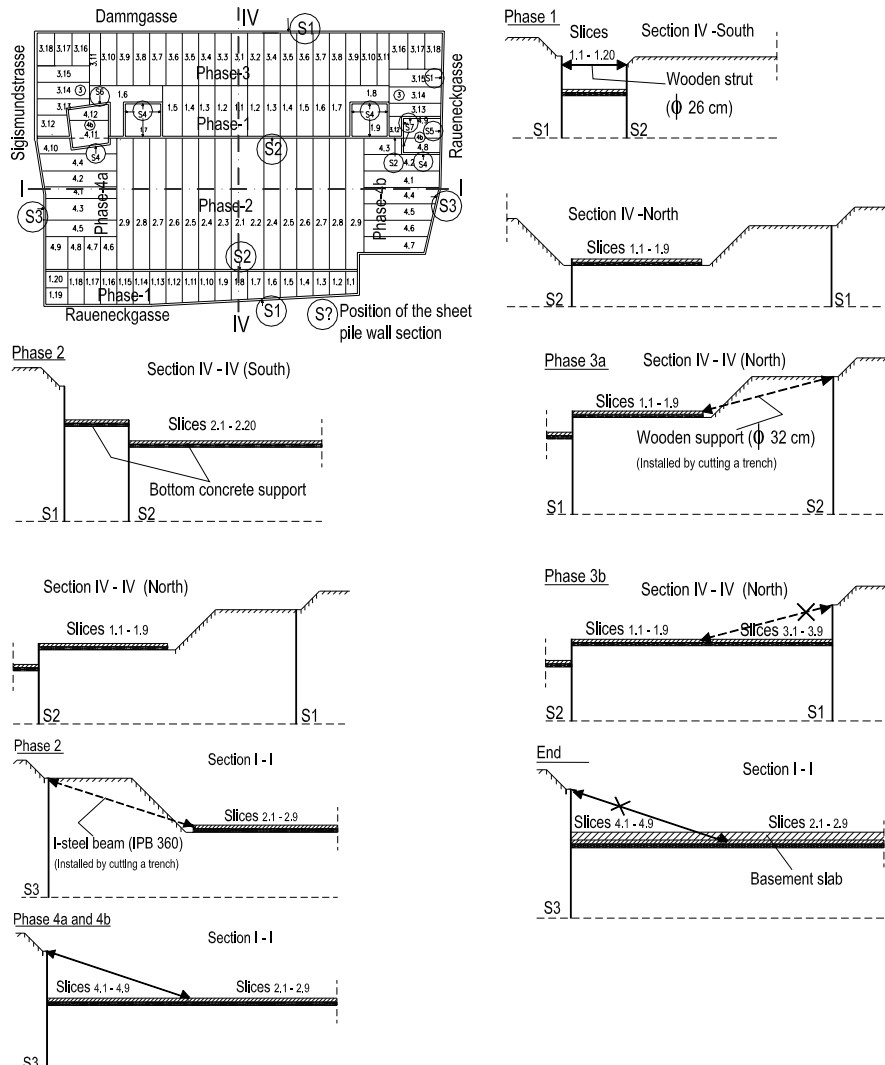


Fig. 4.85. A typical section (North - South and West - East) showing the excavation phases



Fig. 4.86. Overview of the excavation site



Fig. 4.87. Excavation and placement of the bottom slab in slices

Site condition

Altogether 3 boreholes were drilled, 5 test pits were excavated, 5 cone penetration test were conducted on the site for the purpose of exploring the soil and investigat-

ing the groundwater condition. Two additional bore logs were also available from old soil exploration on the site. Their locations are shown in Fig. 4.84. The site investigation revealed 2.6 to 5.3 m fill material comprising gravel, sand and rubble from old buildings, overlaying soft lacustrine deposit to a depth of 12 to 30 m. Beneath the lacustrine soil, a moraine comprising sandy and silty gravel was encountered to a depth of 20 m up to a depth greater than 30 m. Though it was not bored at this site, a boulder clay is believed to be found beneath the moraine. Fig. 4.88 is a typical bore log and cone penetration result along with the distribution of the water content with the depth.

Immediately after the boring a water level at 1.6, 1.4, and 1.05 m below the ground in the fill layer at boreholes BK1, BK2 and BK3 respectively was observed. A confined water pressure was encountered at a depth of 22 m at BK2 and at a depth of 21 m at BK3 and raised to a height of 2 m and 12.2 m below the surface respectively. The old bore hole B13 showed three water levels at 2.5 m, 6.0 m and 8.5 m below the surface level. In order to investigate the groundwater condition seriously during the excavation and to avoid the ambiguity shown in the other boreholes, additional 4 standpipes deep in the fill layer and one piezometer deep in to the moraine layer (24 m deep) were installed (see Fig. 4.83 for locations of the standpipes).

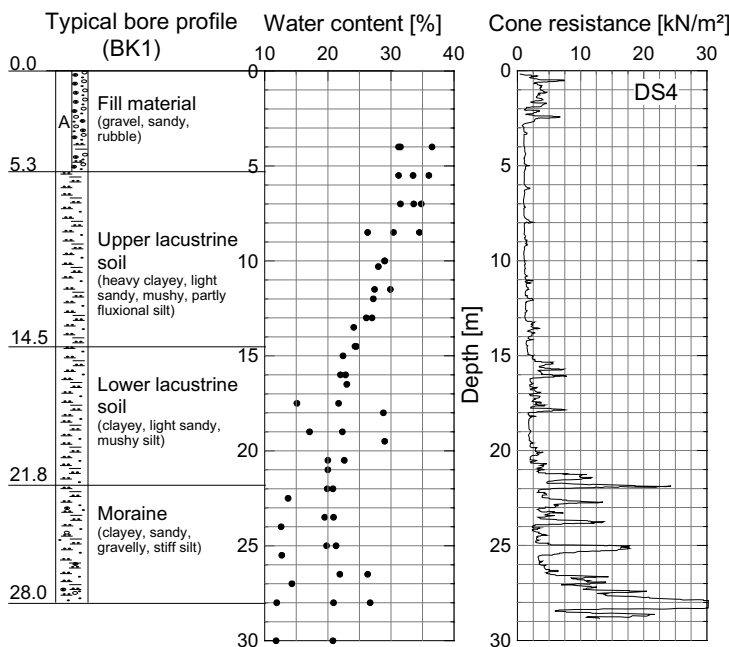


Fig. 4.88. Typical soil profile and properties

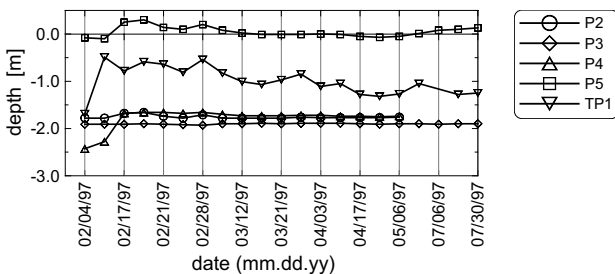


Fig. 4.89. Observations of the groundwater level during excavation

The result of the groundwater observations are shown in Fig. 4.89. The shallow standpipes P2, P3 and P4 showed almost a constant water level at about 2 m below the ground surface on average. The standpipe P5, which is located on the courtyard showed a higher water level which is at about the surface level. This may not be other than a local reservoir in this area. The deep piezometer showed a confined water that had on average a head of 1 m below the surface. The fluctuation of the water level in TP1 is related to the fluctuation of the water level of the Constance lake. The highest and the middle water level of the Constance lake is located at 396.56 and 395.56 MSL respectively, or in other words, 1 m and 2.15 m below the ground surface in reference to the average surface level at the site (397.50 MSL).

Instrumentation and monitoring

Instrumentation was used to record the wall movement, the settlement of the nearby existing buildings, the heave of the basement slab, the pore pressure in the lacustrine soil layer and the reaction forces between the wall and the basement slab and the propped support. Wall movement was measured in two ways. The top of the wall was monitored using geodometer at 27 points. The wall deflection was measured using 6 inclinometers which provides a result to an accuracy of ± 1 mm. The settlement at 50 locations near the existing buildings were monitored using surface surveying starting prior to the beginning of the construction activities at the site. The potential heave of the basement slab was measured using surface surveying at 6 points. In addition to the groundwater observation, pore water pressure was also measured at the inner side of the sheet pile wall at 3 points. The results of the monitoring are described below:

Settlements near existing buildings. Fig. 4.90 shows the measured vertical surface movement starting from prior to the beginning of the excavation in Nov. 1996. A maximum surface settlement of 23 mm was recorded at measuring point HP4 in southern part of the Raueneckgasse street, in which about 25% of the settlement has already occurred during the wall installation. At the opposite street, Dammgasse, a maximum settlement of 3 mm was measured, whereas at Sigis-

mundstrasse a maximum settlement of 14 mm was recorded. In eastern part of the Raueneckgasse street a maximum settlement of 4 mm was observed. At points far from the wall (16 - 25 m) no significant surface settlement was measured, even a heave of 3mm was recorded at measuring point HP16.

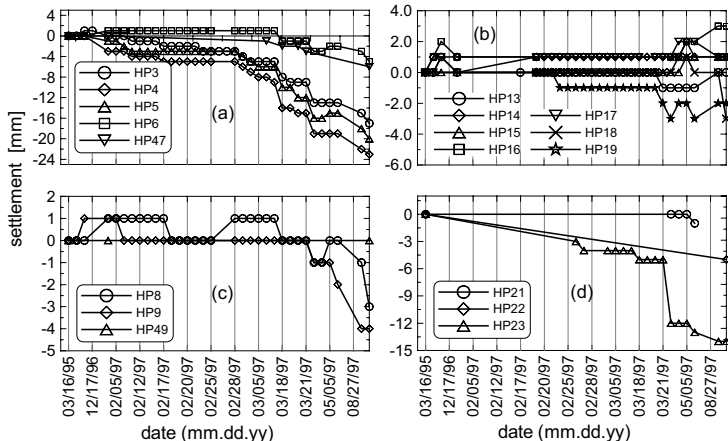


Fig. 4.90. Settlements near the existing buildings: a) Raueneckgasse-south, b) Dammgasse, c) Raueneckgasse-east, and d) Sigismundstrasse

Wall displacement at the top. The movement of the wall head was measured using geodometer, which measures the wall head movement in the three directions (x-y-z). The wall head movement at selected points are given in Fig. 4.91.

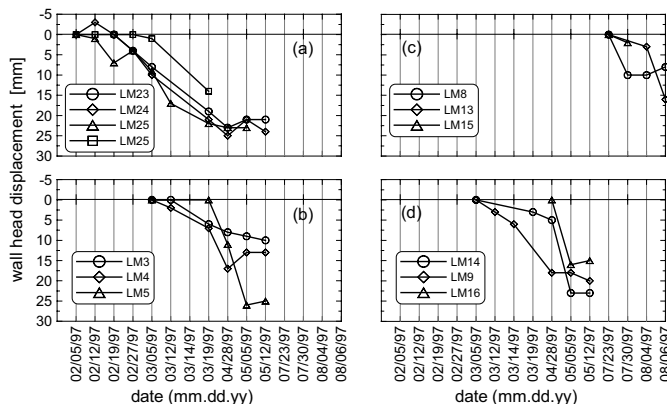


Fig. 4.91. Observed movement of wall head towards excavation: a) Raueneckgasse - South, b) Dammgasse, c) Raueneckgasse - east, d) Sigismundstrasse

Wall deflection. The observed horizontal deflection of the sheet pile wall at the various stages of excavation and support at the measuring locations MS2, MS4, MS3 and MS6 (Fig. 4.83) are shown in Fig. 4.92. It was reported that there were difficulties in the interpretation of the inclinometer reading at the location MS6.

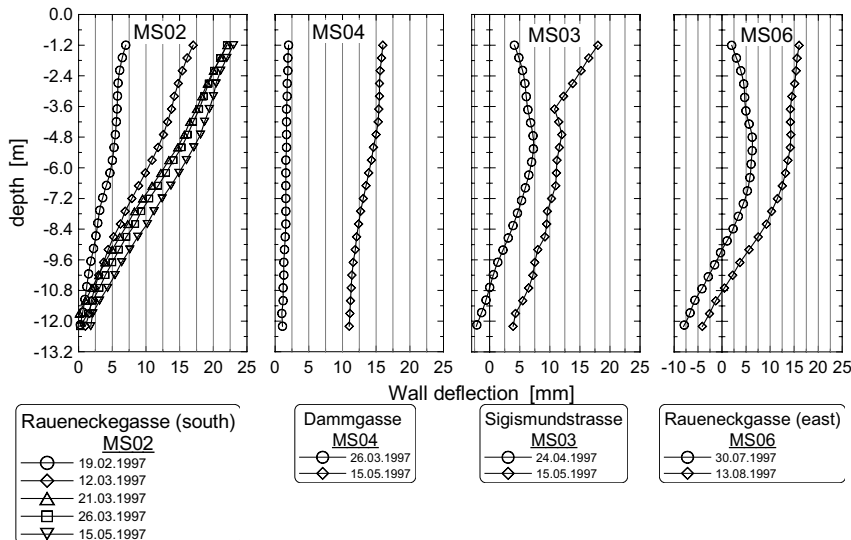


Fig. 4.92. Deflection of the sheet pile wall towards excavation at (MS02, MS04 and MS03)

Excess pore pressure. The excess pore pressure was measured using pressure transducers and are shown in Fig. 4.93. It can be shown from the figure that the measurements were started a bit late. The first measurement (25.02.1997) was carried out after almost the excavation of phase 1a and phase 1b had been completed. It was also reported that the initial readings were influenced by the installation process (Kempfert + Partner 1994-1998).

Reaction forces. A reaction force of 159 and 222 kN/m² was measured between the I-steel propped support and the wall at the location KM1. At the same location a reaction pressure of 23.5 kN/m² was recorded between the bottom slab and the wall at the end of excavation but before the removal of the propped support, and 5.5 kN/m² after placement of 60 cm thick basement concrete slab of the underground floor and the removal of the steel support.

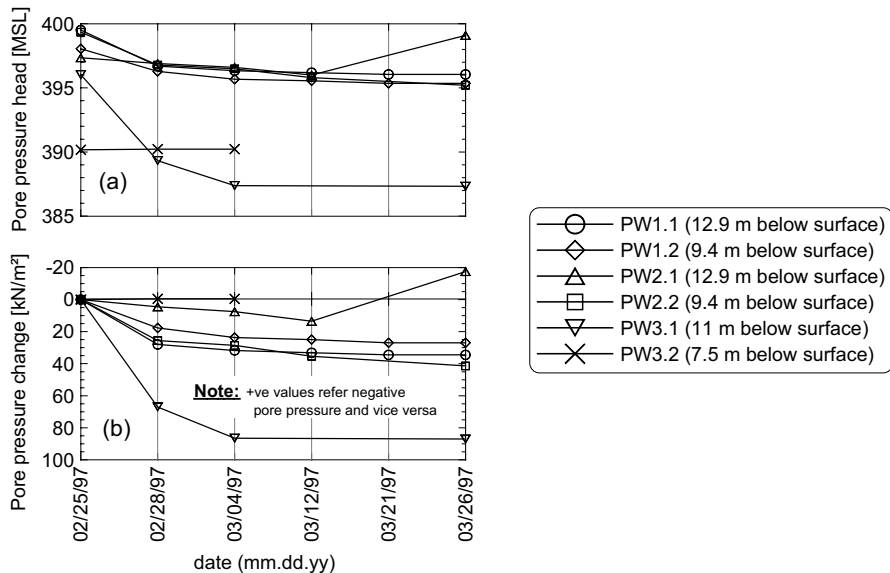


Fig. 4.93. Pore pressure during the excavation) Absolute pore pressure head above sea level (MSL),b) Excess pore pressure

Back analysis of the excavation project using the FEM

Model geometry. The back analysis is carried out using the two-dimensional FE-program PLAXIS 8.1 professional version. A plane strain analysis is adopted using 15 node triangular elements. The hardening soil model (HSM) is used to simulate the behaviour of the soils in all the layers, whereas the Mohr-Coulomb Model (MCM) is adopted to simulate the contact behaviour. The structural elements are assumed to behave elastically. The first step in any FE-analysis of geotechnical problem is to convert the data from the geotechnical reports to a simplified soil profile, idealize the structural elements and to determine the extent of the model geometry. Fig. 4.94 shows the section through site (South-north section) showing the idealized soil profile, arrangement of the structural elements and sequences of the excavation. A similar west-east section is also shown in Fig. 4.95. These sections are identified as section IV-IV and I-I on the site plan (Fig. 4.85).

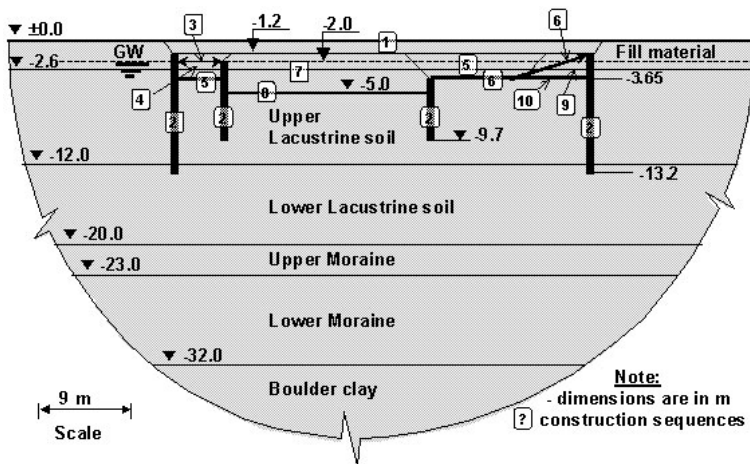


Fig. 4.94. Section through the site (south-north), soil profile and construction sequence

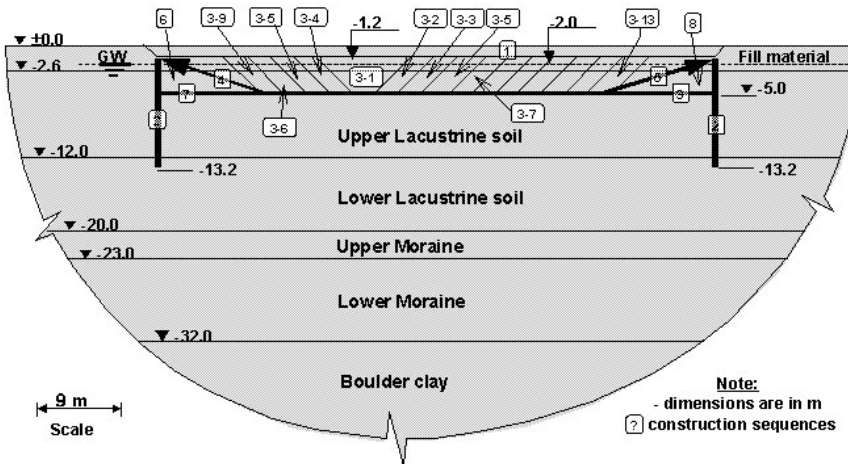


Fig. 4.95. Section through the site (west-east), soil profile and construction sequence

The corresponding finite element model and its mesh are shown in Figs. 4.96 and 4.97. These figures are zoomed in order to show the main part of the model that consist the structural elements, the loads, the soil layers and the excavated section. The geometry of the excavation, the arrangement of the sheet piles and the sequences of the excavation did not allow the use of the advantage of the symmetrical model. That is why the system as a whole have been modeled in the analysis. The size of the models are chosen according to the recommendation of

the working group “Numerics in Geotechnic“ (Meißner 2002) and the parameter study in section 4.9.2. The finite element mesh at south-north section is extended to a depth of 82 m where a fixed boundary is imposed and a zero horizontal displacement is imposed at a distance of 82 m from the edge of the wall. The size of the model as a whole is 204 m wide and 82 m high (Fig. 4.96). Similarly, The finite element mesh at west-east section is extended to a depth of 125 m and to a distance of 120 m from the edge of the wall (all in all 300×125 m) (Fig. 4.97). Since the excavation site was surrounded by existing buildings, a surcharge load of 33 kN/m^2 and 23 kN/m^2 at the southern and northern side (Fig. 4.96) respectively have been applied at the level of the underground floor. Similarly, a load of 20 kN/m^2 and 32 kN/m^2 at the western and eastern side of the excavation (Fig. 4.97) respectively have been applied on the model. The weight of the soil above the underground floor is considered in the calculation of the surcharge loads. In both cases a traffic load of 10 kN/m^2 has been applied between the wall and the existing buildings.

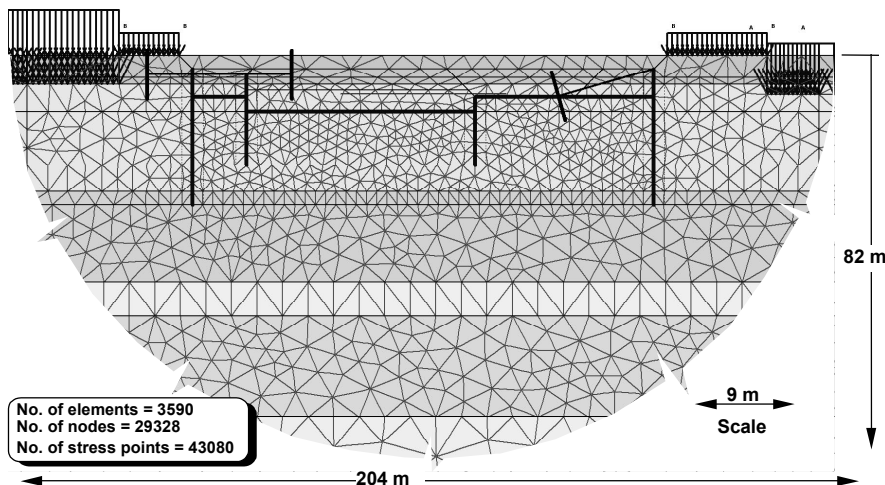


Fig. 4.96. Main part of the finite element mesh: south - north section

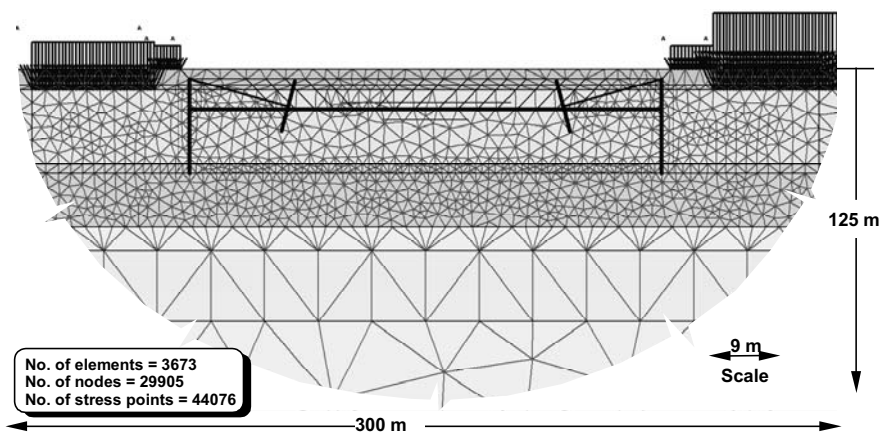


Fig. 4.97. Main part of the finite element mesh: west-east section

Material properties. As it was already mentioned at the beginning of this section, the HSM is the main constitutive model that is used to simulate the behaviour of the soil. The soil parameters required for the FE-computation with the hardening soil model under drained condition are given in Table 4.11. The PLAXIS program provides an option of performing an undrained analysis using the effective strength and stiffness parameters (Section 3.3.2). Hence, the parameters in Table 4.11 may also be used for the consolidation analysis. The program accepts the effective stiffness parameter and calculates the bulk modulus according to the Hook's law of elasticity. The excess pore pressures are calculated from the volumetric strain rate, the bulk modulus of water and the porosity of the soil medium. The layers of the lacustrine soils and the fill material only are assumed undrained in the consolidation analysis, whereas the other layers remain drained. Although the boulder clay layer is relatively impermeable, it is assumed drained, taking into account the long calculation time needed and numerical instability during the consolidation analysis. Since the boulder clay is located at deeper depth (> 32 m), where the influence of the stress change becomes minimum, ignoring its undrained behaviour may not significantly affect the overall result.

The soil parameters of the lacustrine soil layers are directly taken from intensive laboratory tests on undisturbed soil samples from the site and are calibrated using a finite element simulation of the laboratory tests (section 3.3). The soil parameters of the remaining layers are derived from penetration and sounding field tests documented in the geotechnical reports after converting them to suit for HSM.

A separate material set is defined for the interface elements. The shear parameters of the contact elements are adopted from the corresponding layers of soils after reducing the values by a factor of 1/3, whereas the stiffness of the soil layers are adopted as it is (see section 3.2.5). The secant modulus E_{50} of the correspond-

ing soil layer and a Poisson's ratio $\nu = 0.35$ are used as stiffness parameters for the MCM of the interface elements.

The material properties of the structural elements are given in Table 4.12. All the structural elements are assumed to behave elastically.

Table 4.11. Soil parameters for the HSM for drained and consolidation analyses

a) Unit weight, permeability and earth pressure at rest

Soil layer	depth [m]	γ_{sat} [kN/m ³]	γ_{unsat} [kN/m ³]	k_x [m/d]	k_y [m/d]	K_0^{nc} [-]
Fill material	±00.0 - -02.6	17.0	20.0	8.64E-5	8.64E-5	0.577
Upper lacustrine soil	-02.6 - -12.0	19.5	19.5	8.64E-5	8.64E-5	0.590
Lower lacustrine soil	-12.0 - -20.0	19.5	19.5	8.64E-5	8.64E-5	0.546
Upper moraine	-20.0 - -23.0	20.0	20.0	8.60E-3	8.60E-3	0.463
Lower moraine	-23.0 - -32.0	21.0	21.0	1.0	1.0	0.405
Boulder clay	-32.0 - -82.0	22.0	22.0	8.60E-6	8.60E-6	0.500

b) Stiffness parameters

Soil layer	depth [m]	E_{50}^{ref} [kN/m ²]	E_{oed}^{ref} [kN/m ²]	E_{ur}^{ref} [kN/m ²]	p^{ref} [kN/m ²]	ν_{ur} [-]	m [-]
Fill material	±00.0 - -02.6	6000	6000	30000	100	0.20	0.700
Upper lacustrine soil	-02.6 - -12.0	3578	2653	19170	100	0.20	0.730
Lower lacustrine soil	-12.0 - -20.0	5367	3980	28982	100	0.20	0.730
Upper moraine	-20.0 - -23.0	24000	24000	120000	100	0.20	0.500
Lower moraine	-23.0 - -32.0	28000	28000	140000	100	0.20	0.500
Boulder clay	-32.0 - -82.0	40000	40000	20000	100	0.20	0.800

c) Strength parameters

Soil layer	depth [m]	c' [kN/m ²]	ϕ' [°]	ψ' [°]	R_f [-]
Fill material	±00.0 - -02.6	10.0	25.0	0.0	0.90
Upper lacustrine soil	-02.6 - -12.0	13.2	25.3	0.0	0.82
Lower lacustrine soil	-12.0 - -20.0	14.1	27.0	0.0	0.82
Upper moraine	-20.0 - -23.0	5.0	32.5	2.5	0.90
Lower moraine	-23.0 - -32.0	5.0	36.5	6.5	0.90
Boulder clay	-32.0 - -82.0	10.0	30.0	0.0	0.90

Table 4.12. Material properties of the structural elements

Structural element	Type	EA [kN/m°]	EI [kNm ² /m°]	w [kN/m ²]	ν [-]	$L_{spacing}$ [m]
Sheet pile wall	Hoech 134	3.591E6	53550.0	1.3	0.30	-
Bottom slab	Concrete slab, d = 25 cm	7.500E6	39063.0	6.3	0.20	-
	Concrete slab, d = 30 cm	9.000E6	67500.0	7.5	0.20	-
Strut	Wooden plumb, d = 26 cm	9.557E4	-	-	-	2.5
Propped support	Wooden plumb, d = 32 cm	1.448E5	-	-	-	2.5
	I-Steel beam (IPB 360)	9.503E5	-	-	-	4.0

Preliminary analysis and results. A preliminary analysis of the excavation is carried out using the finite element models shown in Fig. 4.96 & 4.97 and the material properties in Table 4.11 & 4.12. In all the computation cases present in this section, a hydrostatic groundwater is assumed at a depth of 2 m below the surface. Both drained and undrained (consolidation) analysis are performed separately.

The new professional version of PLAXIS v8.1 provides an option for performing a consolidation and simultaneous loading in the sense of changing the load combination, stress state, weight, strength or stiffness of elements activated by changing the load and geometry configuration or pore pressure distribution by means of stage construction. This is very important in regard to excavation, because the excavation usually takes some days or weeks or in extreme case also some months, and the pore pressure has the possibility to dissipate already during the excavation. This option of consolidation and simultaneous excavation was utilized in the back analysis of the project. The undrained behaviour was ignored in the first 4 calculation phases.

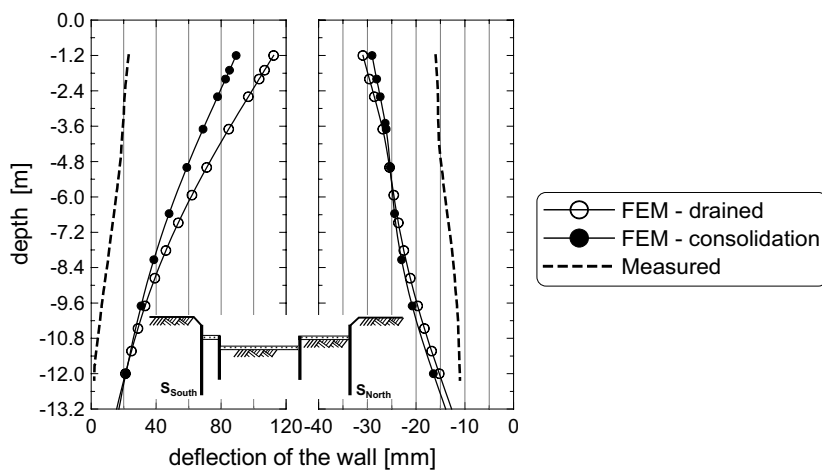
South-North Section (Section IV-IV): The main construction phases are shown in Figs. 4.85 and Fig. 4.94. The construction stages followed in the FE-computation are the same as those described above, but they are simplified and optimized as shown in Table 4.13 (consolidation analysis). The construction stages followed in drained analysis (13 phases) are the same as in the consolidation analysis (Table 4.13) but in the absence of the consolidation time.

Fig. 4.98 shows the calculated displacement of the wall at the end of the excavation stage. Both drained and consolidation analyses results are presented in the diagram. It can be seen from the figure that the FEM - computation shows an excessive displacement than it was measured at the field. A maximum displacement of 112.3 mm (drained) and 79.3 mm (consolidation) at the top of the southern outer wall is computed compared to the measured top displacement of 23 mm. Similarly, a displacement of 30.9 mm (drained) and 28.4 mm (consolidation) is computed at the top of the southern outer wall compared to a measured value of 16 mm. As would be expected the consolidation analysis has led to a lesser displacement than the drained analysis.

Table 4.13. Construction stages (Section IV-IV).

Phase 00:	Generate the initial stresses
Phase 01:	Activate the surcharge and traffic loads
Phase 02:	1 st excavation to a depth of -1.2 m (1)
Phase 03:	wall installation (2)
Phase 04:	2 nd excavation (3) [4 days]
Phase 05:	strut installation (3) [4 days]
Phase 06:	3 rd excavation (4) [7 days]
Phase 07:	installation of bottom slab (5) [8 days]
Phase 08:	4 th excavation (5) and strut removal (3) [4 days]
Phase 09:	bottom slab installation (6) and strut (6) [5 days]
Phase 10:	consolidation time [6.5 days]
Phase 11:	5 th excavation (7) [11 days]
Phase 12:	bottom slab installation (8) [12 days]
Phase 13:	consolidation time [6 days]
Phase 14:	6 th excavation (9) [17 days]
Phase 15:	bottom slab installation (10) [17 days]
Phase 16:	Removal of the strut (6) [12 days]

N.B.: numbers in () are construction sequences (Fig. 4.94) and numbers in [] are consolidation and execution time

**Fig. 4.98.** Calculated and measured displacement of the wall (South-North Section).

West-East section (Section I-I): The excavation of the west-east section consists of several slices of trenches that were executed on the daily output basis (Fig. 4.85 & 4.95). After each slice of the trench had been cut, it followed immediately the placement of fast hardening concrete bottom slab securing a bottom support to the walls in the south-north direction. The excavation was started at strip No. 2.5 (Fig. 4.85) or sequence No. 3-1 (Fig. 4.95) and proceeded to the left and right alternately towards the berms supporting the walls. An attempt had been done to simu-

late these excavation and construction processes in the FEM-computations. The simulation of excavation of each trench and placing of the slab immediately may have no much influence on the results of a drained analysis. The calculation phases followed during the consolidation analysis are shown in Table 4.14.

Table 4.14. Construction stages (Section I-I)

Phase 00:	generate the initial stresses
Phase 01:	activate surcharge load
Phase 02:	1 st excavation to a depth of -1.2 m (1)
Phase 03:	installation of the walls (2)
Phase 04:	excavation of the first strip 2.5 (3-1) [1 day]
Phase 05:	excavation of the next strip 2.4 (3-2) [1 day]
Phase 06:	consolidation time [1 day]
Phase 07:	excavation of the next strip 2.3 (3-3) [1 day]
Phase 08:	consolidation time [2 days]
Phase 09 - 13:	excavation of the strips 2.6, 2.1+2.7, 2.8, 2.2, 2.4 in succession (3-4) to (3-8) [each 1 day]
Phase 14:	consolidation time [3 days]
Phase 15:	excavation of the next strip 2.5 + 2.9 (3-9) [each 1 day]
Phase 16:	consolidation time [8 days]
Phase 17:	excavation of the next strip 2.6 (3-10) and installation of the left support (4)[1 day]
Phase 18:	consolidation time [4 days]
Phase 19 - 21:	excavation of the strips 2.7, 2.8 2.8, in succession (3-11) to (3-13) [each 1 day]
Phase 22:	installation of the right support (5)[1 day]
Phase 23:	excavation of the strips 4.1-4.9 (6) [10 days]
Phase 24:	placement of the bottom slab (7) [11 days]
Phase 25:	consolidation time [10 days]
Phase 26:	removal of the left support (4)[2 days]
Phase 27:	consolidation time [3 days]
Phase 28:	excavation of the strips 4.1-4.9 (8) [7 days]
Phase 29:	placement of the bottom slab (9) [8 days]
Phase 30:	consolidation time [22 days]
Phase 31:	removal of the right support (5)[2 days]
Phase 30:	consolidation time [4 days]

N.B.: 1) numbers in () are construction sequence (Fig. 4.95) and numbers in are consolidation and execution time.

2) placement of the bottom slab in the previous trench followed during the excavation of the next strip.

The computed and measured displacement of the walls at the end of the excavation stage for the west-east section are shown in Fig. 4.99. Surprisingly, both the drained and consolidation analyses led to almost the same wall displacement, but they are far from the measured value. Compared to the measured value of the displacement (18 mm) at the top of the west wall, a maximum displacement of 76.6 mm (drained) and 78.1 mm (consolidation) is obtained from the FEM-computations. Similarly, a displacement of 76.4 mm (drained) and 71.2 mm (consolidation) is computed at the top of the eastern wall compared to a measured

value of 16 mm. It can also be seen from the figure that the amount and shape of the displacement of the wall are almost identical, as if the excavation was symmetrical in respect to the loading and geometry.

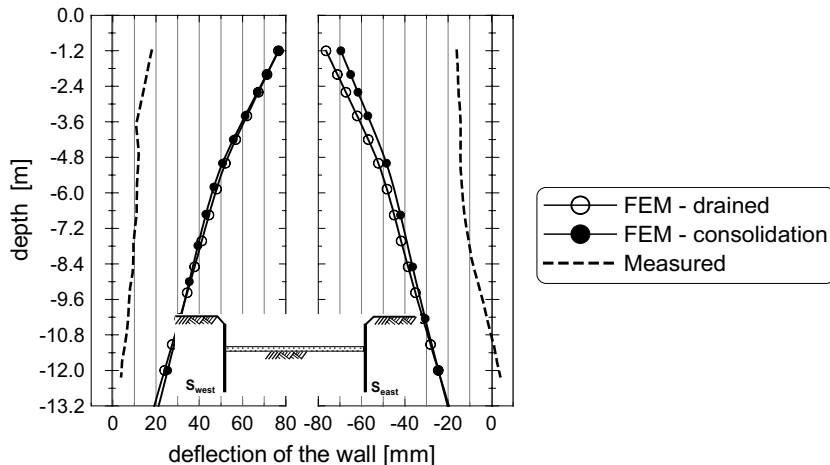


Fig. 4.99. Calculated and measured displacement of the wall (West-East Section).

It would appear from the preliminary analysis and comparison of the measured and computed displacement of the walls that the results did not match each other. The possible cause of the deviation of the FEM - results from the measured values may be summarized in three points as follows: 1) Measured values are incorrect, 2) Soil parameters are underestimated, or 3) Construction details are not simulated correctly.

The probability of mistakes during measuring and interpretations may not be fully ignored. However, the probability of making a mistake that lead to more than 300% differences at all measuring points is very unlikely. The deflection of the wall was measured using inclinometer with an accuracy of ± 1 mm according the geotechnical report. Moreover, the construction was successfully completed without no remarkable damages on the surrounding structures. Therefore, point 1 may be ruled out as possible source of deviation of the results. To investigate the other two points as the main causes of the problem, a parameter study on a simplified geometry has been carried out and is presented in the section below.

Parameter study on simplified model geometry. In order to investigate the possible causes of deviations of the FE-computation results and the measured values, a simplified model geometry (Fig 4.100) is selected for further parametric study. The parameter study includes influence of the interface properties, the groundwater conditions, the stiffness of the soil, and an aspect of constructional procedures. All the FEM-computations has been performed under drained condition following the calculation phases in Table 4.15. Hence, the material properties in Table 4.11 are adopted as a reference parameters.

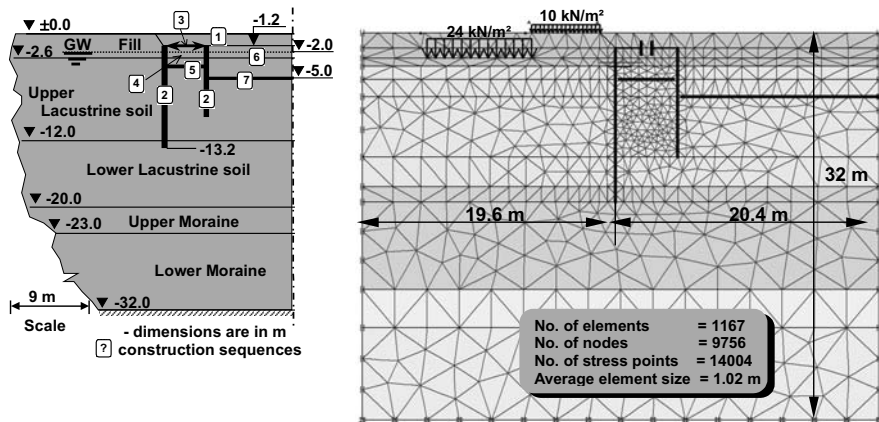


Fig. 4.100. Section and FE-mesh for the parametric study of the project

Table 4.15. The construction phases for the parametric study[“]

Phase 00: generate the initial stresses	Phase 05: installation of bottom slab (5) and removal of the strut (3)
Phase 01: activate the surcharge load	Phase 06: 3 rd major excavation (6)
Phase 02: 1 st excavation to a depth of -1.2 m (1)	Phase 07: placement of the bottom slab (7)
Phase 03: installation of the walls (2)	
Phase 04: strut installation (3) and 2 nd excavation (4)	

The interface behaviour: In this section the possible influence of the interface properties has been examined by varying the shear parameter of the interface and the virtual thickness of the interface. The following cases are investigated:

- Case 0: Reference case ($R_{\text{inter}} = 0.33$ and Virtual thickness factor = 0.10 (default value))
- Inter-case 1: $R_{\text{inter}} = 0.50$
- Inter-case 2: $R_{\text{inter}} = 0.75$
- Inter-case 3: $R_{\text{inter}} = 1.00$
- Inter-case 4: Virtual thickness factor = 0.05
- Inter-case 5: Virtual thickness factor = 0.20

Note that the factor R_{inter} was only applied on the shear parameters.

Fig. 4.101 shows the influence of the variation of the interface properties at three selected points, namely, at wall head (A), at wall toe (B) and around 6.5 m behind the wall (C). It can be noted that varying the value of R_{inter} from the reference value of 0.33 to 1.00 led to a reduction of wall displacement by about 25% at A, no significant change at point B, up to 40% reduction of the surface settlement at C. These changes are not large enough to bring the computed displacements to the measured values. Compared to the reference values, no significant change is

observed for the cases of varying the virtual thickness of the interface from the default value 0.1 to 0.05 and 0.20. Therefore, one may rule out the interface properties as a main source of the differences between the calculated and measured results, though it might contributes its part to the problem.

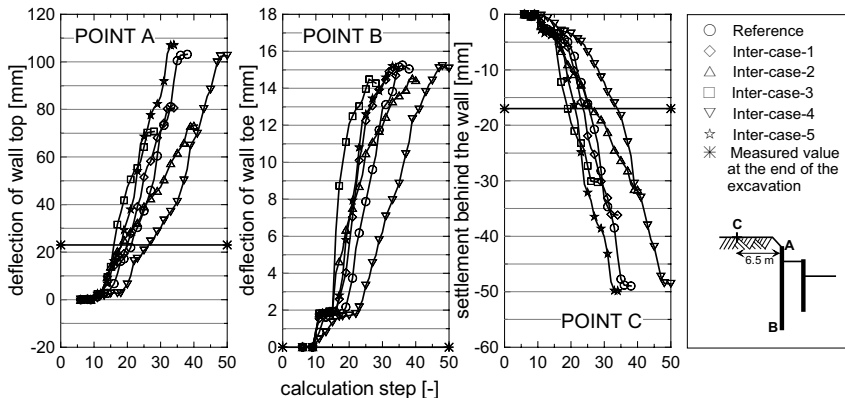


Fig. 4.101. The influence of the interface properties

The stiffness of the soil: It is well known that the modulus of deformation of the soil strongly influences the calculated behaviour of the excavation. The differences between the measured and calculated deformations, not only by excavations but also by shallow foundations, are usually related in the literature to the lack of estimating the deformation modulus correctly from laboratory test results. To examine the effect of the stiffness parameters based on the practical project, the following cases has been investigated:

- Case 0: Reference case
- SS-case 1: Increase the E_{50} and E_{oed} of the fill, the upper and the lower lacustrine layers by a factor of 1.5 and the E_{ur} by a factor of 1.3
- SS-case 2: Increase the above stiffness parameters by a factor of 4
- SS-case 3: Increase the stiffness of the fill layer by a factor of 4

Fig. 4.102 shows that the stiffness values of the upper three layers should increase by a factor as high as 4 in order to arrive at computed deformations that are fairly comparable with the measured values. An efficiency of deformation reduction up to 73% is achieved in the case of increasing the stiffness values by a factor 4 (SS-case-2). The assumption that the fill layer can be stiffer than usually would have taken due to the existing buildings and asphalt streets (SS-case3) does not help to reduce the deformations to a level of the measured values. The parameter variations has clearly shown the influence of the stiffness parameters, however, whether this was the main source of the difference between the computed or the measured values should be proven.

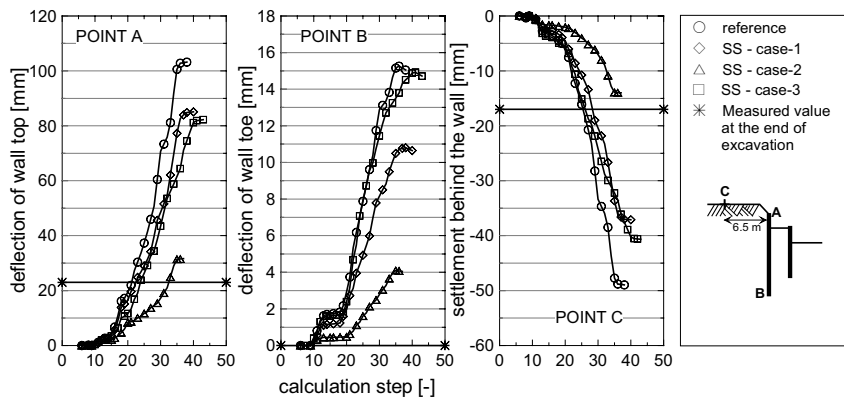


Fig. 4.102. The influence of the stiffness parameters

The groundwater condition: The reference computation is carried out by assuming a hydrostatic groundwater level at 2 m below the ground surface for all soil layers. In the geotechnical report, however, different groundwater levels are indicated for different layers. A free water in the fill layer at -2 m depth on average and a confined groundwater in the moraine layer was encountered, but it was not well known which water table governed in the relatively impermeable layer of the lacustrine soft soil. A drainage filter was also constructed just behind the sheet pile wall to a depth of 1.2 m below the wall, in order to relieve the wall from groundwater fluctuations. These variations of the groundwater condition together with groundwater flow analysis had been considered in the study and they are categorised as follows:

- GW-case 1: GW flow analysis instead of hydrostatic groundwater
- GW-case 2: Consider the drop of the GW due to drainage filter
- GW-case 3: Assume the GW table at -2 m for the fill layer, at -1 m for the moraine layer and interpolation between the two for the lacustrine layers
- GW-case 4: Assume the GW table at -2 m for the fill layer, at -12 for the moraine layer and interpolation between the two for the lacustrine layers.

Fig. 4.103 shows no significant change of the deformations at point A and C due to the groundwater flow analysis but there is up to 45% reduction of the deformation at point B when compared to the reference values. The second case of the GW analysis shows a 22% and 17% reduction of the wall displacement at points A and B and an increase of the settlement at C by about 11%. The GW-case 3 shows no significant influence at points A and C but a reduction of the wall toe displacement by about 31%. The most noticeable effect can be observed from the GW-case 4 analysis results. As it can be seen from the Fig. 4.103, there is a 50 - 65% reduction of the deformations at the given points. In general, the above results show that the importance of the detailed information of the groundwater condition and the type of analysis.

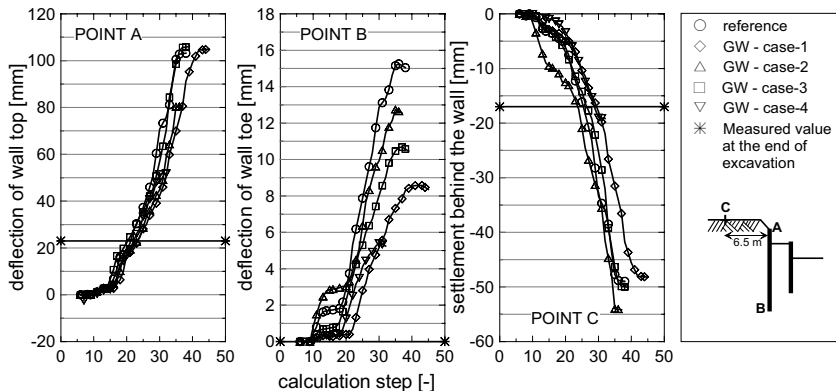


Fig. 4.103. The influence of the groundwater conditions

Other Factors: To this group belong the effect of the plastic behaviour of the sheet pile wall, the no surcharge effect, the effect of considering the surcharge as a rigid body in stead of distributed load, the effect of replacing the bottom slab with a fixed strut, the effect of shifting the transition between the upper and lower lacustrine layer to -9.7 m from the -12.0 m depth below the ground surface and, increasing the stiffness of the lower lacustrine layer by a factor of 3 (after shifting the layer).

Others-case 1: Plastic behaviour of the sheet pile wall. Most often the assumption of the elastic behaviour of the wall might be sufficiently enough for practical purposes. To examine the possible effect of the plasticity, the material behaviour of the wall was defined as elastoplastic by defining an additional parameters: the maximum bending moment of $M_p = 505 \text{ kNm/m}$ and the maximum axial force of $N_p = 3612 \text{ kNm/m}$ (Profile ARBED AZ18-240). The analysis result (Fig. 4.104 - top) shows no influence of this variant on the displacement of the wall and the settlement of the ground surface.

Others-case 2: Without surcharge load. A surcharge load of 24.4 kN/m^2 and a traffic load of 10 kN/m^2 was assumed in the computation of the reference case at a depth of -2 m and at the ground surface respectively. To see the possible effect of these loads, they are set to zero. The result (Fig. 4. 104-top) shows about 20% less displacement at A and about 30% less settlement at C, but no effect on the wall displacement at B.

Others-case 3: Simulation of the building load with a rigid porous body. A cluster was defined which is equal to the building width and 2.0 m deep below the ground surface with a porous linear elastic material property ($\gamma = 18 \text{ kN/m}^2$ and $E = 1.0 \times 10^7$). This is equivalent to the total weight of a 3 storey building ($\approx 36 \text{ kN/m}^2$). This assumption led to a negligible effect at point A and B, but to about 40% settlement reduction at C (Fig. 4. 104-top).

Others-case 4: The bottom slabs assumed as fixed struts instead of plates. The bottom slabs is represented by a plates in the reference case. This may have a negative effect, because the slab plates are automatically connected (either fixed

or hinged) to the wall, i.e., the wall may move upward when the slab moves, which does not mirror the situation in the field. The hinge connection is chosen in this study. The advantage of such plates is their flexibility and stability effect because of their weight. An alternative to the simulation of the bottom slab is to introduce a fixed support, but this option do not allow any horizontal movement.

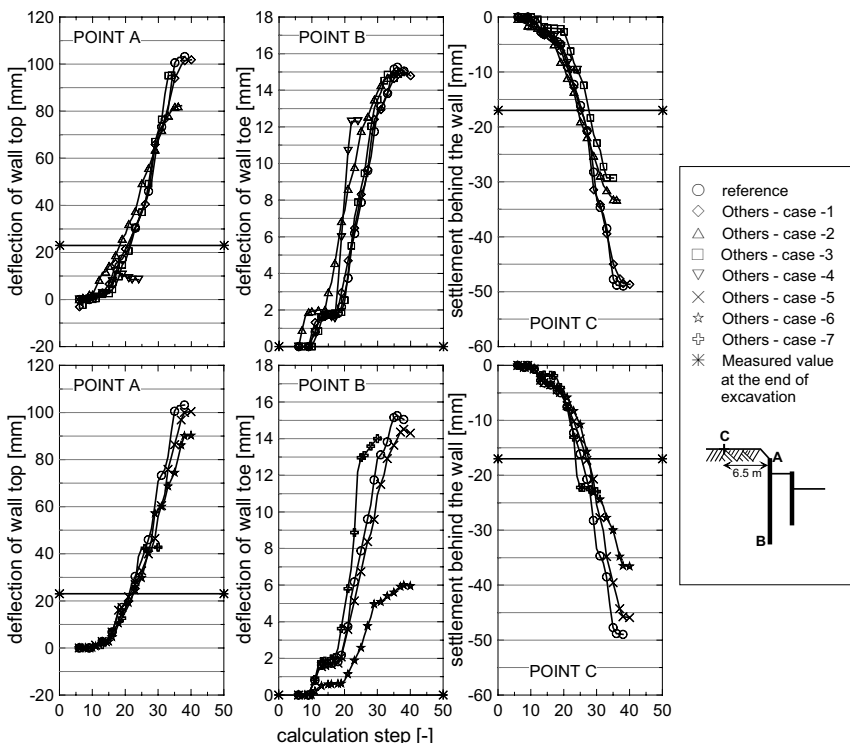


Fig. 4.104. The influence of other factors on deformation behaviour of the wall and the soil.

The comparative effect of both options are investigated under the “others-case 4”, and the results are shown in (Fig. 4.104-top). At first glance, it would appear that this option would be the most effective means of reducing the displacements, as the displacements at A, B and C are reduced by about 92%, 18% and 80% respectively compared to the reference value. There is even 50% less displacement of the wall at A. However, looking at Fig. 4.105, one can easily observe a shape of the computed displacement of the wall which completely oppose to the shape of the measured displacement. The fixed struts at the level of the bottom of excavation (sequence (5), Fig. 4.100) provide non-yielding support to both wall, even it holds back the internal wall. The whole system above the excavation level reacts rigid, but this does not show the reality, and therefore should be ruled out from the options.

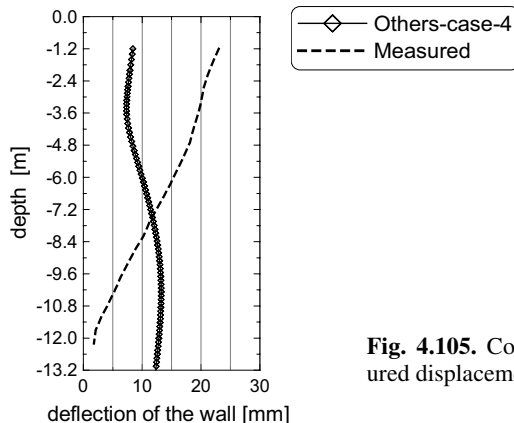


Fig. 4.105. Comparison of the computed and measured displacement of the wall (Others-case-4)

Others-case 5: Shifting the depth of the transition from the upper to the lower lacustrine soil layer to a depth of -9.7 m. It can be seen from the measured values that almost no displacement was recorded at the toe of the outer sheet pile wall (south), indicating a possible fixed support of the wall around the foot. In order to provide a fixed support at the foot, the layer of the lower lacustrine soil was shifted upward to a depth of -9.7 m below the ground surface. If one closely examine the cone penetration field test results, there is a room for possible variation of the boundaries of the layers. However, this option alone did not help to avoid the computed wall displacement at the toe of the wall (Fig. 4.104-bottom).

Furthermore, one more variation was investigated by improving the stiffness of the lower lacustrine layer by a factor of 3 under the name “Others-case 6“ in addition to the shifting of the layer. This option provides a 56% reduction of the wall displacement at B (Fig. 4.104-bottom), whereas its effect at points A and C are moderate.

Others-case 7: Allowing the bottom slab support to effect earlier (3D effect). At last but not least, the 3D effect is investigated. As shown in Fig. 4.85, the excavation was executed in slices of trenches based on daily output. Immediately after excavation of each trench, a fast hardening concrete was placed which provided a bottom support to the wall in south - north directions, before the next excavation had been proceeded. The measured wall displacements at different construction stages also clearly show the effect of the bottom slab, in which a buckling of the sheet pile wall at the level of the bottom slab can be seen. In other words, the slab was already in effect before the end of the excavation. Such excavation procedure is a 3D problem, and can be best solved using 3D-finite element program. However, in this 2D study an earlier effect of the bottom slab was assumed by means of activating it after excavating half of the soil mass but before the end of excavation in each excavation phase.

It appears from Fig. 4.104-bottom that the computed result nears the measured value at point A and C, whereas it shows a little influence at point B. However, it should be noted that the assumption that the supporting effect of the slab starts af-

ter 50% excavation of the soil mass in the corresponding cluster, is purely a rough estimate. Therefore, additional investigation using FE-3D-programm is required before this factor can be used in the 2D-analysis of excavations. That is, the calculation phases 04 to 07 in (Table 4.15) is changed as shown in Table 4.16 below.

Table 4.16. Modified construction phases for the analysis of “Others-case 7“

Phase 00: generate the initial stresses	Phase 05: activate the bottom slab (5), rest
Phase 01: activate surcharge load	excavation (4) and removal of
Phase 02: 1 st excavation to a depth of -1.2 m (1)	the strut (3)
Phase 03: installation of the walls (2)	Phase 06: 3 rd major excavation (6) to half
Phase 04: strut installation (3) and 2 nd excavation (4) to half of its depth	of its depth
	Phase 07: activate the bottom slab (7) and rest excavation (6)

End analysis results. Once the possible impact of the different parameters, construction and groundwater condition has been studied, the next step was to make use of this parameter study to analysis the actual project. Although all the cases studied above might have impact on the deformation behaviour of the excavation, the last case “Others-case-7“ in combination with the case “Others-case-6“ has been identified as the major important factor. The earlier effect of the bottom slab has a major influence on the wall displacement at the top, and improving the stiffness of the soil around the toe will have an effect on the toe displacement. A combination of these two factor might lead to a result comparable with the measured values. Thus, the following cases had been considered for the final analysis of the excavation project in question:

- Final-case-1: the same as “Others-case-7“ in the parameter study
- Final-case-2: the same as “Final-case-1“ but with combination with “Others-case-6“ in the parameter study
- Final-case-3: the same as “Final-case-2“ but with the consideration of the drop of the groundwater table behind the wall due to the drainage filter.

Both drained and consolidation analyses using the FE-models in Fig. 4.96 & 4.97 and the modified parameters and construction stages have been carried out.

Wall Displacements: Fig. 4.106 shows the computed and measured displacements of the southern and the northern walls for the cases described above. It appears from this figure that the consolidation analysis provides a lesser displacement than the drained analysis as would expected. It is also interesting to observe that the first case (Final-case-1: consolidation) led to a displacement at the top which is comparable to the measured values, but it shows more displacement at the toe. However, combining this effect with improving the stiffness of the lower lacustrine soil (Final-case-2: consolidation) still results more computed displacement at the toe of the southern wall and a lesser displacement at the toe of the northern wall than the measured value. The possible explanation can be the difference in soil profile at this particular points. The third variant (Final-case-2) shows no significance effect, and it was neglected in the consequent presentation.

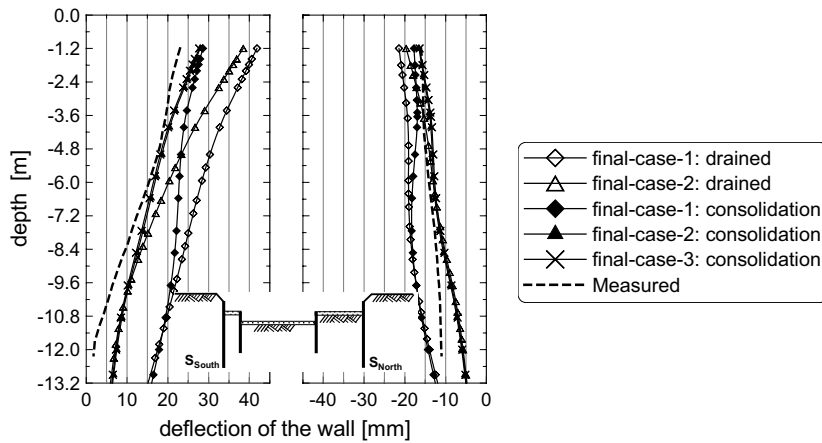


Fig. 4.106. Computed and measured wall displacements (South-north section)

The computed displacement of the west-east walls for the variant “Final-case-2“ only is shown in Fig. 4.107. It can be seen from this figure that the computed displacement from the consolidation analysis matches fairly well the measured displacement of the wall. The shape of the measured displacement of the eastern wall does not match with the computed shape. The toe of the wall also shows movement in the direction of the soil mass. A difficulty of interpretation of the inclinometer measurement at this location was reported in the geotechnical report (Kempfert + Partner 1994-1998), hence the comparison with the computed displacement should take this into account.

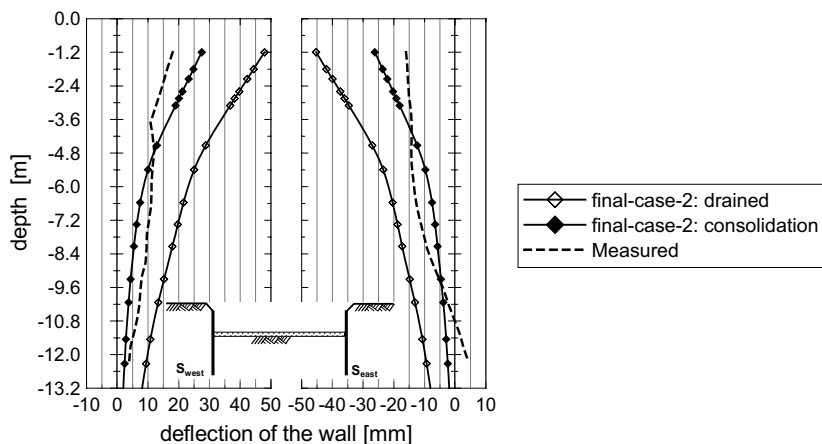


Fig. 4.107. Computed and measured wall displacements (West-east section)

Wall Head Displacement: The measured displacements of the wall head at selective points (LM23 to LM26) on the southern wall compared to the computed displacements are shown in Fig. 4.108. It can be seen from the figure that the consolidation analysis (Final-case-2) result fairly matches with the observed displacements.

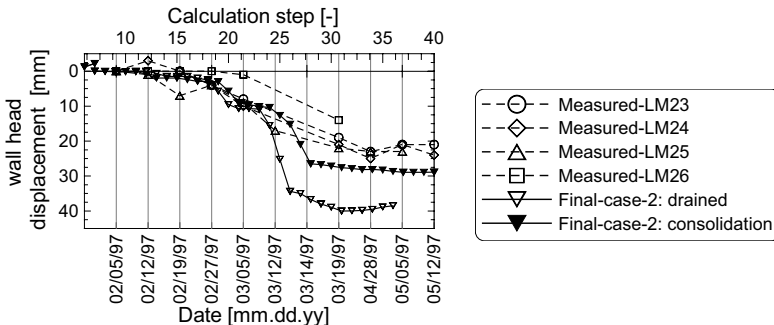


Fig. 4.108. The wall head displacement

Surface Settlement Behind the Wall: Two representative computed settlements from drained and consolidation analysis are presented in Fig. 4.109 for the variant “Final-case-2”. Fig. 4.109a shows the computed ground surface settlement at the location in front of the existing building which is 6.5 m behind the southern wall (Raueneckegasse) and the measured settlements at the locations HP4 and HP5 (see Fig. 4.83). The course of the computed and measured settlement curves is more or less similar. It should be noted that the computed settlements are given in terms of the calculation steps, whereas the measured settlements are drawn based on the real construction time. However, one can clearly identify the different construction phases from the course of the curves, and one may easily compare the computed and measured results. Moreover, the computed settlements up to the installation of the walls (inclusive) has been set to zero, whereas the measured settlements are displayed from the beginning of the construction. For example, a total settlement of about 5 mm was measured at HP4 immediately after the installation of the wall, and adding this value to the computed settlement will result even to a better agreement of the computed and measured settlements.

Similarly, Fig. 4.109b shows the computed ground surface settlement behind the western wall (Sigismundstrasse) at a distance of 10.5 m compared to the measured settlements at measuring points HP23 and HP21. The consolidation analysis result shows a good agreement with the measured value as far as the course of the settlement curves is concerned.

As would be expected, the drained surface settlement is less than the settlement from the consolidation analysis. As can be seen from Fig. 4.109, the difference of the settlements is higher in the west-east section than that the south-north section, which indicates the effect of the simulation of the excavation of each slice, subsequent placement of the bottom slab and simultaneous consolidation.

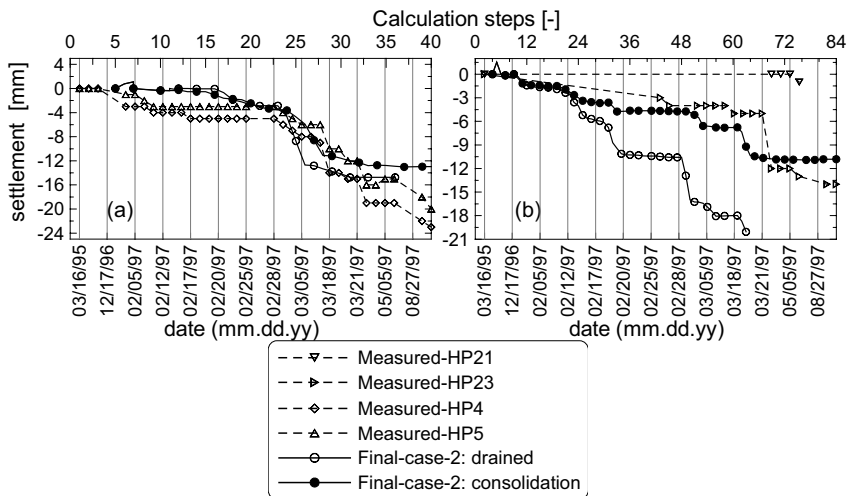


Fig. 4.109. Computed and measured settlements: a) behind the southern wall; b) behind the western wall

Pore Pressure: The calculated excess pore pressure at three locations and at two different depths are shown in Fig. 4.110. It appears from the figure that there is fair agreement between the measured and computed values, though the measurement of the excess pore pressure was not carried out to the end of the excavation.

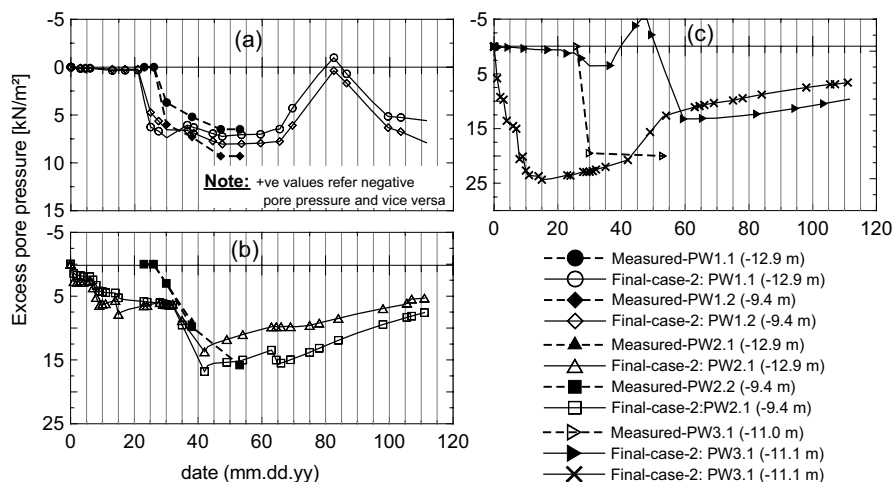


Fig. 4.110. Computed and measured pore pressure

4.12.3 Project-II: Markgrafenstrasse - Constance

Introduction

The excavation site is located in a built up area in southern Germany in the city of Constance. It was intended for the basement of a multi-storey residential apartment and the construction work was completed in 1993. The site plan together with site investigation and instrumentation locations is shown in Fig. 4.111. The excavation is 5.4 m to 6.8 m deep, and covered an area of 55 m x 55 m at the longest side. The site is surrounded by 1- to 6-storey (with one basement floor) residential buildings as shown in Fig. 4.111. All buildings are rested on raft foundation. At two sides (along MS2 and MS5), the excavation was very close (1.2 to 1.5 m) to the existing buildings.

Site condition

The site investigation revealed a ground comprising upper lacustrine silty clay of thickness 3 to 4 m with low to medium plasticity and soft to stiff consistency, overlying very soft lower lacustrine clay of thickness 6 to 8.5 m. Beneath the lower lacustrine layer is a low plastic lacustrine clay mixed boulder clay of thickness 2 to 3.5 m overlying moraine gravel. Although no investigation was made to estimate the extent of the moraine layer, it is believed from the experience that it extends at least up to a depth of 32 m below the ground surface. Beneath the moraine layer, a boulder clay layer is usually assumed in Constance area. The groundwater is assumed to be located at 2 m below the ground level.

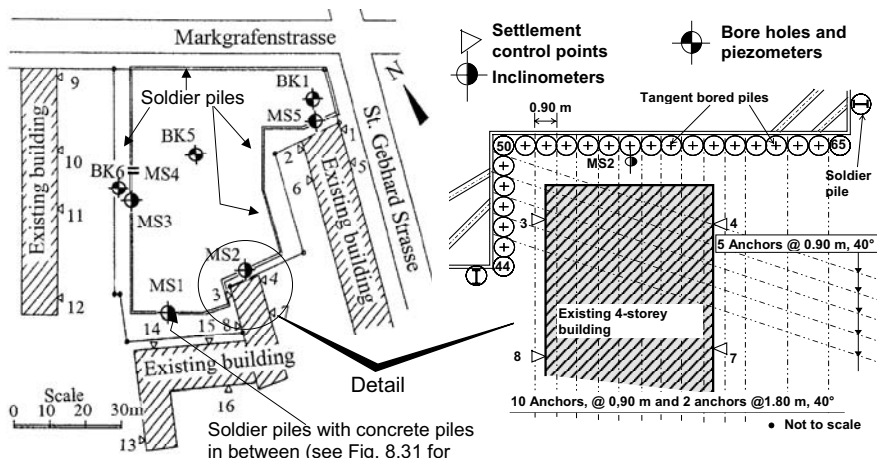


Fig. 4.111. Site plan, location of boreholes and instrumentation

Support system

The excavation was supported by three types of wall systems. The larger part of the excavation, i.e., the west-northern side (along MS3 &MS04), the north-eastern side (parallel to markgrafen street) and part of the east-southern side (Fig. 4.111) were supported by soldier piles with timber sheeting. The soldier pile was made up of IPB 600 I-steel beam section, and it was placed in a pre-bored 90 cm diameter concrete footing which penetrates 2.5 m deep inside the moraine layer starting just below the excavation bottom. The piles were located at a spacing of 2 and 2.5 m.

In the south-western side (along MS01), the excavation was supported in a similar way as above with soldier piles, but concrete pile sheeting instead of the timber sheeting. One 75 cm diameter reinforced concrete piles and two 62 cm diameter concrete piles (Fig. 4.112) were placed between the soldier piles. These concrete piles penetrated 2 m below the excavation depth.

The rest of the excavation (along MS02 and MS05) were supported by 0.90 m diameter tangent bored concrete piles (see detail on the left side of Fig. 4.111). The piles penetrate 2 - 3 m into the moraine layer.

All the wall systems were supported by ground anchors of the type “Techno-Anchor, 6φ 12 St 1420/1579“ inclined at 40° below the horizontal at a spacing of 0.9 m in the case of tangent concrete piles and 2 to 2.5 m in the case of soldier piles. The anchors are extended 3.8 to 4.5 m deep into the moraine layer. All anchors were supposed to be pre-stressed to a load of 80-100% of their design load. The walls were supported by struts at all internal corners.

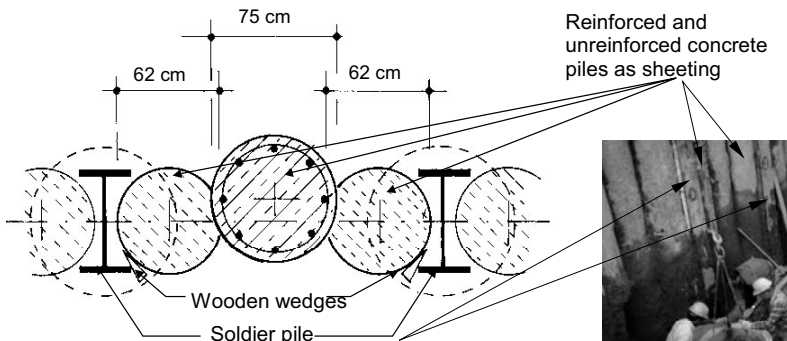


Fig. 4.112. Detail of support along the side where MS01 is located (Fig. 4.111)

Monitoring results

Surface settlements. The settlements at 16 locations near the existing buildings were monitored using surface surveying starting prior to the beginning of the construction activities. The locations of the measuring points are shown in Fig. 4.111.

Fig. 4.113 shows the result of settlement monitoring. As shown in Figs. 4.113a, c & d, no significance settlement was recorded at the corresponding measuring points. On the contrary, unlike the expectation a maximum settlement of 12 to 55 mm was measured at measuring points 3, 4, 7 and 8 (Fig. 4.113b), where there was a very stiff wall system on this side of the excavation. As shown in Fig. 4.113b about 80% of the settlement occurred during the installation of the anchors. The cause of this problem was reported and discussed by Kempfert and Stadel 1994; Kempfert 1997. Also Kempfert and Gebreselassie 1999 tried to follow the settlement due to anchor installation of this project using a combination of analytical and numerical methods.

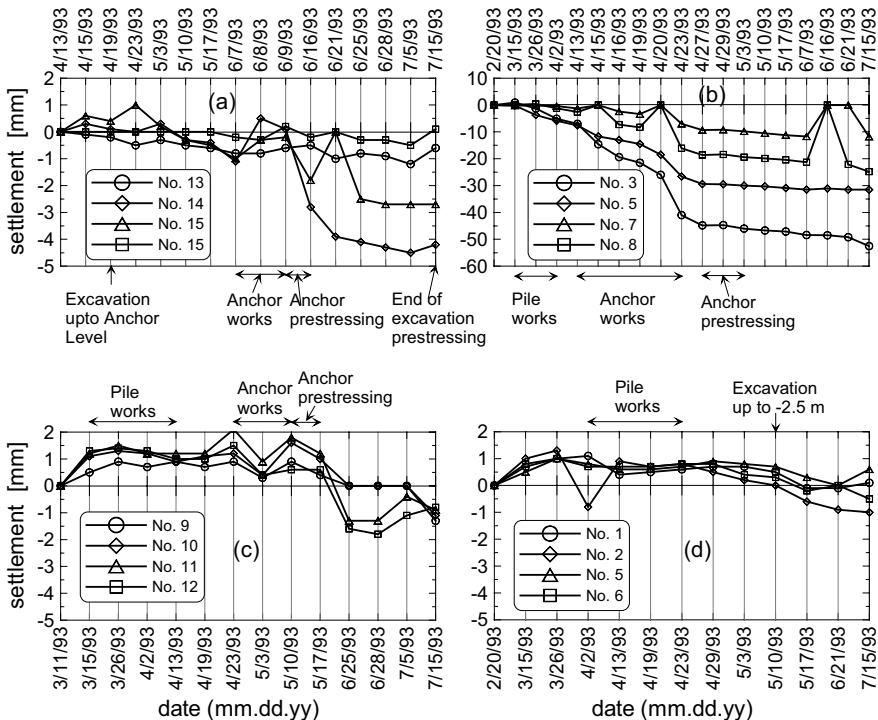


Fig. 4.113. Measured settlements around the existing buildings

Wall deflection. The deflection of the wall was monitored by means of inclinometers at five locations. The results of the inclinometer measurements at three measuring points (MS01, MS02 and MS03) are given in Fig. 4.114. As can be seen from this figure, the walls deflect toward the soil due to the anchor pre-stressing, showing that the soil in the upper layers could not bear the load. The anchors were pre-stressed to a force of 80-100% of the design load, i.e., 400, 630 and 429 kN at MS01, MS02 and MS03 respectively. The subsequent measure-

ments also show no significant change of the deflection of the wall even at the end of the excavation.

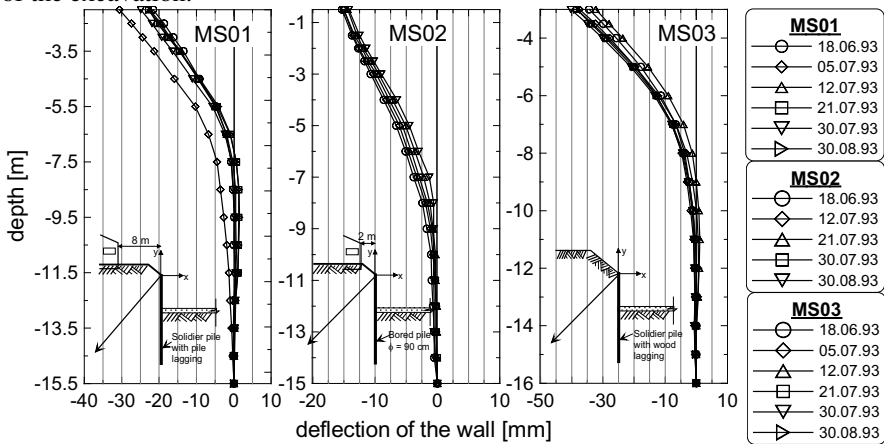


Fig. 4.114. Measured deflection of the wall

Anchor force. The anchor forces were also measured at different time of the construction stages. As shown in the Fig. 4.115, the anchor had yielded slightly during the subsequent excavations showing a drop of 37, 20 and 29 kN at the measuring points MS01, MS02 and MS03 respectively.

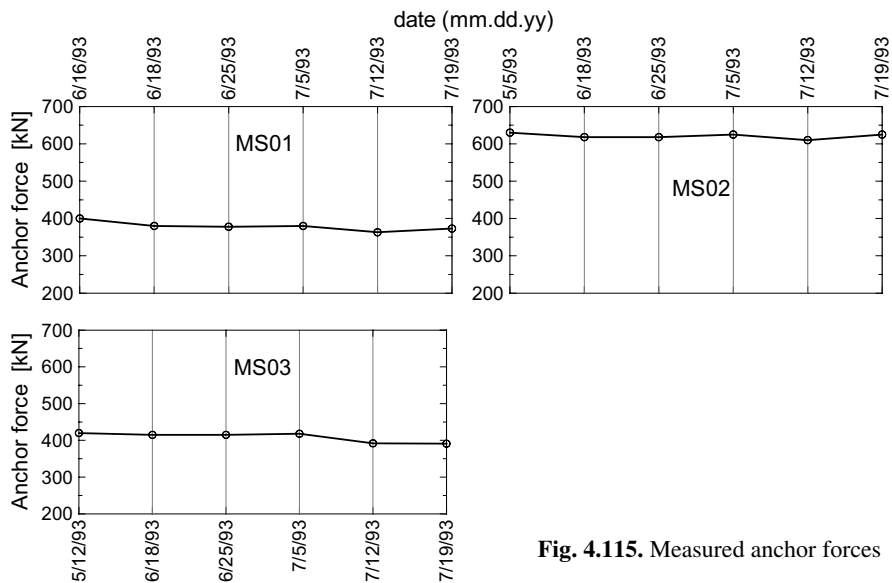


Fig. 4.115. Measured anchor forces

Back analysis of the excavation project-II using the FEM

Model geometry and the finite element mesh. Three sections, namely, section through the inclinometer measuring points MS01, MS02 and MS03, are selected for the back analysis of the excavation project using the FEM (PLAXIS V8), because there are three different wall systems at these locations and settlement and wall deflection measurements are available. The soil profile at these section is more or less the same. The idealized soil profile, arrangement of the structural elements, sequences of the construction and zoomed finite element mesh at the sections MS01, MS02 and MS03 are drawn in Figs. 4.116, 4.117 & 4.118 respectively.

The size of the models is chosen according to the recommendation of the “Working Group Numeric in Geotechnical Engineering” (Meißner 2002; Gebreselassie 2003)) and the parameter study in Section 4.9.2. The finite element mesh at MS01 and MS02 is extended to a depth of 60 m where a fixed boundary is imposed and a zero horizontal displacement is imposed at a distance of 110 m behind the edge of the wall. A symmetrical axis is defined at a distance of 28 m from the wall, where only no horizontal displacement is imposed. The size of the models as a whole is 138 m wide and 60 m high (Figs. 4.116 & 4.118). Similarly, The finite element mesh at MS03 is extended to a depth of 45 m and to a distance of 100 m behind the edge of the wall (all in all 117 × 45 m) (Fig. 4.118). A symmetrical axis is defined at a distance of 17 m from the edge of the wall.

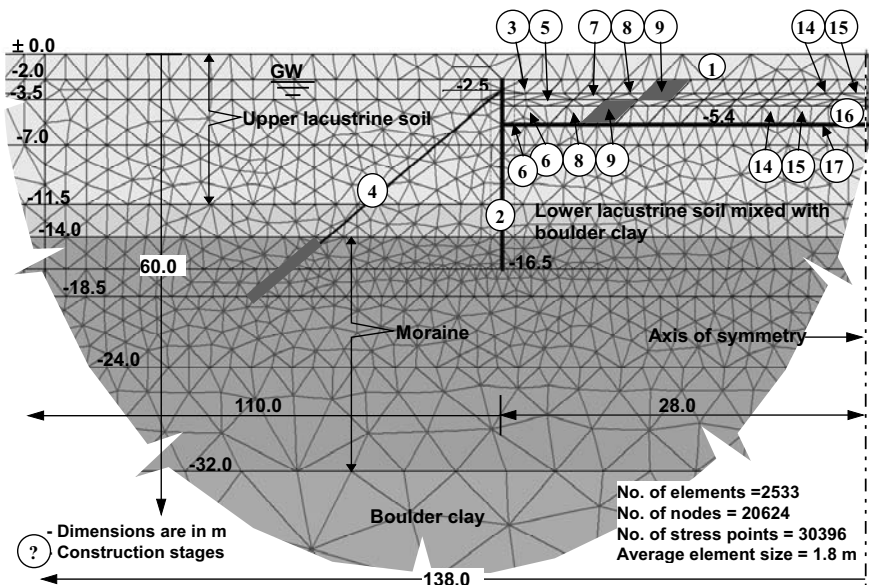


Fig. 4.116. Model geometry, excavation sequences and the finite element mesh for the section through MS01

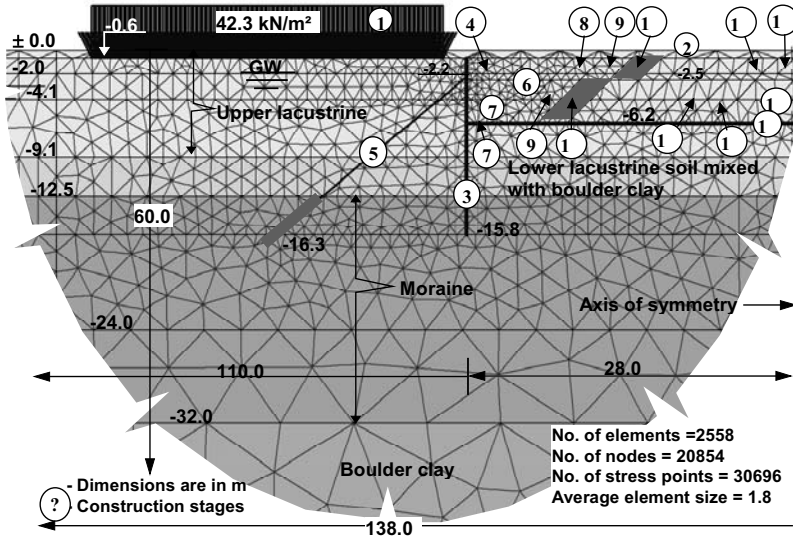


Fig. 4.117. Model geometry, excavation sequences and the finite element mesh for the section through MS02

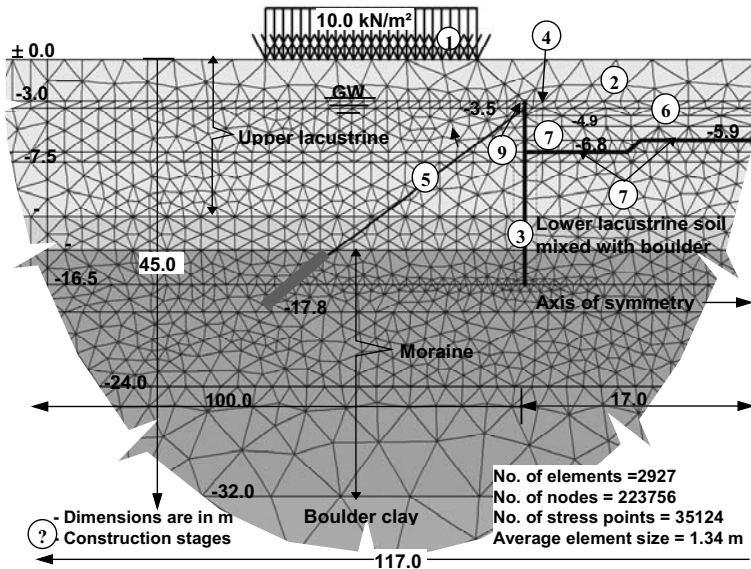


Fig. 4.118. Model geometry, excavation sequences and the finite element mesh for the section through MS03

At section through MS01, the load from the one-storey building is ignored with the assumption that the weight of the soil above the basement floor shall play the same purpose. A surcharge load of 42.3 kN/m^2 is applied at MS02 to simulate the load from the existing 4 - storey building. At section MS03, a traffic load of 10 kN/m^2 is applied to simulate the only traffic load on the road behind the walls. The influence of the existing building at this section is ignored.

Material properties. Like project -I, the HSM iss used as main constitutive model to simulate the behaviour of the soil. The soil parameters required for the FE - computation with the hardening soil model for drained and consolidation analyses are given in Table 4.17. In the first reference analysis of the project the upper and lower lacustrine soil layers are taken as one layer. The soil parameters for the other layers are adopted from the geotechnical report (Kempfert + Partner 1991-1993) after adjusting them to suit the material model. In the absence of comparative triaxial and compression tests, the reference value of the constrained modulus for the other layers is assumed to be equal to the reference value of the 50% secant modulus.

The layers of the lacustrine soil and the lacustrine soil mixed with boulder clay are assumed undrained in the consolidation analysis, whereas the other layers remain drained. Hence, the moraine and boulder clay soil layers in the undrained analysis shares the same parameters as in the drained analysis (Table 4.17). Although the boulder clay layer is relatively impermeable, it is assumed drained, for the same reason given in section 4.11.2.

Similar to the project-I, a separate material set is defined for the interface elements. The shear strength reduction factor of $1/3$ is assumed for the lacustrine and the lacustrine mixed with boulder clay layer, whereas a factor of $2/3$ is taken for the moraine layer. As explained in project -I, the stiffness of the contact surface remains the same as the surrounding soil.

The equivalent modulus of elasticity of the soldier pile (IPB 600) with timber sheeting (MS03) is estimated according the recommendation of the Working Group "Numerics in Geotechnics" 2001 of the German Society of the Geotechnical Engineers from the equation:

$$E_{\text{equivalent}} = \sqrt{\frac{E_{st}^2 \cdot A_{st}^3}{12a^2 \cdot I_{st}}} \quad (4.67)$$

and the equivalent thickness of the wall from the equation:

$$d_{\text{equivalent}} = \frac{E_{st} \cdot A_{st}}{a \cdot E_{\text{equivalent}}} \quad (4.68)$$

where E_{st} , A_{st} , and I_{st} are the modulus of elasticity, the cross sectional area and the moment of inertia of the I-steel beam respectively, and a is the spacing between the I-beams. The soldier pile was placed in a 90 cm concrete footing starting just below the excavation bottom up to 2.5 m deep in the moraine layer. Hence, a separate material property is defined for the lower part of the soldier pile. The com-

combined modulus of elasticity of the steel and the concrete footing is estimated based on the weighted average as follows

$$E_{combined} = \frac{E_{st} \cdot I_{st} + E_{con} \cdot I_{con}}{I_{combined}} \quad (4.69)$$

The equivalent modulus of elasticity is then estimated from Eq. 4.56 by substituting the $E_{combined}$ and $I_{combined}$ in place of the E_{st} and I_{st} .

The soldier with concrete pile sheeting (MS01) is assumed to react together against bending. Hence, the stiffness of the upper part of soldier pile with concrete pile sheeting is taken as the sum of the stiffness of the steel beam and the three concrete piles. The stiffness of the lower part is estimated analogue to the lower part of the soldier pile with concrete footing (MS03).

The bottom slab is simulated as a plate and the stiffness parameters are estimated accordingly. The material properties of all the structural elements are given in Table 4.18 & 4.19. All of them are assumed to behave elastically.

Table 4.17. Soil parameters for the HSM for drained and consolidation analyses

a) Unit weight, permeability and earth pressure at rest

Soil layer	depth [m]	γ_{sat} [kN/m ³]	γ_{unsat} [kN/m ³]	k_x [m/d]	k_y [m/d]	K_0^{nc} [-]
Lacustrine soil	00.0 - -11.5	19.5	19.5	8.64E-5	8.64E-5	0.629
Lacustrine soil mixed with boulder clay	-09.1 - -14.0	20.0	20.0	8.64E-6	8.64E-6	0.531
Moraine	-12.5 - -32.0	21.0	21.0	1.0	1.0	0.391
Boulder clay	-32.0 - -60.0	22.0	22.0	8.60E-6	8.60E-6	0.500

b) Stiffness parameters

Soil layer	depth [m]	E_{50}^{ref} [kN/m ²]	E_{oed}^{ref} [kN/m ²]	E_{ur}^{ref} [kN/m ²]	p^{ref} [kN/m ²]	ν_{ur} [-]	m [-]
Lacustrine soil	00.0 - -11.5	3785	2901	14285	100	0.20	0.900
Lacustrine soil mixed with boulder clay	-09.1 - -14.0	15000	15000	75000	100	0.20	0.900
Moraine	-12.5 - -32.0	63250	63250	316230	100	0.20	0.500
Boulder clay	-32.0 - -60.0	40000	40000	200000	100	0.20	0.800

c) Strength parameters

Soil layer	depth [m]	c' [kN/m ²]	ϕ' [°]	ψ' [°]	R_f [-]
Lacustrine soil	±00.0 - -11.5	20.1	23.2	0.0	0.82
Lacustrine soil mixed with boulder clay	-09.1 - -14.0	10.0	28.0	0.0	0.82
Moraine	-12.5 - -32.0	1.0	37.5	7.5	0.90
Boulder clay	-32.0 - -60.0	10.0	30.0	0.0	0.90

Table 4.18. Material properties of the walls and the bottom concrete slab

Structural element	Type	<i>EA</i>	<i>EI</i>	<i>w</i>	<i>v</i>
		[kN/m°]	[kNm²/m°]	[kN/m²]	[–]
Soldier pile with timber sheeting:	Upper IPB 600	2.836E6	1.7969E5	1.753	0.30
	Lower IPB 600 and Concrete	1.100E7	3.8612E5	8.040	0.25
Soldier pile with concrete sheeting:	Upper IPB 600 and Concrete	2.136E7	8.0966E5	13.90	0.25
	Lower IPB 600 and Concrete	1.100E7	3.8612E5	8.040	0.25
Tangent bored piles	Concrete $\phi = 90$ cm	2.120E7	1.0740E6	11.70	0.20
Bottom concrete slab	Concrete $d = 30$ cm	9.000E7	6.7500E4	7.5	0.20

Table 4.19. Material properties of the support system

Structural element	Type	<i>EA</i> [kN/m°]	<i>L_{spacing}</i> [m]
Anchor (MS01)	Techno-anchor 6φ12 St 1420/1570	71252.0	2.00
Anchor (MS02)	Techno-anchor 6φ12 St 1420/1570	158333.0	0.90
Anchor (MS03)	Techno-anchor 6φ12 St 1420/1570	71252.0	2.00
Grout body	Cement grout	100000.0	-

The FE-calculation phases. A preliminary analysis of the excavation is carried out using the finite element models shown in Figs. 4.116 to 4.118 for the sections through MS01, MS02 and MS03 respectively and using the material properties in Tables 4.17 to 4.19. Both drained and consolidation analyses are performed separately. In all the computations, a hydrostatic groundwater is assumed. The idealization of the construction stages are presented in the following sub-sections.

Section through MS01: The construction stages at the section through MS01 are shown in Fig. 4.116. The excavation was started at the corner, extended side wise, and then proceed in slices in a step form toward the middle of the excavation by stabilising the slopes and immediate placement of the bottom concrete slab (see Fig. 4.119). The exact day to day activities were not documented or they are not included in the geotechnical report available to the author. However, an attempt has been done to idealize the construction stages in the computation based on the information from the field measurements and photos. These idealised computation phases and the corresponding consolidation and execution times are presented in Table 4.20. As already mentioned in Section 4.11.2, it is possible to perform a construction stage and a consolidation process simultaneously, i.e., the excess pore pressure starts to dissipate immediately after the start of the excavation.

The construction stages for the drained analysis are the same as the consolidation analysis less the consolidation steps.

**Fig. 4.119.** View of the construction stages**Table 4.20.** Construction phases for the consolidation analysis (MS01)

Phase 00: generate the initial stresses	Phase 11: Consolidation [2 days]
Phase 01: 1 st pre-excavation to a depth of -2.0 m (1)	Phase 12: the next slice excavation to a depth of -3.5 m (7) [1 day]
Phase 02: wall installation (2)	Phase 13: the next slice excavation to a full depth of excavation (8) on daily output basis [1 day]
Phase 03: 2 nd excavation to a depth of -3.0 m and 3.5 m wide (3) [2 days]	Phase 14 - 16: excavation proceed in slices in a stair case form toward the middle of the excavation (9)-(11). The bottom slabs of the previous slices have been activated during the excavation of the next slice [each 1 day]
Phase 04: Consolidation [48 days]	Phase 17: Consolidation [2 days]
Phase 05: Anchor installation (4) [2 days]	Phase 18 - 22: same as phases 14 - 16 but slices (12) - (16) [each 1 day]
Phase 06: Anchor pre-stressing (4) [2 days]	Phase 23: placement of the last bottom slab (17) [2 days]
Phase 07: Consolidation [10 days]	Phase 24: Consolidation [45 days]
Phase 08: 3 rd excavation to a level of -4.0 m and 5 m wide (5) [30 days]	
Phase 09: Consolidation [4 days]	
Phase 10: 4 th excavation to a level of bottom excavation but only 3.5 m wide(6) and at the same time installation of the bottom slab (6) [2 days]	

N.B.: numbers in () are construction sequence (Fig. 4.116) and those in [] are consolidation and execution time

Section through MS02: Fig. 4.117 shows the general construction sequences at the section through MS02. Similar to the section at MS01, the excavation was started near the wall by first excavating a small working space for the installation of anchors and then proceeded further till the bottom of the excavation in a width of about 3.5 m. Once this area was secured and a bottom concrete slab (fast hardening cement) was placed in position, the excavation continued in slices in a step form toward the middle of the excavation by stabilising the slopes and immediate placement of the bottom slab. These construction procedures are idealised in the consolidation analysis of the project at this section as given in Table 4.21. Again the construction stages for the drained analysis are almost the same as for the consolidation analysis less the consolidation steps.

Table 21. Construction phases for the consolidation analysis (MS02)

Phase 00: generate the initial stresses	bottom slab (7) [2 days]
Phase 01: activate the surcharge(1)	Phase 12: Consolidation [2 days]
Phase 02: 1 st pre-excavation to a depth of -0.6 m (2)	Phase 13: the next slice excavation to a depth of -2.5 m (8) [1 day]
Phase 03: wall installation (3)	Phase 14: the next slice excavation to a full depth of excavation (9) on daily output basis [1 day]
Phase 04: 2 nd excavation to a depth of -2.5 m and 3.5 m wide (4) [2 days]	Phase 15 - 17: excavation proceed in slices in a stair case form toward the middle of the excavation (10)-(12). The bottom slabs of the previous slices have been activated during the excavation of the next slice [1 day each]
Phase 05: Consolidation [9 days]	Phase 18: Consolidation [2 days]
Phase 06: Anchor installation (5) [10 days]	Phase 19 - 22: same as phases 15 - 17 but slices (13) - (16) [1 day each]
Phase 07: Anchor pre-stressing (5) [7 days]	Phase 23: placement of the last bottom slab (17) [2 days]
Phase 08: Consolidation [50 days]	Phase 24: Consolidation [45 days]
Phase 09: 3 rd excavation to a level of -4.1 m and 5.6 m wide (6) [4 days]	
Phase 10: Consolidation [3 days]	
Phase 11: 4 th excavation to a level of bottom excavation but only 3.5 m wide (7) and at the same time installation of the	

N.B.: numbers in () are construction sequence (Fig. 4.117) and those in [] are consolidation and execution time

Section through MS03: At this section, only few construction stages are enough (Fig. 4.118), because the excavation in slices parallel to the walls along MS01 and MS02 can not be modelled with 2D-FE-programs. This is similar to the section IV-IV in project-I (see Section 4.11.2). One slice excavation parallel to the walls at section MS01 or MS02 can reach the whole excavation width at section through MS03. In fact, the 3D-effect remain the same as in section IV-IV in project-I. Hence, it is assumed that the bottom slab will start to effect after 50% of the soil mass above it will have been removed. Table 4.22 shows the idealised calculation stages for the consolidation analysis. These construction phases are also valid for the drained analysis with the exclusion of the consolidation steps.

Table 4.22. Construction phases for the consolidation analysis (MS03)

Phase 00: generate the initial stresses	Phase 08: Anchor pre-stressing (5) [5 days]
Phase 01: activate the surcharge load (1)	Phase 09: Consolidation [38 days]
Phase 02: 1 st pre-excavation to a depth of -3.0 m (2)	Phase 10: 3 rd excavation to a level of -4.9 m (6) [12 days]
Phase 03: wall installation (3)	Phase 11: final excavation to a level of bottom excavation (7) and at the same time installation of the
Phase 04: 2 nd excavation to a depth of -3.5 m and 3.5 m wide (4) [6 days]	bottom slab (7) [12 days]
Phase 05: Consolidation [4 days]	Phase 12: Consolidation [45 days]
Phase 06: Anchor installation (5) [17 days]	
Phase 07: Consolidation [2 days]	

N.B.: numbers in () are construction sequence (Fig. 4.118) and those in [] are consolidation and execution time.

In all the cases the computed displacements till the installation of the wall (inclusive) has been set to zero.

Results of the back analysis. The first analysis carried out is the reference case with the soil profile, finite element model, the material properties and the construction stages discussed and presented in the preceding sections. This reference case is hereafter called as “case-1”. In the reference case, the lacustrine soil is assumed to be consisted in one layer in order to start with the worst condition. However, experience from project-I and also from geotechnical report of this project show that there might exist two layers of the lacustrine soil; the upper and the lower layers with different soil properties. Hence, a second case is defined as “case-2”, which separates the lacustrine soil into the upper and lower lacustrine soils. The separation occur at a depth of -3.5, -3.0, and -4.5 m below the ground surface at the sections through MS01, MS02 and MS03 respectively. The soil parameters of the upper lacustrine layer remain unchanged, but for the lower lacustrine soil layer the material parameters from similar situation at project-I (Dammgasse) for the reference case are adopted (refer to Table 4.11). The only difference is that the lower lacustrine soil layer at Dammgasse was encountered at deeper depth than here at Markgrafenstrasse.

The third and last case, known as “case-3”, is same as case-2 but with increased stiffness parameters of the lower lacustrine soil by a factor of 3. The results of the analyses are presented and compared with the measured values in three groups, namely, deflection of the wall, surface settlement and anchor forces.

Wall deflection: Fig. 4.120 shows a comparable presentation of the calculated and measured deflection of the wall at the end of the excavation at section through MS01. The result of the drained analysis are shown on the left and the consolidation analysis on the right. As can be seen from the figure, the result of the drained analysis of “case-1” shows a deflection of about 5.7 mm more at wall head in the direction of the soil mass and about 7.2 mm more below the bottom of the excavation in the direction of the excavation as compared to the measured deflection. The second drained analysis “case-2” shows a deflection of about 4.1 mm less at the top, whereas the deflection below the bottom of excavation remains almost the same as in “case -1”. Increasing the stiffness of the lower lacustrine layer “case-3” did not help much in reducing the bending and displacement of the wall below the bottom of excavation to the minimum level of the measured value, whereas at the top of the wall it led to deflection about 10.1 mm less than the measured value. Hence, this option is neglected in the consolidation analysis of this section and the other two sections.

In contrary to the drained analysis, the result of the consolidation analysis shows a fixed end support of the wall below the bottom of excavation and it matches exactly to the measured deflection in the case of the variant “case-2”. A possible reason for the difference in the results of the drained and consolidation analyses can be the negative excess pore pressure that still exist below the bottom of the excavation at the end of the construction or at the time of the last measurement.

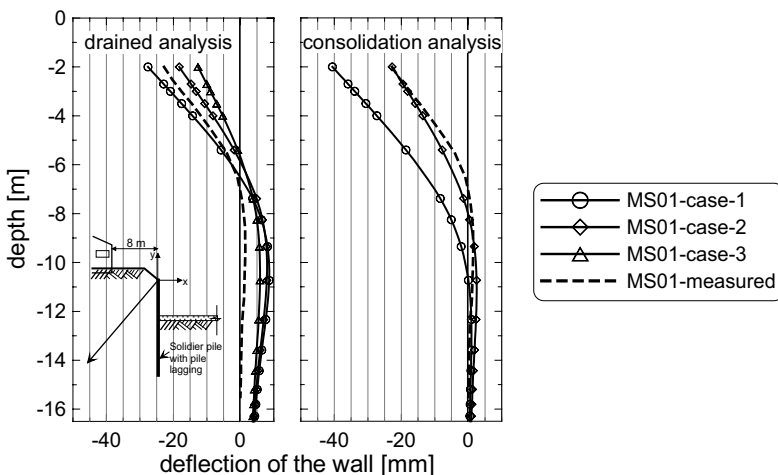


Fig. 4.120. Measured and computed deflection of the wall at section through MS01

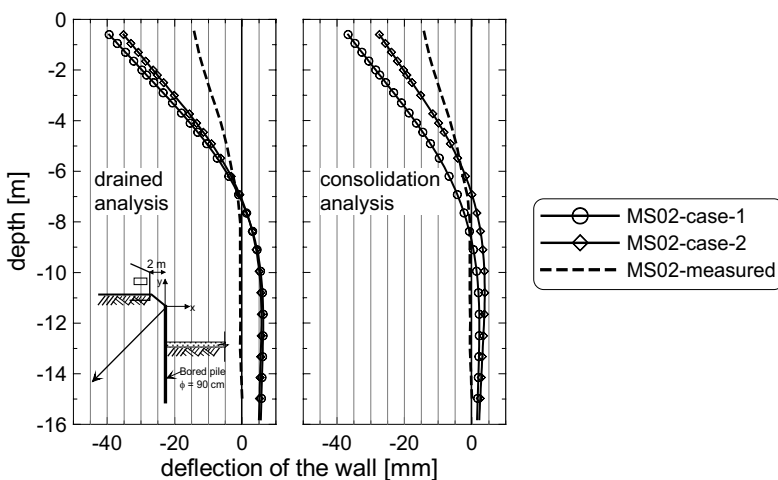


Fig. 4.121. Measured and computed deflection of the wall at section through MS02

The result of the drained analysis of the section through MS02 (Fig. 4.121-left) shows more than double deflection at the top and wall displacement below the bottom of excavation level in both the variants (case-1 and case-2) as compared to the measured values. Again, the results of the consolidation analysis (Fig. 4.121-right) shows a relatively better match, but it is still far from the measured deflection. The existing building at this section is located very near to the wall at a distance of 2 m. The foundation of the building and the walls of the basement floor might contributed to the stiffness of the whole system and reacted rigidly to the

anchor pre-stressing, hence smaller measured deflection of the wall at the top. If the possible increase in the stiffness of the soil layer up to the depth of the basement floor would be considered in the FEM-computations, the deflection of the wall will definitely come close to the measured value.

A very surprisingly result is to see in Fig. 4.122. This figure shows the result of the drained analysis (left) and the consolidation analysis (right) of the section through MS03. The result of the consolidation analysis “case-2“ matches almost 100 % to the measured deflection of the wall.

In general, it would appear that the measured deflection of the wall can fairly be approximated with FE-computations, specially by means of the consolidation analysis and with the application of the soil parameters according to the „case-2“.

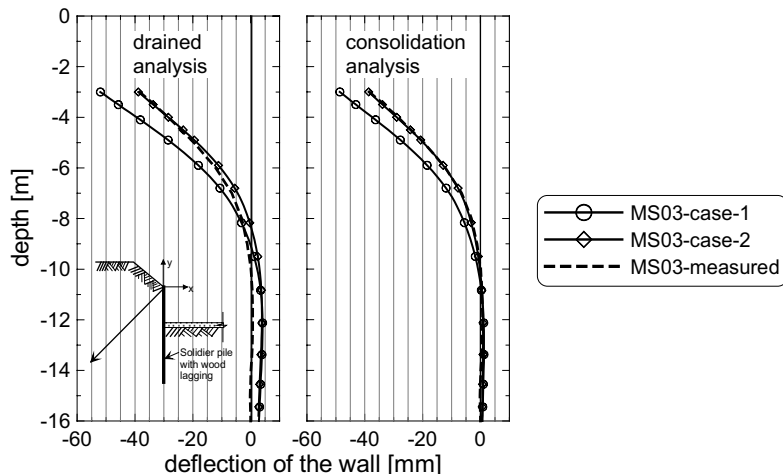


Fig. 4.122. Measured and computed deflection of the wall at section through MS03

Settlement at the ground surface: The computed settlements from the drained analysis at all sections and for all cases are presented in Fig. 4.123 compared to the measured settlements. The computed settlements are plotted as a function of the calculation steps and the measured settlement as a function of the date of measurements. At first glance, it seems difficult to compare the results, but they can be compared based on the course of the settlement curves. The arrows in the diagrams may help to approximately indicate the time point of the start of the anchor installation in the field and in the FE-calculations.

The measured settlements at the sections MS01 and MS03 are as such very minimum (max. 4 mm at MS02). The computed settlements are (case-1 and case-2) relatively more than the measured settlements, but they remain in the minimum ranges (max. 8 mm at ME01). The reason for excessive settlements at the section through MS02 is already explained and corresponding sources in literature are referred in Section 4.11.3.4. Above 80% of the settlement occurred during the anchor installation. This part of the settlement can not be modelled directly by means

of the 2D-FE-computations. An approach to approximate such settlements at re-entry corners based on 2D-FE-analysis and analytical means are given in Kempfert and Gebreselassie 1999. Therefore, there is no wonder to observe the large difference between the measured and computed settlements in Fig. 4.123 at a section through MS02. However, if one ignores the part of the settlements during the anchor installation and shift the settlement curves upward, a fair match of the computed and measured settlements may be obtained. Note also that the computed settlements of the first three calculation phases are not included in the diagrams.

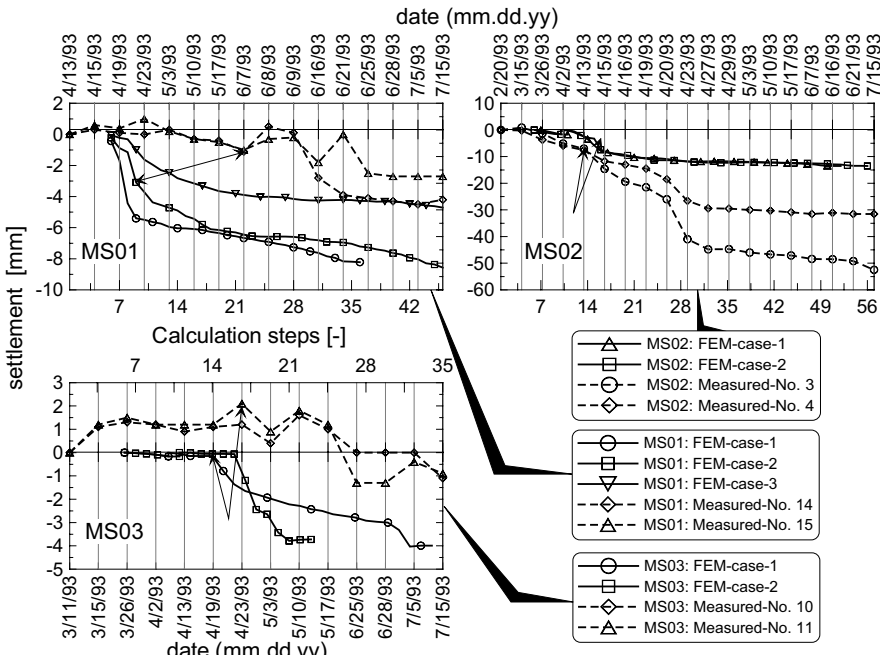


Fig. 4.123. Measured and computed settlements based on drained analysis

A further observation from Fig. 4.123 is that no significant difference is observed from the computed settlements of case-1 and case-2 at all three sections. This indicates that only the upper lacustrine layer mainly contributes to the settlements at the ground surface.

The settlement results from the consolidation analysis compared to the measured results are plotted in Fig. 4.124. The computed results at all sections show up to 2 - 6 mm heave during the anchor pre-stressing. Although such heave due to horizontal loading is theoretically possible, no remarkable heave was recorded during the surface surveying. The course of the computed settlement after anchor pre-stressing, however, resembles the measured settlement lines.

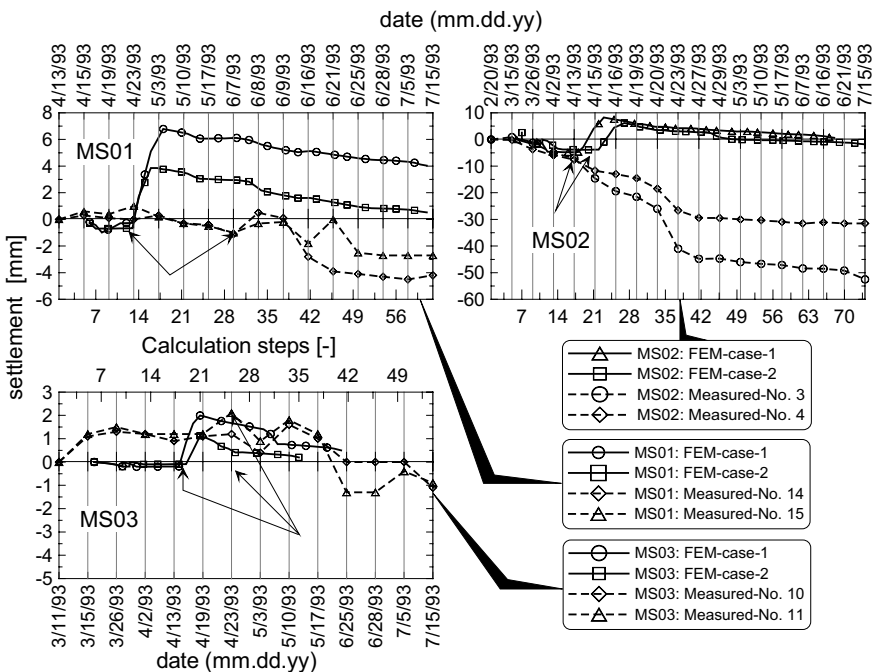


Fig. 4.124. Measured and computed settlements based on consolidation analysis

Anchor forces: The computed anchor forces (Fig. 4.125) from the drained analysis show an increasing trend during the various construction stages, whereas the anchor forces from the consolidation analysis show a slight drop during the excavation stages immediately after pre-stressing, rises very slowly to the position of the pre-stressing force at section through MS01 and MS02, and remains constant at section through MS03. In general, one can say the consolidation analysis can fairly estimate the development of the anchor forces during the various construction stages.

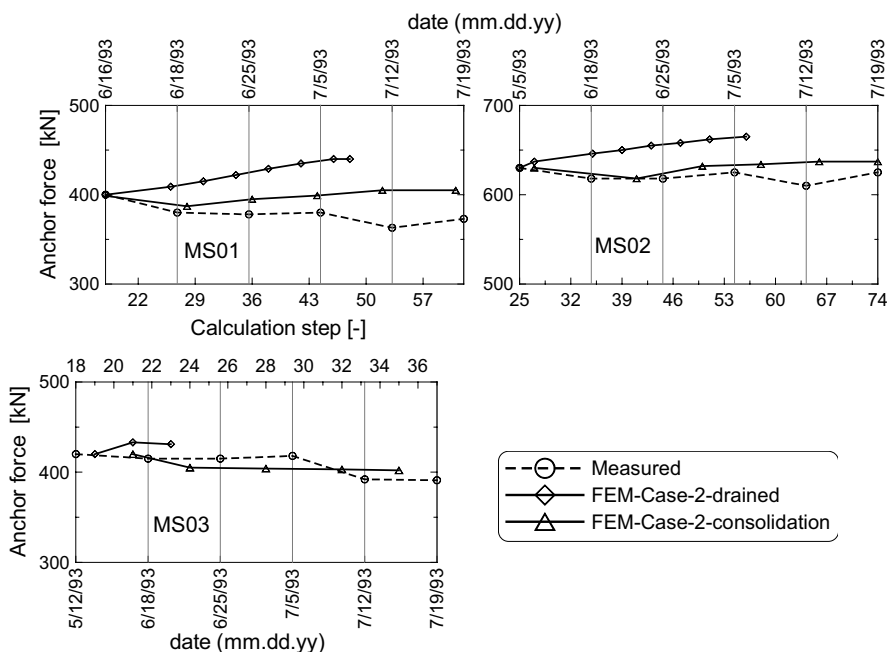


Fig. 4.125. Measured and calculated anchor forces

4.12.4 Project-III: Seeuferhaus – Constance

Introduction

Up to 9 m deep excavation was executed in 2002 for the shopping center building locally known as Seeuferhaus in Constance city near the lake Constance. The excavation was 100 m long and 50 to 100 m wide and carried out in two parts (Fig. 4.127). Part I of the excavation includes two basements part II only one basement. The underground condition in city Constance and the surroundings is known of a deep and soft deposit of lacustrine soil.

Underground conditions

The ground consists of 5 layers (Fig. 4.127). The upper most layer is 3.0 to 4.5 m thick fill material (layer I), of which 2 to 3 m was already cut off within the premise of the construction site. Beneath the fill layer is a layer (layer II) which consists silty fine to medium sand alternatively and it is underlain by soft lacustrine deposit (layer III) starting from a depth about 5.5 to 9 m below the ground surface. The lacustrine soil changes its consistency from soft to stiff in the transition zone starting from approximately a depth of 20 m in the north and 35 m in the south be-

low the ground surface and it strongly consists sand and gravel parts (layer IV). From a depth of 28 to 32 m in the north and 50 m in the south downwards, the bore profile is dominated by a stiff to very stiff ground moraine (layer V).

The upper groundwater level was located at about 3 m below the ground surface during the exploration. A second confined groundwater was also encountered in the ground moraine whose water head reached 1 m below the ground surface.

The results of a number of field and laboratory soil tests are summarized in Fig. 4.126. The natural water contents varies between 35 and 15% and shows a general decreasing trend with depth. The liquid limit in the upper part varies in the range of 40 % which can be classified as lean clay (CL) according to DIN 18196. Starting from a depth of approximately 14 m, the lacustrine soil becomes CL-ML with falling liquid limit value due increasing amount of silt and fine sand.

There were very limited and highly strewing values of the undrained shear strength from the field vane tests available during the preliminary design phase. Therefore, supplementary field vane tests had been conducted during the construction phase and the low undrained strength of the underground had been approved, which is typical in this area.

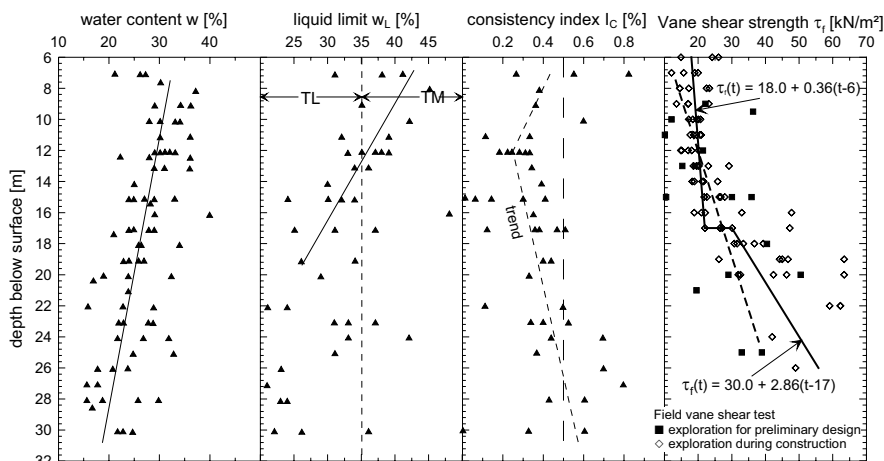


Fig. 4.126. Soil properties

Project description

The trapezoidal shaped layout of the excavation (Fig. 4.127) consists of a rectangular portion (Part I) with an excavation depth of 9.1 to 9.9 m that accommodates two basement floors and a triangular portion (Part II) with a depth of 5.8 to 8.0 m (Fig. 4.128). The two excavation parts were executed successively. The construction plan included the installation of the sheet pile walls first and placement of approximately 130 bored piles that extends deep into the moraine layer starting from

the existing preliminary excavation level at a depth of about 3 m below the ground surface.

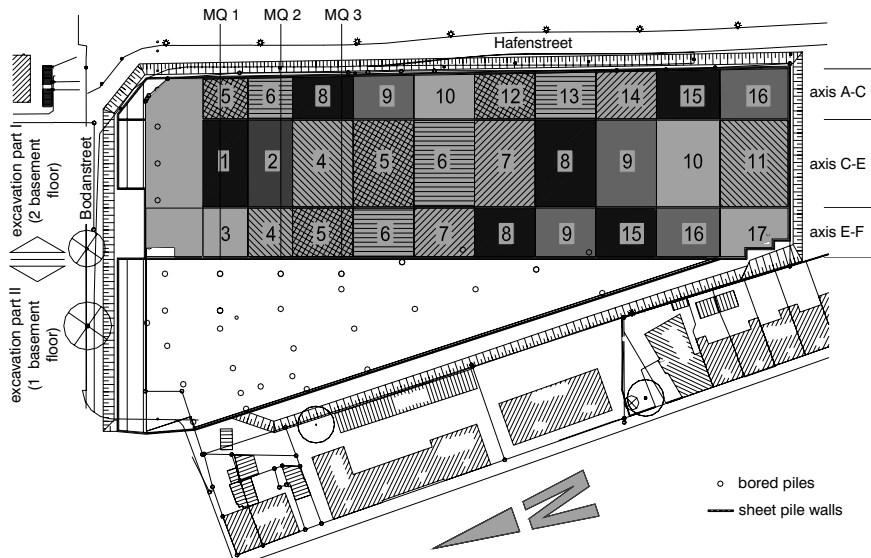


Fig. 4.127. Layout showing succession of the excavation

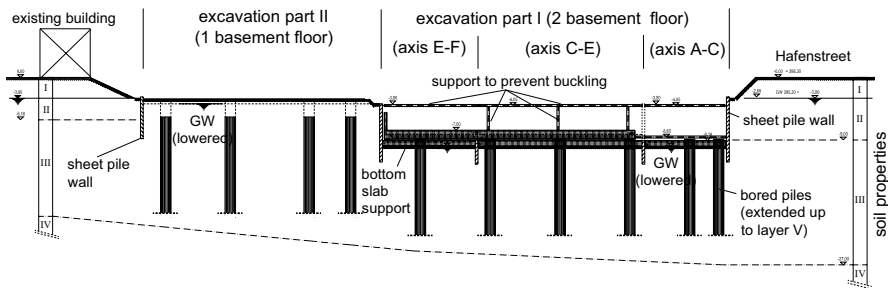


Fig. 4.128. Section MQ1 through excavation

To reduce deformations in the soft lacustrine layers, the excavation part I was again partitioned in three longitudinal strips by means of intermediate sheet pile wall following the orientation of the pile grid system (Fig. 4.127). The sheet pile walls were supported at the top about 4 m below the ground surface by steel struts and at the bottom of excavation by lean concrete slab. Since the bottom support

was intended to contribute to safety against basal and overall failure at the same time, it was connected to the piles and supposed to overcome tensile stresses.

The excavation had been proceeded successively in blocks as shown in Fig. 4.127. The steps followed are indicated by numbers in the layout. Starting from slope in the north, the excavation was proceeded first in the middle strip (Part I, axis C-E) in slices and immediately followed cutting of the exposed part of the piles and placement of the 0.7 m bottom unreinforced concrete slab based on daily construction capacity (Fig. 4.130). The construction work continued in the outer strip near the excavation part II and then to the outer strip near the hafen street. Fig. 4.129 shows an overview of the execution of the excavation in strips and blocks at different construction stages. Some construction details are also illustrated in Fig. 4. 130.

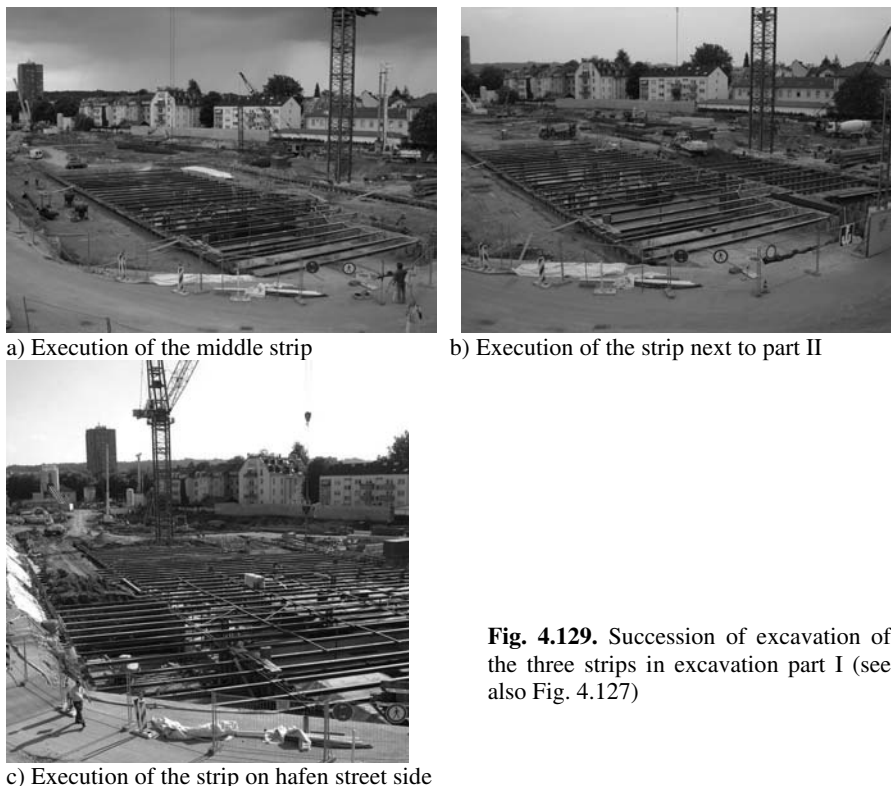


Fig. 4.129. Succession of excavation of the three strips in excavation part I (see also Fig. 4.127)



Fig. 4.130. Some details of construction works with blockwise excavation and bottom slab placement

Monitoring results

The excavation was equipped with monitoring instrumentation such as inclinometers to measure the horizontal movement of the soil behind the external retaining walls, surveying instruments to control the settlements behind the wall, extensometer to control heave, piezometer to follow the change in pore pressure and load transducers for measurements of strut forces. Figs. 4.131 and 4.132 show typical results of horizontal soil movement and pore pressures at sections MQ3 and MQ2 through the excavation in transverse direction (refer to Fig. 4.127). It appears from Fig. 4.131 that the pore pressure dropped slightly at the beginning of the excava-

tion of the middle strip and remains more or less stable until the excavation of the outer strips had been started at a later time where a further sudden drop of the pore pressure was observed. However, the pore pressure had established to its steady state after few days. Similar development of the pore pressure was also observed at section MQ2 (Fig. 4.132) and other measuring points.

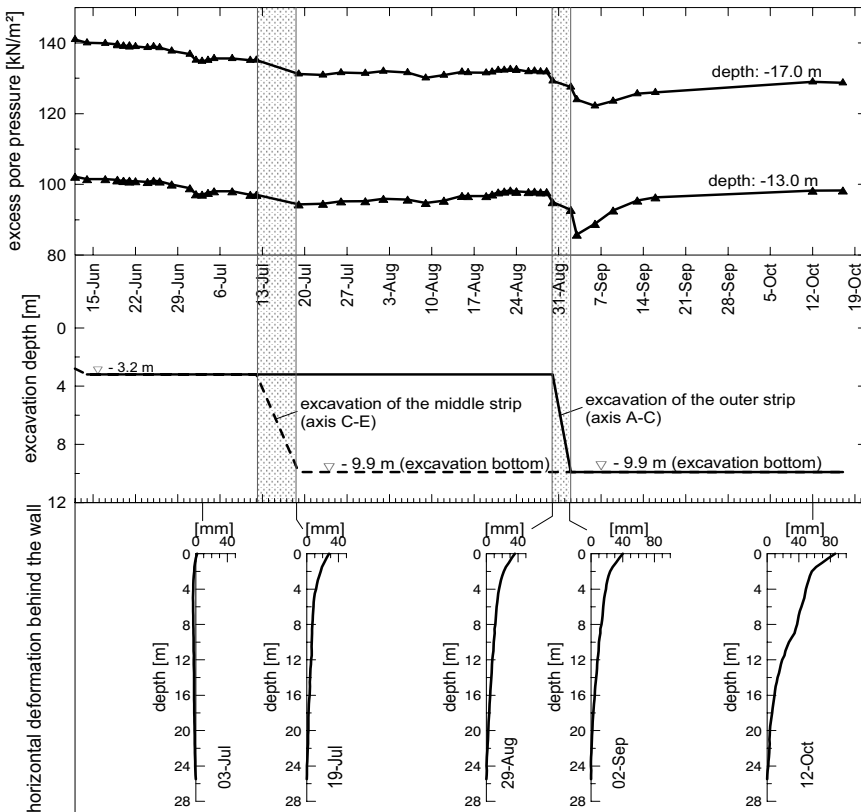


Fig. 4.131. Development of pore pressure and horizontal wall deformation behind the wall at section MQ3

The inclinometers were located just few centimeters behind the outer sheet pile wall. The result of the inclinometer measurement in Fig. 4.131 and 4.132 show that the soil behind the outer sheet pile wall had started to move toward the excavation first after the begin of the execution of the outer strips. During the excavation of the middle strip however no significant wall movement was observed as it can be witnessed from the figures. This kind of trend had also been observed at other measuring points. A maximum horizontal wall movement of about 86 mm was measured at measuring point at section MQ3. However, had it not for the spe-

cial construction method followed in this project, excessive deformations would have occurred.

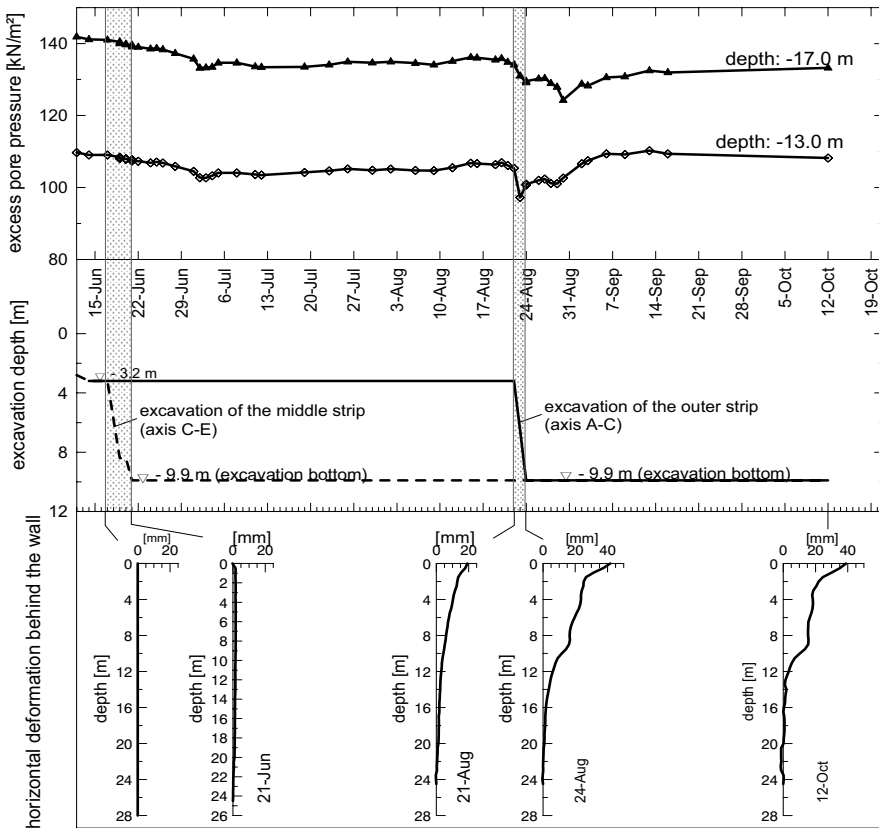


Fig. 4.132. Development of pore pressure and horizontal wall deformation behind the wall at section MQ2

The sensitivity of soft lacustrine soils to excavations can be seen Fig. 4.133. Although the deformed wall was an intermediate sheet pile, which had had not a consequence to the nearby structures, the danger of excavation in soft ground is clear to see.



Fig. 4.133. Excessive deformation and collapse of an intermediate sheet pile wall

4.12.5 Project-IV: Seearkaden Starnberg

Introduction

In execution of the 7.3 m deep excavation for a 4-storey shopping center building known as Seearkaden with two underground basements in Starnberg in southern Germany, a construction method was chosen, by which the excessive deformations of the excavation could to a large extent be prevented. By applying a consistent monitoring method, introducing a bottom support in form of a soilcrete which is anchored by tension injection piles deep in the lacustrine soil layer, and dividing the excavation site into different construction segments, the high safety requirements for the nearby buildings could successfully be fulfilled. The case history is adopted from Katzenbach et al. 1992.

Underground conditions

The site is located in the area of a former glacier lobe in the proximity of a lake-shore, where at the edge of a glacier lake clay and silt had been deposited. This is also typical for many other lakes on the foot of the Alps in southern Germany.

The exploration of the underground shows a 5 m thick middle dense gravel layer overlain by 2 m thick fill material and underlain by a deep lacustrine soft soil (Fig. 4.134). In between the upper and lower lacustrine layer, there exists a thin

dense gravel layer at a depth 16 to 17 m. Due to its middle density are all neighboring building are founded on the upper gravel layer.

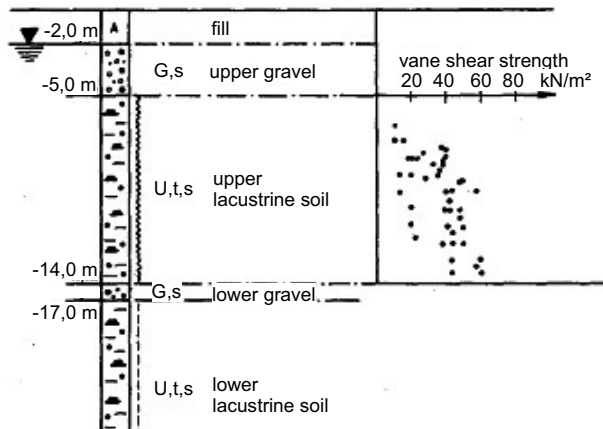


Fig. 4.134. Soil profile and distribution of the field vane shear strength

The upper lacustrine soil is believed to be young and normally consolidated. It has a consistency of soft to very soft with tendency to flow. It is light plastic soil with liquid limit between 20 and 30 %, plasticity index between 4 and 13% and undrained shear strength between 10 and 60 kN/m².

The lower lacustrine layer have more or less similar properties as the upper layer in regard to the consistency and grain size distribution except that it is relatively stiffer than the upper one. The undrained shear strength of the lower lacustrine is estimated to be:

$$c_u = 35 + 0.25 \cdot \gamma' \cdot z \leq 80 \text{ kN/m}^2 \quad (4.70)$$

The groundwater is located at a depth of 2 m below the ground surface, however, the groundwater in the lower gravel layer is found to be confined.

Project description

Relaying on the relatively thick layer of load bearing gravel layer, it was initially planned to proceed the excavation in a conventional way, where a 17 m long and watertight sheet pile wall tied back by ground anchor was used to support the excavation. The sheet pile was installed using a high frequency vibration and partly pressed into the ground using a heavy equipment on the side of the excavation near historical old buildings. During the installation of the sheet pile walls, the soft lacustrine soil had already started to react. With proceeding of the excavation in small sections, the cofferdam-like anchor-soil-sheet pile wall-block system tended to move on the top of the upper lacustrine clay in the direction of the excavation

and received almost no earth reaction below the bottom of excavation, even before the excavation reached the bottom of the gravel layer. It is first after refilling of the first excavation part and pre-stressing the ground anchors, it was possible to bring the wall to its original position.

To fulfil the requirement for a very limited deformations and to avoid damages on existing buildings, the method of execution was modified and adjust to accommodate the difficult situation in-situ. The excavation was first divided into three blocks using a diaphragm wall as shown in Fig. 4.135 (block 1 to 3) in order to minimise the simultaneous mass movements. Moreover, a 2 m thick soilcrete composed of 4600 single columns was installed at the bottom of the excavation from a preliminary excavation level at a depth of 1.5 m below the ground surface.

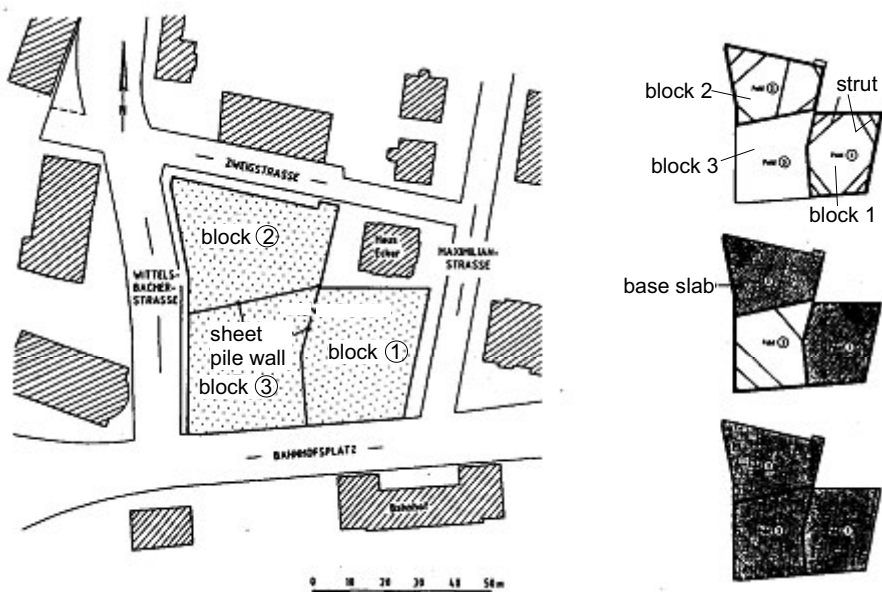


Fig. 135. Layout, partition of the excavation in blocks and construction steps (Seekaden Starnberg)

The soilcrete serves on one hand as bottom support to the sheet pile wall and on the one hand as load bearing slab to prevent the basal and deep seated failure. To optimise the application of the soilcrete, it was anchored downwards using 1400 micro injection piles which reaches 17 m deep into the relatively stiff lacustrine layer (Fig. 4.136).

After the completion of the above preliminary preparation measures, a further partial excavation was executed to install a reinforced concrete wales and steel tube struts. Due to the small number of struts and their arrangement at the excavation corners, the construction obstacles could be avoided which is a common problem in braced excavation.

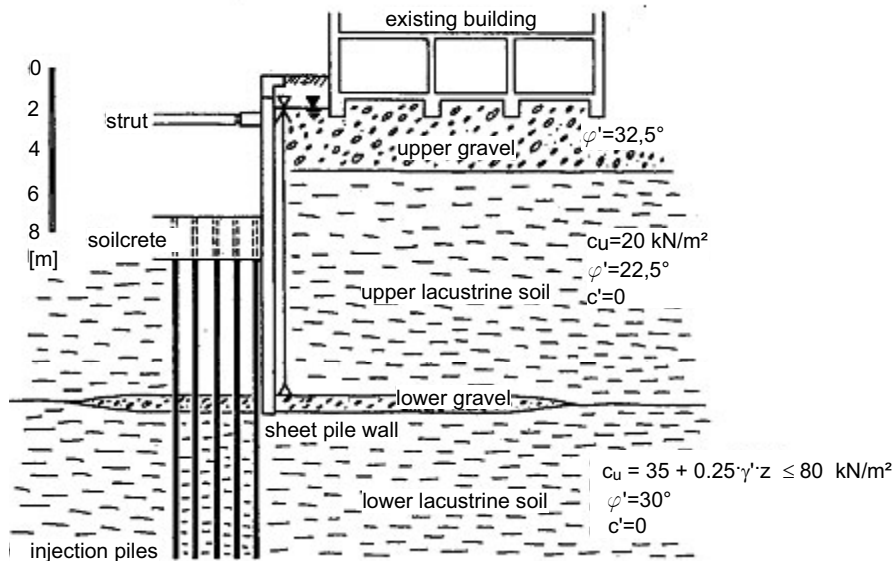


Fig. 4.136. Section through the excavation site

Monitoring results

The horizontal deformations of the sheet pile walls had been controlled by inclinometer that extended to a depth of 30 m below the ground surface. Typical inclinometer measuring points are indicated in Fig. 4.137. The movement of the head of the sheet pile and the diaphragm walls were measured by geodetic instruments. The maximum horizontal displacement of the wall towards the excavation was about 1 cm. The plots of the deflection of the wall in Fig. 4.137 illustrate the effectiveness of the soilcrete as bottom support. The reaction forces in all the struts had been controlled using a load transducer. Fig. 4.138 shows a typical result of strut monitoring. The measured strut forces lie between 1000 to 2000 kN and did not exceed the computed values. The peaks and downs in Fig. 4.138 shows the effect of temperature on strut forces.

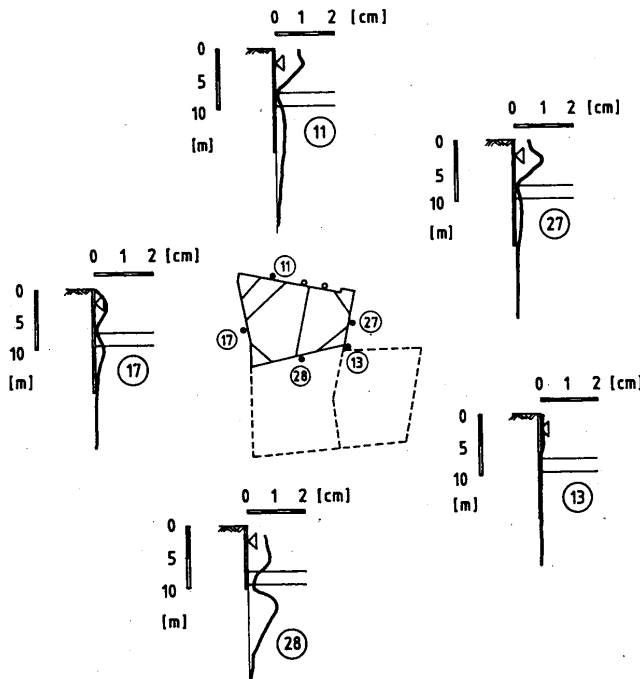


Fig. 4.137. Deformation of the walls at different points in block 2

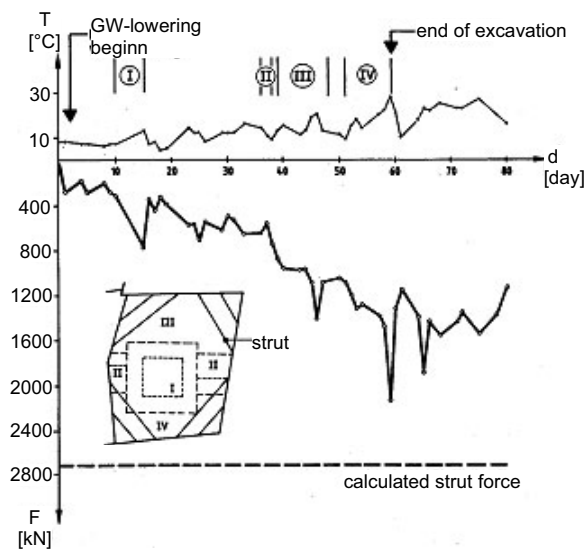


Fig. 4.138. Measured strut force in the course of the construction

At the end of the excavation, a maximum heave of about 5 mm was measured, but it had been reduced back to zero after the construction of the foundation of the building had been finished.

Similarly, settlements of the nearby existing structures were controlled up to a distance of 90 m away behind the excavation walls. Some typical results of settlements of the neighbouring buildings standing directly behind the excavation are shown in Fig. 4.139. At the building nearest to the excavation, a total settlement of 12 mm was measured as a result of the soilcrete installation, full excavation and the load from arcade building. The building had experienced a tilting of 1:2200 but did not suffer any damage.

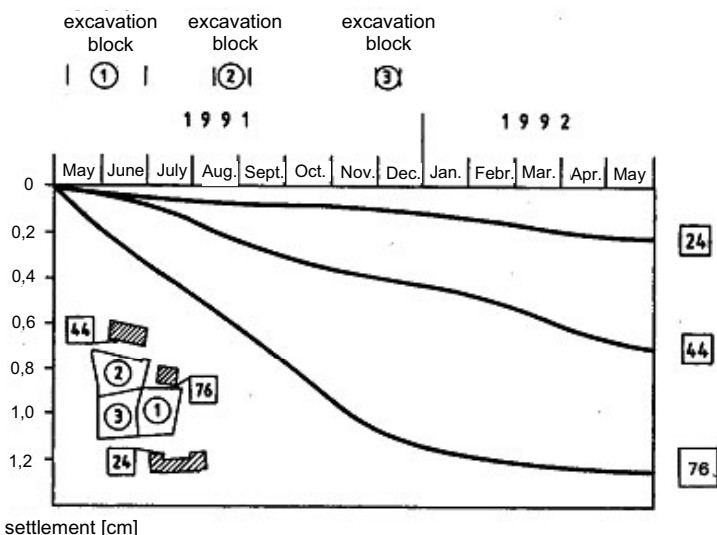


Fig. 4.139. Measured settlements near existing buildings

4.12.6 Project-V: Karstadt building in Rosenheim

Project description

This is about a project for extension of the Karstadt shopping building in Rosenheim in southern Germany built in 1994. The building consists partly one and partly two basements which required an excavation of 9 and 6.7 m respectively below the ground surface. The underground condition at the site is described in the next section. This case history is adopted from Ostermayer and Gollub 1996.

Historically, buildings in Rosenheim are founded on load bearing gravel layer with box type foundation (crawl space). The buildings built after the 2nd world war however are founded on the gravel layer with a compensated basement floor,

so that only slight uniform settlement may arise in the remaining gravel layer above the soft lacustrine soil.

It is for the first time that a 9 m deep excavation was executed in Rosenheim for two basement floors for the Karstadt building in 1968/70. During the demolition of the old building on the site, cracks had been registered in the nearby existing buildings. With advance of the excavation, the cracks developed further and the damage even reached buildings far away from the excavation. The installation of a diaphragm wall with ground anchor embedded in the bearing gravel layer could not avoid the excessive deformation, so that the excavation had to be flooded and filled back. It is after the use of a top-down construction method that the excavation was successfully completed.

About 25 years later, the construction work for the extension of the Karstadt building was started in 1994. North of the existing Karstadt building it was required to extend the building with one basement floor in construction part BT 1/2 (\approx 6.7 m deep) and two basement floor in BT 3 (\approx 9.0 m deep), whereby cultural protected façade of the old houses in Munich street should remain maintained (Fig. 4.140).

In the construction part BT 3 (9.0 m deep), where the excavation reached the soft lacustrine soil layer, the excavation was supported by 88 cm diameter bored tangent piles, whereas the rest of the excavation (BT 1/2, 6.7 m deep) was supported by different systems: underpinning with soilcrete, bored tangent piles ($D = 88$ and 40 cm) as shown in Fig. 4.140. On the side of the existing Karstadt building no support was required because of the existing diaphragm wall.

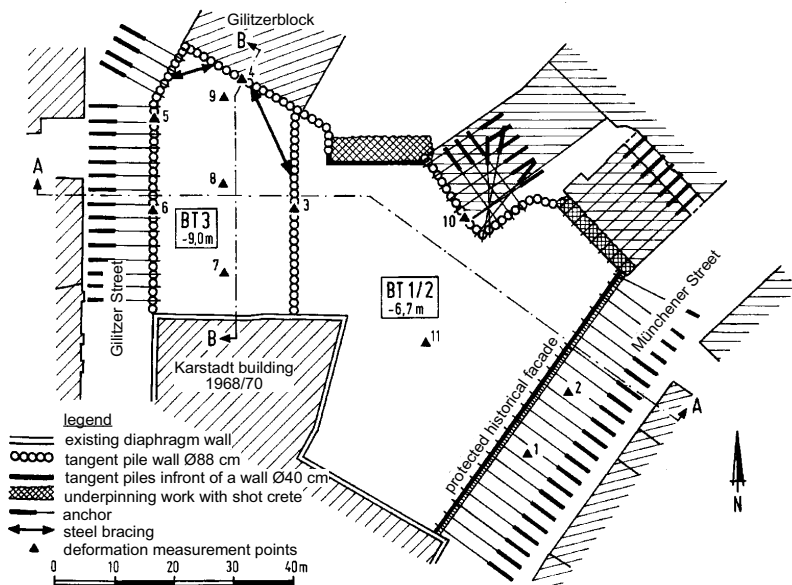


Fig. 140. Excavation layout and partitioning (Karstadt building Rosenheim)

To keep the deformations as minimum as possible, a special precaution was necessary in the deep excavation part BT 3. This includes a tie back support of the pile wall with ground anchor which is embedded in the gravel layer, a strut support at corners (see Figs. 4.140 and 4.141) and a bottom support with 1.5 m thick soilcrete. Moreover, the soilcrete was supported by tension piles which are extended to a depth of 34.0 m below the ground surface (Fig. 4.141).

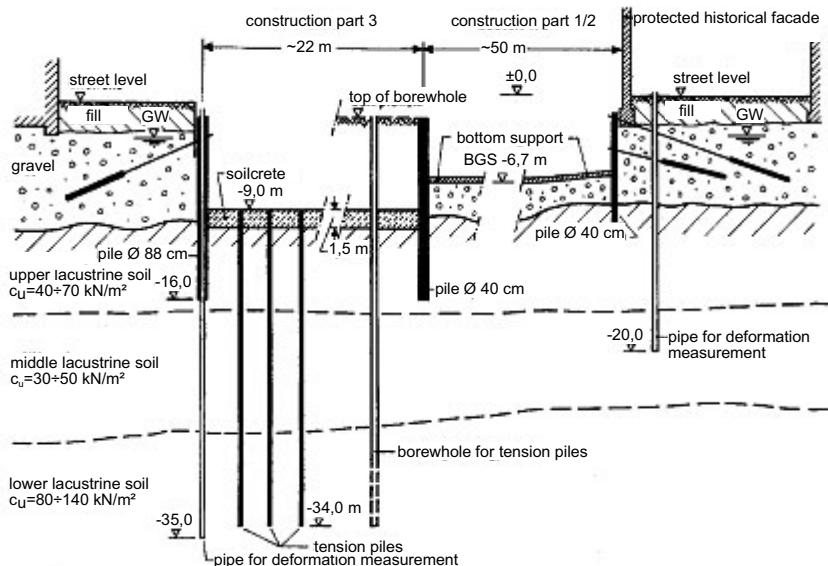


Fig. 141. Section A-A through the excavation (BT 3 and BT 1/2)

The bottom of excavation in BT 1/2 (6.7 m deep) remains within the gravel layer. The retaining walls made of the pile wall and the underpinning were supported by two layered ground anchor (Fig. 4.142). To avoid an excessive horizontal displacement of the wall-soil-anchor-block system towards the excavation due to the presence of the soft lacustrine deposit 2 m below the excavation bottom, a 25 cm thick reinforced concrete was installed at the bottom of the excavation in slices.

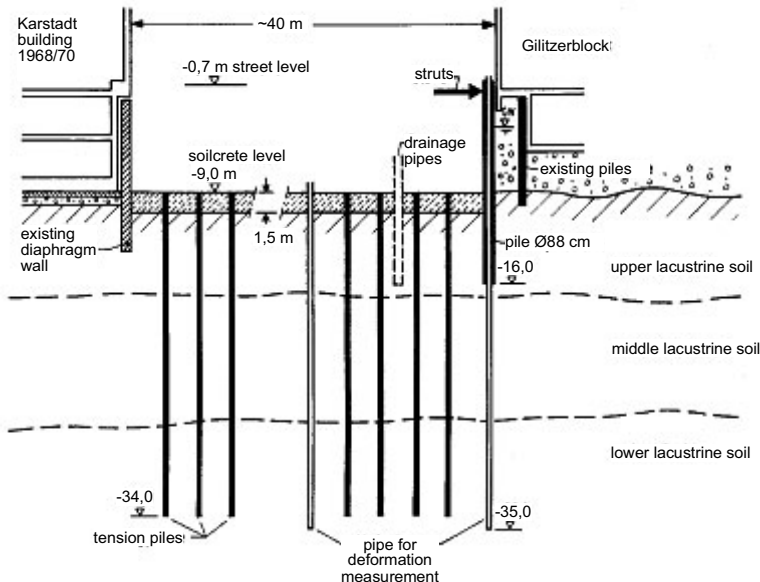


Fig. 142. Section B-B through the excavation (BT 3)

The underground condition

The underground conditions at the site is characterised by 8 to 10 m deep gravel layer underlain by a very deep lacustrine deposit (Fig. 4.143). It is believed that the lacustrine deposit may have a thickness of 140 to 190 m. Similar to the other previous projects (section 4.12.2 – 4.12.5), the lacustrine soil is a post glacial deposit with sand or/and silt seems and thin layers in between and it is highly compressible, possesses very low shear strength as well as it is very sensitive. The normal groundwater level in the area is located at a depth of 2 to 3 m below the ground surface.

The field vane shear test result in Fig 4.143 show a linear increase of the shearing strength by about 3.0 kN/m² per meter depth, which is typical for normally consolidated soils. The strength drops strongly in the middle lacustrine layer between 17 and 20 m depth and starts to increase thereafter until it joins the trend lines of the linear increase in strength in the upper lacustrine layer at approximately 27 m. The possible reason for the drop of the vane strength is that the middle lacustrine layer was underconsolidated, i.e., the consolidation of the layer under own weight was not completed. The remaining excess pore pressure (stagnation gradient) may have contributed to drop of strength. Fig. 4.143 Also shows the distribution of the natural water content, the plasticity index as well as the consistency index with depth.

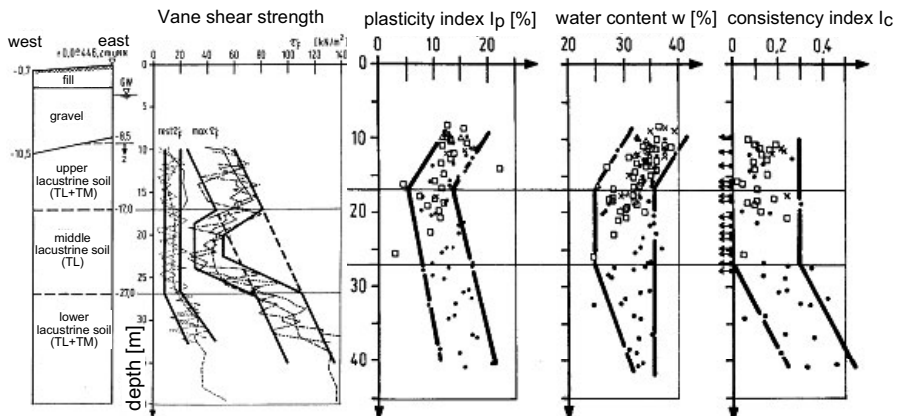


Fig. 4.143. The underground condition and soil properties

Results of deformation measurements

For monitoring of the deformations and displacements of the retaining structures and the soil, 7 inclinometers were installed at different points around the excavation: measurement points 1 and 2 (20 m deep) in Munich street behind the wall; 3, 4, 5, 6, and 10 through the pile walls up to a depth of 35 m. Extensometers are also installed at four different positions within the excavation (Fig. 4.139 to 4.142).

The deformation measurements in BT 3 show a displacement of the pile wall in the direction of the retained soil as result of the installation of the soilcrete. During the consequent excavation phases, however, a very small amount of displacement of the walls in the direction of the excavation had been observed. A 15 mm horizontal displacement of the pile wall at the measuring point 4 (Fig. 4.144) and 18 mm at point 5 (Fig. 4.145) in the direction of the soil were registered after the installation of the soilcrete. Similarly, a heave of the pile about 3 mm at point 4 and 17 mm at points 5 and 6 were recorded. The displacement of the walls in soil direction and the small amount of the heave of the piles are related to the installation of the soilcrete in soft cohesive soils, which could not be avoided despite the careful execution of the installation.

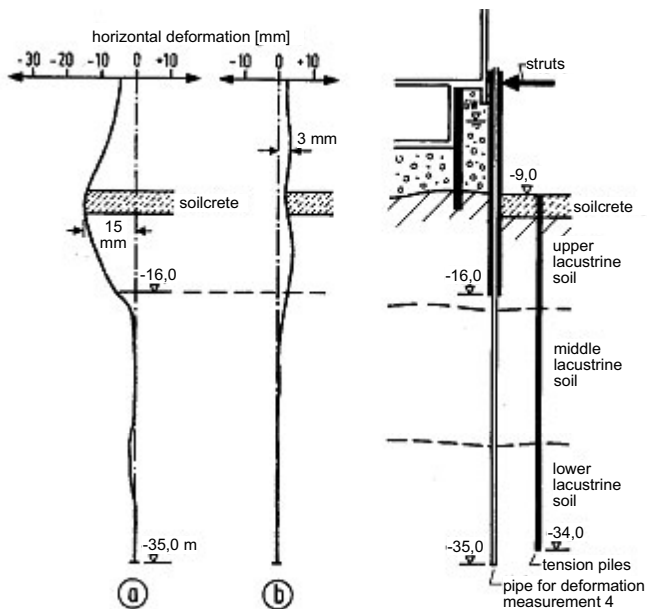


Fig. 144. Horizontal deformation of wall at measuring point 4, BT3: a) after the installation of a soilcrete as a bottom support and the tension piles from the ground surface before excavation had begun, b) full excavation

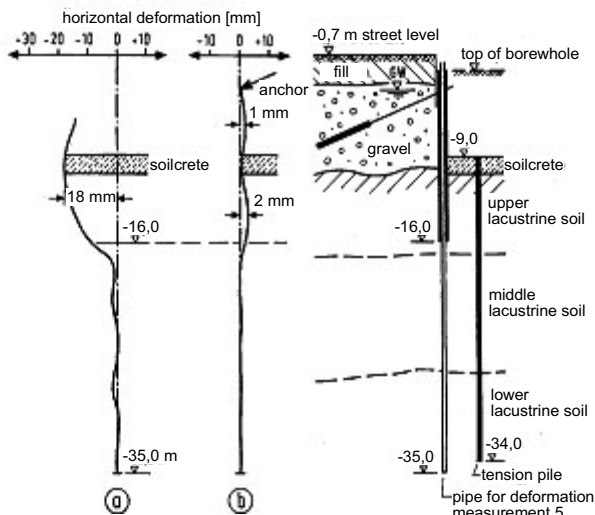


Fig. 145. Horizontal deformation of wall at measuring point 5, BT3: a) after the installation of a soilcrete as a bottom support and the tension piles from the ground surface before excavation had begun, b) full excavation

Since the pile walls in BT 3 are pushed back during the soilcrete installation, predominately horizontal wall displacement of 1 to 3 mm was measured after the end of the excavation in this part of the site.

The measurements at points 1 and 2 behind the 40 cm diameter pile walls show a very small amount of horizontal displacement of about 3 mm toward excavation after the end of the 6.7 m deep excavation. Obviously, the installation of the bottom reinforced concrete support in slices had contributed in preventing the movement of the anchored soil block system.

Heave measurements at the centre of the excavation BT 3 show 10 mm total heave of the soilcrete, which resulted from stress relief in the upper and middle lacustrine soil layers, whereas only about 1 mm heave was recorded in the lower lacustrine soil layer approximately below 25 m. Upon loading from the weight of the new building, a total settlement of 10 to 13 mm was measured which is approximately equal to the measured heave.

5 Shallow foundations on soft soils

5.1 General

Shallow foundations are common type of foundations on soft soils. Indeed the magnitude of the settlement and the appropriate settlement prediction plays an important role in order to prevent structural damages to newly erected buildings or existing neighbouring buildings. For that matter, the following well-known damage-producing deformation forms should be studied:

- Sagging,
- Hogging,
- Entrainment settlement,
- Tilting.

In general the expected settlements in shallow foundations on soft soils are substantially high and their magnitude are expected to be in the order of decimetres.

Further information on allowable total and differential settlements are given in section 5.4.4.

The shallow foundations on deep soft layers will in particular demand an intensive geotechnical investigations and planning. In the following the special features of the shallow foundations on soft soils are summarised and research results and our experiences from practical projects (case histories) are presented.

5.2 Historical foundation on soft soil deposits

Depending upon regional experiences and the formation of the soft soil deposits, historical buildings are founded on different forms of foundation elements. An intensive compilation of historical foundations can be found in Oexle 1986; Goldscheider 1993.

According to Borrmann 1992 historical foundations can be divided into four different groups. These are:

- sleeper foundation,
- floating timber pile foundation,
- combined sleeper-floating timber pile foundation,
- combined timbered floating pile-sleeper foundation

Fig. 5.1 illustrates an example of a sleeper arrangements with horizontal load distributing grids.

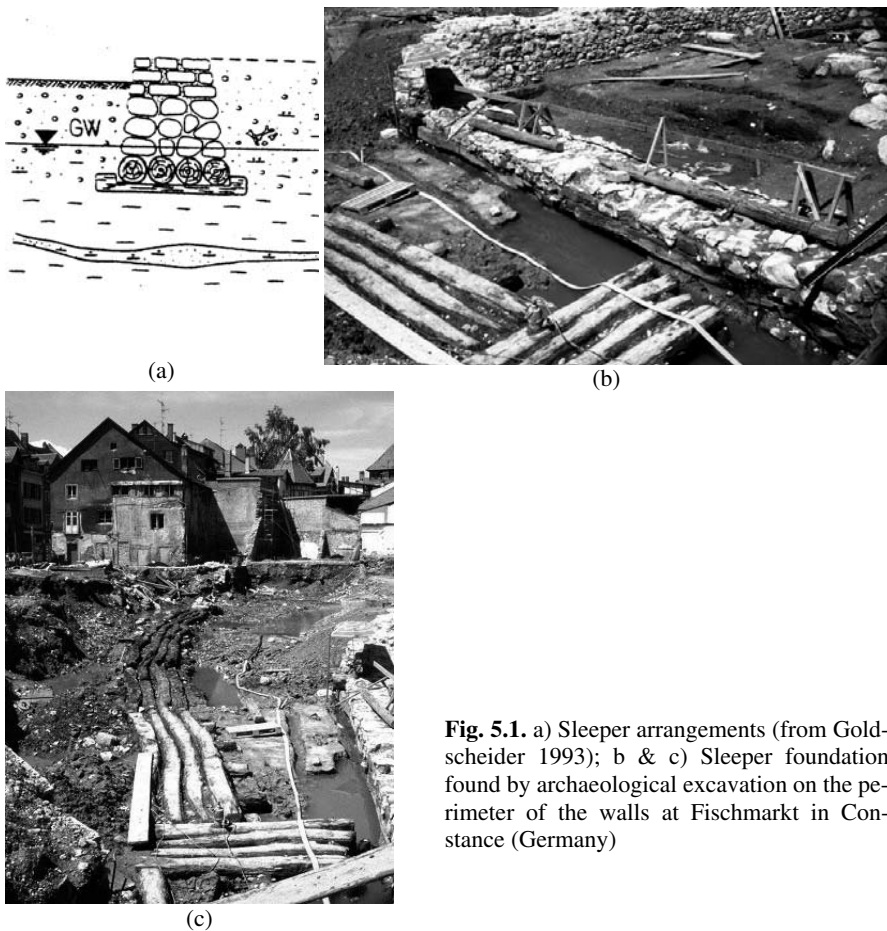


Fig. 5.1. a) Sleeper arrangements (from Goldscheider 1993); b & c) Sleeper foundation found by archaeological excavation on the perimeter of the walls at Fischmarkt in Constance (Germany)

Fig. 5.2 shows some examples of floating timber pile foundation types. In Roman Antique time up to 18th Century, floating timber pile foundation made of round timber logs are rammed vertically close to each other as deep as possible (1-3 m) into the soft ground usually untreated or charred at its tip to protect it against bursting (Fensterbusch 1964). Since floating timber pile foundation does not normally reach the bearing layer, they are assumed as a deep seated shallow foundation at the level of the pile tip in regard to the load transfer mechanism. According to Pieper 1983, floating timber pile foundation are to be categorized rather as ground improvement measures, since they serve as a support for the first layer of masonry foundation and prevent the sinking of the stones into the soft soil.

For a better load transfer, floating timber pile foundations had been used in the period 13th to 19th century. These piles did not however reach or partially reach the bearing layer as shown in Fig. 5.2d & e. Since these piles can only penetrate few meters in the soft underground, they can also be considered as a shallow foundation in regard to the load transfer mechanism.

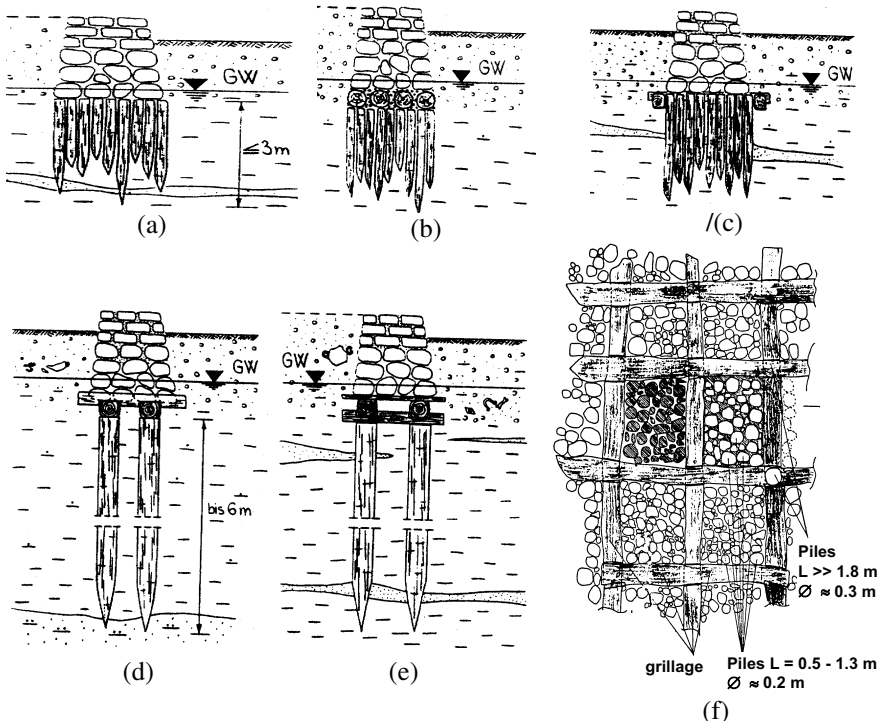


Fig. 5.2. Examples of historical foundations on soft soils; a) floating timber pile foundation; b) sleeper- floating timber pile foundation; c) floating timbered pile-sleeper grid construction; d) floating timbered pile-sleeper grid construction with double and sharp cut planks; e) floating timbered pile-sleeper grid construction (from Goldscheider 1993); f) Top view of floating timbered pile-sleeper grid construction of the Gifhorn castle (from Wichert 1988)

Other shallow foundation forms are masonry foundations with quarry stone or foundation forms with vault type construction between the masonry foundations (Fig. 5.3).



Fig. 5.3. a) Masonry foundation of quarry stone; b) strip footing with vaults in between

In a later development of the mere sleeper foundation, an isolated or strip wooden footings were constructed in order to uniformly distribute the load and reduce the settlements of buildings on soft soils (Fig. 5.4). In such kind of foundations, round timber logs are placed parallel side by side and connected together by transverse sleepers. Sometimes the sleeper foundation is wider than the width of the foundation sole in order to reduce the contact stress and distribute the load to a larger surface area. Moreover, the pure sleeper construction prevents the straddling and evading of the foundations and it distributes the settlement uniformly. This type of foundation was mainly used in Germany between 13th and 15th century (Goldscheider 1993).

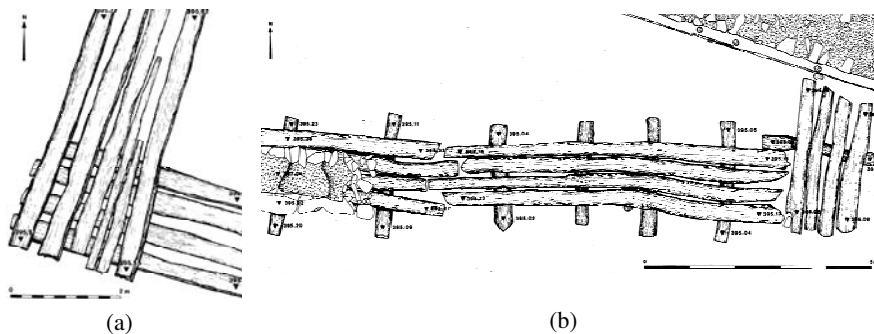


Fig. 5.4. a) Sleeper footing (Goldscheider 1993) b) top view of sleeper construction (Oexle 1986)

5.3 Type of shallow foundations

Modern shallow foundations on soft soils are usually constructed as rigid raft foundation, frequently in connection with a stiffened reinforced concrete basements or an additional basement floors for the relief of the building foundation. A comparative compilation of shallow foundation forms on soft ground can be found in Auvinet 2002 with the following variants (Fig. 5.5):

- raft foundation,
- partially compensated raft foundation ($\sigma_{vo} < \sigma_0$),
- compensated raft foundation ($\sigma_{vo} \approx \sigma_0$),
- overcompensated raft foundation ($\sigma_{vo} > \sigma_0$),

where σ_{vo} = overburden pressure and pre-consolidation pressure,
 σ_b = stresses due to dead and live loads from the buildings,
 $\sigma_0 = \sigma_b - \sigma_u$ = net pressure on the footing,
 σ_u = uplift pressure.

Fig. 5.6 also shows pictures of compensated and overcompensated type of raft foundations.

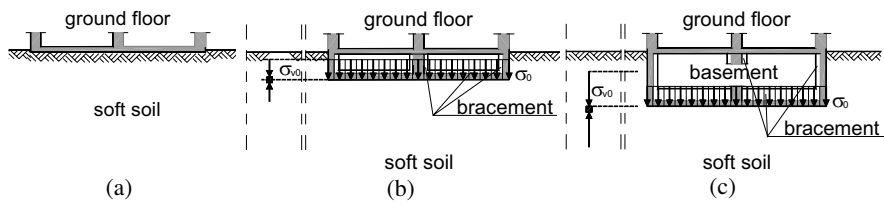


Fig. 5.5. a) Raft foundation; b) partially and/or fully compensated raft foundation; c) overcompensated raft foundation

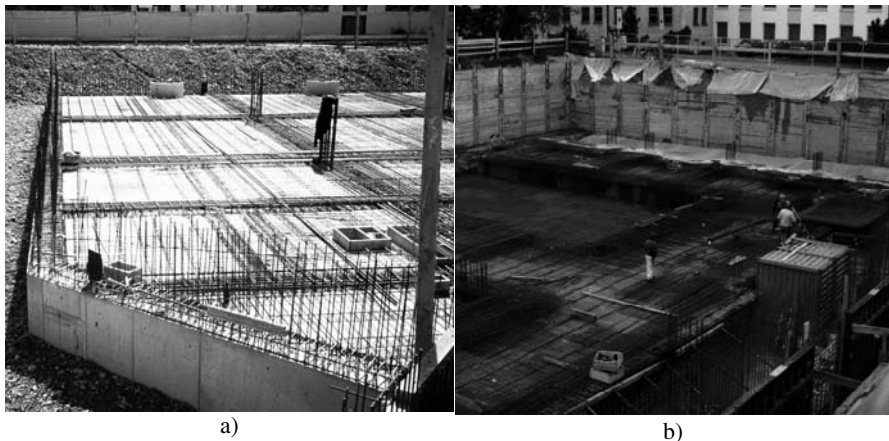


Fig. 5.6. a) Compensated (Fig. 5.5b), b) overcompensated (Fig. 5.5c) raft foundations

The raft foundations (Fig. 5.5a) should preferably be used in soft underground as compared to isolated and strip footings, since the settlement differences based on the largest settlement are about 30 % smaller in raft foundations than in isolated footings. A further advantage of raft foundations is that they can bridge weak spots in the soil.

The compensating box - type shallow foundations shown in Figs. 5.5b&c and 5.6a&b are particularly suitable for soft soils, in which the building load are compensated by the weight of the excavated mass of the soil (Cuevas 1936)). If the overburden pressure of the soil is smaller than the building load, the raft foundation is known as partially compensated (Fig. 5.5b). If on the other hand the overburden pressure of the soil is greater than the building load, it is called overcompensated (Auvinet 2002) (Fig. 5.5c). If the groundwater level is close to the ground surface, such type of foundations should be constructed watertight as waterproof white tub.

A partial soil exchange to improve the carrying capacity of the soft underground is only meaningful, when the thickness of the soft soil layer is insignificance. A limited soil exchange in a deep soft soil layer may only subject the un-

derlain soft layer prone to settlement with an additional pressure and therefore, it has usually rather a negative effect with additional increased settlement.

A further important point in shallow foundations on a deep soft soil deposit is that the load from the superstructure should to some extent be transmitted centric into the basement and/or base plate, otherwise a substantial tilts may be expected.

5.4 Settlement calculations – the serviceability limit state

5.4.1 Soft soils deformation behaviour and calculation methods

The description of the deformation behaviour of soft soils can be found in various literature in soil mechanics. Section 2.6 for example contains a compilation of the deformation behaviour of soft soils. Beyond this, the factors and relationships that particularly target the determination of the settlements of shallow foundations on soft soils are described in the following sections. Thereby, the differences between the stiffness parameters such as the elasticity modulus E , the constrained modulus E_{oed} (oedometer test), deformation modulus E_v (plate load test) and the compressibility modulus E_m have to be distinguished. The later is preferably used for settlement calculation and it can be derived from back analysis of measured settlements of practical projects or adopted from the constrained modulus with due consideration of the empirical correction factor μ as given in Eq. 5.1.

$$E_m = \frac{E_{oed}}{\mu} \quad (5.1)$$

The constrained modulus can be derived from one-dimensional compression test result as a secant modulus as follow (see also Section 2.6):

$$E_{oed} = \frac{\Delta\sigma'}{\Delta\varepsilon} \quad (5.2)$$

The constrained modulus is in general stress dependant, whereby it has to be noted that the strain $\varepsilon = s/h_0$ is not an absolute value, rather it depends on the reference height h_0 . For this reason different forms of deformation parameters in form of the compression index C_c and the swelling index C_s are frequently used in the literature for the settlement calculation (see section 2.4).

5.4.2 Stresses and settlements due to external load

The basis for determination of stress distribution in soil and settlement calculations of building foundations is the well known Boussinesq's 1885 equation for point loads on an elastic-isotropic-half-space. Froehlich 1934 modified the Boussinesq's approach. The background and derivation of the equations can be found for instance in Kezdi 1970; Poulos 2002 and other soil mechanics and foundation

books. By integrating the influence of several point loads, a formula can be derived for calculation of the stresses in an elastic-half-space under any surface load. Selective diagrams and equations are given in the following only for illustration purpose.

Fig. 5.7 shows the most commonly used diagram developed by Steinbrenner 1934 for calculation of stresses in soil under flexible uniform surface load. The corresponding equations are given by:

$$i_i = f\left(\frac{z}{b}, \frac{a}{b}\right) = \frac{\sigma_z}{q} \quad (5.3)$$

$$\sigma_z = \frac{q}{2\pi} \cdot \left[\arctan\left(\frac{a \cdot b}{z \cdot \sqrt{a^2 + b^2 + z^2}}\right) + \frac{a \cdot b \cdot z}{\sqrt{a^2 + b^2 + z^2}} \left(\frac{1}{a^2 + z^2} + \frac{1}{b^2 + z^2} \right) \right] \quad (5.4)$$

The pressure q can be the dead load p or the live load q at surface level or the stresses σ_b , σ_0 or $\Delta\sigma$ under foundations, footings or buildings

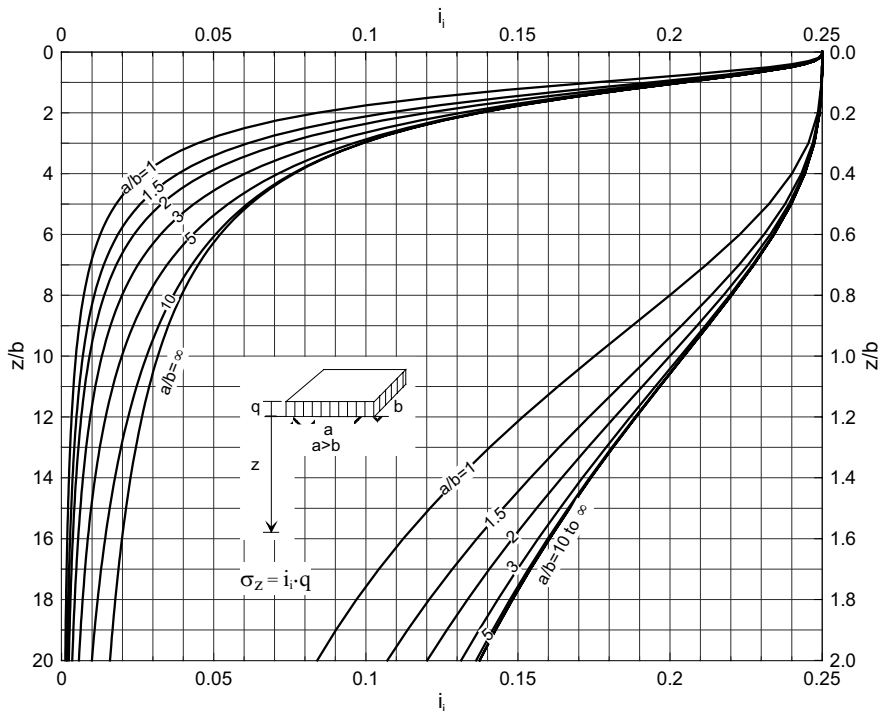


Fig. 5.7. The value of the influence factor i_i for calculation of the vertical stresses σ_z at a depth z in an elastic half space under a corner point or under a point outside or inside of a rectangular flexible foundation subjected to a uniform surface load of q (after Steinbrenner 1934)

Based on the Steinbrenner's diagram (Fig. 5.7), Kany 1974 developed further a diagram for calculation of stresses in soil under rigid uniform surface load at a given characteristic point, which normally find its application in the conventional computation of shallow foundations (Fig. 5.8). At the characteristic point, it is assumed that the settlement of a rigid and flexible raft foundations are identical (Graßhoff 1955). It is a general practice in Germany to determine the settlements of a raft foundation at the characteristic points. The equations used to develop the diagram in Fig. 5.8 are given below.

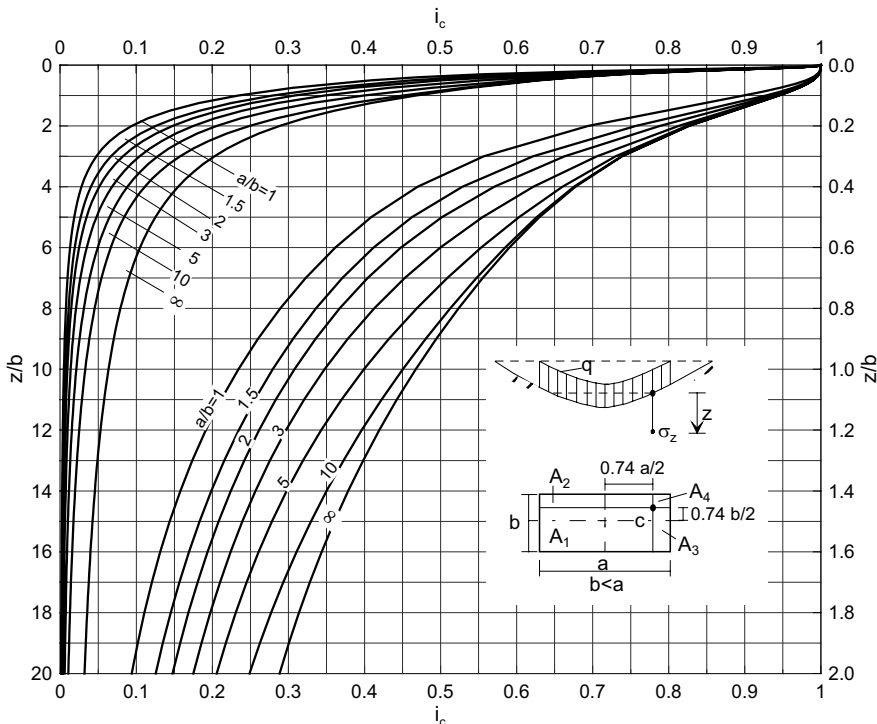


Fig. 5.8. The value of the influence factor i_c for calculation of the vertical stresses σ_z at a depth z in an elastic half space under the characteristic point C of a rectangular rigid foundation subjected to a uniform surface load of q (after Kany 1974)

$$i_c = f\left(\frac{z}{b}, \frac{a}{b}\right) = \frac{\sigma_z}{q} \quad (5.5)$$

$$\sigma_z = \frac{q}{2\pi} \cdot \sum_{n=1}^4 \left[\arctan \left(\frac{a_n \cdot b_n}{z \cdot \sqrt{a_n^2 + b_n^2 + z^2}} \right) + \frac{a_n \cdot b_n \cdot z}{\sqrt{a_n^2 + b_n^2 + z^2}} \cdot \left(\frac{1}{a_n^2 + z^2} + \frac{1}{b_n^2 + z^2} \right) \right] \quad (5.6)$$

For further formulas and nomograms for calculation of stresses in soil due to external load refer to Grasshoff 1954; Grasshoff et al. 1982; Das 1997; Poulos 2002; Tefera and Schulz 1988.

Settlement calculations serve as a basis for verification of the safety of the foundation in the serviceability limit state (SLS). In settlement calculations, it has to be differentiated between overburden pressure due to own weight of the soil, the relief of the pressure due to excavation and the pressure due to building load (Fig. 5.9).

In order to obtain as much as possible a realistic predictions, the settlement should be calculated with due consideration of the primary loading and un/reloading state of the stresses. Based on the theory of elasticity, the settlements of a foundation under axial load may be determined from:

$$s = \sum_i I \left(\frac{\sigma_{z,ur,i}}{E_{oed,ur,i}} + \frac{\sigma_{z,i}}{E_{oed,i}} \right) \cdot d_i \quad (5.7)$$

$$\text{or } s = \sum_i I \left(\frac{\sigma_{z,ur,i}}{E_{m,ur,i}} + \frac{\sigma_{z,i}}{E_{m,i}} \right) \cdot d_i \quad (5.8)$$

where $\sigma_{z,i}$, $\sigma_{z,ur,i}$ = the vertical additional pressure in the primary loading and reloading state of stress on the i^{th} slice,
 d_i = thickness of the i^{th} slice,
 $E_{oed,i}$, $E_{oed,ur,i}$ = the constrained moduli (Eq. 5.2) for the primary loading and un/reloading state of stress of the i^{th} slice respectively,
 $E_{m,i}$, $E_{m,ur,i}$ = moduli of compressibility (Eq. 5.1) for the primary and un/reloading state of stress of the i^{th} slice respectively.

Each stiffness parameters has to be determined at the corresponding stress level. Fig. 5.9 shows the different stress components in soil and the limiting depth. The stress history of a soil element i in the i^{th} slice can be described as follows:

- overburden pressure $\sigma_{v0,i}$ at the middle of the slice at the initial stage,
- stress relief on the slice by $\sigma_{v,i} = \sigma_v \cdot i$ at the end of an excavation, where σ_v is the total stress relief due to the excavation at the foundation level and i is an influence factor for vertical stress distribution under uniform surface load,

- additional pressure $\sigma_{0,i} = \sigma_0 i_i$ on the slice due to the external load, where σ_0 is the average contact pressure (Fig. 5.9),
- the contact pressure extends into two ranges as shown in Fig. 5.9. It starts from the reloading branch (AB) of the load-settlement diagram and it may end on the virgin consolidation line (BC),
- the uplift pressure σ_u at the foundation level,

The vertical additional stress in soil at a depth z in primary loading and reloading state of stress can be given by

$$\sigma_{z,i} = (\sigma_0 - \sigma_v) \cdot i_i = \sigma_I \cdot i_i \quad (5.9)$$

$$\sigma_{z,ur,i} = \sigma_v \cdot i_i \quad (5.10)$$

respectively. If the stress in the soil below the characteristic point is required, the corresponding influence factor i_c should be used instead of i_i . The stress difference $\sigma_I = \sigma_0 - \sigma_v$ can be taken as a net contact pressure.

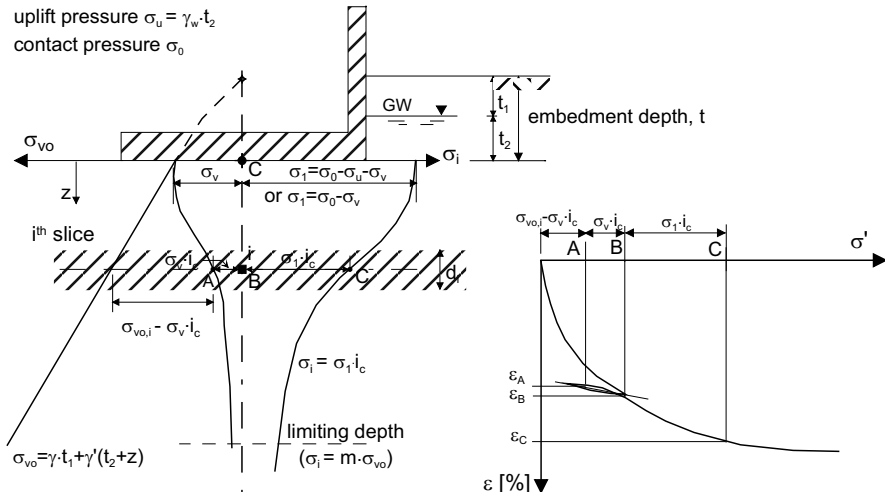


Fig. 5.9. Stress components and their distribution in soil under a shallow foundation

The settlement under the characteristic point of a foundation subjected to uniformly distributed load can also be calculated from:

$$s = \frac{\sigma_I \cdot b \cdot f}{E_{oed}} \quad (5.11)$$

$$s = \frac{\sigma_I \cdot b \cdot f}{E_m} \quad (5.12)$$

where b is the shorter side of the foundation and f is the settlement coefficient according to Fig. 5.10 or Eq. 5.13.

$$s_c = \frac{\sigma_0}{2 \cdot \pi \cdot E_m} \cdot \sum_{n=1}^4 \left[z \cdot \arctan \left(\frac{a_n \cdot b_n}{z \cdot \sqrt{a_n^2 + b_n^2 + z^2}} \right) \right. \\ \left. + a_n \cdot \ln \left(\frac{\sqrt{a_n^2 + b_n^2 + z^2} - b_n}{\sqrt{a_n^2 + b_n^2 + z^2} + b_n} \cdot \frac{\sqrt{a_n^2 + b_n^2} + b_n}{\sqrt{a_n^2 + b_n^2} - b_n} \right) \right] \\ + b_n \cdot \ln \left(\frac{\sqrt{a_n^2 + b_n^2 + z^2} - a_n}{\sqrt{a_n^2 + b_n^2 + z^2} + a_n} \cdot \frac{\sqrt{a_n^2 + b_n^2} + a_n}{\sqrt{a_n^2 + b_n^2} - a_n} \right) \quad (5.13)$$

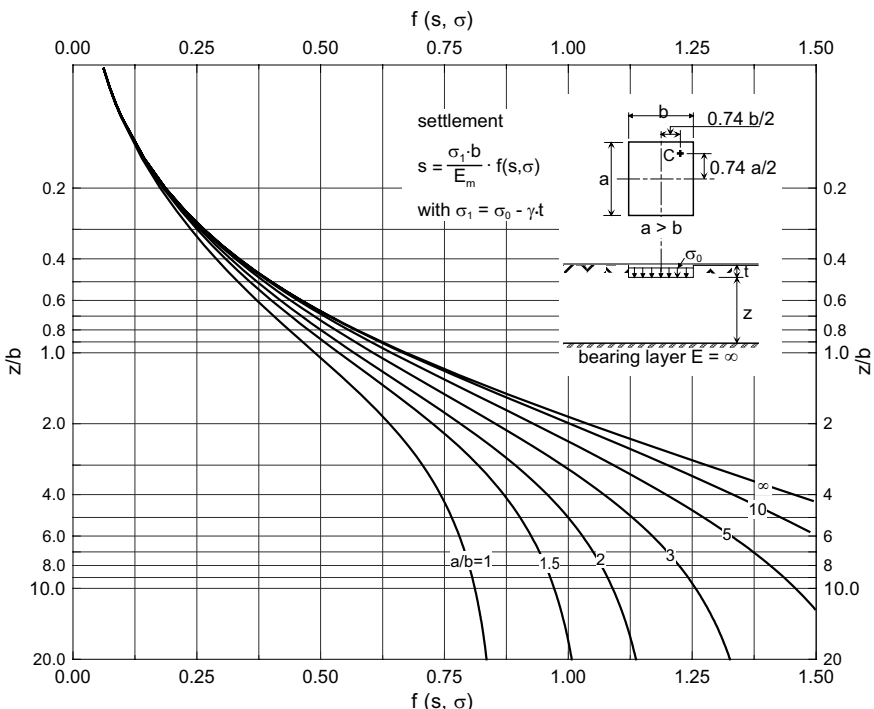


Fig. 5.10. The value of the influence factor f for the calculation of settlement of a rectangular flexible foundation subjected to a uniform surface load σ_0 under the characteristic point C in an elastic-half-space with Poisson's ratio $\nu = 0$ (after Kany 1974)

In case of a layered underground, the settlement is given by:

$$s = \sigma_I \cdot b \cdot \left(\frac{f_1}{E_{oed,1}} + \frac{f_2 - f_1}{E_{oed,2}} + \dots + \frac{f_n - f_{n-1}}{E_{oed,n}} \right) \quad (5.14)$$

E_{oed} can also be replaced by other form of deformation parameter such as E_m .

If the settlement is calculated based on the deformation parameter from the one-dimensional compression test (constrained modulus), it should be corrected by correction factor μ according to the section 5.4.3 (Table 5.3 & 5.4). Thus Eq. 5.7 can be written as:

$$s = \mu \cdot \sum_i \left[\left(\frac{\sigma_{z,ur,i}}{E_{oed,ur,i}} + \frac{\sigma_{z,i}}{E_{oed,i}} \right) \cdot d_i \right] \quad (5.15)$$

The settlement influence reaches only an infinite depth below the foundation level. Hence, the thickness of the compressible layer can be limited to a depth at which the change of stress due to surface load does not exceed for example 20 % of the overburden pressure according to DIN 4019 (see also Fig. 5.9 and Section 5.4.3). The limiting depth usually lies between $z = b$ and $z = 2b$.

Based on back analysis of a number of projects with shallow foundations on lacustrine soil deposit in southern Germany, correction factors μ and m are derived in section 5.5.4 for stiffness and limiting depth respectively.

If a bearing layer (e.g. rock) is encountered at a depth above the limiting depth, the depth to the bearing layer is taken as a limiting depth. If the depth of the foundation and the corresponding stress relief due to excavation is relatively large, a special attention is required in determining the lowest depth considered in settlement analysis.

5.4.3 Time settlement behaviour, magnitude and components of settlements of shallow foundations

In a settlement analysis, it has to be distinguished between the immediate settlement s_0 , the consolidation (primary) settlement s_p and the creep (secondary) settlement s_α as shown in Fig. 5.11.

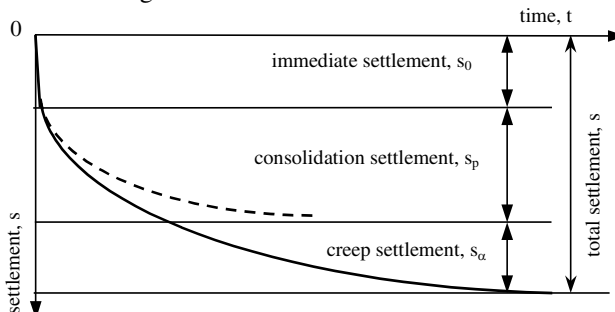


Fig. 5.11. Time-settlement diagram

The in-situ time-settlement relationship of cohesive soil layers can be determined using the simplified Eq. 5.16 according to model theory.

$$t_{c(in-situ)} = t_{c(oed)} \cdot \frac{c_{v(oed)}}{c_{v(in-situ)}} \cdot \frac{l_d^2}{l_d^2} \quad (5.16)$$

where t_c is the time required for primary consolidation, l_d is the drainage path and c_v is the coefficient of consolidation. The results of the back analysis of the case histories in section 5.5 & 5.6 show that the ratio $c_{v(in-situ)} / c_{v(oed)}$ varies approximately between 4 and 5, however, this ratio is often set to unity for practical calculations.

The time-settlement behaviour and the magnitude of the settlement of saturated cohesive soils are usually approximated using the one-dimensional consolidation theory. The important equations of the one-dimensional theory are described in the following. For three-dimensional consolidation, refer to, e.g. Rendulic 1936; Biot 1941; Davis and Poulos 1972).

The settlement at time t can be determined using degree of consolidation $U(t)$ as follows

$$s_t = U_{(t)} \cdot s_p \quad (5.17)$$

where s_p is the settlement at the end of the primary consolidation. According to the conventional Terzaghi's theory, the degree of consolidation for different distribution of the initial excess pore pressures is estimated using the time factor T_v given by:

$$T_v = \frac{c_v \cdot t}{l_d^2} \quad (5.18)$$

$$c_v = \frac{k \cdot E_{oed}}{\gamma_w} \quad (5.19)$$

The time factor is again dependant on the coefficient of consolidation. The coefficient of consolidation is determined using Eq. 5.19 dependant on the permeability and compressibility of the soil. The theoretical relationships between the degree of consolidation and the time factor is given in Fig. 5.12. For the purpose of comparison, this relationship from field observations of settlement according to FGSV 542 1988 is also given in Fig. 5.12.

As already discussed in section 5.4.2, the calculation of settlement is normally based on the linear elasticity theory (Hooke' law) and the stress distribution on the elastic-halfspace. However, it was proved that there exists no exact similarity between the model based on the one-dimensional compression test and the real field condition (Schulze and Muhs 1967) and hence a direct application of the one-dimensional results is only conditionally possible.

For example, Olson 1986; Crawford 1986; Duncan 1993 pointed out that the time dependent settlements can only conditionally predicted based on the coeffi-

cient of consolidation according to Terzaghi's theory. The values of the coefficient of consolidation derived from back calculation of settlement measurements are 6 to 7 times higher than those obtained from one-dimensional compression tests in laboratory according to Becker and Lo 1981; Oteo et al. 1979. Moreover, the assumption that the permeability and stiffness of the soil remains constant throughout the consolidation process does not reflect the real behaviour of soft soils (Ulrich 1980; Magnan et al. 1979; Mitchell 1993). These facts are exemplary demonstrated in Table 5.1 & 5.2, which show settlement observations compared to predicted settlements of selected projects.

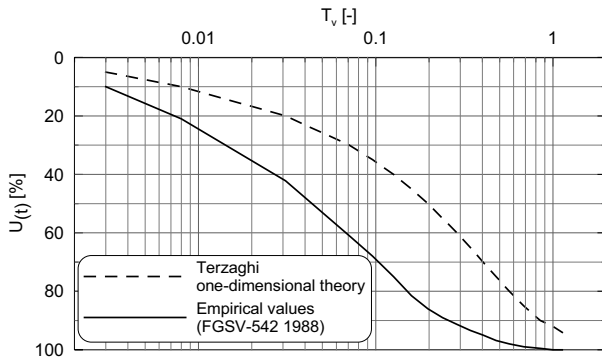


Fig. 5.12. Solution of one-dimensional consolidation based on Terzaghi's theory and field settlement observations

Table 5.1. Measured and predicted consolidation time (Lunne et al. 1982)

Project	Consolidation time [Months]	
	observation	prediction based on Terzaghi's theory
1	9	96
2	20	29
3	40	120

Table 5.2. Measured and predicted primary settlement (Maschwitz and Richwien 1979)

Project	Settlement [cm]	
	observations	Prediction based on oedometer test
1	60	89
2	15	35

The extraction of undisturbed soil samples in soft soils is associated with setbacks and requires a special handling. According to Bjerrum 1973, mechanical disturbances of soft clay during the extraction, transport and mounting in laboratory apparatus may lead to the breakdown of the structure of the soil and hence

loss of the pre-consolidation history of the deposit (see also Section 2.2). This will have in turn an influence on the compressibility behaviour of the soil as shown in Fig. 5.13. Settlement prediction based on results of laboratory tests on such specimens may lead to a higher settlement.

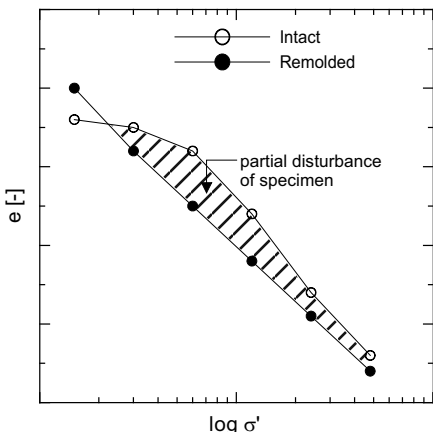


Fig. 5.13. Comparison of one-dimensional compression behaviour of intact and remolded samples of soft clay (after Leroueil and Vaughan 1990)

Scherzinger 1991 collected undisturbed lacustrine soil samples and had performed among others a one-dimensional compression tests. The samples had been preserved under the in-situ stress condition and water content during transportation until the laboratory tests by means of special pressure cells (see section 2.2). According to Scherzinger 1991, the compression index C_C determined in laboratory from such high quality undisturbed samples with step wise increasing the load after the end of primary consolidation (EOP) shows a good agreement with the in situ C_C -values. On average a ratio of 0.94 is found between the laboratory and in-situ compression indexes.

Most often several silt and sand seams are encountered in nature in post glacial deposits such as lacustrine clays. Such kind of seams can not sufficiently be modelled in laboratory using small scale standard compression test ($h = 1.4\text{--}2\text{ cm}$, $D = 7\text{--}10\text{ cm}$). Walker and Morgan 1977 reported on the basis of settlement measurements on an embankment on clay layer that the measured consolidation settlements are 200 times faster than those predicted from laboratory tests due to the silt and sand seams in-situ (Fig. 5.14).

Jagau 1990 and Scherzinger 1991 measured an excess pore pressure in lacustrine soft soil layer in southern Germany and they came to the conclusion that this soils are not still fully consolidated under their own weight despite of the silt and sand seams. It seemed that the silt and sand seams are fully embedded in the clay which makes horizontal drainage impossible. On the other hand, Klob 1992 tried to prove based on settlement observations that the seams of silt and sand can enhance the consolidation process by means of horizontal drainage, which influences the time-settlement behaviour and reduces the time for primary consolidation by a factor of 10.

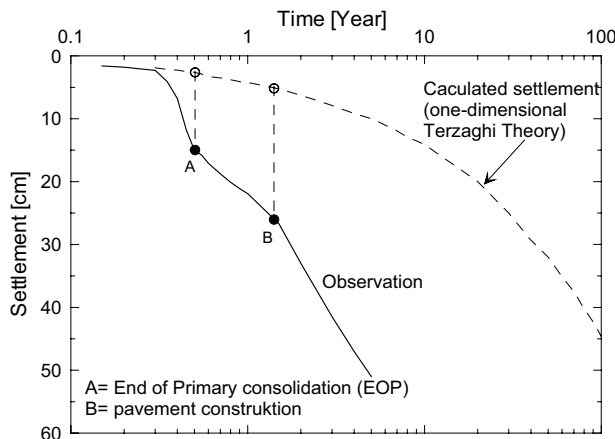


Fig. 5.14. Comparison of measured and calculated settlements of an embankment on silty clay with silt and sand seams (after Walker and Morgan 1977)

Furthermore, the state of knowledge of the influence of the limiting depth, which is the lowest level considered in settlement analysis of deep soft soil deposit, is not sufficient (Altes 1976). The limiting depth seems to depend on soil characteristics such as structure resistance, initial hydraulic gradient, compressibility as well as geometrical parameters such as the size, form and depth of foundation (Kézdi 1976). Seycek 1991 reported, however, that the lowest level considered in settlement analysis is independent from the compressibility of the soil. DIN 4019 recommends to limit the thickness of the compressible soil to a depth, at which the additional pressure due to the building load does not exceed 20 % of the overburden pressure (see Fig. 5.9). Several authors (Egorov 1977; Altes 1976) show that the settlement calculation assuming the lowest level according to DIN 4019 leads to a larger settlement than the observed settlement (see also section 5.5.4). For this reason the determination of the lowest level as well as the settlement calculation shall either be modified by considering the structural resistance (Seycek 1991) or the initial hydraulic gradient (Maslov and Le Ba Lyong 1986).

According to Mitchell 1993, the following are the reasons why the commonly used constitutive models for soil compression and consolidation may not give suitable representation of the actual behaviour:

- The relationship between the void ratio and the effective consolidation pressure is not linear, as is assumed for the Terzaghi consolidation theory.
- Changes in void ratio, compressibility and hydraulic conductivity during the consolidation are neglected or not properly taken into account.
- Secondary (creep) compression is often neglected, and models for taking into account are of uncertain validity.
- Soil properties differ among the strata making up the soil profile and within the individual strata themselves. There is also a substantial effect

of the sample disturbance and the applicability of the sample characteristics to the real soil profile in-situ.

- Boundary conditions are uncertain or unknown, especially drainage boundaries.
- Although one-dimensional analyses are often used, two- and three-dimensional effects may be important.
- The stress increments may not be known with certainty.

In the literature, there are two approaches so far used to improve the settlement predictions. The first one is the introduction of the correction factor as shown in Eq. 5.20 to the settlement calculated based on conventional oedometer tests (Skempton and Bjerrum 1957; Scott 1963; Tomlinson 1986). Table 5.3 shows the correction factors for different soil types according to Tomlinson 1986. Eq. 5.1 can also be used instead of Eq. 5.20.

$$s = \mu \cdot s_{cal} \quad (5.20)$$

DIN 4019 also recommends this method and suggests a modified correction factors according to Table 5.4.

Table 5.3. Correction factors for settlement predictions (after Tomlinson 1986)

Soil type	Correction factor μ
Very sensitive clays (soft alluvial, estuarine and marine clays)	1.0 to 1.2
Normal consolidated clay	0.7 to 1.0
Overconsolidated clay (London clay, Weald, Kimmeridge, Oxford, and Lias clays)	0.5 to 0.7
Heavily overconsolidated clays (glacial till, Keuper Marl)	0.2 to 0.5

Table 5.4. Correction factors for settlement predictions (DIN 4019)

Soil type	Correction factor μ
Sand and silt	2/3
Normally consolidated and light overconsolidated clays	1.0
Heavily overconsolidated clays	0.5 to 1.0

The second approach is the modification of the consolidation theory, e.g. through rheological models, which considers the secondary settlement and the rate of settlement.

In the following are constitutive laws for one-dimensional compression summarized by Soumaya 2005. Fig. 5.15 shows different models that describe the deformation of the soil grain according to different principles. The constitutive law developed so far for one-dimensional compression can be grouped according to Lerouil et al. 1985 in four categories as shown in the following functions:

$$f(\sigma'_v, e) = 0 \quad (5.21)$$

$$f(\sigma'_v, e, t) = 0 \quad (5.22)$$

$$f(\sigma'_v, e, \dot{\sigma}_v, \dot{e}) = 0 \quad (5.23)$$

$$f(\sigma'_v, e, \dot{e}) = 0 \quad (5.24)$$

For example, Eq. 5.21 represents the classical Terzaghi's theory, in which a linear relationship is assumed between the effective consolidation pressure and the void ratio.

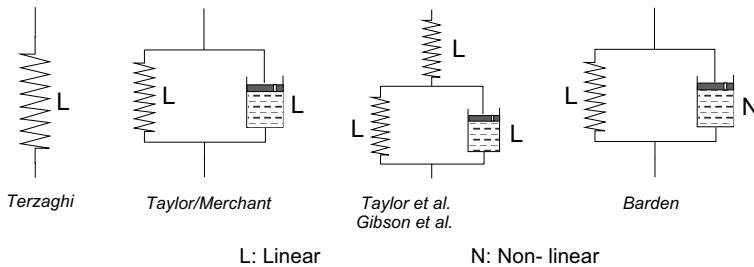


Fig. 5.15. Some typical rheological models for description of the deformation behaviour of soils

Among others, Buisman had already in 1936 asserted that the soil deforms further under constant effective pressure and the classical theory is unsuitable to describe the overall behaviour of the cohesive soils. The compression model (Eq. 5.22) developed by Bjerrum 1967 considers the dependency of the void ratio on effective consolidation pressure and time (Fig. 5.16). The deformation path ABCD consists of three ranges: the elastic range AB, the elasto-plastic range BC and the viscous range CD.

To explain the material behaviour shown in Fig. 5.16, Bjerrum 1967 divides the deformation into an immediate and delayed settlement. The definitions of these terms are given in Fig. 5.16b in comparison with the definitions of primary and secondary settlements.

If a normal consolidated soil is left under constant effective stress σ'_A for a long period of time, it will continue to settle (creep settlement or aging). If the soil is subjected to an additional effective stress $\Delta\sigma'$, it pursues the path ABCD and reacts rigidly until it reaches an apparent pre-consolidation pressure σ'_B . During further loading beyond point B, the void ratio-pressure line joins the line of the immediate compression (primary consolidation line) (Fig. 5.16).

Although the Bjerrum model contain some interpretation difficulties regarding the exact location of the transition from primary to creep consolidation, it extremely contributed to deep understanding of the essential aspects of consolidation. These are the apparent overconsolidation phenomena due to secondary con-

solidation, the existence of parallel equal-time compression lines, which means that the coefficient of secondary consolidation is constant independent of stress level, even if stress varies with time, and the last aspect is that the model is constructed using the three widely known material constants C_c , C_s and C_a .

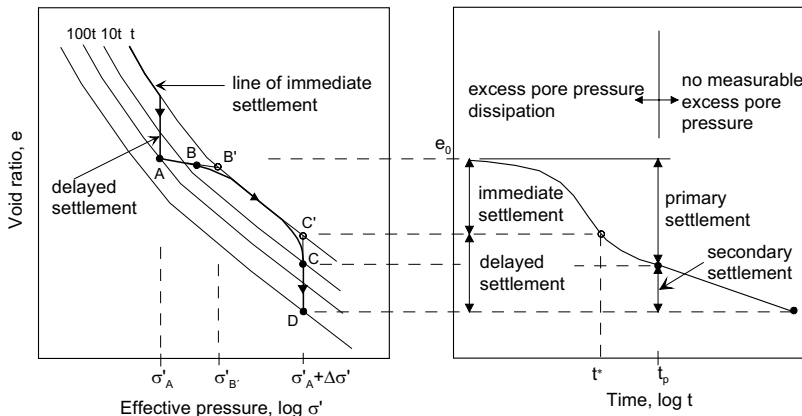


Fig. 5.16. Geological history and compressibility model proposed by Bjerrum 1967 for a normally consolidated clay; a) consolidation processes of a compressible soil layer, b) definition of the settlement components.

On the basis of the Bjerrum model (Fig. 5.16), Garlanger 1972 formulated the following compression equations with the assumption that a soil element with state point (e, σ') at any position in the layer will trace the path AB'C'D,

$$-\frac{de}{dt} = \alpha \frac{1}{\sigma'} \left(\frac{\partial \sigma'}{\partial t} \right) + \frac{\beta}{t^*} e \left(\frac{e}{e_{R'}} \right)^{\gamma} \left(\frac{\sigma'}{\sigma'_{R'}} \right)^{\delta} \quad (5.25)$$

where α , β , γ and δ are constants dependent on C_c , C_s and C_α and t^* is the time from which viscosity starts to act (point C' in Fig. 5.16a), although this model is not in a position to describe possible viscous behaviour during the consolidation phase.

Imai 1995 classified the one-dimensional compression into three components (Fig. 5.17): irrecoverable compression de_{ir} , recoverable elastic compression de_e and irrecoverable viscous compression de_v under constant effective stress. The first two components can experimentally distinguished by carrying out a stress recovery (unloading) test from B to C, but experimental distinction between irrecoverable plastic and viscous compression in path AB cannot be made, because time-independent plastic component cannot be measured during time-dependant compression. Imai 1995 considered the compression during the path AB as an elasto-viscous phase, because the consolidation compression of soils is time-dependent and the transition from the elasto-viscous phase (AB) to the pure viscous phase in the secondary compression part (BD) will be smooth.

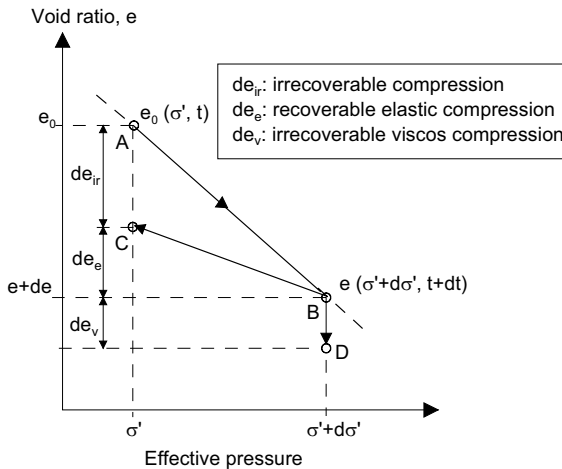


Fig. 5.17. Components of one-dimensional compression
(after Imai 1995)

The idea that the elasto-viscous behaviour governs the compression during the path AB is first suggested by Taylor and Merchant 1940 (Fig. 5.15)) and can be described using the equation

$$de = \left(\frac{\partial e}{\partial \sigma'} \right)_t d\sigma' + \left(\frac{\partial e}{\partial t} \right)_{\sigma'} dt \quad (5.26)$$

The first term on the right hand side corresponds to elasticity and the second to viscosity. Eq. 5.26 is the first extension of the conventional consolidation theory that takes into account the creep compression. Zeevaert 1985 suggested a non-linear relationship for the viscous part of Eq. 5.26 which considers creep during and after the consolidation phase.

In order to take into account the viscosity from the very beginning of the consolidation, i.e. the path ABC'D in Fig. 5.16, Mesri and Rokshar 1974 developed an equation.

$$\left(\frac{\partial e}{\partial t} \right)_{\sigma'} = - \frac{0.434 \beta \cdot C'_\alpha}{t} \quad (5.27)$$

with

$$\beta = \frac{e_0 - e}{e_0 - e_p} \quad (5.28)$$

where e_0 and e_p are void ratio at initial and at the end of the primary consolidation respectively and C'_α is the coefficient of secondary consolidation during the primary consolidation phase. At the end of primary consolidation $C'_\alpha = C_\alpha$.

For the determination of C'_α Mesri and Choi 1985 introduced the following relationship:

$$C_\alpha / C_c = C'_\alpha / C'_c = \text{constant} \quad (5.29)$$

This means that the ratio between the creep coefficient and the compression index of a given soil type is independent from e and σ' . According to Mesri and Choi 1985, the values of C_α/C_c range from 0.02 to 0.10 for variety of natural soils including peats, organic silts, highly sensitive clays, as well as granular materials. For a majority of inorganic soft clays $C_\alpha/C_c = 0.04 \pm 0.01$, and for highly organic plastic clays $C_\alpha/C_c = 0.05 \pm 0.01$.

According to Leinenkugel 1976, the values of C_α/C_c are dependent on the coefficient of viscosity I_v and the angle of overall shearing strength φ'_s

$$C_\alpha / C_c = 2I_v \tan \varphi'_s \quad (5.30)$$

If typical values of I_v and φ'_s for normally consolidated clays ($I_v = 3\%$ and $\varphi'_s = 26^\circ$) are inserted into Eq. 5.31, $C_\alpha/C_c = 0.03$.

To include the influence of other factors on the deformation behaviour of soil (e.g. the rate of deformation), compression models in Eqs. 5.23 and 5.24 are suggested, with which different behaviours can be combined for the compression path AB (Fig. 5.17).

Yin and Graham 1989 developed a general viscous-elastic and viscous-elastic-plastic constitutive model using the concept of “equivalent time” in continuous loading. They used a separate equation for purely elastic unloading. Such kind of approach can be described using the function in Eq. 5.23. Klobe 1992 developed further the Yin and Graham model as a rate dependent compression law, which can be described by the equation

$$R(\sigma'_v, \dot{e}, \dot{\sigma}'_v, \ddot{e}) = 0 \quad (5.31)$$

Eq. 5.31 contains the first and second derivative of the void ratio in respect to time and the rate of the stress relief during the unloading phase. Based on Eq. 5.31, Klobe extended the Buisman equation (Eq. 5.32) for prediction of settlement during the secondary consolidation phase, i.e.,

$$\dot{s}(t) = \frac{H \cdot C_B}{t} \quad \text{or} \quad s(t) = H \cdot C_B \cdot \ln \frac{t}{t_p} \quad (5.32)$$

with the equation

$$s(t) = H \cdot C_B \cdot \ln \frac{t - t_I}{t_p - t_I} \quad (5.33)$$

where C_B is called the Buisman faktor, H is the thickness of the compressible layer t_p is the consolidation time and t_p is a constant integration factor. t_p is determined in such a way that the calculated settlement will agree with the measured settle-

ments. The value ($H \cdot C_B$) can be determined with the help of Eq. 5.32 and settlement measurements.

With this model it is possible to predict the influence of a small stress relief or load increase (e.g. because of renovation measure) on the secondary settlement, which is important from practical point of view.

Since old and insufficiently founded buildings are primarily affected by creep phenomenon, the viscose behaviour that expresses itself by creep, relaxation and strain rate should be taken into account (Krieg 2000). The relationships between compression, creep, relaxation and increase in the rate of strain is shown Fig. 5.20.

The settlement-pressure lines under different strain rates can be expressed with the equation

$$\sigma'_0 = \sigma'_i \left(\frac{\dot{\varepsilon}_0}{\dot{\varepsilon}_i} \right)^{I_v} = \sigma'_i \left(\frac{t_i}{t_0} \right)^{I_v} \quad (5.34)$$

where σ'_i is the reference pressure at the strain rate of $\dot{\varepsilon}_i$, I_v is the viscosity index and t_0 is a reference time. The primary consolidation time t_p can serve as a reference time in case of compression tests with incremental load increase (Gudehus 2001).

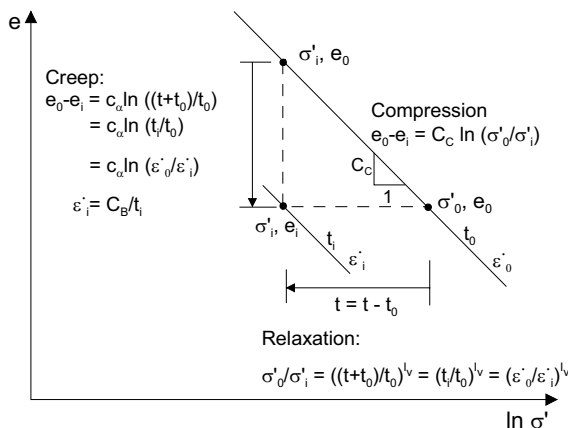


Fig. 5.18. Relationships between compression, creep, relaxation and rate of strain (after Krieg 2000).

With the help of Eq. 5.34 and the equation for the calculation of the creep compression, i.e.,

$$\Delta e_v = C_a \ln \frac{t + t_i}{t_i} \quad (5.35)$$

where v indicates the creep as well as the viscous compression, Krieg 2000 developed the following equation for the determination of the change of the void ratio due to change of stress during the creep phase:

$$\Delta e_i = C_\alpha \ln \frac{t + (1/R)t_0}{(1/R)t_0} \quad (5.36)$$

where $R = (\sigma'_i / \sigma'_o)^{l_v}$.

Based on this concept, Krieg 2000 suggested a new stabilisation procedure for historical buildings, with which the creep settlement can effectively be brought to an end.

5.4.4 Allowable settlements, tilts and angular distortions

Deformations of the underground, here predominantly settlement, may lead to a strain in the superstructure, which may in turn lead to a redistribution of stresses in soil. Thus, there exist an interaction between the soil and structure. This is commonly called as soil-interaction and applies equally to isolated footings, a system of isolated and strip foundations, raft foundations, pile foundations and last but not least foundations of neighbouring buildings.

Total uniform settlements are less dangerous for buildings than differential settlements, tilt, angular distortion and angular strains. The following presentations are largely taken from Fischer 2006.

Fig. 5.19a shows schematic presentation of differential settlements, tilting and angular distortions. The differential settlement results angular rotation and bending in reference to the initial position of the foundation. The course of the curvature can be approximated analogue to the deflection of a tendon. The following relationship are given for the radius of curvature of a curve between two inflection points (Fig. 5.19c):

$$R^2 = \left(\frac{l_{2,5}^2 / \cos \theta}{2} \right)^2 + (R^2 - 2 \cdot R \cdot \Delta s_{max} \cdot \cos \theta + \Delta s_{max}^2 \cdot \cos^2 \theta) \quad (5.37a)$$

$$R = \left(\frac{\frac{l_{2,5}^2 / \cos^2 \theta}{4} + \Delta s_{max}^2 \cdot \cos^2 \theta}{2 \cdot \Delta s_{max} \cdot \cos \theta} \right) \quad (5.37b)$$

For very small value of θ and $\Delta s^2 \ll R$, Eq. 5.37b can be simplified to:

$$R \approx \frac{l^2}{8\Delta s} \quad (5.37c)$$

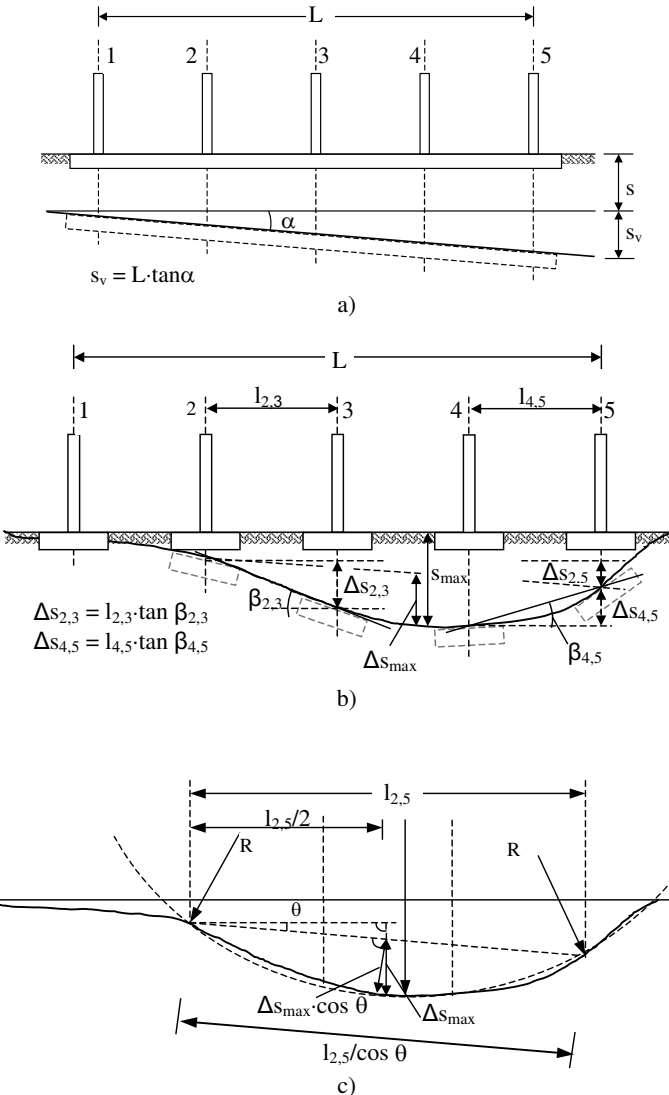


Fig. 5.19. a) Tilt due to differential settlement; b) angular distortion and deflection; c) definition of the radius of curvature

The allowable settlement does not only depend on static criteria, but also on the function of the structure (serviceability limit state). For example, for a tower foundation that settles uniformly, statically relevant specification of the allowable settlement may not be required. However, pipe lines connected to external pipe lines may determine the allowable settlement.

Different requirements for structures, for instance, on the one hand the demand for crack free structure in regard to its water tightness, and on the other hand allowing a small aesthetic cracks deliberately to save on foundation cost, requires different criteria for allowable differential settlements. These will however induce an additional stress restraint in the structure, if the settlement leads to sagging or hogging and they are primarily responsible for damage of a structure. Examples of crack propagation in an idealised structure or structural elements as a result of settlements giving rise to sagging or hogging are demonstrated in Fig. 5.20. Some practical illustrations of the different settlement forms are also given in Fig. 5.21.

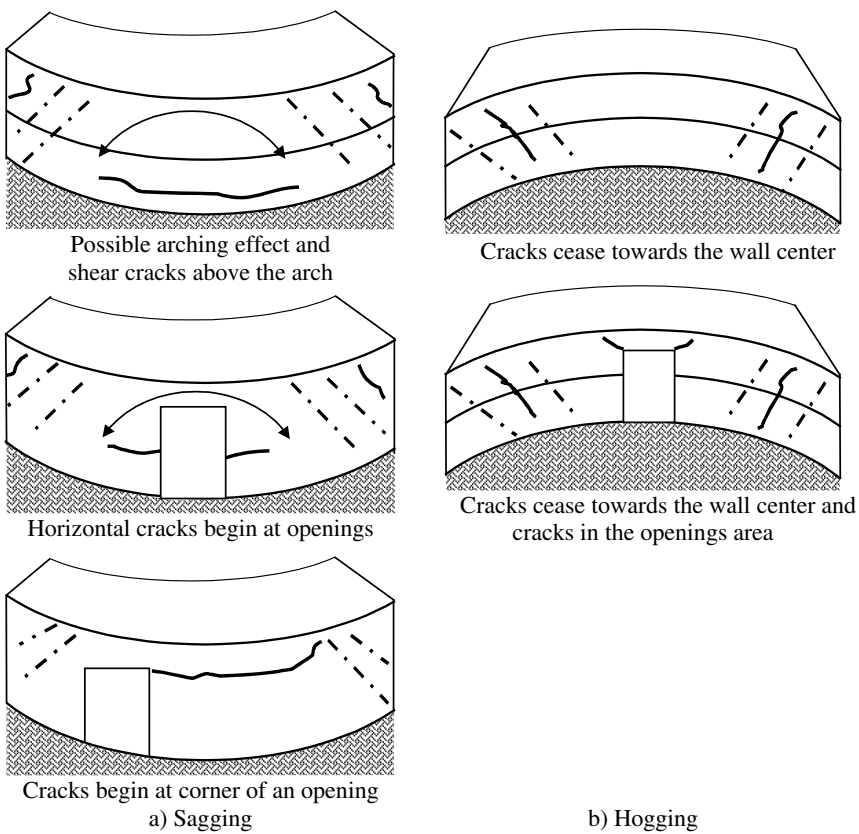


Fig. 5.20. Crack propagation due to sagging and hogging settlements

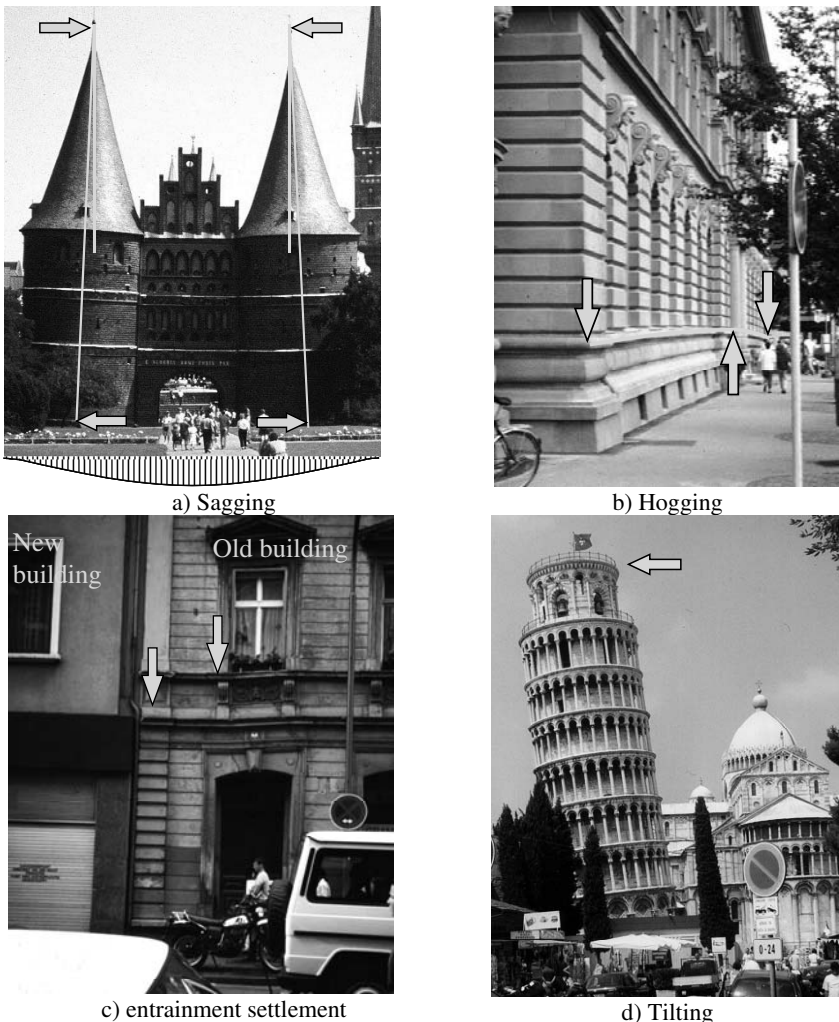


Fig. 5.21. Illustrations of the effect of different settlement forms on buildings

The bending of the foundation structure arising from sagging or hogging settlements may lead to an additional stress in the structure or structural elements depending on the stiffness of the structure. Whereas an ideal flexible structure can follow the curvature of the settlement trough without significant additional stresses, rigid structures are subjected to additional stresses.

The terms “flexible” and “rigid” express two extreme cases of the stiffness of structures. In reality, however, the stiffness of most buildings made of brick walls or solid reinforced concrete walls or reinforced concrete frames lies between these two extreme cases. Such buildings may follow up the curvature to certain degrees

without damage taking place. The degree of static determinacy of a structure can also affect the capacity of the structure to absorb the additional stresses developed due to differential settlements and distortions. It is widely known that statically determinant structures may better adjust to the curvatures of sagging or hogging than statically indeterminate structures.

The angle of distortion between individual foundation elements (Fig. 5.19b), which go beyond a rigid body tilt, is decisive for the allowable differential settlement.

The condition of a building in which it becomes uninhabitable or unusable, i.e. if the serviceability limit state fails, shall be taken as criteria for a building damage, but not the limit state at collapse of the structure. Differential settlements as a result of inhomogeneities in the underground are to be borne free of crack by the building to some extent through geometrical arrangements and selection of type of construction material only. The damage risk is higher by a quick loading than by slow incremental loading. Some examples of crack propagation and means of controlling the inclination of buildings are shown in Figs. 5.22 & 5.23.

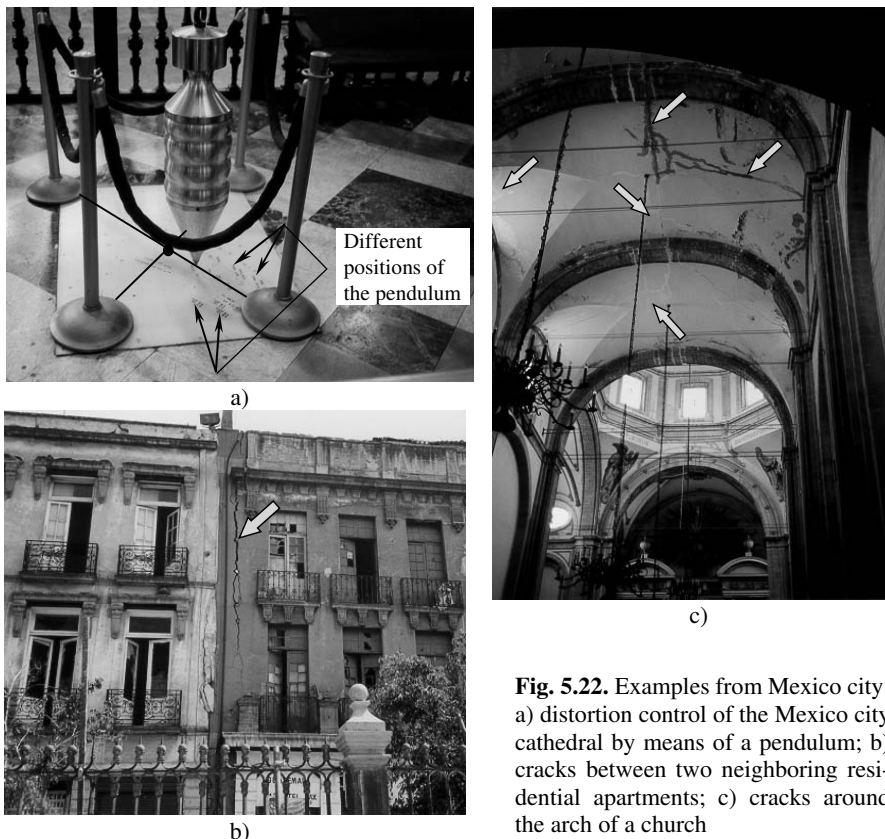


Fig. 5.22. Examples from Mexico city:
 a) distortion control of the Mexico city cathedral by means of a pendulum; b)
 cracks between two neighboring residential apartments; c) cracks around
 the arch of a church

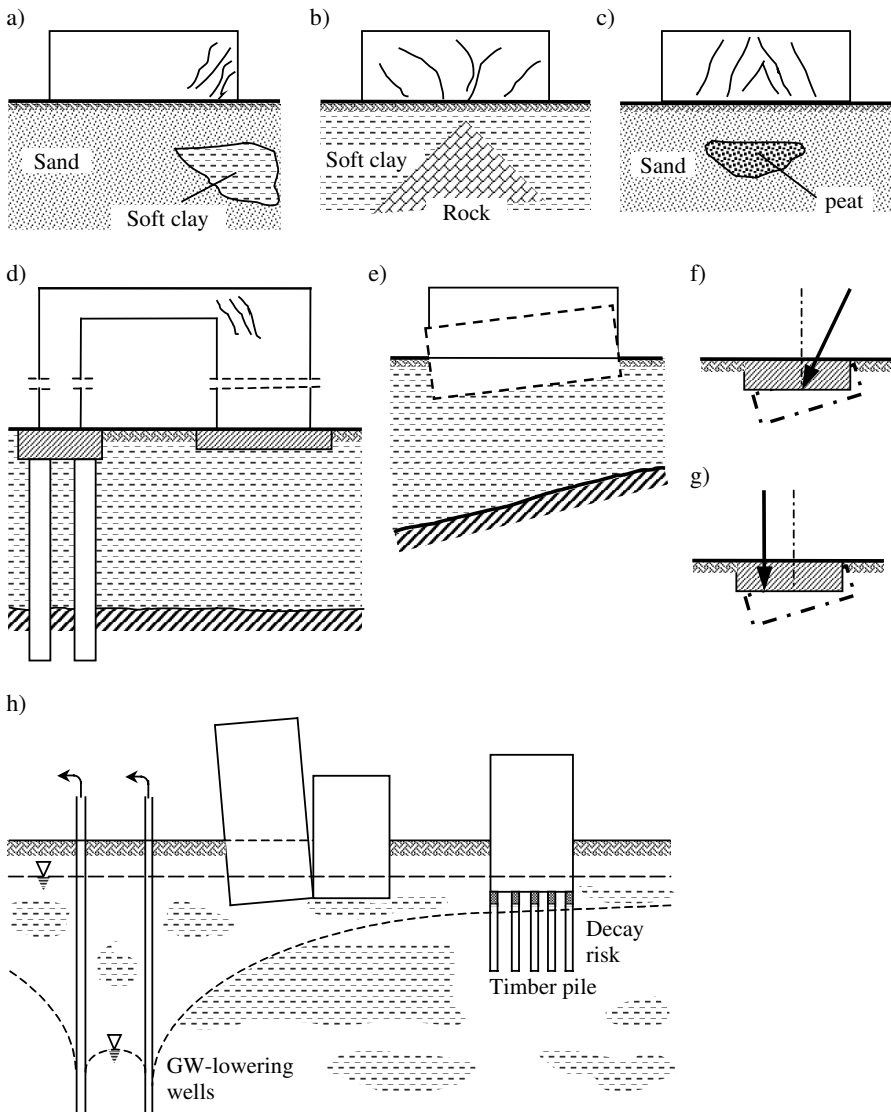


Fig. 5.23. Some illustrations of causes of differential settlements and crack propagation

In defining the criteria for allowable differential settlement, the effect of adjacent buildings (Fig. 5.24) must be considered where applicable. For this reason it is recommended to arrange a settlement barrier at a zone, where the stress in underground changes suddenly and to a larger extent. (e.g. one-story buildings near a high rise buildings).

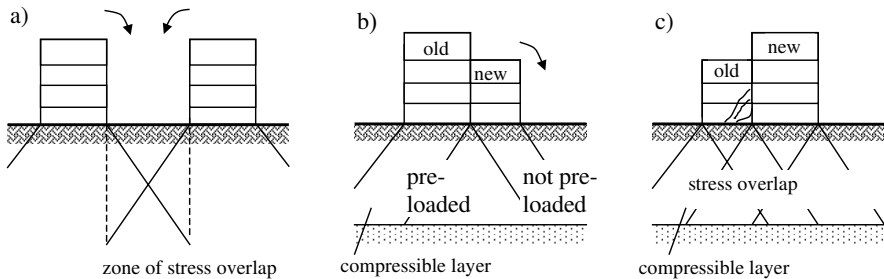


Fig. 5.24. Interaction between adjacent structures

In the literature, different damage limiting criteria are given at which building damage can be tolerated or a complete damage is to be expected. Since the determination of the damage limiting values is difficult for different structures in connection with the construction materials used and the underground condition at the site, and hand it is difficult to determine which deformations, tilting or distortions can be tolerated or can cause damage, the limiting values given in the literature differ from each other substantially. The permissible angular distortions of foundations of neighboring structures are also formulated as a limiting value beside the limiting values for differential settlement. A further parameter, namely the radius of curvature can also be derived from the settlement trough where the sagging can be approximated as a part of a circle.

The limiting values given in Table 5.5 for the case of settlements arising to sagging can be divided into empirically determined values and values determined based on settlement measurements. These are:

- empirically determined values according to Skempton and McDonald 1956; Bjerrum 1963; Burland et al. 1977; Smoltczyk 1990, and
- values determined based on settlement measurements according to Terzaghi 1948/1961; Leussink 1954; Schultze 1967; Sherif 1973; Pfefferkorn 1994; Meyerhoff 1953; Polsin and Tokar 1957.

These limiting values developed based on a general underground condition can also be used for normally consolidated soft soil deposits. Irrespective of the limiting values, however, the additional stresses developed due to differential settlement or angular distortions causing damage to the building on soft underground may be overcome by constructing a rigid monolithic foundations such as box or basements reinforced concrete foundations.

Table 5.5. Allowable differential settlements and angular distortions

			Sagging settlement			
			Differential settlement [%]	Differential settlement Δs [cm]; L [m]	Angular distortion $\tan \beta [-]$	Radius [km]
Nendza 1982	Terzaghi 1948	limiting value of Δs derived assuming length of structure L = 35 m	5.0 to 2.0	1/350 to 1/875	2.5 to 6	
	Leussink 1954		5.0 to 2.0	1/350 to 1/875	2.5 to 6	
	Russ. Norm 1955		12.0 to 5.0	1/146 to 1/350	1 to 6	
	Meyerhoff 1953		6.0	1/292	2.2	
	Rausch 1955		3.0	1/583	4.0	
Skempton and McDonald 1956 (based on statistical analyses of infilled framed structures)	isolated footings	derived from the limiting value $\Delta s/l = 1/500$ and safety factor of $\eta = 1.5$	60· s_{max}	clay	3.6	
	raft foundations			sand	2.4	
	box foundation		40 to 60· s_{max}	clay	2.4 to 6.0	
				sand	1.6 to 3.6	
	isolated footings	derived from the limiting value $\Delta s/l = 1/300$	40 to 60· s_{max}	clay	4.0 to 6.0	
	raft foundations			clay	4.5	
				sand	3.0	
				clay	4.5	
				sand	3.0	
	no crack				1/500	
Polshin and Tokar 1957	light crack				1/300	
	structural damage				1/150	
	Industry and public buildings	steel and reinforced concrete frames	clay, dense sand	(1/500)·L		
			plastic clay	(1/500)·L		
	Masonry walls	brick walls supported by columns at corners	clay, dense sand	(1/143)·L		
			plastic clay	(1/1000)·L		
	Overhead cranes	more story public buildings	clay, dense sand	L/H<3	(1/3333)·L	
				L/H>5	(1/2000)·L	
		one story buildings	plastic clay	L/H<3	(1/2500)·L	
				L/H>5	(1/1430)·L	
		plastic clay, dense sand		1/1000		
Sowers 1957	steel frames			(1/133)·L		
	reinforced concrete frames			1/500		
Meyerhoff 1953	frames			1/400		
	Infilled frames			1/300		
	masonry walls			1/1000		
Terzaghi 1961				(1/2000)·L		
Leussink 1963/1967	high rise buildings			2.0	1/250	1.0

Table 5.5. (cont.)

Schultze 1957			2.0
Mayer and Rüsch 1967			1/300
Bjerrum, 1963 (extension of Skempton)	damage limiting values	structures in general	1/150
		bearing walls	1/300
		framed structures	1/600
	Safety limiting values	no cracks	1/500
		brick walls $h/l < 1/4$	1/150
		settlement sensitive machines	1/750
Fjeld 1963	L/H = 2		1/200 to 1/300
	L/H = 4		< 1/200
Sherif 1973	isolated footings	$50 \cdot s_{\text{mittel}}$	
	raft foundations	$33 \cdot s_{\text{mittel}}$	
Schultze 1974			1/125
Grant et al. 1974	isolated footings	clay	5.0
		sand	3.0
	raft foundations	clay	5.0
		sand	3.0
	framed structures		1/300
	load bearing walls		1/300
Burland 1977	Wall element	Masonry walls	< 1/1000
		Infilled frames	$1/1100 < \Delta s/l < 1/650$
		reinforced concrete	< 1/1250
Rybicki 1978	general limit values		< 0.5
	mining area		5.0
Nenzda 1982	general limit values		5.0
	brick walls with reinforced concrete roof slab		1/800 3.0
	reinforced concrete frame		1/800 3.0
Smoltczyk 1990	collapse		$\geq 1/100$
	structural	severe	1/100 to 1/170
		moderate to severe	1/170 to 1/250
	architectural	slight to moderate	1/250 to 1/500
		slight	1/500 to 1/1000
	no damage		$\leq 1/100$
Dulácska 1992			1/500
EVB 1993			2.0
Pfefferkorn 1994			1/1000

Table 5.5. (cont.)

MacLeod et al. 1980	masonry wall with tensile strength $f_{bt} = 1.5 \text{ N/mm}^2$	L/H = 2	uniform load	0.027·L to 0.095·L 1/833 to 1/250
			point load	0.016·L to 0.068·L 1/3125 to 1/599
	homogeneous soil	L/H = 5	uniform load	0.020·L to 0.063·L 1/581 to 1/220
			point load	0.009·L to 0.028·L 1/2778 to 1/763
	Inhomogeneous soil, uniform load, L/H = 2			0.010·L to 0.042·L 1/3125 to 1/700
DIN 4421 1982	structural frame of group II and III			$\Delta s = 0.025 \cdot L \leq \text{max. } \Delta s = 0.50$
Euro code 1997	isolated footings			2.0
	isolated footings on sand			1.9
	infilled frames, masonry walls	SLS		1/2000 to 1/300
		ULS		1/150
	general limit values			1/500

SLS = serviceability limit state; ULS = ultimate limit state

Table 5.6. Permissible settlement criteria for hogging type of settlement

			Differential settlement Δs [cm]	Angular distortion $\tan \beta$ [-]	Radius [km]
Schultze and Horn 1990 (derived from Bjerrum 1963)	damage limit	structures in general		1/300	
		walls		1/600	
		infilled frames		1/1200	
	safety limit	no crack		1/1000	
		brick walls h/l < 1/4		1/300	
	settlement sensitive machines			1/1500	
Burland et al. 1977	Wall element			< 1/1000	
Rybicki 1978	mining areas				2.0
MacLeod et al. 1980	masonry walls ($f_{bt} = 1.5 \text{ N/mm}^2$), inhomogeneous soil, L/H=2 and uniform load			0.06	1/7143 to 1/4762
	homogeneous soil	L/H=2	masonry walls ($f_{bt} = 1.5 \text{ N/mm}^2$) with point load	0.01 to 0.013	1/2380 to 1/2000
		L/H=5		0.006 to 0.017	1/2000 to 1/1205
Nendza 1982					2.0
Dulácska 1992					1/1000

In many cases the respective limiting values are derived from statistical analysis (e.g. Skempton 1956; Terzaghi 1948; Grant 1974 etc.) or settlement measurements (e.g. Leussink 1963). For the more critical hogging settlement of structures, however, allowable limiting values are hardly available in the literature. Hence, the allowable settlement criteria in Table 5.6 are exclusively derived from the val-

ues for sagging settlements. For example, Schultze and Horn 1990 divided the limiting values for sagging from Bjerrum 1963 by two to get the limiting values for hogging settlements as shown in Table 5.6.

Contrary to the empirically derived limiting values, Burland 1977 developed procedures for determination of the limiting values for infilled walls, masonry walls, reinforced concrete walls and beams based on theoretical approach with the help of the Timoschenko differential solution for beams (Fig. 5.25).

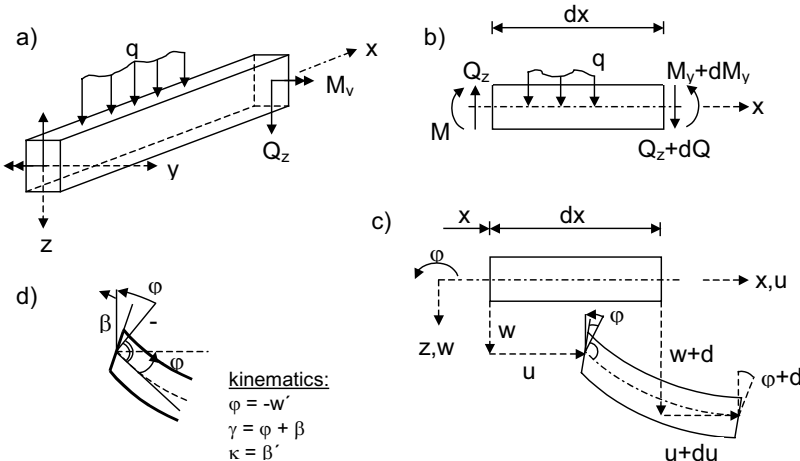


Fig. 5.25. Beam in shear: a) geometry; b) section forces; c) deflection; d) kinematics

The followings are the assumptions in Timoschenko's beam solution:

- elastic material property (Hook's Law),
- linear stress distribution (Navier),
- no change of the section thickness during deformation,
- superposition of the deformations due to bending and shear forces,
- an average value of shear strain γ_{xy} ,
- no arching effect ,
- negligible normal deformation,
- 2nd order derivation.

The deflection of a girder beam supported at the two ends consists two components, namely the deflection as a result of the bending and shear forces, and can be given as function of the strain at rupture of the material used and the ratio of the depth to length of the beam element. Based on the virtual work, the deflection is given by:

$$f_l = \int_y \frac{\delta M \cdot M}{EI(x)} dx + \int_y \alpha_k \cdot \frac{\delta Q \cdot Q}{GA(x)} dx \quad (5.38)$$

where α_k is known as a shear coefficient and it is given by (see also Table 5.7):

$$\alpha_k = \frac{1}{\alpha_s} = A \cdot \int_A \frac{S^2}{I^2 \cdot b^2(x)} dA \quad (5.39)$$

Table 5.7. Shear coefficient as a function of the shape of the cross section

Cross section	Shear coefficient κ
	1.2
	$\alpha_k \approx \frac{\sum A}{A_s}$

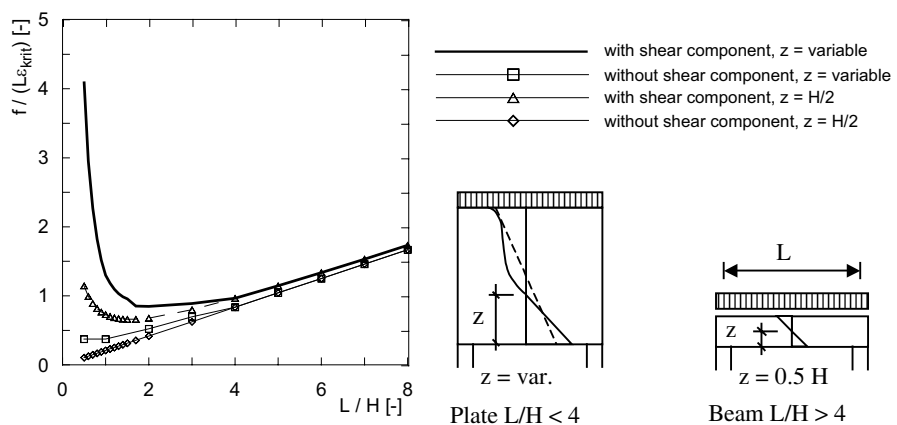


Fig. 5.26. Relative critical deflection of a reinforced concrete element ($E/G = 2.6$) for the case of sagging settlement

It appears from Fig. 5.26 that the shear deformation component cannot be neglected at least for plate elements and the assumption that the neutral line of the plate element is located at the middle of the plate (i.e. $z = 0.5 \cdot h$) does not reflect the reality.

For the determination of the damage limiting values, the following strains at rupture are assumed:

- Masonry: $\varepsilon_{krit} = 0.0075\%$
- Reinforced concrete: $\varepsilon_{krit} = 0.003\% \text{ to } 0.005\%$

The derived values are more conservative than those derived from settlement measurements and statistical methods. Thus, Franke 1980 suggested that the limiting values given by Burland 1977 should be used for spread foundations only, whereas those values developed empirically by Bjerrum 1963 can be used for isolated footings.

It should be noted that the values in Table 5.5 & 5.6 suggested by different authors reflect the local soil conditions, the construction methods and peculiarities and hence they do not claim a general validity, rather they should be understood as reference values.

Further information on allowable differential settlements and angular distortion can be found in Placzek 1982 including settlements as a result of shrinkage. With the condition that the volume decrease ΔV is equal to the amount of water evaporated, the settlement due to shrinkage can be approximated from:

$$s = \frac{\Delta m_w}{\rho_w \cdot A} \quad (5.40)$$

where Δm_v is the amount of water evaporated in a given time interval, ρ_w is the density of the water dependent on temperature and A is the surface area subjected to evaporation (Fig. 5.27).

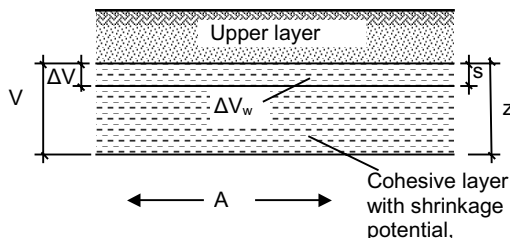


Fig. 5.27. Volume change due to shrinkage

Moreover, settlements are possible, if the roots of trees near a building extend deep into the soft soil layer and suck water depending on season and the requirement for its growth. A case history of settlement arising from shrinkage of the soil due to deep rooted tree near a building is given in Section 5.8.

5.5 Case histories of buildings on raft foundations

5.5.1 General

In the following are presented 10 case histories of buildings with raft foundations on soft lacustrine clay in southern Germany near the lakes in front of the Alps (see also Soumaya 2005; Soumaya and Kempfert 2006). A number of field observations show that the calculated settlements using the standard method of settlement analysis are on average 50 % larger than the actually measured settlements. Hence, the main objective of this section is to describe the considerable discrepancy between measured and predicted settlements by means of back analysis of practical projects and laboratory test program. The laboratory test program includes standard consolidation test (STD) and constant rate of loading consolidation test (CRL). The influences of the load increment and the loading rate on the soil deformation behaviour have been intensively investigated. Finally, recommendations for the practice are given how to determine compressibility parameters and hence to improve the settlement prediction.

5.5.2 Soil condition

The soils near the lakes in front of the Alps such as lake Constance locally known as “Bodensee” belong to the pre- and postglacial deposits (Fig. 5.28).

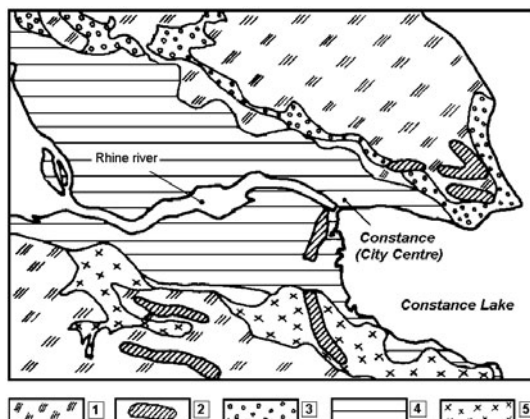


Fig. 5.28. Geological soil map around the lake constance, southern Germany: 1) lacustrine clay (pre-glacial sediments), 2) moraine, 3) gravelly moraine, 4) lacustrine clay (post glacial, holocene sediments), 5) Loam (post glacial, holocene sediments)

In geotechnical terms, the lacustrine clay deposit contain silty clays to sandy silts of low plasticity with soft to very soft consistency and a water content of 25–50 %. The undrained shear strength c_u varies between 10 and 40 kN/m². Some details about the material behaviour of the lacustrine clays can be found in chapter 2. Because of their low strength and high compressibility, the lacustrine clays in southern Germany are generally considered as difficult soils in foundation engineering. The most and common type of foundation of normal buildings on lacustrine soft deposits in this area is the raft foundation.

The underground condition of the 10 projects from different sites in the region presented in the following are almost the same, so that the settlements of the buildings can directly be compared and analyzed to obtain a general picture of the deformation behaviour of soft soil in southern Germany.

5.5.3 Review of settlement observations

Method

The principle of back analysis can be expressed in either of the modified forms of Lambe's 1973 equation (Lerouil and Tavenas 1981):

$$\text{observation} + \text{soil Parameter} \Rightarrow \text{validated theory} \quad (5.41)$$

$$\text{observation} + \text{theory} \Rightarrow \text{empirical soil parameter} \quad (5.42)$$

Nevertheless, the conventional theories are widely used in the geotechnical practice to estimate the primary and secondary settlement as well as the rate of consolidation. In this section, however, the approach in Eq. 5.42 is used together with the available long-term settlement measurements and the standard methods to obtain representative deformation parameters and taking into account the choice of an “appropriate theory” to describe the soil response.

Back-analysis procedures

The field observations are analyzed using the method developed by Asaoka 1978. This method enables to determine the final settlement s_∞ and the coefficient of consolidation c_v for a give settlement observations with time. After evaluating the final settlement for all measurement points of every single project, a settlement isolines map is plotted to interpolate the final settlement \bar{s}_∞ at the so called the characteristic points at which the settlement of the raft is usually calculated according to the German practice (e.g. Fig. 5.30). At the characteristic point, it is assumed that the settlement of a rigid and flexible raft foundations are identical Graßhoff 1955.

Using the c_v -values derived from the measured settlements, the field primary settlement s_p can be estimated. By inserting the measured primary settlement s_p into the well known Eq. 5.43 and assuming that the ratio C_c/C_s remains the same

for in-situ soil condition and a specimen in laboratory, an average value of in-situ compression index can be approximated.

$$s = s_p = \frac{H}{1+e_0} \left[C_s \cdot \log \frac{\sigma'_{vc}}{\sigma'_{v0}} + C_c \cdot \log \frac{\sigma'_{v0} + \Delta\sigma}{\sigma'_{vc}} \right] \quad (5.43)$$

where H is the thickness of the compressible layer, e_0 is the initial void ratio, σ'_{v0} is the effective overburden pressure after excavation, and σ'_{vc} is the preconsolidation pressure which is assumed to be equal to the overburden pressure before excavation in normally consolidated soil deposits and $\Delta\sigma$ is an average increase of pressure due to external surface load in the compressible layer and it can be estimated using the Simpson's rule.

It should be mentioned here that the settlement measurements in all the projects treated hereafter was started after the raft foundation was in place on a compacted granular fill. Hence, considerable amount of immediate settlements had already occurred prior to the start of any of the measurements in addition to the elastic settlements due to recompression. Therefore, the largest part of settlement occurs entirely along the virgin compression line and hence the error that may arise from the assumption of $C_c/C_s = 4.8$ can be neglected.

Furthermore, all measured settlements beyond the primary consolidation time t_p is used to estimate an average field coefficient of secondary consolidation C_α from the equation:

$$C_\alpha = \frac{1}{H} [(s - s_p) / \log(t/t_p)] \quad (5.44)$$

in which s is the measured settlement corresponding to time t , where $t > t_p$. In this way the field it is possible to separate the primary and secondary settlements as well to determine the actual rate of deformation and compare them with the corresponding values from standard laboratory tests.

Case 1: A Student hostel building

This case history deals with a students dormitory in Constance, southern Germany. The building consists of 9-storey and a basement floor and it rests on 36 m thick lacustrine clay layer (Fig. 5.29).

Settlements were measured at six points on the raft for 884 days immediately after the raft foundation was in place. Fig. 5.30 shows the observed time-settlement curves and the settlement contours along the raft surface.

Using the Asaoka's method, the settlements at all measurement points is estimated so that an average final settlement of about 6.2 cm at the characteristic points can be interpolated. This value is 35 % smaller than the calculated settlement $s_{cal} = 9.5$ cm using the standard method of analysis.

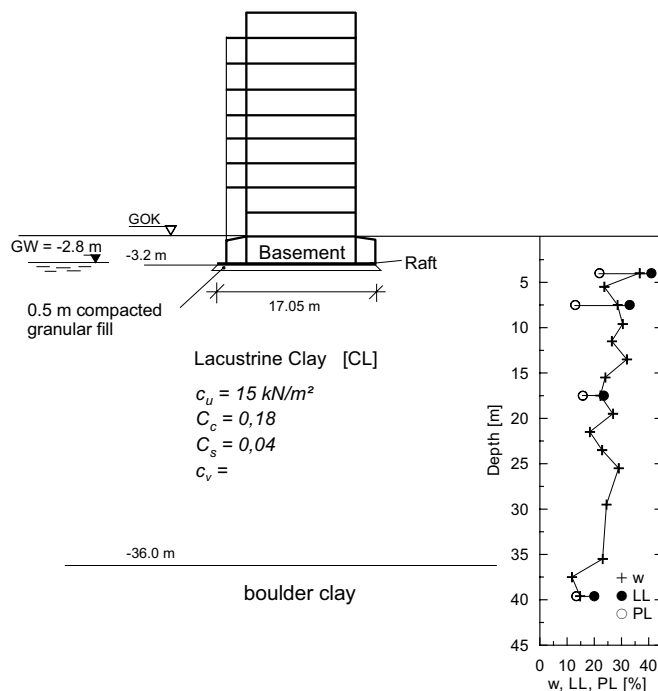


Fig. 5.29. Soil condition, case 1

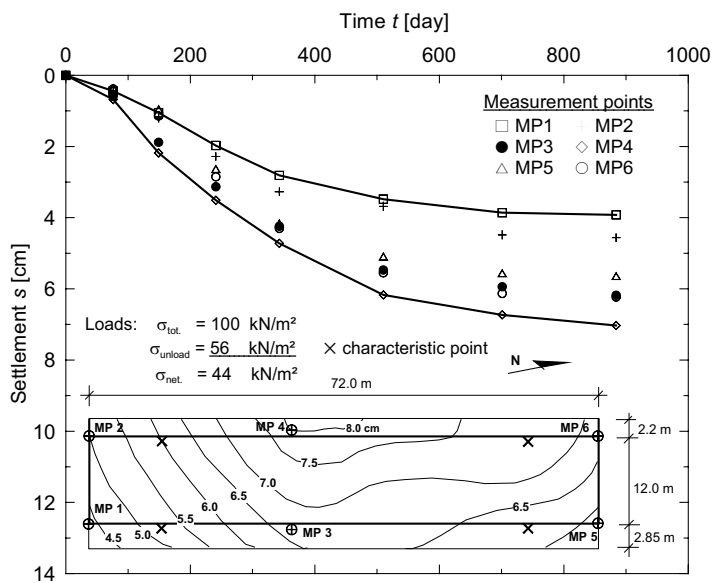


Fig. 5.30. Measured settlements and the foundation plan, case 1

Furthermore, an average value of the coefficient of consolidation $c_v = 32 \text{ m}^2/\text{year}$ is derived assuming a two way drainage path of length 17.4 m each. Substituting the measured settlement $s_p = 6.2 \text{ cm}$ into Eq. 5.43, an average field compression index $C_c = 0.104$ can be obtained. Further, using the field c_v -value, a field consolidation time of $t_p = 748$ days is estimated for this particular project. Again by substituting the measured settlement corresponding to the field consolidation time $t_p = 748 \text{ days}$ into Eq. 5.44, an average field coefficient of secondary consolidation $C_\alpha = 0.0048$ can be determined.

In the following case histories, only the soil conditions and the settlement records are presented and the results of the back analysis are summarized in section 5.5.4.

Case 2: An office building with underground parking garage

The second case history deals with an office building in city of Constance, southern Germany. The building consists of 5-storey in the southern part and 4-storey in the north part with a basement and an underground parking garage and it has S-form ground plan. Its 0.5 m thick raft foundation lies on a 1 m thick well-compacted granular fill. The subsoil investigation by means of borings and soundings to a depth of about 41 m revealed a lacustrine soft clay deposit with a thickness of 31 to 38.5 m below the ground surface (Fig. 5.31). The lacustrine clay layer is believed to be normally consolidated and has an average water content of 30 % and an undrained shear strength of 20 kN/m².

The measured settlements at 12 monitoring points over a period of 961 days are shown in Fig. 5.32. The same procedure as in the case 1 is followed to perform the back analysis.

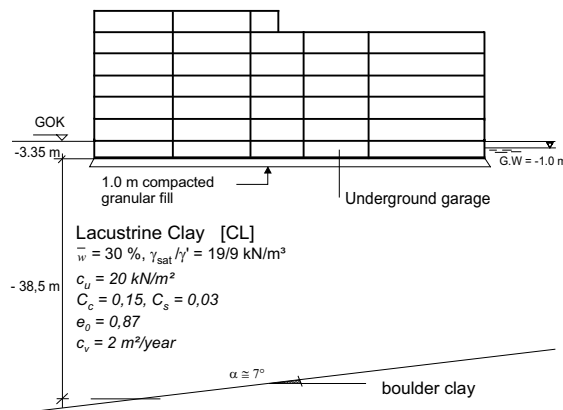


Fig. 5.31. The soil condition, case 2

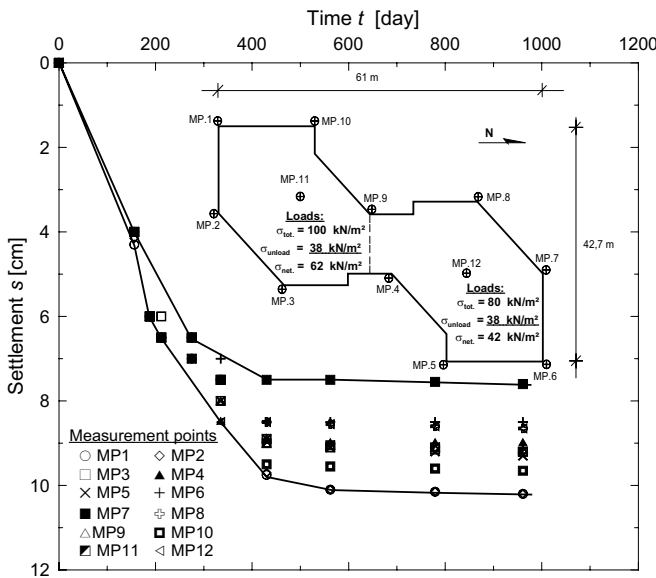


Fig. 5.32. Measured settlements and the foundation plan, case 2

Case 3: The Apartment and commercial building

The case history is about an apartment and commercial building in Radolfzell, Germany that has 7 floors and two basements. The lower basement is intended for underground parking garage. The building has a base dimension of $21.5 \times 21.8 \text{ m}^2$ with a total load of 126 kN/m^2 . It is founded on a 0.8 m thick raft foundation that rests on a 0.5 m thick well-compacted granular fill.

During the subsoil explorations using 3 borings and 2 test pits, a lacustrine soft clay layer with a thickness of 11 m was encountered underlying a boulder clay layer of unknown thickness (Fig. 5.33).

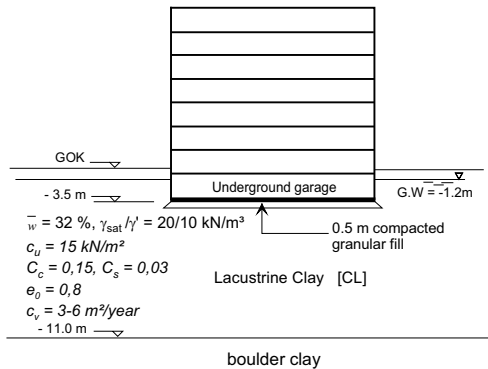


Fig. 5.33. The soil condition, case 3

The settlement was measured at the raft center over a period of 378 days only (Fig. 5.34). In this case study, the observation time was not long enough to analyze the field secondary settlement fairly. Nevertheless, the primary consolidation of compressible layer was completed within the observation time.

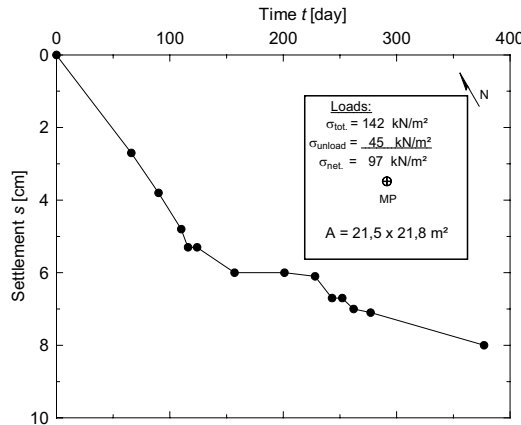


Fig. 5.34. Measured settlements and the foundation plan, case 3

Case 4: Administration building

The 4-storey administration building with underground parking garage in this case history has a base dimensions of $17.0 \times 12.4 \text{ m}^2$ with a total load of 72 kN/m^2 . It is founded on a 0.5 m thick raft that rests on a 0.5 thick well-compacted granular fill.

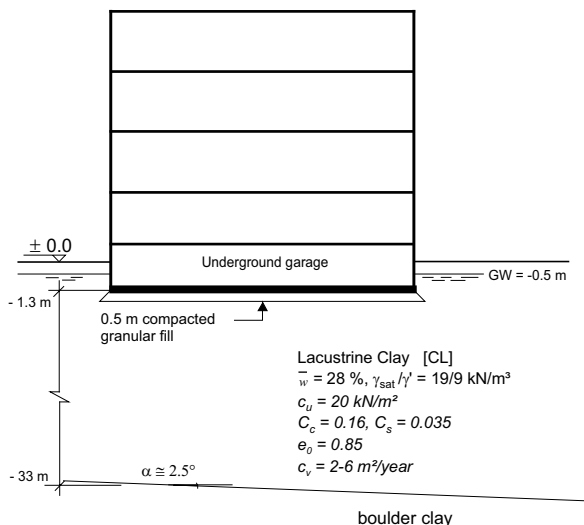


Fig. 5.35. The soil conditions, case 4

The subsoil consists of a soft, low to middle plastic lacustrine clay with a thickness exceeding 30 m (Fig. 5.35). The undrained shear strength is estimated to be about 20 kN/m^2 and the average natural water content is about 28 %.

The settlements of the building had been monitored at the four corners of the building over a period of 2343 days (Fig. 5.36).

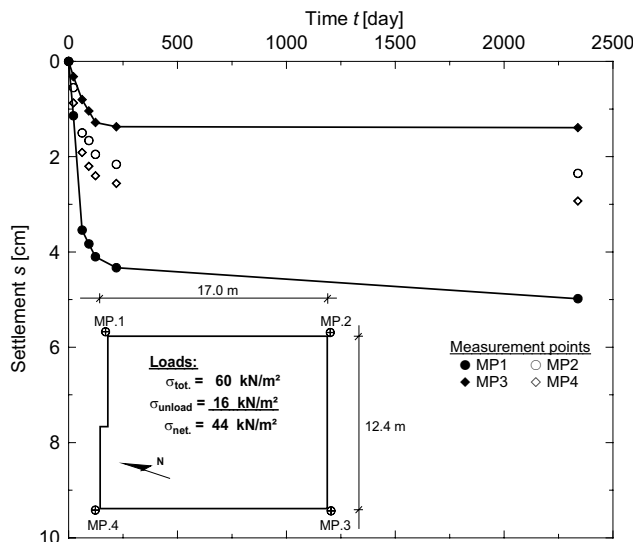


Fig. 5.36. Measured settlements and the foundation plan, case 4

Cases 5 and 6: Two office buildings

These case histories are about two adjacent office buildings in the city of Constance, Germany. Each building is 3-story high and has an underground parking garage and an attic. The buildings are founded on adjacent but separate raft foundation. Each raft has a base area of $19 \times 28 \text{ m}^2$ and subjected to an average total load of 65 kN/m^2 . The rafts are analyzed separately with due consideration of the interaction of the two buildings.

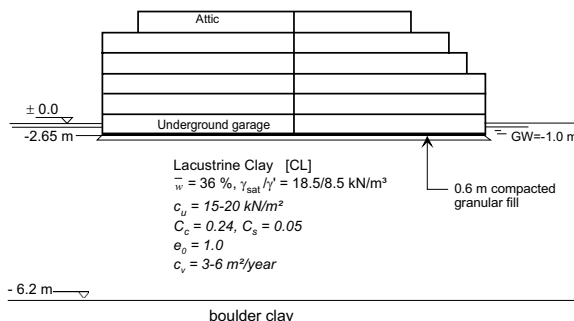


Fig. 5.37. The soil condition, cases 5 and 6

The subsoil conditions and some soil properties are given in Fig. 5.37. The lacustrine soft clay layer is limited to a depth of about 6.2 m where a boulder clay was encountered beneath it.

The settlements of the two buildings were monitored at 10 measurement points over a period of 780 days (Fig. 5.38).

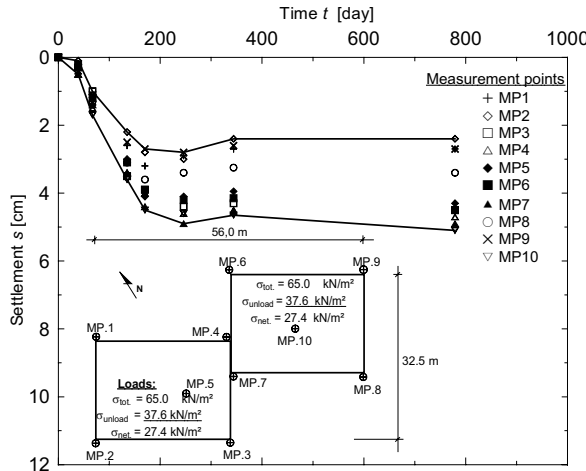


Fig. 5.38. Measured settlements and the foundation plan, cases 5 and 6

Case 7 and 8: Office and storage buildings

The underground condition of the office (case 7) and the storage (case 8) buildings are more or less similar and is shown in Fig. 5.39. Contrary to the previous case histories, a layer of soft, middle plastic lacustrine clay up to a depth of 18 m followed by soft, low plastic lacustrine clay up to a depth of 28 m was encountered during boring to a depth of 33 m. Beneath the lower lacustrine layer is boulder clay. Each building has 3-storeys, a basement for an underground parking garage. The raft foundation of the office building has a rectangular form with a size of $38.5 \times 18.6 \text{ m}^2$ and is subjected to an average total load of 71.5 kN/m^2 . The storage house has an L-form with a total load of 68 kN/m^2 . The raft foundation of both buildings are located at a depth of 2.0 m below the ground surface, i.e. the weight of the excavated soil mass is about 27 kN/m^2 at the foundation level.

The settlements of both buildings had been recorded at six and eight points respectively over a period of 952 days as shown in Figs. 5.40 & 41.

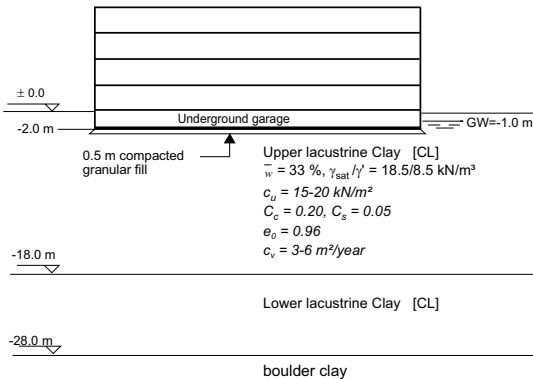


Fig. 5.39. The soil conditions, cases 7 and 8

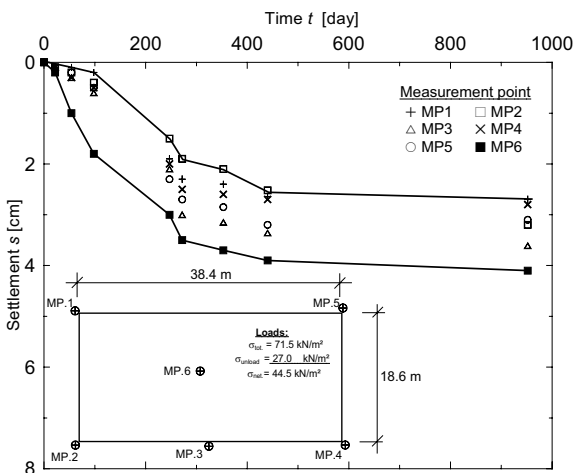


Fig. 5.40. Measured settlements and the foundation plan, case 7

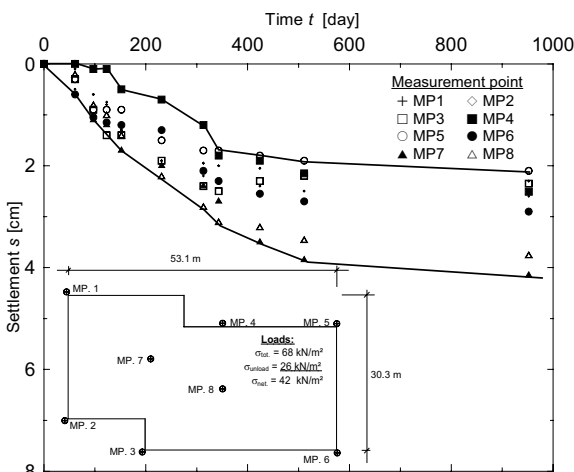


Fig. 5.41. Measured settlements and the foundation plan, case 8

Case 9: Office and administration building

This is again a 4-storey building with basement on a lacustrine soil layer in Constance city. The raft foundation has an irregular shape and is subjected to total load of 87 kN/m^2 (Fig. 5.42). The foundation is located at a depth of 2.5 m and the groundwater at 0.5m below the ground surface. The stress relief due to excavation is therefore about 26 kN/m^2 at the foundation level.

The subsoil conditions were explored by two borings to a depth of about 35 m where a deep boulder clay layer had been reached. Between the ground surface and the moraine layer is a layer of soft, middle plastic lacustrine clay. The site is located closer to the northern coast of the Rhine river similar to the buildings in cases 7 and 8. Therefore, the geotechnical properties are similar to those shown in Fig. 5.39.

Because of its low strength and high compressibility, the soft layer was pre-loaded for six months with a 2 m high granular fill which has an equivalent surcharge load of about 40 kN/m^2 . A total 5 cm settlement was measured during this pre-loading period. Taking into account the pre-consolidation pressure and the stress relief due to excavation, about 55% of the total building load seems to lay on the recompression branch of the time-settlement curve. The recorded settlements of the building at 6 points on raft and for a period of 1675 days are shown in Fig. 5.42.

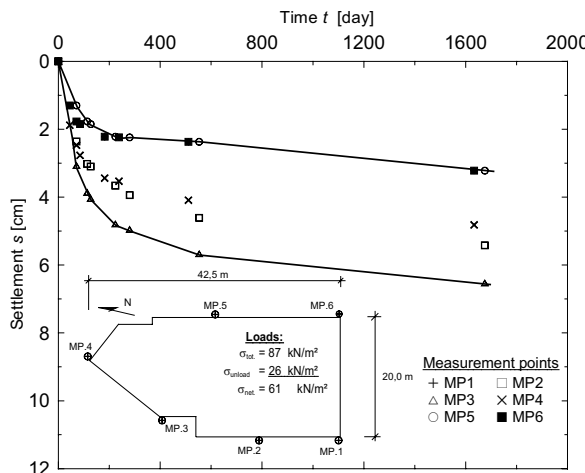


Fig. 5.42. Measured settlements and the foundation plan, case 9

Case 10: Service and administration building

The last case history in this category deals with a service and administration building in Constance city. It has 5-storeys and a basement with a $36.6 \times 27.9 \text{ m}^2$ rectangular raft foundation and a total load of 84 kN/m^2 (Fig. 5.43).

The subsoil condition had been investigated by means of 4 boreholes to a depth of about 20 m and 13 soundings to a depth of 6 m. Also at this site a layer of soft, middle plastic lacustrine clay was encountered up to the end of the borehole. The soil properties are very close to the properties shown in Fig. 5.39, simply because the building is located at the other side of the street opposite to the buildings in cases 7 and 8.

The settlements of the building measured at 6 points over a period of 474 days are shown in Fig. 5.43. Similar to the case 3, the field secondary settlement cannot be fairly analyzed because of the relatively short observation time.

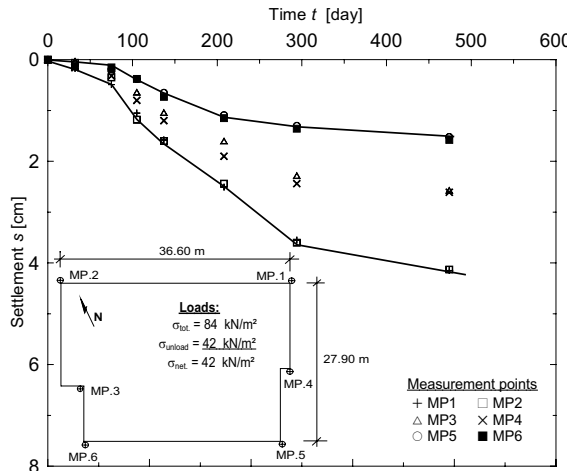


Fig. 5.43. Measured settlements and the foundation plan, case 10

5.5.4 Summary of the back analyses results

By applying the methods explained previously, the field values of the final field settlement \bar{s}_∞ and the field coefficient of consolidation c_v and consequently the primary field settlement s_p as well as the consolidation time t_p for all the case histories has been determined. By substituting these values in Eqs. 5.43 & 5.44, the average field compression index C_c and the average field coefficient of secondary settlement C_α can be estimated. The results of the back analysis for the case of primary consolidation are summarized in Table 5.8.

Using estimated values of the field coefficient of the secondary consolidation and the compression index in Table 5.8, the ratio C_α/C_c can be approximated as shown in Table 5.9.

Table 5.8. Back analysis results for the primary consolidation case

Case	S_{cal} [cm]	$C_v(\text{field})$ [m ² /y]	$t_p(\text{field})$ [day]	$S_p(\text{field})$ [cm]	$C_c(\text{field})$ [-]	$C_c(\text{field})/C_c(\text{lab})$ [-]
1	9.5	32.0	748	6.15	0.104	0.65
2	12.7	43.4	365	9.1	0.126	0.70
3 ¹⁾	11.6	19.5	275	7.4	0.128	0.71
4	7.5	36.4	677	4.6	0.080	0.62
5	7.1	3.1	318	4.4	0.145	0.63
6	7.1	3.1	330	4.7	0.155	0.67
7	6.8	41.6	445	4.0	0.118	0.59
8	7.1	33.0	560	4.1	0.115	0.58
9	7.3	41.8	670	4.85	0.166	0.75
10	6.7	15.8	380	4.7	0.160	0.69

¹⁾ The settlement in case 3 was calculated at the raft center and not at the characteristic point since the settlement was measured at this point only.

Table 5.9. Back analysis results for the secondary consolidation case

Case	C_α (field)	C_c (field)	C_α/C_c (field)
1	0.0027	0.104	0.038
2	0.0026	0.126	0.021
3	0.0027	0.128	0.021
4	0.0016	0.080	0.020
5	0.0034	0.145	0.023
6	0.0036	0.155	0.023
7	0.0027	0.118	0.023
8	0.0027	0.115	0.023
9	0.0039	0.166	0.023
10	0.0038	0.160	0.024
average	0.0030	0.130	0.024

From the above back analysis of the 10 case histories of buildings on raft foundations above a compressible lacustrine clay, the following conclusions can be drawn:

- For the investigated cases the ratio of observed to calculated primary settlements as well as the compression indexes is on average 0.67.

$$\mu = \frac{S_{p(\text{measured})}}{S_{p(\text{calculated})}} = \frac{C_{c(\text{field})}}{C_{c(\text{Laboratory})}} \approx 0.70 \quad (5.45)$$

- From the back analysis of the projects, the factor m for the limiting depth according to section 5.4.2, Fig. 5.9 is found to be on average $m = 0.26 \approx 0.25$.
- Except for cases 5 and 6, the values of the field coefficient of consolidation c_v are 4 to 15 times higher than the laboratory values. However, the laboratory and field c_v -values are identical in the cases 5 and 6. This is because a comparatively thin clayey layer is located between the raft foundation and the stiff boulder clay and the consolidation can obviously be assumed as one-dimensional. Similar field observation was reported by Terzaghi and Peck 1967.
- Data about the secondary settlement can be obtained since the time for primary consolidation t_p for all cases lies within the observation time. The short observation time in some cases are attributed to the fact that they were monitored by practicing engineers for controlling purposes and not for research purposes. On the basis of the available long-term observation, a field coefficient of secondary consolidation C_α can be determined using the Eq. 5.45 for all cases with an average value of 0.003. Thus, the normally consolidated lacustrine clay in southern Germany is subjected to a low secondary consolidation according to Mesri's 1973 classification.
- The ratio C_α / C_c seems to be constant with an average value of 0.024, which is slightly below the lower limit of the equation

$$C_\alpha / C_c = 0.04 \pm 0.01 \quad (5.46)$$

proposed by Mesri and Choi 1985 for inorganic soft clays.

5.5.5 Effect of load increment and rate on settlement prediction

Incremental loading test (IL-test)

According to Soumaya 2005, the first explanation for the discrepancies between the measured and calculated settlement is the overestimation of the compression index C_c determined from standard one-dimensional consolidation tests based on the incremental loading ($\Delta\sigma/\sigma = 1$) after 24 h. That means the compression at the end of 24 h is taken in the derivation of the compression index instead of the compression at the end of the primary consolidation (EOP), which exaggerates its value. Experiences show that (Soumaya 2005), the time t_p for the primary consolidation of specimen of soft clay in laboratory usually lie between 10 and 240 min. Based on this fact, Soumaya 2005 carried out a number of one-dimensional consolidation tests on high quality specimens of lacustrine clay in order to determine the ratio of C_{c-EOP} / C_{c-24h} .

It should be noted here that the end of primary consolidation is determined by measuring the excess pore pressure at the undrained end of the bottom of the oedometer cell. Fig. 5.44 shows a typical load-settlement-lines based on both standard 24 h- and EOP-compression. The load increment is $\Delta\sigma/\sigma = 1$ in both cases. The analysis of a number of laboratory tests on the lacustrine clay specimen from

southern Germany shows that the ratio of C_{c-EOP}/C_{c-24h} lies between 0.84 and 0.92. These values are much higher than the average factor 0.67 found in Section 5.5.4 between the field and laboratory compression indexes of the ten case histories.

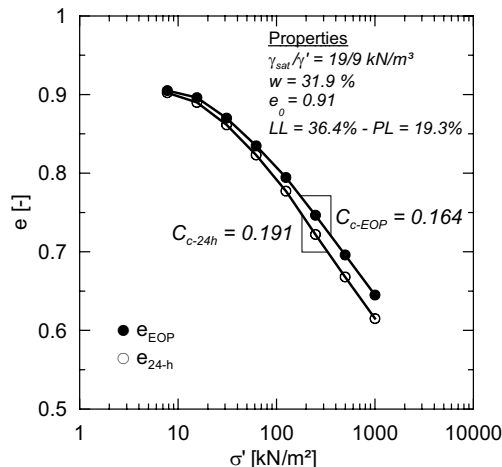


Fig. 5.44. Typical time – settlement lines based on 24h- and EOP-compressions curves for lacustrine soft clay in southern Germany

Thus, it appears that the overestimation of the laboratory C_c -value cannot be clarified using the standard consolidation test only. For this reason, Soumaya 2005 carried out further a series of consolidation tests with small load increments to study the effect of load increment on the determination of the compression index.

A typical load-settlement diagram of two oedometer tests on similar specimens but with different load increments is shown in Fig. 5.45. Both specimens were subjected to a preconsolidation pressure of 62.5 kN/m^2 incrementally. Starting from the preconsolidation pressure, the specimens were loaded incrementally up to a pressure of 125 kN/m^2 , whereas one specimen was loaded with standard increment $\Delta\sigma/\sigma = 1$, the other one was loaded with an increment of $\Delta\sigma/\sigma \approx 0.1$. Each increments was effected after the end of primary consolidation (EOP). The EOP was controlled using the excess pore pressure measured with a pore pressure transducer at the undrained end of the oedometer cell.

It is evident that the soil response depends on the load increment. If the load increment is large, the structure of the soft soil may be destroyed under the massive pressure. The influence of the load increment on the compression behaviour can be quantitatively examined by determining the C_c -values for different load increments. The C_c -value for the standard load increment $\Delta\sigma/\sigma = 1$ and 24h-compression (path AD in Fig. 5.45) is found to be $C_{c-24h} = 0.132$, whereas for EOP-compression (path AC) it is $C_{c-EOP} = 0.111$. On the other hand, the C_c -value decreases to 0.103 in the case of a load increment of $\Delta\sigma/\sigma \approx 0.1$ (path AB) and EOP-compression.

Taking in mind that the ratio of the total building load and the initial overburden pressure at the middle of the compressible soil layer of the demonstrated case histories varies between 0.3 and 0.6, the following question can be posed: what

would happen to the compression index value, if for example the specimen is loaded to half of the load (93.75 kN/m^2) at once (path AB'). It appears from the Fig. 5.45 that the point B' will be overlooked by doubling the load but the C_c -value remains the same. However, the use of small load increment can better trace the consolidation line.

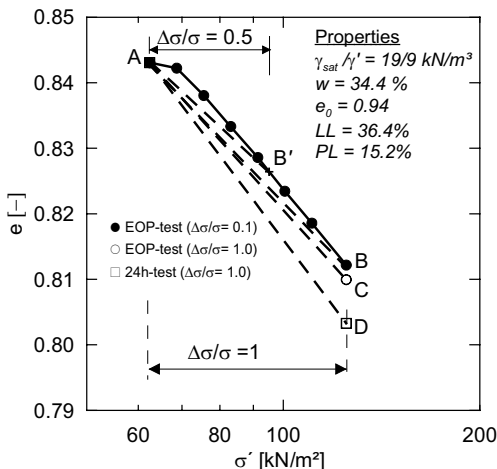


Fig. 5.45. Load-settlement diagram for two tests with different load increments

Constant rate of loading test (CRL-test)

Although the consolidation tests with small load increments can better describe the compression behaviour of soft soils, they can not be applied for the engineering practice because such test required a long time. Alternatively, a constant rate of loading test (CRL) may offer several advantages over the conventional incremental test (IL) (Aboshi et al. 1970; Janbu et al. 1981). In addition to the advantage of the short testing time, CRL-test provides a continuous tracing of the compression line. Therefore, Soumaya 2005 suggested to use the CRL-test for estimation of the compression parameters of soft soils.

The influence of the rate of loading on the compression behaviour is a vital question in the CRL-tests. At the present no general criteria is available for the selection of an appropriate loading rate, because all the criteria in the literature are established by comparing results of CRL-tests at different loading rates with results of standard consolidation test regardless of the shortcomings of the standard consolidation test. Soumaya 2005 used the following simple procedure to estimate the required rate of loading for the CRL-test from the field measurements based on the well-known model law for consolidation given in Eq. 5.16. To apply Eq. 5.16, however, the construction time $t_{c(in-situ)}$ and the field coefficient of consolidation $c_{v(in-situ)}$ must be known. Inserting these field values together with the corresponding laboratory values into Eq. 5.16, the time $t_{c(oed)}$ required in laboratory for the same degree of consolidation in-situ can be estimated.

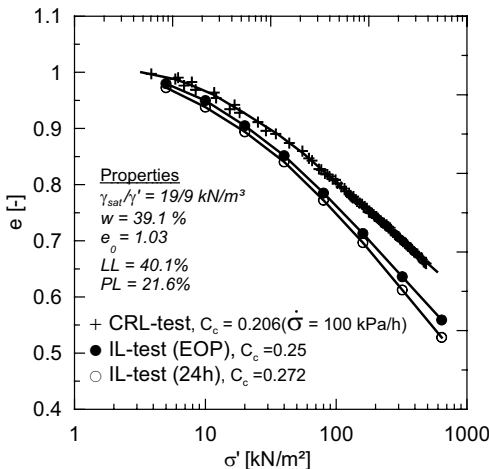


Fig. 5.46. Comparison of the load-settlement lines from the CRL- and IL-tests for the lacustrine clay in southern Germany

However, it should be noted that the model similarity can only apply, when the specimen in laboratory is subjected to the same load as the soil in-situ. Thus, the laboratory rate of loading can now be estimated by dividing the total building load with the laboratory time $t_{c(\text{load})}$. For example, an approximate loading rate of about $120 \text{ kN}/\text{m}^2/\text{h}$ is derived for the first case history (case 1). Similarly, the laboratory rate of loading for all case histories is found to vary between 80 to $140 \text{ kN}/\text{m}^2/\text{h}$. Under this rate of loading, Soumaya 2005 conducted a series of CRL-tests. A comparative presentation of the load-settlement lines from the CRL-tests and IL-standard tests on similar specimens are shown in Fig. 5.46.

The CRL-tests using the rate of loading calibrated to the field condition led to an average ratio of $\mu = C_{c-\text{CRL}}/C_{c-\text{IL}(24h)} = 0.74$, which is very close to the average ratio of $\mu = C_{c(\text{field})}/C_{c(\text{lab})} = 0.70$ obtained from the back analysis of the 10 case histories in section 5.5.4.

5.6 Two case histories with excessive settlements

5.6.1 General

Similar to the previous 10 case histories, these two projects are also located in the city of Constance. They are built on raft foundation on lacustrine soil deposit. As already mentioned in Section 5.5, experience in this area shows that the calculated settlements using the compression parameters from the standard consolidation test are on average 50 % higher than the measured settlements. Hence, the acquired experience in predicting settlements in this region is assumed satisfactory for most practical cases, since the calculated settlements usually lies on the safe side. However, a long-term observations of an office building and a storage tank showed that the measured settlements of both structures is about 2 to 3 times higher than the

predicted values in the design phase. In the following, the two cases are presented and the cause of the excessive settlements investigated.

5.6.2 Case A: office building

The first case history in this group deals with an office building with 4-story and a basement and has a base area of $20 \times 34.4 \text{ m}^2$ and a total load of 97 kN/m^2 . It is founded on a 0.5 m thick raft foundation that rests on a 2.5 m thick well-compacted granular fill. Hence, a net pressure of about 62.6 kN/m^2 is transmitted to the underground (Fig. 5.47).

The subsoil consists a layer of soft, middle plastic lacustrine clay to depth of 28 m followed by soft, low plastic lacustrine clay up to the end of the borehole depth. (Fig. 5.47).

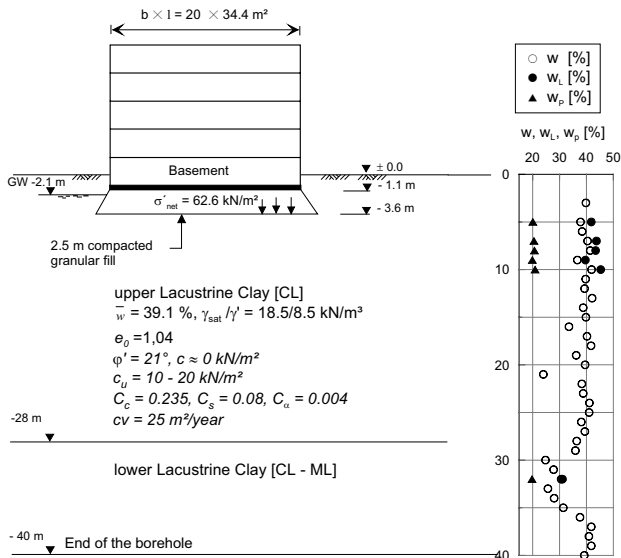


Fig. 5.47. The subsoil condition, case A

Immediately after the raft foundation was in place, settlements had been recorded at nine points over a period of about 13 years (≈ 4670 days). The measured settlements are given in Fig. 5.48. Similar to the case histories in Section 5.5, the field settlements are analyzed using the Asaoka's 1978 method.

Using this method the final settlements at all measurement points are estimated with an average of about 69 cm at the center of the raft. This value is about 2.5 times higher than the predicted settlement ($s_{\text{cal.}} = 27.5 \text{ cm}$). The field value of the coefficient of consolidation $c_v = 25 \text{ m}^2/\text{year}$ assuming a one way drainage and a

thickness of 7.5 m for the compressible soil layer is about 5 higher than the laboratory value.

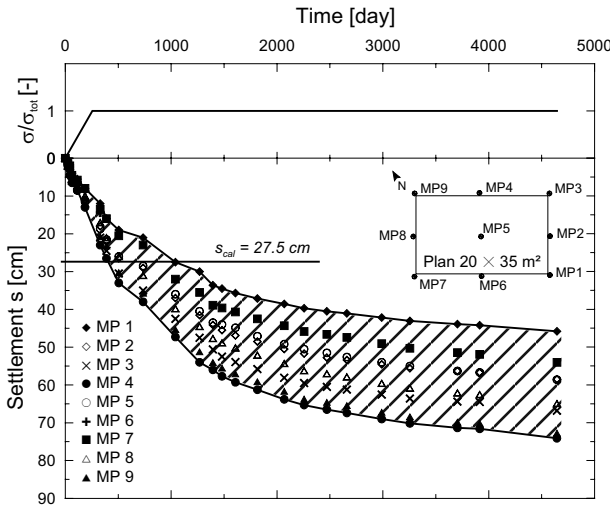


Fig. 5.48. The measured settlements and the foundation plan, case A

The reason for the excessive settlement beyond the calculated settlement can only be presumed that the soil in the vicinity of the foundation might undergo a local failure arising to plastic deformations.

The ultimate bearing capacity can be conventionally calculated using the well known equation:

$$q_{ult} = c \cdot N_c \cdot v_c + \gamma_D \cdot D \cdot N_q \cdot v_q + 0.5 \cdot B \cdot \gamma \cdot N_\gamma \cdot v_\gamma \quad (5.47)$$

Under undrained conditions Eq. 5.47 becomes:

$$q_{ult} = 5.14 \cdot v_c \cdot c_u + \gamma_D \cdot D \quad (5.48)$$

Using the effective shear parameters an ultimate bearing capacity of $q_{ult} \approx 455 \text{ kN/m}^2$ is estimated. On the other hand a much lower $q_{ult} \approx 140 \text{ kN/m}^2$ is obtained for the short-term condition. Hence, the total safety factor (FS) varies between 1.14 and 3.7.

However, the designer calculated the allowable load assuming a total safety factor of 2, because he thought that the soil is partially consolidated and the shear strength is improved due to the compacted granular fill. It is quite evident from the measured settlements that the calculated allowable load is in question and a partial shear failure may not be excluded. It is believed that the net pressure on the compressible layer was underestimated. Since the weight of the compacted granular fill is greater than the weight of the removed soft soil, the difference between the weights may be assumed as an additional load on the underground, which was not taken into account in the design phase.

The plastic deformations cannot be predicted using the conventional analytical methods. Hence, a numerical analysis method is used to investigate the excessive settlement arising from the possible plastic failure (refer to Section 5.6.4)

5.6.3 Case B: Storage tanks

The second case history deals with storage tanks. The structure consists of three juice containers with a total storage capacity of $3 \times 225 = 675 \text{ m}^3$. The subsoil investigation up to a depth of 10.5 m revealed lacustrine sediment layer of 2.5 m thick underlain by about 2.5 m thick silty sand layer. Beneath the silty sand layer follows the lacustrine soft clay (Fig. 5.49).

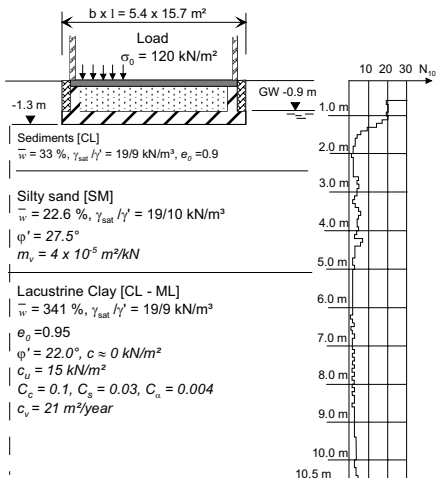


Fig. 5.49. The subsoil conditions, case B

The settlement record at 4 measurement points for a period of 7 years immediately after the raft foundation was in place are shown in Fig. 5.50. Using the Asaoka's method, a final settlements of 22 cm at the southern side and 13 cm at the northern side with an average value of 17.5 cm are interpolated. This value is about twice higher than the predicted settlements ($s_{cal} = 9 \text{ cm}$).

Because the analysis of this project has been carried out in terms of total stresses, possible effect of local shear or progressive failure was excluded. Soumaya 2005 supposed that the reason for the discrepancy between measured and calculated settlements is that the underground is subjected to a fast loading due to a quick filling of the tanks. To verify this assumption the use of numerical methods is inevitable, because the conventional methods cannot consider the influence of loading rate on the compression behaviour of soils. From project documents it was found that the storage tanks were approximately filled within 7 months after the beginning of the construction. This piece of information is used to derive the average rate of loading that is used later in the numerical analysis (see section 5.6.4).

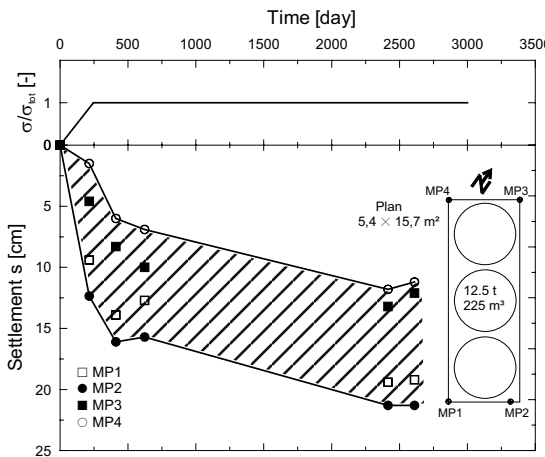


Fig. 5.50. The measured settlements and the foundation plan, case B

5.6.4 Numerical analysis

The two projects are analyzed using the finite element method with the program “PLAXIS” using a constitutive soil model the so called soft soil creep model (SSCM). The required soil parameters are taken from Figs. 5.47 & 5.49

The results of the FE-analyses of the first project are shown in Fig. 5.51 in a form of time-settlement-lines and they are compared to the measured settlements at the measurement point 5. Fig. 5.51 also shows the course of the total safety factor with time.

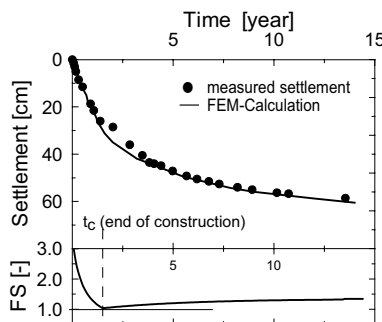


Fig. 5.51. Measured against computed time-settlement-lines and time-dependent total safety factor, case A

The FE-analysis show a good agreement with the measurements. This is partly because the input parameters are estimated from the settlement back analysis of the project. The plot of the safety factor FS shows that the foundation is nearly approaching failure (i.e. $FS = 1.1$) 1.5 years after the beginning of the construction.

This may explain the reason for the excessive measured settlements, because the underground is possibly undergone plastic deformations. The safety factor of buildings (ultimate limit state) on soft soil deposits is presented in section 5.9 separately.

Fig. 5.52a shows the computed and measured time-settlement-lines of the storage tank. The settlement at the center of the raft foundation is interpolated from the settlements at the corners. The upper and lower lines correspond to a loading rates of 0.57 kN/m²/day and 0.72 kN/m²/day respectively. These load rates has been chosen with the assumption that the tanks were filled in a period of 165 to 215 days.

It is obvious that the response of soft soil depends on the rate of loading. Such behaviour can be demonstrated schematically with the help of the effective stress paths for each loading rate as shown in Fig. 5.52b. The faster the load, the closer be the effective stress path to the critical state line due to the developed excess pore pressure, and hence larger deformations. This fact helps to explain the significant settlements of the tanks that could not be predicted using the conventional methods in the design phase.

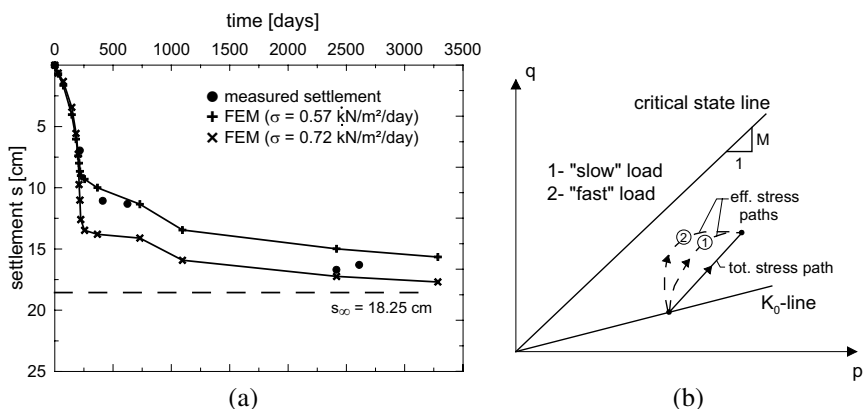


Fig. 5.52. a) Comparison of the measured and computed settlements of the tank foundation
b) Dependency of the stress paths on the rate of loading

5.7 Case history of an embankment

The case history is about an earth embankment on Highway 99A, approximately 25 km south-east of downtown Vancouver, Kanada. The embankment was built in 1971 on Salish sediments which include all postglacial terrestrial sediments and postglacial marine sediments. In engineering term the underground is a silty clay of low plasticity with an average natural water content of 45%, liquid limit of 36% and plasticity index of 11% and it is classified as soft soil. The

groundwater is located just below the ground surface. Beneath the soft soil, a very dense silty gravel was encountered. This case history is adopted from Crawford and DeBoer 1987; Crawford and Campanella 1991; Crawford et al. 1994. Therefore, refer to this literature for more and detail information. Fig. 5.53 shows the geometry of the embankment, the underground conditions as well as the loading stages and corresponding settlement measurements.

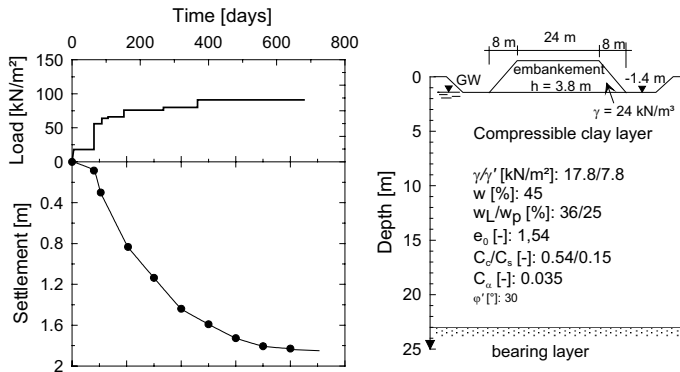


Fig. 5.53. Embankment on Highway 99A, Vancouver, Canada (after Crawford and DeBoer 1987): a) load-settlement curves; b) the geometry and the underground condition

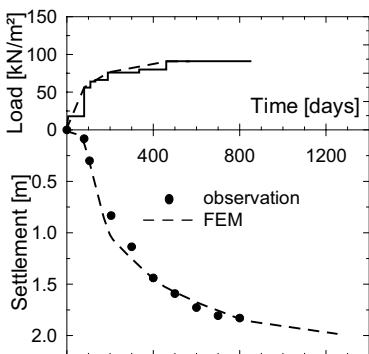
According to Crawford et al. 1994 the total calculated settlement using the conventional methods but with corrected field curves is 1.2 m. On the other hand a final measured settlement of 2.0 m can be extrapolated from Fig. 5.53a. Crawford et al. 1994 concluded that a significant part of the measured settlement may have been due to lateral spreading under the shoulders of the fill. They also observed from pore pressure measurement that the embankment was approaching failure. It is known that shear strains are greatest as failure approaches. Therefore, they conducted a finite element consolidation analysis to assess the influence of lateral spreading on vertical movements beneath the shoulders of the embankment where the settlements were measured and verified the discrepancy between the measured and predicted settlement values.

Soumaya 2005 carried out once again a finite element back analysis of the embankment based on the data from Crawford and DeBoer 1987; Crawford and Campanella 1991; Crawford et al. 1994 using the FE-computer program “PLAXIS V8”. As a constitutive soil model the so called soft soil creep model (SSCM) was used (refer to Chapter 3 for constitutive soil models). The average coefficient of consolidation was determined from the settlement measurements using the Asaoka 1978 method. Furthermore, an average value of the constrained modulus E_{oed} was estimated using Eq. 3.33 and the compression index C_c in order to determine the coefficient of permeability k required in the FE-computation with the help of Eq. 5.19. The soil parameters, geometry and load input parameters are summarised in Table 5.10.

Table 5.10. Parameters for FE-back analysis of the embankment of the Highway 99A, Vancouver, Canada

Parameter	Symbol	Calculation method	
		Analytical	FEM
Soil parameters	Void ratio	e_0 [-]	1.540
	Compression index	C_c [-]	0.540
	Swelling index	C_r [-]	0.150
	Coefficient of secondary consolidation	C_α [-]	0.035
	Angle of overall shear strength	ϕ'_s [°]	30.00
	Coefficient of pore pressure	A [-]	0.700
	Poisson's ratio	ν [-]	0.400
	Equivalent coefficient of consolidation	c_{ve} [m²/year]	70.00
Load and geometry input parameters	Coefficient of permeability	k [m/day]	-
	Net pressure	σ_0 [kN/m²]	91.0
	Stress relief due to excavation	σ_v [kN/m²]	11.0
	Pre-consolidation pressure	σ_{vor} [kN/m²]	85.0
	Layer thickness	H [m]	21.6
	Drainage path	l_d [m]	10.8
	Loading time	t_c [year]	0.85 (variable)

The comparison of the measured against the computed settlements is shown in Fig. 5.54. It appears from the figure that there is an excellent agreement between the measured and the FE-computed settlements. The FEM is also in a position to simulate very well the loading stages of the embankment fill.

**Fig. 5.54.** Computed and measured settlements of the embankment of the Highway 99A, Vancouver, Canada

5.8 Case history of settlement due to shrinkage

The one-story gas transfer station building in Constance city with a base area of $9.82 \times 9.24 \text{ m}^2$ (Fig. 5.55a) showed an excessive total and differential settlement,

although the load transmitted into the soft ground was marginal. The settlement measurements over a long period of time showed that the settlement did not come to rest and the building settled further with a rate of settlement that dependant on seasonal variations. The excessive settlement in particular the differential settlements subjected the gas pipelines around the walls to an additional tensile strains. As consequence the pipe lines was maintained and some of them totally replaced. However, the building continued to settle even after the maintenance causing a horizontal displacement and tilting of the building in the north west direction. The situation could not be explained by means of the classical settlement calculations, even with due considerations of the correction factors for in-situ case for the region.

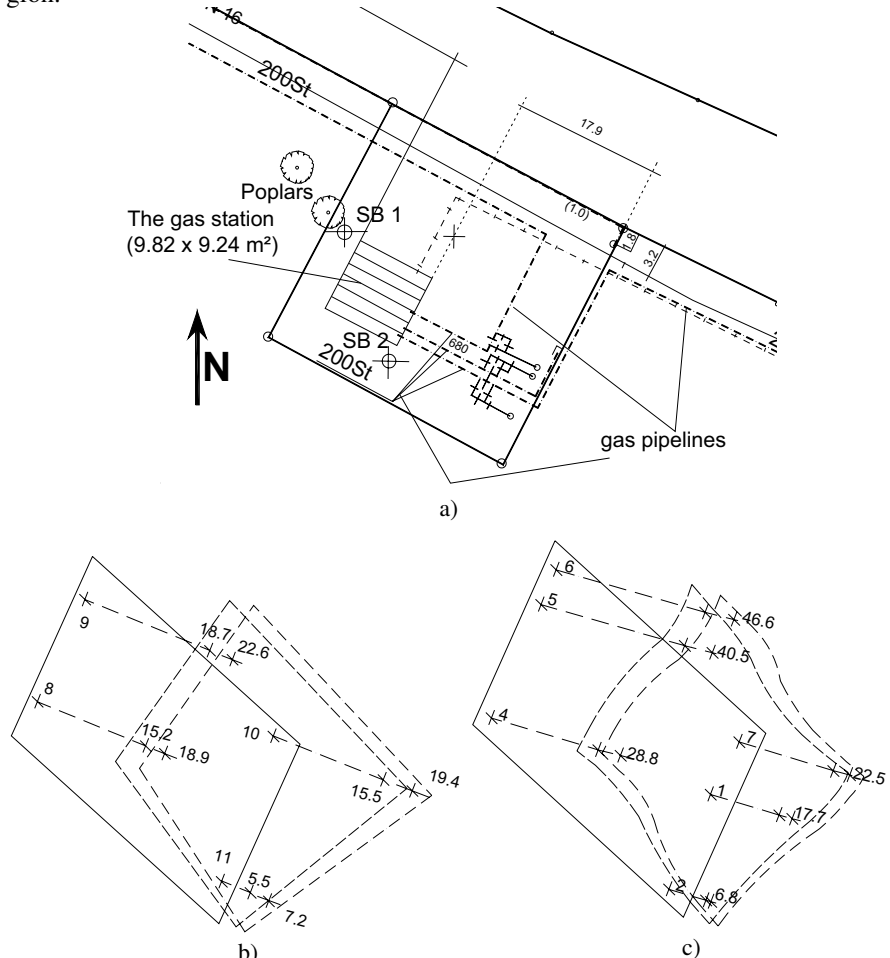


Fig. 5.55. a)The top view of the gas transfer station building and the gas pipelines; b) measured settlements (cm) in form of isometric view; c) measured relative settlements (mm) in the last one year in form of isometric view

As shown in Fig. 5.55b, a maximum total settlement of 22.6 cm was measured at the north-west corner of the building (point 9). This gives a differential settlement $\Delta s = 15.4 \text{ cm}$ in comparison with point 11 diagonally at the other corner. Fig. 5.55c also shows the relative settlement of the raft foundation within one year of time. A maximum relative settlement up to 4.7 cm was measured in a period of one year.

The first suspicion for the cause of the differential settlement was the two popular trees near the building in the north west direction (Fig. 5.55a). These type of trees are known of their deep root and require large amount of water for their growth. In order to clarify this suspicion, two boreholes (SB1 and SB2, see Fig. 5.55a) were drilled to a depth of 8 m below the ground surface. The two boreholes revealed an upper clayey fine to medium sand layer up to a depth of 1.2 m followed by a lacustrine clay to the end of the borehole. The boreholes show no variation in soil profile at the two location.

The determination of the natural water content of the soil at every meter depth showed that the water content of the lacustrine soil layer in SB1 is 3% lower than that in SB2 on average. This difference is nothing but due to the sucking of the water by the trees during the dry seasons.

In order to determine the volume change behaviour of the lacustrine soil layer, shrinkage limit test was conducted and the result shows a water content at the shrinkage limit $w_s = 18.6\%$. The shrinkage limit test shows not only the change in consistence from solid state to the plastic state, but also the volume change behaviour of the soil. Hence, from this test a bilinear relationship can be derived between the volume change of the specimen and its water content (Fig. 5.56).

For a natural water content difference $\Delta w = 3\%$, there is a volume change of $\Delta V = 0.74 \text{ cm}^3$ according to Fig. 5.56. In percentage, this volume change is about 3.9%. Assuming an influence zone of the roots of the tree up to 6 m depth, the one-dimensional compression of the soil layer can be approximated to 23 cm. Therefore, this shows that the settlement due to shrinkage of the soil is in the order of decimetres.

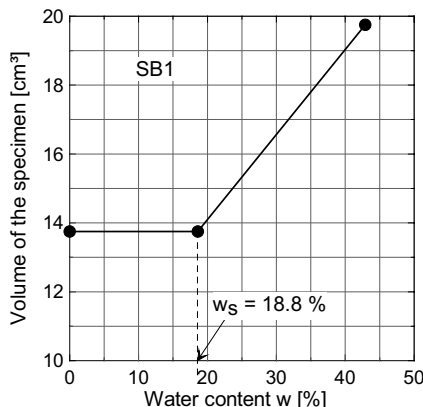


Fig. 5.56. Volume change – water content relationships

5.9 Safety of shallow foundations

Conventionally, the load-carrying capacity (ultimate limit state, ULS) and the settlement (serviceability limit state, SLS) of a shallow foundation are determined separately independent from each other. The verification of the bearing capacity assumes an ideal-plastic behaviour, whereby an ultimate load σ_{max} is calculated without the consideration of the deformation behaviour. On the other hand, the common settlement calculations are based on elastic behaviour and ignore the plastic deformations. A schematic presentation of both procedures are given in Fig. 5.57.

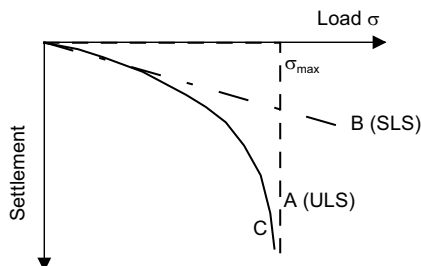


Fig. 5.57. Schematic presentation of the maximum load in ultimate limit state, ULS (ideal-plastic) and settlement in serviceability limit state, SLS (elastic)

According to Fellenius 1927; Bishop 1955, the total safety factor is defined as:

$$FS = \frac{\tau_f}{\tau_m} \quad (\text{Fellenius-law}) \quad (5.49)$$

where τ_f is the ultimate shear strength of the soil and τ_m is the mobilised shear strength due to an additional load from the structure.

Similarly, the safety factor can also be defined using the deviatoric stress q as follows:

$$FS_{(t)} = \frac{(q_f)_t}{q_t} = \frac{M \cdot p'_t}{q_t} \quad (5.50)$$

where q_t and p'_t are the deviatoric stress and the mean stress at a time t and M is the slope of the failure line. Fig. 5.58 illustrates both definition of the total safety factor (Eqs. 5.49 & 5.50). The required total safety factor is normally greater than 1.5. Refer to Section 5.6 for calculation of bearing capacity of a raft foundation.

The index t in Eq. 5.50 indicates the time dependency of the total safety factor. It is of great important for foundations on soft soils to know the development of the safety factor with time during the construction (loading) as well as during the consolidation phases in order to avoid a critical situations.

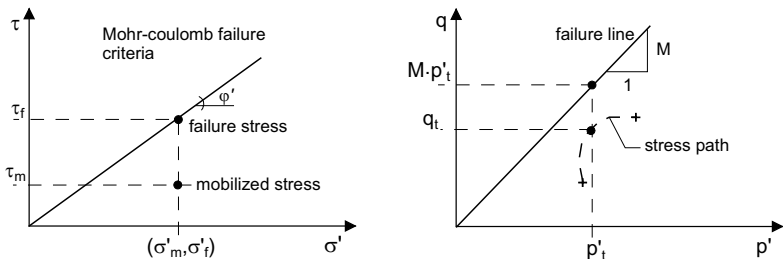


Fig. 5.58. Definitions of the safety factor: a) τ - σ' diagram; b) p' - q diagram

Fig. 5.59 shows the course of the safety factor with time for the project in case 3 (section 5.5.3). It appears from Fig. 5.59 that the building had enough reserve. A critical situation is already reported in section 5.6 for that project in case A, where the building would have come to failure nearly 1.5 years after start of the construction (see also Fig . 5.51).

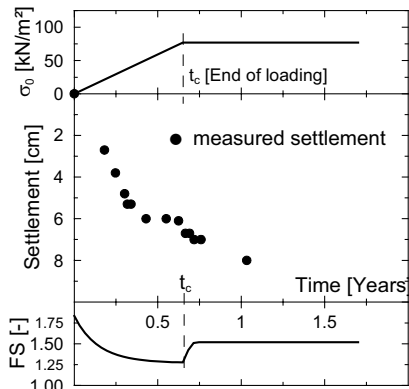


Fig. 5.59. The course of the safety factor of a raft foundation

5.10 Design of raft foundation

5.10.1 General

The common methods of analysis, i.e., the subgrade reaction and the elastic-half-space methods are also commonly used for analysis of raft foundations on soft soils provided that the underground is far from failure. The subgrade reaction method is developed based on the assumption that the contact pressure distribution is proportional to the settlement of the foundation and the underground can be simulated by several independent springs. The fundamentals of the elastic-half-space method is first formulated by Ohde 1942. It is based on the assumption that deflection of the raft conforms with the settlement trough of the underground.

Both methods may supply different results. An agreement of the results of both methods depends on the distribution of the applied load and the rigidity of the plate.

In practice a constant subgrade modulus for the whole width of the plate is frequently used as a first approximation. The subgrade modulus can be derived using the closed formulas (Eqs. 5.11 or 5.12) for settlement calculations. Setting $f \approx 1$ and applying the definition of the modulus of the subgrade reaction according to Winkler 1867, i.e.,

$$k_s = \sigma_0 / s \quad (5.51)$$

the subgrade modulus can be written in terms of constrained or deformation moduli and the width of the plate as follows:

$$k_s = E_{oed} / b \text{ bzw. } k_s = E_m / b \quad (5.52)$$

Since the first approximation in the analysis of a raft foundation does not represent the real condition in comparison to the elastic-half space method, it is a common practice to introduce 2nd approximation of the distribution of the subgrade modulus based on the contact pressure distribution according to Boussinesq 1885, where a higher value of the subgrade modulus is used at the edge areas and a lower value at internal area. Both approaches are schematically illustrated in Fig. 5.60. Increasing the subgrade modulus at the edge leads to a reduction of stress peaks arising from the theoretical equations for elastic half-space, which cannot occur due to yielding or flow of the soil at edges. Such reduction affects the contact pressure distribution up to a distance of 10 % of the foundation width measured from the edge of the plate (Schultze 1961). This is examined further in the following.

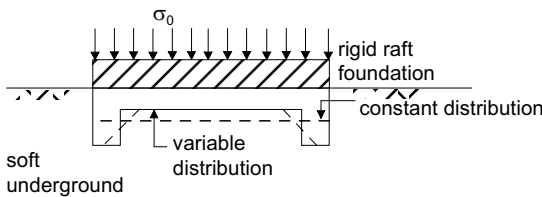


Fig. 5.60. Two approaches of the subgrade modulus method of analysis of raft foundations

5.10.2 Parameter study

The results of a parameter study for an idealised foundation and underground conditions shown in Fig. 5.61 are summarised in the following. The aim of the study is to show the extent of the influence of the soil stiffness on the flexural stress and settlement of the foundation.

The following variations are examined in the parameter study:

- Variant 1: constant subgrade modulus throughout the foundation width,

- Variant 2: variable subgrade modulus, in which its value is doubled at the edge areas (up to a distance of $0.1 \cdot b$ from the edge),
- Variant 3: the same as variant 2 but the subgrade modulus increased by factor 2.5 and 5.0 at the edge areas,
- Variant 4: subgrade modulus corrected on the basis of the elastic-half-space method,
- Variant 5: elastic half-space method.

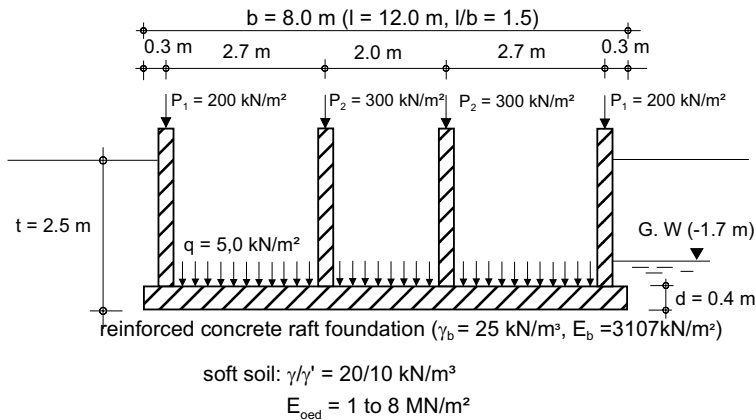


Fig. 5.61. An idealised foundation and underground conditions for a parameter study

The stiffness of the soft underground is described by the constrained modulus E_{oed} and it is varied between 1, 2, 4 and 8 MN/m^2 within each variant mentioned above. The settlements are calculated using Eq. 5.11 so that the corresponding subgrade modulus can be derived from Eq. 5.51. The calculated settlements and the corresponding subgrade moduli are summarised in Table 5.11.

Table 5.11. Subgrade moduli for an average contact pressure of $\sigma_0 = 132 \text{ kN/m}^2$

$E_s [\text{MN/m}^2]$	$s [\text{m}] (\text{Eq. 5.11})$	$k_s [\text{MN/m}^3] (\text{Eq. 5.51})$
1	0.294	0.45
2	0.147	0.90
4	0.074	1.80
8	0.037	3.60

Fig. 5.62 shows the results of the parameter study regarding the bending moments of the plate. The influence of the assumed different distribution of the subgrade modulus on the bending moments can clearly be seen in Fig. 5.62.

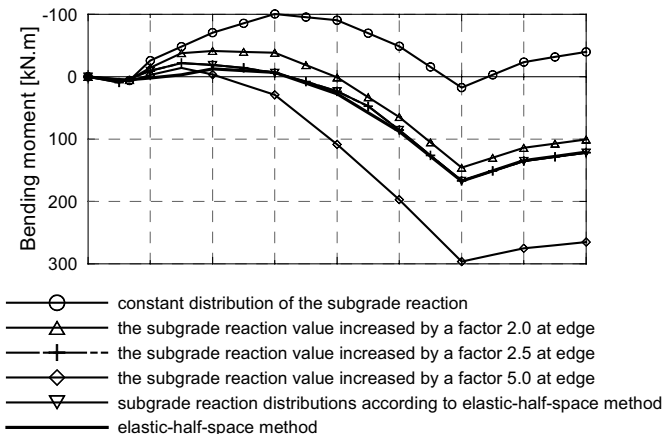


Fig. 5.62. Bending moments of a raft foundation by different distribution of subgrade reaction

In general, the following conclusions can be drawn from the parametric study:

- The magnitude of the modulus of the subgrade reaction has no significant influence on bending moment of raft foundation on soft soils,
- On the other hand, the distribution of the subgrade reaction will have a determining influence on bending moment of the plate,
- A good convergence to the result of the elastic half-space method can be achieved, when the average modulus of subgrade reaction (Eq. 5.51) is increased by a factor of 2.5 at the edge of the raft foundation,
- The assumed strip width 0.1b ($b = \text{width of the plate}$) at the edge of the plate, where an increase of modulus of the subgrade reaction is required, can lead to a realistic result.

5.10.3 Numerical analysis using the FEM

In addition to the parameter study in section 5.10.2, FE-computations using the program system “PLAXIS-3D-Tunnel” had been conducted. The soft underground is simulated by the so called constitutive soft soil creep model (SSCM), whereby creep effect is ignored in order to compare the results with analytical method, since in the later case the creep effect cannot be considered in the calculation.

The necessary constrained modulus is taken from the parameter study in section 5.10.2. Other input parameters such as the compression and swelling indexes C_c and C_s respectively are estimated from Eqs. 3.33 and 3.34. A comparative presentation of the various computation results is shown in Fig. 5.63. The distribution of the subgrade reaction is here assumed constant throughout the width of the plate.

According to Graßhof 1978 and Kany 1974, the most probable bending moment line may lie between the two extreme lines calculated using the subgrade re-

action and the elastic-half-space methods, which can also be confirmed to a large extent in Fig. 5.63.

Basically, the above example shows that the computation of the plate using the subgrade reaction method with constant distribution of the subgrade modulus throughout the width of the plate exhibits larger deviation from the FE-results. This is mainly because the subgrade reaction method does not take into account the influence of the pressure overlapping of the neighbouring loads and hence it cannot simulate the sagging type of contact pressure distribution. According to Amann and Breth 1977, these shortcomings can be eliminated, if a variable subgrade reaction is used over the stretch of the plate on the basis of the form of the settlement trough. Usually a linear increase of the subgrade reaction is used with double value at the edge of the plate (Fig. 5.60).

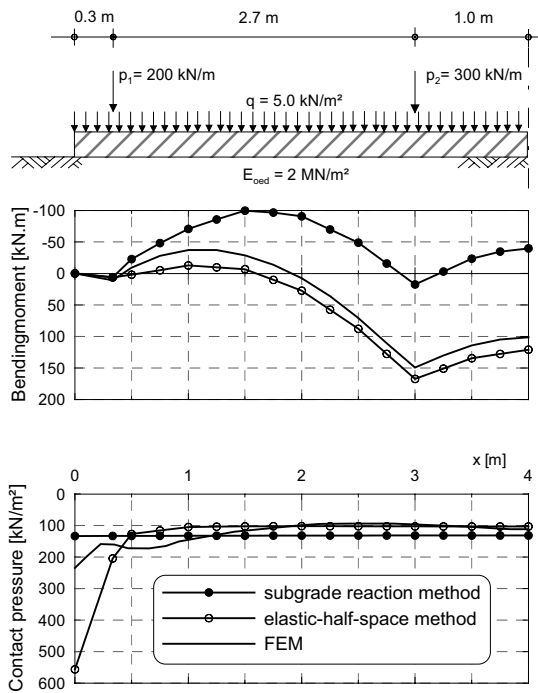


Fig. 5.63. Comparison of different methods of calculation of raft foundation on soft soil

It appears from Fig. 5.64 that a good agreement can be reached between the results of the FE-computation and the subgrade reaction method, if the subgrade reaction is increased by a factor of 1.75 and 3.5 at the edge and corner respectively for a strip width of 0.1·b and if it is redistributed at the centre of the plate according to Eq. 5.53a.

$$k_{s,e} \cdot A_e + k_{s,r} \cdot A_r + k_{s,m} \cdot (A - A_r - A_e) = k_s \cdot A \quad (5.53a)$$

where $k_{s,e}$, $k_{s,r}$, $k_{s,m}$ are the modulus of the subgrade reaction at the edge, at the corner and in the middle of the plate, and A_e , A_r , A are the corresponding surface areas. The corresponding values of the the subgrade moduli and areas for the example in Fig. 5.64 is given as follows:

$$2.45 \cdot 2.56 + 1.225 \cdot 26.88 + 0.7 \cdot 66.56 = 0.9 \cdot 96 \quad (5.53b)$$

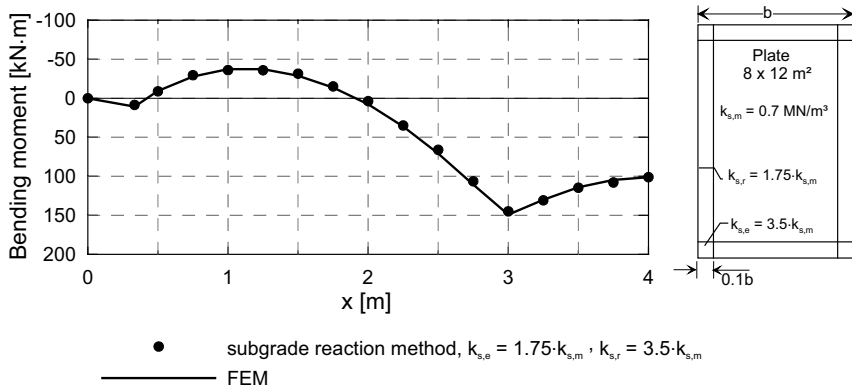


Fig. 5.64. Comparison of the FEM with the modified subgrade reaction method

5.10.4 Verification of the modified subgrade reaction method on selective projects

General

The recommended modified subgrade reaction method of analysis of raft foundations on soft soils in section 5.10.3 is examined once again in the following based on practical projects. For this purpose two projects, namely the projects in case 3 and 7 in section 5.5.3 are selected.

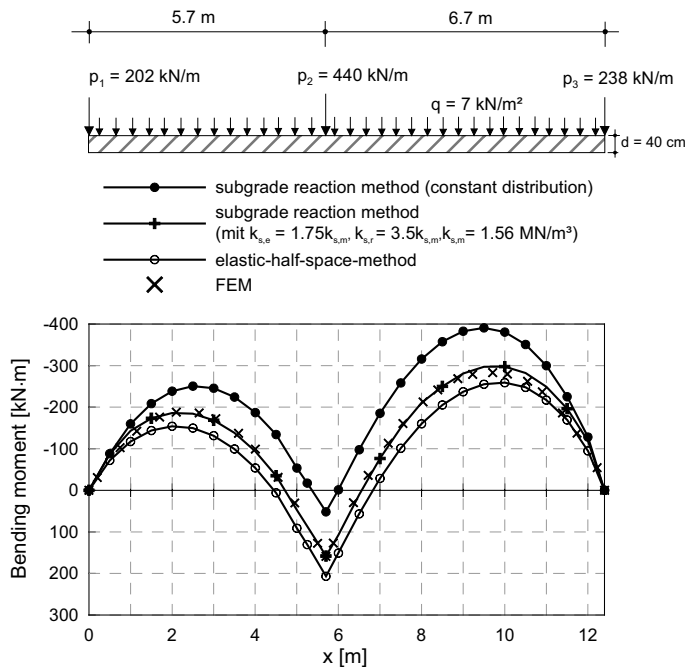
Case 4 (section 5.5.3)

The foundation at this project consists of a reinforced concrete raft of rectangular shape and it supports three walls in the longitudinal direction. For further information on boundary and underground conditions (see section 5.5.3). For the determination of the mean value of the subgrade reaction using Eq. 5.51, the end settlement must be first extrapolated from settlement measurements. The input parameters for the numerical and analytical methods are summarised in Table 5.12.

Table 5.12. Soil parameters used in the comparative analyses of the project 4

Method	Parameter	Remarks
Subgrade reaction	$k_s \approx 1900 \text{ kN/m}^3$	$s_\infty = 4.1 \text{ cm}, \sigma = 77.5 \text{ kN/m}^2$
Elastic-half-space	$E_s = 4000 \text{ kN/m}^2$	$E_m = E/\mu, \mu = 0.7$
Finite element	$C_c = 0.13$ $C_s = 0.03$ $C_B = 0.003, C_\alpha = 0.0015$	$C_\alpha = C_B/(I+e_0)$, with $e_0 = 0.9 \sim 1$ for lacustrine clay

A comparative presentation of the bending moment lines of the raft foundation calculated using the different methods are shown in Fig. 5.65. As it can be seen from the diagram, the subgrade reaction method with constant value of the subgrade modulus fails to give a comparable bending moment with the FEM. However, if a modified subgrade reaction distribution ($k_{s,e} = 1.75 \cdot k_{s,m}$, $k_{s,r} = 3.5 \cdot k_{s,m}$) is used, a better agreement can be achieved between the two methods as shown in Fig. 5.65.

**Fig. 5.65.** Comparison of bending moments according to the different method of analyses, case 4 (section 5.5.3)

Case 7 (section 5.5.3)

The foundation at this project is made up of reinforced concrete raft of rectangular shape and it is stiffened in both directions by cross walls as shown in Fig. 5.66 (left). The final settlements at each measuring points are extrapolated from the measured settlements (Fig. 5.66 (right)). The settlement trough shows almost a flat curvature indicating that the raft foundation behaves almost rigid.

A summary of the input parameters for the comparative analyses are given in Table 5.13. The load from the superstructure are simplified as line loads in longitudinal and traverse directions.

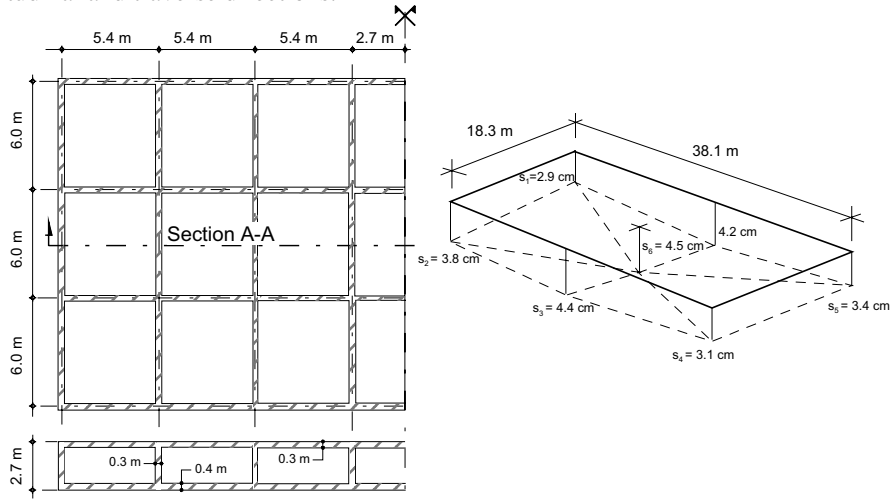


Fig. 5.66. Plan and cross-section of a raft foundation and measured settlement, project 7

Fig. 5.67 shows the bending moment lines of the raft foundation at section A-A calculated according to the different methods. It can be seen from the diagram that the bending moment lines from the modified subgrade reaction and the FEM match very well. On the other hand, the subgrade reaction method with constant distribution of the subgrade modulus gives a higher span moment and a lower support moments than the FEM.

Table 5.13. Soil parameters used in the comparative analyses of the project 7

Method	Parameter	Remarks
Subgrade reaction ($k_s = \text{constant.}$)	$k_s = 1640 \text{ kN/m}^3$	$s_\infty = 4.37 \text{ cm}, \sigma = 71.5 \text{ kN/m}^2$
Modified subgrade reaction	$k_{s,e} = 4627, k_{s,r} = 2314, k_{s,m} = 1322 \text{ kN/m}^3$	$k_{s,e} = 1.75 k_{s,r} = 3.5 k_{s,m}$
Finite element	$C_c = 0.12, C_s = 0.025$ $C_B = 0.003, C_\alpha = 0.0027$	$C_\alpha = C_B/(1+e_0)$, with $e_0 = 0.85$

The settlements according to the different methods are plotted against the measured settlements in Fig. 5.68. It is remarkable to observe that the settlements calculated using the constant subgrade modulus show a convex form whereas the settlement lines using a modified distribution of the subgrade modulus show a concave form.

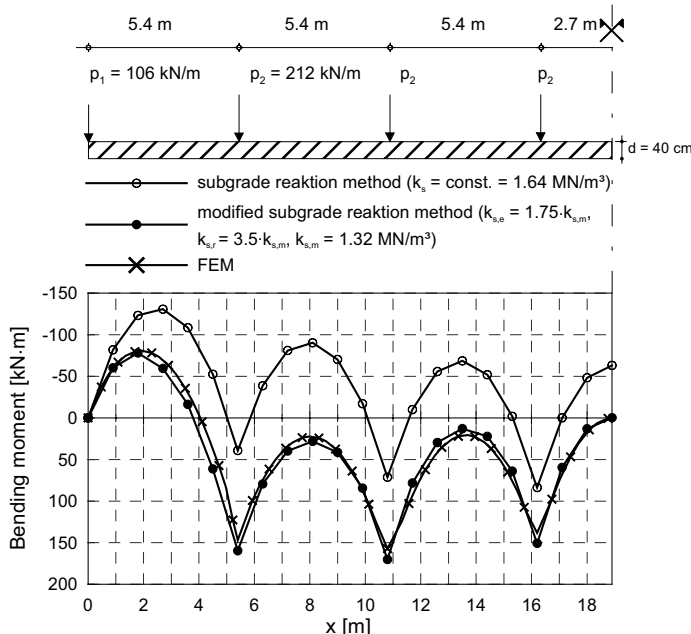


Fig. 5.67. Comparison of the bending moments at section A-A according to the different methods of analyses, case 7 (Section 5.5.3)

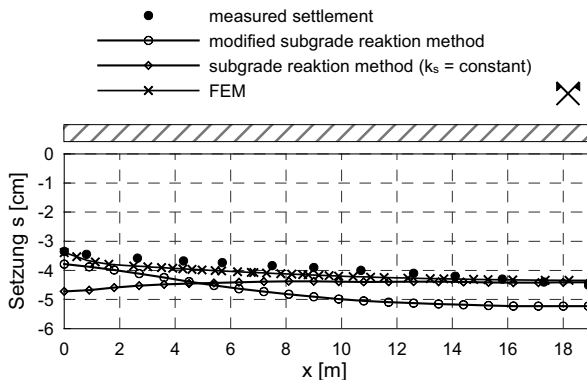


Fig. 5.68. Comparison of the measured and calculated settlements at section A-A, case 7

The settlement trough determined using the FEM shows the best agreement with the end settlement extrapolated from the settlement measurements. On the other hand the settlement using the modified distribution of the subgrade modulus show relatively larger values than the measured settlements, but it runs parallel to the measured settlement line.

5.10.5 Effect of creep of the soil on flexural stress of a plate

For the two projects in cases 4 and 7 (Section 5.6), a comparative FE-computations has been carried out with and without the effect of creep of the soft underground. The bending moment lines are determined at the end of the consolidation period and after 30 years. The result show no significant effect of the creep of the soft soil on the flexural stress of the raft foundations.

5.11 Summary and recommendations

From the foregoing investigations and huge experiences gathered from numerous practical projects, the following recommendations are given for the prediction of settlements on the basis of soil exploration and laboratory test results as well as the design and analysis of shallow foundations (spread foundations, raft foundations, box-foundations, etc.) on soft soils (see also Soumaya 2005):

1. Determination of compression parameters:

- In estimating the compression parameters of soft soils from the standard oedometer tests, the compression at the end of the primary consolidation (EOP-compression) are recommended instead of the standard compression after 24 h,
- It is advisable to determine the EOP-compression using Taylor's method, because the EOP-compression determined according to Casagrande may contain additional creep compression, thus may underestimate the stiffness of the soil,
- A realistic determination of the compression parameters can be effected using the EOP-consolidation tests with a small load increment (e.g. $\Delta\sigma/\sigma = 0.1$), but it is time consuming,
- As much as possible a constant rate of loading consolidation test should be used for the derivation of the compression parameters, because this type of test can better simulate the true in situ load boundary conditions. A suitable rate of loading for instance for the lacustrine soil in southern Germany lies between 70 and 140 kN/m²/h.

2. Determination of settlement and bearing capacity:

- If the settlement of shallow foundations on soft soils is calculated using the compression parameters derived from standard oedometer tests, the

settlement should be corrected by a factor μ , for example, $\mu = 0.70$ for lacustrine soft clay in southern Germany,

- For the description of the time-settlement behaviour of the soft soil, it is recommended to use the empirical values of the coefficient of consolidation c_v derived from settlement observations, because c_v -values from standard consolidation tests on lacustrine clay scatter extremely and supply no reasonable prediction,
- If a soft subsoil is quickly loaded (e.g., embankment construction), the influence of the load rate on the compression of the underground should be taken into account, which cannot be considered with the conventional methods of calculations.
- During the transfer of the load from superstructure to the soft underground, the bearing capacity of the underground is to be verified for all drainage conditions of the respective time point, in order to avoid large unrecoverable settlements damage of the structure. If necessary, it recommended to consider the partial drainage conditions.

3. Analysis and design of raft foundations

- The design of a relatively rigid raft foundation on soft soils can either be made using the elastic-half-space method or the modified subgrade reaction method with a variable distribution of subgrade modulus ,
- As modified design approach, the modulus of subgrade reaction can approximately be increased by a factor of 1.75 and 3.5 at the edge and corner areas respectively with a strip width of $0.1 \cdot b$ (b = width of the plate) and correspondingly reducing its value at the centre area (see Fig. 5.64) in order to obtain a realistic section forces of the plate.

6 Pile foundation

6.1 Introduction

Pile foundation is a broader field, therefore only a selective part is going to be presented in this chapter. An overview of the pile foundation can be found for example in Tomlinson 1994; Kempfert et al. 2003. Hence, this chapter focuses specially on questions relating with pile foundations in soft underground. Independent from this, however, an overview of pile systems has been compiled, whereby some part of the contents has been taken from Kempfert et al. 2003.

Piles, as an important type of deep foundation, are generally used to transfer axial and horizontal building loads over low strength soil layers or through water body into load bearing strata. Typical applications are:

- single pile foundations for the transfer of single loads
- pile group foundations for surface loads, and
- combined pile-raft-foundations as a special type of pile foundation, with additional transfer of load through contact pressure between the raft and the soil between the piles.

The requirements for a pile or a pile foundation are governed primarily by the type of structure, the construction methods and the low strength subsoil conditions. Only actual piles will be discussed in this chapter, excluding construction methods such as vibrated concrete piles, slurry trench elements, caisson foundations, or columns constructed by jetting methods. Some information on column type foundation can be found in chapter 7.

A long tradition exists in Germany in applying codes to the design and construction of various pile types. In the mean time several European Codes have now been developed on pile foundations, such as:

- EN 1536: Bored piles
EN 12 699: Displacement piles
EN 14199: Micropiles
EN 12 794: Precast concrete piles

Recommendations on design and dimensioning of pile foundations can be found in the following codes:

- EN 1997-1: Geotechnical Design Part 1: General Rules (Eurocode).
EN 1993-5: Design of steel structures Part 5: steel sheet pile walls and steel piles.
DIN 1054: Ground verification of the safety of earthworks and foundations (German national code).

Other publication of importance on pile foundations are:

- Subcommittee on field and laboratory testing: Axial Pile Loading Test – Part 1: Static Loading (ISSMFE 1985).
- Recommendations for pile foundation (DGTT AK 2.1 2006).
- Guidelines for the design, dimensioning and construction of combined pile-raft-foundations (CPR guideline) (DIBt-DGTT-DAFStB 2002).

In the various countries different safety concepts have been used for the design of pile foundations based on total and/or partial safety factors. In the following sections, partial safety concepts will be considered, which applies to the entire design of engineering structures within Europe. However, country specific differences has been anticipated, which can be referred to where appropriate, because there exist, for example, years long experience with the regulations of DIN 1054 in Germany. This approach is approximately equivalent to the design approach 2* of European code (see also section 1.2)

6.2 Pile types and construction methods

6.2.1 Selection of appropriate pile type

Table 6.1 contains a summary of pile types with a comparison of their advantages and disadvantages. Apart from economical considerations, the selection of the pile type also depends on the soil and groundwater conditions, building loads, space requirements, proximity to buildings and the sensitivity of the structure to settlement..

Table 6.1. Advantages and disadvantages of different pile types

Pile Type	Advantage	Disadvantage
Displacement piles		
Timber pile	Good drivability, high elasticity, easy to handle and to cut, high life span below water, relatively inexpensive	Fast destruction due to rotting in air, not drivable in dense soil, limited load bearing capacity and length
Steel pile	High material strength and elasticity, large choice of different profiles, little damage during transport; can be easily extended, base reinforcement by wings possible; good driving characteristics, little vibration during driving, can be connected easily; batter up to 1:1; length depending upon driving resistance	Relatively high material costs, danger of corrosion, danger of abrasion by sand, H-sections can deflect or twist during driving

Table 6.1. Continued

Pile Type	Advantage	Disadvantage
Reinforced concrete pile	Production in practically any length and strength; resistant to sea water; good soil compaction during driving; easy to connect with building; high load bearing capacity; batter up to 1:1	Heavy and difficult to handle, sensitive to bending, e.g. during transportation hardening and installation; danger of fracture; heavy driving equipment necessary; problems when encountering obstacles; stronger vibrations during driving and possibly noise disturbance
Prestressed concrete pile	Same as for reinforced concrete piles; high resistance to buckling and bending, high load bearing capacity; batter same as for reinforced concrete pile	Same as for reinforced concrete piles
Cast-in-place displacement piles	Good compression of the surrounding soil and thus high load bearing capacity, low settlement, expanded base possible; length can be adapted to requirements	Noise and vibration during driving; danger of damaging fresh neighbouring piles; limited batter, problems when encountering obstacles; sensitive to shear forces; quality depends on experience of crew, particularly in granular soils with high groundwater; lengths up to approx. 25 m; batter up to approx. 4:1
Full displacement bored piles (Screwed cast-in-place piles)	High load bearing capacity due to displacement and compaction of the surrounding soil; high skin friction due to rough or helical pile shaft; little removal of soil low risk of settlement of neighbouring buildings; little noise and vibration during installation	High torque required, production problems similar to bored piles; problems with drilling obstacles (no chiseling possible); limited batter up to approx. 4:1
<hr/>		
Bored piles		
Bored pile	Largely without vibration and noise; during drilling control of soil conditions and therefore optimal adjustment of length possible; flexible working height (e.g. under bridges or roofs); large depths with large diameters possible; drilling obstacles can be handled e.g. through the use of chisels; expanded base possible; normal lengths (dependent on the drilling procedure) up to approx. 30 m; larger lengths possible with telescopic drilling	Loosening of soil possibly during installation, quality very dependent on manufacturing process and operating personnel; possible problems or risks: placement of concrete under water (tremie method) particularly for piles with small cross sections difficult; during pulling of casing development of vibration or pulling of reinforcement can be possible; hydraulic failure possible, if outside water levels are higher than in casing; During boring without casing (in unstable ground support with slurry) danger of the loose rock falling into the drill hole; limited batter up to approx. 4:1

Table 6.1. Continued

Pile Type	Advantage	Disadvantage
Micro piles	Depending on type of micro pile Largely without vibrations; very flexible, any inclination possible; GEWI piles easily extendable by sleeve connections; relatively high load bearing capacity by post grouting	Cannot tolerate bending; in very soft soils danger of buckling

Fig. 6.1 illustrates the allocation of the pile types to the corresponding European Codes for pile installation.

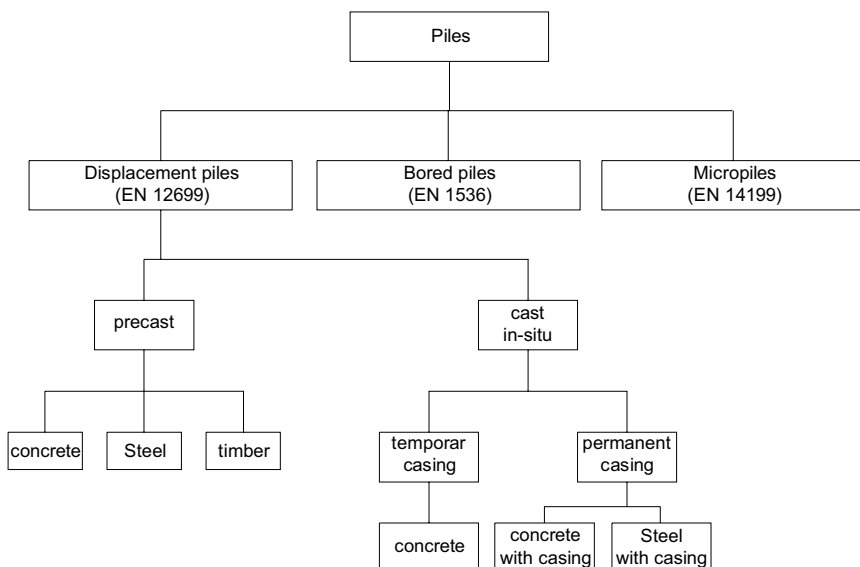


Fig. 6.1. Overview of the pile types; bored pile according to EN 1536, displacement pile according to EN 12699 and micropiles according to EN 14199

6.2.2 Displacement piles

General

The basic principle of displacement piles (driven piles) is based on the assumption that the soil displaced by the pile or the driven casing increases the lateral stresses in the surrounding soil generally causing:

- densification and prestressing in cohesionless and unsaturated cohesive soils and
- excess pore pressures in saturated cohesive soils.

Basic information on displacement piles can be found in EN 12699 and Van Weele 2003.

Timber piles are only used today for small buildings (Fig. 6.2) or for temporary structures, such as form work and crane foundations, and will therefore not be discussed in this chapter.



Fig. 6.2. Floating timber pile foundation near lake shore for a small industrial building

Prefabricated steel piles

a) Steel piles in general: Steel piles are either the original rolled steel sections or assembled steel sections. They can be driven to a maximum inclination of 1:1. Steel piles can be grouped on the basis of their cross section into H-piles, pipe piles and square shaped piles. There are also piles made from various sheet pile sections and piles with and without closed end (Fig. 6.3). The piles can be extended by splicing if required. Today, piles are typically spliced by welding. The splices must have the same compressive, tensile and bending strength as the original section.

If fin like expansions are used to reinforce a pile along the shaft or the base, they must be arranged symmetrically and welded to the pile. The welds must be strong enough to resist the expansion forces developing during the formation of the soil plug and when high driving resistances are experienced. In piles with an expanded base the formation of a soil plug must be ensured by using appropriate construction measures. Construction details for an expanded pile base, as derived from tests, can be found in De Beer 1986. In granular soils the bearing capacity can be increased by more than 100% using these methods. In stiff clays cross-section expansions should be geared more towards an increase of the shaft resis-

tance rather than end bearing; open sections with larger shear area should be selected. Today it is generally more economic to use longer single section piles than piles with costly base expansions. For steel piles installed in aggressive soil or water, increased corrosion must be expected. Protective coatings or special alloys may delay the corrosion process.

Because of the high strength of steel piles, damage only occurs under extreme loading, e.g. during driving in hard or bouldery soil layers such as very coarse gravel or glacial tills. Profiles which are too light can roll up along their base or can become twisted along their axis. For driven steel pipe piles stabilizing cross braces across the base are only required in exceptional cases, e.g. in particularly dense or stiff soils they might not be needed. Base expansions therefore should always be combined with cross braces.

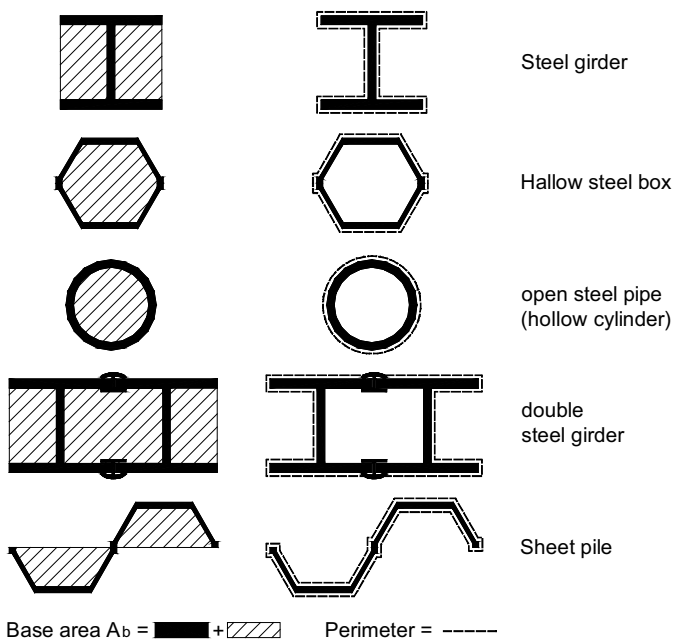


Fig. 6.3. The pile base and surface friction area of steel piles



Fig. 6.4. Anchor pile for sea wall, driven with an hydraulic pile driver

b) Ductile cast iron piles: Ductile cast iron is a highly resistant material, which provides good driveability and high corrosion resistance for piles. Compared to steel St. 37, ductile cast iron is chemically and mechanically very stable. The ductile properties are due to spherical graphite nodules, which ensure a more even stress distribution and therefore a more even load transfer than the laminated graphite in gray cast iron. The original brittle material is transformed into a material which can sustain very high loads.

The normal length of individual pile elements is 6.0 meters. Shorter elements are also available for installation in restricted spaces. With simple conical socket joints almost any pile length can be achieved. During driving a rigid connection will be produced which exhibits the same strength in tension and in compression as the actual pipe section. Due to the low weight of ductile cast iron pipe piles they can be installed with light and flexible equipment causing minimal noise and vibrations (Hettler 1990). To improve their structural strength, the piles can be filled with concrete after removal of the soil plug. The bearing capacity can be increased by external grouting. Working loads for externally grouted piles are between 300 to 700 kN for a pile diameter of 118 mm and up to 1300 kN for a diameter of 170 mm. The piles can be used as tension piles if they are filled with concrete containing tensile reinforcement.

c) Franki type steel pipe piles: An installation method was recently developed, where steel pipe piles can be installed with minimal noise and vibration using a procedure similar to that of cast-in-place displacement piles (Franki type piles). The steel pipe piles are driven in sections with a small drop hammer inside the pile casing. After reaching the required depth the piles can be loaded immediately, as the steel tubing remains in the ground. If necessary, the piles can be filled with reinforced concrete (See Fig. 6.5). These steel pipe piles can be installed with small specialized equipment, which allows working in limited space conditions. If, for example, head space is limited inside buildings, several short pipe sections can be

successively installed and spliced by welding. In suitable soil conditions an expanded base can also be produced to increase the end bearing capacity. Allowable bearing capacities for piles with 4.0 m embedment in a load bearing granular soil may range between 250 and 300 kN for a pile diameter of 270 mm and between 450 and 480 kN for a diameter of 360 mm.

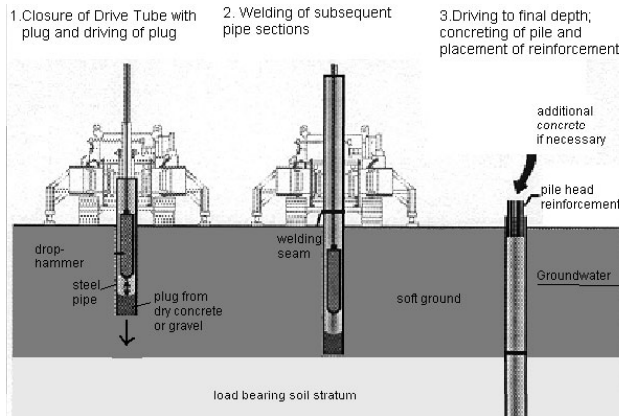


Fig. 6.5. Installation method of a Franki type steel pipe pile, (after company brochure) and example of installation with limited headroom

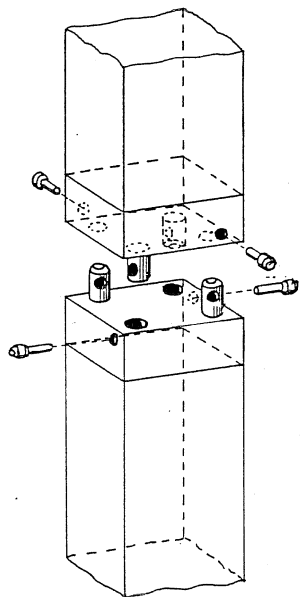
Precast concrete piles

Prefabricated reinforced concrete piles may be solid or hollow with square, rectangular, polygonal or circular cross sections, with or without prestressing. The following requirements must be considered in accordance with EN 12794:

- The longitudinal reinforcing bars should be at least 8 mm in diameter with at least one bar in each corner of rectangular cross sections or at least six bars distributed over the perimeter of circular cross sections.
- In the area of the pile head, transverse reinforcement should be arranged over a length of at least 750 mm with a minimum of nine stirrups.
- In the area of the pile base, transverse reinforcement is to be arranged over a length of at least 200 mm with at least five stirrups.



Fig. 6.6. Driving of a reinforced concrete piles on a batter with an hydraulic pile driver (photo: "Centrum Pfähle")



a)

b)

Fig. 6.7. Splicing system "Centrum Pfähle". a) detail of system, b) spliced pile section

- In the remaining portion of the pile shaft, transverse reinforcement should be equally distributed with a minimum distance between stirrups of 300 mm.

The pile lengths can be adapted to local conditions by using various types of splicing systems, which permit different lengths of prefabricated elements to be joined during the driving process. A typical splicing system is shown on Fig. 6.7. The splices must be designed for the same load as the remaining pile shaft. Such piles are particularly suitable for small construction sites, and for locations where the pile lengths cannot be exactly predicted. Another major advantage is, that low headroom pile drivers can be used, allowing installation in areas with limited space.

Prestressed Concrete Piles have been used extensively in the Netherlands (see Van Oudenallen 1999). The main requirements are:

- Minimum longitudinal reinforcement is approximately 0.5% of the pile cross section for shorter piles and 0.6% for longer piles.
- Transverse reinforcement is required only in the pile head and pile base area, and not over the entire length.

According to DIN 12794 the cross sectional area of the prestressing steel should be greater than 0.1% of the cross sectional area of the pile shaft for pile lengths less than 5.0 m and greater than 0.2% for pile lengths > 10 m. Clustered prestressing elements are not permitted. The spacing between the prestressing bars must be wide enough to allow placement and compaction of concrete to be carried out satisfactorily and to achieve a good bond between the concrete and the prestressing bars.

Concrete piles manufactured by centrifugal force are hollow in their center. At the same time excess water and fines are transferred towards the center, resulting in a very good grain size distribution near the pile surface, which constitutes the load bearing portion of the cross section. Depending on the application, conical or cylindrical piles are manufactured with external diameters of 240, 350, 450 and 600 mm. All of these piles can be spliced by welding of the prestressing bars. Good quality control of the installed piles is possible by inspection of the hollow core using mirrors.

The highest risk of damaging prefabricated piles occurs during transport and driving. Transverse cracking and microfissuring can occur due to improper handling. Transverse cracks can be identified by visual inspection on the construction site and the damaged piles can be discarded. This is not possible for microfissures. During pile installation the number and size of cracks and fissures can potentially increase causing corrosion of the reinforcement and spalling of the concrete due to penetrating groundwater. According to Van Weele 1994 considerable tension forces can develop in heavy piles, during driving with light drop hammers, particularly when ram helmets with hard packings are used and soft layers are penetrated. Tension cracks may then develop (Kempfert et al. 2003).

Pressure grouted displacement piles

Pressure grouted displacement piles are prefabricated piles with an extended base. The resulting annulus along the shaft is pressure grouted during installation. In the past, before the termination of the respective patents, this type of pile was known as an MV-pile. Today these piles are called vibro injections piles, or RI or RV-piles. RI-piles are used in tension under cyclical loads and also occasionally for compressive loading (Schmidt and Seitz 1998). They consist of steel sections (steel St 37 and St 52) with a collar welded to the lower end (Fig. 6.8). Two injection tubes are attached along the flange web transitions of each pile. Because grout is injected during the vibration process, driving is easier and a tight contact with the surrounding soil can be achieved with time. Typically, the grout consists of a water cement mix with the addition of small quantities of bentonite. During load tests very high ultimate tension capacities of approximately 2000 to almost 5000 kN were recorded (Brem and Wooge 1997).

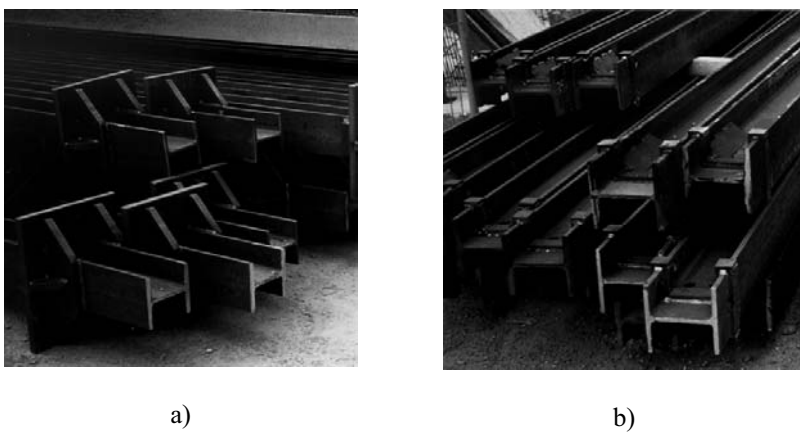


Fig. 6.8. a) RI-pile heads, b) RI-pile shoes

Cast-in-situ concrete displacement piles (Driven cast-in-situ concrete piles)

Two major types of cast-in-place concrete displacement piles can be identified on the basis of the driving process:

- Driving inside the casing (Franki type pile)
- Direct driving of casing (Simplex type pile)

Both pile types and their construction methods are shown in Fig. 6.9. In the Franki type method (Compacto Piles) the steel casing is closed at the base by a concrete or gravel plug. The casing diameter ranges between 335 and 610 mm. A single drop hammer is used. In the Simplex type method a thick walled steel casing protected by a ram helmet is driven directly into the ground. The driven casing, with a diameter between 340 and 720 mm, is closed by a base plate. For the

Franki type pile an expanded base is normally created in the ground. A partial driven base expansion can also be achieved with the simplex pile. A maximum inclination of 4:1 is possible for both pile types.

Due to compaction during driving of the concrete shaft the shaft resistance can be also increased. In soft ground only plastic concrete should be used for the shaft. In fine grained soils with $c_{u,k} \leq 15 \text{ kN/m}^2$ concrete should not be placed against the soil, but should be supported during placement by a liner or other appropriate measures. According to EN 12699 the minimum reinforcement is 0.5% of the pile diameter. For longitudinal reinforcement at least four bars with a diameter of 12 mm should be used, with a clear distance of at least 100 mm between the longitudinal bars of the reinforcing cage. For aggregates with a maximum grain size of 20 mm the minimum clear distance can be 80 mm. The minimum diameter of the transverse reinforcement should be 5 mm.

A new variation of driven cast-in-place concrete piles is the so called adhesion bond pile. The initial construction is similar to the Franki type pile with the creation of an expanded base. However, during placement of the soft concrete in the pile shaft, the casing must not be pulled, and subsequently a steel section is placed into the fresh concrete and driven through the completed expanded concrete base to the required depth. The steel section serves as an extension of the pile in dense sand as well as reinforcement to the pile shaft. Sufficient concrete cover is given due to the wall thickness of the driven casing. The adhesion bond pile has the same capacity in compression as a Franki type pile of the same concrete area. During tensile loading the steel section connects the expanded concrete base to the shaft, thus activating an additional soil wedge above the base.

Driven cast-in-place concrete piles are very susceptible to deficiencies in workmanship. Damage may occur when concrete is placed too late or when pulling of the casing has been delayed. Because the concrete is no longer plastic at this stage and has become very stiff it will stick to the inside wall of the casing and during pulling it will be dragged up without flowing back to its original position. The concrete will crack and the pile surface will be damaged. As a result, the compressive strength of the concrete is reduced and the corrosion protection of the reinforcement is no longer guaranteed (Hilmer 1991).

Other causes of damage may include:

- Low consistency of the concrete, with for example insufficient workability.
- Sloughing of soil and necking of concrete during placement causing exposure of the reinforcement ("cauliflowering") when the overlying column of concrete is too low to provide the necessary excess pressure to support the exposed soil face.
- An excess head of groundwater pressure of approximately 20 meters in coarse sands and gravel, which may cause hydraulic failure of the concrete plug into the driven casing.
- Too small a distance between adjacent piles. Due to compaction and displacement of the soil during driving, previously installed piles may be uplifted, damaging fresh concrete. The sequence of driving should be such, that previously installed piles will be affected as little as possible.

- Damage to the reinforcement cage during compaction of the concrete. Due to driving inside the casing, the reinforcement can be bent and pushed sideways into the surrounding soil (Hilmer 1991).

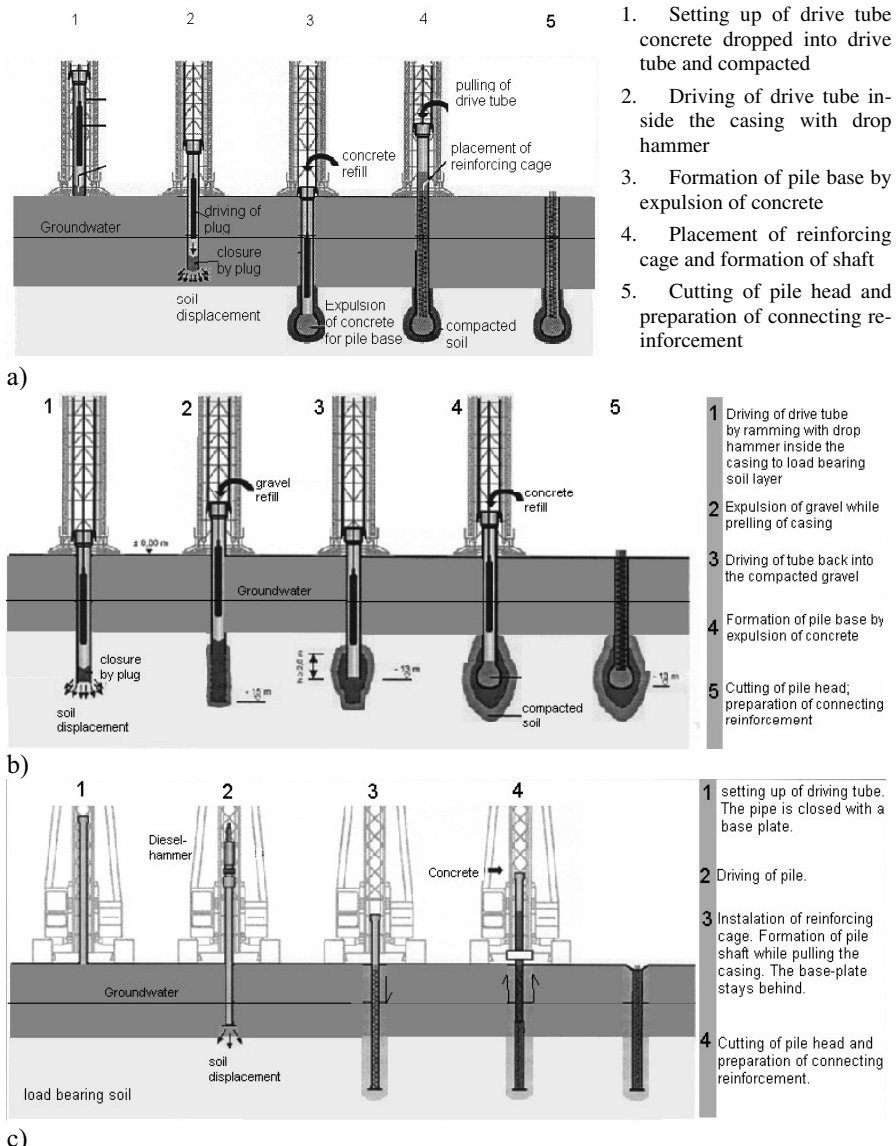


Fig. 6.9. Installation method of driven cast in place concrete piles (compacto piles): a) standard Franki pile, b) Franki pile with gravel precompaction, c) Simplex pile (company brochure of Franki Foundation)



Fig. 6.10. Installation of Simplex piles
(photo: Franki foundation)



Fig. 6.11. Damaged pile shafts of a driven cast in place concrete pile group for a pier foundation

Installation of displacement piles

Displacement piles can be installed by driving, vibrating, jacking or screwing, with complete displacement of the soil. Cross sectional area, length, type of driven material and soil conditions are particularly important with respect to the choice of driving technology. Information on methods and equipment can be found for e.g. in Kempfert et al. 2003. The pile installation can be further optimized by dynamic pile testing during driving (see section 6.4.3). Preferably drop hammers and dynamic hammers should be used, because with these methods the driving energy can be clearly evaluated. This is particularly important, if driving criteria is derived from pile load tests.

The pile spacing must be sufficiently large and the driving sequence such that adjacent piles or structures will not be damaged due to driving related compaction and displacement of the soil. The minimum spacing should be $\geq 3D_s$ for displacement piles without an expanded base and $\geq 2D_b$ for piles with an expanded base,

baut not less than 1.0 meter. For cast-in-place-displacement piles, EN 12699 suggests that the piles should not be installed within a distance of six pile diameters to adjacent piles without a permanent casing, as long as the concrete has not reached sufficient strength, or unless sufficient experience has been obtained on the construction site. As long as the soil within the length of the shaft has a critical undrained shear strength of $c_u \leq 50$ kPa, the distance between freshly installed cast-in-place-displacement piles without a permanent casing should be increased as shown on Fig. 6.12. When dry compacted concrete is used for the pile shafts, the distances obtained from Fig. 6.12 can be reduced by 50%.

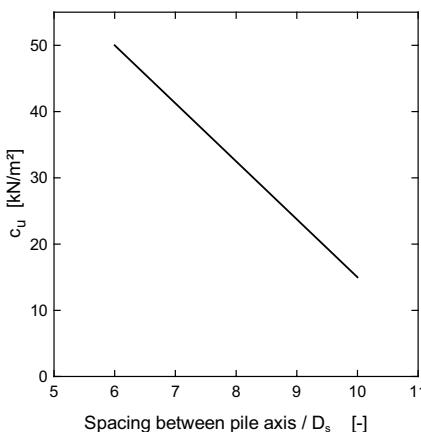


Fig. 6.12. Minimum distance between fresh driven cast-in-place concrete piles without permanent casing, after EN 12 699

Prefabricated piles can be installed with vibrating pile drivers in gravels and sands with rounded grain shapes. This method is not suitable in gravels and sands with angular grains or in dry and highly cohesive soils, or in dense soils where particle rearrangement is not possible. In well graded soils in particular densification near the base of the pile may be such that vibratory driving must be discontinued. The vibratory method is most efficient in soils with high water contents. If possible, high frequency vibrators, with frequencies between 30 and 50 Hz should be used to limit the occurrence of damaging resonance effects on buildings. Maximum amplitudes normally occur during startup and shut down of vibratory pile drivers. Equipment with controllable centrifugal forces should therefore be utilized.

In dense to very dense granular soils and stiff to hard cohesive soils pile driving is very difficult and is often not possible unless special methods as listed in Table 6.2 are applied.

Table 6.2. Suitable driving aids in different soil types

Driving Aid	Soil Types	Tools
Flushing with compressed air	sand	jet pipes
Jetting with water		
Low pressure 10-50 bar	sand, gravel	
Medium pressure 50-200 bar	silt, loam	jet pipes
High pressure 200-500 bar	clay, marl	
Preboring		
Unloading $\phi < 150$ mm	sand, gravel	auger
Stress release $\phi < 400$ mm	sand, gravel	
Blasting		
Loosening by blasting	rock, marl	drill rods
Soil exchange		
Trenching	bouldery soils	clam shell, hydraulic hoe

More details can also be found for example in Döbbelin and Rizkallah 1996.

a) Jetting: During jetting the soil will liquefy and particles will rearrange, reducing the penetration resistance at the pile base. During low pressure jetting the jetting pressure at the jet point is around 10 to 20 bar. Depending on the pressure and jet point diameter (typically in the order of 25 to 40 mm), water quantities of between 200 to 500 l/min per jet point will be pumped into the ground. Low pressure jetting is used primarily in dense, cohesionless soils. In contrast, with high pressure jetting pressures between 350 to 500 bar are applied, permitting the use of smaller water quantities (approximately 10 to 50 l/min). During high pressure jetting the soil will be precut and the particles rearranged, reducing the shaft resistance of a pile. High pressure jetting can be used effectively in very dense soils. Instead of water, air can also be used for jetting. Typically, the bearing capacity of a pile is substantially reduced due to jetting. (Kempfert et al. 2003).

b) Preboring: When driving of steel sections, a compacted soil plug forms at the base of the pile, which may impede the pile installation. In such cases, and in very dense soils, e.g. stiff to hard clays, shales, slates, marls, sandstone, limestone and when encountering obstructions, predrilling is commonly used, which after loosening of the soil, permits driving without difficulties. Predrilling should be stopped about 1.0 meter above the pile base, to ensure sufficient embedment depth.

c) Loosening by Blasting: In highly overconsolidated soils, in clay stones and in banks of limestone or sandstone, piles can be installed only after loosening by blasting. When using blasting, the rock will be loosened but not removed. Piles should be driven as soon as possible after blasting, to avoid possible redensification of the fractured rock.

Full displacement bored piles (Screwed cast in-situ piles)

Full displacement bored piles are screwed piles which are installed by screwing and thrusting a closed steel pipe into the ground without excavation of any soil.

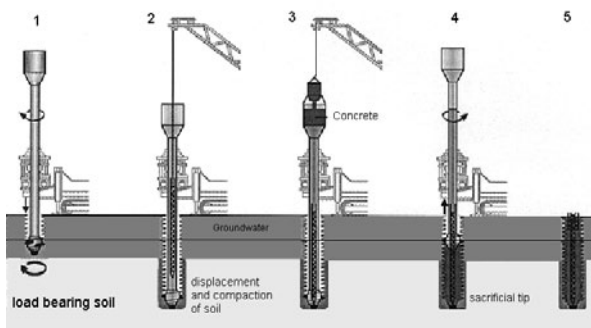
The soil is displaced by means of a special driving tube, which is closed off by a water tight pile tip. The pile tip may consist for example of a dead base plate with helical flanges or a cutter head. By regular pulling and twisting of the tube, the cutter head between tube and pile tip creates a pile shaft with external helices. Alternatively, the base of the driving tube may contain a flange with a limited number of helices, and a displacement element. On reaching the final depth, a reinforcement cage is placed inside the tube and after being filled with concrete, the tube is pulled. Screw piles must have an outer diameter of at least 300 mm. The driving tubes can be spliced to obtain the required pile length.

The following conditions must be considered during construction (Buchmann and Steiner 1996):

- Penetration is not possible in very dense sand and gravel, stiff to hard clays or weathered rock. It is very difficult to drill through very dense interbedded soil layers.
- Obstacles, such as old foundations or construction debris, must be removed before pile installation.
- Due to the full displacement of the soil, considerable heave must be expected in the vicinity of the pile. This effect must be accounted for, particularly in soft soils and when piles are to be installed immediately adjacent to fresh cast-in place concrete piles.
- The drilling equipment requires a stable working base with an area of at least 6 by 10 metres and sufficient moving space.
- The diameter of the reinforcement cages is small due to the dimensions of the driving tube so that only relative small bending moments can be resisted by the pile, for example due to lateral loading from active and passive earth pressures.

The construction systems available on the market place differ in the design of cutter head, the pile diameter and the direction of screwing during installation and pulling of the drive tube. In the following section three methods are shown.

a) Atlas pile: Atlas piles have been used in Europe and Australia since the 1980's. During the installation of Atlas piles (Fig. 6.13) a steel tubing with a cutter head and a single thread screw blade is twisted into the ground by a powerful rotary drive, applying a large vertical pressure at the same time. The cutter head is closed off by a water tight sacrificial base tip. The torque and the vertical load applied during installation can be measured and compared to the drilling records. Once the required depth is reached, the reinforcement cage is installed. The tube and a funnel extension attached to its top are filled with a soft KR concrete, with a maximum aggregate size of 16 mm. By twisting backwards and pulling the driving tube, the base tip can be disconnected. The concrete in the driving tube fills the space created by the cutter head. As a result of the single thread screw blade at the cutter head, a continuous helical concrete flange of approximately 50 mm thickness is created along the pile shaft, which gives an appearance similar to a wood screw (Fig. 6.14).



1. Screwing of cutter head into the ground under a large vertical pressure
2. After reaching final depth, installation of reinforcing cage
3. Filling of tube and funnel extension top with soft KR concrete
4. Untwisting and pulling of tube, while placing of concrete
5. Pile is completed. Additional short head reinforcement can be installed.

Fig. 6.13. Installation stages of an Atlas pile (company brochure of Franki Foundation)

The diameter of the pile shaft is dependent on the size of the exchangeable cutter head. Screwing the cutter head into the ground requires a very large torque, up to 400 kNm, to displace and compact the surrounding soil. As Atlas piles can be installed with practically no vibration and little noise, this pile type can be used immediately adjacent to buildings or structures which are sensitive to vibration. The minimum distance to existing structures is 800 mm. The load transfer is primarily due to shaft resistance, as is obvious from the shape of the pile.

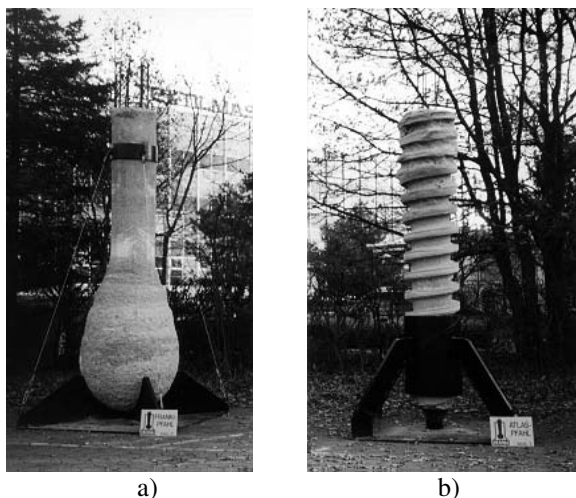


Fig. 6.14. Excavated driven cast-in-place concrete pile (a) and Atlas Pile (b) (photo: Franki Foundation)

b) Fundex pile: Fundex piles are constructed by driving a casing with a smooth surface. The casing is closed off at its base by a sacrificial cast iron pile tip, which also acts as a drill bit with a diameter that, depending on the pile diameter, is up to 60 mm larger than the attached casing. The tip facilitates penetration and displacement of the soil, which because of its helical shape, displaces the soil initially

into a downward and then into a lateral direction. Fundex piles have diameters between 380 and 440 mm.

The tube is twisted into the ground by applying a torque of between 120 to 360 kNm, and a vertical load utilizing the self weight of the drill rig (Schmidt and Seitz 1998). The encountered soil strata can be identified from the activated installation pressure. After reaching the required depth, a reinforcing cage and concrete is placed in one operation without interruption. The casing is then pulled in a twisting movement, causing the tip to disconnect and to remain in the ground as an expanded base. The casing is pulled in stages. During each stage the casing is partially pushed back to densify the concrete in the shaft, thus creating a profiled shaft surface. Fundex piles can be produced almost without vibration and at a low noise level.

c) SVV pile: SVV piles are constructed by screwing the casing, a displacement element and a drill bit clockwise into the ground. The displacement element ensures a constant diameter for the completed pile (Buchmann 1993). By using a water tight sacrificial base plate, the soil is completely displaced by the pile during installation. After reaching the required depth, a reinforcing cage is placed and concrete is pumped into the casing at high pressure.

The base plate is disconnected by a short anticlockwise twist and remains in the ground. The casing is subsequently pulled while twisting in the same direction as during installation, which is different to the other pile systems. Other than this, in terms of vibration, noise and construction time, this pile type is similar to the other methods.

d) Problems and Deficiencies: Full displacement bored piles may be affected by the following problems and deficiencies, in addition to those listed in section 6.2.2 for cast-in-place displacement piles.

- If the helical auger is too long the soil near the base may loosen rather than being densified, and may slump into the created cavity.
- in very dense sand the drilling tools may heat up to temperatures which affect the quality of the concrete and may also damage the pile tip.

6.2.3 Bored piles

Principles of construction

Drilled piles are typically constructed by cutting and removing the soil within the protection of a casing which should be driven beyond the excavation depth. Densification of the soil surrounding the pile shaft or below the pile base does not occur, as no soil displacement and no major dynamic action in the ground takes place. For casings with a constant diameter installed without major lateral movement, the lateral stresses in the ground will exhibit minimal change if the pile is installed properly. If a drill bit with an overcut is used, an annulus is created along the shaft, which in cohesive soils may remain open and in granular soils may fill up with loose material. In both cases, the annulus causes a decrease in the lateral in-

situ stresses and possibly loosening of the surrounding soil. After pulling the casing the horizontal stresses will be governed by the hydraulic pressure of the fresh concrete. At the pile base the soil is unloaded in the vertical direction which may not lead to loosening of the soil below the pile base, however.

During installation of piles in cohesive soils without a casing, deformation and thus softening of the soil may occur, resulting in a decrease in the bearing capacity. The pressure of the fresh concrete cannot offset these effects. However, when using a bentonite slurry to support the hole, expansion and softening of the soil will be reduced considerably.

When drilling piles with continuous flight augers the surrounding ground is supported by the soil contained between the auger blades. It can be assumed that some lateral densification of the soil can occur due to the volume displacement by the auger stem and that therefore softening of the soil can be averted. When a drill casing is vibrated into the ground, loose to medium dense soils may densify, resulting in an increase in bearing capacity.

Improper procedures, for example excavation ahead of the casing, may lead to loosening in granular soils. This not only causes a reduction of pile capacity and excessive pile settlements, but also subsidence of the soil surface. Loosening of the soil can also be induced if water levels in the drill hole are maintained too low, or if the auger is pulled out too rapidly.

Construction methods for bored piles (see also EN 1536)

Fig. 6.15 to 6.18 illustrates the most commonly used construction methods for drilled piles and their applications.

(a) Standard piling methods using Kelly drill

- borehole supported with casing (Fig. 6.16)
- borehole supported with bentonite slurry (Fig. 6.17)

(b) Grab construction methods

- with casing oscillator (Fig. 6.18)
- with continuous flight auger (SOB pile) (Fig. 6.19)

Other characteristic features of cased drilled piles are:

- The purpose of the casing is to prevent loosening of the soil during drilling in the vicinity of the pile, thus the inclination of the pile must be greater than 4:1. In order to minimize disturbance of the soil, the casing must also be kept ahead of the excavation during drilling. In soft cohesive soils and in granular soils, particularly in fine sands and silts below the groundwater table, the casing should be advanced by at least one pile radius. If hydraulic uplift at the base is to be expected, or in very soft and liquified soils, the advancing distance of the casing should be even larger.
- Below the groundwater table and for artesian conditions an excess pressure head must always be maintained in the drill hole by using water or some other liquid (generally bentonite slurry) to prevent hydraulic failure at the base of the drill hole. Any washing of soil particles into the borehole by water flow must be avoided.

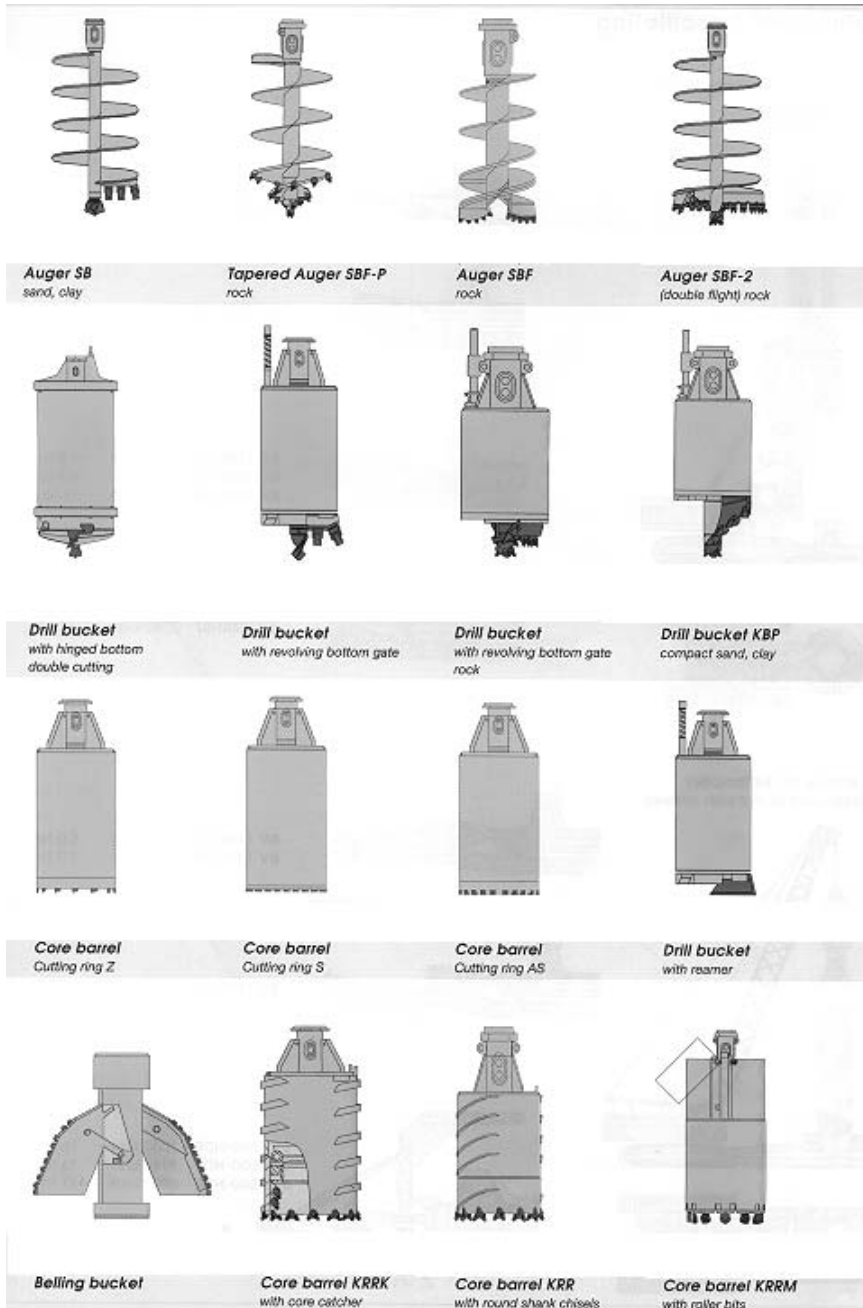


Fig. 6.15. Rotary drilling equipment for installation of bored piles (courtesy: Bauer construction company)

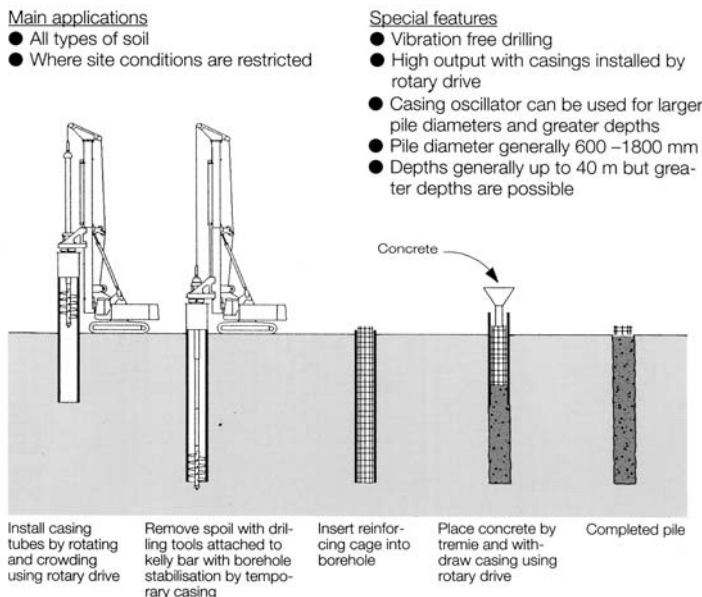


Fig. 6.16. Cased Pile installation with Kelly rotary drilling (courtesy: Bauer construction company)

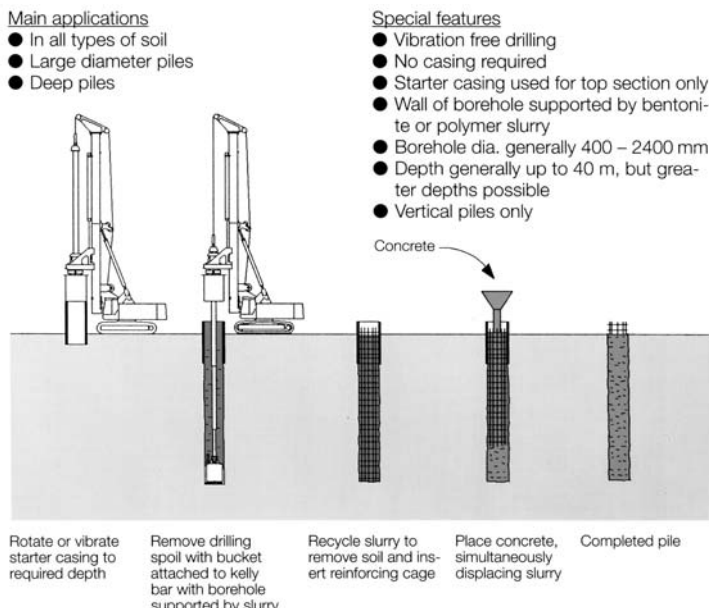


Fig. 6.17. Pile installation with Kelly rotary drilling supported by bentonite slurry (courtesy: Bauer construction company)

Main applications

- Soil such as sand and gravels with high demands on casing technology
- Where it is economically viable to use chisels to break up bedrock and boulders

Special features

- Minimum distance to existing buildings is required
- Pile diameters generally ranging from 620 to 2000 mm
- Depths generally up to 50 m.

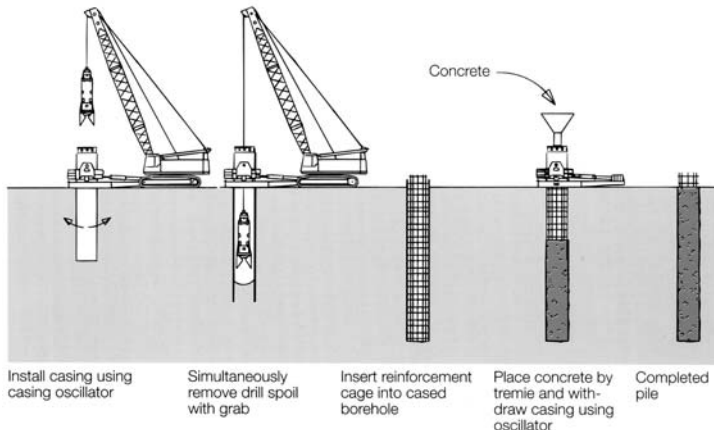


Fig. 6.18. Percussion drilling with cable dredger and casing machine (courtesy: Bauer construction company)

Main applications

- All types of soil
- Restricted sites

Special features

- Vibration free
- Reinforcement can be pushed or vibrated into the fresh concrete
- Pile bore diameters from 400–1000 mm
- Depths generally up to 18 m

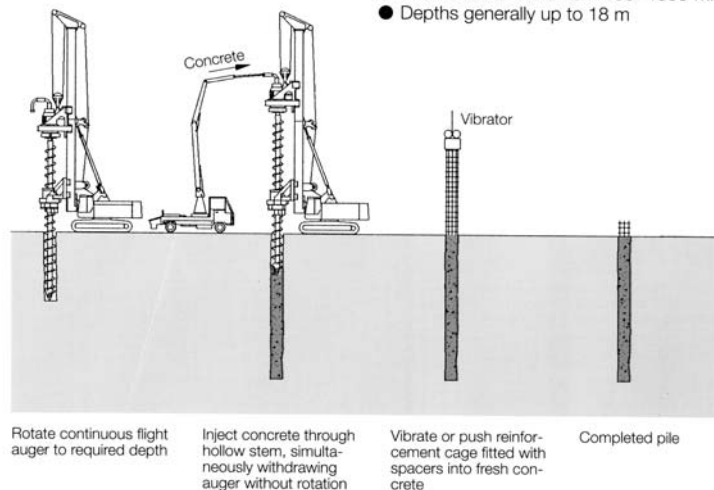


Fig. 6.19. Auger bored piles (SOB Pile) (courtesy: Bauer construction company)

- After the casing has reached the final depth, the soil must be carefully excavated to the base of the casing. To avoid an accumulation of loose soil below the pile base, concrete must be placed immediately after completion of final excavation. As a rule, drilled piles must be finished within the same day.
- Over cutting at the base of the casing must be kept at a minimum to prevent loosening of the soil in the vicinity of the pile.

Uncased boreholes supported by a stabilizing liquid are particularly important for the installation of large diameter piles.

- Stabilizing liquids are typically bentonite water slurries, often with various additives.
- Slurry supported drill holes are excavated by auger, grab construction or the air lifting method with roller bits (see Kempfert et al. 2003).
- In soft cohesive soils with $c_u \leq 15$ kPa, piles should not be drilled without a casing.

Holes drilled with continuous flight augers are supported by the soil resting on the auger blades. Two methods can be identified: drilling with small a diameter hollow stem and drilling with a large diameter hollow stem. Piles drilled with a large diameter hollow stem are also called partial displacement drilled piles. For piles drilled with a small diameter hollow stem the auger diameter ranges between 400 and 1000 mm, with inner diameters of the hollow stem between 100 and 150 mm. After reaching the final depth, concrete is pumped through the stem into the hole while the auger is pulled. The rate of pulling must be sufficiently slow, to prevent the development of suction at the base of the auger and the resulting sloughing of soil into the hole. A reinforcing cage can then be vibrated into the fresh concrete. The volume of the soil excavated during drilling depends on

- The diameter of the hollow stem: the larger the diameter, the less soil will be excavated, and the more soil is laterally displaced and compacted;
- The continuity of drilling rate (Stocker 1986).

The following should be also considered:

- Continuous flight augers should not be used in poorly graded granular soils with a shape factor $U \leq 3$ below the groundwater table and in very soft cohesive soils with $c_u \leq 15$ kPa.
- Pile depths are limited by the height of the drill rig and the length of the auger.
- Construction must be continuously monitored.
- The concrete, exiting at the base of the auger stem must be under sufficient pressure, to ensure that the space created during pulling of the auger is filled immediately with fresh concrete.

The combination of a cased borehole with continuous flight auger drilling is called the “twin rotary head method” which forms a continuous pile wall. By using two independent drive systems, one for the casing and one for the auger, they can be constructed so slimly that piles can be installed immediately in front of the walls of existing buildings. Pile depth is governed by the height of the drill rig. Pile diameters range between 200 and 500 mm.



Fig. 6.20. Hollow stem auger sections

Under-reamed/belled bored piles

In sufficiently stable soils drilled piles can be constructed with an expanded base. Deposits with gravel inclusions should be avoided. The bellng bucket must ensure that a concentric base can be created. It is important that the expansion of the bell beyond the pile shaft can be monitored and controlled during construction. Before placement of concrete, the pile base should be carefully inspected to ensure that the base is free of debris or loose soil. In North America it is common practice to lower persons in cages into the hole to view it and if necessary clean any debris from the base. Dry cement or lean concrete is also placed along the base to solidify any wet soil before placement of the structural concrete. When constructing an expanded base below the groundwater table the base cavity must be stabilized by a sufficiently large hydraulic pressure in the borehole. The shaft of piles with an expanded base should always be supported by a casing. The slope of the foot expansions should be greater than 3:1 in granular soils and 2:1 in cohesive soils. In compression piles the base expansion generally does not require reinforcement.

Recommendations for reinforcement and concrete work

As a rule, high slump concrete with a slump of 100 to 150 mm should be used for drilled piles, without addition of super plasticizers: The slump of the concrete placed in holes stabilized by bentonite slurry should be 120 to 150 mm. The concrete cover of the reinforcement should be at least 50 mm and for concrete placed in a slurry supported hole at least 70 mm, to prevent inclusions of bentonite slurry within the concrete. During placement of concrete the following should be ensured:

- the concrete reaches the base of the borehole in its original mix design and consistency;

- the concrete does not segregate nor becomes contaminated;
- the concrete column is not disconnected, and does not experience a reduction in cross section.

Hoses or funnels used for pumping the concrete, must reach down to the base of the drill hole and during concrete placement must always be immersed in fresh concrete. When placing concrete below the groundwater table or within a bentonite slurry the tremie method must be used, ensuring that the tremie pipe is pulled only after immersion of at least 3 meters in the fresh concrete.

In fine grained soils with $c_u < 15$ kPa the concrete cannot be placed against the soil, it must be supported by liners.

The column of the fresh concrete in the casing should be high enough to provide a sufficient concrete pressure to balance the groundwater pressure and to prevent soil from sloughing into the hole. The concrete pressure is sufficiently high if equilibrium with the lateral pressures can be demonstrated for the plane case. The concrete strength of drilled piles, according to EN 1536, should be classified between C 20/25 and C 30/37. In North American practice, for high quality concrete piles, concrete with a 28 day strength of at least 50 MPa should be used. For additional comments on materials and fabrication see “Recommendations for Design, Manufacture and Illustration of Concrete Piles” prepared by the American Concrete Institute Committee 543.

To ensure that the concrete within the pile shaft is not contaminated, concrete must be pumped until the entire contaminated concrete has risen to the top of the concrete column, above the cut off level of the pile. Before placing the concrete, the tremie pipe must be plugged with an appropriate material to prevent mixing of the concrete with the water or slurry. The initial charge should contain a mix with higher cement content or, alternatively, cement grout to reduce the wall friction in the tremie pipe. For drilled concrete piles, the longitudinal reinforcement should consist of ribbed steel bars of at least 16 mm diameter (EN 1536 recommends 12 mm). The clear distance between reinforcing bars should be at least twice the maximum grain size of the aggregates. The transverse reinforcement should consist of stirrups or spirals, with a diameter of at least 6 mm and a maximum spacing of 250 mm. Inclined piles should always be reinforced. For tension piles, the tensile reinforcement should be constant over the entire length of the drilled pile. The reinforcing cage should be stiffened and suspended in such a way, that during transport and placement no permanent deformations occur. To ensure that during placement of the concrete and pulling of the casing the reinforcing cage maintains its planned position, a flat iron cross should be mounted at the lower end of the cage. The reinforcement can be installed into the fresh concrete, possibly assisted by slight vibration, if the minimum concrete cover and the intended location can be guaranteed.

Problems and damage

a) Cased bored piles: As explained previously, the casing should be in advance of the boring to prevent loosening of the soil during the drilling process. If this cannot be assured, slumping of soil into the borehole may occur in soft soil and high

groundwater conditions, as shown in Fig. 6.21a. During pulling of the casing, water which accumulates outside of the casing may narrow or widen the cross section of the concrete column (Hilmer 1991).

Another reason for damage to drilled piles and other cast-in-place concrete piles, is the occurrence of hydraulic failure along the pile base. With grab or rotary drilling methods the water pressure is reduced in the hole during pulling of the drilling tool. This piston effect depends on the cross section, shape and surface roughness of the drilling tool and on rate of pull and it may lead to softening of the ground as soil particles are sucked up. Large negative excess pore pressures in the hole may initiate hydraulic failure, further loosening the surrounding ground. In Hartung 1993 results from model tests are shown, which are summarized in the following:

- The negative excess pore pressure decreases exponentially with the difference in cross sectional area between borehole and drilling tool. The larger the gap between the casing and the drilling tool the smaller the excess pressure. The shape of the drilling tool has little influence.
- The pulling velocity is very important, resulting in negative excess pore pressures which increase by the square of the pulling velocity. For example, tripling of the pulling velocity increases the negative excess pressure by a factor of nine.
- If the gap is clogged by debris, the negative excess pressure increases by a factor of three.
- During cleaning of the borehole the casing advance becomes zero, with a high risk of hydraulic failure.

It has been frequently found that as a result of large negative excess water pressures, piles turned out too short, even though drilling had occurred to the planned depth. Below the pile base sand is usually encountered which originate from layers two metres above the base. Most likely, the sand was sucked from the outside of the casing into the borehole during the pulling of the drilling tool. The ground was loosened over the entire length of the pile, with a reduction in bearing capacity and large settlements (See also Fig. 6.21b). In a former German Code, it was suggested that the ratio of the radius of the drilling tool to the radius of the casing should be less than 0.8, to avoid these piston effects. Modern drilling tools, often do not comply with this recommendation. It must therefore be assumed that the piston effect can not always be avoided.

The occurrence of necking or voids in pile shafts manufactured with high slump concrete is often encountered when the concrete column within the casing becomes too low during pulling, or when the concrete supply is interrupted (Hilmer 1991).

b) Uncased, slurry supported bored piles: To prevent bentonite or bentonite soil inclusions in the pile concrete, the bentonite slurry should be checked before placement of the concrete with respect to contamination and a possible increase of slurry density, and replaced if necessary. Damage can also occur along the perimeter of the hole during the installation of the reinforcing cage.

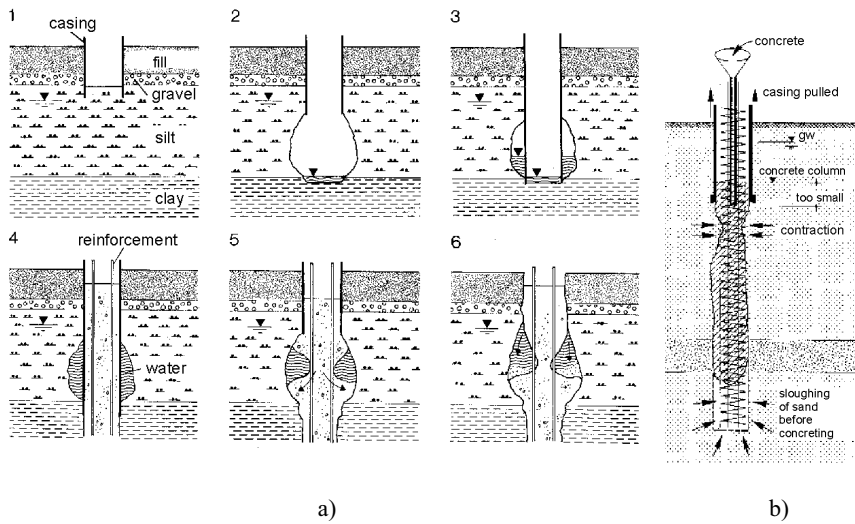


Fig. 6.21. Potential damage to bored piles: a) casing following drilling advance, b) cave-in along pile shaft with reduction of pile cross section and hydraulic failure at base before placement of concrete (after Hilmer 1991)

c) Uncased continuous flight auger piles and partial displacement piles

- Voids and necking of the pile shaft may occur when the pumping pressure of the concrete is less than the hydrostatic concrete pressure and the pulling velocity of the auger is not precisely adjusted to the rate of placement of the concrete.
- When drilling through obstacles or dense sand deposits only a small auger penetration rate can be achieved. The soil on the auger blades is therefore transported to the surface without replacement from below, resulting in voids and deficient support of the borehole. The effect of rotation without penetration is even worse in sands below the groundwater table and in soft soil layers which, by slumping towards the auger, cause loosening of the surrounding ground (Hilmer 1991). This may result in settlement of the piles and the adjacent soil.

Pressure grouting of the pile base and pile shaft

Pressure grouting of the pile base and pile shaft can be applied to prefabricated concrete piles installed into cased boreholes or to cast-in-place piles, which have been constructed by using cased or uncased (continuous flight auger) drilling (Schmidt and Seitz 1998). The specification for pressure grouting of the base and the shaft are contained in EN 1536. Pressure grouting can be applied for cast-in-place concrete piles only after the concrete has set. Only permanent grout pipes

are permitted, which should be adapted to the grouted area and the surrounding soil. Pressure grouting of the base can be carried out:

- by using a flexible bladder, which can be installed together with the reinforcement cage and permits distribution of the grout over the entire base area, or
- by sleeved perforated cross pipes, which are installed along the pile base (see EN 1536).

Pressure grouting of the shaft can be carried out with grout pipes which are attached either to the reinforcing cage, the reinforcing pipe or the prefabricated concrete element of the pile (see EN 1536). When both, the base and shaft are to be grouted, the shaft should be grouted first. Preloading of the pile base can be achieved by flexible pressure bladders or by rigid cylinders with movable pistons (pressure pots). These elements are installed in the drill hole with the reinforcing cage. After placement of the concrete piles they are expanded by pumping cement slurry into these units. The downward reaction force causes prestressing of the pile base. The reaction force in the upward direction is resisted by the shaft friction. The base expansion is discontinued, as soon as a heave of not more than 2 mm is recorded at the pile head. Pressurizing of the base can be also controlled by measuring the volume of cement grout injected and the pressure applied. Instead of pressurized bladders or pressure pots, grout pipes with sleeve valves near the pile base can also be used.



Fig. 6.22. Grouting of base and shaft (left) in drilled piles; detail of shaft-grouting (right), (photo: M. Stocker)

The shaft resistance provides a significant part of the pile resistance, particularly for large embedment lengths. An increase in the lateral stresses from pressure grouting along the pile shaft will therefore result in considerable improvement of the pile bearing capacity. Pressure grouting along the pile shaft is carried out by means of thin plastic tubing with sleeve valves, which are attached to the reinforce-

ing cage. Each grout location is supplied by individual feeder pipes (Schmidt 1996). The number of grout valves depends on the soil conditions and the proposed improvement in the bearing capacity. Normally, two valves at the same level are positioned opposite to each other and the valves in the adjacent levels are rotated by 90°. Roughly, one valve per 4 m² of shaft area should be provided. After initial hardening of the pile concrete, the concrete cover of the valves is fractured by the application of high water pressure. It is important that fracturing occurs at the right point in time. Cement mortar is then injected, which exits through the fractured concrete of the pile. The pressure and volume of the grout, as well as the water cement ratio (< 0.7) and grouting rate (l/min) must be assessed on the basis of experience, depending on local conditions and required strength increase. Typically, a grouting pressure of 20 bar and a grout volume of 100 kg per valve is applied.

For pressure grouted drilled piles the following observations were made after they were excavated (Schmidt 1996):

- The concrete cover of the reinforcing cage had spalled off over an area of 1.0 to 2.0 m² per valve, and was pushed laterally into the soil; the resultant void was filled with cement providing corrosion protection for the reinforcing steel.
- Generally, the cement mortar had spread from the pile surface into the soil, cementing sand and gravel particles onto the pile shaft. The resulting shell was about 20 mm thick.
- Layers of clean gravel had been grouted, producing an approximately 100 mm thick cemented slab up to a distance of two meters from the piles.
- Most natural sand and gravel deposits cannot be grouted with cement mortar. In these soils, the grout spreads along the pile shaft, increasing the contact pressure between the pile and the soil. Cohesive soils cannot be grouted at all. Pressure grouting leads to displacement of the soil by cracking. In rock pressure grouting of the shaft is almost impossible, and generally not required, as the shaft resistance is activated by interlocking with the rock.

6.2.4 Micropiles

Since micropiles are used in the so called “raft foundation on floating injection piles (RFIP)“ (section 6.8 and 6.9), which is a suitable foundation system for deep layered soft soil, this pile type is treated in detail in the following.

According to the European Code EN 14199, “micropiles” include drilled piles with a diameter of less than 0.3 m and displacement piles with a diameter of less than 0.15 m. Examples are, “root piles”, which have been known for decades, and the more recently developed one bar piles, pipe piles and steel tube piles. The major advantage of micropiles is that they can be installed largely without noise and vibration in a restricted space. Load transfer into the ground is achieved by pressure grouting with concrete or cement mortar. The following differentiation can be made:

- Cast-in-place piles, with continuous longitudinal steel bar reinforcement manufactured with concrete or cement grout. The minimum shaft diameter is 150 mm, with a concrete cover of 30 to 45 mm, depending on the aggressiveness of the surrounding soil or groundwater.
- Composite Piles, which are characterized by load bearing members made of reinforced concrete or steel, with a minimum diameter of 100 mm. The load bearing member is placed either into a drilled hole or manufactured with an expanded base, for example as a pressure grouted driven pile. The borehole can be filled with concrete before placement of the load bearing member.
- The space occupied by pressure grouted piles can be created either by drilling, driving or vibratory methods. The soil can be excavated by inner and outer flushing methods (“wash boring”). Wash borings alone are not permitted for creating the hole. When drilling below the groundwater table, an excess pressure must be applied to prevent soil from sloughing back into the drill hole. The borehole should be cleaned of all drilling debris before placement of the load bearing member.

When “pressure grouting” the grout is injected at a pressure greater than the hydrostatic pressure, either by air or by liquid pressure. During creation of the shaft the grouting pressure should be at least 5 bar within the region of load transfer.

During second stage grouting, grout is injected when the grout of the first grouting phase has hardened. The type of grout, pressure and quantities must be adapted to the subsoil and the local conditions. The second stage grout must be such that fractured zones will be refilled. Second stage grouting cannot be applied to loaded piles. For second stage grouting special grout tubes are used which allow application of pressures of up to 50 to 60 bar.

The GEWI Pile is a composite pile manufactured in the following stages:

- Drilling of a cased hole, often by wash boring methods.
- Installation of the GEWI steel bar elements into the borehole filled with cement grout, which can be extended if required by means of couplings.
- Pulling of the drill casing and initial pressure grouting.
- Second stage pressure grouting, once or several times (primarily in cohesive soils).

Figs. 6.23 and 6.24 illustrates the micropile system. In cohesive and granular soils the cement grout is injected through the drill casing. Second stage grouting in cohesive soils results in fracturing of the hardened cement at the locations of the grout valves (See Fig. 6.25). Subsequent multistage grouting is possible by means of a second stage grouting system. Standard corrosion protection of the steel bar is provided by a cover of cement mortar of at least 20 mm thickness. For double corrosion protection, a threaded steel pipe is installed in addition to the cement grout, as shown in Fig. 6.24b. The load transfer occurs by bonding with the ribbed steel surface along the pile shaft.



Fig. 6.23. Completed GEWI piles with postgrouting hoses

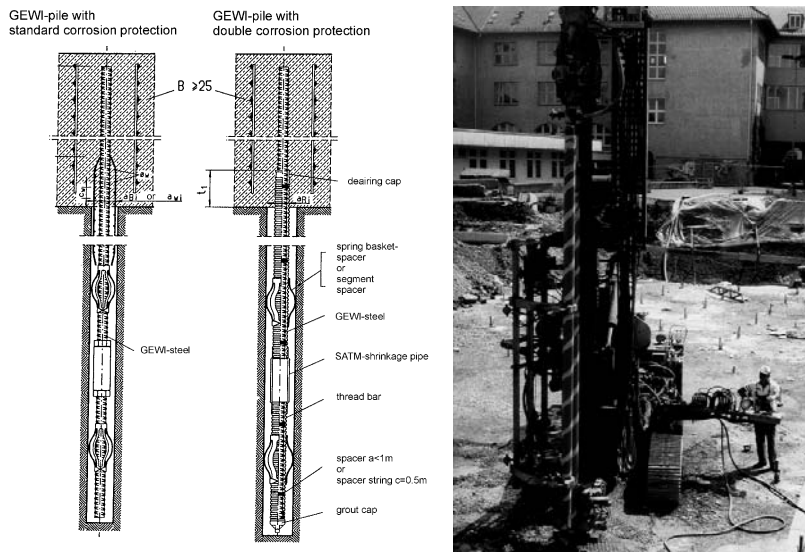


Fig. 6.24. GEWI pile; basic corrosion protection (left); double corrosion protection (center); installation by drilling (right)

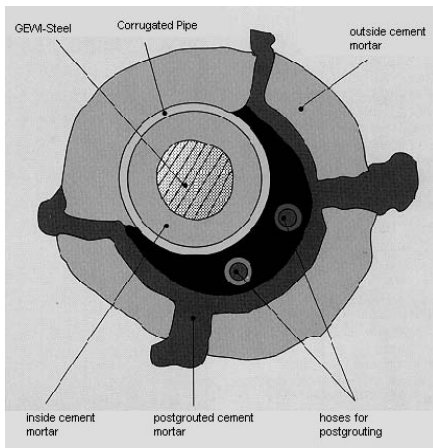


Fig. 6.25. Section through a postgrouted GEWI pile (company brochure DYWIDAG)

6.3 Pile bearing behaviour

For the axial resistance of single piles two components should be considered:

- Internal Pile Capacity (Structural Capacity of Pile): the pile must resist building loads and loads occurring during the construction stages without being damaged in anyway. The design must comply with the appropriate structural codes and will therefore not be discussed further in this section.
- External Pile Capacity (Load transfer capacity from the pile into ground): Strength and deformation properties of the substrata (soil and rock) must be such that the anticipated loads can be transferred by a single pile into the ground without failure or excessive settlement. (Failure and performance criteria must be fulfilled).

The external capacity in the axial direction of a single compression pile is made up of two components, the base resistance $R_b(s)$ and the shaft resistance $R_s(s)$.

The active pile resistance depends on the pile settlement and can be described by a resistance-settlement curve (RSC). Fig. 6.26a shows that the shape of the RSC for end bearing q_b and for shaft resistance (skin friction) q_s is different, q_b is almost parabolic, whereas q_s can be approximated by a bi-linear elasto-plastic configuration. Therefore, only the skin friction pile exhibits a true failure condition in which no further load increment can be achieved. Hence,

$$R = R_b(s) + R_s(s) \quad (6.1)$$

and in the ultimate limit state (ULS)

$$R = R_b + R_s = q_b \cdot A_b + \sum q_{s,i} \cdot A_{s,i} \quad (6.2)$$

The larger the end bearing component the less a true failure state, as defined above, can be achieved (see Fig. 6.26c). In order to specify the pile resistance for the ultimate state (ULS), it is common practice to assume a limiting settlement as a criterion, often defined by $s_{ult} = s_g = (0.1) D$. Many suggestions for the theoretical prediction of the external pile capacity can be found in the literature. Theory of elasticity based on the Mindlin equations and numerical methods with non-linear material characteristics have been used in these predictions.

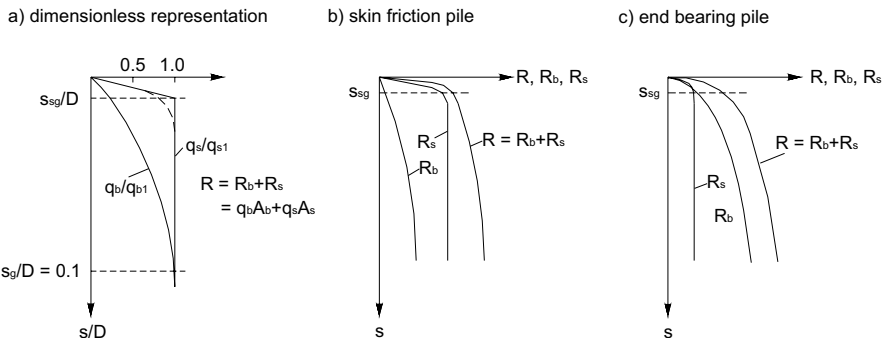


Fig. 6.26. Qualitative load-settlement-curves of a pile for point resistance and shaft resistance. a) dimensionless representation, b) friction pile, c) end bearing pile

Critical discussions of rigid-plastic and linear-elastic-plastic models can be found in Kempfert 2001. In summary, it was concluded, that numerical methods even with the application of non-linear material characteristics do not provide satisfactory results. This was demonstrated for sand in more detail in Gudehus 1980. Reasons for such behaviour are as follows:

- When installing of piles in the ground by driving, jacking, vibrating or drilling the properties of the ground will be changed from those valid for the at rest (K_0) conditions prior to installation, into a state which is difficult to evaluate.
- Pile loading causes changes in the ground which cannot be considered using the methods originally derived for shallow foundations. Because of the much larger overburden stresses at the level of the pile base, pile end bearing stresses greater than 1 to 2 MN/m² are encountered where the compressibility of sands and gravels is increased due to grain fracturing (e.g. De Beer 1963, Linder 1977, Vesic an Clough 1968). In conjunction with these processes the angle of friction below the pile base changes with increasing load and the frictional behaviour of the soil can no longer be represented by a linear failure surface.
- During pile loading in compression the soil adjacent to the pile tip is pushed upward by the volume of the pile penetrating into the ground under loading, as well as by the volume increase occurring in dense soils when the soil below the tip is approaching a state of failure. These upward movements load

the soil above the pile tip adjacent to the pile shaft and result in an increase in lateral stress in the lower shaft portions (Eigenbrod 1998) (See Fig. 6.27). The increase in lateral stress is associated with an increase in shaft resistance in the lower shaft sections once critical deformations are exceeded (Eigenbrod et al. 2001).

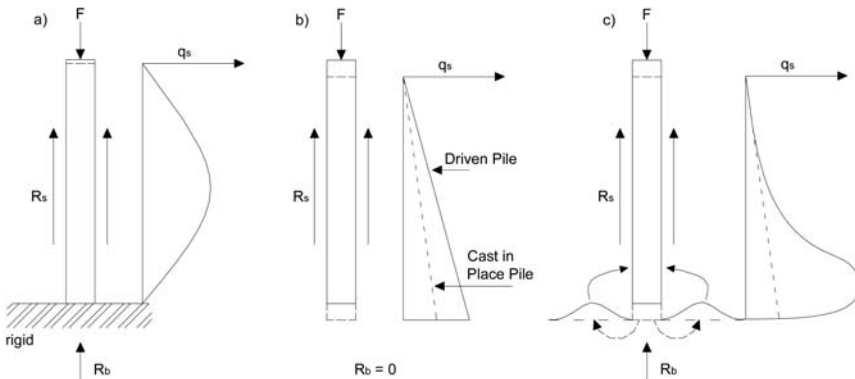


Fig. 6.27. Shaft resistance and end bearing dependent on relative deformations between the pile and the soil. a) rigid base, elastic pile $R_b > R_s$; b) floating pile, zero end bearing $F = R_s$; c) shaft resistance and end bearing in elasto-plastic soil $R_s = f(R_b)$

- d) In contrast to the interpretation in c) (Fig. 6.27c) some other opinions (Kempfert 2001) relating to the interaction between skin friction and base resistance are shown in Figs. 6.28 to 6.30
- e) By comparison, the skin friction of tension piles is not affected by this mechanism and is therefore smaller than for compression piles where end bearing is mobilized during tip deformations when a critical value is exceeded.
- f) For piles founded in a rigid material (e.g. rock), which does not allow deformations of the pile tip during compressive loading, a parabolic distribution of shaft resistance occurs with zero shaft resistance at the base and at the top, because at the base the differential movements between the pile and the soil are zero (by definition in a rigid base) and at the top because the lateral stresses are zero due to the zero overburden stress (Kezdi 1964).

According to German Code DIN 1054, it is normally not allowed to determine the axial pile capacities using theoretical soil mechanics based calculation methods or with empirical formulae, because the various factors, particularly those related to the pile installation cannot be adequately considered with these methods. In contrast, the European Code EN 1997-1 permits the design of piles on the basis of soundings (semi-empirical methods), as is common practice outside Germany. In Germany, because of the wide variability of geological conditions, only pile tests are considered sufficiently reliable, as they can take into account local characteristics, such as pile type, pile installation method and ground conditions.

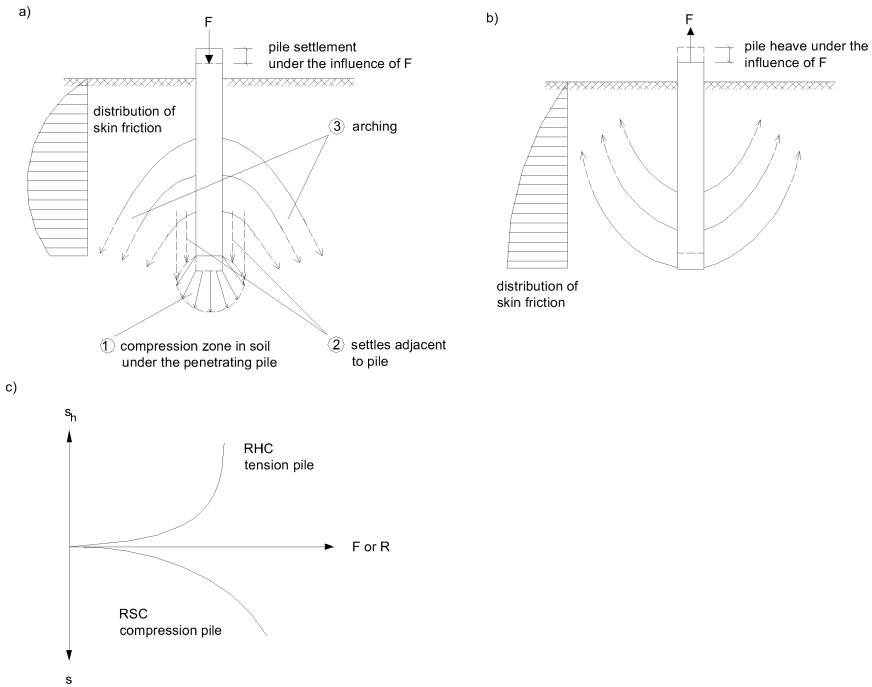


Fig. 6.28. Load transfer models for piles in compression and in tension. a) compression pile; b) tension pile; c) load-deformation-curve for compression pile and tension pile

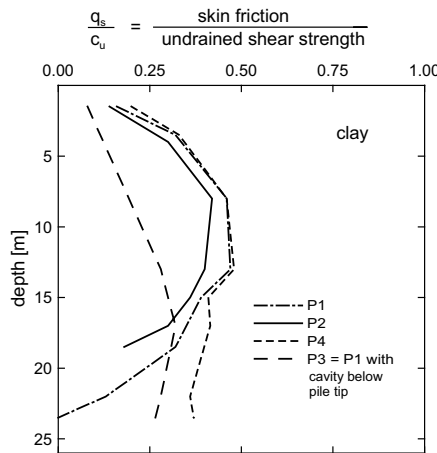


Fig. 6.29. Measured skin friction distribution for drilled piles (after O'Neill et al. 1972); shaft resistance of pile P3 only decreases slightly because of void below the base of the pile

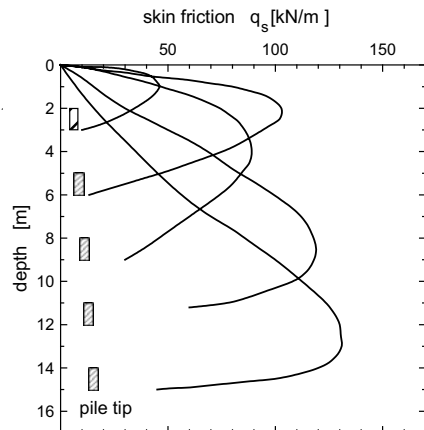


Fig. 6.30. Measured skin friction in sand for displacement piles (after Vesic 1963)

However, when designing pile load tests for foundations with very few piles where pile tests are not economical, or for offshore foundations where pile tests cannot be carried out, suggestions for calculating pile capacities are shown below.

In the ultimate limit state design (ULS) and the serviceability limit state (SLS), the pile foundations can also be designed using the partial safety factor concept (section 1.2) similar to design of shallow foundations

6.4 Axial pile resistance

6.4.1 General

According to the European Code EN 1997-1 and in particular the German Code DIN 1054, the pile resistance should preferably be determined on the basis of pile load tests. Pile load tests are normally carried out by static test loading, with incremental load increases. Although pile load tests are very costly, they can provide economic advantages and a better assessment of the pile quality. However, dynamic pile testing methods are becoming increasingly important in determining the integrity and resistance of piles.

Before carrying out a load test, careful planning of the pile test is required, including a series of preparatory investigations:

- The load test should be carried out at a location with representative soil conditions; type and method of construction of test piles should be at least similar to the foundation piles.
- The Magnitude and type of load transfer should be estimated. One should be determine whether axially loaded piles carry the loads primarily by end bearing or by shaft resistance. If one of these components is dominant the load test should be adjusted accordingly.
- If special test piles are installed, large deformations can be permitted during the load test.

For each geotechnically typical zone and for each pile type, at least one static pile load test should be carried out. For micropile foundations at least two piles, or a minimum of 3% of the total number of piles should be tested by static load tests. The pile test should be carried out on the basis of the ISSMFE recommendation "Axial Pile Loading Test" (ISSMFE Subcommittee on Field an Laboratory Testing 1985). In Germany pile load tests should primarily be based on DGTT AK 2.1 2006, and on the numerous publications on pile load testing.

6.4.2 Pile resistance from static Load Tests

Because a foundation design should be based on the results of pile load tests, the tests should be carried out prior to the design. Structural piles can be used as test piles, if the resulting changes in bearing characteristics are considered in the de-

sign of the foundation. Nevertheless, it is recommended, that separate test piles are installed for static load tests if possible.

For prefabricated displacement piles, base resistance and shaft resistance cannot be measured separately without excessive effort, so generally only the total pile resistance is determined. This is also the case for simple load tests on drilled and pressure grouted piles. However, particularly for drilled piles, end bearing and shaft resistance should be measured separately: By determining the deformation changes along the length of the pile, the axial load in the pile can be estimated, taking into account the cross sectional area of the pile and an average modulus of elasticity. Suggestions for instrumentation can be found in DGGT AK 2.1 2006. In addition, pressurized bladders at the pile base can be used as shown on Fig. 6.31.

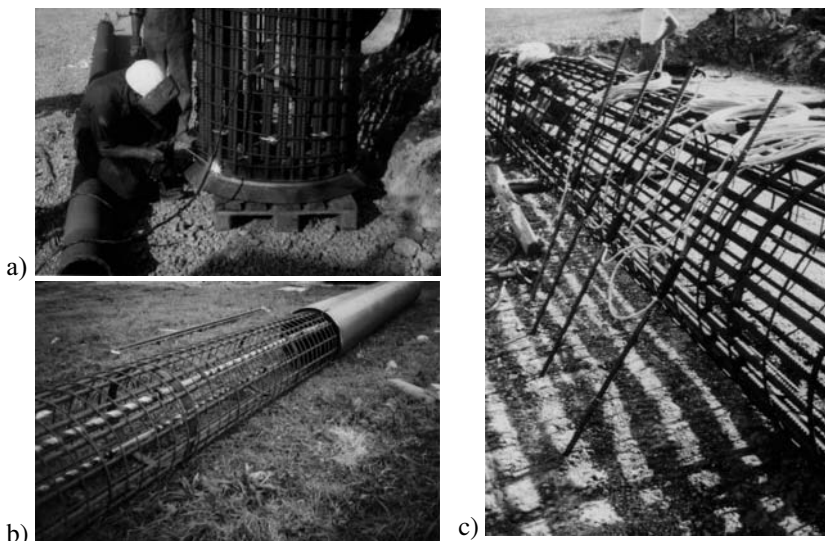


Fig. 6.31. Instrumentation for the measurement of point resistance and skin resistance. a) pressure cell, with strain gauges just above base; b) measuring tubes with strain gauges; c) measurement of pile deformations at various points with strain gauges mounted on reinforcement cages

To minimize the interaction between reaction piles and test piles, a minimum distance between the test pile and the anchor zones of the reaction piles must be maintained, as shown in Fig. 6.32.

A separation between end bearing resistance and shaft resistance is often achieved, particularly for displacement piles, by loading the pile first in tension and subsequently in compression. From the tension test the ultimate shaft resistance in tension $q_{s,t}$ is obtained; from the second test the end bearing resistance is calculated, assuming that shaft resistance in tension and in compression is approximately the same. It has been shown, for example in Mazurkiewicz 1975 and in Koreck, that after a change in load direction the shaft resistance in sand $q_{s,l}$ typi-

cally decreases. The above procedure therefore provides end bearing values q_{bl} , which are too large compared to the situation in which the compression loading is not preceded by tension loading. It was suggested by Gudehus 1980 that with reversal of the stress path, the sand contracts, causing a decrease in lateral stress along the pile shaft after each load change. The error due to this effect is large only if the shaft resistance in the sand is large compared to the total pile resistance. However, because displacement piles typically show only minimum embedment in load bearing strata, the error in most cases is small.

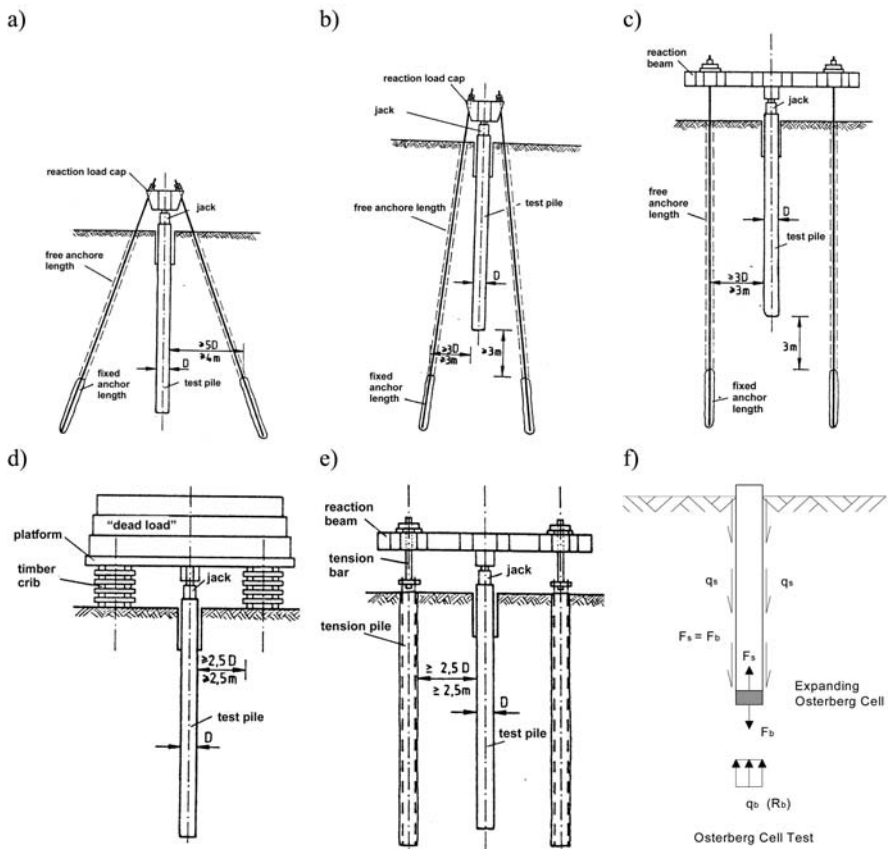


Fig. 6.32. Minimum distances between the anchors of the load frame and the test pile (after DGGT AK 2.1 2006) for a) radial arrangement of inclined grout anchors with shallow anchor zones; b) radial arrangement of inclined grout anchors with deep anchor zones; c) parallel arrangement of grout anchors with deep anchor zones; d) points of support for dead load system; e) load frame with tension piles; f) Osterberg – Cell

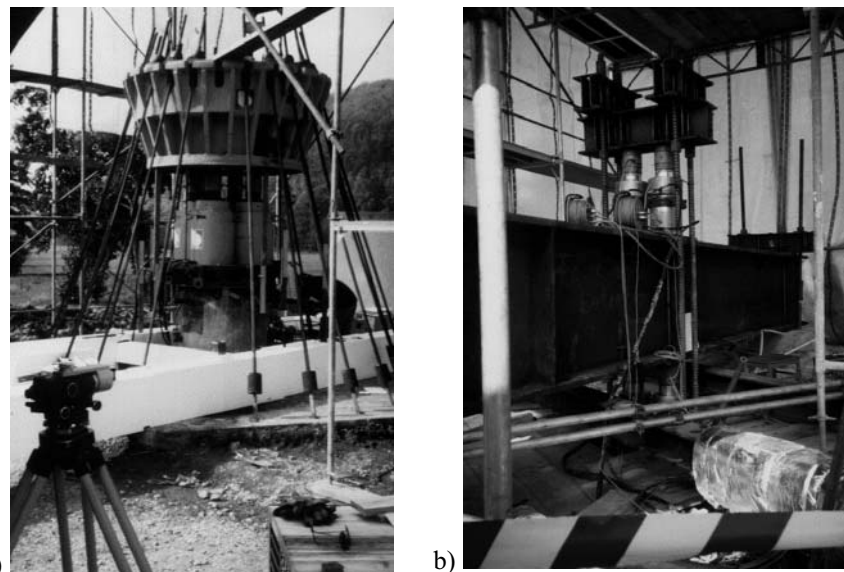


Fig. 6.33. Load frame and loading devices for axial pile load test. a) load test according to Fig. 6.32a; b) loading arrangement for cyclic loading with alternative compression and tension loads

In the late 1980's Osterberg developed a new, relatively low cost testing method (Osterberg 1994 and 1998), by incorporating a sacrificial hydraulic jack ("Osterberg-cell"), placed near or at the base of the pile to be tested. With the Osterberg-cell method (short: "O-cell method") a separation of the shaft and base behaviour, and other results, important for assessing the quality of the pile, can be obtained. In comparison to conventional top down load testing methods, no reaction system is required, thereby considerably reducing the cost of pile load testing, (See Fig. 6.32). The method is applied primarily for cast in place concrete piles but can also be used for testing driven piles (Osterberg 1994).

During testing the load is applied incrementally by increasing the pressure in the O-cell. This causes the O-cell to expand, pushing the pile shaft above the cell upward and the pile base downward. Measurements typically recorded are: the O-cell pressure (the test load), upward movement at the pile head, upward and downward movements at the O-cell and expansion of the O-cell. The O-cell load versus the upward movement of the O-cell top represents the shaft resistance-deformation curve of the pile shaft. The O-cell load against the downward movement of the O-cell base is the base-resistance-deformation curve of the pile base. Typical load-deformation curves are shown on Fig. 6.34. Because the buoyant weight of the pile above the O-cell must be subtracted from O-cell load to obtain the shaft resistance of the pile, the maximum shaft resistance is less than the maximum base resistance. Such direct information on shaft resistance and base resistance of a pile cannot be obtained from conventional top down load tests. Ex-

amples for O-cell load testing can be found, for example in Fellenius 2001 and Fellenius et al. 1999.

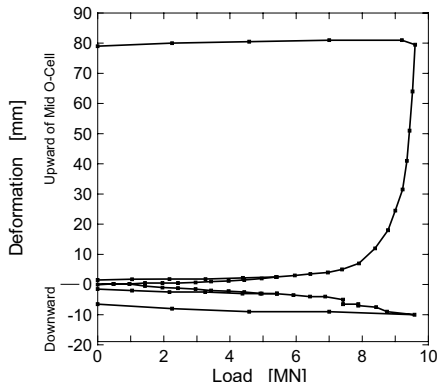


Fig. 6.34. Pile test result for an Osterberg-Cell

For conventional top down test loading of piles, hydraulic jacks are used. The loads are monitored by pressure cells; deformations are measured with dial gauges (0.01 mm precision), LVDT's (sensitive to temperature changes) and as an independent control with precision levels (0.1 mm precision). The two loading procedures typically used in Europe are as follows:

- Incremental load increase, in which the subsequent load increment is applied after the deformations have completely stabilized;
- Loads are increased in equal time intervals, regardless of settlement, e.g. every hour.

According to DGGT AK 2.1 2006 the number of load increments should be such that the expected ultimate pile resistance R_g can be reached in approximately eight equal load increments, as shown in Fig. 6.35. The regular load increments should be preceded by a smaller preload, which is defined as the zero value, to stabilize the load arrangement and to set the displacement gauges to zero. At the level of the design load (approximately at $0.5 R_g$), an unloading stage should be incorporated; the load at the various load stages should be maintained until rate of deformation has decreased to 0.1 mm per five minutes. In order to determine the creep behaviour for all load levels, the same time interval should be selected at each level. Different procedures are prescribed for load testing of drilled piles in EN 1536.

To determine creep deformations and long term performance, longer waiting periods to those defined previously should be maintained. At higher load levels, the rate of loading should be sufficiently slow, for example by applying the load increment within a period of five minutes to allow dissipation of the creep deformations.

When time is limited, loading should be carried out above the design load by the constant rate of penetration method (CPR test), to determine the ultimate pile capacity, with a rate of displacement of less than 0.2 mm/min.

In North America pile load tests are generally performed in accordance with ASTM Designation D-1143, which contains seven separate procedures, as listed in the following:

1. “Standard Loading Procedure”—a slow constant load method using eight equal load increments to twice the design load. Total test duration is 48 to 72 hours, or more.
2. “Cyclic loading”—the “Standard Loading Procedure” method with unloading and reloading cycles added.
3. “Loading in Excess of Standard Test Load”—after finishing the “Standard Loading Procedure”, the pile is reloaded to failure or to a predetermined maximum load.
4. “Constant Time Interval Loading” a constant load method in ten equal increments of load to twice the design load. The increments are applied every 60 min. regardless of settlements. The method is similar in all other aspects to the “Standard Loading Procedures” method.
5. “Constant Rate of Penetration Method” (CRP) requires the use of a special pump that can provide a constant flow of oil to the jack. Usual penetration rate is between 0.25 and 0.5 mm/min. Total test duration is 2 to 3 hours.
6. “Quick Load Test Method” a constant load method using many small load increments applied at constant short time intervals. The test is carried out to failure, or to a predetermined maximum load. Total test duration is 3 to 6 hours.
7. “Constant Settlement Increment Loading Method”—a special method, where the applied load increments are varied to achieve approximately equal settlements per load increment. The settlement increment is chosen to be about 1% of the pile head diameter.

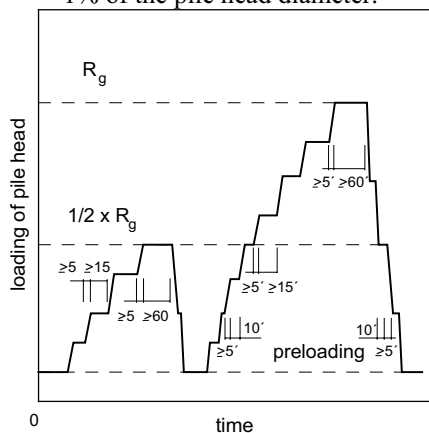


Fig. 6.35. Recommendation for the selection of load increments (after DGQT AK 2.1 2006)

Monitoring of loads and deformations should occur simultaneously for each load stage in intervals of 0, 2, 5, 10, 20, 40, 60, 90, 120, 180 minutes etc. to facilitate plotting the rate of creep in a semi-log graph.

It should be pointed out again, that equal duration per load stage should be maintained over the entire load range. The influence of the preceding load stages

on the subsequent ones can then be compared at each level. Failure caused by exceeding the shear strength of the soil is indicated by sudden increases of settlement velocities, which can only be readily recognized when equal time intervals are used. Otherwise, it may be necessary to decrease the load increments, due to the rapidly increasing settlements as failure is approached. With the CRP method, according to Whitaker and Cooke 1961 and ASTM Designation D-1143, only the ultimate pile resistance R_g can be determined reliably, but the associated settlements might be too small. For a more realistic assessment of the load-settlement behaviour, it has been recommended in Whitaker and Cooke 1966, that a load controlled load stage is included by maintaining the load at a constant level until the settlements have fully stabilized. Therefore, at the same load the differences in settlements between load controlled and deformation controlled tests can be recognized.

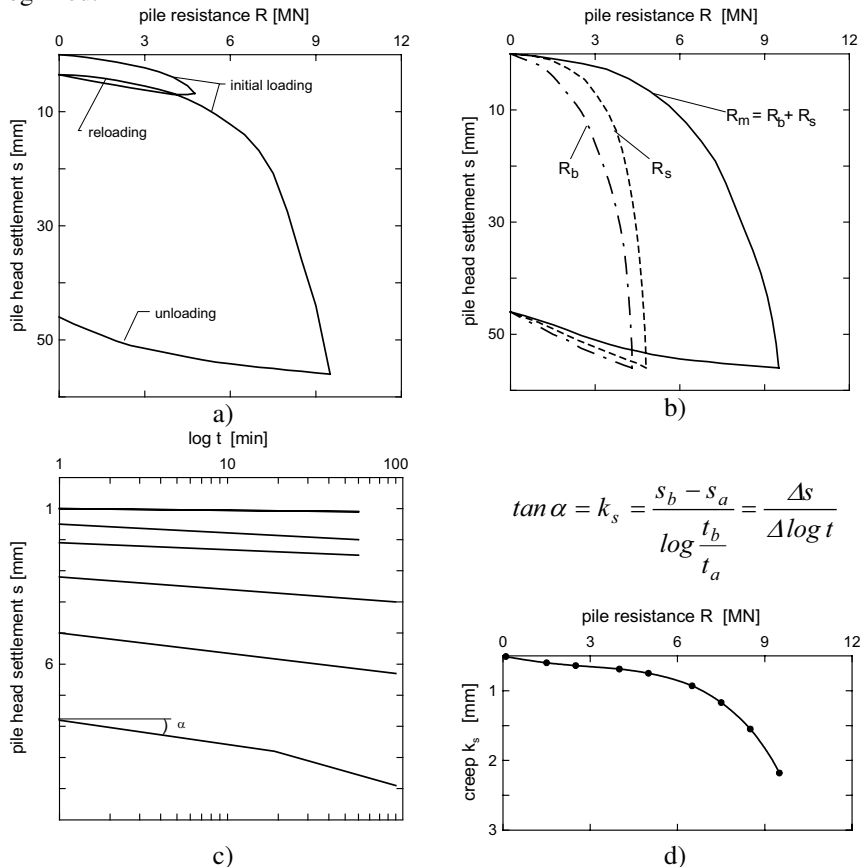


Fig. 6.36. Analysis and representation of pile load test results (after DGGT AK 2.1 2006). a) pile resistance settlement curve; b) separate representation of point resistance and skin resistance; c) creep curves at different load levels; d) creep versus respective pile load levels

Evaluation and presentation of pile load test results depends on the purpose of the test, the type of tests and the type of instrumentation. Examples are given above in Fig. 6.36.

The ultimate axial pile resistance R_g or $R_{ult,i}$ can be evaluated from the load-deformation diagrams obtained by the pile load tests. The procedure of how to determine the ultimate pile resistance has not yet been uniformly defined.

The German Code DIN 1054 specifies the following: "The ultimate load is the load at which during testing a compression pile clearly settles, or alternatively, a tension pile heaves noticeably. In the resistance-settlement diagram the ultimate load is the point at which, the flatter branch of the curve changes into a steeper portion with increasing deformations". According to Smoltczyk 1985, Eq. 6.3 can also be applied to define the ultimate load. The ultimate resistance R_g can also be equated to the creep resistance R_c . The creep resistance R_c can be obtained by plotting the settlement $s_{i,30}$ during the last 30 seconds of load stage No. i as a function of the pile resistance R .

If during load testing of compression piles the ultimate pile resistance $R_{ult,i}$ cannot be clearly identified from the load-settlement curve, the ultimate settlement s_{ult} can be calculated from Eq. 6.3 according to the German Codes for almost all pile types.

$$s_{ult} = (0.10) D_b \quad (6.3)$$

Numerous rules and recommendations are summarized in Kempfert 2001 based on Fellenius 1975 and Vesic 1975 about how to determine the ultimate pile resistance, referring primarily to smaller pile diameters less than 0.5 m.

If during pile load testing only small settlements occur, the ultimate resistance can be extrapolated according to Rollberg 1976 as shown in Fig. 6.37.

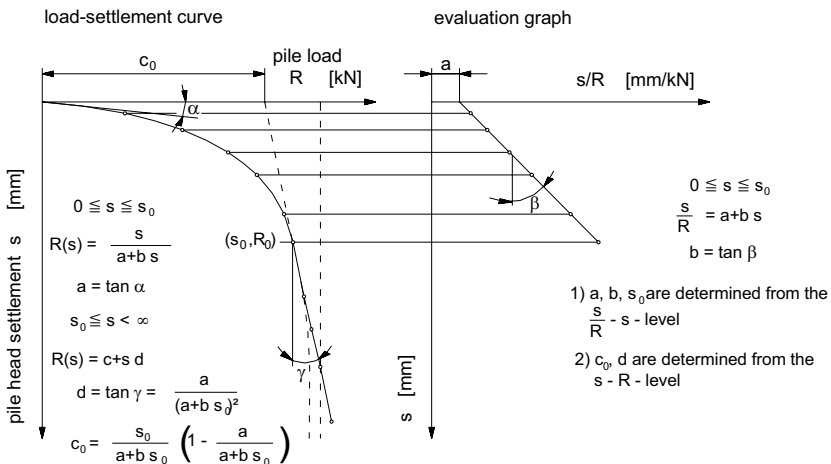


Fig. 6.37. Extrapolation of a load test results using the improved hyperbolic method (after Rollberg 1976)

6.4.3 Dynamic pile testing

Background

Dynamic, non-destructive testing methods are an alternative to the laborious static axial pile load tests. During dynamic testing a dynamic impact load is applied to the pile, which is of the same order of magnitude as the future working load, but only acts for milliseconds. The impact load is in equilibrium with the acceleration dependent inertia force, the velocity dependent damping force and the settlement dependent soil resistance. Conclusions on the bearing capacity are theoretically possible if the correlation between pile movements and forces is known. The deformations along the pile shaft and the acceleration are measured over time. For integrity testing, only the acceleration distribution over time is of interest. In total the following information can be obtained:

- For the total system: the effect of properties of the pile, the soil and the drop hammer, as well as development of the driving resistance with time.
- From the strata: the dynamic pile driving record.
- For the drop hammer: then effective driving energy and efficiency of driving.
- For the pile cap: the performance and rigidity.
- From the development of pile impact and dynamic pile resistance: refusal and effectiveness of redriving.

The applicability of dynamic pile tests is defined in EN 1997-1, DIN 1054 and in DGGT AK 2.1 2006. According to this code it is permissible to apply a dynamic load of the same order of magnitude as the later working load and to derive the pile resistance from a dynamic pile test when static pile load tests of a comparable pile-soil-system are available for calibration.

All evaluation methods are based on the theory of one-dimensional wave propagation theory: due to the impact of the drop hammer or due to any other dynamic excitation an impact wave is transferred into the pile, which depends on soil response, experiences a characteristic change. Generally, a portion of the impact load reaches the pile base and will be reflected as a tension wave. After time $T = 2L/c$ (where c is the propagation velocity of the wave [m/s], a material constant) the reflection wave causes a movement of the pile head, which can be measured.

Integrity tests using this method are useful for quality control and performance evaluation.

Dynamic pile load tests

During pile driving when the drop hammer hits the pile head, movements of the pile result. If the pile is not embedded in the soil, the velocities caused by the impact wave are proportional to the force on the pile head:

$$F = \frac{E_b \cdot A_Q}{c} \cdot v \quad (6.4)$$

where

- v = velocity, proportional to the induced force
- A_Q = cross sectional area of pile
- c = wave propagation velocity in m/s; $c = 2L/T$

The proportionality factor $E_b A_Q / c$ is called the impedance Z and is a measure of the pile quality and therefore also the total dynamic resistance of the pile. The impedance Z comprises stiffness and mass distribution of the pile.

$$Z = \frac{E_b \cdot A_Q}{c} \quad \text{or} \quad Z = c \cdot \rho \cdot A_Q \quad (6.5)$$

where

- E_b = dynamic modulus of elasticity of pile material; $E_b = c^2 \rho$
- ρ = density of pile material

As soon as the pile penetrates the ground, the movement is resisted by shaft resistance. As a result the velocity of the pile decreases and becomes smaller than v . The skin friction also causes refraction, which can be recognized at the pile head as deviations of the normal force and velocity from the proportionality. The deviation of the velocity from the proportionality indicates how much the pile is embedded in the soil. Therefore, the reflection of the wave at the pile base is also depended on the magnitude of the pile movement and the pile base resistance which is activated by the pile movement. Hence, the reflection at the pile base provides information about the magnitude of the base resistance.

The total penetration resistance of the pile-soil-system can be determined from the reflection at the base, which is dependent on the shaft resistance and the base pressure.

$$R_{tot} = \frac{1}{2} [(F_1 + Z \cdot v_1) + (F_2 - Z \cdot v_2)] \quad (6.6)$$

where

- F_1 = impact force
- v_1 = velocity of impact
- F_2 = measured force of wave reflected at the base
- v_2 = velocity of wave reflected at the base

The force $F(t)$ can be calculated from the measured strain $\varepsilon(t)$ using the correlation $F(t) = E_b A_Q \varepsilon(t)$. The respective velocities $v(t)$ can be obtained from the time integral of the measured acceleration $a(t)$.

Using the direct methods the capacity for the static resistance R_{stat} is calculated from the total penetration resistance R_{tot} . The dynamic component R_{dyn} , which occurs only during driving as a result of inertia and damping forces, must be subtracted from the total resistance of the soil:

$$R_{stat} = R_{tot} - R_{dyn} \quad (6.7)$$

where

- R_{stat} = available static resistance
- R_{tot} = total dynamic resistance
- R_{dyn} = dynamic resistance

One should therefore attempt to determine the dynamic component of the resistance as precisely as possible from the measurements of force and velocity at the pile head, in order to identify the effective static pile resistance. Two methods are commonly used:

- Direct method (e.g. CASE, TNO)
- Expanded evaluation method (e.g. CAPWAP, TNOWAVE)

For further details for evaluation and interpretation of dynamic pile load tests, refer for example to Kempfert et al. 2003, DGQT AK 2.1 2006.

6.4.4 Pile resistance against horizontal loadings

For bearing behaviour of piles subjected to horizontal loading see for example Tomlinson 1994; Kempfert et al. 2003.

6.4.5 Determination of pile resistance

General

As already mentioned, the static and dynamic pile load tests are the safe method for the determination of the pile bearing capacity or pile resistance (see also DGQT AK 2.1 2006)

There are several methods in the literature for calculation of pile resistance, in particular the limit resistance of displacement piles. These are selectively summarised in the following, whereby the presentations are partially adopted from Witzel 2004.

According to Poulos 1989, the calculation methods presented in the subsequent sections are classified into three categories. The first category consists of empirical methods which are based on soil field and laboratory investigations. These methods are used commonly in practice all over the world. The calculation methods in the second category are developed based on a higher theoretical background, however, they are usually simplified for practical purposes. The third category consists of numerical calculation methods.

Table 6.3 shows the allocation of the calculation methods presented in the foregoing sections to the corresponding category. Detail presentation of the methods can be found in Witzel 2004.

Based on cone penetration test (CPT) results and the hyperbolic method (Fig. 6.37), Behnke and von Bloh 1998 developed a method for prediction of the pile resistance-settlement lines.

Table 6.3. Classification of the different methods for determination of the axial pile resistance (after Poulos 1989)

Category		Method
1	empirical methods	Based on in-situ tests: Laboratory and field tests: CPT, SPT, PMT c_u (α -Method), I_D , D , I_c
2a	theoretical methods	Methods using effective stresses (β -Method)
2b	theoretical methods	Methods using effective stresses with consideration of the hole space enlargement within the pile base
3	numerical methos	Finite Element Method (FEM) Boundary Element Method (BEM)

Empirical methods

a) Calibration on cone penetration test (CPT): The empirical method for prediction of the ultimate pile capacity from CPT is the most used method internationally. This method is usually used for piles in non-cohesive soils. Specially in north European countries such as the Netherlands, Belgium and Norway the method is widely spreaded and partially implemented in corresponding codes. The method refers primarily to displacement piles.

a1) pile base resistance: For the determination of pile base resistance, the mean value of the characteristic cone resistance of the CPT q_c at pile base (e.g. Schram Simonsen and Athanasiou 1997; Mets 1997; Bustamante and Ganeselli 1982; Schröder 1996) or at a defined area around the pile base (Bartolomey 1997; Mandolini 1997; Zweck 1980) is used, whereby the value is multiplied by an empirical reduction factor ω_b . The factor ω_b takes into account the globally different influences on the base resistance of displacement piles.

$$q_b = \omega_b \cdot q_c \quad (6.8)$$

Some of the required reduction factors for determination of pile base resistance based on the mean CPT results are given in Table 6.4 and Fig. 6. 38 comparatively.

According to Kraft 1990, special attention is required on the difference in cone form, rate of penetration and scale factor, when transferring the CPT results to base resistance of displacement piles. Advanced approaches which take into account more influence factors for prediction of the pile base resistance can be found, for e.g. in De Beer 1971/72; DIN V ENV 1997-3:1999-10;. Holeyman et al. 1997.

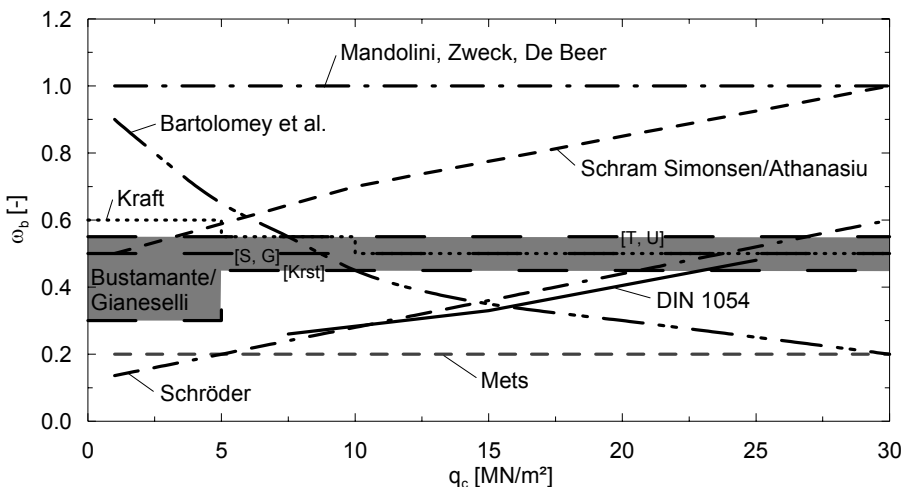


Fig. 6.38. Reduction factor ω_b for determination of pile base resistance compiled from literature (displacement piles)

Table 6.4. Reduction factors ω_b for determination of the mean pile base resistance

Reference	Schram Simonsen and Athanasiu 1997	Bartolomey et al. 1997	Kraft 1990	Mets 1997	Bustamante and Frank 1997, 1999; Fascicule 62-V	Mandolini 1997	Zweck 1980; De Beer 1971, 1972	Schroeder 1996	DIN 1054:2003-01
Soil type	-	-	ncs	-	C, M G, S chalk	ncs gran.	-	reinforced concrete	ncs
Pile type	-	-	Steel pipe	-	-	-	-	reinforced concrete	-
q_c [MN/m ²]	1) 2)	1) 1)	1) 0.55	1)	1) 0.20 0.55 0.50	3) 1.00 1.00	4)	1) 1)	1)
≤ 1	0.50	0.90							
2.5	0.53	0.80	0.60			0.30			-
5	0.59	0.65							
7.5	0.64	0.55							0,26
10	0.70	0.45							
12	0.76								
15	0.85	0.35				0.45			0,33
20	1.00	0.30	0.50						
25									0.48
> 30			0.20						-

1) mean value of q_c at a depth of pile base

2) mean value of q_c at a depth of $1 \cdot D_b$ above and $4 \cdot D_b$ below the pile base

3) mean value of q_c at a depth of $4 \cdot D_b$ above and $1 \cdot D_b$ below the pile base

4) mean value of q_c at a depth of $8 \cdot D_b$ above and $3.75 \cdot D_b$ below the pile base

Abbreviations to the type of soil: C = clay, M = silt, G = gravel, S = sand, ncs = non-cohesive soil

a2) *Pile shaft resistance:* There are two group of methods used for determination of the characteristic pile shaft resistance based on CPT results. The first group applies the mean characteristic cone resistance q_c of CPT as input parameter for the calculation, whereas the second group takes the measured local skin friction f_s of CPT as a basis for the calculation. In both cases, the result of CPT must be reduced by empirical factors $\omega_{s,f}$ and $\omega_{s,q}$ according to Eq. 6.9a & b.

$$q_s = \omega_{s,q} \cdot q_c \quad (6.9a)$$

$$q_s = \omega_{s,f} \cdot f_s \quad (6.9b)$$

Some of the required reduction factors $\omega_{s,q}$ for determination of pile shaft resistance based on the mean CPT results are given in Table 6.5 and Fig. 6. 39 comparatively.

Table 6.5. Reduction factors $\omega_{s,q}$ for prediction of the mean pile base resistance based on cone resistance of CPT along the pile shaft (displacement piles).

Reference	Schram and Athanasiu 1997	Simonsen 1997	Mandolini 1997	Heijnen 1985; Schröder 1996	DIN 1054: 2003-01	ENV 1997-3:1999-10
Soil type	-	nbs	nbs	reinforced concrete	nbs	nbs
Pile type	-	-		reinforced concrete	reinforced concrete	Steel girder
q_c [MN/m ²]					1)	
1	0.010	0.020				
2		0.015			0.010	
5					S/ S.g	
10	0.007	0.012	0.010		0.0093	0.005
15					gS	0.0075
20	0.005	0.009			0.005	
25					G	
30		0.007				

1) If a cone resistance $q_c \geq 15$ MN/m² of the CPT is measured for a continuous depth interval ≥ 1 m, then take $q_c \leq 15$ MN/m² for this interval
If the depth interval with $q_c \geq 12$ MN/m² < 1 m, then take $q_c \leq 12$ MN/m² for this interval.

According to ENV 1997-3:1999-10, the reduction factor for determination of pile shaft resistance in cohesive soils should be supplemented as described below. According to this method, no shaft resistance should be considered for piles in peat soil. In clay and silt soils with cone resistance > 1 MN/m², a factor of 0.035 can be used, whereas for cone resistance ≤ 1 MN/m² an increase of the factor with depth according to Eq. 6.10 can be taken.

$$5 < z/D_{eq} < 20 \quad \omega_{s,q} = 0,025 \quad (6.10a)$$

$$z/D_{eq} \geq 20 \quad \omega_{s,q} = 0,055 \quad (6.10b)$$

where z/D_{eq} is the ratio of the depth below the surface and the equivalent pile diameter.

Bustamante and Frank 1997/99 introduced a method according to France code Fascicule 62-V, which in turn is based on in-situ pile load tests (Bustamante and Ganeselli 1982).

Table 6.6. Reduction factor $\omega_{s,q}$ for the determination of pile shaft resistance using the mean characteristic cone resistance of CPT along the shaft of the pile and the maximum shaft resistance according to Bustamante and Frank 1997/99

Pile type	Soil type	Clay and silt			Sand and gravel			
		q_e [MN/m ²]	< 3	3 – 6	> 6	< 5	8 – 15	> 20
Closed steel pipe	$\omega_{s,q}$		–	1/120	1/150	1/300	1/300	1/300
	$q_{sl,max}$ [kN/m ²]	15		40	80	–	–	120
Rammed precast concrete pile	$\omega_{s,q}$		–	1/75	–	1/150	1/150	1/150
	$q_{sl,max}$ [kN/m ²]	15		80	80	–	–	120

Table 6.7. Reduction factor $\omega_{s,s}$ for the determination of pile shaft resistance based on the local skin friction f_s of CPT

Reference	Soil type	Pile type	f_s [MN/m ²]					
			≤ 0.02	0.04	0.06	0.08	0.10	> 0.12
Meyerhof 1976	nbs	-				1		
Mets 1997	-	-				0.8		

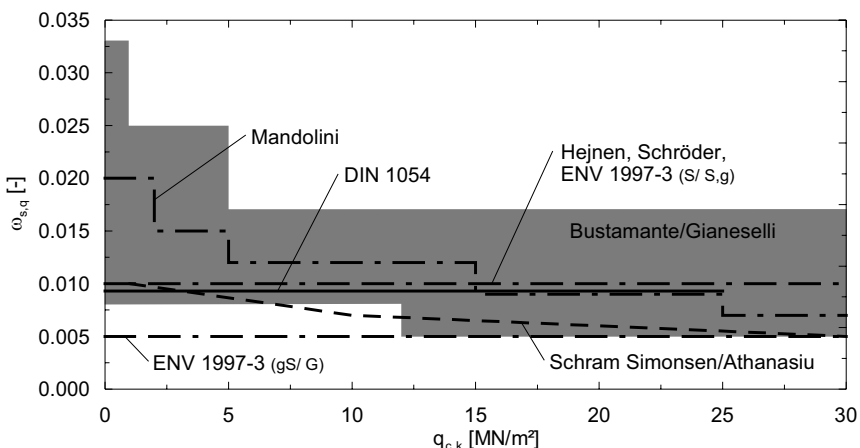


Fig. 6.39. Reduction factor $\omega_{s,q}$ for the prediction of pile shaft resistance (displacement piles)

b) Calibration on standard penetration test (SPT) or pressiometer (PMT): Detail of this method can be found in Witzel 2004.

c) Calculation procedure in Germany: It is almost the same as in a), where table values are given for different type of piles. These table values are in turn derived empirically from a correlation of large number of pile load tests with CPT test results (refer to DIN 1054 and DGQT AK 2.1 2006).

d) Empirical method, α -Method: This is a semi-empirical method which is developed based on the undrained shear strength of cohesive soils. In this method time plays a decisive role, because, on one hand, the bearing capacity of displacement piles in cohesive soil can be increased due to the consolidation process after the driving, on the other hand it was observed that the bearing capacity of piles in stiff cohesive soils decreases with time (Tomlinson 1994) (also compare with section 6.4.6). According to Budhu 2000, this method is applied to determine the initial bearing capacity (short term bearing capacity) in cohesive soils. However, the approaches presented hereafter in this section to estimate the end pile bearing capacity (long term) is based on empirical correlation between the pile base and shaft resistance with the undrained shear strength of cohesive soils.

d1) Pile resistance: In the literature, for e.g., API RP 2A 1989; Burland 1973; Findlay 1997; Gwizdala 1997; Kempfert 2001; Mandolini 1997; Poulos 1989; Schram Simonsen and Athanasiu 1997; Skov 1997, the Skempton 1959 approach is used, where the pile base resistance of a displacement pile in the ultimate limit state according to Eq. 6.11 for piles with $t/D_b \geq 3$.

$$q_b = \alpha_b \cdot c_u = 9 \cdot c_u \quad (6.11)$$

where c_u is the undrained shear strength of undisturbed soil at a depth of the pile base, t is an embedment depth in the bearing layer, and D_b is pile diameter.

For piles with $t/D_b < 3$, values for α_b are given by Prakash and Sharma 1989 as shown in Table 6.8. Fleming et al. 1992 also suggested a reduction of the factor α_b for embedment length in load bearing clay layer between $0 \leq t/D_b \leq 3$.

Table 6.8. Values of α_b for different ratio of embedment depth to the pile diameter

α_b	t/D_b				
	0	1	2	3	≥ 4
Prakash/Sharma (1989)	6.2	7.8	8.5	8.8	9.0
Fleming et al. (1992)	6.0	7.0	8.0	9.0	9.0
Budhu (2000)	6.0	7.2	8.4	9.0	9.0

Budhu 2000 developed an equation (Eq. 6.12) which gives values of α_b closer to Prakash and Sharma 1989.

$$\alpha_b = 6 \cdot \left(1 + 0,2 \frac{t}{D_b} \right) \quad (6.12)$$

Eq. 6.11 is valid for $\alpha_b \leq 9$ and $q_b \leq 3.8 \text{ MN/m}^2$

Briaud 1985 further developed the Skempton 1959 method by considering the rate of loading, since soil sample for determination of undrained shear strength in laboratory usually comes to failure within approximately 10 min. On the other hand, it has been observed from pile load tests that the failure usually occurs within 0.13 sec after loading. The increase of the undrained shear strength with decrease of time to failure can be quantified as follows:

$$\frac{c_{u1}}{c_{u2}} = \left(\frac{t_2}{t_1} \right)^n \quad (6.13)$$

where

c_{u1} and c_{u2} are the undrained shear strength at time t_1 (pile load test) and t_2

(Laboratory test condition) respectively,

t_1 and t_2 are the time to failure in the case of pile load test ($t_1 = 0.13$ sec) and laboratory test ($t_2 = 10$ min) respectively, and

n is the viscosity exponent.

Assuming Eq. 6.11 is valid,

$$q_b = 9 \cdot \left(\frac{10 \cdot 60}{0,13} \right)^n c_u \quad (6.14)$$

Eq. 6.14 gives values of α_b from 10.7 for $n = 0.02$ (stiff clay) to 21.0 for $n = 0.10$ (soft soil).

d2) *Pile shaft resistance*: The pile shaft resistance is directly correlated with undrained shear strength through the adhesion coefficient α_s according to Eq. 6.15.

$$q_s = \alpha_s \cdot c_u \quad (6.15)$$

Required values of the adhesion coefficient α_s are given in Table 6.9 and Fig. 6.40.

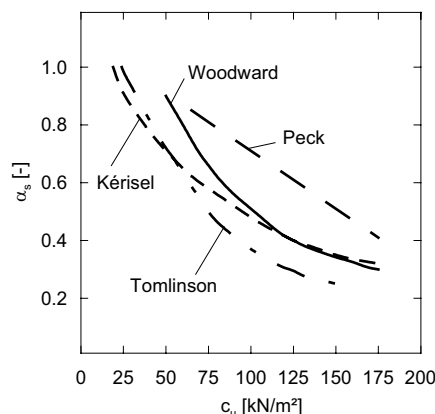


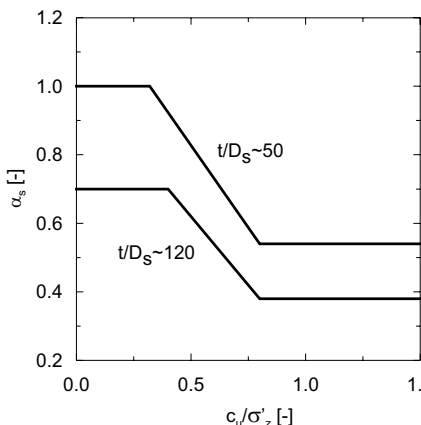
Fig. 6.40. Adhesion coefficient α_s according to McClelland 1974

Table 6.9. Values of the adhesion coefficient α_s (displacement piles)

α_s	Remarks	Reference
$m \cdot r$	$m = 0.8-1.0$ for concrete dependant on the texture of the surface $m = 0.7$ for steel $r = 0.4$	Skov 1997
0.4	$c_u > 100 \text{ kN/m}^2$	Lehane 1997
1.0	$c_u < 30 \text{ kN/m}^2$	
1.0	$c_u \leq 25 \text{ kN/m}^2$	Mandolini 1997
$1.0 - 0.011 \cdot (c_u - 25)$	$25 \text{ kN/m}^2 < c_u < 70 \text{ kN/m}^2$	
0.5	$c_u \geq 70 \text{ kN/m}^2$	
0.6-0.8	Overconsolidated lacustrine soils	Findlay et al. 1997
1.0	$c_u \leq 35 \text{ kN/m}^2$	Poulos 1989
0.5	$c_u \geq 80 \text{ kN/m}^2$	
	linear interpolation between the values for $L/D > 50$	
$1.5 \cdot \tan \delta'$	Long term bearing capacity with: δ' = effective angle of skin friction	Clark and Meyerhof 1972
0.8	Reinforced concrete (3 months after ramming and $c_u \leq 50 \text{ kN/m}^2$)	Broms 1981
0.5	Steel (6 months after ramming and $c_u \leq 50 \text{ kN/m}^2$)	

Adhesion coefficients for piles with conical toe are given in Tomlinson 1994 as a function of the embedment depth into the bearing clay layer and overlaying layer.

According to Semple and Rigden 1984/86, the adhesion coefficient α_s can be given as a function of the ratio of the embedment depth to pile diameter and normalised undrained shear strength as shown in Fig. 6.41.

**Fig. 6.41.** Adhesion coefficient α_s according to Semple and Rigden 1984/86

The method recommended by the American Petroleum Institute for planning, design and construction of stabilized oil plate forms (*API RP 2A 1989*) also considers the dependency of the adhesion coefficient α_s on the normalized undrained strength as given in Eq. 6.16.

$$\alpha_s = 0.5 \cdot \left(\frac{c_u}{\sigma'_z} \right)^{-0.5} \quad \text{for} \quad \left(\frac{c_u}{\sigma'_z} \right) \leq 1.0 \quad (6.16a)$$

$$\alpha_s = 0.5 \cdot \left(\frac{c_u}{\sigma'_z} \right)^{-0.25} \quad \text{for} \quad \left(\frac{c_u}{\sigma'_z} \right) > 1.0 \quad (6.16b)$$

The above method is however only secured at the moment for steel pipe piles with open end.

Fleming et al. 1992 asserted that the shaft resistance of a pile is not only dependant on the shear strength of the soil, but also on the loading history of the soil which can be expressed by the overconsolidation ratio (OCR). Assuming that $\alpha_s = 1.0$ for normal consolidated clay, the following relationships for the factor α_s can be developed based on test results.

$$\alpha_s = \left(\frac{c_u}{\sigma'_z}_{nc} \right)^{0.5} \cdot \left(\frac{c_u}{\sigma'_z} \right)^{-0.5} \quad \text{for} \quad \left(\frac{c_u}{\sigma'_z} \right) \leq 1.0 \quad (6.17a)$$

$$\alpha_s = \left(\frac{c_u}{\sigma'_z}_{nc} \right)^{0.5} \cdot \left(\frac{c_u}{\sigma'_z} \right)^{-0.25} \quad \text{for} \quad \left(\frac{c_u}{\sigma'_z} \right) > 1.0 \quad (6.17b)$$

The subscript nc in Eq. 6.17 represents for normal consolidation state of the soil.

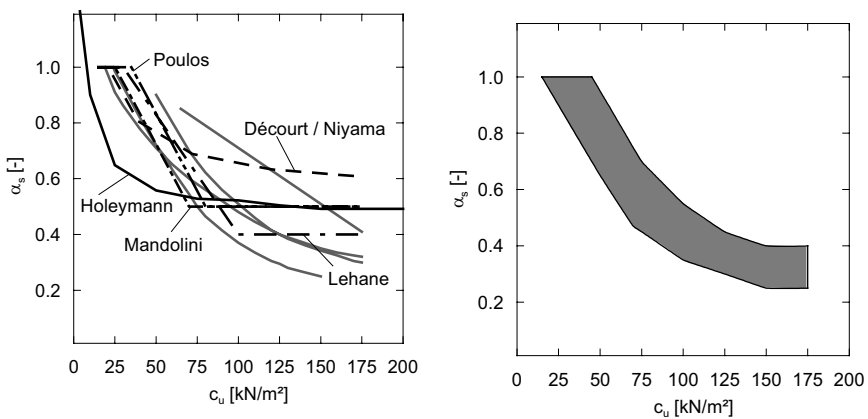


Fig. 6.42. Relationship between the adhesion coefficient α_s and the undrained shear strength c_u (displacement piles)

On the contrary, Randolph et al. 1979 found out from numerical investigation with consideration of the effect of pile ramming that the normalised undrained shear strength is independent from degree of overconsolidation. This means that α is independent from OCR for the case of total stress analysis.

A comparative overview of the commonly used methods for determination of the pile resistance of driving piles are shown in Fig. 6.42a in addition to those given in Fig. 6.40. The different relationships can be summarized as shown in Fig. 6.42b, where a possible zone for the value of the adhesion coefficient α_s is given.

For piles with $t/D_b > 3$, the base resistance q_{bl} is uniformly given in the literature as 9 times the undrained shear strength at a depth of the pile toe. Similar approaches are also used, for example, in France code Fascicule 62-V and Décourt and Niyama 1994. Few methods only approximate the base resistance coefficient $\alpha_b > 9$.

Theoretical methods with effective stresses

Pile base resistance: In this group of methods, the pile base resistance is usually approximated according to modified bearing capacity theory of shallow foundations as shown in Eq. 6.18. As it can be seen from Eq. 6.18, the width component of the equation is ignored, because of the relatively small pile width compared to pile depth.

$$q_b = N_q \cdot \sigma'_v + N_c \cdot c' \quad (6.18)$$

where,

N_q, N_c bearing capacity factors according to Table 6.10,
 σ'_v effective vertical stress in soil at a depth of the pile base.,
 c' effective cohesion of the soil.

This method is predominately used in literature for pile in non-cohesive soils, because the α -Method is usually preferred for piles in cohesive soils. However, as a matter of completeness, the bearing capacity factor N_c is also treated in this section.

For the following reasons, a direct adoption of the classical bearing capacity factors for the shallow foundations N_q and N_c is not possible:

- The base resistance in ultimate limit state does not increase indefinitely with the embedment depth of the pile contrary to what it is expected from the classical bearing capacity equation. At a definite depth onwards the base resistance remains constant (Meyerhof 1976; McClelland 1972; API RP 2A 1989).
- The angle of friction of soil around the pile base changes during pile installation due to high stress condition. The classical bearing capacity factor N_q cannot directly be adopted for piles with the governing angle of friction during the installation process

The relationship between the bearing capacity factors N_q and N_c is given by:

$$N_c = (N_q - 1) \cdot \cot \varphi' \quad (6.19)$$

Table 6.10. Bearing capacity factors N_q und N_c for displacement piles

N_q, N_c	Figure / Tabelle	Reference
$N_q = f\{\varphi'; t/D_b\}$	Fig. 6.43 und Table 6.10	Berezantzev et al. 1961
$N_q, N_c = f\{\varphi'\}; t/D_b$	Fig. 6.43	Meyerhof 1976
$N_q = f\{\varphi'\}$	Fig. 6.43	Schram Simonsen and Athanasiu 1997
$N_q = f\{\text{soil type}; \delta\}$	Table 6.14	McClelland 1974
$N_q = f\{\text{soil type}; \delta\}$	Table 6.14	API RP 2A 1989

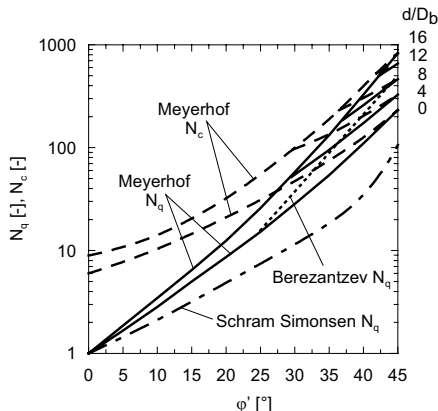
The most commonly used method for determination of the bearing capacity factor N_q for piles is that recommended by Berezantzev et al. 1961. This method takes into account the relationships between the friction angle of the soil φ' , the ratio of the pile embedment depth to its diameter t/D_b and the bearing capacity factor N_q . The values of N_q in Fig. 6.43 must be reduced relative to the ratio of the embedment depth to the pile diameter (Table 6.11).

The decessive factor in determination of the bearing capacity factor N_q is reasonable approximation of the effective friction angle which is affected by pile installation. This is because N_q is very sensitive to the angle of friction φ' . A small change in φ' can lead to a large change in the bearing capacity factor.

According to the Poulos and Davis 1980, the effective friction angle after pile installation can be approximated from:

$$\varphi' = \frac{\varphi'_I + 40}{2} \quad (6.20)$$

where φ'_I is effective friction angle before the pile installation.

**Fig. 6.43.** Values of N_q and N_c for displacement piles

Meyerhof 1976; McClelland 1974; API RP 2A (1989) suggest a maximum value for the characteristic pile base resistance $q_{b,max}$ at a depth of the pile toe.

$$q_{b,max} [MN/m^2] = 5 \cdot N_q \cdot \tan \varphi' \quad (6.21)$$

where N_q is the bearing capacity factor for short piles ($d/D_b \leq d_{crit}/D_b$)

Table 6.11. Correction values for the bearing capacity factor N_q as a function of t/D_b according to Berezantzev et al. 1961

t/D_b	φ'				
	26°	30°	34°	37°	40°
5	0.75	0.77	0.81	0.83	0.85
10	0.62	0.67	0.73	0.76	0.79
15	0.55	0.61	0.68	0.73	0.77
20	0.49	0.57	0.65	0.71	0.75
25	0.44	0.53	0.63	0.70	0.74

Pile shaft resistance: The calculation of shaft resistance using theoretical soil mechanics methods was originally based on the strength equation along the pile-soil-interface with friction angle φ , adhesion c_a and normal stress $\sigma_x = K \cdot \sigma_z$.

$$q_s = \sigma_x \tan \varphi + c_a = K \sigma_z \tan \varphi + c_a \quad (6.22)$$

A simplified formula that can be applied for both cohesive and non-cohesive soils is given as follows:

$$q_s = \gamma z \tan \varphi K = \gamma z \beta \quad (6.23)$$

In cohesionless and normally consolidated clay soils, Eq. 6.24 is commonly used:

$$\beta = K \tan \varphi = K_0 \tan \varphi = (1 - \sin \varphi) \tan \varphi \approx 0.25 \quad (6.24)$$

For cohesionless soils approximately a constant skin friction can be assumed beyond a critical embedment ratio ($t/D_s \approx 15$), similar to the base resistance. For these conditions typical β -values are not available. K can be estimated on the basis of experience, from K_o -value, the pile type and the size, and compressibility of the soil. The maximum K -value can be less than the K_o -value for drilled piles; for displacement piles in dense sand the values of K can range between $4 \cdot K_o$ up to $K_p = \tan^2(45 - \varphi/2)$ near the ground surface. As a result of the larger soil displacement for closed end pile sections. K -values are markedly larger than for open section displacement piles. For cohesive soils the β -values are summarized from the literature as shown in Table 6.12.

For very long open end steel pipe piles (e.g. offshore steel pipe piles), design parameters are given by McClelland 1974; API RP 2A 1989 as shown in Table 6.13. In case the soil builds a strong graft within the pipe, the whole area of the circular cross section can be taken as area of the base resistance similar to solid piles. However, if the soil does not build a graft within the pipe, the ring cross section of the pipe is taken as the area for transfer of the base resistance.

Table 6.12. β -values for cohesive soils compiled from the literature

Cohesive Soil	K	β	Pile Type	Reference
normally consolidated. $I_L > 0.25$	(1 - sin ϕ)	approximately 0.25	slender piles	[11]
		0.3 with $l = 15$ m		[58]
		0.15 with $l = 60$ m		[58]
overconsolidated. $I_L > 0.25$ ($c_u = 50$ to 120 kN/m 2)	(1 - sin ϕ) \sqrt{OCR}	0.5 to 2.5	displacement piles	[58]
		0.5 to 1.5		bored piles [58]
London clay ($I_L \approx 0.0$) $K_0 \approx 3$	(1 to 2) K_0	1 to 2	displacement piles	[11]
	(0.7 to 1.2) K_0	0.7 to 1.4		bored piles [11]

[11]: Burland 1973; [58]: Meyerhof 1976

Table 6.13. Design parameters for bearing resistance of driven steel pipe pile in sand (Pile base and shaft resistance)

Density	Soil type	API RP 2A 1989	McClelland 1974	Friction angle between pile surface and soil	API RP 2A 1989	McClelland 1974	API RP 2A 1989	McClelland 1974
		$q_{s,max}$ [MN/m 2]		δ [$^\circ$]	N_q [-]		$q_{b,max}$ [MN/m 2]	
Very loose	S							
loose	SM	0.0478	0.0538	15	8	8	1.9	2.2
medium dense	M							
loose	S							
medium dense	SM	0.0670	0.0753	20	12	12	2.9	3.2
dense	M							
medium dense	S							
dense	SM	0.0813	0.0915	25	20	20	4.8	5.4
dense	S							
very dense	SM	0.0957	0.1076	30	40	40	9.6	10.8
dense	G							
very dense	S	0.1148	–	35	50	–	12.0	–

Numerical methods

Numerical methods such as the Finite Element Method (FEM) or Boundary Element Method (BEM) are powerful methods to solve a complex problems and they find more acceptance in engineering practice. The finite element method is also used in geotechnical engineering since 30 ago to study the bearing capacity and the resistance-settlement behaviour of piles. A reasonable result can be achieved with the finite element calculation, if the soil properties do not essentially change during the installation of the pile (e.g. bored piles).

The description of the soil properties and the influence zone is very difficult. The soil surrounding the pile is displaced and compacted during driving the pile and consequently its property changes strongly. This change in the property of the surrounding soil has a decisive influence on the bearing capacity of piles. The numerical simulation of the displacement effect is not yet clear. Some literature on this topic are summarised in the following.

It is believed that the soil maintains the stresses due to pile driving even after complete installation of the pile, which possibly affect the resistance-settlement behaviour of the pile. Although Vesic 1977b; Poulos 1987 pointed out the importance of the residual stresses for the resistance-settlement behaviour of piles, most of the methods used are based on residual stress free piles. According to Holloway et al. 1978, the ignorance of the residual stresses after the pile installation may lead to overestimation of the shaft resistance and underestimation of the base resistance, thus a false distribution of the real part of the resistance in the ultimate limit state.

As simpler first approximation, Poulos 1987 suggested that the residual stresses in the pile subsequent to installation can be estimated by using static analysis in which the pile (at final penetration) is loaded to failure in compression and then unloaded back to zero. The stresses which remains in the pile after such static analysis can be taken as an approximation of the residual stresses due to driving effect for further numerical calculation of the bearing capacity of the pile. A computer program TAPILE had been developed to perform the static analysis, which requires the following input parameters:

- the distribution of the Young's modulus (or shear modulus) and Poisson's ratio of the soil with depth along and beneath the shaft,
- the distribution of the limiting shaft resistance along the pile for both tension and compression loading, and
- the limiting base resistance of the pile for both tension and compression loading

The Poisson's ratio of the soil is not an important parameter in the analysis and may be estimated (e.g. 0.3 for piles in sand, 0.5 for piles in clay under undrained conditions) The limiting shaft and base resistance are usually assessed either by total stress analysis for piles in clay or by an effective stress analysis which can be applied to shaft resistance in either clay or sand and to base resistance in sand.

Altaee et al. (1992b) introduced a numerical analysis for the simulation of the installation and loading processes for cast-in-situ concrete displacement piles. The boundary condition and the results of analysis is given in detail in Altaee et al. 1992a. The calculation was conducted using the finite element method, whereby a plastic material behaviour of the soil was simulated. The critical state is used as a boundary surface. The required model parameters had been derived from cone penetration test (CPT) (Altaee et al. 1992a) and standard penetration test (SPT) as well as values from own experience and literature from comparable soil condition. The initial stress (before pile installation) was generated based on the in-situ density obtained from the field test, the groundwater condition and K_0 value.

The excess pore pressure developed in the surrounding soil due to pile driving can be estimated according to Desai 1978 based on the cavity expansion approach. The results of this approach can be used as initial condition for finite simulation of the resistance-settlement behaviour of piles.

According to Desai 1978, the pile driving produces different stress and excess pore pressure conditions. The soil material directly near the pile are near to failure (Zone I). Next to this zone up to a distance approx. equal to r_0 from pile axis exists a zone where the soil is in plastic condition (Zone II). Thereafter is the elastic zone (Zone III) (Fig. 6.45).

As simplification to the more complicated cavity expansion approach, i.e. indefinite expansion of the cavity, it can be assumed instead a cylindrical cavity expansion which is equal to the volume of the fully installed displacement piles (Fig. 6.44). Moreover, it is assumed that the main part of deformations occur in the horizontal direction, which does not hold true for areas around the pile head and toe. However, the simplification leads to a realistic solution according to Desai 1978.

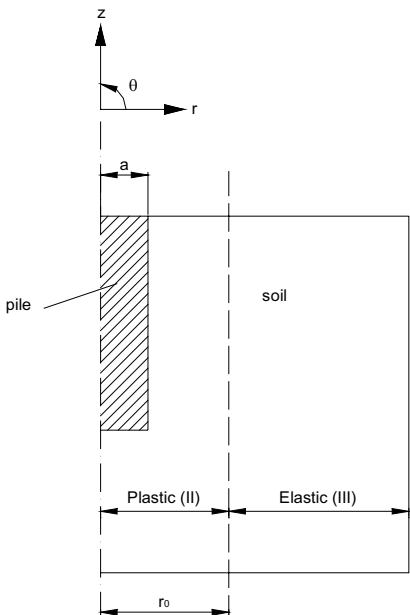


Fig. 44. Simulation of pile driving by cavity expansion (after Desai 1978)

The presented approaches for numerical simulation of displacement piles are normally not yet convenient for practical applications. Satisfactory results can be achieved for bored piles, if the numerical model is calibrated on the basis of pile load test.

6.4.6 Change of the bearing capacity of piles with time

It is generally known that the bearing capacity of pile, especially displacement piles increases with time. In the past it has already been observed that the shaft resistance increases up to 250% (Witzel 2004).

Chow et al. 1996 analyzed pile load test results of different piles: steel, reinforced concrete, timber piles in saturated and unsaturated carbonate free sand. They found out that the shaft resistance increases with time, whereas the base resistance remains constant. There are three hypothesis which may explain this phenomenon, whereby the third hypothesis provides a plausible explanation of the increase in shaft resistance.

1. Chemical processes, in particular corrosion of steel piles.
2. Change in sand property arising from ageing of the sand.
3. Long term increase of the horizontal stress in soil σ'_h (radial stresses surrounding the pile).

Chow et al. 1996 observed a regular increase of the bearing capacity in the first five years after the installation of the pile. The values of the shaft resistance follows a semi-logarithmic line with time after the pile installation. The quotient $R_s(t)/R_s(t = 1d)$ increases with each logarithmic cycle between 25 and 75% as shown in Eq. 6.24.

$$\frac{R_s(t)}{R_s(t = 1d)} = 1 + A \cdot \log\left(\frac{t}{t = 1d}\right) \quad (6.24)$$

where A is an empirical factor with an average value of 0.5 (± 0.25)

The above equation is plotted in Fig. 6.45 for the total pile resistance ($Q_T = R$) and the shaft resistance ($Q_S = R_s$) for displacement piles in non-cohesive soils.

Based on different pile load tension tests in northern Germany, Berger 1986 quantified the effect of the time on bearing capacity of driving tension piles with a time factor $Z(t)$. The increase in pile resistance within the first 14 days can remain unconsidered, so that the shaft resistance can be estimated from Eq. 6.25.

$$R_s(t) = R_s \cdot (Z(t) - 0.82) \leq 1.32 \cdot R_s \quad (6.25)$$

where

$R_s(t)$ limiting shaft resistance at time t

R_s calculated value of shaft resistance

$Z(t)$ time factor according to Eq. 6.26

$$Z(t) = C \cdot \frac{(e^{\alpha t} - e^{-\alpha t})}{e^{\alpha t} + 0.5e^{-\alpha t}} \quad (6.26)$$

C constant ($C = 0.5$)

α constant ($\alpha = 1/45$)

t number of days after the end of pile driving.

It is already discussed that the shaft resistance of piles in short term (undrained condition) can be better expressed by the undrained shear strength of the soil c_u (α -Method). With increasing time however the effective shear parameters φ' and c' (β -Method) seems to better describe the shaft friction behaviour of piles.

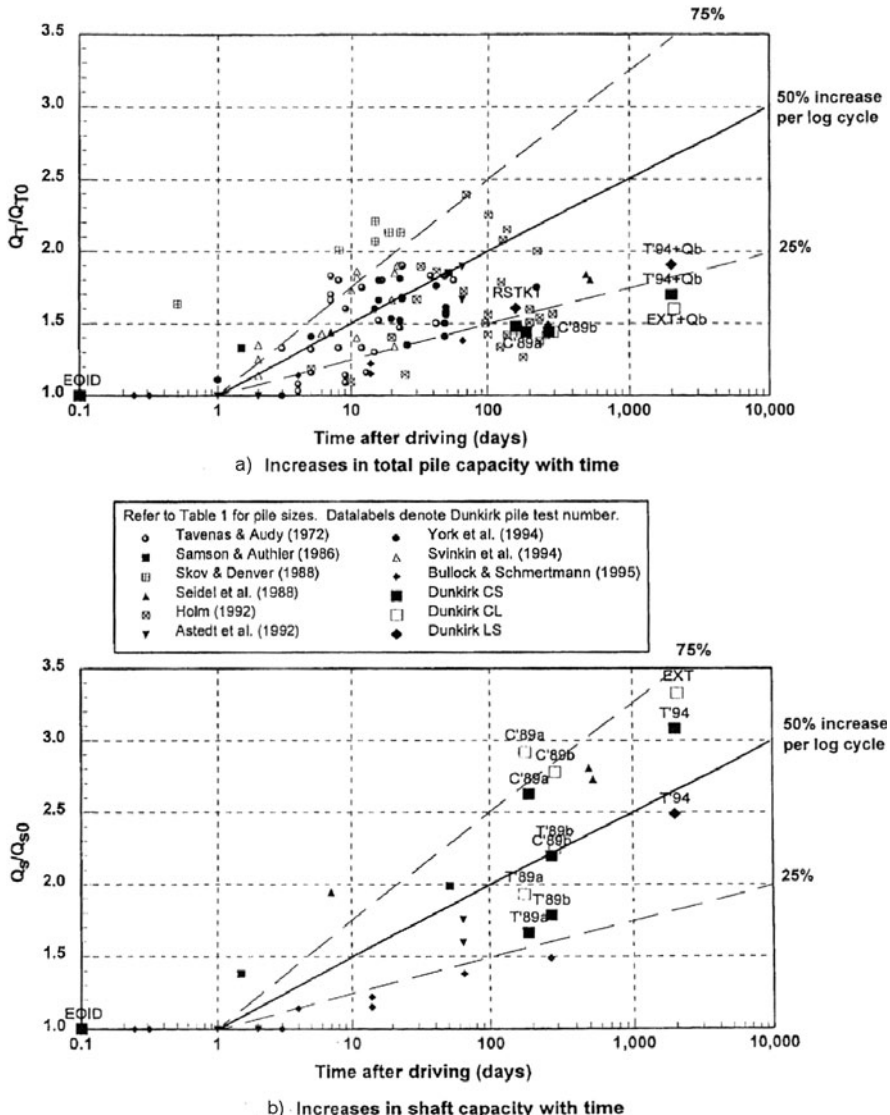


Fig. 6.45. The increase in pile resistance of displacement piles in non-cohesive soils (after Chow et al 1996)

According to Vesic 1975; Jardine and Chow 1996, the increase in shaft resistance can be controlled by the following time factor T :

$$T = (4 \cdot c_h \cdot t) / D^2 \quad (6.27)$$

where

c_h coefficient of horizontal consolidation of the soil

t time after pile installation

D Pile diameter

Jardine and Chow 1996 had observed that 70% of the maximum observed bearing capacity of closed steel piles and steel pipe piles with strong graft of the soil within the pipe can be activated by time factor $T = 10$. The increase in bearing capacity ceased by a time factor of about $T \approx 100$.

According to Tomlinson 1994, the increase in bearing capacity can be observed in soft cohesive soils only, whereas a decrease in bearing capacity may occur in stiff cohesive soils after long period of time. (Table 6.14).

Table 6.14. Decrease in bearing capacity of displacement piles (after Tomlinson 1992)

Pile type	Soil type	Decrease in bearing capacity ¹⁾	Reference
Driven precast reinforced concrete	London clay	10 – 20 % 9 months after the 1 st pile load test	Meyerhof/Murdock (1953)
	Aarhus (Septarian) clay	10 – 20 % 3 months after the 1 st pile load test	Ballisager (1959)
Driven steel pipe pile	London clay	4 – 25 % 12 months after the 1 st pile load test	Tomlinson (1970)

¹⁾ the 1st pile load test had been conducted one month after driving of the pile

6.5 Negative skin friction

6.5.1 General

The effect of the negative skin friction on pile foundations arises from a relative displacement of the soil and the pile in axial direction. This relative displacement is normally caused by settlement of a compressible soil layer, which in turn may be resulted for example due to additional surface loads, consolidation of the compressible soil layer or groundwater level fluctuations (Fig. 6.46). The weight of the compressible soil layer and the layer above it will hang on the pile shaft due to the skin friction and produces a down-drag force on the pile. This skin friction is op-

posite to the shaft resistance arising from pile settlement only, therefore, it is designated as negative skin friction. A negative skin friction may also be developed in tension piles in bottom slabs anchorage system due to heave of the soil surrounding the pile.

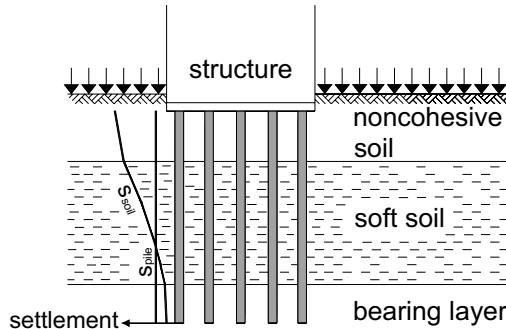


Fig. 6.46. Settlement of the soft soil layer due to consolidation, groundwater lowering, etc.

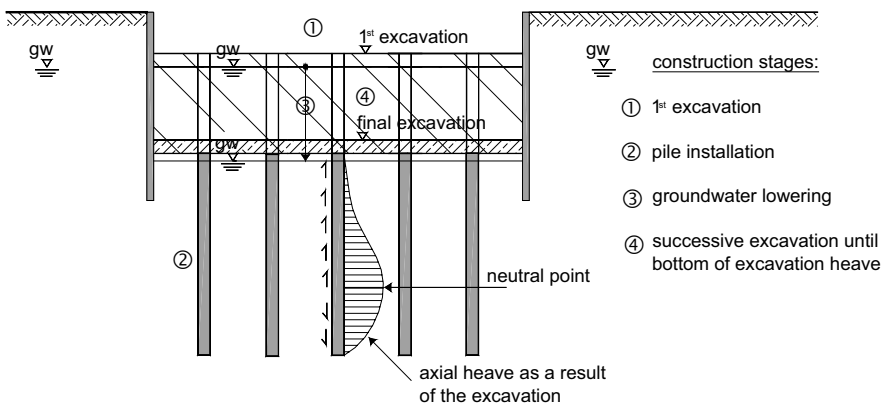


Fig. 4.47. Heave in bottom slab anchorage system

The negative skin friction can be estimated using the total safety factor concept in different ways. The two commonly used procedures are:

- reduction of the pile resistance by an amount equal to the downdrag force (reduced pile bearing capacity). or
- increase of the pile load by amount equal to the downdrag force.

This leads to different total safety factors for the pile foundation.

According to the new partial safety factor principle, however, the negative skin friction on piles is clearly defined as an action, which leads to an additional down-drag force F_n on piles. For the practical verification of safety of the pile founda-

tion, a distinction should be made between the serviceability and ultimate limit states (SLS and ULS respectively), in which each limit state requires different input value of negative skin friction.

6.5.2 Neutral point

The actions arising from the negative skin friction together with the actions from the structural loads are in equilibrium with pile base resistance depending on the settlement. Fig. 6.48 shows an illustration of the interrelationship between these forces for two cases:

- when the action F_a from structural load is relatively low and thus small pile settlement s_a , the part of the actions arising from the negative skin friction F_n becomes larger and the influence of τ_n extends further deep,
- On the other hand, a large actions from structural load F_b may give rise to a higher pile settlement and can lead to the mobilisation of the shaft resistance q_s due to the relative movements between soil and pile.

The point where the negative skin friction changes over to positive shaft resistance is called the neutral point.

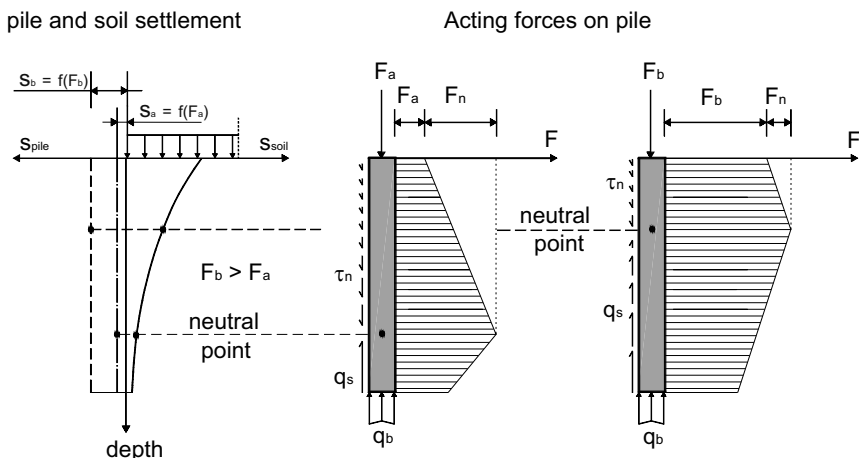


Fig. 6.48. Qualitative illustration of the interrelationships between the pile resistance, actions from structural load, negative skin friction and the neutral plane of piles in homogeneous soil (Kempfert et al. 2003). Note: only a change in axial pile direction is presented in the diagrams

6.5.3 Actions arising from negative skin friction

An appropriate estimation of the negative skin friction τ_n on a pile requires the following information:

- the distribution of the pile settlement with depth,
- the distribution of the settlement of the compressible soil layer with depth,
- the relative displacement of the pile and the soil, and
- mobilisation functions for τ_n and q_s , if necessary

Essentially, there are two approaches usually used in the literature for the determination of the characteristic value of negative skin friction τ_n :

- The total stress method for cohesive soils:

$$\tau_n = \alpha \cdot c_u \quad (6.28)$$

where α is a factor which determines the magnitude of the characteristic skin friction τ_n for cohesive soils and c_u is the characteristic undrained strength of cohesive soils.

The value of α depends on the properties of the pile material and the surrounding soils and lies between 0.15 and 1.60 (Table 6.15). DIN 1054:2005-01 sets $\alpha \approx 1.0$.

Table 6.15. Compilation of the α -values for different soil types

Soil type	α	Reference	Remark
Sandy silt	0.50-1.70		Compression end pile
	0.65-1.60	Endo et al. 1969	Inclined compression end pile
	0.50-1.30		Friction pile
Silty clay	0.27-2.13	Little et al. 1989	Compression end model pile
	0.40-0.50	Little 1994	Field measurements
Clay	0.17-0.22	Puri et al. 1991	Model piles
	0.16-0.43	Mohan et al. 1981	
	0.40-0.61	Fellenius 1971	Field test
London Ton	0.65-0.85	Tomlinson 1970	Long/short bored piles
	0.50-0.60		Grouted piles
	0.30	Burland et al. 1966	Field test
Clay	1.00	Auvinet et al. 1981	Driven piles
Soft clay ($c_u = 50 \text{ kN/m}^2$)	1.00/0.80/0.50	Broms 1966	Timber piles
			Bored concrete piles
			Bored steel piles
peat	0.42	Cognon 1972	Field measurements
	1.00	Weiß 1974	Timber piles
-	0.30-1.50	Broms 1979	Statistical derivation

- The effective stress method for cohesive and non-cohesive soils:

$$\tau_n = K_o \cdot \tan \varphi' \cdot \sigma'_v = \beta \cdot \sigma'_v \quad (6.29)$$

where σ'_v is the effective vertical stress, K_0 is the coefficient of the earth pressure at rest, ϕ'_k is the characteristic value of the angle of internal friction and β is a factor which determines the magnitude of the characteristic skin friction τ_n for cohesive and non-cohesive soils.

Depending on the type of soil, the value of β varies between 0.1 and 1.0 (Table 6.16). Most often a value of $\beta = 0.25$ to 0.30 is used for non-cohesive soils.

Table 6.16. Compilation of the β -values for different soil types

Soil type	β	Reference	Remark
Brocken rock	0.40	Kempfert 2001	For single pile with a settlement rate of about 10 mm/year
Sand, gravel	0.35	Kempfert 2001	For single pile with a settlement rate of about 10 mm/year
Brocken rock	0.40	Kempfert 2001	For single pile with a settlement rate of about 10 mm/year
Sand, gravel	0.35	Kempfert 2001	For single pile with a settlement rate of about 10 mm/year
Sand	0.35-0.50	Broms 1979	
	0.26-0.79	Lebegue 1964	
	2·(tan ϕ'_k - tan 24°)		increase with depth
	0.26-0.52	Bakholdin 1974	decrease with depth (concrete pile)
	0.30-0.40	Garlanger 1974	Steel pile
	0.40	York 1974	Steel pile
	0.60	Kishida 1976	alluvial sand in Japan
Sand, gravel			
Very loose	0.35	Bustamante 1999	
loose	0.45	Bustamante 1999	
medium dense	0.45	Briaud et al. 1991	Bored piles
dense	1.00	Bustamante 1999	
very dense	0.50- >1.00	Briaud et al. 1991	Bored piles
Silt, silty sand ($I_p = 0.05-30$, $I_c = 0$)	<0.10-0.35		Compression end piles
	0.20-0.40	Endo et al. 1969	inclined compression end piles
	0.15->0.40		friction piles driven piles
Loess	0.18	Grigorian et al. 1975	Reinforced concrete piles
Silt	0.25-0.30	Kempfert 2001	For single piles, derived empirically
	0.25-0.30	Broms 1979	
	0.20-0.25	Fellenius 1971	Field test
organic silt ($I_p = 60\%$, $I_c = 65\%$)	0.30	York 1974	Steel pile
Silt-clay			
Very soft	0.20-0.25	Fellenius 1971	Driven reinforced concrete piles
soft	0.10-0.15(0.20)	Bustamante 1999	Bored driven piles
stiff	0.15-0.20(0.30)	Bustamante 1999	Bored driven piles
very stiff	0.20 (0.30)	Briaud et al. 1991	Bored driven piles

Table 6.16. Continued

Soil type	β	Reference	Remark
Clayey silt	0.19	Gant 1959	driven piles
	0.41-0.56	Bozozuk et al. 1979	compression end piles
	0.44-0.60		friction piles driven steel piles
Lean clay	0.20		For single piles, derived empirically
Medium plastic clay	0.15	Kempfert 2001	
Plastic clay	0.10		
Ton ($I_p = 30 \%$, $I_c = 0-50 \%$)	0.20	Little 1994	Steel and reinforced concrete piles
normalkonsolidiert $w_L \leq 50 \%$ $w_L > 50 \%$	0.30	Kempfert 2001	with a settlement rate of about 10 mm/year
	0.20		
Kaolin	0.18	Kempfert 2001	Model test on a vertical single pile
	0.24-0.29	Kempfert 2001	
Soft clay	≤ 0.25	Burland 1973	Measurments on steel piles Statistically derived from large scale tests
-	0.25	Broms 1979	general assumption in canada,
Soft clay	0.20-0.30	Meyerhoff 1976	The lower value is valid for a depth < 15 m and the upper value for a depth > 60 m
Kaolin ($I_p = 13 \%$, $I_c = 0 \%$)	0.15-0.18	Shibata et al. 1982	Small scale model tests on steel piles
Bangkok clay ($I_p = 30-45 \%$, $I_c = 0 \%$)	0.15-0.20	Indraratna 1992	Measurments on steel piles
marine clay (very soft to soft)	0.18	Bozozuk 1972	Reinforced concrete piles
	0.24-0.30		Model piles
Clay ($I_p = 20-30 \%$, $I_c = 50 \%$)	0.20-0.25	Takashi et al. 1974	
	0.20	Garlanger 1974	Field tests
	0.30	Johannessen et al. 1965	Driven steel pile
		Kishida et al. 1974	alluvial clay in Japan (general assumption)
Organic soil	0.10-0.15 (0.20)	Bustamante 1999	Bored driven piles
	0.15		Driven piles with open ends
	0.20	Briaud et al. 1991	Driven piles with close ends
	0.15		Bored pilesl
Sonstiges	β	Quelle	
Coated with asphalt	0.02	Briaud et al. 1991	
Betonite slurry	0.05	Briaud et al. 1991	

The negative skin friction of a non-cohesive fill material above the compressible layer may lead to a large effects of actions on the pile, therefore, the resulting characteristic effects of actions should not be greater than the overburden weight

of this layer. This regulation, however, is only meaningful for closely placed piles in a group.

The influence of the negative skin friction extends up to the neutral point. In reality, however, there exist a transition zone where the negative skin friction changes over to positive shaft resistance and this transition is usually assumed as linear. Fellenius 1972 called the transition zone a neutral plane. Within the transition zone, the negative skin friction is therefore not fully mobilised. The length of the neutral plane depends on the relative displacement between pile and soil (Fig. 6.49). The smaller the angle α between the intersecting settlement lines of the pile and soil, the more will be the transition zone from negative to positive skin friction.

For practical applications, the neutral point only is assumed without the transition zone between τ_n and q_s . The maximum effects of action on the pile in axial direction occurs in each case at this point, since the total downdrag force of the downward directed actions arising from the negative skin friction increases and no load reduction can take place up to this point, since no pile resistance is mobilised. Furthermore, the settlement of the pile coincides with the settlement of the surrounding soil at the neutral point.

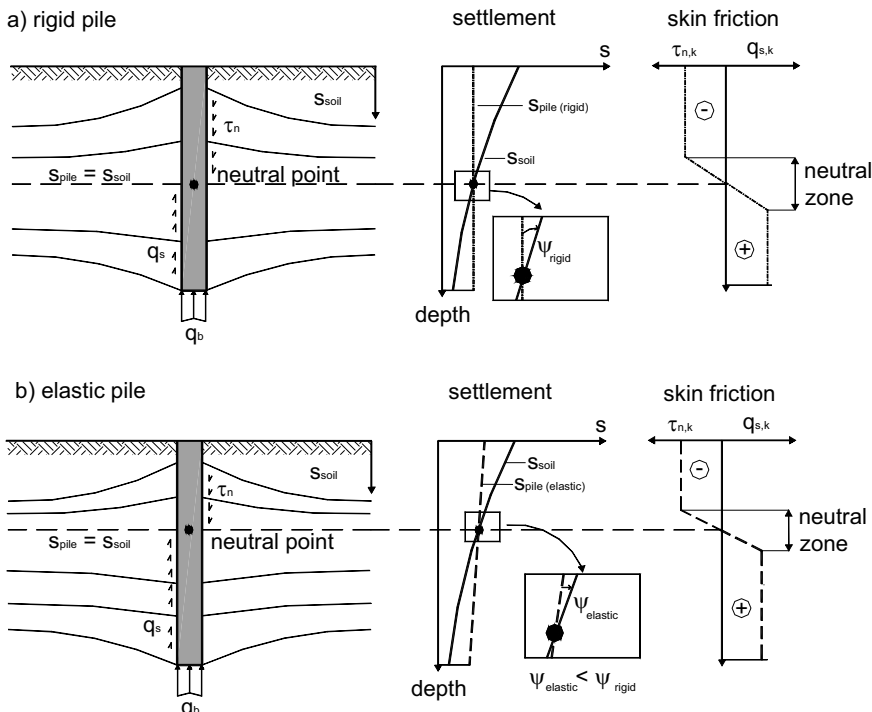


Fig. 6.49. Overview of the negative skin friction and the mobilisation of the pile shaft resistance depending on the intersection angle of the settlement lines of the pile and soil ψ , a) a rigid pile, b) elastic pile (originally from Fellenius 1972, adopted from Kempfert 2005)

The neutral point is located near the pile toe in case of end bearing piles, whereas it is usually located in the above half of the pile in case of friction piles.

In the determination of the location of the neutral point in the serviceability limit state (SLS) and hence the magnitude of the action F_n , it is usually recommended to calculate the settlement of the surrounding soil s_n using the characteristic parameters for the final condition (drained condition), i.e., with due consideration of the consolidation and creep settlement. A comparison of the pile settlement s and the settlement of the soil s_n gives the location of the neutral point.

In the ultimate limit state ULS, it is recommended to set the pile settlement s_{ult} according to the selected pile bearing capacity calculation method in ULS in the determination of the location of the neutral point and the magnitude of the actions $F_{n,ult}$. A comparison of s_{ult} and s_n gives the location of the neutral point in the ULS, which can be located differently as that in the SLS.

The estimated pile settlements in the ULS do not normally occur in reality under the applied working loads (characteristic actions). The verification of the bearing capacity in ULS thus takes place on basis of a fictitious deformation state.

For closely spaced piles in a pile group, the negative skin friction can be reduced due to group action. If, as a result of negative skin friction, the allowable pile loads are exceeded and too many additional piles may therefore be required, the negative skin friction can be reduced or eliminated by construction measures, such as coating of the pile shaft with bitumen or by the application of collars.

6.6 Lateral loads and settlement bending

The effects of lateral pressure on piles are also called passive horizontal loads. Lateral loads can be caused for example by lateral deformations due to asymmetrical surface loads or by large asymmetrical excavations, if the pile is tied into firmer ground at its base. Similarly, batter piles can experience loading during vertical ground movements. In soft soils such deformations commonly cause bending of the piles as shown in Fig. 6.50.

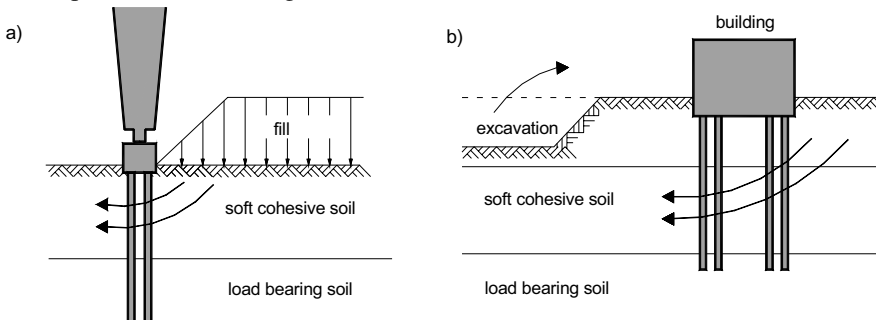


Fig. 6.50. Examples of the development of lateral pressure on pile foundations caused by:
a) asymmetrical surcharge, b) excavation on one side only

Along slopes lateral loading of pile foundations can occur, even if soft layers are not encountered, particularly if the piles are used as stabilising elements.

Lateral loads on piles can be predicted from three dimensional finite element models or by the methods suggested in FGSV 1994.

Pile foundations may fail due to lateral loads after longer time periods. The cause for these failures are not clearly understood. The deformations can be grouped according to the time sequence in which they occur:

- shear deformations at constant volume during load application
- deformations due to consolidation of the soil
- long term creep deformations

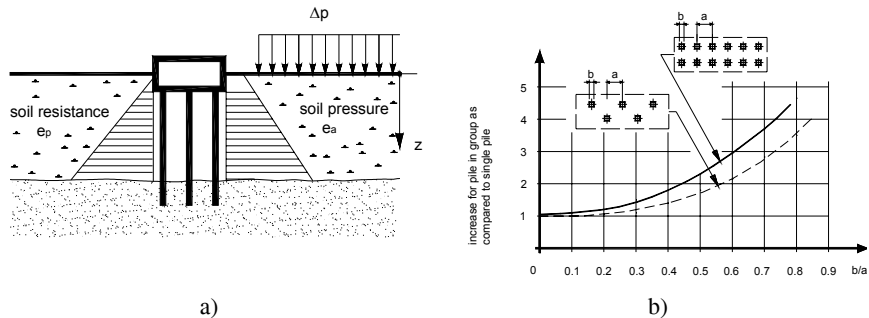


Fig. 6.51. a) Layout for comparison of earth pressures; b) increase in the effect of differential earth pressure on a single pile depending on the geometry of the pile group (after Meyerhof 1959)

In order to calculate the magnitude of the lateral loads, two extreme cases may be considered:

- the soil flows around the pile, loading the pile with the flow pressure p_f
- the pile is loaded by the resultant earth pressure Δe , which is the difference between active and passive earth pressure.

The smaller of the two values is governing. Various suggestions for the flow pressure p_f in case of (a) can be found in the literature, e.g.,

$$p_f = (3 \text{ to } 10) \cdot c_u \quad (6.30)$$

According to FGSV 1994 a characteristic flow pressure can be used where:

$$p_f = 7 \cdot c_u \quad (6.31)$$

The characteristic resultant earth pressure according to case (b) can be calculated from:

$$\Delta e = e_a - e_{pv} \quad (6.32a)$$

$$e_a = \gamma \cdot z + \Delta p - 2c_u \quad (\text{if } c_u \text{ is used}) \quad (6.32b)$$

$$e_a = \gamma \cdot z \cdot K_a + \Delta p - 2c' \cdot \sqrt{K_a} \quad (\text{if } c' \text{ and } \varphi' \text{ are used}) \quad (6.32\text{c})$$

$$e_a = \gamma \cdot z \cdot K_a + U_c \cdot \Delta p \cdot K_a + (1-U_c) \cdot \Delta p - 2c' \cdot \sqrt{K_a} \quad (\text{for partial consolidation}) \quad (6.32\text{d})$$

$$e_p = \gamma \cdot z \cdot K_p \quad (6.32\text{e})$$

where Δp = surcharge load
 U_c = degree of consolidation
 K_p = 1.0

The characteristic horizontal load on a single pile is then calculated from:

$$E_h = \Delta e \cdot a \quad (6.33)$$

For loading width “ a ” the smallest of the following values are governing: pile spacing; three times the pile diameter; thickness of the cohesive soil layer; or total width of the pile group divided by the number of piles. The lateral load also depends on the distance between the pile and the surcharge responsible for the lateral load. Noticeable lateral deformations should be expected within distances of up to twice the thickness of the soft soil layer. For larger distances it is recommended (FGSV 1994) that lateral pressures should be applied as listed in Table 6.17.

Even if no lateral loads on the piles were calculated, piles in soft, cohesive soils should always be designed for minimum bending moments as shown in Fig. 6.52.

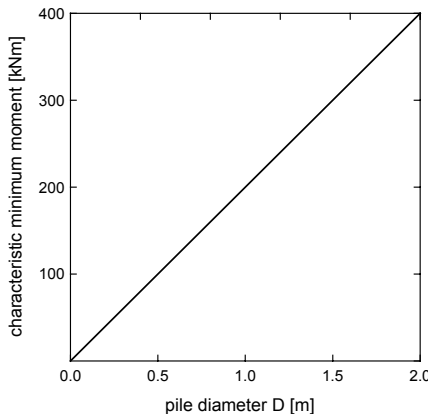


Fig. 6.52. Characteristic minimum pile moment (after Meyerhof 1959)

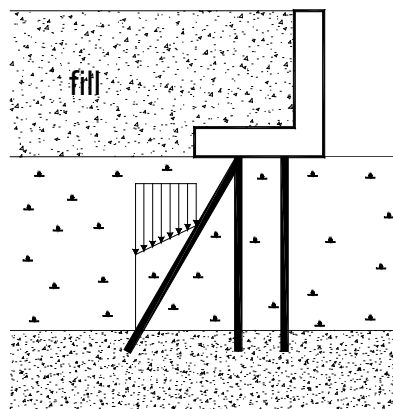


Fig. 6.53. Effect of negative skin friction on raking piles (after Meyerhof 1959)

Table 6.17. Effect of lateral earth pressure changes on distant pile foundations (from FGSV 1994)

Distance [m]	10 to 25		25 to 40	
thickness of the soft soil layer [m]	15-30	5-15	15-30	5-15
reduction of the resulting earth pressure (%)	10-20	5-15	5-15	approx. 5

The lateral pressure on the piles can be reduced by the following measures:

- soil exchange or soil improvement
- placement of fill before installation of the piles
- preloading
- reduction of the slope height
- flattening of slopes
- arrangement of collar piles, which shield the structural pile from the soil deformations.

Factors, which may cause the bending of piles due to settlement are shown schematically in Fig. 6.53. For batter piles the effects of the horizontal component from the pressure by soil flow (Eq. 6.31), or the earth pressure difference according to Eq. (6.32) and of the vertical components from the vertical surcharge can be applied over an influence width per pile of $3D_s \leq 3 \text{ m} \leq \text{pile spacing}$. The vertical components acting on the piles must be less than the pressure from the soil flow according to Eq. 6.31.

6.8 Special pile foundations in deep soft soil deposits

While classical foundation stabilisation methods such as soil replacement, vibro-compaction, etc., are normally not reliable in deep layered soft soils, standard pile foundation with bored and displacement piles embedded deep in bearing layer are usually used, provided that they remain economically feasible.

Besides floating piled raft foundation (section 6.9) which are commonly used in deep soft soil layer, other special pile foundation systems are also applied frequently in such type of soils. These special foundation systems are used on one hand to reduce the settlement through transfer of the stresses into deep bearing layer and on the other hand to avoid the sinking of the raft foundation as a result of consolidation settlement.

In order to reduce settlement and the number of piles used, it can be economical to combine the pile foundation with the so called compensated box type foundation as shown in Fig. 6.54a.

As shown in Fig. 6.54b a small number of piles are arranged to reduce foundation settlement. Since the number of piles is low, the neutral point generally coincides with the pile cap. In that case positive friction is mobilised along the full length of the piles and the piles are in a permanent failure state. Hansbo 1984 called such piles as “creep piles”.

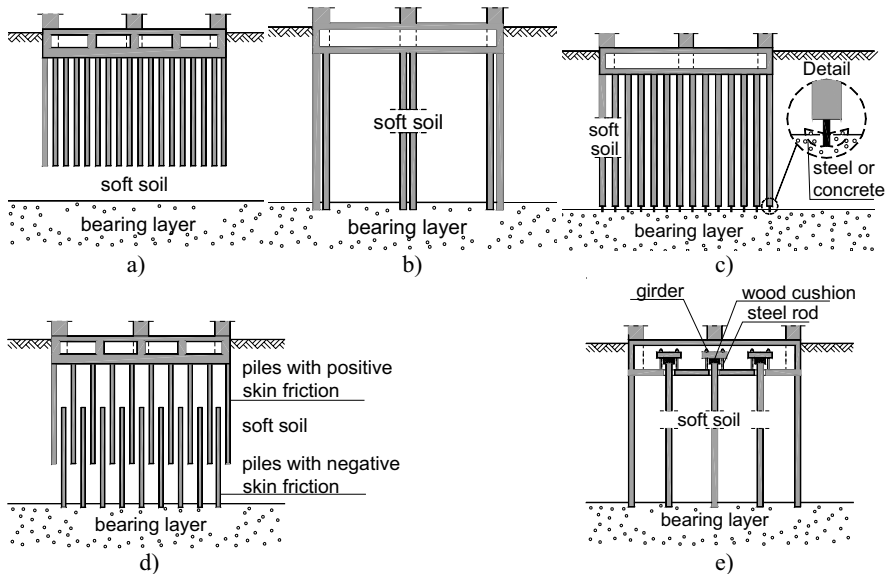


Fig. 7.54. a) Floating piled raft foundation; b) Piled raft foundation with compression pile tip; c) Piled raft foundation with penetrating pile tip; d) overlapped piles (Girault 1964); e) Foundation system with control piles (Flores 1948).

The pile foundation system with a penetration tip shown in Fig. 6.54c was conceived to increase the bearing capacity of friction piles with a controlled contribution of the penetration tip. The diameter of the penetration tip is smaller than the rest of the pile in order to facilitate penetration in the hard layer under combined effect of loading and negative friction and to avoid emersion. The penetration tip can be made of reinforced concrete (Reséndiz 1964; Ellstein 1980) or steel (Reséndiz et al. 1968). In the later case, the bearing capacity of the pile can be better controlled by using a point with a pre-established failure load. Flexibility of the penetration tip consists however a problem during installation of piles (Auvinet (2002).

The pile foundation system with overlapping piles (Fig. 6.54d) (Girault 1964/80) includes conventional friction piles subjected to positive skin friction and used to reduce settlement. Additional settlement reduction follows through friction piles which are embedded in the bearing layer and subjected to negative skin friction. This arrangement not only reduces the increment of stresses in the soil and the corresponding settlement, but also avoids or minimises emersion of the foundation system.

The so called piled raft foundation with control piles (Fig. 6.54e) are equipped at their upper part with a mechanism that controls the load received by each pile. Each pile can also be unloaded by removing the mechanism in order to correct any tilting or emersion of the building. These systems can be sometimes installed during the life of the structure as part of an underpinning process.

Some details of these special foundation system and further references can also be found in Auvinet 2002.

6.9 Raft foundation on floating injection piles (RFIP)

Beside the methods presented in section 6.8, there are other sporadic stabilisation methods in soft underground by using injection with very high pressure known as “soil fracturing”, see for e.g. Santoyo and Ovando-Shellye 2002.

Kempfert 1986 reported for the first time in Germany the positive experiences with “Raft foundation on Floating Injection Piles (RFIP)“ in soft lacustrine soil deposit, which is technically extreme economical due to the considerable settlement reduction compared to shallow foundations and pile foundation. In the mean time the RFIP has been practised by a number of projects. The settlement reduction effect of RFIP compare to shallow foundation is shown in Fig. 6.55. For standard piled raft foundation with bored piles, refer for e.g. to Moermann 2002; Hanisch et al. 2002; Reul 2000; Katzenbach and Arslan 1999; El-Mossallamy 1996; Hanisch et al. 2002.

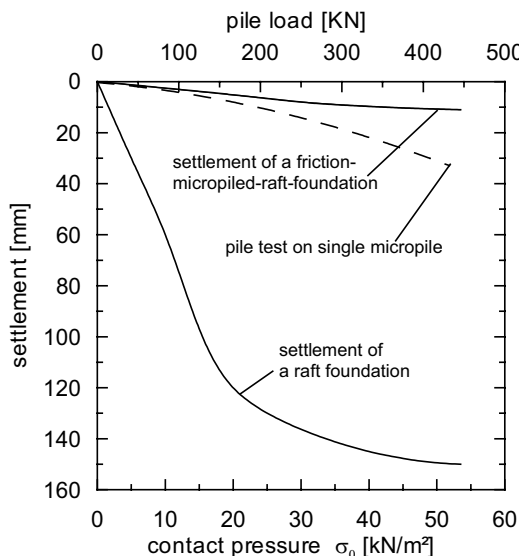


Fig. 6.55. Comparative presentation of the settlement reduction effect of the RFIP foundation system using a project example (project IIa, section 6.10.3) (after Boehm 2006)

Fig. 6.55 shows a settlement reduction up to about 90% with RFIP system compare to a shallow foundation.

For the favourable geotechnical condition of the RFIP system in soft underground contribute mainly the following two effects (Fig. 6.56):

a) Horizontal soil hardening: The high injection pressure (up to 80 bar) results a horizontal hardening in the soft soil with a favourable change of the initial stress conditions.

b) Formation of a lateral sheet of mortar: Similarly, the high injection pressure may also produce predominantly vertical lateral sheet of mortar (Fig. 6.56) around the pile diameter in the soft soil, which on one hand increases the horizontal soil hardening and on the other hand enlarges the pile shaft surface area.

Experiences and some research results of the RFIP can be found in Kempfert and Böhm 2003; Böhm 2006.

The RFIP system consists of mainly:

- Micropiles as injection piles (frequently steel rod) with a length between 15 and 25 m and diameter between 15 and 30 cm arranged uniformly in a quadratic grid system with a spacing of 1 to 3 m. The injection followed under pressure in one to three injection horizons.
- Reinforced concrete raft in which the pile head is connected to its reinforcement.
- Depending on the form of the foundation layout, the soil condition and the pile grid system additional compensated box type reinforced concrete frame as underground floor can be appropriate.

Fig. 6.57 illustrates schematically the mode of function of the elements of the RFIP system.

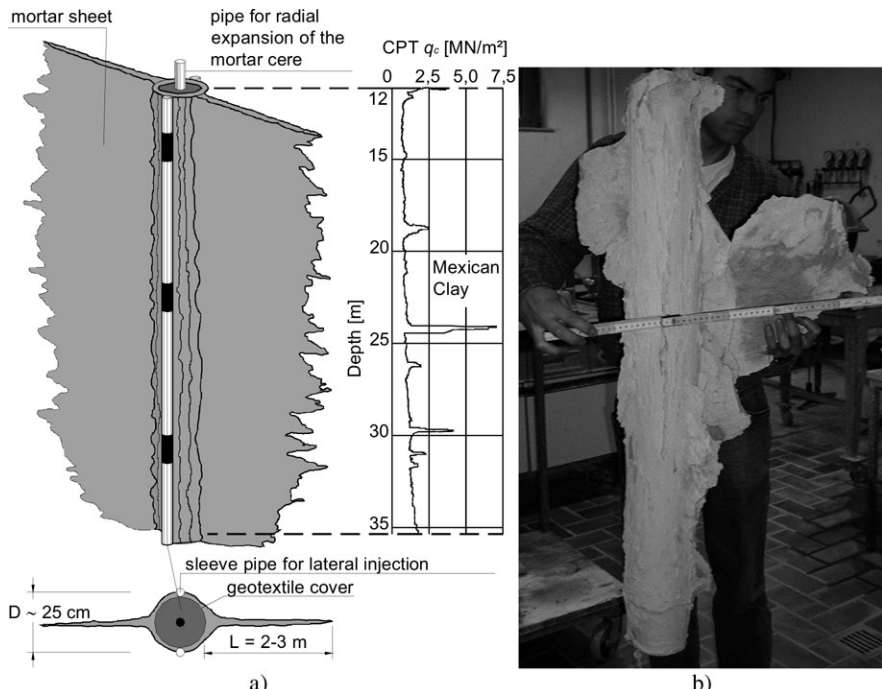


Fig. 6.56. Formation of lateral sheet of mortar in soft soils: a) dimensions of an excavated injection body (after Santoyo and Ovando-Shellye 2002), b) Injection pile with lateral mortar sheet from a large scale model tests (after Böhm 2006)

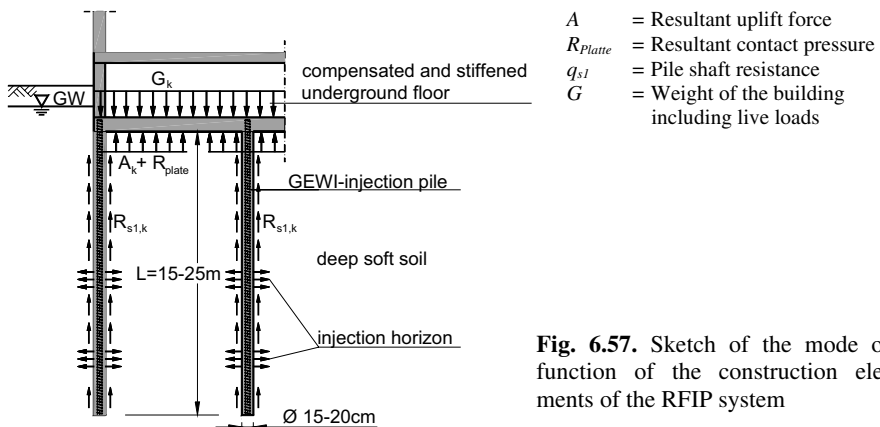


Fig. 6.57. Sketch of the mode of function of the construction elements of the RFIP system

For details on grouted micropiles refer to e.g. Bruce and Juran 1997; Amour et al. 2000; Kempfert 2001; Kempfert et al. 2003 and section 6.2.5. An important element for the settlement reduction effect of the RFIP is the type and size of the pile as well as the degree post grouting. The more the realised grout material, the larger will be the soil improvement and stabilisation effect of the soft soil. Since the grout material (cement suspension or cement mortel) distributes it self to a larger area around the injection pile, the cavities in soil are filled with the grout and a better bond can be achieved between the pile and the surrounding soil. According to Bruce and Juran 1997, a grout with a lower pressure but applied slowly has a better hardening effect in the soil than a grout with high pressure and applied very fast. Presumably, the structure of the soil may be disturbed and break apart by the quickly applied high pressure, and hence thin but several a ramification of the cement suspension my be formed in the soil. On the other hand, by slowly applied lower grout pressure, a thick but few suspension ramifications can be formed without disturbing the soil (Fig. 6.56), which eventually form a bearing slice (sheet) that serves as a load transfer element. For this reason, repeated post grouting increases the effectiveness of the RFIP system.

By the practical projects in case histories, section 6.10, a grout pressure between 25 and 30 bar and a grout volume up to 0.015m^3 per meter pile length had been used depending on the post grouting series in the installation of the GEWI injection piles. The one up to three times post grouting had been conducted with a pressure of about 40 bar, whereby a high pressure up to 80 bar were necessary to burst open (crack) the pile concrete or the hard cement.

There are two main application forms for the RFIP foundation system as shown in Fig. 6.58.

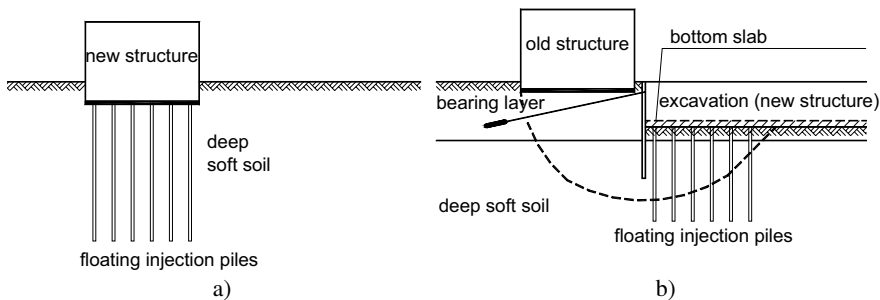


Fig. 6.58. Application forms for the RFIP foundation system: a) foundation of a new structure, b) Excavation and protection of old structures

The increase in the stiffness of the soft layer due to the stabilisation effect of the injection pile grid system leads to settlement reduction and improvement of the serviceability of the system. On the other side, the hardening effect in the soil due to the grouting pressure may increase the strength of the soil surrounding the pile and lead to the improvement of the bearing capacity of the soil, whereby the safety against bearing capacity failure in short term for a shallow foundation for the boundary condition shown in Fig. 6.58a is not adequate without additional construction measures. Another practical application shows Fig. 6.58b, where injection piles can be used to protect an excavation against bottom heave and global bearing failures.

The case histories in section 6.10 limits itself to the experiences with the stabilising injection piles, with one exception, i.e., the project with driven piles, since the soil straining and prestressing effect of the injection piles can be controlled relatively through the injection pressure. Therefore, this does not mean that another type of piles or column type elements that have soil displacement effect do not produce a similar or partially comparable effects as the injection piles. The stabilisation effect of each system should however be examined separately, because the favourable geotechnical effects of the RFIP system presented here may not directly apply to other projects offhand.

6.10 Case histories on RFIP-foundation system

6.10.1 General

Kempfert 1986 reported the first positive experience in stabilising RFIP foundation system for an abutment of an old railway bridge in soft soil deposit in southern Germany. In the mean time, there are very good experiences with this foundation system, which are compiled and analysed in the following. Beside the projects with RFIP system, one project with precast reinforced displacement floating piles is also presented for purpose of comparison.

Following are compiled experiences in four practical projects with stabilising floating piled raft foundation. Thereby, it should be distinguished between:

- Foundation of new structures with RFIP system,
- Foundation of new structures with stabilising floating piled raft foundation (precast reinforced displacement piles), and
- Stabilisation of excavations and protection of old structures with RFIP system.

The boundary conditions and the acquired experiences together with some measurement results are summarised in the following. Here, the settlement reduction factor is defined as:

$$\beta_s = \frac{\text{Settlement of a shallow foundation}}{\text{Settlement of a RFIP - foundation}} \quad (6.34)$$

For further information and details refer to Kempfert and Böhm 2003; Böhm 2006.

6.10.2 Project I (RFIP-foundation system)

Introduction

A one lane old steel frame bridge founded on timber logs has to be replaced by two lane new railway bridge made up of reinforced concrete. The new bridge has a span length of about 130 and 20 m (Fig. 6.59). The dimension and load had been changed against the original bridge due to an arrangement of a footpath by the west abutment, so that the foundation of the old bridge was replaced by RFIP system.

Soil conditions

The soil profile is shown in Fig. 6.60. The groundwater is located at a level of the average river water level which is approximately 0.5 m above the bottom of the foundation mat. The soft soil layers reach up to 50 m depth below the surface. Fig 6.60 also illustrates the distribution of the water content w , the consistency index I_c and the undrained shear strength c_u with depth.

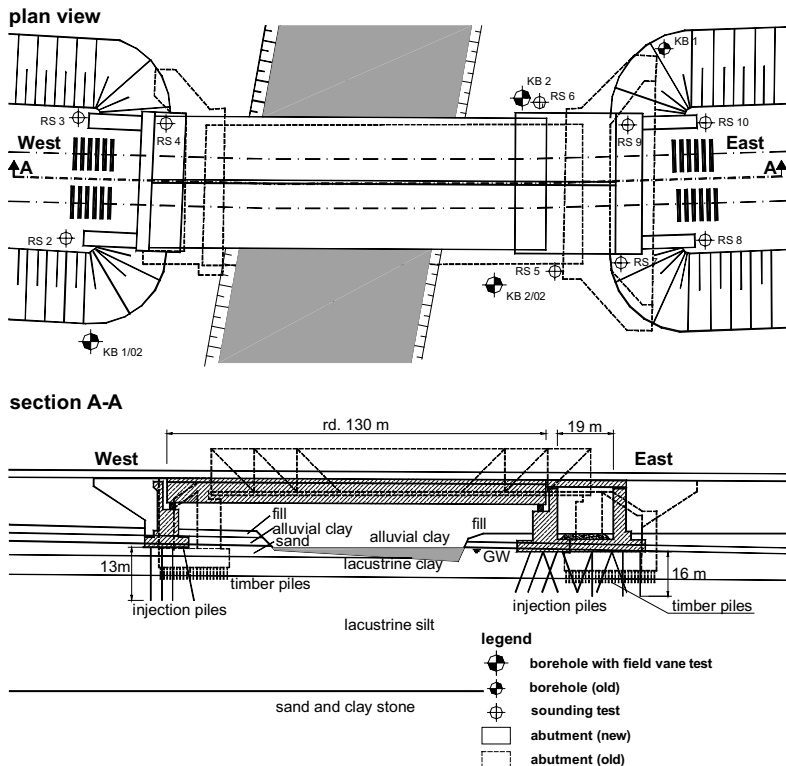


Fig. 6.59. Plan view and section in long direction as well as arrangement of the injection piles (project I)

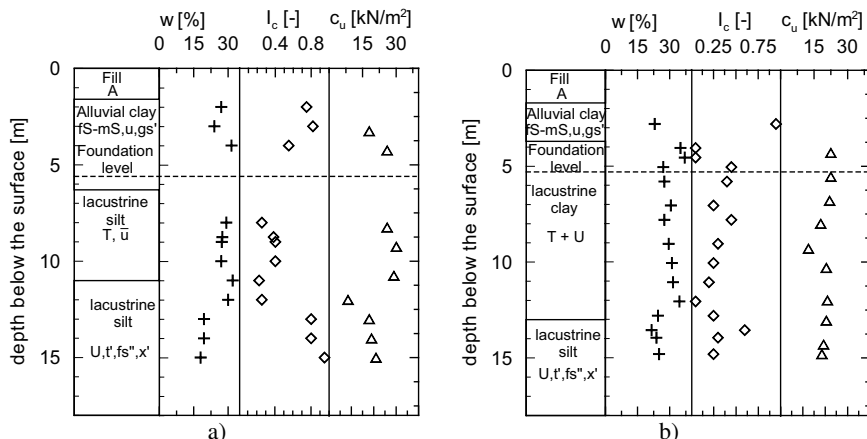


Fig. 6.60. The distribution of the water content, consistence index and undrained shear strength: a) West abutment, b) East abutment (after Kempfert 1986)

The foundation system

The abutments and the piers are founded on RFIP foundation system. The injection piles are made of a grouted single steel bar with a hole diameter of $\varnothing = 0.11$ m and a length of 13 and 16 m at west and east abutments respectively. The hole was drilled with rotary drill under wash boring. The injection piles penetrated 5 to 6 m into the lacustrine silt layer (Fig. 6.59).

Settlement measurements

The restoration of the bridge was executed in two phases, in order not to obstruct the railway operation at least at one truck. The settlement was measured at different points for both construction phases during the construction as well as operation (Fig. 6.61).

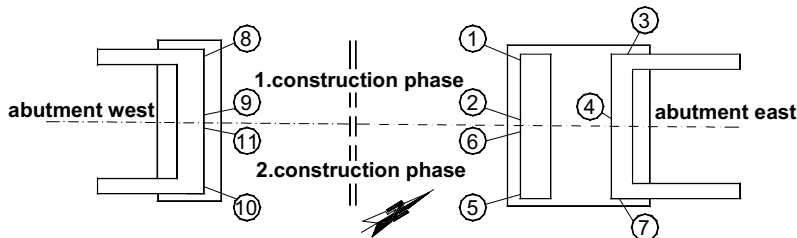


Fig. 6.61. Arrangement of settlement measuring points around the abutments

The predicted settlement was around 25 mm. The measured settlements at the west and east abutments are shown in Figs. 6.62 and 6.63 respectively. The maximum settlement at the west and east abutments amounts to 12 and 21 mm respectively. Further information on the project are summarised in tab. 6.18.

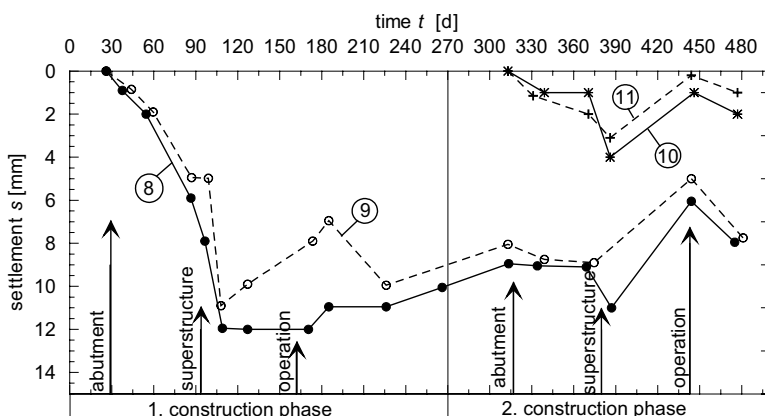


Fig. 6.62. Settlement measurement at west abutment (after Kempfert 1986)

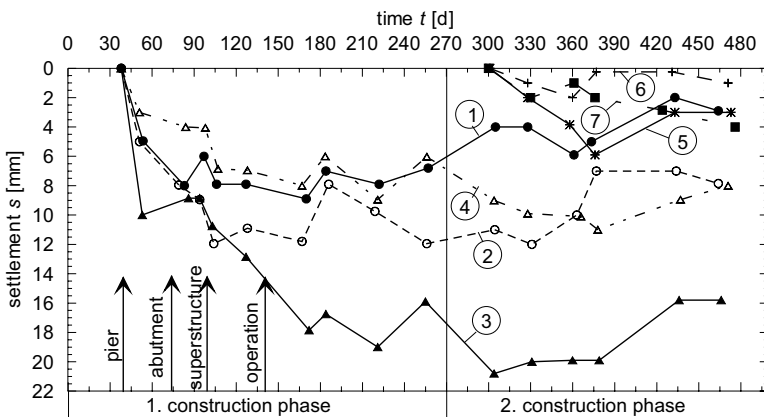


Fig. 6.63. Settlement measurement at east abutment (after Kempfert 1986)

Table 6.18. Summary of important parameters of project I

Structural boundary conditions	
1. Height of abutment	approx. 8 m
2. Average surface load at foundation level	approx. 260 kN/m ²
3. Excavation	-
4. Pre-load	Weight of old bridge and embankment
5. Thickness of the soft soil layer (Lacustrine clay)	Up to 50 m 50 m under GOK
6. c_u -value (min./max./middle)	7 / 25 / 18 kN/m ² (reduced according to nach Bjerrum)
7. Groundwater level	GW etwa in Höhe Gründungssohle
Construction boundary condition of the injection piles	
8. Injection pile system	Single steel rod grouted piles: system Bauer
9. Pile length [m]	16 m/18 m for west/east abutments
10. Borehole diameter [m]	110 mm (Internal diameter)
11. Drilling method	Rotary drilling with wash boring
12. Injection pressure [bar]	Simply filled
13. 1 st postgrouting pressure [bar]; amount [l]	15 to 20 bar, not available
14. 2 nd postgrouting pressure [bar]; amount [l]	Not conducted
Project analysis	
15. Settlement measurement	12 to 22 mm at most
16. Maximum measurement duration	Up to 16 months after abutment installation
17. Number of pile load test	3
18. Average skin friction	Sand $q_{s1} = 100 \text{ kN/m}^2$; Upper lacustrine clay $q_{s1} = 55 \text{ kN/m}^2$; Lower Lacustrine silt $q_{s1} = 180 \text{ kN/m}^2$

6.10.3 Project II (RFIP)

General

The project consists of several single buildings within a complex that includes old and new buildings. The location of the subprojects are shown in Fig. 6.64. The indices a, b and d indicates the order of the execution of the project. By one old building with shallow foundation denoted here as subproject II^d, the compressibility modulus was back calculated based on partially measured and partially approximated settlements values. This subproject is used for comparison of the settlements of RFIP foundation system with shallow foundation.

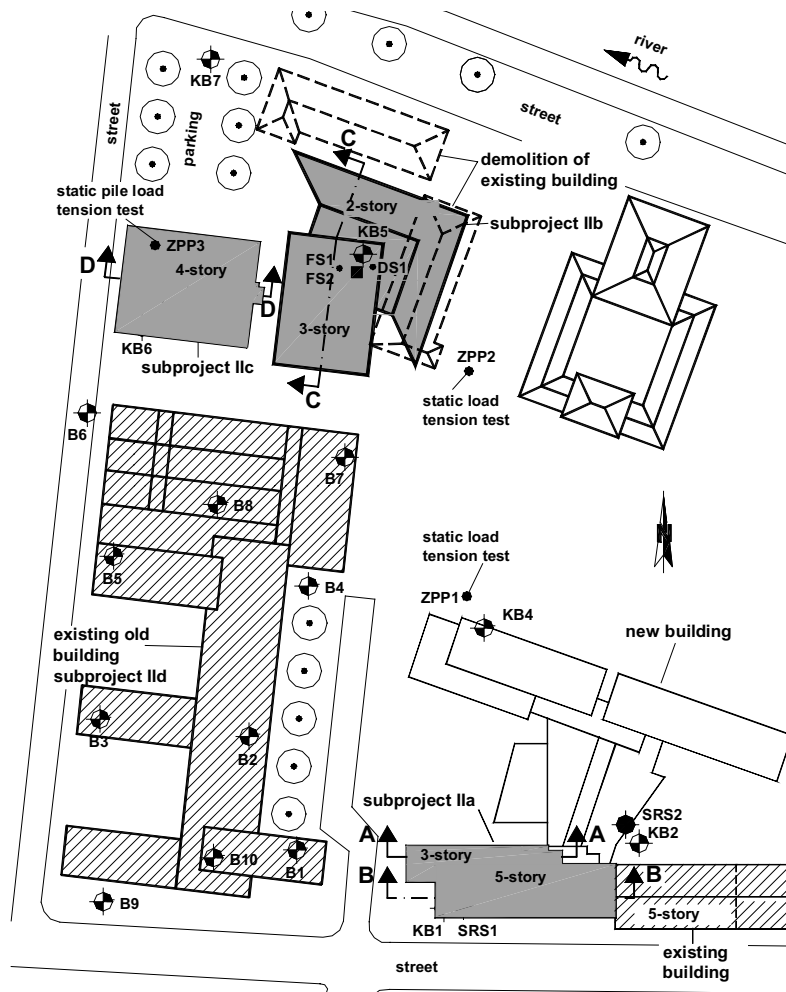


Fig. 6.64. An overview plan of project II (subproject IIa, IIb, IIIc and IVd) and different location of boreholes, sounding tests and pile load tests.

Underground conditions and soil parameters

The underground soil consists of predominantly lacustrine clay with partly sand and silt seems (Fig. 6.66). The grain size distribution of the lacustrine deposit is also illustrated in Fig. 6.65. The lacustrine is overlain by fill material of 2 m thick and underlain by moraine. The thickness of the soft soil deposit varies between 22 m (Fig. 6.66a) and 34 m (Fig. 6.66b). The distribution of the water content is also shown in Fig. 6.66. The average water content lies between 25 and 35% with exception of few point with water content above 65%. This is mainly due to organic content of the lacustrine soil at this depth.

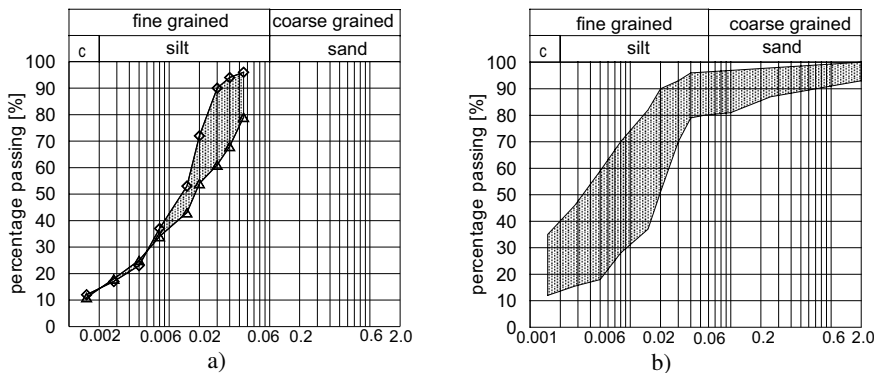


Fig. 6.65. Ranges of the grain size distribution (project II); a) upper lacustrine clay, b) lower lacustrine clay

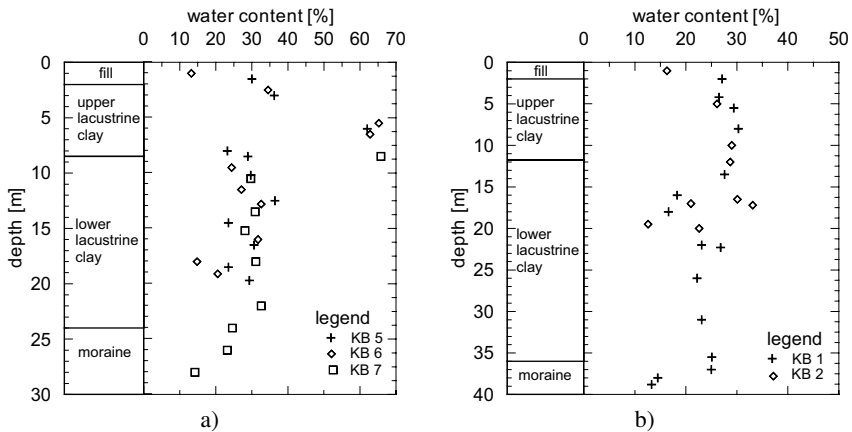


Fig. 6.66. Water content distribution with depth (project II): a) KB 5, KB 6 and KB 7 (sub-project IIb und IIc), b) KB 1 and KB 2 (subproject IIa)

Fig. 6.67a illustrates the results of field vane test as undrained shear strength c_u as well as the reduced undrained shear strength τ_f according to Bjerrum (1973) at

the locations FS 1 and FS 2 that extend up to a depth of 10 m below the surface. Similarly, Fig. 6.67b shows the cone penetration test result, which clearly shows the presence of sand and silt seems with in the lacustrine soil layer. The soil parameters according to the geotechnical report of the project are summarised in Table 6.19.

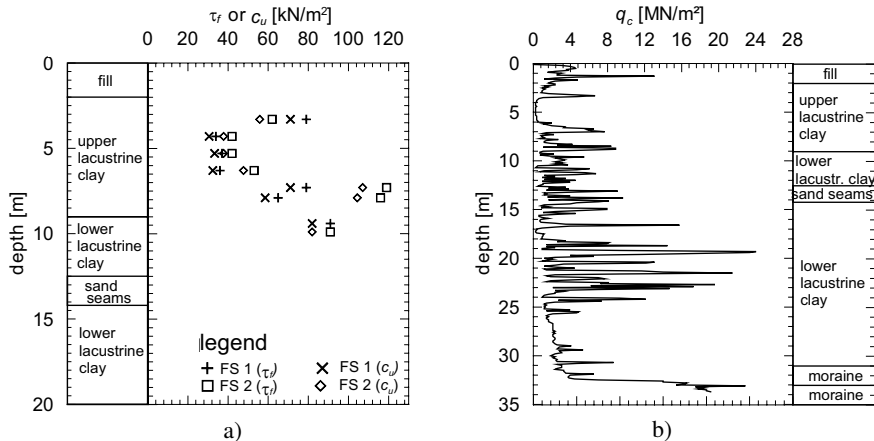


Fig. 6.67. a) Undrained shear strength derived from field shear vane test (FS 1 and FS 2),
b) Cone penetration test (DS1)

Table 6.19. Soil parameters from geotechnical report

Soil layer	γ / γ' [kN/m ³]	w [%]	E_{oed} [MN/m ²]	ϕ' [°]	ϕ_u' [°]	c' [kN/m ²]	c_u [kN/m ²]
Fill material	20 / 10	13.2	5	30.0		0	
Upper lacustrine soil	19 / 9	22 - 42	2 - 6	25	0	5	
Sand and silt seems	20 / 10	17 - 30	6	30		0	
Upper lacustrine soil	20 / 10	20 - 37	8	25	0	15	30
Moraine	22 / 12	20.1	30			-	-

Groundwater situation

The groundwater adjusts it self to the water level fluctuation of near river the Rhein, though a bit delayed. The daily fluctuations during and after the construction are shown in Fig. 6.68 at a location of the projects IIa and IIc under the foundation bottom and the river Rhein.

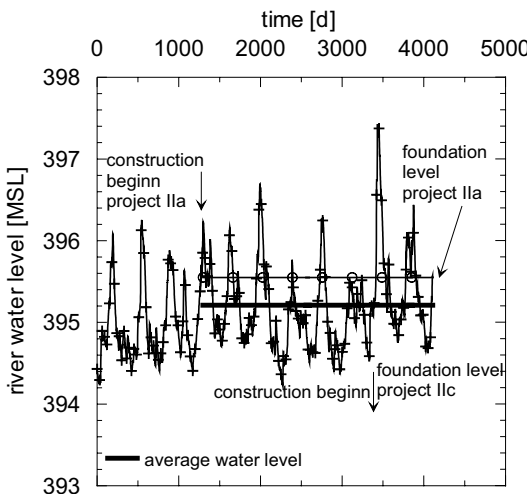


Fig. 6.68. Daily fluctuation of the ground and river water levels (project II)

Subproject IIA

a) Foundation system: The location of the subproject IIA is indicated in Fig. 6.64. Moreover, Figs. 6.69 and 6.70 also illustrates the plan view and section through the building in long direction of the subproject (compare with Fig. 6.64).

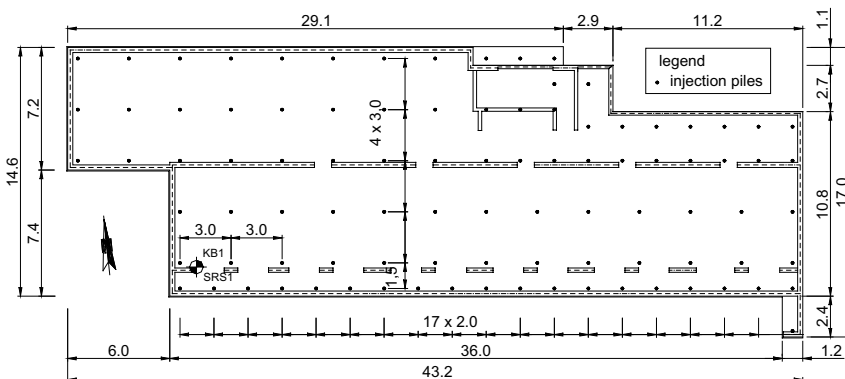


Fig. 6.69. Plan view of the raft foundation and arrangements of the injection piles (project IIA)

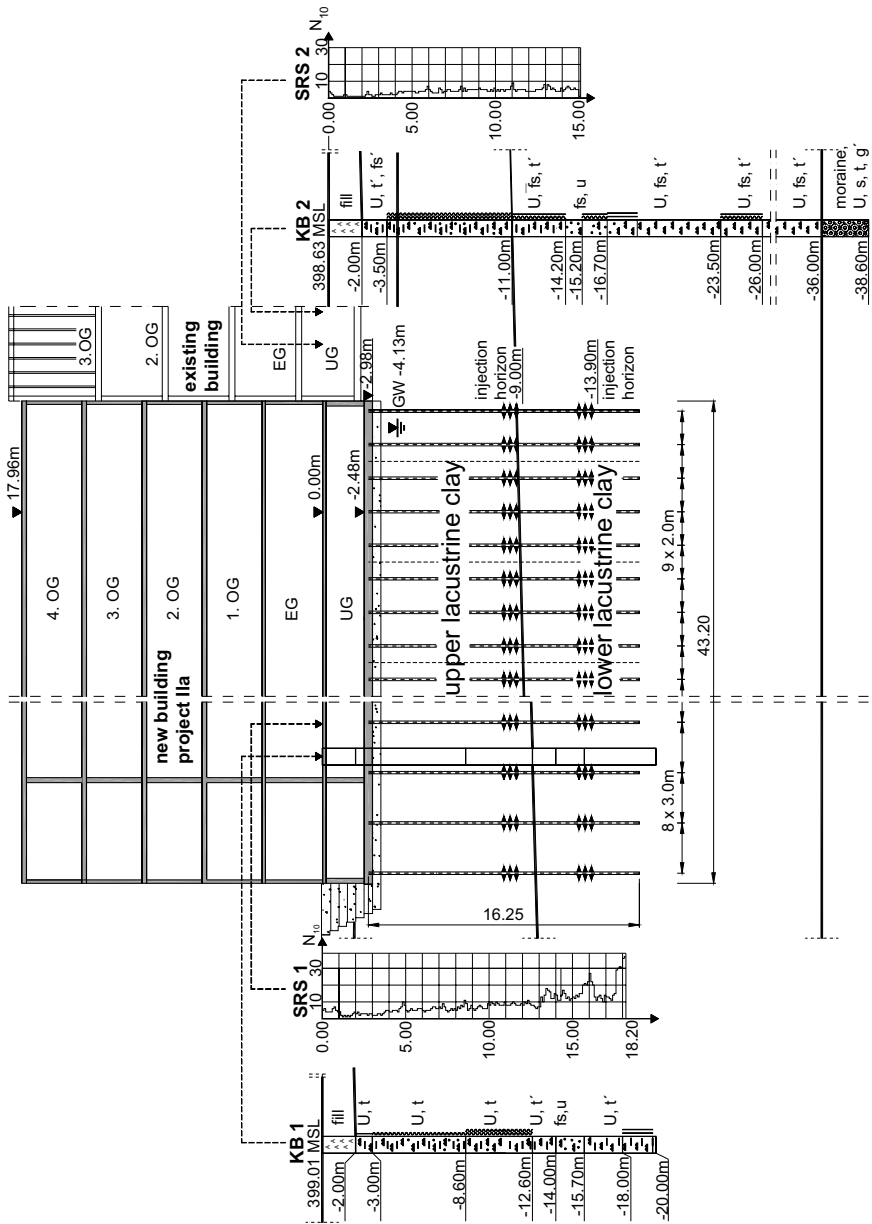


Fig. 6.70. Soil profile and section through the structure in long direction (project IIa)

The building of the subproject IIa was founded on RFIP foundation system with 95 injection piles with a total length of 16 m of which 5 m length of the pile is embedded into the lower lacustrine clay. The centre to centre spacing of the piles was 3 m and reduced to 2 m along the nearby street and around the stair case as well as elevator locations (Fig. 6.69). The equivalent radius r_c of the influence zone of a single pile with quadratic grid system is approximated to be 1.12 to 1.69 m, which gives a pile density of $5.77 \text{ m}^2/\text{pile}$.

The injection piles consists of the type GEWI Piles (System DYWIDAG., BSt 500 S/Ø bar = 50 mm) with a borehole diameter of 110 mm carried out with a rotary drill method. Fig. 6.71 shows excavated injection piles with pile head plates as well as an overview of the foundation. General information on the subproject and some construction data are given in Table 6.20. The installation of the GEWI injection pile had been carried out with casing and filled with C 25 concrete class under very small pressure. The injection pressure to burst open the fresh concrete (maximum the next day after the installation) was average 25 and 30 bar in the upper and lower horizon respectively. A cement suspension Z 45F with an injection pressure of 27.5 and 38.3 bar in the upper and lower horizon respectively. The maximum post grouting injection pressure lay around 80 bar. Average consumption of cement suspension for installation of the pile and post grouting lay around $0.015 \text{ m}^3/\text{pile length}$.

The equivalent diameter of the injection pile can be calculated form the average consumption of cement suspension as $d_{not grouted} = 0.145 \text{ m}$ and $d_{grouted} = 0.173$. The expansion of the borehole of each pile was about 2.8 cm.



Fig. 6.71. Partially excavated injection pile with pile head plates and an overview of the foundation

Table 6.20. Summary of general information and construction data on the subproject IIa

Structural and soil conditions		
1	Average size of the building	43 m x 15 m
2	Number of story	5 to 3 story and 1 underground floor
3	Average load on the foundation	15 kN/m ² x 6 = 90 kN/m ²
4	Stress relief due to excavation	≈ 59 kN/m ²
5	Preloading	no
6	Soft soil thickness	Up to 30 m below the surface
7	c _u -value (min/max.)	20 – 40 kN/m ²
8	Groundwater conditions	3 m below the surface on average at level of the raft
Injection pile installation characteristics		
9	Pile system	GEWI injection pile (System DYWIDAG)
10	Pile length	16 m
11	Borehole diameter	146 mm (lost end with 150 mm)
12	Drill technik	Displacement rotary drill
13	Spacing	2.5 to 10 m
14	Injection horizon	9 m and 13 m below the level of the raft foundation [12 to 16 m below surface]
15	Injection fill pressure	Simply filled without pressure
16	Burst open pressure	25.4 bar (upper horizon)/29.7 bar (lower horizon)
17	1 st post grouting, injection pressure	27.5 bar (upper horizon)/38.3 bar (lower horizon)
18	Amount of grout (1 st post grouting)	52.4 l (upper horizon) / 62.1 l (lower horizon)
Project analysis		
19	Calculated settlement as shallow foundation	70 to 150 mm
20	Calculated settlement as RFIP	20 to 40 mm
21	Settlement measurements	5.2 to 18.5 mm (see Fig. 6.15a & b)
22	Settlement reduction factor, β _s	8.1 to 13.5
23	Maximum measurement period	11 year
24	Number of pile load tests	2
25	Average skin friction	Upper lacustrine: q _s = 60 to 96 kN/m ²

b) Prediction and measurement of settlements and forces on pile head: The calculated expected settlements for the RFIP foundation system lay between 20 and 40 mm with the assumption that the raft and the pile can share the load from the superstructure to 50%.

The measured settlements and the forces on head of selective injection piles together with building loads according to the construction stages are shown in Fig. 6.73. The location of the measurement points are indicated in Fig. 6.72. However, the settlement measurements had been started first after completion of the construction of the underground floor, the ground floor and some walls of the 1st floor, and hence the initial settlements are simply extrapolated as shown in Figs. 6.73 & 6.74.

legend

- = injection piles
- [PF1] = load tranducer (on pile head)
- ② ▼ = settlement measuring point till the completion of 3rd floor
- MP104▼ = settlement measuring points for long term monitoring
(approx up to 5 years after completion of the building)

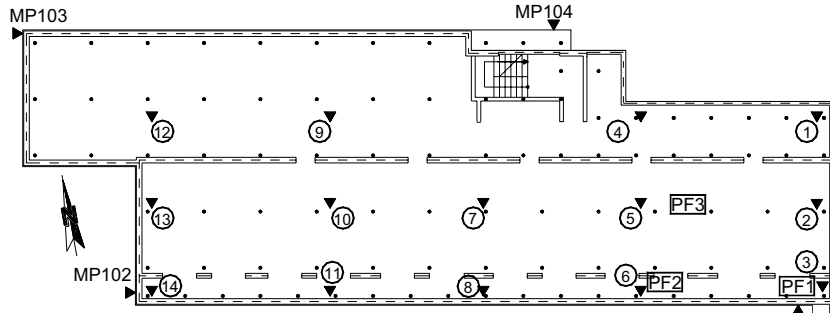


Fig. 6.72. Plan view of the foundation and arrangement of the monitoring points (subproject IIa)

The measured settlement are extrapolated according to Sherif 1973 which gives a settlement of 5.2, 12.3, 17.5 and 18.5 mm at measuring point MP 103, MP 101, MP 102 and MP 104 respectively. The maximum load on pile head (pile No. 3) was measured to be 55 kN within the measurement period.

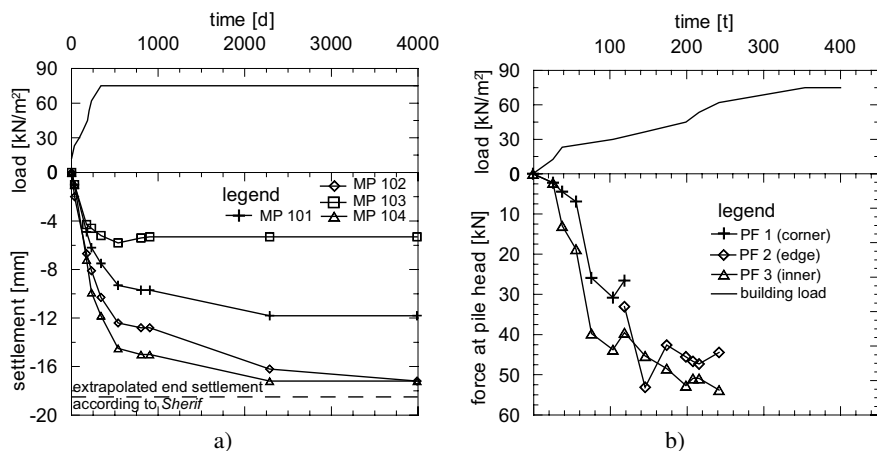


Fig. 6.73. a) Measured settlements (a) and the force at pile top (subproject IIa)

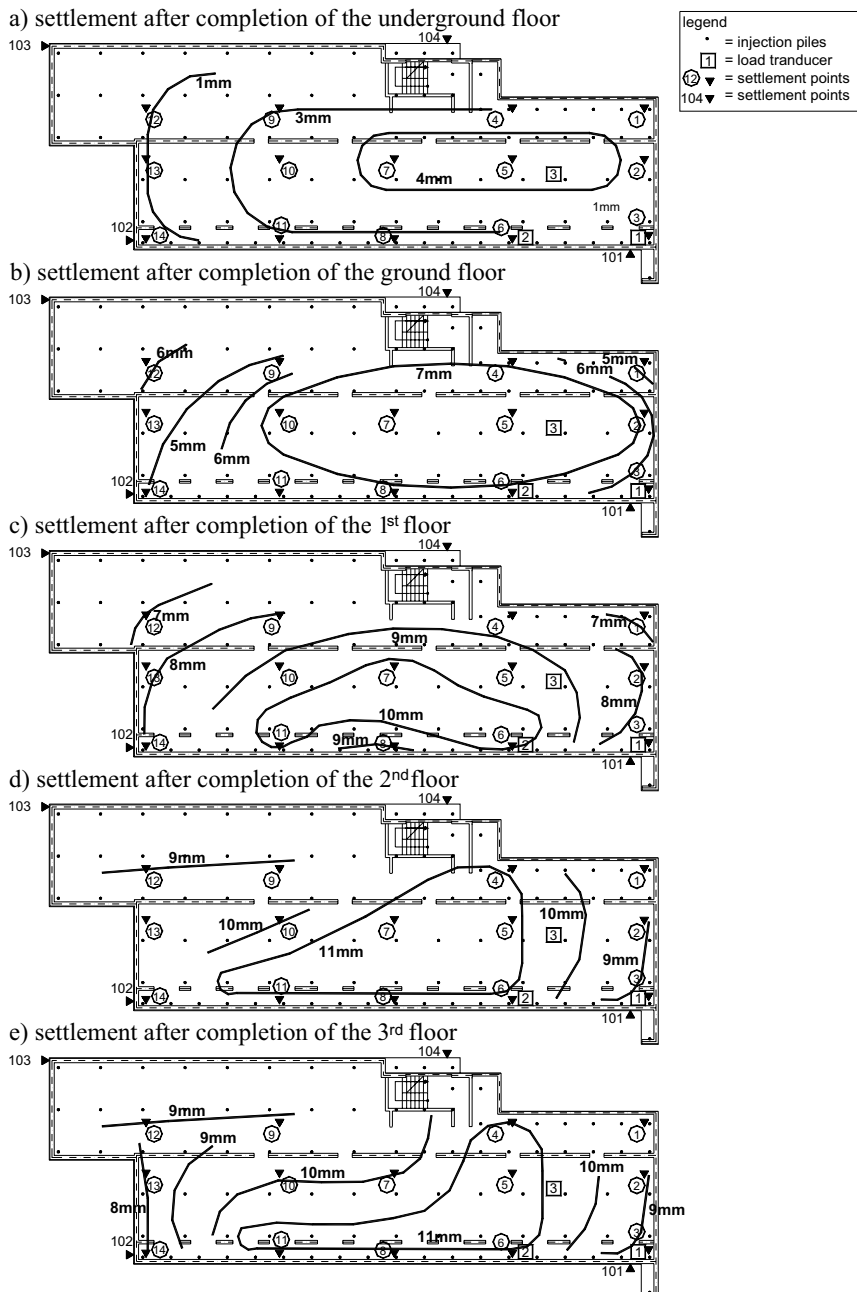


Fig. 6.74. Settlement contour of the raft at different construction stages (subproject IIa).

The measured absolute settlements of the raft foundation after completion of each floor from the ground floor to 3rd floor are drawn in Fig. 6.74 as a contour of equal settlements. At the middle of the raft it formed a settlement trough after the completion of the underground floor. Starting from the completion of the 1st floor, the settlement trough remains unchanged (Fig. 6.74)

Subproject IIb

a) **Foundation system:** The position of the subproject can be seen in Fig. 6.64. The foundation layout and cross section through the building are also shown in Figs. 6.75 & 6.76 respectively. Alternative to the foundation system of the subproject IIa, the RFIP system in this subproject was combined with girder beams (see Fig. 6.76). 65 injection piles had been installed under the beam girder in the short and long directions at a spacing of 5 and 2.5 m in the rectangular shaped foundation and 8 and 11 m in the L-shaped foundation. The radius of the influence area r_c of each pile lays between 2.8 and 1.4 in the rectangular region and between 4.5 and 6.2 m in the L-shaped region. The density of the piles lays between 9.7 m²/pile in rectangular foundation area and 40 m²/pile in the L-shaped foundation area.

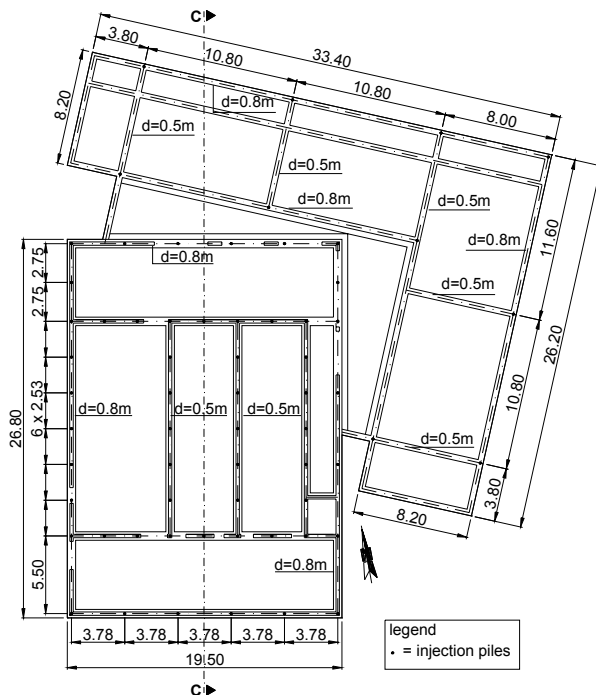


Fig. 6.75. Foundation layout and arrangements of beam girders above the injection piles (subproject IIb)

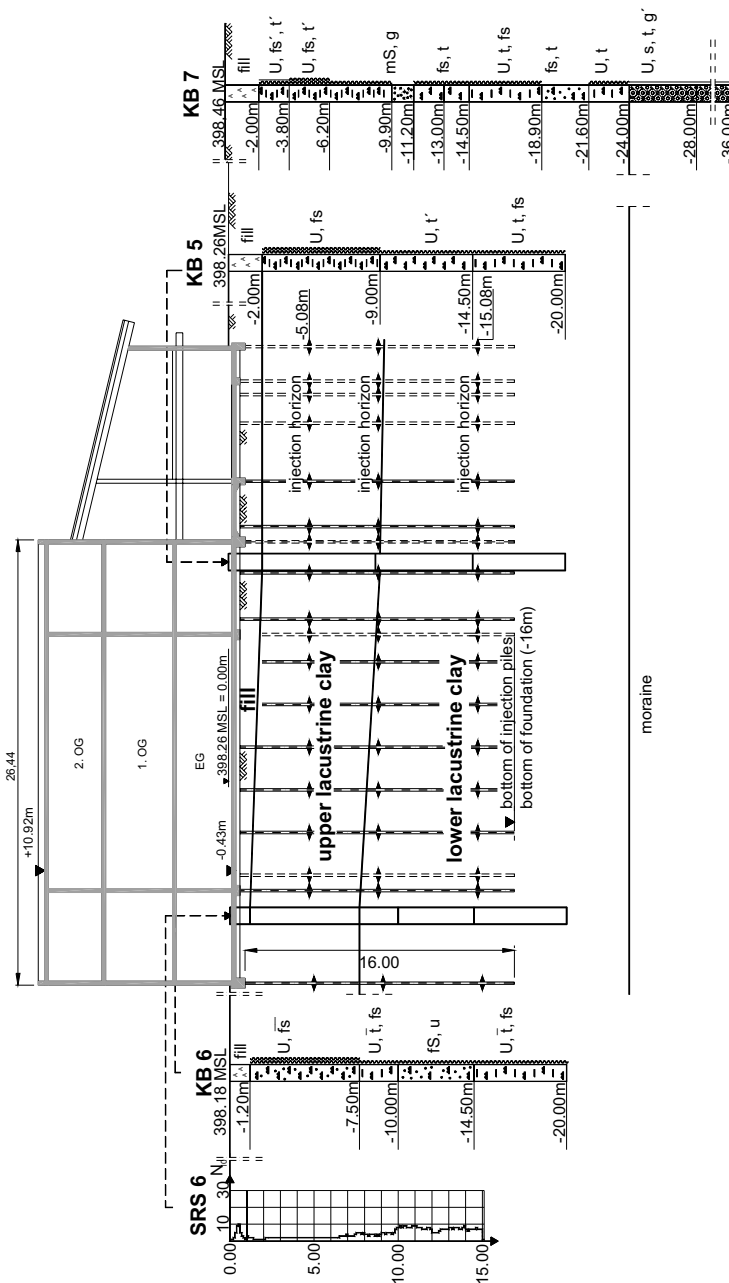


Fig. 6.76. Underground profile and section C-C in long direction (subproject IIb)

The injection piles consists of the type GEWI Piles (System DYWIDAG., BSt 500 S/Ø bar = 50 mm) with a borehole diameter of 130 mm carried out with a rotary drill method. The injection pile has a length of 16 m, 8 m of which is embedded in the lower lacustrine soil (Fig. 6.76).

Because of the large difference in the load from the rectangular and the L-shaped buildings, a hinge was built between the two foundations, so that the different settlement of the buildings would not influence each other. Further general information on the subproject and data on the construction of the foundation are compiled Table 6.21

Table 6.21. Summary of general information and construction data on the subproject IIb

Structural and soil boundary conditions		
1	Average size of the building	$\approx 33 \text{ m} \times 13 \text{ m}$
2	Number of story	2 story without underground floor
3	Average load on the foundation	30 and 15 kN/m ²
4	Stress relief due to excavation	No
5	Preloading	$\approx 20 \text{ kN/m}^2$ (partly due to 2-story old building)
6	Soft soil thickness	up to 30 m below the surface
7	c _u -value (min/max.)	20 – 40 kN/m ²
8	Groundwater conditions	on average 3 m below the foundation level
Injection pile installation characteristics		
9	Pile system	GEWI injection pile (System DYWIDAG)
10	Pile length	16 m
11	Borehole diameter	120 mm (lost end with 130 mm)
12	Drill technik	displacement rotary drill
13	Spacing	1.5 x 2.0 m and 3.0 x 3.0 m
14	Injection horizon	5, 9 and 14 m below the level of the raft foundation
15	Amount of grout / injection pressure	700 l / 10 – 15 bar
16	1 st post grouting (burst open pressure)	29, 30 and 57 bar in the upper, middle and lower horizon respectively
17	Amount of grout (1 st post grouting)	45, 51, and 31 l in the upper, middle and lower horizon respectively
Project analysis		
18	Calculated settlement as shallow foundation	up to 150 mm
19	Calculated settlement as RFIP	20 to 40 mm
20	Settlement measurements	12 to 24 mm (extrapolated end settlement)
21	Maximum measurement period	10.5 years
22	Settlement reduction factor, β_s	6.3 to 12.5
23	Number of pile load tests	2
24	Average skin friction	Upper lacustrine: $q_s = 104 \text{ kN/m}^2$

b) Settlement prediction and measurements: The settlement of the foundation with the RFIP system was calculated to be 20 to 40 mm. It was assumed that 2/3 of the building load goes to the injection piles and the rest is carried by the bear girder.

Measured settlements at four corner point (Fig. 6.77a) are plotted in Fig. 6.77b dependant on the average building load. The measured values agrees with the predicted values, although the secondary settlement was not yet closed. The measured settlements were extrapolated according to the Sheriff 1973 method to obtain the end settlements. These are 11.7, 19.7 and 24.1 mm at measurement points MP1, MP2 and MP3 respectively.

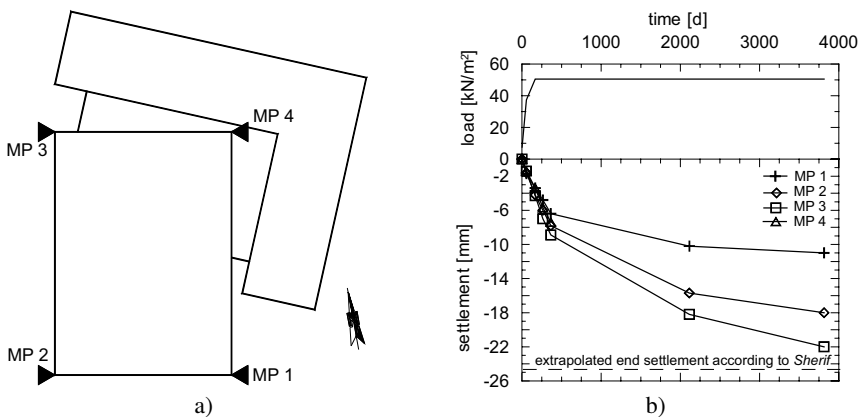


Fig. 6.77. a) Layout of measurement points, b) time-settlement diagram (subproject IIb)

Subproject IIc

a) Foundation system: The position of the subproject can be seen in Fig. 6.64. The foundation layout and section through the building and foundation are also shown in Fig. 6.78 & 6.79. The raft foundation is located 4.2 m below the ground surface and it is about 12 m far from the subproject IIb, that was built 6 years before. In order to protect the structure from an uplift pressure, the 0.6 m thick raft foundation was extended about 0.6 m beyond the external walls. The groundwater fluctuates itself with the water level of the river Rheine and it is located at a depth of 1.4 m above the foundation level on average. By high water level (H WL) and low water level (L WL), the groundwater is located at a depth of 0.3 m below the ground surface and at foundation level respectively (see Fig. 6.79).

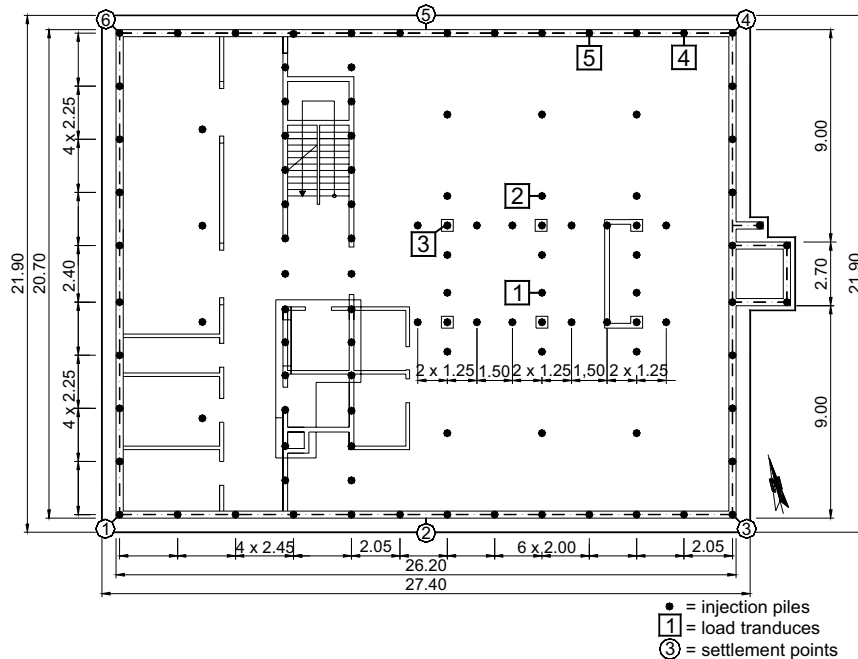


Fig. 6.78. Foundation layout with injection piles arrangements (subproject IIc)

The subproject is founded on RFIP system with 111 injection piles of the type GEWI Piles (System DYWIDAG., BSt 500 S/Ø bar = 50 mm). The foundation is rested on 1 m thick compacted gravel fill. The boreholes for the installation of the injection piles were made with auger drilling. The injection pile has a length of 15 m, 4 m of which is embedded in the lower lacustrine soil (Fig. 6.79).

The injection piles are arranged at center to center distance of 4 m at the middle of the foundation and 2.25 m at the external walls. At location of stair cases, elevator and others, the spacing is reduced to 1.25 m. The radius of the influence area r_c of each pile lays between 1.4 and 4.5m.

The injection piles had been filled with C 25 concrete without pressure and the 1st post grouting followed with cement suspension ($w/c = 0.6$) under a pressure of 35 bar on average. General information on the subproject and data on the construction are compiled in Table 6.22.

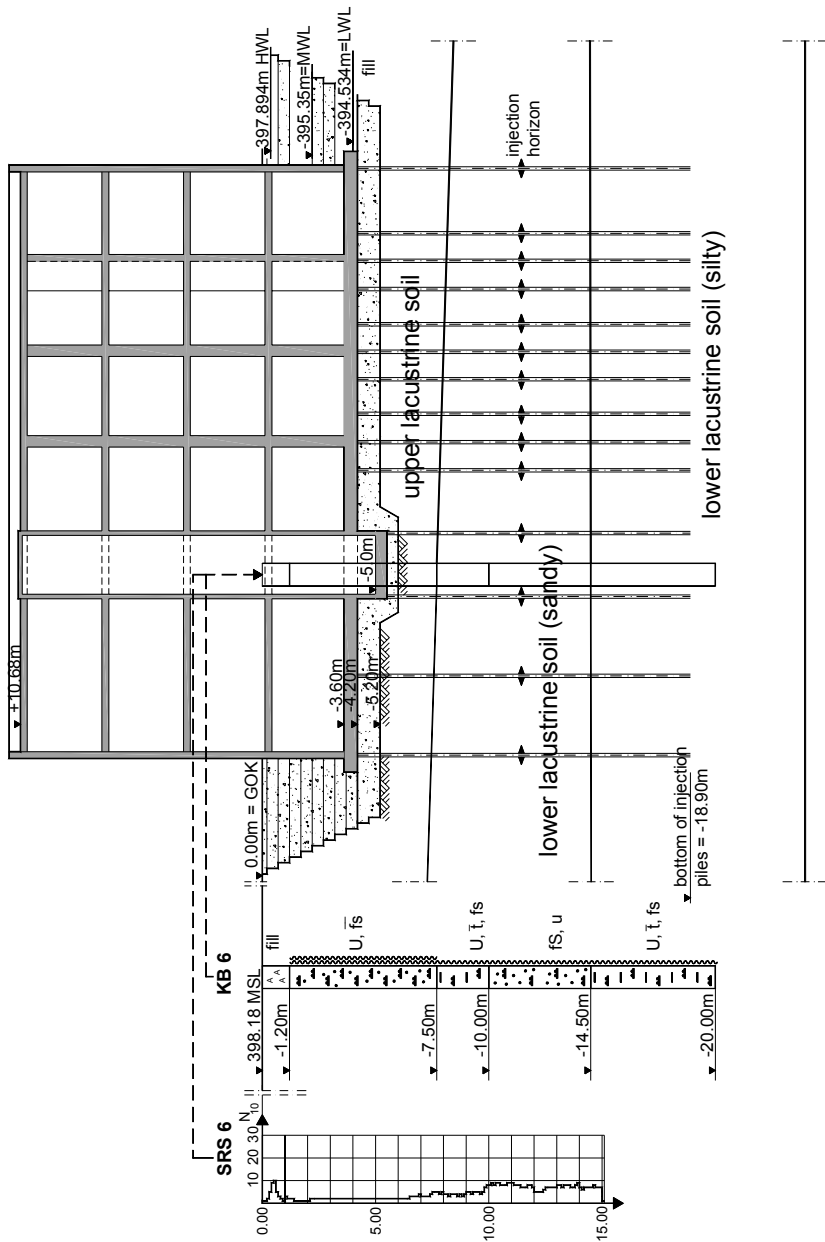


Fig. 6.79. The underground profile and section D-D through the building (subproject IIc)

Table 6.22. Summary of general information and construction data on the subproject IIc

Structural and soil boundary conditions		
1	Average size of the building	27 m x 22 m
2	Number of story	4 story including 1 st underground floor
3	Average load on the foundation	85 kN/m ²
4	Stress relief due to excavation	≈ 40 kN/m ²
5	Preloading	no
6	Soft soil thickness	up to 30 m below the surface
7	c _u -value (min/max.)	20 – 40 kN/m ²
8	Groundwater conditions	on average 1.4 m above the foundation level
Injection pile installation characteristics		
9	Pile system	GEWI injection pile (System DYWIDAG)
10	Pile length	15 m
11	Borehole diameter	130 mm (lost end with 220 mm)
12	Drill technik	augur boring
13	Spacing	partly 1.25 and 2.25 to 4 m
14	Injection horizon	12 m below the the raft foundation
15	Amount of grout / injection pressure	500 l / 0 – 5 bar
16	1 st post grouting / burst open pressure	28 to 38 bar / 31 - 35 bar
17	Amount of grout (1 st post grouting)	60 l
Project analysis		
18	Calculated settlement as shallow foundation	up to 200 mm
19	Calculated settlement as RFIP	Up to 50 mm
20	Settlement measurements	8 to 22 mm (extrapolated end settlement)
21	Settlement reduction factor, β_s	9.1 to 15
22	Maximum measurement period	5 years
23	Number of pile load tests	1
24	Average skin friction	Upper lacustrine: q _s = 104 kN/m ²

b) Settlement prediction and measurements and forces on pile head: The settlement of the foundation with the RFIP system was calculated to be 20 to 40 mm with the assumption that that 2/3 of the building load goes to the injection piles and the rest is carried by the raft. The measured settlements are shown in Fig. 6.80a. Since the first measurement was carried out first after the completion of the underground floor, the ground floor and some of the wall of the 1st floor, the initial settlement was approximated to be 4 to 5 mm and added to the measured values. The maximum measured settlement which is about 22 mm remains far below the predicted value. The measured extrapolated final settlements approximated according to Sherif 1973 are 8.5, 15.5, 15.4, 22.2, 19.5 and 13.4 at the measuring points MP1, MP2, MP3, MP4, MP5 and MP6 respectively.

Fig. 6.80b shows the measured forces on the top of selective piles. The maximum force 297 kN was measured at edge pile 5.

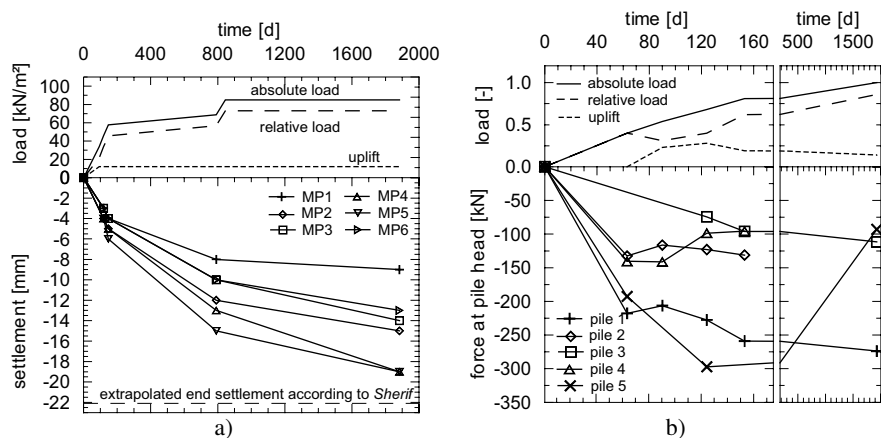


Fig. 6.80. a) Time-settlement diagram, b) Forces on pile top (subproject IIc)

Back calculation of the compressibility modulus (subproject IIc)

The compressibility modulus E_m is estimated from the settlement measurements on an existing old building founded on shallow foundation within the premise of the project II. Refer to Fig. 6.64 for the location of the old building. Each floor is assumed to transmit a load of 15 kN/m². The estimated contact pressure and the corresponding calculated settlement for each part of the building are shown in Fig. 6.81. The groundwater is assumed at a depth of 3 m below the ground surface, i.e., at foundation level and it is the same as the average water level of the Rheine river.

The back calculation of the compressibility modulus is performed using the closed equations with a limiting depth of about 0.7 times the width of the building part and with consideration of stress relief due to excavation. The results are summarised in Table 6.23

Table 6.23. Back calculation of compressibility modulus from measured settlement and estimated contact pressure

Building part	I	II	III	IV	V	VI
Settlement [cm]	12-16	4-8	13-17	14-18	4-8	8-12
Contact pressure σ_0 [kN/m ²]	60	70	50	50	50	50
Compressibility modulus E_m [kN/m ²]	2.7-3.6	7.8-15.7	1.4-1.9	1.3-1.8	3.0-6.1	2.4-3.6

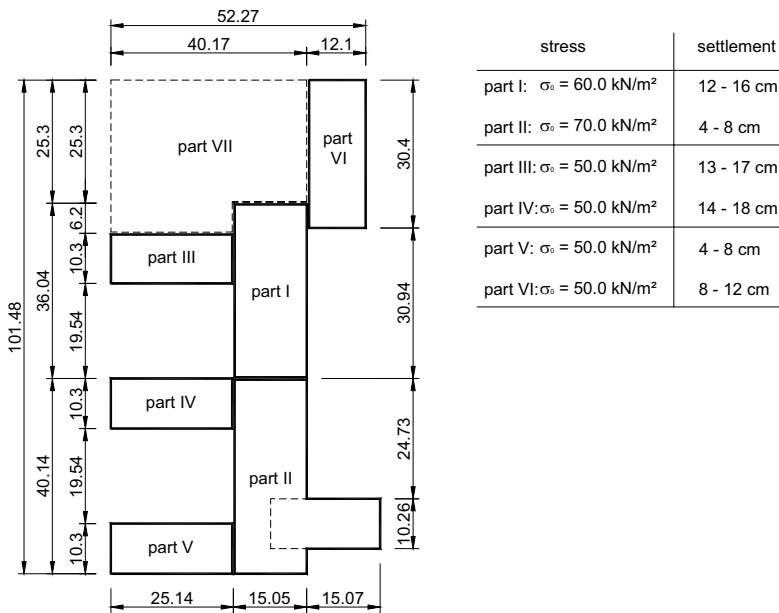


Fig. 6.81. Foundation layout, estimated contact pressure and the corresponding measured settlement of an old building (subproject IIId)

6.10.4 Project III (Floating displacement piles)

General

This project is a 3 story building without underground floor and it is constructed with steel frame structure (Fig. 6.82 & 6.83).

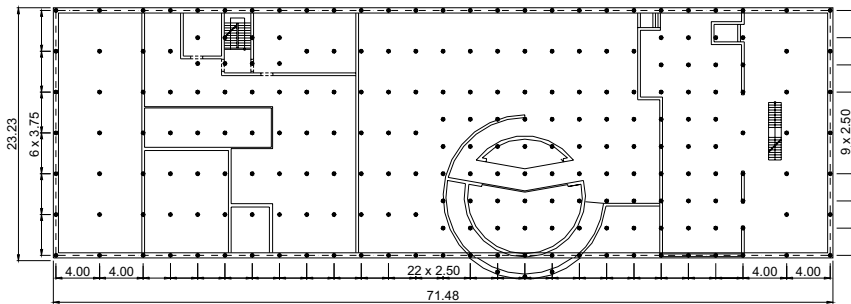


Fig. 6.82. Foundation layout and arrangement of the precast displacement piles (project III)

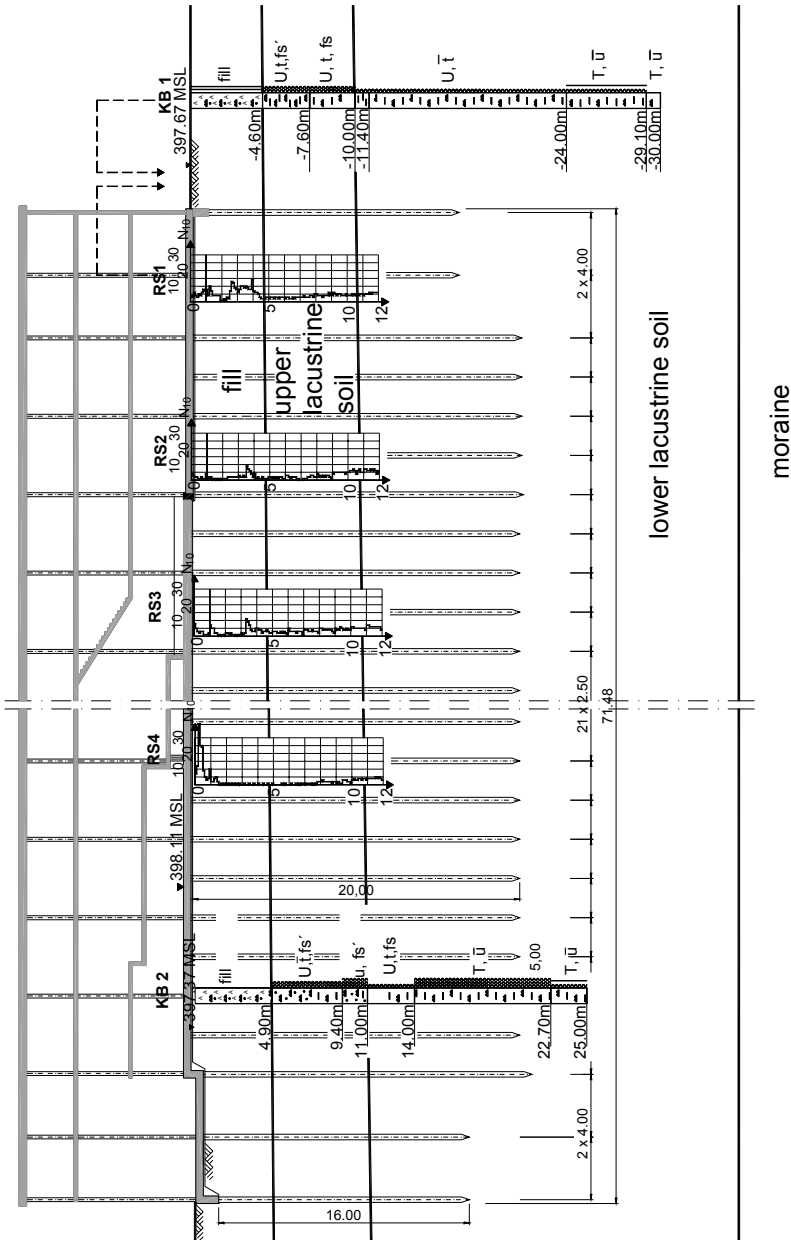


Fig. 6.83. Underground profile and section through the building (project III)

Soil conditions

The underground profile is shown in Fig. 6.83. The groundwater is encountered at a depth of 3 m below the ground surface. The simplified soil profile, the distribution of the natural water content and the consistency index with depth are illustrated in Fig. 6.84 and the corresponding main soil parameters according to geotechnical report of the project is given in Table 6.24.

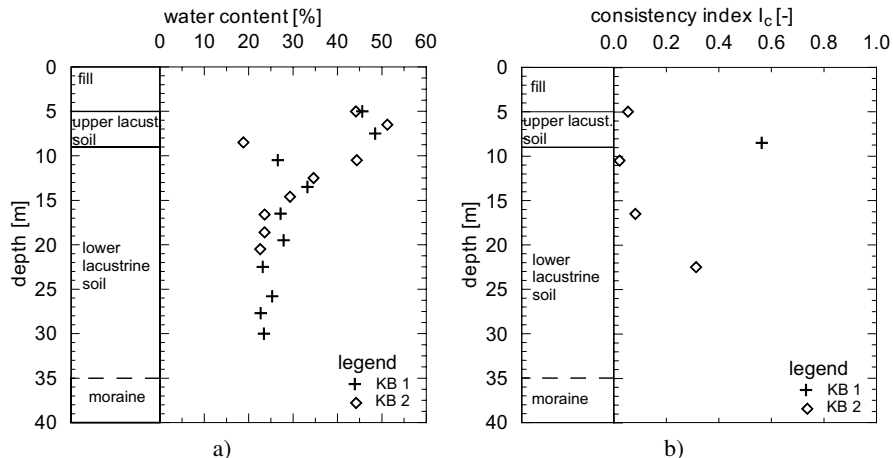


Fig. 6.84. The distribution of the natural water content and consistency index (project III)

Table 6.24. Back calculation of compressibility modulus from measured settlement and estimated contact pressure

Soil layer	γ/γ' [kN/m ³]	w [%]	I_c [-]	E_{oed} [MN/m ²]	φ' [-]	c' [kN/m ²]
Fill material	17/7	-		1-5	22.5	0-5
Upper lacustrine soil	18/8	38.6	0.136	2-4	10	4
Lower lacustrine soil	19/9	24.9	0.139	8-10	17	8

Foundation system

The building in this project is founded on a 220 floating precast concrete driven piles in combination with a raft foundation. The piles have a diameter of $\emptyset = 35$ cm and a length of 16 and 20 m. They are arranged at a spacing of 2.5 and 3.5 (Fig. 6.82). The radius r_c of the influence area of each pile lays between 1.4 and 2.1m. It was assumed that 25 % the building load goes to the raft foundation and the rest is carried by the floating driven piles. The general information on the project and data on the construction are compiled together in Table 6.25.

Table 6.25. Summary of general information and construction data on the project III

Structural and soil boundary conditions		
1	Average size of the building	72 m x 23 m
2	Number of story	3 story
3	Average load on the foundation	60 kN/m ²
4	Stress relief due to excavation	no
5	Preloading	information not available
6	Soft soil thickness	up to 40 m below the surface
7	c _u -value (min/max.)	information not available
8	Groundwater conditions	on average 1.0 m below the foundation level
Injection pile installation characteristics		
9	Pile system	precast reinforced concrete
10	Pile length	15 m
11	Borehole diameter	350 mm
12	Installation method	driven pile
13	Spacing	2.5 and 3.75 m
Project analysis		
14	Calculated settlement as shallow foundation	up to 150 mm
15	Calculated settlement as floating piled raft foundation	up to 50 mm
16	Settlement measurements	up to 82 mm, extrapolated end settlement 165 mm
17	Maximum measurement period	1 year
18	Settlement reduction factor, β_s	0.9
19	Number of pile load tests	6
20	Allowable load/ultimate load/skin friction	292-398 kN / 400 kN / q _s = 17.5 kN/m ²

Settlement measurements

The predicted settlement lay around 150 mm for a shallow foundation without any stabilisation measure under a surface load of 50 kN/m².

Settlement of the building was monitored at 9 points along the perimeter of the building (Fig. 6.85a). The measurement was started first after the installation of raft foundation and the last measurement was 6 months after completion of the building. The measured settlements shown in Fig. 6.85b indicate that the primary consolidation at the time point of the last measurement was not closed. It appears that there was no clear settlement reduction effect of the floating driven piles compared to shallow foundation. The extrapolated measured settlement according to Sheriff 1973 method lies around 165 mm which is a bit larger than the calculated settlement for shallow foundation.

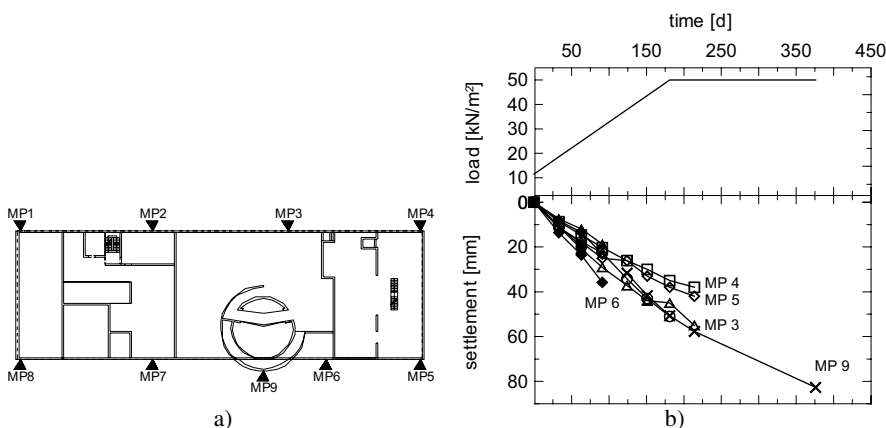


Fig. 6.85. a) Arrangement of the measuring points, b) time-settlement and time-load diagrams (project III)

6.10.5 Project IV (excavation and old building stabilisation with RFIP)

General

For an extension of an existing 10-story building, a new building was constructed as shown in the foundation layout in Fig. 6.86. The new building is rested on shallow foundation 2 m below the foundation level of the existing building.

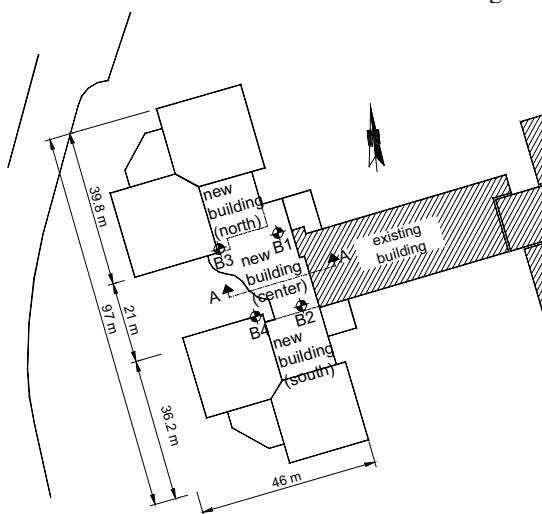


Fig. 6.86. Plan view of the existing and the new buildings with locations of boreholes (project IV)

Underground condition

The underground condition was explored by means of 4 borings (B1 to B2) and 12 field shear vane tests up to a depth of 22 to 25m (see Fig. 6.86 for location of boreholes and Fig. 6.87 for soil profile). Beneath the 2 m thick fill material is a sandy, silty, gravel (river gravel) which has a thickness of 5.5 m. Underneath the river gravel layer is a lacustrine clay soil whose consistency varies from very soft to soft (Fig. 6.87). The groundwater is located at a depth of 0.8 m below the ground surface. The distribution of the undrained shear strength c_u determined from the field vane shear test and after reducing its value by a factor according to Bjerrum 1973 is shown in Fig. 6.88. It can be seen from Fig. 6.88 that c_u increases with the depth from about 30 kN/m² at a depth of 9 m below the surface to about 60 kN/m² at a depth of 19 m. The soil parameters according to geotechnical report are shown in Table 6.26.

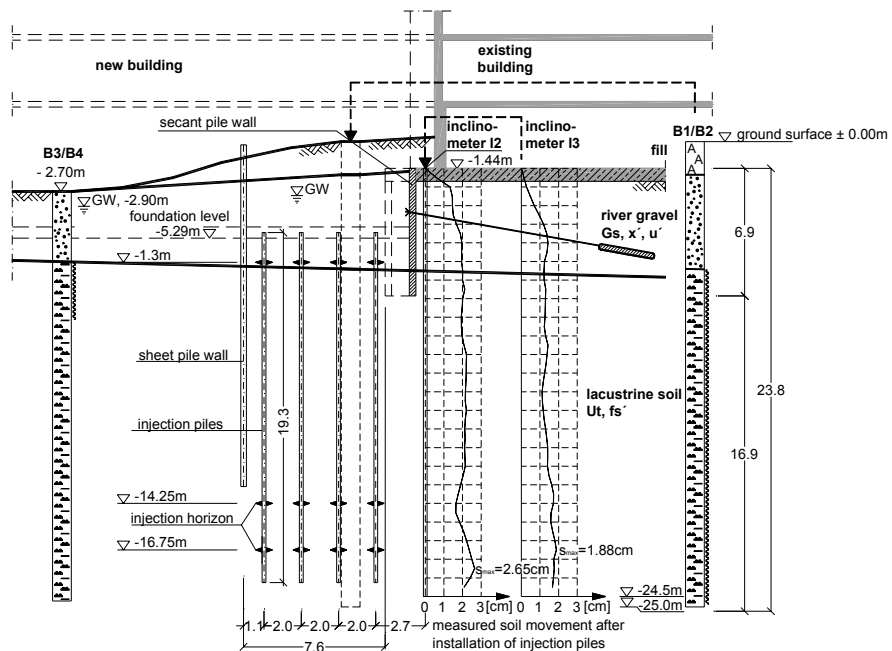


Fig. 6.87. Underground profile and section A-A through the foundation (project IV)

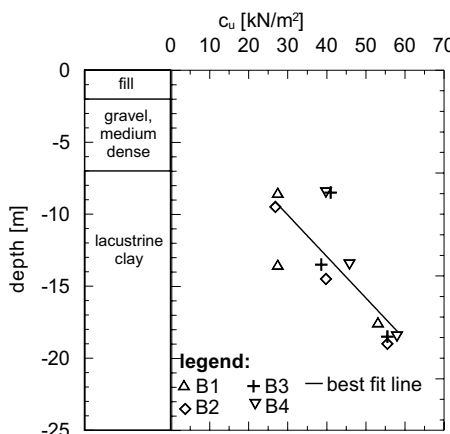


Fig. 6.88. The distribution of the undrained shear strength c_u with depth (project IV)

Table 6.26. Soil parameter as given in the geotechnical report of the project

Soil layer	γ/γ' [kN/m³]	φ' [-]	c' [kN/m²]
Fill material	20/10	20	0
River gravel	21/11	35	0
Lacustrine soil	19/9	-	refer to Fig. 6.30

Foundation system and execution

The aim of the stabilisation measure with the injection piles (see Fig. 6.87) in the vicinity of the 10-story building was to improve the strength and stiffness of the soft soil deposit, in order to avoid bottom heave failure, since the safety of the existing building was not guaranteed without this measure. 85 injection piles were installed at rectangular grid system of 2 m x 1.8m (Fig. 6.89) with a length of 19.3 m below the raft foundation level. The injection was carried out in three horizon which are located at depth of 1.3, 14.3 and 16.8 m below the foundation level.

The injection piles are installed in a borehole of 133 mm diameter and they are injected under pressure up to three times at three injection horizon.

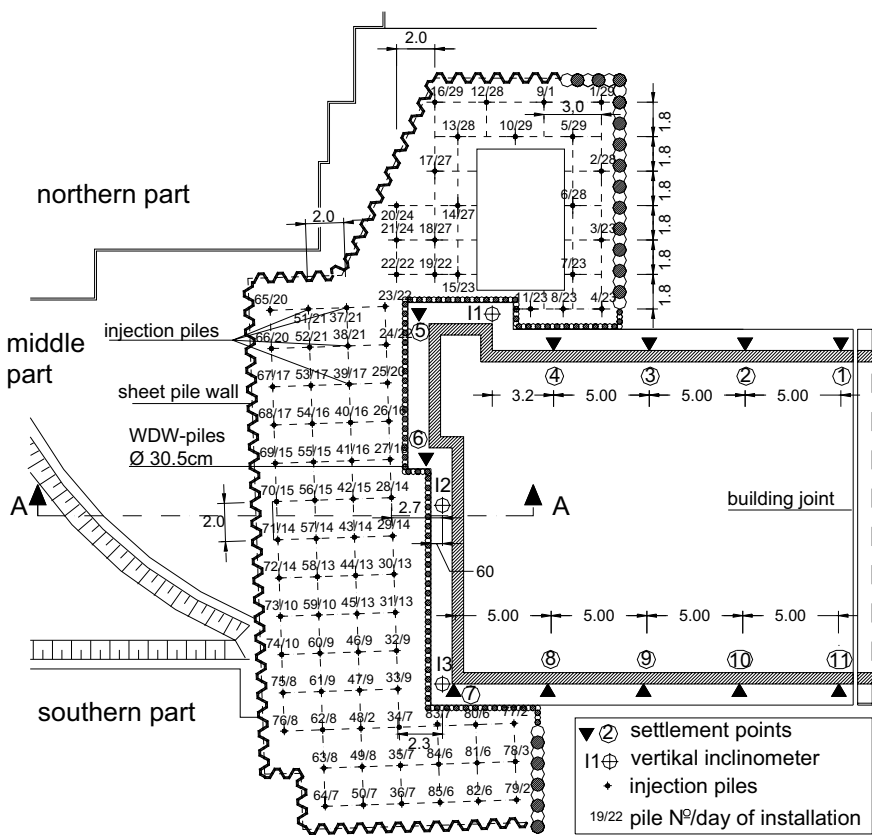


Fig. 6.89. Layout of stabilisation of the open excavation and injection piles grid system (project IV)

The general information on the project and construction data are compiled in Table 6.27. Fig. 6. 90 also shows a photo of the existing 10-story building and the construction measure for its stabilisation.

Table 6.27. Summary of general information and construction data on the project IV

Structural and soil boundary conditions		
1	Average size of the building	12 m x 40 m
2	Number of story	10-story
3	Average load on the foundation	150 kN/m ²
4	Stress relief due to excavation	no
5	Preloading	no information available
6	Soft soil thickness	up to 40 m below the ground surface
7	c _u -value (min/max.)	28 – 60 kN/m ²
8	Groundwater conditions	on average 0.8 m below the ground surface
Injection pile installation characteristics		
9	Pile system	GEWI injection pile (System DYWIDAG)
10	Pile length	19 m
11	Borehole diameter	130 mm (lost end with 220 mm)
12	Drill technik	auger boring
13	Spacing	1.8 m x 2.0 m
14	Injection horizon	1.3, 14.25, and 16.75 m below the raft foundation
15	Amount of grout / injection pressure	300 l / -r
16	1 st post grouting / burst open pressure	19 to 26 bar / 13 to 16 bar
17	Amount of grout (1 st post grouting)	4.5 l/length of meter
18	2 nd post grouting / burst open pressure	30 to 32 bar / 24 to 29 bar
19	Amount of grout (2 nd post grouting)	3.8 l/length of meter
Project analysis		
21	Maximum settlement RFIP	11 mm
22	Maximum measurement period	120 days
23	Number of pile load tests	-

**Fig. 6.90.** a) Existing building with excavated injection piles, b) Injection pile head and stepwise installation of the raft foundation (project IV)

Inclinometer and settlement measurements

To follow up the settlement and displacement of the existing building, three vertical inclinometer were installed and settlement was measured at 11 points along the perimeter of the building. The location of the measurement points are shown in Fig. 6.31. The results of the settlement measurements are plotted in Fig. 6.91.

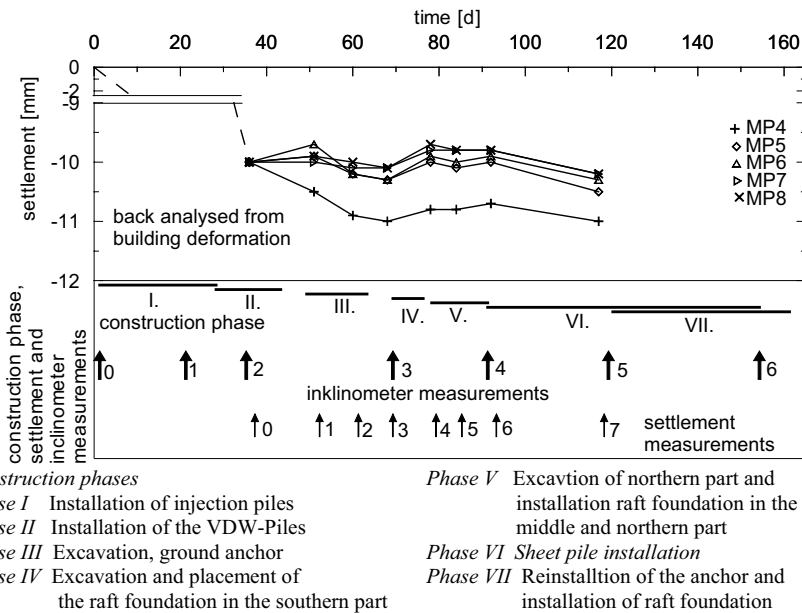


Fig. 6.91. The result of settlement measurements dependant on the construction stages

The horizontal deformation of the underground in the direction of the existing building are also shown in Fig. 6.87. A horizontal displacement of 10 to 27 mm was measured in the direction of the existing building. It appears that the injection piles had resulted in the improvement of the strength and stiffness of the soft underground through the injection pressure as well as the prestress condition due to the existing building.

The recorded settlements 10 to 15 mm on the existing building are more or less the same that caused during a comparable standard pile installation. Hence, the efficiency of the construction measure to stabilise the existing building is confirmed through the settlement measurements. With this measure the safety of the building was ensured during all construction stages.

6.10.6 Summary

The analysis of the measured settlements on the practical projects with the RFIP foundation system show that this type of foundation is proved to be excellent. Compared to shallow foundation, a settlement reduction factor β_s between 3 to 10 had been achieved through the stabilisation measure using the floating injection piles in normally consolidated soft soil deposit. The length of the injection piles (GEWI piles) varies between 10 and 20 m and the piles are installed in 1 to 3 injection horizon, which are grouted one to three times.

In contrast to the RFIP foundation system, the application of precast reinforced concrete driven pile (project III) show no settlement improvement compared to shallow foundation. Therefore, the RFIP system is also proved to be a better foundation stabilisation method compared to reinforced concrete driven piles in normally consolidated soft soils. The injection piles showed a very good results not only by individual pile load tests but also as a stabilising floating piled raft foundation.

In all the above presented projects, the following trend was observed during the installation of the injection piles:

- There exist an interaction between the injection piles, because a higher injection pressure had been observed during the grouting of a neighbouring injection piles within a group than in a single injection piles,
- Radical deformation of the soil was measured during the grouting process,
- A higher injection pressure was required in the lower injection horizon than the horizon located at a shallow depth. This again shows the dependency of the injection pressure on the available stress and stiffness of the soil.

The special favourable effect of the RFIP foundation system may arise from the following bearing mechanisms:

a) Skin friction on pile shaft: The pile carry part of the applied load through the skin friction, which builds itself along the contact between the pile and the soil depending on the vertical and horizontal stress levels.

b) Horizontal soil hardening: The cavity expansion due to the 1st injection and consecutive post grouting results a horizontal hardening in the soil. As a result of the cavity expansion of the pile, the soil surrounding the pile is subjected to a higher stress, which results a consolidation of the surrounding soil and thus improvement of the soil bearing and deformation behaviour: a reduction of the water content as a result of the increasing density of the soil and an increase in strength and stiffness of the soil. It is presumed that the cavity expansion due to the first injection pressure is approximately uniformly distributed along the pile length, whereas it concentrates itself in the region around the injection horizon during the post grouting.

c) Vertical mortar sheet: Likewise, a vertical mortar sheet may be formed around the pile surroundings in the soft soil layer due to the high injection pressure, which on one hand increases the horizontal restrain in the soil and on other hand clearly enlarges the skin surface area (see Fig. 6.56). By the first injection process, a vertical mortar sheet forms first, since the horizontal stresses are normally less than the vertical stresses and the grout suspension finds its way in a direction of minimum resistance. However, since the horizontal stresses increase after the first injection, a horizontal wings of mortar sheet can be formed and propagated during the consecutive post grouting.

d) As a result of the effects in b) and c), the soil stiffness increases and stresses in the soft soil layer reduces to hydrostatic stress condition, which results in an effective transfer of the external load under the raft foundation of the building that cause a minimum settlement. The load sharing factor between the injection piles and the raft lies between about 0.25 and 0.75 to 0.75 and 0.25 depending on the different boundary conditions.

7 Soil stabilisation with column-like elements

7.1 General

Constructions of roads, railways and other engineering structures on soft soils usually involves with problems such as excessive settlements, deformations and stability problems. To avoid or reduce such problems, there are several measures in geotechnical engineering, in which the soil improvement and stabilisation is one of them. Soil improvement and stabilisation is a broad field which may include different methods and techniques. Fig. 7.1 illustrates and categorises the different methods known in the international literature. This chapter, however, limits itself to soil stabilisation methods using pile/column like elements.

Ground improvement methods using column-like elements are used on an increasing scale in geotechnical engineering since the late 1960's. They are applied in road and railway embankments as well as in foundation of tanks, warehouses and light buildings. The basic principle of these techniques is to relieve the load on the soft soils without altering the soil structure substantially. This is achieved by installing column- or pile-type structures in a grid pattern into a bearing layer. On top of the columns a load transfer mat consisting of geotextile or geogrid reinforcements or a rigid plate is placed. The stress relieve of the soft soils results from a redistribution of the loads in the embankment through the arching effect, which is additionally stabilised by the geotextile/geogrid reinforcement by means of the so called the membrane effect. As a result the compressibility of the improved or composite ground can be reduced and the bearing capacity and shear strength increased. The consolidation of the soft soils can also be accelerated and thus the settlements after construction may be minimised considerably, since most column-type structures act as a vertical drain.

7.2 Reinforced embankments on pile-like elements

7.2.1 General

In recent years a new kind of foundation, the so called “geosynthetic-reinforced and pile-supported embankment” (GPE) has been developed (Fig. 7.2). Pile like elements (e.g. concrete piles, grouted stone columns, walls etc.) are placed in a regular pattern through the soft soil down to a lower load-bearing stratum. The construction and design principles of the various types pile-like elements is pre-

sented in the following subsequent sections. In this section the load transfer mechanism of a reinforced embankment on pile like system is described.

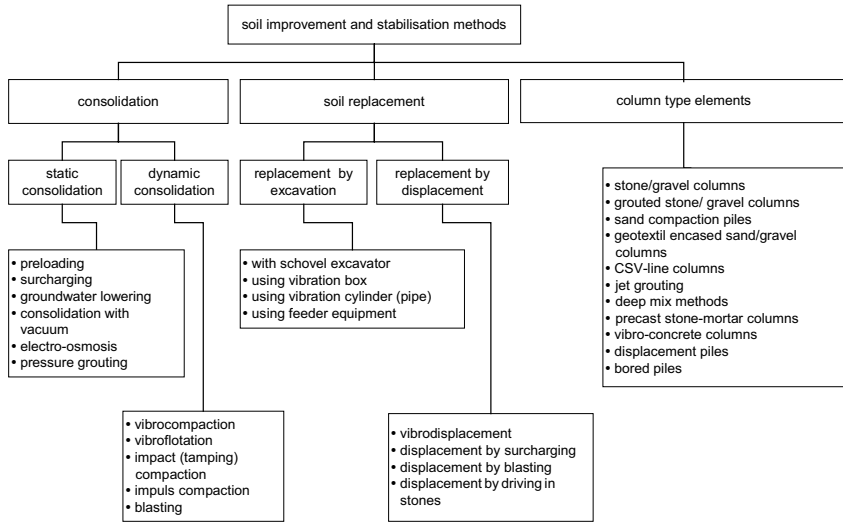


Fig. 7.1. Overview of the soil improvement and stabilization techniques

Above the pile heads, a reinforcement of one or more layers of geosynthetics (mostly geogrids) is placed. In areas with soft subsoil this type of underground improvement techniques have important advantages over the conventional embankment foundation from the technical, ecological and financial point of view. The application of such system of foundation is growing in geotechnical engineering very fast. (see e.g. Alexiew and Vogel 2001).

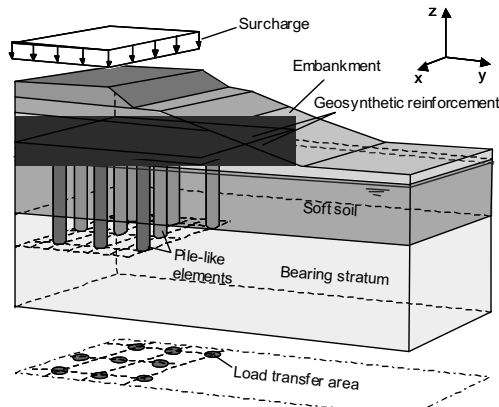


Fig. 7.2. A system of geosynthetic-reinforced and pile-supported embankment

7.2.2 Load transfer mechanism

The stress relief on the soft soil layer arises from an arching effect in the reinforced embankment above the pile head and a membrane effect of the geosynthetic reinforcement (Fig. 7.3) (Kempfert et al. 2004; Zaeske 2001). Due to the higher stiffness of the columns relative to the surrounding soft soil, the vertical stresses from the embankment and the surcharge load are concentrated on the piles, simultaneously soil arching develops as a result of differential settlements between the stiff column heads and the surrounding soft soil.

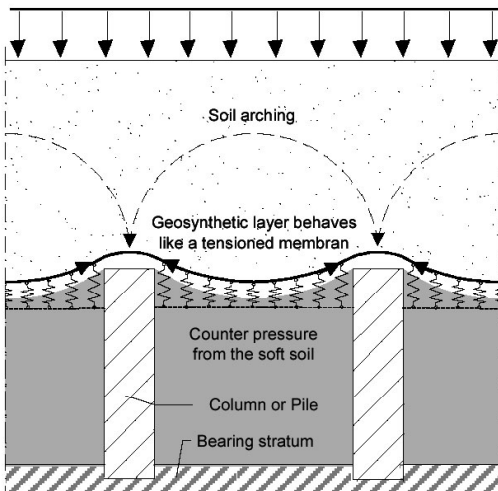


Fig. 7.3. The load transfer mechanisms

The 3D-arch spans the soft soil and transfers the applied load into the piles, where they are further transmitted down to the bearing stratum. The stress distribution can be calculated in various ways. Fig. 7.4, for example, shows a system consisting of several arches as a shell element (Zaeske 2001; Zaeske and Kempfert 2002). At the apex of the arch, the radial stress σ_r is equal to the vertical stress σ_z in Cartesian coordinate system (Fig. 7.4). The equilibrium of the forces in radial direction leads to the following general differential equation, which is a function of the vertical stresses $\sigma_z(z)$ (Zaeske, 2001):

$$-\sigma_z \cdot dA_u + (\sigma_z + d\sigma_z) \cdot dA_o - 4 \cdot \sigma_\phi \cdot dA_s \cdot \sin\left(\frac{\delta\Phi_m}{2}\right) + \gamma \cdot dV = 0 \quad (7.1)$$

where

$$\begin{aligned} dA_u &= (r \cdot \delta\Phi)^2 \\ dA_o &= (r + dr)^2 \cdot (\delta\Phi + d\delta\Phi)^2 \approx 2 \cdot d\delta\Phi \cdot r^2 \cdot \delta\Phi + 2 \cdot dr \cdot r \cdot \delta\Phi^2 + r^2 \cdot \delta\Phi^2 \end{aligned} \quad (7.2a)$$

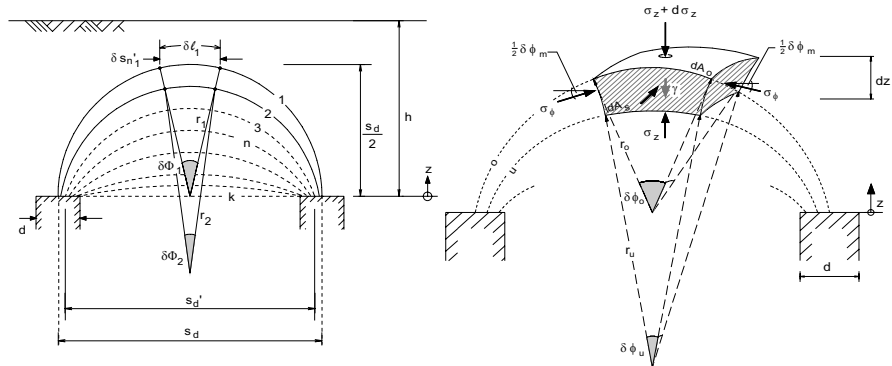


Fig. 7.4. Theoretical arching model (after Zaeske and Kempfert 2002)

$$\begin{aligned} dA_s &= (r + \frac{1}{2}dr) \cdot (\delta\Phi + \frac{1}{2}d\delta\Phi) \cdot dz && \approx dz \cdot r \cdot \delta\Phi \\ dV &= (r + \frac{1}{2}dr)^2 \cdot (\delta\Phi + \frac{1}{2}d\delta\Phi)^2 \cdot dz && \approx dz \cdot r^2 \cdot \delta\Phi^2 \end{aligned} \quad (7.2b)$$

For the part of the embankment above the arch, a constant stress distribution due to the traffic load and a linearly increasing stress distribution due to soil own weight is assumed. After simplification and solving the differential equation (Eq. 7.1) and finding the limit as $z \rightarrow 0$, an equation for estimation of the effective stress σ_{zo} on the top of the soft soil layer can be derived:

$$\sigma_{zo} = \lambda_1^\chi \cdot \left(\gamma + \frac{p}{h} \right) \cdot \left(h \cdot (\lambda_1 + t^2 \cdot \lambda_2)^{-\chi} + t \cdot \left(\left(\lambda_1 + \frac{t^2 \cdot \lambda_2}{4} \right)^{-\chi} - (\lambda_1 + t^2 \cdot \lambda_2)^{-\chi} \right) \right) \quad (7.3)$$

where

$$\begin{aligned} \chi &= \frac{d \cdot (K_{crit} - 1)}{\lambda_2 \cdot s_d} \\ \lambda_1 &= \frac{1}{8} \cdot (s_d - d)^2 \\ \lambda_2 &= \frac{s_d^2 + 2 \cdot d \cdot s_d - d^2}{2 \cdot s_d^2} \\ K_{crit} &= \tan^2 \left[45^\circ + \frac{\varphi'}{2} \right] \end{aligned} \quad (7.4)$$

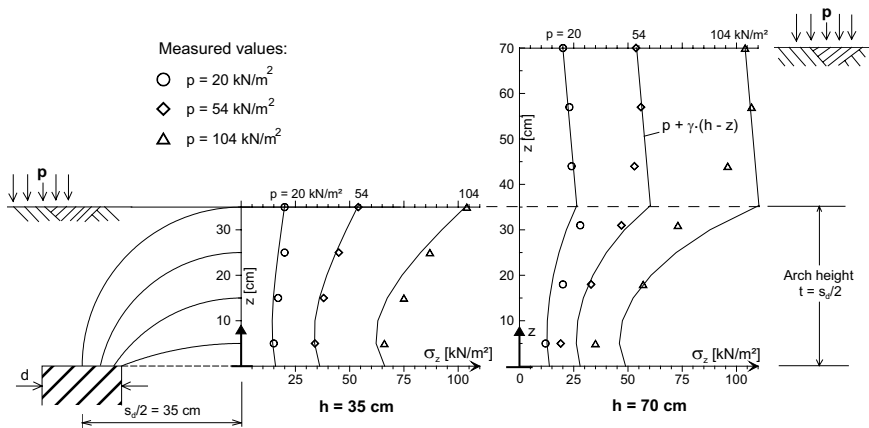


Fig. 7.5. Comparison of the measured and calculated stresses in the reinforced embankment: (height of the embankment $h = 35$ and 70 cm)

Simplified dimensionless diagrams for estimation of σ_{zo} can also be found in Zaeske and Kempfert 2002; Zaeske 2001; EBGEO - DGGE 2003. Fig. 7.5 shows a comparison of the analytically calculated stresses with the result of model tests.

The loading system of the geosynthetic reinforcement (Fig. 7.6) can be expressed by the differential equation (Eq. 7.5) of an elastic cable supported at two ends, in which the vertical deflection z and the horizontal force H are the unknown variables (Zaeske, 2001; Zaeske and Kempfert, 2002).

$$\frac{d^2 z}{dx^2} = \frac{q_z}{H} + \frac{C \cdot z}{H} \quad (7.5)$$

with

$$H = \frac{2 \cdot \int_0^i \sqrt{1 + (z_w')^2} \cdot dx + 2 \cdot \int_i^j \sqrt{1 + (z_p')^2} \cdot dx - l_0}{2 \cdot \int_0^i (1 + (z_w')^2) \cdot dx + 2 \cdot \int_i^j (1 + (z_p')^2) \cdot dx} \cdot J \quad (7.6)$$

where

$$z_w(x) = A_{1,W} \cdot e^{\alpha_W \cdot x} + A_{2,W} \cdot e^{-\alpha_W \cdot x} - \frac{\beta_W}{\alpha_W^2} \quad 0 \leq x \leq i \quad (7.7)$$

$$z_w'(x) = \alpha_W \cdot (A_{1,W} \cdot e^{\alpha_W \cdot x} - A_{2,W} \cdot e^{-\alpha_W \cdot x})$$

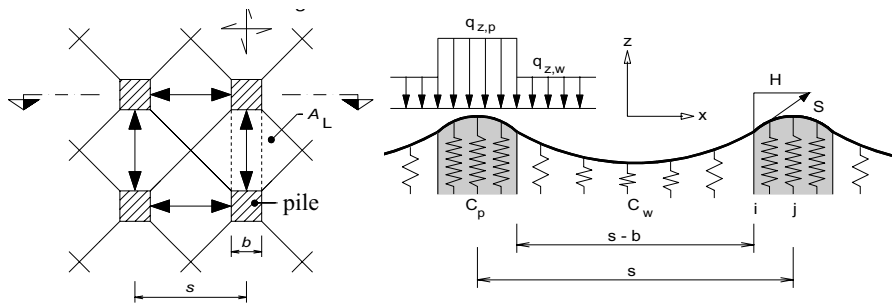


Fig. 7.6. The load system of the membrane (Geosynthetic reinforcement)

$$z_p(x) = A_{1,p} \cdot e^{\alpha_p \cdot x} + A_{2,p} \cdot e^{-\alpha_p \cdot x} - \frac{\beta_p}{\alpha_p^2} \quad i \leq x \leq j \quad (7.8)$$

$$z_p'(x) = \alpha_p \cdot (A_{1,p} \cdot e^{\alpha_p \cdot x} - A_{2,p} \cdot e^{-\alpha_p \cdot x})$$

and

$$\alpha_w^2 = \frac{C_w}{H}; \quad \alpha_p^2 = \frac{C_p}{H} \quad (7.9a)$$

$$\beta_w = \frac{q_{z,w}}{H}; \quad \beta_p = \frac{q_{z,p}}{H} \quad (7.9b)$$

$$A_{1,w} = A_{2,p} \cdot \frac{\alpha_p}{\alpha_w} \cdot \frac{e^{(\alpha_w - \alpha_p) \cdot i} \cdot (e^{2 \cdot \alpha_p \cdot (i-j)} - 1)}{e^{2 \cdot \alpha_w \cdot i} - 1} \quad (7.9c)$$

$$A_{2,p} = \frac{e^{\alpha_p \cdot (2 \cdot j + i)} \cdot (e^{2 \cdot \alpha_w \cdot i} - 1) \cdot (\alpha_p^2 \cdot \beta_w - \alpha_w^2 \cdot \beta_p)}{\alpha_p^2 \cdot \alpha_w \cdot (L_1 + L_2)}$$

$$L_1 = (\alpha_p - \alpha_w) \cdot (e^{2 \cdot (\alpha_p + \alpha_w) \cdot i} + e^{2 \cdot \alpha_p \cdot j}) \quad (7.9d)$$

$$L_2 = (\alpha_p + \alpha_w) \cdot (e^{2 \cdot \alpha_p \cdot i} - e^{2 \cdot (\alpha_p \cdot j + \alpha_w \cdot i)})$$

J in Eq. 7.7 is the stiffness of the geosynthetic membrane and C_p and C_w in Eq. 7.9a are the subgrade reaction (spring constants) of the pile and the soft soil layer respectively (see Fig. 7.6).

The resultant tensile force in the reinforcement membrane S is then given by:

$$S(x) = \varepsilon(x)/J = H \cdot \sqrt{1 + z'^2(x)} \quad (7.10)$$

For dimensionless diagrams for design of geosynthetic supported embankments on pile-like elements in soft soils, refer to EBGEO,DGTT 2003; Zaeske and Kempfert, 2002; Zaske 2001.

7.3 Stone columns and sand compaction piles

7.3.1 General

Stone columns and sand compaction piles represent the most known column-type technique for improving soft soils. They possess high compressive strength and stiffness relative the soft soil. They do not only serve the function of reinforcement and drainage, but they also increase the bearing capacity and reduce the settlement of the soft ground. Depending on the type of installation method, the soil around the column is compacted due to the displacement of the soil during installation, and hence improved stiffness of the soil.

Various installation methods are used world-wide, for instance, the vibro-replacement method (Fig. 7.6), the vibro-compaction method, the vibro-composer method and ramming by dropping hammer (15 to 20 kN), etc.

The effectiveness of the load redistribution to the columns mainly depends on the lateral support from the surrounding soft soil. The lateral support is expressed by means of the undrained shear strength. According to German regulations, the application of stone columns is generally limited to soils with undrained shear strength $c_u \geq 15 - 25 \text{ kN/m}^2$ (FGSV 1979). Stone columns are also occasionally used in very soft soils with an undrained shear strength $c_u < 10 \text{ kN/m}^2$ (Raju 1997). Generally, however, there is a risk in installing stone columns in sensitive or organic soils.

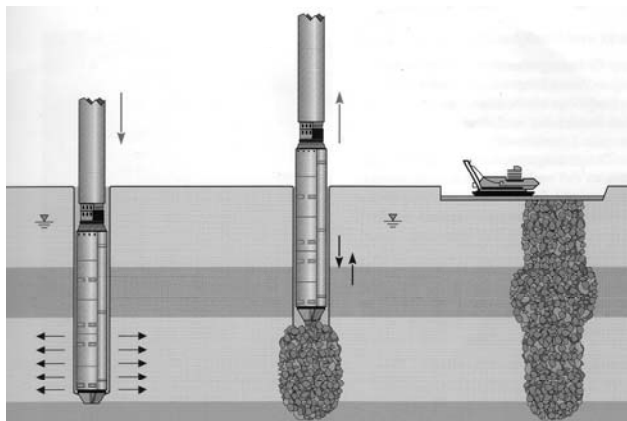


Fig. 7.7. Vibro-replacement method (Photo: Keller Grundbau)

7.3.2 Principles of design and analysis

General

Since control of the soil improvement attained with the gravel columns is only possible with a relatively large expense and effort, a simplified and reliable calculation procedures are inevitable, which may help to minimize the control measurements and hence the cost of the project. An overview and comparison of existing design methods is given for instance by Soyez 1987; Bergado et al. 1994; Priebe 1995. Most design methods are based on the ‘unit cell concept’, i.e. a cylinder of composite ground enclosing the tributary soil and a column is considered. The effect of soil improvement is usually expressed by the so called settlement reduction factor (soil improvement factor) β , which is defined as:

$$\beta = \frac{\text{settlement of unimproved soil}}{\text{settlement of improved soil}} \quad (7.11)$$

Several methods for calculating this factor and thus designing the column grid are available in literature. The most commonly used analytical approach in Europe is that of Priebe 1995.

In the design of gravel columns two limit cases has to be differentiated. These are the single column under a single foundation pad and raster of columns under an infinitely long rigid or flexible plate. However, none of the two cases may happen in practice. Therefore, one has to choose the design method which approximates realistically the given situation for a particular project. can accomplish therefore only by use more near in each case of the border line lying a simplified calculation with an approximation character. If one considers limit case of a single column, the calculation concentrates mainly on the load-carrying capacity of the column. On the other hand, a raster of columns require the analysis the deformation behaviour of the improved underground.

Bearing capacity of a single column

Gravel columns may undergone failure in one of the following forms as shown in Fig. 7. 8: bulging, shear, or punching failure.

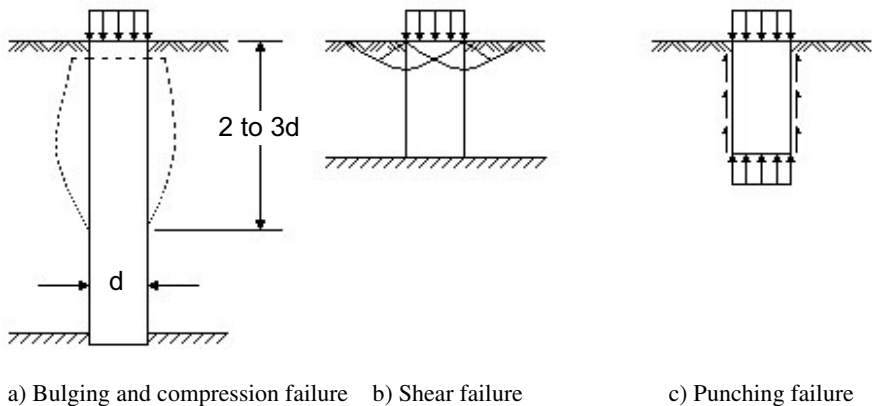
Bulging or compression failure. Analogue to the effective shear parameters in a specimen in a triaxial test, the maximum effective pressure on the column can be expressed by:

$$\sigma'_{v,max} = \tan^2 \left(45 + \frac{\varphi_c}{2} \right) \cdot \sigma'_{h,max} = K_{p,c} \cdot \sigma'_{h,max} \quad (7.12)$$

Where

$\sigma'_{v,max}$ = maximum vertical effective pressure on the column,

$\sigma'_{h,max}$ = maximum horizontal effective pressure on the surrounding soil,



a) Bulging and compression failure b) Shear failure c) Punching failure

Fig. 7.8. Failure mechanism of a single gravel column in soft soil

ϕ_c = angle of internal friction of the column material,

$K_{p,c}$ = the coefficient of the passive earth pressure of the column material in Rankin's special case

Analogue to a pressuremeter cell, the maximum horizontal effective pressure on soil may be given by

$$\sigma'_{h,max} = p_{max} - u \quad (7.13)$$

$$p_{max} = (\sigma'_{h,0} + u_0) + k \cdot c_u \quad (7.14)$$

Where p_{max} is the absolute stress in the surrounding soil at limit state, u is the pore pressure in the column material, $\sigma'_{h,0}$, u_0 are the initial horizontal stress and pore pressure in soil before column installation, c_u is the undrained shear strength of the soil and k is called influence factor. There are different recommendation for the influence factor k in literature.

$$k = 1 + \ln \left[\frac{E_s}{2 \cdot (1 + \nu_s) \cdot c_u} \right], \quad \text{or} \quad k = 1 + \ln \left[\frac{E_s}{3 \cdot c_u} \right], \quad \text{or} \quad k = 6.18 \quad (7.15)$$

where E_s and ν_s are the modulus of elasticity and the Poisson's ratio of the soil respectively. More equations for the influence factor can be found in Bergado et al. 1994.

Shear failure. This type of failure can be examined by taking an axis symmetrical composite column-soil unit cell system with a cone type of rupture surface as shown in Fig. 7.7b. Ignoring the shear stresses on column skin and the shear deformation along the rupture surface and assuming a constant volume, the maximum effective vertical pressure $\sigma'_{v,max}$ on the column can be estimated from:

$$\sigma'_{v,max} = c_u \cdot \left[\frac{\sigma}{c_u} + \frac{2}{\sin(2 \cdot \delta)} \right] \cdot \left[1 + \frac{\tan \delta_c}{\tan \delta} \right] \cdot \tan^2 \delta_c, \quad \text{mit } \delta_c = 45 + \frac{\varphi_c}{2} \quad (7.16)$$

where σ is the applied external pressure on the improved soil.

Punching failure of a floating column. The resistance of the column against punching arises from the skin friction and the base resistance. Ignoring the weight of the column, the minimum length of a column required to avoid a punching failure is given by:

$$L_{min} = \frac{l}{2} \cdot R_c \cdot \left(\frac{\sigma_{v,0}}{c_u} - g \right) \quad (7.17)$$

The longer the column the smaller will be the base resistance. The maximum length of the column at which the base resistance will no more exists may be calculated from:

$$L_{max} = \frac{l}{2} \cdot R_c \cdot \frac{\sigma_{v,0}}{c_u} \quad (7.18)$$

where $\sigma_{v,0}$ is the vertical stress on the top of the column and R_c is the radius of the column. A length of column beyond the maximum length will not have any advantage. Hence, the optimum length of the column lies between these extreme values, i.e. $L_{min} \leq L \leq L_{max}$.

Design of column groups

The two main aspects of the design of column groups are the determination of the settlement reduction effect in the compressible layer and the improvement in the load bearing capacity of the whole system. The assumption in the analysis and design of the column group in this section is that the columns reach the bearing layer.

The columns are usually arranged either in triangular, quadratic or hexagonal grids. Each grid pattern have an axis symmetrical influence zone cylindrical in shape usually referred as a unit cell with an equivalent diameter d_e equal to 1.05, 1.13 and 1.29 times the column spacing for the case of triangular, quadratic and hexagonal grids respectively.

Following assumptions are made in the following approach to determine the settlement reduction effect of the gravel columns:

- The columns penetrate the compressible layer fully,
- No immediate and secondary settlement,
- The foundation plate is assumed rigid
- Both the column and the soil settles together, i.e., $s_c = s_s$

Because of their higher stiffness the columns share a larger proportion of the applied load and relieves the compressible layer. The equilibrium of the external

pressure $\Delta\sigma_0$ and the vertical reaction stresses $\Delta\sigma_{v,c}$ and $\Delta\sigma_{v,s}$ on the column and the soft soil may give rise to the following equation:

$$\Delta\sigma_0 \cdot A_e = \Delta\sigma_{v,c} \cdot A_c + \Delta\sigma_{v,s} \cdot (A_e - A_c) \quad (7.19)$$

Refer to Fig. 7.13 for the definition of the variables in Eq. 7.19.

The effect of the soil improvement due to the installation of gravel columns can mainly be expressed in terms the settlement reduction factor β (Eq. 7.11) and the stress concentration factor n given by:

$$n = \frac{\sigma_c}{\sigma_s} \quad (7.20)$$

Although the influence of the column installation on the property of the soil negatively or positively have not been sufficiently studied, it is assumed that the soil will retain its original property. Because of the same surface settlement of the column and the soil, the settlement of the whole composite system is mainly arise from the soil. Assuming the stiffness of the soil remain constant before and after the soil improvement, the following relationship can be derived:

$$\beta = \frac{\sigma}{\sigma_s} = 1 + (n-1) \cdot a_c, \quad a_c = \frac{A_c}{A_e} \quad (7.21)$$

The main assignment is then the determination of the parameter n dependent on the area replacement ratio a_c . There are generally two approaches available to solve this problem. The first approach assumes a plastic failure of the column until it becomes to equilibrium condition as a result of the consolidation of the surrounding soil, whereas the second approach assumes elastic property of the column and the soil.

The plastic failure approach. This model considers the soil surrounding the column as a cylindrical pipe with a thick wall and has the soil parameters E_s and v_s . In developing the model, the following was assumed for the contact system between the column and the soil.

- The surface settlements of the column and the soil are the same,
- The plastic failure of the column material follows that of the soil,
- An incompressible column material and a volume constant deformation behaviour,
- The soil behaves linear elastic with constant modulus of elasticity and Poisson's ratio with depth,
- The cross section remains uniform,
- The same unit weight of the soil and the column material.

Priebe 1995 considers the pipe with a thick wall as infinitely long and subjected to the following internal pressure:

$$\Delta\sigma_h = \Delta\sigma_{h,c} - \Delta\sigma_{h,s} \quad (7.22)$$

with

$$\Delta\sigma_{hc} = K_{ac} \cdot \sigma_c = \tan^2 \left(45 - \frac{\phi_s}{2} \right) \cdot \sigma_c \quad (7.23)$$

$$\Delta\sigma_{hs} = \sigma_s \quad (7.24)$$

where $\Delta\sigma_{hc}$ is a change of horizontal pressure of the column on the soil and $\Delta\sigma_{hs}$ is the change of the horizontal resistance of the soil. Assuming the soil at the transition zone to the column exercises a hydrostatic pressure due to installation process, Priebe 1995 set $\Delta\sigma_{hs} = \sigma_s$. With a further assumption that the outer surface of the pipe will not undergo a radial deformation, the settlement reduction factor can be expressed as:

$$\beta = \frac{\sigma}{\sigma_s} = 1 + a_c \cdot \left[\frac{0,5 + f(v, a_c)}{K_{ac} \cdot f(v, a_c)} - 1 \right] \quad (7.25)$$

with

$$f(v, a_c) = \frac{1 - v^2}{1 - v - 2v^2} \cdot \frac{(1 - 2v) \cdot (1 - a_c)}{1 - 2v + a_c} \quad (7.26)$$

The soil improvement factor β can also directly be read from Fig. 7.9. Further approaches and models to estimate the degree of the soil improvement using the gravel column can be found in Gruber 1995; Bergado 1994; Soyaz 1987; Smolcicky 1983; Van Impe and De Beer 1983; Goughnour 1983; Ghionna and Jamolkowski 1981; Vautrain 1980. See also Madhav et al. 1996 who took into account a linear increase of the modulus of elasticity of the column material with depth.

The linear elastic approach. One of the possible models in this approach introduces an equivalent elasticity modulus for the composite column-soil system. It is the weighted average of the elasticity modulus of the column material and the soil and it given by:

$$\bar{E} = \frac{E_c \cdot A_c + E_s \cdot (A_e - A_c)}{A_e} \quad (7.27)$$

and the factor β can be written as:

$$\beta = 1 + a_c \cdot \left(\frac{E_c}{E_s} - 1 \right) \quad (7.28)$$

Further approaches using linear elastic behaviour can be found in Balaam and Booker 1976.

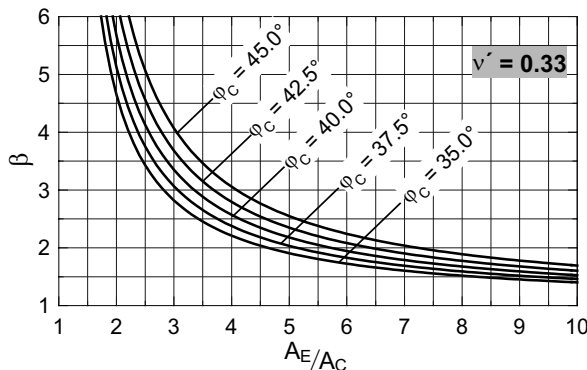


Fig. 7.9. The settlement reduction factor

Improvement of the safety and stability of the composite system. Beside the reduction of the settlement, the sand/gravel columns will help to improve the stability of the foundation (Priebe 1995; Aboshi et al. 1979; Di Maggio 1978). In order to conduct the stability analysis with a homogenous soil layer, Di Maggio 1978 suggested an equivalent unit weight as follows:

$$\bar{\gamma} = \gamma_c \cdot a_c + \gamma_s \cdot (1 - a_c) \quad (7.29)$$

Further equivalent parameters for cohesion and internal angle friction are also given in Priebe 1995; Di Maggio 1978 as follows:

$$\bar{c} = (1 - m) \cdot c_s + m \cdot c_u \quad (7.30)$$

$$\tan \bar{\varphi} = (1 - m) \cdot \tan \varphi_s + m \cdot \tan \varphi_u \quad (7.31)$$

where m is the part of the load carried by the column. Di Maggio 1978 set $m = a_c$, whereas Priebe 1995 took into account the effect of the load redistribution on the column and he suggested the following relationship:

$$a_c = m_{min} \leq m \leq m_{max} = \frac{A_c \cdot \sigma_c}{A_e \cdot \sigma} \quad (7.32)$$

Aboshi et al. 1979 introduced an equivalent shear resistance along the failure surface as follows:

$$\bar{\tau} = (1 - a_c) \cdot \tau_s + a_c \cdot \tau_c \cdot \cos \alpha \quad (7.33)$$

with

$$\tau_c = \sigma_{c,z} \cdot \cos \alpha \cdot \tan \varphi_{c,r}, \quad \sigma_{c,z} = \sigma_c + \gamma'_c \cdot z, \quad \tau_s = c_u \quad (7.30)$$

Where τ_s , τ_c are the shear stresses in soil and in column along the failure surface, $\sigma_{c,z}$ is the normal stress in column at a depth of z, τ_s is the inclination of the failure surface from the horizontal and $\varphi_{c,r}$ is the residual angle of internal friction of the column material.

7.4 Geotextile encased sand/gravel columns (GEC)

7.4.1 General

The foundation system with geotextile encased sand or gravel columns (GEC) is a new soil improvement method and it is primarily used for improvement of foundations of road embankments in Germany, Sweden and the Netherlands since the last decade (Raithel 1999; Raithel et al, 2004). Recently, it is also used in dike constructions and land reclamation (see for example section 7.9.1). Basically, this method is an extension of the well known stone column and sand compaction pile foundation improvement techniques. The only difference is that the column in this new method is encased with geotextile with high tensile strength. Contrary to the conventional sand/gravel columns, the GEC system can be used in very soft soils ($c_u < 15 \text{ kN/m}^2$) such as peat or very soft silt/clay as well as sludge because of the lateral support provided by the geotextile casing. In the following the essential features of the bearing and deformation behaviour of the GEC-system are described.

7.4.2 Installation method

There are two methods of installation of the GEC-system that are usually used in practice. These are the displacement (Fig. 7.9a) and the replacement (Fig. 7.9b) methods. With the replacement method, an open steel shaft (usually $\emptyset = 150 \text{ cm}$) is driven deep into the bearing layer and the soil within the shaft is removed by auger boring as shown in Fig. 7.9b. Whereas by the vibro displacement method, a steel shaft (about $\emptyset = 80 \text{ cm}$) with a conical end that has two flaps and close upon contact with the soil is inserted and vibrated down to the bearing layer displacing the soft soil. In both cases, the open geotextile sack is then placed in the shaft and filled with sand or gravel while the shaft is pulled out slowly under vibration in order to reach a maximum possible compaction of the fill material. Figs. 7.10 and 7.11 also show schematically the displacement and the replacement method of installation of the GEC system respectively.



Fig. 7.10. The installation method of the GEC-system: a) the displacement method; b) the replacement method

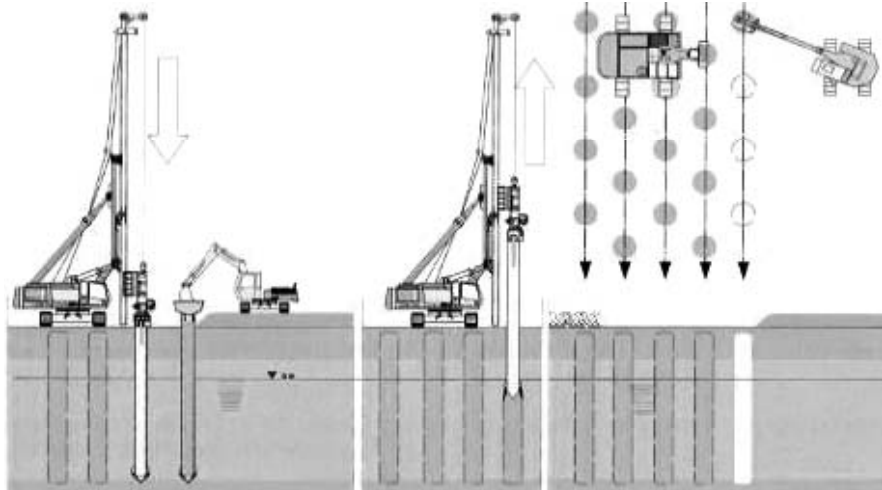


Fig. 11. Schematic presentation of the displacement method of installation

The replacement method is preferred for soils with relatively higher penetration resistance or when vibration effects on nearby buildings and road installations have to be minimised. The advantages of the vibro-displacement method compared to the replacement method are: i) faster and more economical column installation, ii) the soil surrounding the column will be pre-stressed due to the displacement of the soil, and iii) no need of soil disposal. Obviously, there are also disadvantages of the displacement method such as the development of the excess pore pressure during penetration, the effects of vibrations on the surrounding and the deformations due to the volume of the displaced soil.

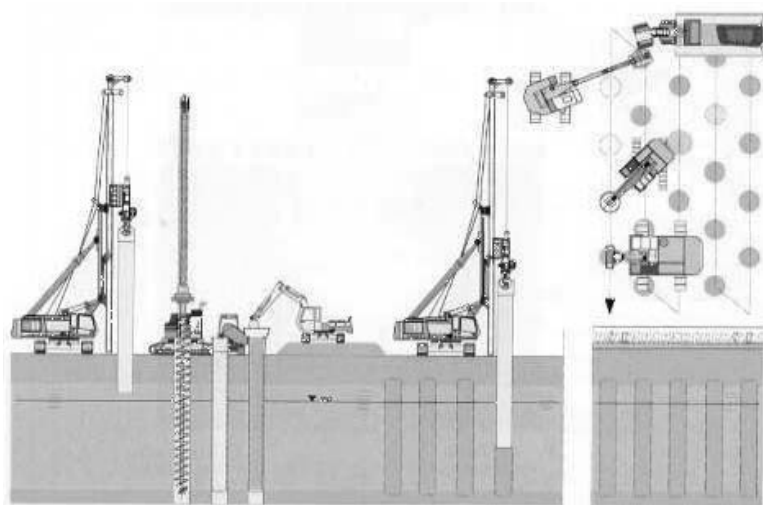


Fig. 7.12. Schematic presentation of the replacement method of installation

7.4.2 The bearing system of the GEC

With the foundation system GEC gravel/sand-columns are installed into a bearing layer to relieve the load on the soft soils. Due to the geotextile casing in combination with the surrounding soft soils the column becomes a radial support, whereas the casing is strained by hoop stresses (Raithel et al. 2005; Raithel 1999). In contrary to the conventional stone/gravel or sand compaction columns, a special range of application of the GEC-system such as in very soft soils ($c_u < 15 \text{ kN/m}^2$) like peat or very soft silt/clay as well as sludge is possible. This is mainly due to the supporting effects of the geotextile casing.

In a non-encased column, the horizontal support of the soft soil must be equal to the horizontal pressure in the column otherwise failure of the column is inevitable. In a GEC-system however the horizontal support of the soft soil can be much lower due to the geotextile casing. The horizontal support depends also on the vertical pressure over the soft soil, which can be much smaller. As a result a stress concentration on the column head and a lower vertical pressure over the soft soil and therefore a large settlement reduction may be achieved. To withstand the high ring forces, the geotextile casings are manufactured seamless. Beside transferring the load down to the bearing layer, the columns simultaneously functions as vertical drains.

The GEC are arranged in a regular rectangular or triangular grid system. The influence area A_e of a single column A_c in triangular grid is for example a hexagonal area, which can be transformed into an equivalent circular area (Fig. 7.13 right). The influence area is also called the unit cell concept which contain the column and the soil in influence zone.

7.4.3 The analytical calculation approach

The analytical axial symmetric model according to the ‘unit cell concept’ is shown in Fig. 7.13 together with the essential load and boundary conditions (Raithel et al. 2005; Raithel 1999).

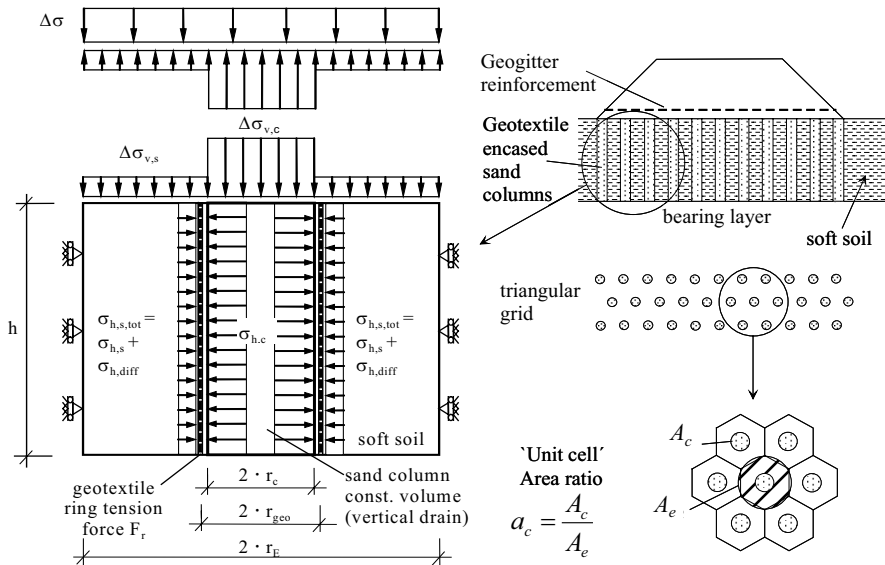


Fig. 7.13. An analytical model for the design and analysis of GEC system (Raithel 1999)

Beside the boundary conditions in Fig. 7.13, the following assumptions are considered in deriving the analytical model:

- equal settlement of the column and the soft soil,
- negligible settlement of the bearing layer below the column base,
- within the column the coefficient of active earth pressure $K_{a,c}$ applies,
- the earth pressure at rest with $K_s = K_{0,s} = 1 - \sin\varphi$ can be assumed, if replacement type of installation method is employed, and an increased coefficient of earth pressure $K_s = K_{0,s}^*$ for displacement method,
- linear-elastic behaviour of the geotextile,
- for the analysis and design of the foundation, the drained (end) condition is decisive, because it gives the maximum settlement and hoop tensile stress.

The model is developed based on the conventional calculation models for stone columns and sand compaction piles by, for example, Priebe 1976; Ghionna and Jamiolkowski 1981. The equations are extended and complemented to include the effect of the geotextile coating. For consolidation analysis and settlement calculations, the conventional calculation methods for foundations can be used.

The equilibrium of the external pressure $\Delta\sigma_0$ and the vertical reaction stresses $\Delta\sigma_{v,c}$ and $\Delta\sigma_{v,s}$ on the column and the soft soil may give rise to the following equation:

$$\Delta\sigma_0 \cdot A_e = \Delta\sigma_{v,c} \cdot A_c + \Delta\sigma_{v,s} \cdot (A_e - A_c) \quad (7.34)$$

Refer to Fig. 7.13 for the definition of A_c and A_e .

Assuming that $\Delta\sigma_{v0,c}$ and $\Delta\sigma_{v0,s}$ are the initial vertical stresses in the column and the soft soil layer, the corresponding horizontal stresses can be written as:

$$\Delta\sigma_{h,c} = \Delta\sigma_{v,c} \cdot K_{a,c} + \sigma_{v0,c} \cdot K_{a,c} \quad (7.35a)$$

$$\Delta\sigma_{h,s} = \Delta\sigma_{v,s} \cdot K_{0,s} + \sigma_{v0,s} \cdot K_{0,s}^* \quad (7.35b)$$

If the replacement installation method is used, $K_{0,s}^*$ should be substituted by $K_{0,s}$ in Eq. 7.35. Assuming a linear-elastic behaviour, the hoop tensile force ΔF_r in the geotextile coating with a radius r_{geo} can be given as a function of the lateral strain and the stiffness J of the geotextile as follows:

$$\Delta F_r = J \cdot \varepsilon = J \cdot \frac{\Delta r_{geo}}{r_{geo}} \quad (7.36)$$

Using the formula for boiler cylinder, the hoop force can be converted to horizontal stress $\Delta\sigma_{h,geo}$ as follows:

$$\Delta\sigma_{h,geo} = \frac{\Delta F_r}{r_{geo}} \quad (7.36)$$

The sum of the stresses in the horizontal direction immediately near the coating results a stress difference $\Delta\sigma_{h,diff}$ which has an effect the soft soil and leads to horizontal deformation until a corresponding additional earth pressure is mobilised (mobilisation of the passive earth pressure partially) in the soft soil layer to bring the horizontal stresses in equilibrium. The stress difference $\Delta\sigma_{h,diff}$ is given by Eq. 7.38 and demonstrated in Fig. 7.14:

$$\Delta\sigma_{h,diff} = \Delta\sigma_{h,c} - (\Delta\sigma_{h,s} + \Delta\sigma_{h,geo}) \quad (7.38)$$

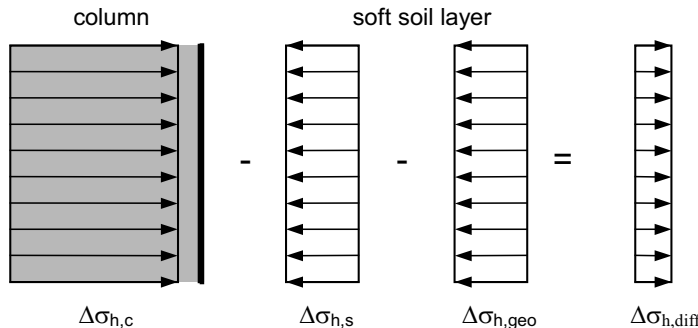


Fig. 7.14. Horizontal stresses at the transition between the column and the soft soil

The stress difference results a lateral expansion of the column. This horizontal deformation Δr_c and the settlement of the soft soil layer s_s can be calculated using the equations for a radial and longitudinal loaded hollow cylinder according to Ghionna and Jamiolkowski 1981 as:

$$\Delta r_c = \frac{\Delta\sigma_{h,diff}}{E^*} \cdot \left(\frac{1}{a_c} - 1 \right) \cdot r_c \quad (7.39)$$

and

$$s_s = \left(\frac{\Delta\sigma_{v,s}}{E_{oed,s}} - 2 \cdot \frac{1}{E^*} \cdot \frac{\nu_s}{1-\nu_s} \cdot \Delta\sigma_{h,diff} \right) \cdot h \quad (7.40)$$

Herein

$$E^* = \left(\frac{1}{1-\nu_s} + \frac{1}{1+\nu_s} \cdot \frac{1}{a_c} \right) \cdot \frac{(1+\nu_s) \cdot (1-2\nu_s)}{(1-\nu_s)} \cdot E_{oed,s} \quad (7.41)$$

where ν_s is the Poisson's ratio and $E_{oed,s}$ is the constrained modulus of the soft soil layer.

If a constant volume of the column material is assumed the following relationship can be formulated between the vertical settlement and the lateral expansion of the column:

$$s_c = \left(I - \frac{r_0^2}{(r_0 + \Delta r_c)^2} \right) \cdot h_0 \quad (7.42)$$

It should be noted that Eq. 7.42 shows a pure geometric relationship. That means, if the calculation is to be carried out for several load increments, the initial height h_0 and the initial radius r_0 must be newly calculated for each load increment.

Compatibility of the horizontal deformations requires that

$$\Delta r_c = \Delta r_{geo} + (r_{geo} - r_c) \quad (7.43)$$

As mentioned above, it is assumed that the settlement of the column and the soft soil layer is equal, i.e.

$$s_c = s_s \quad (7.44)$$

Using Eqs. 7.35, 7.36 and 7.43

$$\Delta\sigma_{h,geo} = \frac{J \cdot [\Delta r_c - (r_{geo} - r_c)]}{r_{geo}^2} \quad (7.45)$$

Inserting Eq. 7.45 into Eq. 7.38 and make use of stress difference in Eq. 7.36 and the equilibrium Eq. 7.33, the horizontal deformation of the column can be calculated from:

$$\Delta r_c = \left(\frac{1}{\frac{E^*}{(1/a_c - 1) \cdot r_c} + \frac{J}{r_{geo}^2}} \right) \cdot \left[K_{a,c} \cdot \left(\frac{1}{a_c} \cdot \Delta\sigma_0 - \frac{1-a_c}{a_c} \cdot \Delta\sigma_{v,s} + \sigma_{v,0,c} \right) - K_{0,s} \cdot \Delta\sigma_{v,s} - K_{0,s}^* \cdot \sigma_{v,0,s} + \frac{(r_{geo} - r_c)}{r_{geo}^2} \cdot J \right] \quad (7.46)$$

But Eq. 7.46 is dependant on the unknown variable $\Delta\sigma_{v,s}$. Hence, substituting Eq. 7.42 and 7.39 into Eq. 7.44, the following relationship for the determination of the part of the pressure on the soft soil layer $\Delta\sigma_{v,s}$ can be derived:

$$\left\{ \frac{\Delta\sigma_{v,s}}{E_{oed,s}} - \frac{2}{E^*} \cdot \frac{V_s}{1-V_s} \cdot \left[K_{a,c} \cdot \left(\frac{1}{a_E} \cdot \Delta\sigma_0 - \frac{1-a_E}{a_E} \cdot \Delta\sigma_{v,s} + \sigma_{v,0,c} \right) - K_{0,s} \cdot \Delta\sigma_{v,s} - K_{0,s}^* \cdot \sigma_{v,0,s} + \frac{(r_{geo} - r_c) \cdot J}{r_{geo}^2} - \frac{\Delta r_c \cdot J}{r_{geo}^2} \right] \right\} \cdot h = \left[I - \frac{r_c^2}{(r_c + \Delta r_c)^2} \right] \cdot h \quad (7.47)$$

which is again dependant on Δr_c . Therefore, Eqs. 7.46 and 7.47 should be solved iterative. Since the solution of these equations manually is cumbersome and time consuming, it is advisable to use a computer program.

The constrained modulus $E_{oed,s}$ of the soft soil layer plays a significant role in Eqs. 7.47 and 7.46 and hence the determination of its value realistically as a function of the existing stress level p^* is very important. According to Ohde 1939 (Eq. 2.76) the stress dependency of the constrained modulus can be given by:

$$E_{oed,s} = E_{oed,s}^{ref} \cdot \left(\frac{\sigma^*}{p_{ref}} \right)^m \quad (7.48)$$

where $E_{oed,s}^{ref}$ is the reference constrained modulus at a reference pressure of p_{ref} .

Immediately near the encased column, there is an increase of horizontal stress (Eq. 7.37), which leads to an increase of the mean stress in the soft soil layer for a constant vertical stress. For estimation of the mean stress the following equation can be used.

$$\sigma_{1,2}^* = \frac{1}{2} \cdot \left\{ \left(\Delta\sigma_{v,s} + \sigma_{v,0,s} \right) + \left[K_{0,s} \cdot \Delta\sigma_{v,s} + K_{0,s}^* \cdot \sigma_{v,0,s} + \Delta\sigma_{h,Dif} \right] \right\} + c \cdot \cot \varphi_s \quad (7.49)$$

where σ_1^* and σ_2^* are the stresses before and after load change respectively. The mean stress σ^* is the given by:

$$\sigma^* = \frac{\left(\sigma_2^* - \sigma_1^* \right)}{\ln \left(\frac{\sigma_2^*}{\sigma_1^*} \right)} \quad (7.50)$$

The average value, i.e. $\sigma^* = (\sigma_2^* + \sigma_1^*)/2$ may also give adequate result for practical purposes.

For an extension of the calculation model to layered soft underground and for a simplified calculation model, refer to Raithel et al. 2005; Raithel and Kempfert 2000; Raithel 1999.

7.5 CSV Method

7.5.1 General

The combined soil stabilisation with vertical columns (CSV) is a method, whereby small diameter columns of a dry binder or binder-sand mixture are installed using a displacement auger. Cement and lime are usually used as binders material. The columns with a diameter of 12 to 18 cm are arranged at a centre to centre distance of 0.5 to 1.5 m in a quadratic or triangular grid system. According to DGQT AK 2.8 2002, the centre to centre distance should not exceed three times the column diameter. The CSV-method can be used in very soft to stiff cohesive soils, loose granular soils and organic soils (Scheller and Reitmeier 2001). The stabilisation effect of the CSV arises from a combination of densification, pressurisation, load concentrations on the columns and dewatering due to the hydration process. The most common applications of the CSV-method are foundations of railway and highway embankments, building foundations and slope stabilisation. The advantages of the CSV-method are low equipment and mobilization costs, vibration free

installation, high flexibility in design and application, its application in organic soils and no need of material disposal.

7.5.2 The method of installation

Dry binders or binder-sand mix are inserted into the ground using a continuous flight auger. The auger consists a pressure bit at its end that displaces the ground laterally and compacts the stabilised soil. The auger runs through a material funnel and transports the dry binder or binder-sand mix into the cavity both during the downward and upward movements. The surrounding soil acts as a casing for the transport of the dry mix. If the soil is not firm enough to fulfil this task, the quantity of material input will be adjusted to create the necessary casing for a smooth and satisfactory transport of the dry material (Scheller and Reitmeier 2001). Fig. 7.15 shows a schematic presentation of the installation process and an excavated column during the installation.

The equipment required to install CSV-columns is relatively simple and light (Fig. 7.16). The hydraulic crawler rig with approximately 30 tons can operate on marginal ground. Adjustments can be made during the installation of the CSV-columns to confirm with the existing soil condition. It is generally possible to achieve a production of 40 to 70 m of column length per hour and per rig, but the production can significantly be increased under favourable soil conditions.

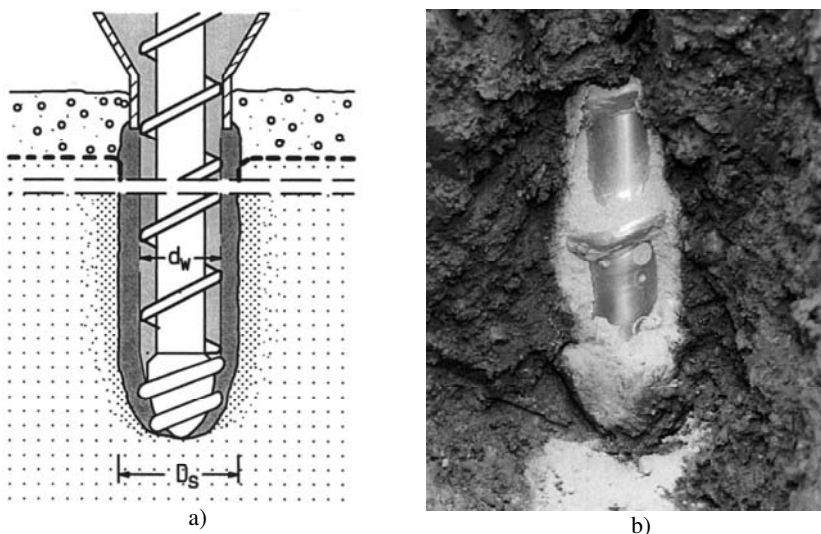


Fig. 7.15. a) The installation process; b) exposed auger during material transport (Courtesy: Bauer construction company)

7.5.3 The bearing system

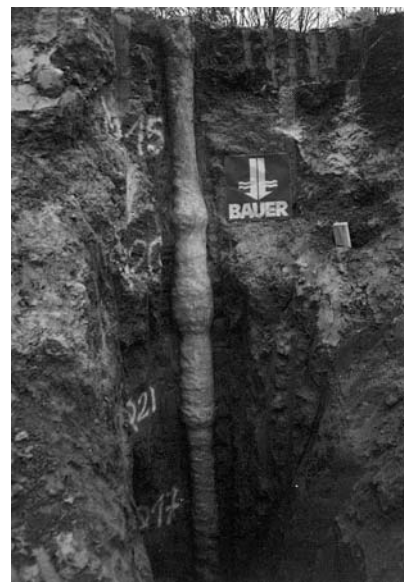
The bearing mechanism of the CSV-method arises from several superimposing effects. These include: compaction of the stabilised and the surrounding soils, dewatering due to the hydration process and load concentration on the CSV-column because they are more rigid and strong than the surrounding soft soil. According to Scheller and Reitmeier 2001 and DGGT AK 2.8 2002, there are two types of columns, namely, Type A and Type B. Type A columns are made of materials which have a chemical or physical effect on the surrounding soil but without developing its own strength. There exist an effect of dewatering, heating and ion transfer on the mechanical properties of the surrounding soil, but it is limited to the direct vicinity of the column. Type B columns are made of hydraulic binders and harden through hydration with pore or groundwater. Such type of columns are capable of carrying loads. A typical mix design consists of 20 to 30% Portland cement and 70 to 80% well graded sand. Assuming a water-cement ratio $w/c = 0.25$, one meter of column requires 1.5 to 2.0 litters of water for hydration. Type B columns are more frequently used in recent years than Type A columns.

According to DGGT AK 2.8 2002, the amount of the load concentration on the columns that reach the bearing layer depends on:

- the ratio of the cross sectional area of the column and its influence area,
- the stiffness of the column and its length,



a)



b)

Fig. 7.16. a) CSV-installation equipment; b) exposed CSV-column (Courtesy: Bauer construction company)

- the ratio of the stiffness of the column to the surrounding soil,
- the effect of load transmitting bearing layers or structural elements on the top of the column.

The structural load on soft underground stabilised with CSV-columns are transmitted to the bearing layer predominantly through the columns, where the columns are installed closed each other and reach the bearing layer (Fig. 7.17a). In this case the soft soil layer has no significant influence on the bearing behaviour of the system. Therefore, the bearing behaviour at or below the base of the columns governs the load-settlement behaviour of the stabilised foundation.

On the other hand, the interaction between the structure and the foundation system with floating type columns is complicated. For columns made of hydraulic binders with a higher stiffness and a rigid cap above them, the structure-foundation-soil interaction behaviour may be assumed similar to a combined pile-mat foundation. By closely placed floating columns (maximum spacing less than the perimeter of a single column), the whole stabilised area reacts as a homogeneous block. The bearing resistance results from the skin friction along the perimeter of the block ($2 \cdot (B + L) \cdot l_c$) and end resistance over the base area ($B \cdot L$), where B and L are the width and length of the block respectively and l_c is the length of the column (Fig. 7.13b).

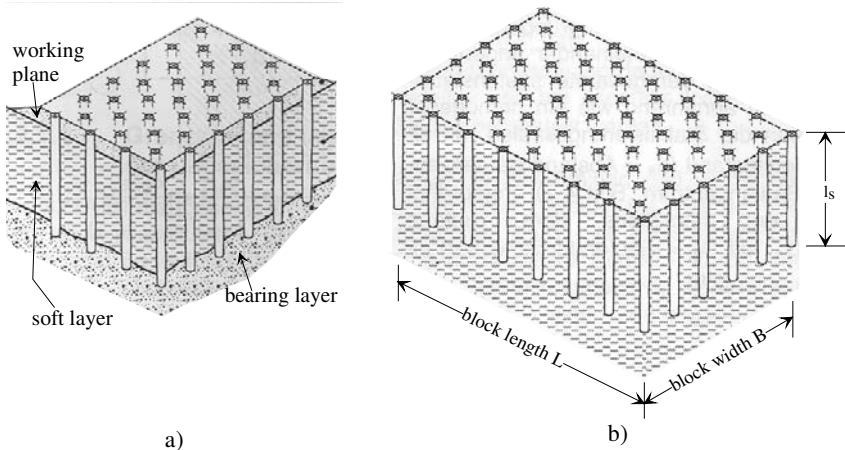


Fig. 7.17. a) CSV-Columns resting on bearing layer, b) Floating CSV-Columns acting as a block (adopted from DGQT AK 2.8 2002).

7.5.4 Design and analysis

Based on their experience, Scheller and Reitmeier 2001 reported that the 28 day compressive strength of the CSV-Column can reach 10 to 30 MN/m² and able to carry a structural load up to 450 kN/m². To best of our up to date knowledge, there

is no general procedure for the design and analysis of CSV-system of foundation improvement. The following design guidelines are wholly adopted from a technical bulletin of the Germany Society of Geotechnical Engineers, DGQT AK2.8 2002 and apply only for the Type B columns. The bulletin differentiates further between two categories of the Type B columns. These are:

- B1: the CSV-columns are made up of non-cohesive granulate material such as sand with effective internal friction angle φ' and dilatancy angle ψ .
- B2: the CSV-columns are made up of hard granulate-binder mix with a higher unconfined compressive strength, i.e. the influence of the internal friction of the granulate material is here negligible.

The design and verification of the safety of the CSV-system are based on the partial safety concept (refer to section 1.2) and are divided into different categories according to the failure and limit state condition. The general inequality equation is given by:

$$E_d \leq R_d \quad (7.51)$$

i.e., the design value of actions should not exceed the design value of resistance. Refer to DIN 1054 in regard to the determination of the design values of actions. In the following the determination of the characteristic and the design value of resistance only are presented.

Safety against internal column failure. The verification of the safety against internal failure of a column is based on the assumption that the structural loads are carried wholly by the columns. The characteristic value of the resistance $R_{c,k}$ for type B1-column is given by:

$$\begin{aligned} R_{c,k} &= A_c \cdot \sigma_0 = A_c \cdot (\gamma \cdot z + 2 \cdot c_{u,k}) \cdot K_p \\ &= A_c \cdot (\gamma \cdot z + 2 \cdot c_{u,k}) \cdot \tan^2 \left(\frac{\pi}{4} + \frac{\varphi'_k}{2} \right) \end{aligned} \quad (7.52)$$

The corresponding design value of the resistance is given by:

$$R_{c,d} = \frac{I}{\gamma_{Ep}} \cdot \lambda_{3D} \cdot R_{c,k} \quad (7.53)$$

where $c_{u,k}$, φ'_k are the characteristic values of the undrained strength and the effective internal angle of the column material respectively, A_c is the cross-sectional area of a single column, γ_{EP} is the partial safety factor for passive resistance ($\gamma_{EP}=1.4$, 1.3, and 1.20 for the load cases LF1, LF2 and LF3 respectively according to DIN 1054 2005) and λ_{3D} is a factor for three-dimensional case ($\lambda_{3D} \geq 1.0$) (Brauns 1978).

Similarly, for type B2-column,

$$R_{c,k} = A_c \cdot q_{u,k} \quad (7.54)$$

$$R_{c,d} = \frac{I}{\gamma_q} \cdot R_{c,k} \quad (7.55)$$

where q_{uk} is the characteristic values of the unconfined strength of the column material and γ_q is the partial safety factor ($\gamma_q = 2.0, 2.0$, and 1.5 for the load cases LF1, LF2 and LF3 respectively according to DGGT AK2.8 2002).

Safety against external bearing capacity. Whereas a monolithic sinking of the B1-columns as a result of failure of the surrounding soil is improbable, B2-columns should be verified for safety against such failure. There is no closed formula for the determination of the load-settlement behaviour of B2-columns. They are instead designed based on empirical values from comparable underground conditions similar to piles and the design is checked during construction using a quality inspection load tests. The design value of the resistance of end B2-columns is given by:

$$R_{cp,d} = \frac{I}{\gamma_{cp}} \cdot R_{cp,k} \quad (7.56)$$

where $R_{cp,k}$ is the characteristic value of the resistance obtained either from empirical values or from load test results and γ_{cp} is partial safety factor (for a number of load tests $n = 2$, $\gamma_{cp} = 1.4$ and for $n \geq 3$, $\gamma_{cp} = 1.25$ according to DGGT AK2.8 2002).

Floating B2-columns together with the base slab can be loaded to their maximum external bearing capacity ($E_d \leq R_{cp,d} = R_{cp,k}$), provided that the base slab can share the external load.

Stability of slopes and foundations. The stability of slopes and foundations on underground stabilised with CSV-columns should be verified against rupture failure of the whole system. The overall stability of the foundation with B1-columns can be proved similar to stone and sand columns (section 7.3). According to the art of loading which depends on the type of the failure mechanism, the construction steps, etc., those columns subjected to axial compressive stress, shear stress and tensile stress should be differentiated. The resistance of the columns is therefore calculated according to the art of the loading.

In the verification of the overall stability of slopes and foundations with both B1 and B2 type columns, the compaction effect of the installation process on the soil between the columns should be taken into account. The improvement effect of the compaction can be expressed in terms of the effective cohesion c or the undrained strength c_u as follows:

$$\begin{aligned} c &= c_0 \cdot \exp(\Delta e / C_c) \\ c_u &= c_{u,0} \cdot \exp(\Delta e / C_c) \end{aligned} \quad (7.57)$$

where c_0 and $c_{u,0}$ are the initial effective cohesion and the undrained strength of the unimproved underground, Δe is the change in void ratio due to the installation process of the columns and C_c is the compression index. Similarly, the corresponding improvement in the stiffness of the soil may be estimated by:

$$E_{oed} = E_{oed,0} \cdot [1 - \frac{\Delta e}{I + e_0}] \cdot \exp(\Delta e / C_c) \quad (7.58)$$

where $E_{oed,0}$ and e_0 are the initial constrained modulus and void ratio of the soil before the installation of the columns.

Settlement analysis: The settlement of B1 type columns can be calculated analogue to the sand and gravel columns (section 7.3). For B2-columns, however, the total settlement s consists of three components, i.e.,

$$s = s_z^{ES} + s_B^{ES} + s_G \quad (7.59)$$

where s_z^{ES} is the compression of individual column, s_B^{ES} is the settlement of an individual column and s_G is the settlement due to group effect. Similar to pile groups, the base of equivalent raft foundation for the calculation of the group settlement are shown in Fig. 7.18.

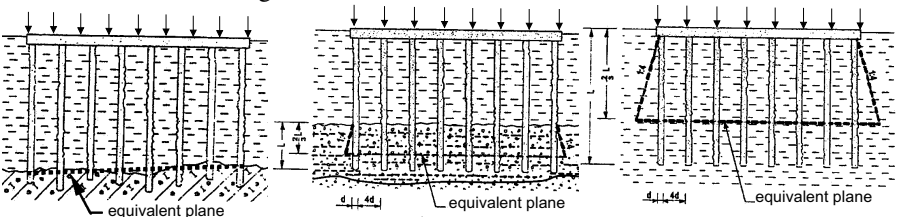


Fig. 7.18. Equivalent planes for calculating settlement of column groups

7.6 Deep mixing method (DMM)

7.6.1 Introduction

A further possibility of ground improvement is the installation of stabilisation columns in the soft ground without the displacement effect on the surrounding soil during the production. The columns serve as a reinforcement to the soft underground due to their higher stiffness as compare to the soil. The mechanical installation method follows by means of a rotary mixing tool, with which a binder or a binder mix is inserted and mixed with the soil.

There are two major categories of deep mixing method: dry soil mixing and wet soil mixing Table 7.1. As the name implies the dry mixing works with dry binders

where as the wet mixing works with slurry of the binders. Lime, cement or lime-cement mix are usually used as a binder.

Table 7.1. Classification of Deep Mixing Method (after Aoi 2002)

Binder	Condition	How to feed	Method
Lime	Dry	Screw feeding (mechanical)	DLM - Deep Lime Mixing Method
		Compressed air (pneumatic)	DJM – Dry Jet Mixing Method
	Cement		Nordic method (Europe)
Cement	Wet		DJM – Dry Jet Mixing Method
		Pumping (liquid feeding)	CDM – Cement Deep Mixing
			European method – Flight auger type

Similar to the CSV-columns, the columns may not always be treated as a load transferring piles, even when cement is used as a binder. Partly it is not the load carrying capacity of a single column of importance, but the improvement of the strength and stiffness of the soil due to mixing with the binder.

The main purposes of deep soil mixing are the following: settlement reduction, increase of stability, prevention of sliding, application as retaining structure, vibration reduction, liquefaction mitigation and remediation of contaminated ground (Holm 2001).

7.6.2 Dry deep mixing method

General

The dry deep mixing method has been developed in Sweden and Japan almost parallel in the 1960's. At its earliest development phase lime was used as a binder material, but later cement also came into effect. At present the method is widely spread all over the world with different type of equipment. A dry binder is forced into the ground pneumatically or mechanically using rotary method of penetration. Like the CSV-method the bearing mechanism of the dry deep mixing method arises from the superimposing effects of compaction of the stabilised soil during mixing, dewatering due to the hydration process and load concentration on the columns because they are more rigid and stronger than the surrounding soft soil. For the hydration process have a water content of at least 20% is required.

Installation procedure and equipment

Fig. 7.19a shows the installation process schematically. In this method a mixing tool is penetrated into the soil down to the desired depth of the column and a dry slaked lime or cement or lime-cement-mixture is injected into the soft ground through holes located just above the horizontal blades of the mixing tool (Fig. 7.19b) with the aid of a compressed air while the tool is withdrawn slowly. There is also a mechanical means of introducing the binder into the ground through

screw feeding. The resulting columns have the same diameter (60 - 100 cm) as the blades of the mixing equipment (Fig. 7.20). Lime - gypsum and lime-fly ash mixture is also used to stabilise soft soils with a high water content (up to 120%) and organic soils with water content of up to about 100% respectively (Broms 1991).

The installation, bearing system and design of dry deep mixing columns can be abundantly found in the literature, for instance, SGE Report 4:95E 1997; Broms 1991; Holm 2001, 2002; Bruce et al. 1998/2002; etc. In the following a summary of the principle of this method is presented.

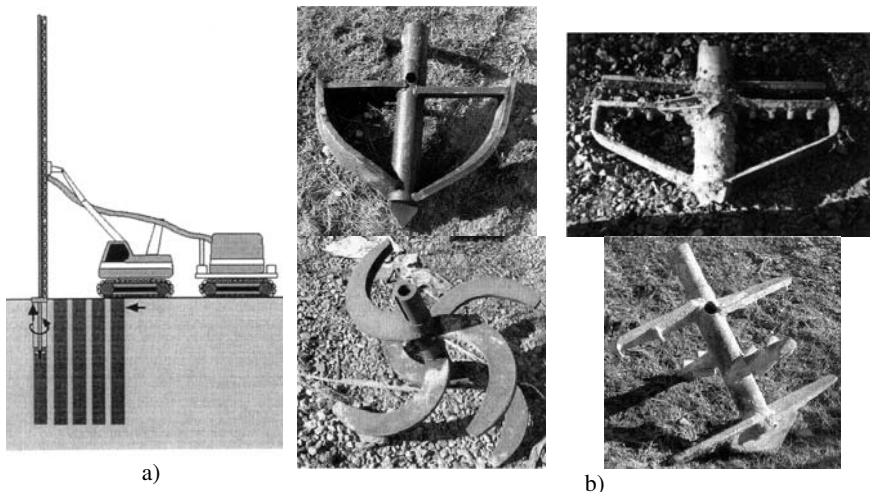


Fig. 7.19. a) Installation of lime column, b) Horizontal blades at the tip of the mixing tool (partly from Topolnicki 2003)



Fig. 7.20. Excavated lime column (after Kempfert and Raithel 2005)

The strength and other properties of the stabilized column

The shear strength of clay stabilized with lime will normally be higher than that of the undisturbed clay about 1 to 2 hours after the mixing. This strength increase is often obtained even when the sensitivity of the clay is high and a large part of the initial shear strength is lost due to the remoulding of the clay during the mixing. The undrained shear strength of the stabilized clay can under favourable conditions be as high as 0.5 to 1.0 Mpa. Normally an increase of 10 to 50 times can be expected, if the initial shear strength is low (10 to 15 kPa). Approximately 1/3rd of the final shear strength is usually obtained after 1 month, and about 3/4th after 4 months. The relative increase of the shear strength decreases in general with increasing liquid limit. The shear strength increases in general with increasing compaction of the stabilized soil (Broms 1991).

The shear strength of the stabilised soil in the columns is not uniform even when the mixing of the binders with the clay is done very carefully. Because of the aggregation, the measured shear strength will vary with the testing method and the size of the tested samples. According to the SGF Report 4:95E 1997, the maximum value of the undrained strength $c_{u,col}$ of the column should not exceed 150 kPa irrespective of the results of laboratory and field tests. The compression modulus of lime columns is approximated to be 50 to 100· $c_{u,col}$, where the lower value is for organic soils and the upper one for silty clay. For lime-cement columns the compression modulus is approximately equal to 50 to 150· $c_{u,col}$.

Assuming an internal friction angle 30° for the column material, the ultimate internal bearing capacity of a single column can be estimated from the expression:

$$\sigma_{ult} = 2 \cdot c_{u,col} + 3 \cdot \sigma_h \quad (7.60)$$

where σ_h is the horizontal pressure between the soil and the columns. The long term creep strength of the columns is usually assumed to be 65% of the ultimate bearing capacity, hence the maximum load on a single column is given by:

$$q_{I,max} = 0.65 \cdot a \cdot \sigma_{ult} \quad (7.61)$$

where $a = A/c^2$ is the area ratio, where A and c are the cross sectional area and the spacing of the columns respectively.

For calculation of the rate of settlement, the permeability of the lime stabilised clay can be assumed to be approximately 1000 times the unstabilised clay. For soils stabilised with lime-cement, the permeability can be assumed to 400 to 800 times the unstabilised soil.

The bearing capacity of the columns

Single columns. The ultimate bearing capacity of a single column is governed either by the shear strength of the surrounding soil (shear failure) or by the strength of the column material (column failure). In case of soil failure, the ultimate bearing capacity of a single column depends both on the skin friction resistance along

the surface of the column and on the end resistance. The short term ultimate bearing capacity of a single column can be expressed as:

$$Q^{col} = (\pi \cdot d \cdot l_c + 2.25 \cdot \pi \cdot d^2) \cdot c_u \quad (7.62)$$

where d is the diameter of the column (usually $d = 0.5$ to 0.6 m), l_c is the length of the column and c_u is the average undrained strength of the surrounding soft soil determined, for example, by fall cone or field tests. In Eq. 7.62 it is assumed that the skin friction is equal to the undrained shear strength c_u and the base resistance is approximated to be $9 \cdot c_u$. The base resistance of floating columns is generally low compared with the skin resistance, while the base resistance of columns that extend down to a bearing layer can be high. A large part of the applying load will then be transferred to the bearing layer through the bottom of the columns. Further details on the bearing capacity of single columns can be found in Broms 1991.

Column groups. Similar to single columns, the ultimate bearing capacity of a column group is governed either by the shear strength of the untreated soil between the columns and the shear strength of the column material. Possible shear failure of a group of columns is shown in Fig. 7.21. The bearing capacity of a group of columns arises from the skin resistance along the perimeter of the column group ($2 \cdot c_u \cdot l_c \cdot (B + L)$) (Fig. 7.17b) and the base resistance of the block, which is 6 to 9 times the undrained strength of the soil c_u . Hence, the total bearing capacity of a group of columns can be written as:

$$Q_{ult}^{group} = 2 \cdot c_u \cdot l_c \cdot (B + L) + (6 \text{ to } 9) \cdot c_u \cdot B \cdot L \quad (7.63)$$

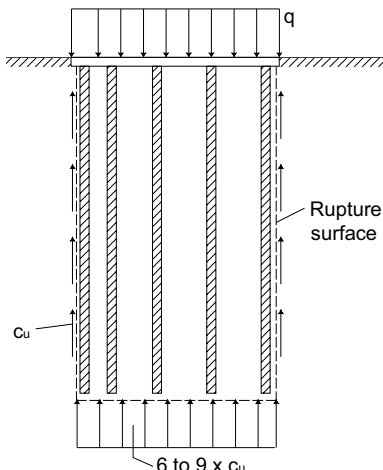


Fig. 7.21. Shear failure of column group as a block

The factor 6 refers to a foundation with $L > B$, whereas the factor 9 can be used for square foundations. However, a relatively large deformation, 5 to 10 percent of the width of the loaded area, is required to mobilise the maximum base resistance. It is therefore proposed to neglect the base resistance in the design (Broms 1991).

The ultimate bearing capacity of a group of columns may also be governed by local shear failure along the edge of the block. This kind of ultimate bearing capacity can be calculated in the same way as the stability of slopes, but it can also be estimated from:

$$q_{ult} = 5.5 \cdot c_{u,av} \cdot (1 + 0.2 \cdot b/l) \quad (7.64)$$

Where b and l are the width and length of the locally loaded area, and $c_{u,av}$ is the average shear strength along the assumed rupture surface.

Settlements of a column group

It is generally reported in the literature that the efficiency of stabilisation columns in reducing the settlement of a foundation ranges between 25 to 80 percent depending on the type of the structure, the property of the untreated soil and the binder used. According to the SGF report 4:95E 1997, the settlement of the columns can be calculated using the following equation:

$$s_1 = \sum \frac{\Delta h}{a} \cdot \frac{q_1}{M_c} \quad (7.65)$$

where Δh is the thickness of the layer, q_1 is the pressure on the columns and M_c is the compressibility modulus of the columns.

Similarly, the settlement of the unstabilised soil can be calculated using the equation:

$$s_2 = \sum \frac{\Delta h}{1-a} \cdot \frac{q_2}{M_s} \quad (7.66)$$

where q_2 is the pressure on the unstabilised soil and M_s is the compressibility modulus of the unstabilised soil. The total applied pressure is then given by $q = q_1 + q_2$.

A first settlement calculation can be made by assuming $q_1 = +q_{1,max}$. The obtained settlement s_1 is then compared to the settlement of the unstabilised soil s_2 . If $s_1 > s_2$, a load distribution can be performed by gradually reducing q_1 and corresponding increasing q_2 , so that $s_1 = s_2$. The settlement s_m is then equal to s_1 and s_2 . If the soil is normally consolidated, the settlement s_m can be calculated from:

$$s_m = s_1 = s_2 = \sum \frac{\Delta h \cdot q}{a \cdot M_c + (1-a) \cdot M_s} \quad (7.67)$$

On the other hand, if $s_1 < s_2$, the columns cannot carry any more load and $s_m = s_2$.

For floating columns, the settlement of the soft soil layer below the base of the column group can be calculated using the standard approach for shallow foundation. The total settlement is the sum of the settlement components.

In most cases the differential settlements are the main cause of damages to the structure. This is primarily governed by the shear deformations in the unstabilised soil between the columns (Broms 1991). The maximum angular rotation α between two column rows will then be proportional to the average shear stress along the perimeter of the reinforced block and the average shear modulus G_s of the unstabilised soil as expressed by the relationship:

$$\alpha = \frac{\tau_{av}}{G_s} \quad (7.68)$$

7.6.3 Wet deep mixing method

General

Increasing use of the wet method of deep soil mixing to improve the engineering and environmental properties of soft or contaminated ground indicates growing international interest and acceptance of this relatively new technology. In this method of ground treatment soils are mixed in-situ with cement or lime-cement mix in a slurry form. Wet deep soil mixing is currently applied for stabilisation of the soil to a maximum depth of about 50 m. The slurry is injected into the soil through hollow rotating mixing shaft with various types of cutting tools at its tip. The mixing shafts are also equipped with continuous or discontinuous auger flights, mixing blades or paddles to increase the efficiency of the mixing process. In some methods, the mechanical mixing is enhanced by simultaneously injecting fluid grout at high velocity through nozzles in the mixing or cutting tools (Topolnicki 2003).

The wet mixing method can be applied in soft clays, silts, fine grained sands and organic soils (peat, sludge, etc.). The use of wet mixing in organic soil however requires a special binders and execution procedures. The mechanical property of the stabilised soil depends on the binder property, on the history of deposition and behaviour of the soil, mixing and curing conditions.

The historical development of the wet deep soil mixing method can be found in Topolnicki 2003. According to FHWA 2000, the wet deep mixing method is classified into two major groups based on the mix operation. These are mechanical mixing and a combined jet and mechanical mixing (Fig. 7.22). Within these groups, there is the possibility of injecting the slurry through the holes along the length of the shaft or the end of the shaft or a combination of both of them.

Installation procedure and equipment

Typical wet deep mixing method equipment consists of a mixing plant to supply slurry of the binder and a mixing machine to inject and mix the slurry into the ground. The plant includes: silos, water tank, batching system, temporary storage tank, slurry pumps and power supply unit. The storage tanks have paddle agitators to keep the component materials from settling out of the slurry. Delivery pumps are duplex or triplex reciprocating piston pumps, or variable speed moyno progressive cavity pumps. Pumping rates typically range from 0.08 to 0.25 m³/min, but can reach up to 1 m³/min for high-capacity mixing tools (Topolnicki 2003).

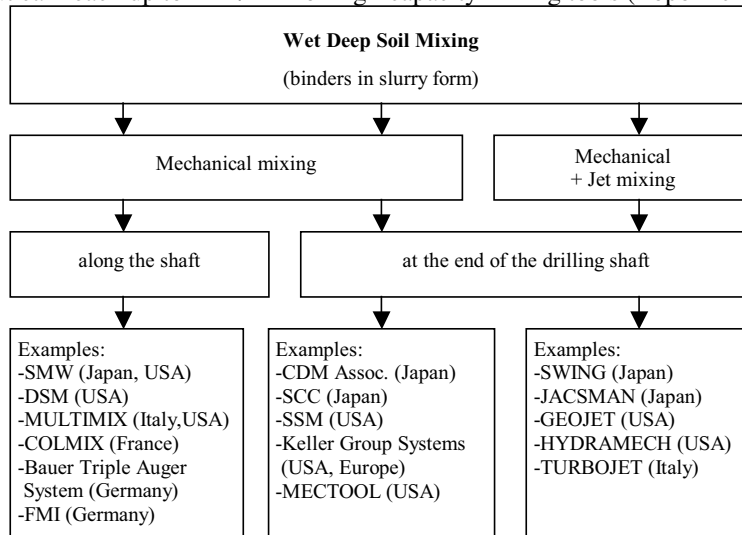


Fig. 7.22. Classification scheme of current operational wet deep mixing methods (after Topolnicki 2003)

The machines that are used for on-land applications usually have 1 to 4 drilling shafts mounted on fixed or hanging leads, and are equipped with specially designed mixing tools (Fig. 7.23). The typical penetration speed is in the range of 0.5-1.5 m/min and is usually increased during withdrawal. The mixing tools are kept in parallel by joint bands mounted at vertical intervals along the drive shafts. With some machines the spacing between individual shafts can be adjusted within prescribed limits to produce overlapped columns. Sophisticated single axis systems with double cutting/mixing blades, spaced 30 cm and rotating in opposite directions, have also been developed in Japan (Horpibulsuk et al. 2002).

For marine applications large execution vessels, equipped with mixing machine, batching plant, storage tanks and a control room, are usually used for rapid treatment of considerable soil volume. The area of treatment in single-stroke operation with 2 to 8 mixing shafts ranges from 1.5 to 9.5 m², and the productivity rates are in excess of 1000 m³ per day.

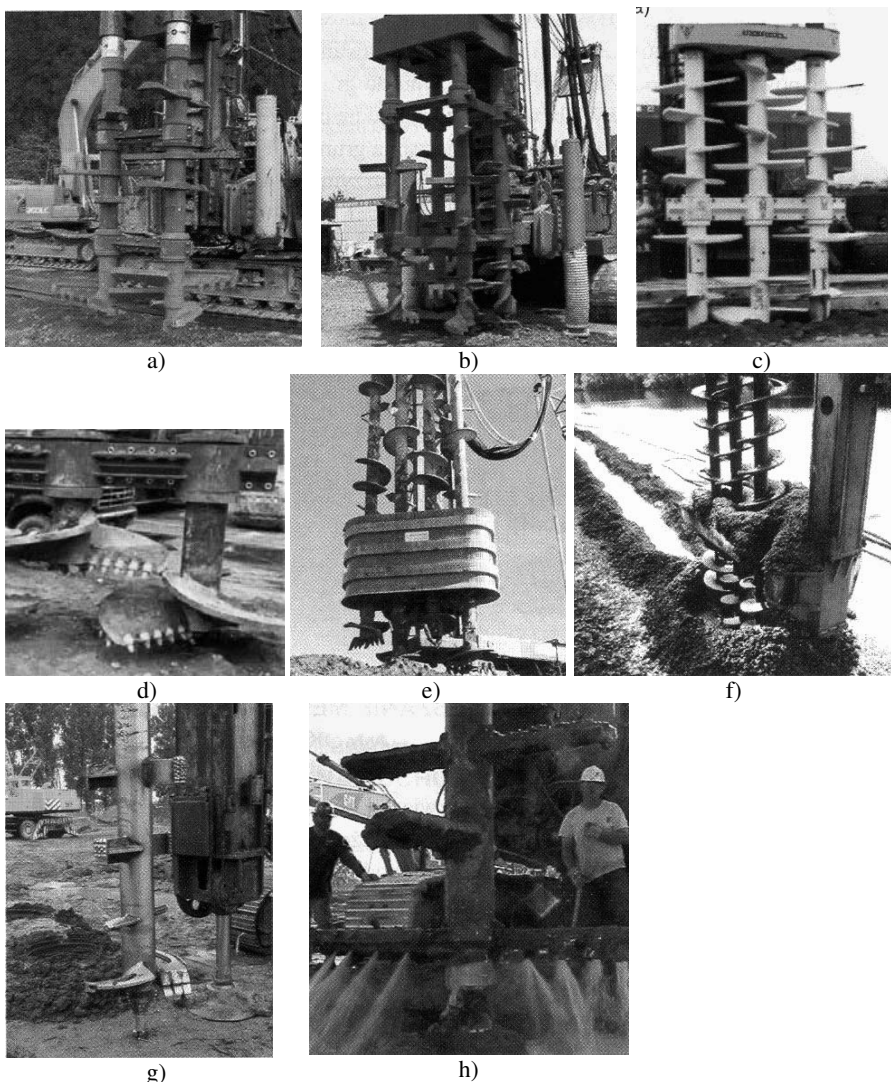


Fig. 7.23. Typical mixing tools (from Topolnicki 2003): a) double axis standard CDM 2 x 1.0 m (CDM Association 2002), b) quadruple axis CDM 4 x 1.0 m (CDM Association 2002), c) triple axis SMW 3 x 1.5 m, d) , e) 0.9 m (Geo-Con-Inc. , f) triple axis 3 x 0.55 m (Bauer), g) single axis 0.8 m (Keller), h) single axis 2.4 m (Hayward Baker/Keller)

The mixing tools for the wet deep mixing method are designed for various improvement purposes and are configured to soil type and available turning equipment. Since there is no one tool that can successfully treat all soils, field adjustments are typical. The mixing tools can be broadly classified into blade based and auger-based constructions (Fig. 7.23).

The typical installation process consists of positioning the mixing shaft(s) above the planned location, penetration of the mixing tool into the ground, verification and improvement of the bottom soil layer, withdrawal, and movement to a new location if necessary. The details of execution depend on the technical features of the equipment, and the site-specific and functional requirements. The delivery of the slurry of the stabilising agent to the subsoil is operator/computer controlled and it is dependant on the energy required for mixing at a specific layer of treated soil. In general, the slurry of the binder can be injected during penetration, withdrawal and restroking.

The homogeneity and strength of a column depends mainly on the efficiency of soil mixing with the binder. This in turn is a function of mixing time, type of mixer, type and behaviour of the soil and the energy with which the slurry is injected into the soil. In order to estimate the energy required for mixing and able to control and alter it on site during execution, a simplified approach has been introduced in Japan based on the so called “blade rotation number” (e.g. CDIT, 2002, see also Topolnicki 2003). The blade rotation number T is defined as the total number of mixing blades passing through the soil during 1 m of single shaft movement and it is expressed as:

$$T = \Sigma M \cdot (R_p/V_p + R_w/V_w) \quad (7.69)$$

for full injection during penetration and the injection hole located below the blades of the mixing tool. Again for full injection during penetration but the injection hole located above the blades of the mixing tool, T is given by:

$$T = \Sigma M \cdot (R_w/V_w) \quad (7.70)$$

For partial injection during penetration and full injection during withdrawal and where the lower injection hole being active during penetration only and the upper one during withdrawal, T can be estimated from:

$$T = \Sigma M \cdot \left(\frac{R_p}{V_p} \cdot \frac{W_p}{W} + R_w/V_w \right) \quad (7.71)$$

where

T = blade rotation number [revolution/m]

ΣM = total number of mixing blades

R_p, R_w = rotational speed of the mixing tool during penetration and withdrawal respectively [revolution/min],

V_p, V_w = penetration and withdrawal velocity respectively [m/min],

W_p = amount of slurry injected during penetration [kg/m^3],

W = total amount of slurry [kg/m^3].

Soil mixing, like other ground improvement technologies, uses indirect control measures to ensure the quality of work and product during execution. The main objective of a control system is to ensure delivery of a correct amount of binder and mixing energy along the installed element. The extent of in-situ mixing opera-

tion monitoring is closely associated with the type of project and the required level of quality control.

Depending on the purpose of the soil improvement using the deep mixing method, conditions of the underground, stability of the foundation and cost of the treatment, different patterns of column installations are used. These patterns include: single columns, group of column, secant columns, tangent columns, etc. (Fig. 7.24).

Square or triangular grid patterns of single or group of columns are usually used when the purpose of the deep mixing is settlement reduction and in some other cases stability improvement. Some common example of application of such patterns are road and railway embankments.

Column walls are used in excavations to stabilize and support open cuts, to protect existing structures with shallow foundations surrounding the excavation from differential settlement and as a seepage barrier. They are also used to increase the bearing capacity of the underground against sliding or lateral forces. Column walls can be constructed either with tangent or secant elements. Secant columns are particularly important when applied as a cut-off wall or as contamination barriers.

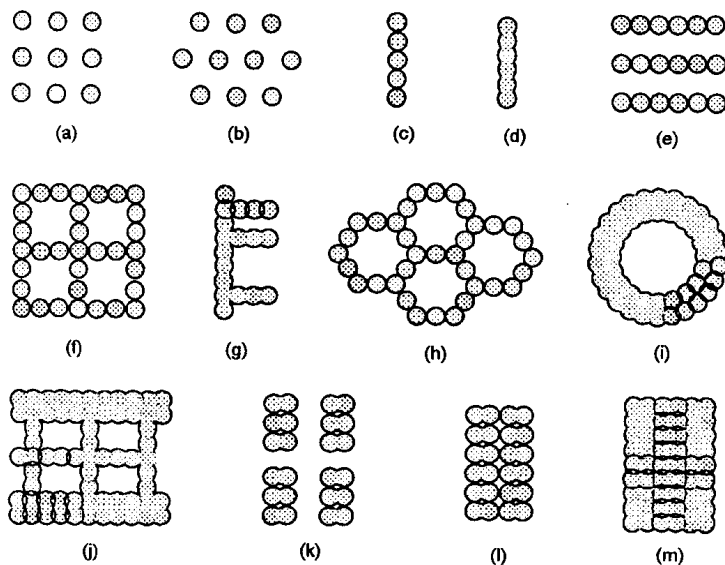


Fig. 7.24. Different patterns of deep soil mixing: a), b) column type (square and triangular grid), c) tangent column wall, d) secant column wall, e) parallel tangent walls, f) tangent walls with a grid system, g) tangent column wall with buttresses, h) circular cells with tangent columns, i) column groups in a ring form, j) lattice type of group of columns, k) group of secant columns, l), m) block made up of secant columns (from Topolnicki 2003).

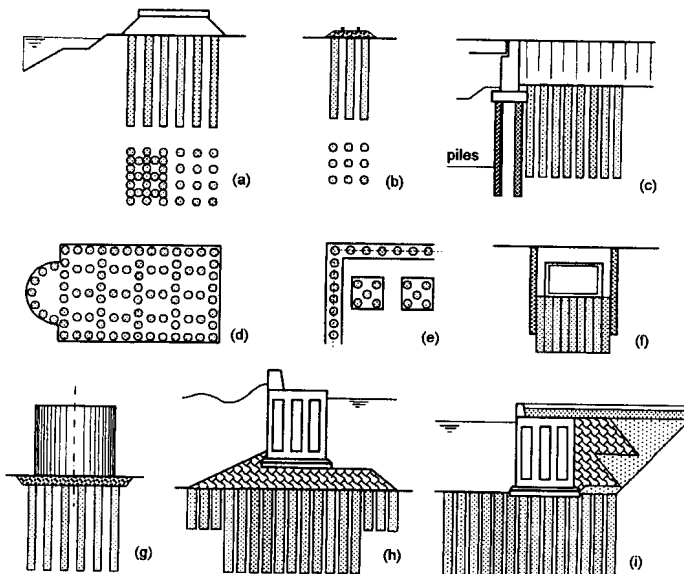


Fig. 7.25. Examples of application of the wet deep soil mixing (from Topolnicki 2003).

Various combinations of columns are also used to build grid, U-form, cellular or circular pattern with tangent or secant columns to improve the interaction with the unstabilised soil. Block of columns may also be used to create massive and stable gravity structures. Different examples of applications are shown in Fig. 7.25. Topolnicki 2003 listed the main merits and demerits of the wet deep mixing as shown listed in Table 7.2 below.

Table 7.2. Main advantages and limitations of wet deep soil mixing (after Topolnicki 2003)

Advantages	Limitations
<ul style="list-style-type: none"> High productivity usually possible, hence economical for large scale projects; Can be potentially used in all types of soils and fills without obstructions; Column spacing and patterns highly variable, arrangements tailored to specific needs; Engineering properties of treated soil can be closely designed; Causes minimal lateral or vertical stress that could potentially damage adjacent structures; No vibration, medium to low noise; Minimum environmental impact; Can be used for on-land, waterfront and marine projects. Quality of treatment verifiable during construction 	<ul style="list-style-type: none"> Depth limitations (depending on the installation method); Not suitable for very dense, very stiff soils or soils with boulders or extremely wet soils; Limited or no ability to install inclined columns (depending on the type of equipment); Uniformity and quality of mixed soil may vary considerably in certain conditions; Columns cannot be installed in close proximity to existing structures (except hybrid mixing); Freeze/thaw degradation may occur; Significant spoil may be produced; Weight of the equipment may be problematic for weak soils (depending on the method); Grout injection pressure may cause heave; Limited ability to treat isolated strata at depth.

Strength of wet deep soil mixing columns

The strength of a single column is governed by the shear strength of the soil (soil failure) or by the shear strength of the column material (column failure). The strength of the column material can be determined in laboratory, for example, using the unconfined compression tests. Field and model investigations and even load tests are often conducted to assist the design procedure.

The strength of the column mainly depends on the type and amount of binder and working specifications; such as the rate of penetration and withdrawal, rotation speed, injection method, mixing tool, water/binder ratio, etc. This requires a good understanding of the complexity of soil-binder physics, chemistry and mechanical property is required.

The strength and deformation parameters can reasonably correlated with the compressive strength of the column material, in other terms the unconfined strength. In practice, the unconfined compressive strength is the key parameter for the current design of stabilized columns due to its simplicity in testing and its cost-effectiveness. At present the unconfined compressive strength of the column material cannot reliably be predicted based the properties of the native soil and the type and amount of the binder. Therefore, it is generally recommended to conduct in advance appropriate trial tests on stabilized soils to obtain more adequate data. At this stage the relationship between the unconfined strength and the binder factor α can be determined. The binder factor α is expressed as the ratio of weight of injected dry binder to the volume of the ground to be treated (Topolnicki 2003).

Topolnicki 2003 compiled the field strength and permeability of wet deep mixing columns from literature for ranges of cement factors and different type of soils as shown in Table 7.3. The corresponding volume ratio defined as the ratio of the volume of slurry injected to the volume of ground to be treated vary greatly and reflect the type of mixing technique used, but it generally lies in the range of 15 to 50% and in most cases between 25 and 40%. The lower volume ratio, the higher will be the efficiency of the mixing mainly due to higher rotational speed or jet assistance.

The relationship between the unconfined compressive strength and other parameters are also compiled in Table 7.4.

Table 7.3. Typical field strength and permeability (after Topolnicki 2003)

Soil type	Cement factor α [kg/m ³]	28-days unconfined compressive strength q_u [MPa]	Permeability k [m/s]
Sludge	250 - 400	0.1 - 0.4	1×10^{-8}
Peat, organic silts/clays	200 - 350	0.3 - 1.2	5×10^{-9}
Soft clays	150 - 300	0.5 - 1.7	5×10^{-9}
Medium/ hard clays	120 - 300	0.7 - 2.5	5×10^{-9}
Silts and silty sands	120 - 300	1.0 - 3.0	1×10^{-8}
Fine-medium sands	120 - 300	1.5 - 5.0	5×10^{-8}
Coarse sands and gravels	120 - 250	3.0 - 7.0	1×10^{-7}

Table 7.4. Typical correlation and data for cement-treated soils (from Topolnicki 2003)

Selected parameters	Expected values/ratios or relationships
Gain in the unconfined compressive strength with time	$q_{u,28\text{ day}} = \text{ca. } 2 \cdot q_{u,4\text{ day}}$ $q_{u,28\text{ day}} = 1.4 \text{ to } 1.5 \cdot q_{u,7\text{ day}}$ (silts, clays) $q_{u,28\text{ day}} = 1.5 \text{ to } 2 \cdot q_{u,7\text{ day}}$ (sands) $q_{u,60\text{ day}} = 1.4 \text{ to } 1.5 \cdot q_{u,28\text{ day}}$ (clays, silts)
coefficient of variation in the unconfined compressive strength	0.2 to 0.6 (typically 0.35 to 0.5), It is lower for laboratory mixed samples than for field samples
Relative strength ratio: core samples to laboratory mixed samples, λ ,	0.5 to 1, lower values for clays higher for sands (1.0 for offshore works in Japan)
core samples to wet grab samples	1 to 1.5
Shear strength (direct shear with no normal stress)	$0.4 \text{ to } 0.5 \cdot q_u$, for $q_u < 1 \text{ Mpa}$ $0.3 \text{ to } 0.35 \cdot q_u$, for $1 \text{ Mpa} < q_u < 2 \text{ Mpa}$ $0.2 \cdot q_u$, for $q_u > 2 \text{ Mpa}$
Tensile strength	$0.08 \text{ to } 0.15 \cdot q_u$, but not higher than 200 kPa . Indirect splitting tests yield lower values than direct uniaxial tests
Secant stiffness modulus E_{50} , at 50 % peak strength	$50 \text{ to } 300 \cdot q_u$, for $q_u < 2 \text{ Mpa}$ $300 \text{ to } 1000 \cdot q_u$, for $q_u > 2 \text{ Mpa}$ (ratio increases with increasing the unconfined strength.)
Axial strain at failure, ε_f : unconfined compression test (crushing failure)	$0.5 \text{ to } 1.0 \%$ for $q_u > 1 \text{ MPa}$ $1 \text{ to } 3 \%$ for $q_u < 1 \text{ MPa}$
confined compression tests (plastic shear)	2 to 5 % (undrained triaxial test)
Poisson's ratio	0.25 to 0.45, typically 0.3 to 0.4

The bearing capacity of the stabilised foundation

If a stabilized soil is likely to behave as a rigid structural member embedded in the ground, its external stability can be evaluated under modes of failure typical for gravity-type structures, including horizontal sliding, overturning, bearing capacity and rotational sliding. Related DM patterns which can be analyzed with this approach comprise mainly block-type improvement and, with certain simplifications, also "blocks" composed of long and short walls, as it has been practiced in Japan for various port facilities (cf. CDIT, 2002). In the latter case, however, is also necessary to examine the extrusion failure mode of untreated soil remaining between the long walls of stabilized soil when subjected to unbalanced active and passive earth pressure, generated for instance by an earthquake (Terashi, Tanaka and Kitazume, 1983).

The principles of calculation of the bearing capacity and settlements of both single columns and column groups from wet deep mixing are similar to that for dry deep mixing columns discussed in section 7.6.2.

7.6.4 Jet pile method

This is another type of deep soil mixing, where a guide hole of 15 to 20 cm is drilled into the soil with auger or boring machines up to the desired depth and a

slit is cut with very high pressurized water by fracturing and churning the surrounding soil. The slit is then injected with binder suspension at high velocity. By rotating the jetting, it is possible to produce a column, also called soilcrete, as large as 2 to 3 m in diameter in soft soils. The compressive strength of the soilcrete is estimated to be in the range of 10 to 50 kN/m² in cohesive soils (Nagaraj and Miura 2001).



a)



b)

Fig. 7.26. Examples of tools for installation of jet piles TURBOJET (Topolnicki 2003)

7.7 Unreinforced pile like elements

7.7.1 Grouted stone/gravel column

Since intermediate layers consisting of organic or very soft to soft soils cannot provide lateral support to the stone columns, the external lateral support can be replaced by an internal bond between the stones. This can be done by introducing cement suspension during the installation of the stone/gravel columns which binds the stones together and form a solid column. The suspension is injected through the injection pipe approximately 4.0 m before the withdrawal of the column material at the apex of the vibrofloat, so that a homogeneous mixture of suspension and column material can be developed. Fig. 7.27 illustrates the installation method of grouted stone columns.

The application of the stone columns are limited to soils with $c_u > 15 \text{ kN/m}^2$, therefore, it recommended to apply the grouted stone columns only for areas with weak soil layers, provided that the thickness of such layers do not exceed 1 m. In this case the grouting shall extend 0.5 m above and below the weak layer.

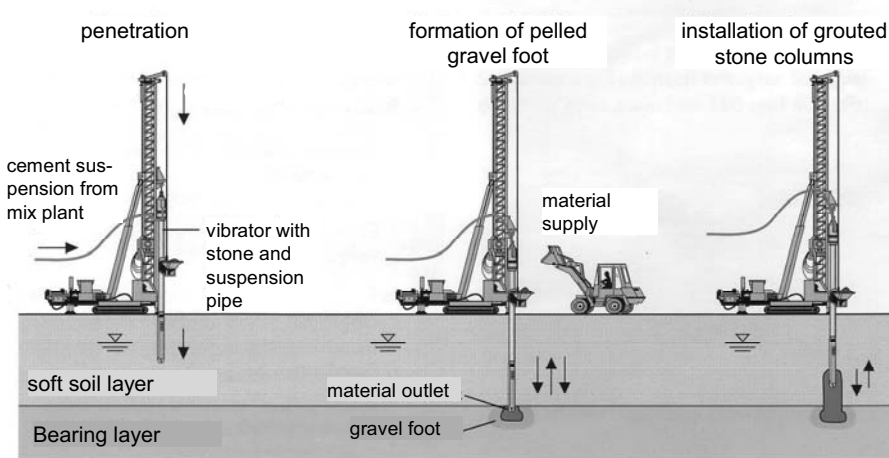


Fig. 7.27. Installation of grouted stone columns (Photo: Keller construction company)

7.7.2 Ready-mixed mortar columns

In the installation of ready-mixed mortar column, the vibroflot first penetrates the soft layer up to the required depth, usually up to a depth of a bearing layer. There a highly compacted gravel or stone foot is produced. The vibroflot is then begins to withdraw and at the same time a ready-mixed mortar is introduced into the hole directly from the surface to the apex of the vibroflot through an air pressure sluice. By alternating pulling and lowering of the vibroflot and simultaneously supplying the mortar a ready-mixed mortar column can be produced.

The range of application of the ready-mixed mortar columns is the same as the grouted stone columns. However, the ready-mixed mortar columns require at least 7 days for curing before they are ready to carry loads. This may lead to longer construction period. The load-carrying capacity of a single ready-mixed mortar column approximately lie between 350 - 400 kN.

7.7.3 Unreinforced concrete columns

The installation of unreinforced concrete columns is the same as the ready-mixed mortar columns except that a ready concrete is used instead of mortar. According to DIN 1045, the concrete should possess a strength class $\geq C\ 12/15$ and $\leq C\ 25/30$ and consistency of KS up to KP. The unreinforced concrete column differs from the ready-mixed mortar column regarding the calculation of the internal bearing capacity. The load carrying capacity of an unreinforced concrete column is approximated to be 600 kN.

The use of unreinforced concrete columns in road and railway embankment is very limited. This is mainly because of the high production cost.

7.8 Displacement and bored piles

Various types of displacement and bored piles are also used to stabilised compressible underground. Since the installation methods, the principles of design and analysis and settlement calculations are similar to the classical pile foundation, reference is given to chapter 6.

7.9 Case histories

7.9.1 Muehlenberger loch - geotextile-encased sand columns (GEC)

General

For the production of a robust aircraft Airbus A380 in Hamburg, Germany, the factory site of the aeroplane dockyard Daimler Chrysler Aerospace (European Aeronautic Defence and Space Company “EADS”) was extended by about 1.4 km² towards the west side. The site, locally known as “Muehlenberger Loch”, is located at the bay area of Elbe river and consists of a tidal mud and marshy area, (Fig. 7.28). The reclamation of the marshy area followed with the construction of a 3 km long polder enclosure that consists 500 m long sheet pile wall and 2500 m long dike founded on over 60 000 geotextile-encased sand columns (GEC). The GEC with a diameter of 80 cm and length between 4 and 14 m below the base of the dike foot reached up to the relatively load bearing sand layer. The dike is the main water front for aeroplane dockyard. Furthermore, another 10 000 columns were also installed to relocate the existing dike ‘Finkenwerder Vordeich’ towards the river Elbe, to avoid sludge replacement, to increase the stability and to decrease the settlements of the dike. The level of enclosed area was increased by drizzling and hydraulic filling of 1×10^6 m³ of sand

The marshy area in the Muehlenberger loch is a sediment from the Elbe river which is deposited over decades. Conventional ground improvement with vibro-displacement piles or stone columns was not possible, because of the low strength of the underground (undrained shear strength $0.4 \leq c_u \leq 10$ kN/m²) (see section 7.4. The condition that the soft soil must not be removed because of ecological reasons, the short construction time and the high tide variation (low and high tides twice a day) were the decisive boundary conditions for the reclamation works.

Because of the high degree of public sensitivity towards any interference with the ecological system of the Elbe river, particularly the area in Muehlenberger Loch, it was agreed to carry out the construction works with the following conditions:



Fig. 7.28. An air view of the marshy area Muehlenberger Loch, the old Airbus premises and the village of Finkenwerder before construction had begun

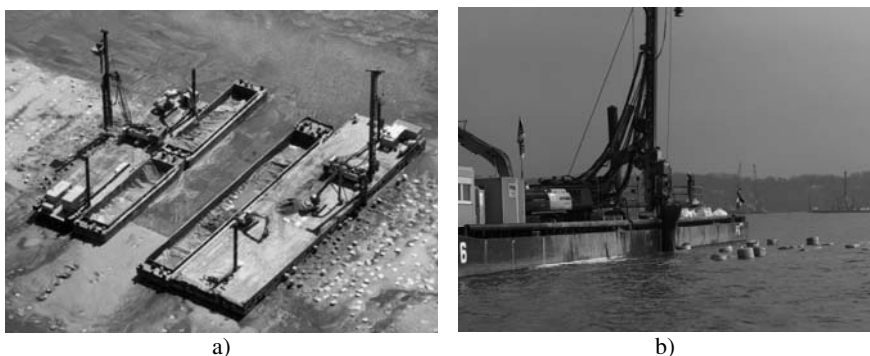


Fig. 7.29. Column installation under water

- No replacement and displacement of the sludge towards the river during reclamation process,
- No discharge of contaminated material into the Elbe River through an excess water used for hydraulic filling,
- Optimisation of sand transport and sand placement. The sand delivered by hopper vessels from the marine borrow pits had to be unloaded immediately after docking. The sand transported from the Elbe island Hahnoefer Sand through dredging pipeline into the construction area (approx. 3 million m³) had to be removed continuously.

Soil conditions

The thickness of the very soft soil layer (sludge) is between 8 to 14 m. The undrained shear strength of the sludge lies between 0.4 and 10 kN/m². Fig. 7.30 shows a typical soil profile and a photographic view of a test pit. It can clearly be seen from the test pit that the consistency of the sludge is almost liquid. Beneath the sludge layer is a load bearing sand layer.

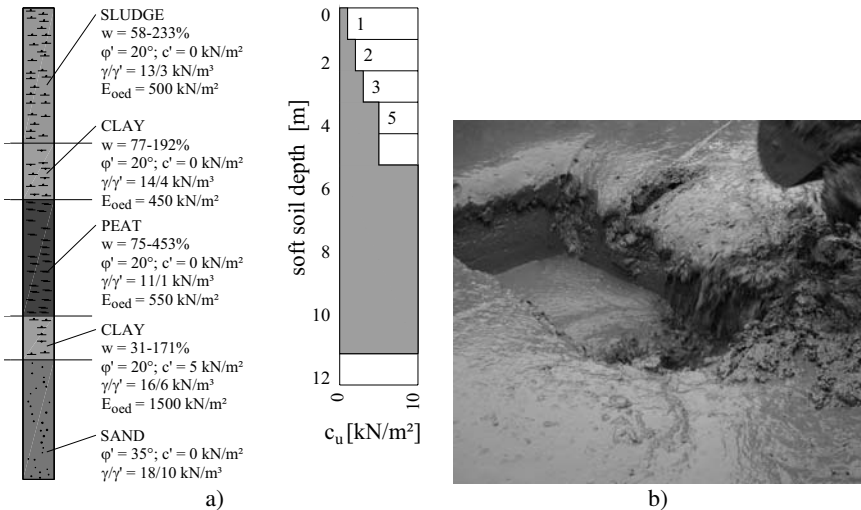


Fig. 7.30. a) Typical soil profile and soil parameters, b) a test pit showing the flow of the sludge

Land reclamation

The original design concept in the tender documents was to enclose the area with 2500 m long temporary sheet pile wall to depth of a 40 m and tied back with anchors connected with raking piles. The wall was intended to serve as a flood protection wall. Having protected by the temporary sheet pile wall, it was planned to maintain a constant water level within the enclosed area, and to fill the first sand layer under water. Eventually, the 1.4 km² reclamation area had to be raised to a height of 5.5 m above sea level by a combination of sand-trickling, sand-sluicing and hydraulic filling. Following a three year consolidation time for the soft soil within the enclosure, a permanent flood control dike would be built to a height of 9 m above sea level and finally the temporary sheet wall and the existing old dike had to be removed.

The original plan was however changed in favour of another fast and economical construction method. This was to enclose the area using a permanent dike founded on GEC-system. The dike had served as polder during the rising of the

1.4 km² construction site to a height of 5.5 m above sea level and as flood protection measure for the future. Hence, the sheet pile wall was no longer necessary and the empoldering function was fulfilled by the dike itself. Compared to the original concept, a considerable amount of sand due to the use of a steeper slope (1:6 against 1:20) could be saved and a high settlement reduction could be reached. Moreover, it was possible to install the GEC-foundation system and rise the dike to a height of 7 meters above sea level within only eight months. Fig. 7.31 shows the top view of the reclaimed area and a photo view of the completed dike from the air.

The construction method with the GEC-foundation system had proved to be superior compared to the original concept for the following reasons:

- 35000 tons of steel was saved, since a sheet pile wall was not necessary,
- 150000 m² reclamation area was saved and 1.1 million m³ less sand was required to fill the dike (steeper slope),
- very small noise pollution (12 vibro displacement machines produced a noise level of 50 dba at a distance of 1000 m),
- reduction of the construction time for the dike from 3 years to 8 months,
- an effective settlement reduction and a high rate of settlement similar to that of vertical drains.

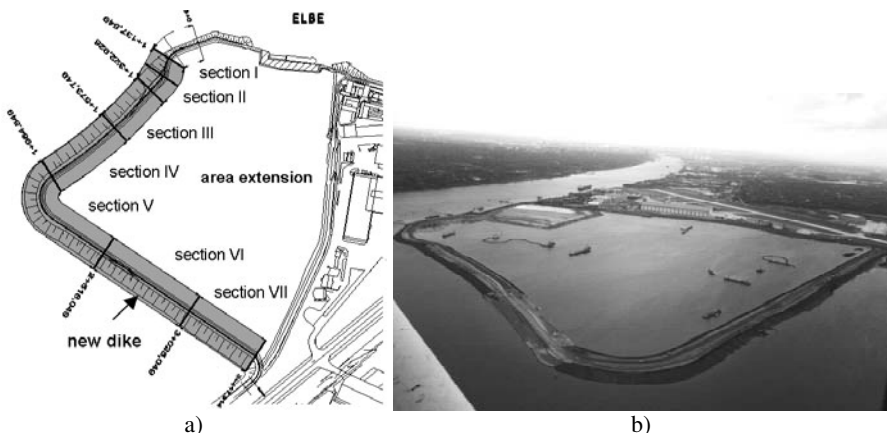


Fig. 7.31. a) Top view of the reclaimed area showing different sections, b) air view of the dike and the polder after nine month

Design and analysis

On the basis of an analytical calculation model (section 7.4) and FEM-analyses for the different parts of the dike, more than 60 000 GEC-columns were designed using a geotextile (Ringtrac) encasing with different stiffness. The stiffness of the geotextile casing was between $J = 1700$ and 2800 kN/m. The maximum hoop

force of the geotextile sack varied between 100 and 400 kN/m. The length of the columns was dependant on the depth of the soft soil along the dike line. The ratio (AC/AE) between the column area AC and the influence area of each column AE was varied between 0.10 and 0.20.

The slope stability of the dike was examined for all construction stages using effective shear parameters φ' and c' as well as excess pore pressure expected at each constructions stage. The slope stability was verified using circular sliding surfaces and a rigid body wedge type failure mechanisms. The 3-dimensional condition of the GEC-foundation system was converted into a 2D plane model by introducing an equivalent plane wall panels. The increase in shear strength due to the concentration of stress on the columns was considered using an equivalent shear parameter according to Raithel (1999). The stability analyses showed that a geocomposite with a high tensile strength (maximum hoop force of 500-1000 kN/m) was required at the symmetry axis of the dike to accelerate the construction of the dike and to obtain a high degree of stability in the initial stage of the construction. It was also necessary to increase the stability since the area behind the dike was to be raised to a height of 5 to 8 m above sea level.

Measurements

Because of the different soil conditions along the dike length, seven measurement cross sections were selected. In each measurement section one earth pressure and one pore pressure transducers at the top of the soft soil layer, two piezometers in the soft soil layer and one horizontal and two vertical inclinometers had been installed to monitor the deformation behaviour. The measurements revealed that the soil conditions was better than given in the tender documents, especially with respect to the consolidation behaviour (see also Raithel et al. (2002)). Due to the high effectiveness of the GEC-foundation system, the dike could be constructed in about 9 months to a height of about 7 m. Therefore, the necessary flood protection was attained after 39 weeks. Measured settlements at dike section VI are shown in Fig. 7.32.

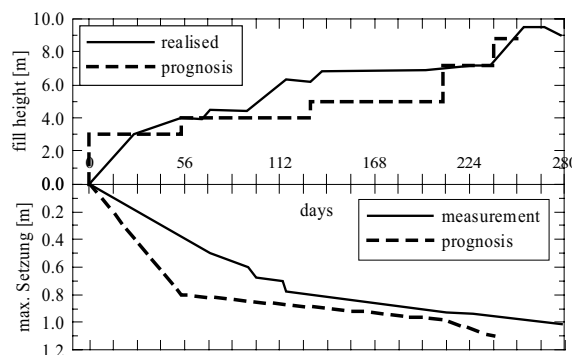


Fig. 7.32. Measured settlements at section VI (see Fig. 7.31)

The dike 'Finkenwerder Vordeich South' is only partly founded on encased columns. In the part outside the main load area vertical drainage is used to accelerate the settlements. Fig. 7.33 shows typical measurement results pointing out the different settlement reduction in the part with encased columns (thickness of soft soil about 7 m) and the part with vertical drainage (thickness of soft soil about 4.5 m).

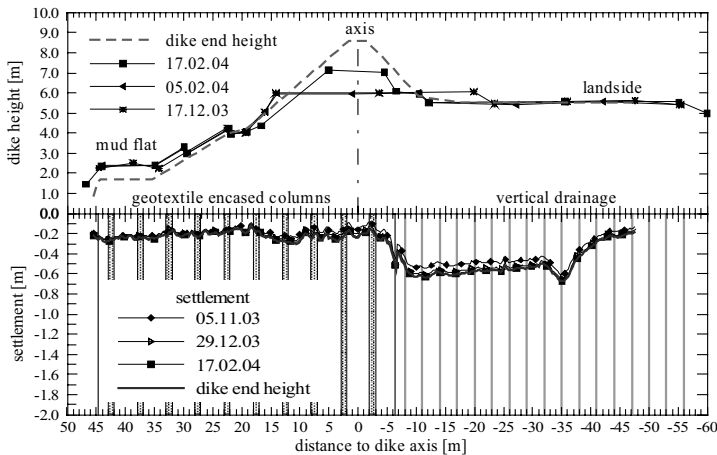


Fig. 7.33. A typical measured settlement at 'Finkenwerder Vordeich'

7.9.2 Hamburg–Berlin railway line: reinforced embankment on pile like elements

General

As part of upgrading the railway line Hamburg-Berlin by the German Rail company, the Buechen-Hamburg and the Paulinenaue-Friesack part of the railway line were upgraded in 2003 to allow a train speed of 230 km/h. Because of the very soft organic soil (peat and mud) layer with insufficient bearing capacity, stabilisation of the embankment foundation was necessary at these two parts.

Buechen-Hamburg line

The part of this line with a total length of 625 m was near the railway station Buechen. The soft underground was stabilised with columns installed using Mixed-in-Place Method (MIP) and the embankment was reinforced with geogrids at its base on the top of the columns (Fig. 7.34). The MIP belongs to the wet deep mixing methods.

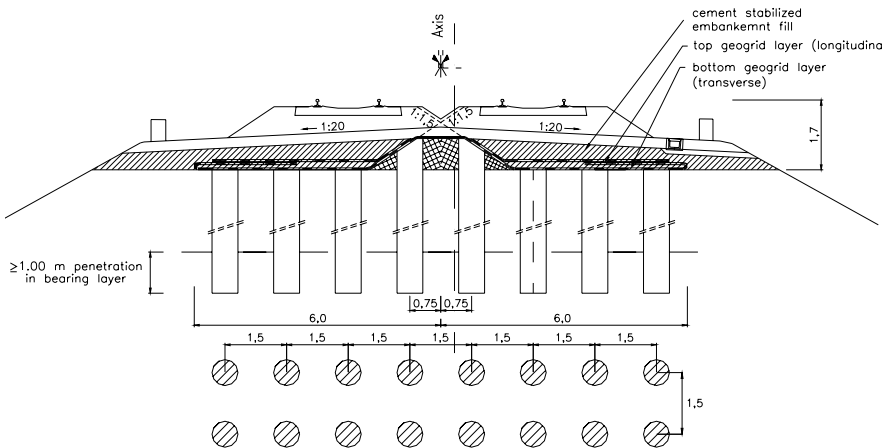


Fig. 7.34. Foundation system at a typical section in Buechen-Hamburg line

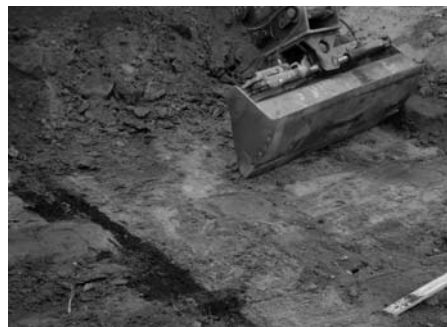
Underground condition. The underground consists of a 3 to 5 m fill of silty and gravelly medium dense sand with slag and organic mixtures underlain by 0.5 to 2 m thick layer of a very soft peat and mud. The peat soil has a water content of 80 to 330% and an organic content between 25 and 80%. Beneath the soft layer a medium dense and slightly silty sand layer with a thickness up to 8 m is encountered followed by a boulder clay with soft to stiff consistency and a water content of 10 to 20%.

Construction. Throughout the upgrading work, a single track operation at a speed of 90 km/h was maintained. The stability of the track during operation was secured by extending the slope of the ballast layer to the base of the embankment (Fig. 7.34). This had made the construction of the geogrid reinforcement across the total embankment width possible. The MIP-columns were installed after excavation of the subbase layer (Fig. 7.35b). Prior to the setting of the MIP material, the columns generally were cut to a level of 1.7 m below top of rail line during the next excavation stage (Fig. 7.35b). The columns adjacent to the embankment symmetrical axis were however left uncut and resulted in a cover less than 1.5 m on top of the columns. Nevertheless, this construction option was favoured over a temporary sheet pile wall, since the retracting of sheet piles could lead to unexpected settlements.

The MIP-columns were installed using a single axis auger (Fig. 7.35a). A cement slurry was injected continuously into the soil during the penetration as well as during the retrieval of the auger. Due to the rotation of the auger, the cement slurry is mixed with the soil. The MIP-technique is free of vibrations and displacements and therefore had no effect on the ongoing railway traffic on the other track. The cement columns (diameter 0.63 m) were installed in a square grid of 1.5 x 1.5 m.



a)



b)

Fig. 7.35. a) Installation of MIP-columns; b) cutting of the MIP-columns

The proportion of the slurry mix (water, cement and bentonite) and the water/binder ratio (approx. 1.0) was determined in laboratory on trial mixed samples. During the 1st soil stabilisation stage (track Hamburg-Berlin), about 800 l/m³ binder were mixed into the soil. During the 2nd stage (track Berlin-Hamburg), the binder was optimised and mixed with the soil to the extent up to a homogenous soil/binder mixture was obtained. This resulted in a variable, soil dependant binder quantity. The depth of the columns was determined on the basis of cone penetration tests prior to column installation. All in all 3260 MIP-columns with a length between 5 and 8 m were installed (total length \approx 21000 m).

On top of the MIP-columns two layers of Fortrac® PVA geogrid type M 400/30-30 had been placed. Since the geogrids are subjected to a load in longitudinal direction only, the short-term tensile strength in transverse direction was taken to be 30 kN/m, whereas the required short-term tensile strength in longitudinal direction was set at 400 kN/m.

The 1st geogrid layer was placed in transverse direction directly on top of the MIP-columns. This geogrid was rolled up near the embankment axis during the 1st construction stage, and later laid across the whole embankment in the 2nd stage. The 2nd geogrid layer was placed in longitudinal direction.

To obtain a uniform bearing platform for the ballast bed, 2.5 to 3% cement was added to the filling material. The top of this cement stabilisation was made rough to ensure a sufficient friction with the upper protective layer. To avoid an influence of hydrolysis of the cement, Polyvinylalcohol was used as geogrid material.

Monitoring. The settlement behaviour of the tracks was monitored by means of geodetic measurements of the position of the outer rail of both tracks. The measurements were carried out at three measurement sections each 20 m in length and consists five measuring points with a spacing of 5 m. These measurement sections were selected at locations with unfavourable soil conditions. The results of the settlement measurements over a period of 6 months train operation are presented in Fig. 3.36. On both tracks the train was operated up to a speed of 160 km/h. Fig. 7.36 shows a maximum settlement of 7 mm in a period of 6 months after reopen-

ing of the track Hamburg-Berlin. This settlement can be considered as small since a settlement of 10 mm to 15 mm can usually occur due to compaction of the ballast bed, the subbase layer and the embankment, even if the soil conditions could be favourable. Furthermore, the geogrids require a small amount of deflection to function effectively.

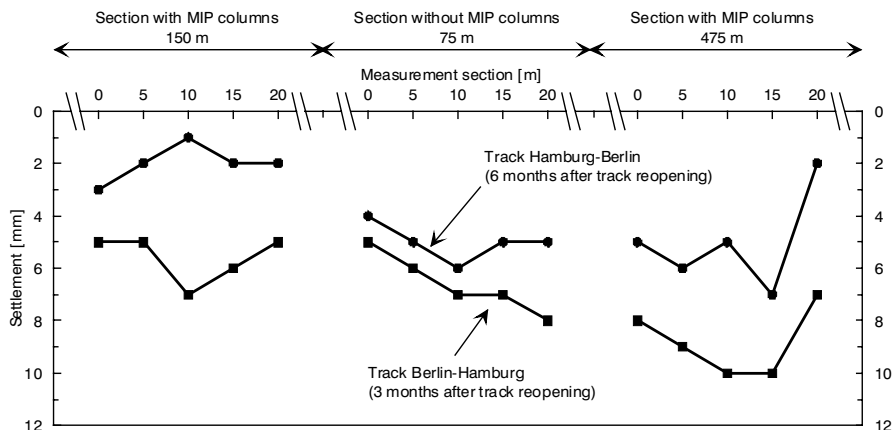


Fig. 7.36. Measured settlement

Section Paulinenaue-Friesack

Westwards of Berlin, at the railway line between Paulinenaue and Friesack, the railway Hamburg – Berlin passes through an area (the so called Havellaendische Luch) with deposits of soft organic soils. This stretch is 13 km long and the soft soil layers have a thickness up to 6.5 m. A dense sand is located beneath the soft layer. The groundwater level is located at the toe of the embankment.

The first upgrading plan. At the time the railway was first constructed 150 years ago, an embankment 2 to 3 m high had been built with a loose sand (Fig. 37a). Since the old railway tracks had suffered considerable settlements in the past, it was necessary to improve the bearing capacity of the embankment. In 1993 to 1995, the railway between Hamburg and Berlin was upgraded to allow a speed of 200 km/h and heavy loads. The typical cross-section of the 1st upgrading work is illustrated in Fig. 7.37b. The section consists of geogrid reinforced embankment, partially grouted stone columns, the soft organic soil (peat) and the dense sand layer at depth with sufficient bearing capacity to carry the total load. The rails were rested on a ballast track.

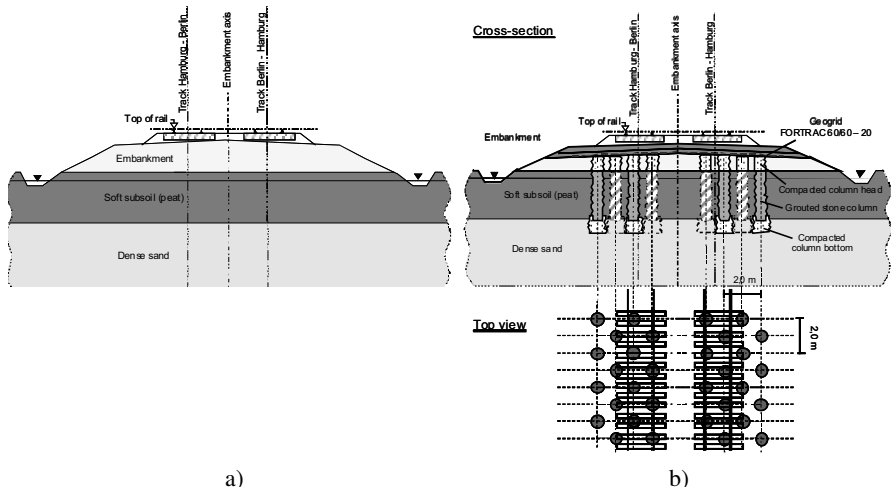


Fig. 7.37. Typical section and soil profile: a) without soil stabilisation measure; b) section according to the 1st upgrading plan

After removing the rails, the ballast bed and the embankment had been removed up to a depth of 1 m below the top of the old rail. As vertical bearing elements, cemented stone columns together with compacted, non cemented stone column at top and at base had been selected. The columns had a diameter of 0.6 m, they are arranged in a triangular grid system with a spacing of 2.0 m and they are extended up to the dense sand layer.

A geosynthetic reinforcement had been laid on the top of the stone columns. The geosynthetic used was of the type biaxial geogrid Fortrac® 60/60 - 20 with an ultimate short-term strength of 60 kN/m in both directions and it had been installed in one layer parallel to the embankment axis. Because of the presence of the temporary sheet pile wall, no overlapping of the geogrids was possible at the middle of the embankment. Moreover, there were no stabilising stone columns close to the the embankment axis. The sheet pile wall had been removed after completion of the track.

Shortly after the end of the first upgrading works, settlements and ballast bed deformations had been observed for the second time. For this reason as well as the general need for further upgrading the track structure for a train speed of 230 km/h, a second upgrading work was planned in summer 2001. As preparation to the second upgrading works, an intensive investigations had been carried out.

Part of the investigation program includes preparation of a 50 m long test excavation while the track remained closed in order to inspect the embankment construction, in particular the status of the geogrid and the cemented stone columns and the subsoil situation (Fig. 7.38a). In the test field, it had been observed that several cemented columns ended below the required height. Non cemented gravel

only was found below the top of the organic soil layer (Fig. 7.38b), while the geogrid was undamaged and in a good condition.



Fig. 7.38. Test filed: a) Temporary sheet pile walls and excavated embankment; b) excavated columns with different heights

The second upgrading plan. In addition to the test field, a number of numerical investigations were carried out and they revealed that the current embankment state would not permit an upgrading of the track for a train speed of 230 km/h. Based on the observations at the test field and the numerical analysis, a modified track structure was planned to rebuilt the embankment first in the test field. The final double track structure which was carried out in summer 2003 is illustrated in Fig. 7.39.

The flat optimised embankment has a height of 2 to 3 m. The lowest working plane was raised from -3.2 m to -2.7 m below the top of the rail to prevent operations below the groundwater level, because groundwater lowering was not allowed to avoid an additional settlement. The old embankment had been removed up to this depth, the piles cut and the organic soil between the columns removed to a depth of -2.8 m below the top of the rail. The soft soil removed between the column was filled with gravel above which a 0.2 m thick mineral layer had been placed. On top of the mineral layer two or three geogrid layers were placed at intervals of 0.3 m vertically. Based on structural analyses biaxial PVA-geogrids had been selected with optimised mesh size, a high-moduli and low-creep, an ultimate tensile strength of 200 kN/m in both longitudinal and transverse direction as well as an ultimate strain of about 5%. The mineral layers between the geogrids consisted of gravelly sand. Finally, the remaining embankment was completed after placement of a 0.4 m thick subbase layer and the rails had been placed on a ballast base.

Between July and September 2003 the entire stretch was rebuilt in only 76 days, while both tracks remains closed. The construction had been executed day and night. All in all 37000 partly grouted stone columns had been excavated, inspected and cut. Fig. 7.40 illustrates the cutting of a column head.

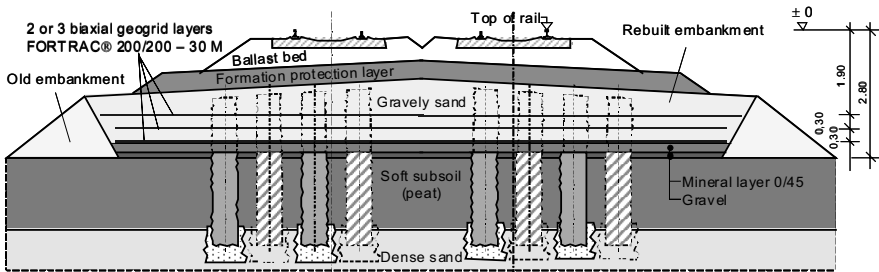


Fig. 7.39. Typical section of the second upgrading works

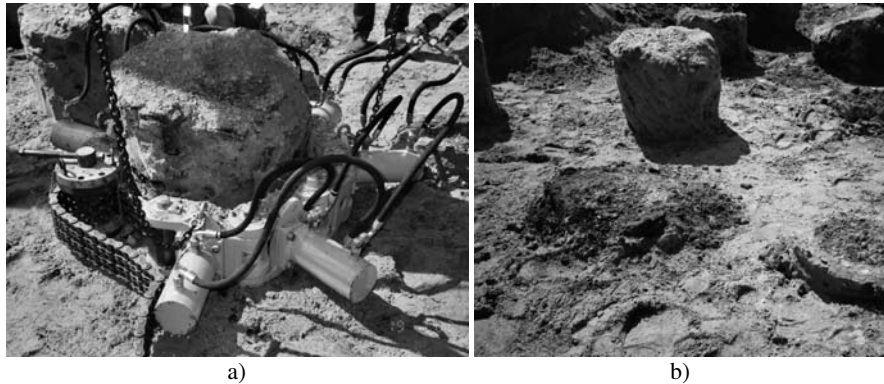


Fig. 7.40. Cutting column heads

The removal of the old embankment had been done in 10 m long sections. The status of the partially grouted stone columns had been examined and well documented for each section. For the case where the excavated columns conditions were as predicted by numerical simulation, three geogrid layers were had been placed. Otherwise, where nearly all columns were intact, only two geogrid layers were necessary. Some figures and facts about the reconstruction works are summarised in Table 7.5. The peak-period demand of construction workers was 450. Both tracks have been in operation since summer 2003.

Table 7.5. Figures and facts about the reconstruction works

Removal of the old embankment	Construction of the new embankment
<ul style="list-style-type: none"> ➤ 23 km overhead contact wire, ➤ 23 km trails in 6 days, ➤ 45.000 m³ ballast, ➤ 115.000 m³ formation protection layer, ➤ 185.000 m³ embankment soil, ➤ 135.000 m² geogrid, ➤ 60.000 m³ excavated soft soil (peat), ➤ 37.000 grouted stone columns had been cut 	<ul style="list-style-type: none"> ➤ 50.000 ton gravel, ➤ 85.000 ton protective mineral layer, ➤ 410.000 m² geogrid, ➤ 400.000 ton embankment soil, ➤ 130.000 ton formation of protection layer, ➤ 23 km ballast bed, trails and overhead contact wire

Monitoring. As check up for the design and verification of the stability as well as the serviceability of the embankment, a monitoring program was installed along three selected sections. A number of vertical and horizontal inclinometers as well as geophones had been installed for the monitoring purpose. Furthermore, the settlements of the rails had also been measured at the selected sections. The long-term monitoring has confirmed the stability and serviceability of the structure. Fig.41 shows typical measured settlements at different vertical locations at section 1 of the Hamburg-Berlin track.

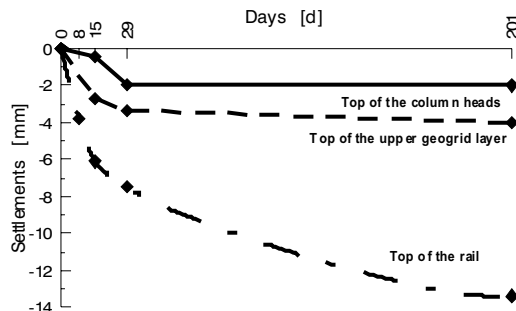


Fig. 7.41. Measured settlement at section 1 of the Hamburg-Berlin track

7.9.3 City road Trasa Zielona in Lublin-Polen: wet deep soil mixing

The weak soil found to a depth of 3 to 8 m consists of loose anthropogenic fill, underlain by 1 to 4 m thick peat and organic clay. The embankment height was 1.3 to 2.5 m and the equivalent live load was 30 kPa. A triangular column grid with spacing 2 m was selected (Fig. 7.42), resulting in soilcrete design strength of 480 to 676 kPa. The required unconfined compression strength was 1.5 Mpa. Altogether 2402 columns with a total length of 15,532 m had been constructed. The final embankment was reinforced with two layers of Tensar geogrid, resulting in the so-called Load Transfer Platform design.

7.9.4 A multistory building on wet deep mixing columns

A multistory building is located in a difficult heterogeneous soil conditions. Beneath a mixed fill, organic clay and some peat was encountered which extends to a depth of 3.5 to about 6.7 m below the final slab foundation level. Below the organic soil layer is fine sand and silt layers of varying thickness, making ordinary piling very expensive due to necessary pile length. Primary calculations also indicated that a direct placement of the foundation slab on the existing soil would lead to large and non-uniform settlements, ranging from 7 to about 50 cm despite of the high stiffness of the slab.

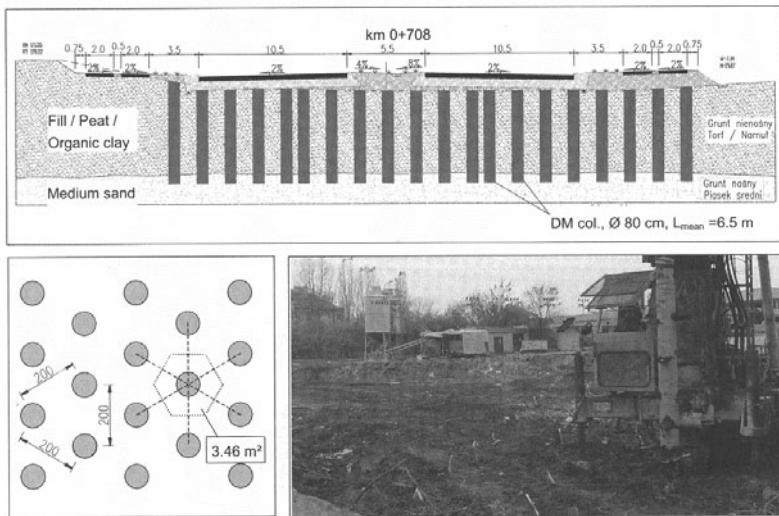


Fig. 7.42. Road embankment supported on wet deep soil mixing columns, Lublin-Polen (Topolnicki 2003)

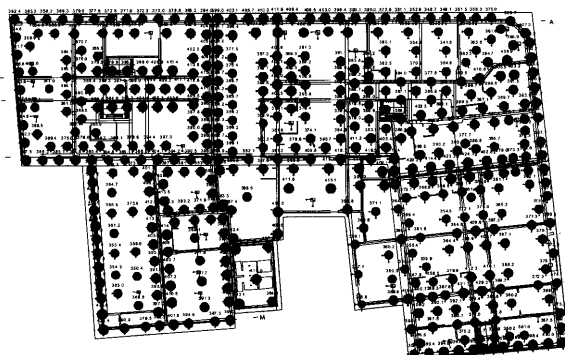


Fig. 7.43. Arrangements of deep soil mixing columns under foundation slab, Kielce-Polen (Topolnicki 2003)

For the outlined design (Fig. 7.43) comprising 461 DM columns with a total length of about 3.280 m, it was necessary to make a good estimate of the expected compressive strength of the soilcrete. Due to heterogeneous soil and the presence of organic layers significant differences in column strength were anticipated. For this reason, maximum factored load acting on a single column was limited to 430 kN, resulting in design compression stress of 0.86 MPa as well as special mixing procedure was adopted at the construction site. The average unit weight of the cement slurry was 1700 kg/m³ and the mean consumption rate was about 180 l/m. According to the accepted design criterion, a partial safety factor of 2.5 was ap-

plied to the maximum factored design stress acting on a single column. This led to compressive strength test on 32 standard cubic samples, extracted from fresh DM columns and tested in uniaxial compression. The mean unconfined compressive strength was 5.72 Mpa and the standard deviation was 2.14 Mpa which results a variation coefficient of 0.38.

7.9.5 Pad and strip foundations on wet deep mixing columns

Strip foundations of varying width between 1.0 and 1.7 m had been designed for loads ranging from 230 to 729 kN/m which gives a pressure of 230 to 430 kPa. There were also 12 types of rectangular pad foundations loaded from 1170 kN to 5670 kN with results a pressure of 310 to 677 kPa. This challenging geotechnical project, originally designed for CFA piles because of expected settlement differences, has been changed in favour of the wet deep mixing stabilization method. The pad and the strip foundations had been designed as shallow foundations supported on DM columns with 80 cm diameter. The assumed column layout under the footings is shown in Fig. 7.44. The number of columns under pad foundations ranges from 3 to 14 and they are selected taking into account the expected internal strength of DM columns and an allowable settlement difference of 5 mm over 6 m span as specified by the client. The maximum design load acting on a single column was limited to 512 kN. This corresponds to compression stress of 1330 kPa for a column with consideration of a reduced diameter due to a slightly aggressive groundwater.

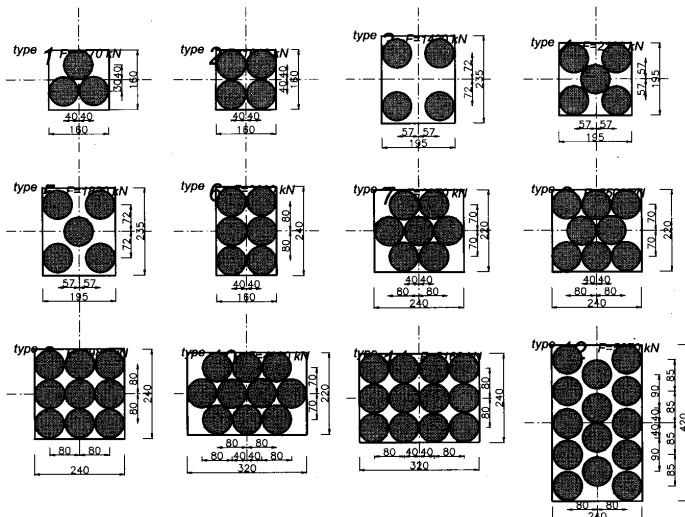


Fig. 7.44. Arrangements of deep soil mixing columns under a pad foundation, Katowice-Polen (Topolnicki 2003)

7.9.6 Highway bridges supported on wet deep mixing columns

Recent works on A2 highway in Poland have initiated new applications for wet deep mixing (DM). After careful analyses it turned out that certain road bridges, originally designed on large diameter piles could be founded on DM columns fulfilling all technical requirements with respect to stability and settlement of the supports and at the same time offering substantial economical savings.

For illustration the solution adopted for bridge WD-105 is presented. The design included soil improvement for 5 bridge supports using 168 DM columns. A typical layout is shown in Fig. 7.45 for the support P3 with 30 columns. Allowable maximum factored load for a single column was 458 kN, resulting in compressive stress of 916 kPa. The required compressive strength was 2.3 Mpa applying a partial safety factor of 2.5. Predicted settlement for the whole support was 0.95 cm.

In order to inspect the actual deformation characteristics of this alternative design, two loading tests on selected single DM columns had been performed. The objective was to determine the load-settlement prediction, rather than to check the bearing capacity as it would be the case for large diameter piles. The loading of the test columns was carried out in 12 steps up to a maximum load of 572 kN, i.e. 150% of maximum characteristic load allowed for a single column which is equal to $458/1.2 = 382$ kN. Each loading step was maintained for at least 30 minutes or until the observed settlement was less than 0.05 mm in 10 minutes.

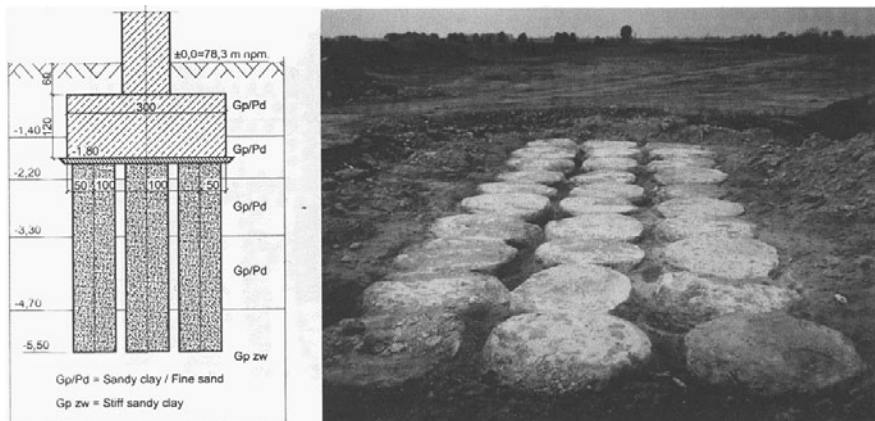


Fig. 7.45. Highway bridge founded on deep soil mixing columns, Polen (Topolnicki 2003)

7.9.7 Restoration of an offshore retaining wall with CSV-columns

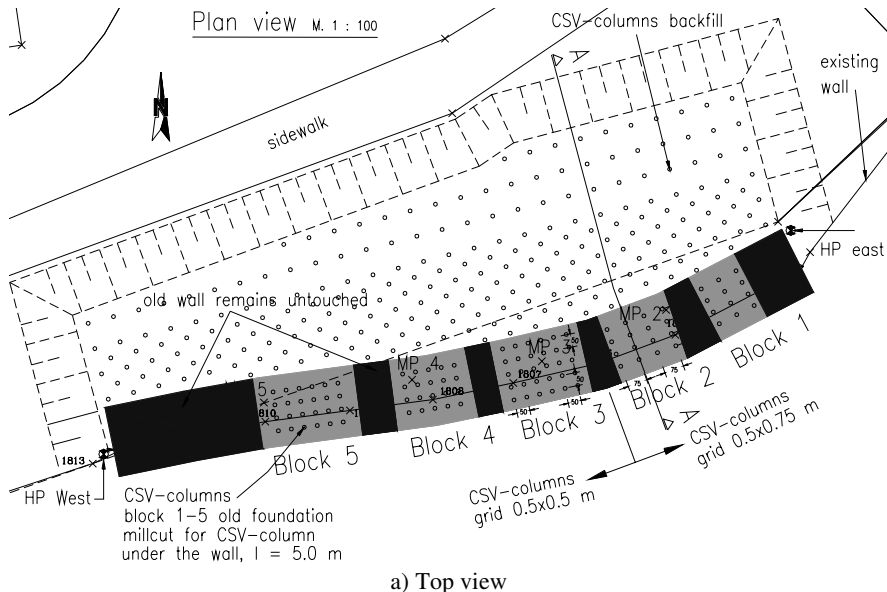
The safety of a masonry wall along the shore of the Constance lake was in danger and had required an immediate restoration. The first recommended measure was to stabilize the backfill area with CSV-columns in order to increase the safety against

overall failure and to strengthen the foundation with injection pile in order to minimize the settlement of the wall (serviceability requirement).

The plan was changed in favour of CSV-method for both the backfill area and the area below the foundation of the wall. The underground consists of mainly soft lacustrine deposit with $w = 35 - 47\%$ and $c_u = 17 \text{ kN/m}^2$. The new restoration measure includes to millcut the existing wall in blocks of $3 \times 2.2 \text{ m}$ large up to the foundation level and introduce CSV-columns (cement as binder material) with a length of 5 m and at grid of $0.75 \times 0.5 \text{ m}$ (Block 1 and 2) $0.5 \times 0.5 \text{ m}$ (Block 3 to 5) as shown in Fig. 7.46. Fig. 7.47 also shows a photographic view of the site and installation of the CSV-columns.

The external bearing capacity of the CSV-columns are approximated by means of load tests according to DGGT AK2.8. Two load tests on single columns had been performed. A settlement of 4.26 and 7.72 mm was measured at a test load of 50 kN. According to the design, the CSV-columns are supposed to carry a total vertical load of 251.5 kN/m , which was proved possible according to the load test results.

The underground below the backfill was also stabilised using CSV-columns which have a length of 8 m each and different spacing with a rectangular and triangular grids as shown in Fig. 7.46. The overall stability calculations of the retaining structure using an equivalent cohesion c_{equ} value of 106 kN/m^2 for 0.75 m triangular grid and 52 kN/m^2 for 1m rectangular grid resulted in a total safety factor of $\eta = 1.54$ which is higher than the required safety factor $\eta_{req} = 1.4$, hence the offshore wall is proved to be safe.



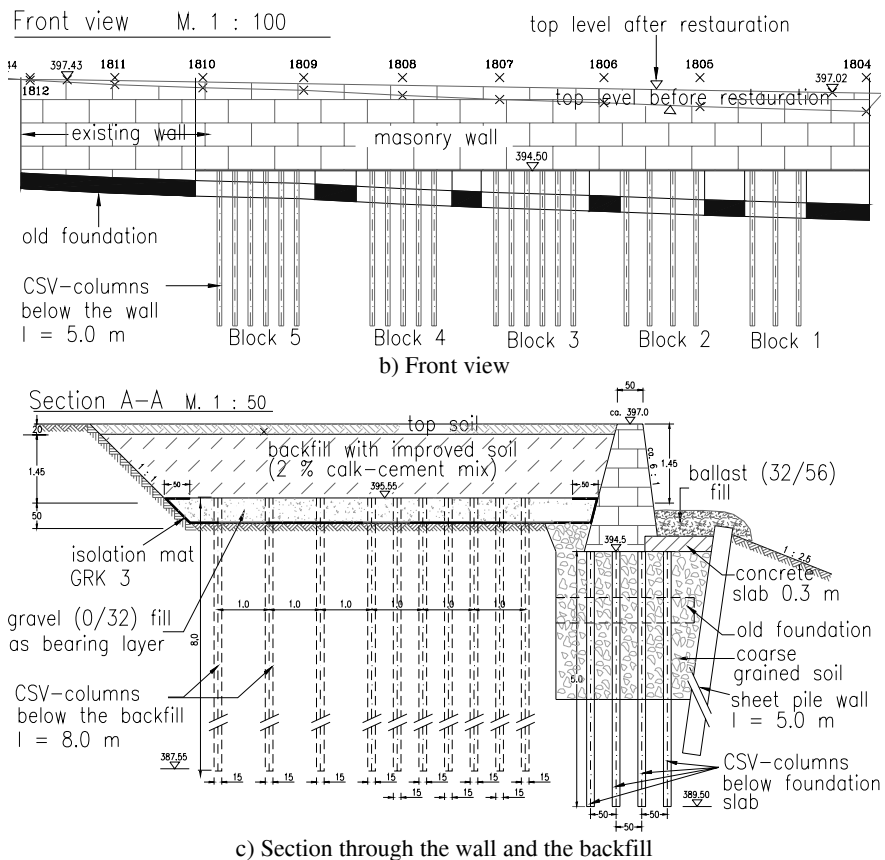


Fig. 7.46. Offshore retaining wall stabilized with CSV-columns



Fig. 7.47. a) Overview of the finished retaining wall, b) CSV-column installation

7.9.8 Stabilisation of 5-storey building foundation and underground parking with CSV-columns

The project consists of a 5-storey apartment building with underground floor (20 x 14 m) and underground parking (30.5 x 17.5 m) with double parking floor (Fig. 7.48) in Constance city, southern Germany. The foundation of the apartment is located at a depth of 1.7 m and that of underground parking at 4.65 m below the ground surface. The construction site is surrounded by existing buildings at a distance of 0.5 to 9 m. The Constance area is known to consist a deep soft lacustrine underground and excavations and foundations in this area are always prone to excessive settlement and deformations. A typical soil profile and sounding test results at the construction site are shown in Fig. 7.50.

To minimise the settlement of the shallow foundation of the 5-storey apartment, a stabilising 237 CSV-columns were installed at a grid system of 1 x 1 m. The CSV-columns have a diameter of 15 cm and a length of 5m each. The mat foundation is rested on the CSV-columns. To design the mat slab, the subgrade reaction is approximated from the expected contact pressure and settlement of single columns. The settlement of a single pile is believed to consist three components: settlement and compression of a single column and settlement due to group effect. The first two components are determined from load test results and they are approximated to be 1 cm. The settlement due to group effect is calculated to be 5 cm. Hence, the total settlement is about 6 cm. Assuming a contact pressure of 100 kN/m², the modulus of subgrade reaction is calculated to be 1.7 MN/m³.

An average value of undrained shear strength $c_u = 27.7 \text{ kN/m}^2$ was estimated from field vane test result for untreated soil. Correcting the field vane strength for the rate of strain according to Leinenkugel 1976, the undrained strength becomes 18.8 kN/m². The degree of hardening due to water absorption of the binding material from the surrounding soil is estimated to be 1%. Due to one-dimensional compression the undrained strength is improved by a factor of 1.4 and becomes 26.3 kN/m² according to Eq. 7.57. Moreover, there will be a soil improvement effect due to shear resistance of the CSV columns which is estimated to be 36.9 kN/m². Therefore, the undrained shear strength of the improved soil is about 63.2 kN/m². This value is however calculated for a grid of 0.8 x 0.8 m. Hence, for grid system of 1 x 1 m a correction should be made accordingly.

As shown in Fig. 7.48, the excavation of the underground parking and the near by existing structures are also protected partly by CSV-columns at a grid of 0.5 x 0.5 m and partly by combination of sheet pile wall and CSV-columns. A typical section through the excavation is shown in Fig. 7.49, where the CSV-columns are arranged to protect the excavation of the underground parking from overall stability failure and at the same time safe guard the safety of the existing structures. Fig. 7.51 also shows the installation process and the CSV-columns after installation is completed. The determination of the degree of soil improvement reached as well as the derivation of the equivalent cohesion and the modulus of the subgrade reaction is same as those CSV-columns used for stabilizing the foundation of the 5-storey apartment discussed above.

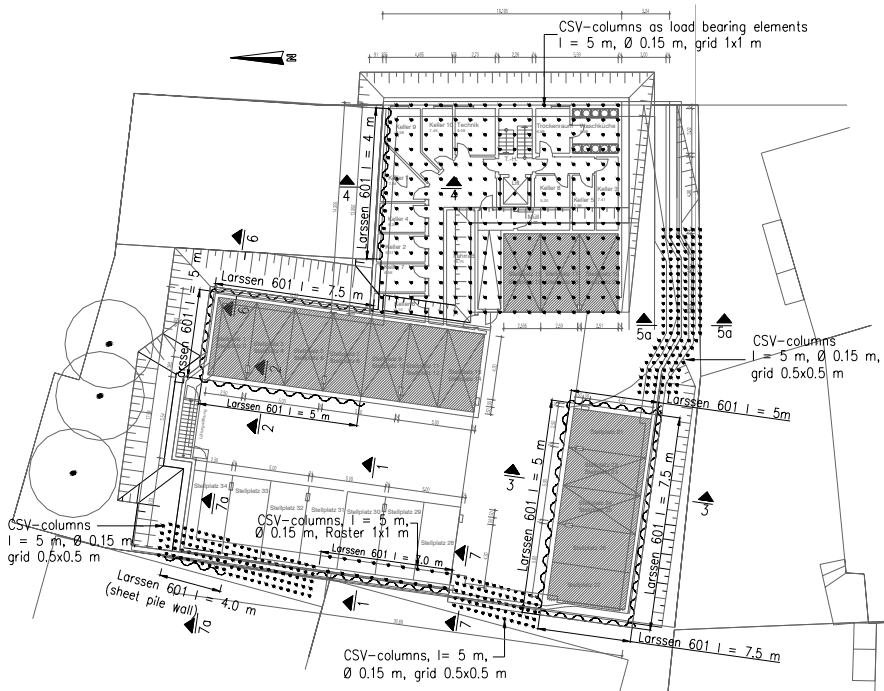


Fig. 7.48. Plan view of foundation of 5-storey apartment building and underground parking stabilized with CSV-columns

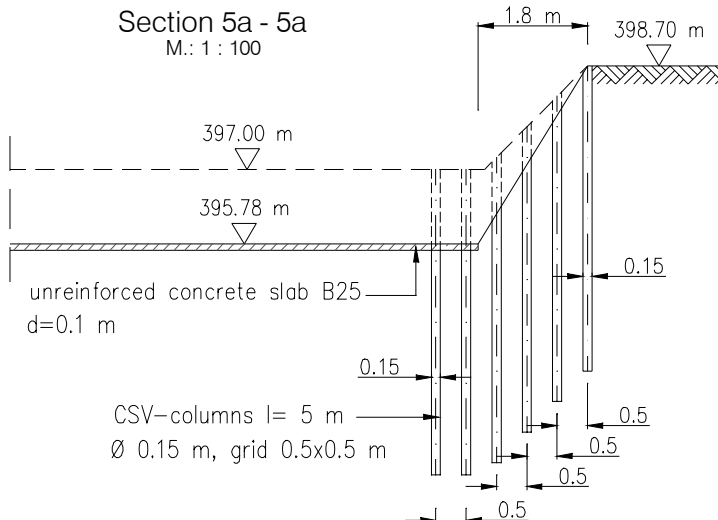


Fig. 7.49. Typical section through the stabilized excavation (Section 5a– 5a, Fig. 7.48)

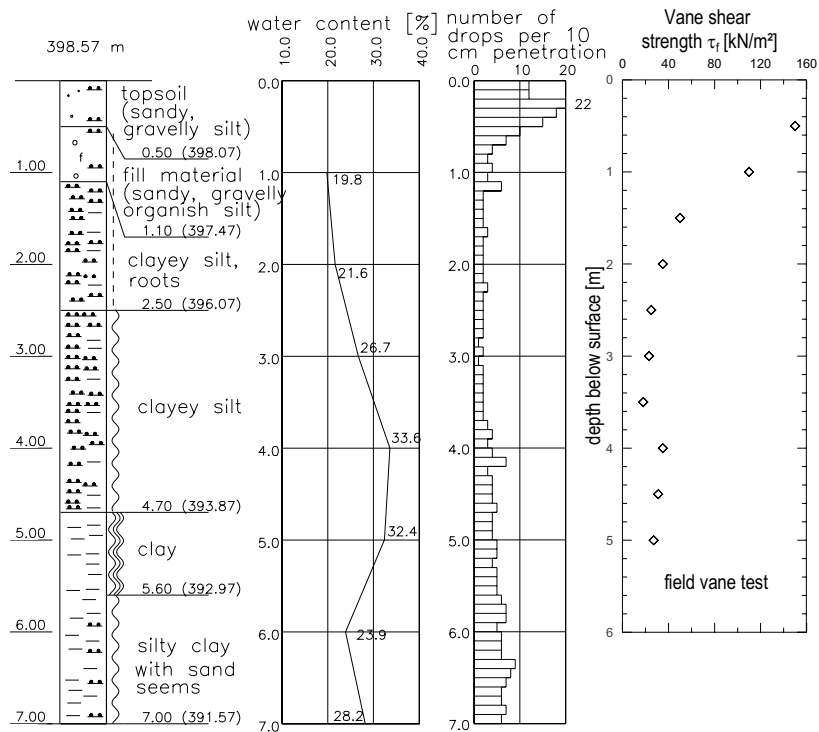


Fig. 7.50. Soil profile and some field test results

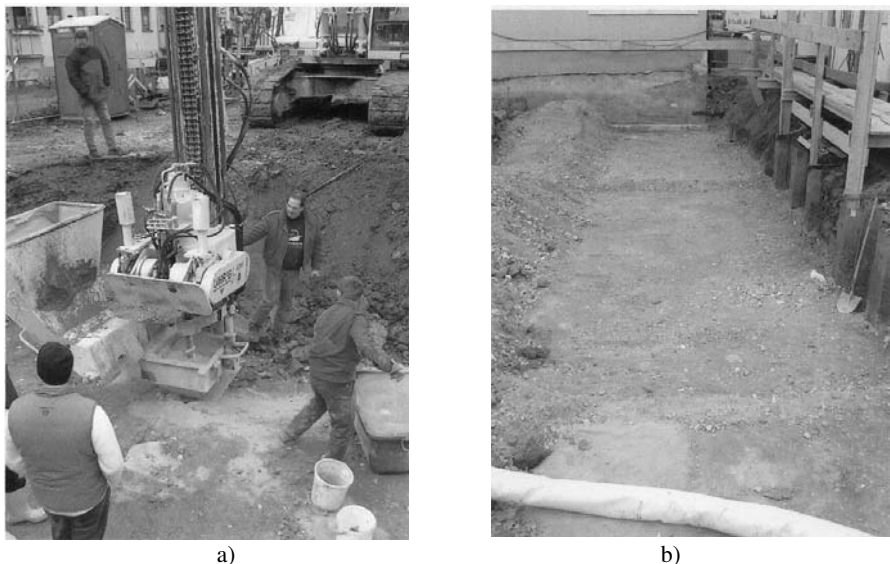


Fig. 7.51. a) Installation of the CSV-columns, b) Work plane after CSV installation

References

- Aboshi H, Yoshikuni A, Mariyama S (1970) Constant rate consolidation test. *Soil and Foundations* 10-1, pp 43 - 56
- Aboshi H, Ichimoto E, Enoki M, Harada K (1979) The „Compozer“ - a method to improve characteristics of soft clays by inclusion of large diameter sand columns. *Proceedings of the International Conference on Soil Reinforcement: Reinforced Earth and Other Techniques*, Vol. 1, Paris, pp 211 - 216
- Alexiew D, Vogel W (2001) Railroads on piled embankments in Germany. Milestone projects, Landmarks in earth reinforcements, ed. by Ochiai et al., Swets & Zeitlinger, pp 185 - 190
- Alphan I (1967) The empirical evaluation of the coefficient K_0 and K_{0r} . *ASCE Soils and Foundations* 7, pp 31 – 40
- Altaee A; Fellenius BH; Evgin E (1992a) Axial load transfer for piles in sand. I. Tests on an instrumented precast pile; *Canadian Geotechnical Journal*. 29, pp 11 - 20
- Altaee A, Evgin E, Fellenius BH (1992b) Axial load transfer for piles in sand. II. Numerical analysis; *Canadian Geotechnical Journal*. 29, pp 21 - 30
- Altaee A, Evgin E, Fellenius BH (1992c) Finite element validation of a bounding surface plasticity model; *Computers & Structures*. Vol. 42. No. 5, pp 825 - 832
- Altes J (1976) Die Grenztiefe bei Setzungsberechnungen. *Der Bauingenieur* 51-3, pp 93 - 96
- Amann P, Berth H, Stroh D (1975) Verformungsverhalten des Baugrundes beim Baugrubenauhub und anschließendem Hochhausbau am Beispiel des Frankfurter Tons. *Technische Hochschule Darmstadt, Heft 15*
- Amann P, Berth H (1977) Über die Setzung von Hochhäusern und die Biegbeanspruchung von Gründungssplatten. *Die Bautechnik* 54-2, pp 37 – 42
- Amour T, Groneck P, Keenley J, Sharma S (2000) Micropile design and construction guidelines implementation manual. Federal Highway Administration, National Technical Information Service, Springfield, Virginia
- Aoi M (2002) Execution procedure of Japanese Dry Method (DJM). Deep Mixing Work Shop 2002, Tokyo
- API RP 2A (1989) American Petroleum Institute; Recommended practice for planning. Designing and Constructing Fixed Offshore Platforms
- Arai K, Jinki R (1990) A lower-bound approach to active and passive earth pressure problems. *Soils and Foundations* 30-4, pp 25 - 41
- Asaoka A (1978) Observational procedure of settlement prediction. *Soil and Foundations*, Japan 18(4), pp 87 - 101
- Asaoka A, Masuo M (1981) Dynamic design philosophy in settlement prediction. Proc. 10th ICSMFE, Stockholm, pp 195 – 198
- Atkinson J, Bransby PL (1978) The mechanics of soils - an introduction to critical state soil mechanics. McGraw-Hill, London

- Atkinson J, Richardson D, Robinson PJ (1987) Compression and extension of K_0 normally consolidated kaolin clay. ASCE, Journal of Geotechnical Engineering Division 113-12, pp 1468 - 1482
- Atkinson J (1993) An introduction to the mechanics of soils and foundations. McGraw-Hill Book Company Europe
- Auvinet G et al. (1981) Negative skin friction in Mexico city clay. Proceedings of the 10th International Conference on Soil Mechanics and Foundation Engineering. Stockholm. Vol. 2, pp 599 - 604
- Auvinet G (2002) Foundations on soft soils in Mexico city. Proc. Intl. Workshop – Technical Committee TC36: Foundation engineering in difficult soft soil conditions, Mexico, pp 124 – 132
- Bakhoidin V et al. (1974) Estimation of negative skin friction on piles and suggestion on its calculation. Fundamenty I Mekhanika Gruntov. No.5, pp 11 - 15
- Balaam NP, Booker JR, Poulos HG (1976) Analysis of granular pile behaviour using finite elements. Proceedings of the International Conference on Finite Element Methods in Engineering. Adelaide, Australia
- Ballisager CC (1959) Bearing capacity of piles in Aarhus Septarian Clay. Danisch Geotechnical Institute. Bulletin No. 7, pp 14 - 19
- Bang S (1985) Active earth pressure behind retaining wall. ASCE Journal of Geotechnical Engineering Division, pp 407 - 412
- Bartolomey AA, Omelchak IM, Ponomaryov AB, Bakhoidin BV (1997) Calculation of pile foundations on limiting states – Russian practice. Design of axially loaded piles – European practice, ed. by De Cock & Legrand, Balkema; Rotterdam, pp 321 - 336
- Bauer E (1992) Zum mechanischen Verhalten granularer Stoffe unter vorwiegend ödemetrischer Beanspruchung. Dissertation. Veröffentlichung des Inst. f. Bodenmechanik und Felsmechanik der Universität Karlsruhe, Heft 130
- Bauer E (1996) Calibration of a comprehensive constitutive equation. Soils and Foundations, 36(1), pp 13 - 26
- Becker DE, Lo KY (1981) Settlement under intermittent loading. Proc. 10th ICSMFE, Stockholm, pp 35 – 40
- Behnke D, von Bloh G (1998) Tragfähigkeitsermittlung von Pfahlgründung durch Drucksondierergebnisse; Vorträge der Baugrundtagung. DGGT. Stuttgart, pp 559 - 576
- Bell FG (1993) Engineering treatment of soils. Spon, London
- Berezantzev VG, Khristoforov VS, Golubkov VN (1961) Load bearing capacity and deformation of piled foundations; V ICSMFE. Vol. 2. Paris, pp 11 - 15
- Bergado DT, Chai JC, Alfaro MC, Balasubramaniam AS (1994) Improvement techniques of soft ground in subsiding and lowland environment. Rotterdam/Brookfield: Balkema
- Berger G (1986) Einfluss der Standzeit auf die Tragfähigkeit gerammter Zugpfähle; Geotechnik 9, No. 1, pp 33-36
- Berner U (1997) Ausführung einer Spundwandbaugrube im Konstanzer Beckenton: Baugruben in Locker- und Festgestein. 3. Stuttgarter Geotechnik-Symposium, pp 227 - 239
- Besler D (1998) Wirklichkeitsnahe Erfassung der Fußauflagerung und des Verformungsverhaltens von geschützten Baugrubenwänden. Schriftenreihe des Lehrstuhls Baugrund-Grundbau der Universität Dortmund, Heft 22
- Bica AVD, Clayton CRI (1998) An experimental study of the behaviour of the embedded length of cantilever walls. Geotechnique 48-6, pp 731 - 745
- Biot MA (1941) General theory of three-dimensional consolidation. J. Applied Physics 12, pp 155 - 165
- Bishop AW (1955) The use of the slip circle in the stability analysis of slopes. Géotechnique 5-1 , pp 7 - 17

- Bishop AW (1958) Test requirements for measuring the coefficient of earth pressure at rest. Proc. of Brussels Earth Pressure Conference, pp 2 - 14
- Bishop AW, Henkel DJ (1962) The measurements of soil properties in the triaxial test. Edward Arnold, London
- Bishop AW (1966) Strength of soils as engineering materials: 6th Rankine Lecture, Geotechnique 16-2, pp 89 - 130
- Bjerrum L, Eide O (1956) Stability of strutteted excavation in clay. Geotechnique 6-1, pp 32 - 47
- Bjerrum L, Simons NE (1960) Comparison of shear strength characteristics of normally consolidated clays. Proc. ASCE Conference on Shear Strength of Cohesive Soils, Boulde, Co
- Bjerrum L (1961) The effective shear strength parameters of sensitive clays. Proc. Of the 5th ICSMFE, Paris, pp. 23 - 28
- Bjerrum L (1963) Allowable settlements of structures. Proc. 3rd European Conf. On Soil Mechanics and Found. Eng'g, Wiesbaden, pp 83 - 118
- Bjerrum L (1964) Observed versus computed settlements of structures on clay and sand. Massachusetts Inst. of Tech. Cambridge Mass. (unpublished lectures)
- Bjerrum L (1967) Engineering geology of Norwegian normally consolidated marine clay as Related to Settlement of Building. Géotechnique 17-2, pp 83 - 118
- Bjerrum L, Clausen C-J F, Duncan JM (1972) Earth pressures on flexible structures, A State-of-the-Art-Report. Proc. 5th European Conference on Soil Mechanics and Foundations Engineering, Madrid, pp 169 - 196
- Bjerrum L (1973) Problems of soil mechanics and construction on soft clay soils and structurally unstable soils (collapsible, expansive and others). Proc. 8th ICSMFE, Moscow, pp 110 – 155
- Böhm F (2006) Zur Wirkungsweise von "schwimmenden" stabilisierenden Verpresspfahl – Plattengründungen bei tiefreichenden Weichschichten. Schriftenreihe Geotechnik, Universität Kassel, Heft 19 (in preparation)
- Bolten MD, Powrie W, Symons IF (1990a) The design of stiff in-situ walls retaining over-consolidated clay: Vol. I, Short term behaviour. Ground Engineering 23-1, pp 34 - 40
- Bolten MD, Powrie W, Symons IF (1990b) The design of stiff in-situ walls retaining over-consolidated clay: Vol. II, long term behaviour. Ground Engineering 23-2, pp 22 - 28
- Boone JS (1996) Ground - movement-related building damage. Journal of Geotechnical Engineering 122-11, pp 886 – 895
- Borchert K-M, Mönnich K-D, Savidis S, Walz B (1998) Tragverhalten von Zugpfahlgruppen für Unterwasserbetonsohlen. Vorträge der Baugrundtagung. DGQT. Stuttgart, pp 529 - 557
- Borrman M (1992) Historische Pfahlgründungen. Institut für Baugeschichte der Universität Karlsruhe, Materialien zur Bauforschung und Baugeschichte, Heft 3
- Boussinesq J (1885) Applications des potentiels à l'étude de l'équilibre et du mouvement des solides élastiques. Paris, Gauthier-Villars
- Bowles JE (1984) Physical and geotechnical properties of soils. McGraw Hill Co. Inc., New York
- Bozozuk M (1970) Effect of sampling, size and storage on test results for marine clay. ASTM, STP 483, pp 121 - 131
- Bozozuk M (1972) Downdrag measurement on a 160-ft floating pipe test pile in marine clay. Canadian Geotechnical Journal. Nr. 5, pp 127 - 136
- Bozozuk M et al.(1979) Analysis of load tests on instrumented steel test piles in compressible silty soil. Behavior of deep foundations. ASTM STP 670. Raymond Lundgren. Ed.; American Society for Testing and Materials, pp 153-180

- Brauns J (1980) Untergrundverbesserung mittels Sandpfählen oder Schottersäulen. Tiefbau, Ingenieurbau, Straßenbau. Bertelsmann Fachzeitschriften GmbH, Jahrg. 22, Heft 8, Gütersloh, pp 678 - 683
- Brem G, Wooge M (1997) Potsdamer Platz Berlin. Bauingenieur 72, pp 53 - 59
- Breymann H (1992) Tiefe Baugruben in weichplastischen Böden. 7.Ch. Veder Kolloquium. TU Graz
- Briaud J-L, Garland E (1985) Loading rate method for pile response in clay; Journal of Geotechnical Engineering, Vol. 111. No. 1, pp 319 - 335
- Briaud J-L, Jeong S, Bush R (1991) Group effect in the case of downdrag. ASCE GSP 27. Geotechnical Engineering Congress, pp 505 - 518
- Brinch-Hansen J, Gibson RE (1949) Undrained shear strengths of anisotropically consolidated clays. Geotechnique, Vol. I, No. 3, pp 189 - 204
- Brinch-Hansen J (1953) Earth pressure calculations. Danish Technical Press, Copenhagen
- Brinkgreve RBJ, Vermeer PA (1992) On the use of cam-clay models. In: GN Pande, S Pietruszczak (eds) Proc. 4th Intl. Symposium on Numerical Models in Geomechanics. Balkema, Rotterdam, pp 557 - 565
- Brinkgreve RBJ, Vermeer PA (1998) Hand book of the finite element code for soil and rock analysis "PLAXIS", Balkema, Rotterdam
- Brinkgreve RBJ (2002) Hand book of the finite element code for soil and rock analysis "PLAXIS" Balkema, Rotterdam
- Britto AM, Gunn MJ (1987) Critical state soil mechanics via finite elements. John Wiley & Sons, New York
- Broms BB (1966) Methods of calculating the ultimate bearing capacity of piles – A summary. Sols-Soils. Vol. 5. No. 18-19, pp 21 - 32
- Broms BB (1979) Negative skin friction. Proceedings of the 6th Asian Regional Conference on Soil Mechanics. Singapore. Vol. 2 pp 41 - 75
- Broms BB (1981) Precast piling practice; Thomas Telford Ltd. London.
- Broms BB (1991) Deep compaction of granular soils. Foundation engineering handbook. H-Y Fang (ed), Chapman & Hall, pp 814 - 832
- Brooks NJ, Spence J (1993) Design and recorded performance of a secant retaining wall in Croydon: Retaining structures. Thomas Telford, London, pp 205 – 215
- Bruce DA, Juran I (1997 a) Drilled and grouted micropiles, state-of-practice review, volume I: background, classification, Cost. Federal Highway Administration, National Technical Information Service, Springfield, Virginia
- Bruce DA, Juran I (1997 b) Drilled and grouted micropiles, state-of-practice review, volume II: design. Federal Highway Administration, Georgetown Pike, USA
- Bruce DA, Juran I (1997 c) Drilled and grouted micropiles, state-of-practice review, volume III: construction, QA/QC, and Testing. Federal Highway Administration, Georgetown Pike, USA
- Bruce DA, Juran I (1997 d) Drilled and grouted micropiles, state-of-practice review, volume IV: case histories. Federal Highway Administration, Georgetown Pike, USA
- Bruce DA et al. (1998) Deep mixing method : A global perspective. Seminar University of Wisconsin
- Bruce DA, Bruce ME, DiMillio AF (2002) Deep mixing: QA/QC and verification methods. Deep Mixing Workshop 2002, Tokyo
- BS Code of Practice No. 2 (1951) Earth retaining structures. Institution of Structural Engineers, London
- Buchmann K-J (1993) Entwicklung und Einsatz des neuen STRABAG Vollverdrängungsbohrpfahles. Pfahl-Symposium. Institut für Grundbau und Bodenmechanik. TU Braunschweig. Heft 41, pp 357 - 368

- Buchmann K-J, Steiner H (1996) Einsatz und Tragverhalten des Vollverdrängungsbohrpfahles bei verschiedenen Bauvorhaben in Norddeutschland. Vortragsband Baugrundtagung. DGGT. Berlin, pp 185 - 192
- Budhu M (2000) Soil mechanics & foundations; John Wiley & Sons. New York
- Burland JB et al. (1966) The behaviour and design of large diameter bored piles in stiff clay. Proceedings of the Symposium on Large Bored Piles. London, pp 51 - 71
- Burland JB (1967) Deformation of soft clay. Ph.D. thesis, Cambridge University
- Burland JB (1973) Shaft friction of piles in clay – a simple fundamental approach. Ground Engineering 6, pp 30 - 42
- Burland JB, Broms BB, De Mello VFB (1977) Behaviour of foundations and structures. IX ICSMFF, Tokyo
- Burland JB, Hancock RJR (1977) Underground car park at the house of commons. London geotechnical aspects. The Structural Engineer 55-2, pp 87 - 100
- Burland JB, Broms BB, De Mello (1977) Behaviour of foundation and structures. Proc. 9th ICSMFE, Tokyo, pp 495 - 547
- Burland JB, Simpson B, St John HD (1979) Movements around excavations in London clay. Design Parameters in Geotechnical Engineering, BGS, London, Vol. 1
- Burland JB, Potts DM, Walsh NM (1981) The overall stability of free and propped cantilever retaining wall. Ground Engineering, London, pp 28 - 38
- Burland JB (1990) On the compressibility and shear strength of natural clays. Geotechnique 40-3, pp 329 – 378
- Bustamante M, GIANESELLI L (1982) Pile bearing capacity prediction by means of static penetrometer CPT. Proceedings of the Second European Symposium on Penetration Testing. Amsterdam, pp 493 - 500
- Bustamante M, Frank R (1997) Design of axially loaded piles – French practice; Design of axially loaded piles – European practice. De Cock & Legrand (eds); Balkema. Rotterdam, pp 161 - 175
- Bustamante M, Frank R (1999) Current French design practice for axially loaded piles. Ground Engineering, pp 38 - 44
- Campanella RG, Vaid YP (1973) Influence of stress path on the plane strain behaviour of sensitive clay. Proc. 8th ICSMFE. Moscow, pp 85 - 92
- Casagrande (1932) Research on the Atterberg limits of soils. Public Roads
- CDIT Coastal Development Institute of Technology (2002) The deep mixing method. AA Balkema Publishers, Japan
- CDM Association (2002) CDM-cement deep mixing bulletin as of 2002
- Chen WF (1975) Limit analysis and soil plasticity. Elasevier, Amsterdam
- Chen WF, McCarron WO (1986) Plasticity modelling and its application to geomechanics. In: Balasubramaniam et al (eds) Proc. Intl. Symposium on Recent Developments in Laboratory and Field Testing and Analysis of Geotechnical Problems, A.A. Balkema, Bangkok, pp 467 - 510
- Chen WF, Mizuno E (1990) Non-linear analysis in soil mechanics. Elsevier, Amsterdam.
- Chow FC, Jardine RJ, Brucy F, Nauroy JF (1996) The effects of time on the capacity of pipe piles in dense marine sand. Proc. 28th Off-shore Technology Conference. OTC 7972, pp 147 - 160
- CIRA (1974) A comparison of quay wall design methods. Report No. 54, Constructional Industry Research and Information Association, London
- Clark JI, Meyerhof GG (1972) The behaviour of piles driven in clay. I. An investigation of soil stress and pore water pressure as related to soil properties; Canadian Geotechnical Journal. 9, pp 351 - 373
- Clayton CRI, Milititsky J, Woods RI (1993) Earth pressure and earth retaining structures. 2nd edn., Chapman & Hall, London

- Clough GW, Woodward RJ (1967) Analysis of embankment stresses and deformations. Journal of the Soil Mechanics and Foundation Division, ASCE 93-SM4, pp 529 – 549
- Clough GW, Duncan JM (1971) Finite element analysis of retaining wall behaviour. Journal of Soil Mechanics and Foundation Engineering, ASCE 97-SM12, pp 657 - 673
- Clough GW, Tsui Y (1974) Performance of tied - back walls in clay. Journal of Geotechnical Division, ASCE 100-GT12, pp 1259 - 1273
- Clough GW, Mana AI (1976) Lessens learned in F.E. analysis of temporary excavation in soft clay. Proc. 2nd Intl. Conference on Numerical Methods in Geomechanics, Blacksburg, pp 496 – 510
- Clough GW, Denby GM (1977) Stabilising wall design for temporary walls in clay. Journal of Geotechnical Engineering Division, ASCE 103-GT2, pp 75 - 90
- Clough GW, Schmidt B (1977) Design and performance of excavations and tunnels in soft clays. A State-of-the-Art Report, International Symposium on Soft Clay, Bangkok
- Clough GW, Smith EM, Sweeney BP (1989) Movement control of excavation support by system by iterative design. In: Kulhawy FH (eds) Foundation engineering: Current Principles and Practices, ASCE 2, New York, pp 869 - 884
- Clough GW, O'Rourke TD (1990) Construction induced movements of in-situ walls. Design and Performance of Earth Retaining Structures, ASCE Geotechnical special publication 25, New York, pp 439 – 470
- Clough GW, Duncan JM (1991) Earth pressures. In: H-Y Fang (eds) Foundation Engineering Handbook, 2nd edn., Chapman & Hall, New York, pp 223 – 235
- Cognan JM (1972) In-situ Measurement of Negative Friction. Ann. Inst. Tech. Bat. Trav. Publ. Nr. 293. Sols and Fondations (89), pp 1 - 12
- Coulomb CA (1773) Essai sur une Application des Regles de Maximis et Minimis à quelques Problèmes de Statique relatifs à l'Architecture. Mémoires de Math. Et Physique. Imprimerie Royale 7, Paris, pp 343 - 482
- Crawford CB (1986) Evaluation and interpretation of soil consolidation. A Symposium on Consolidation of Soil: Testing and Evaluation, ASTM Special Technical Publication 892, pp 71 - 103
- Crawford CB, DeBoer LJ (1987) Field observations of soft clay consolidation in the Fraser Lowland. Canadian geotechnical journal 24, pp 308 - 317
- Crawford CB, Campanella RG (1991) Comparison of field consolidation with laboratory and in-situ tests. Canadian geotechnical journal 28, pp 103 - 112
- Crawford CB, Jitno H, Byrne PM (1994) The influence of lateral spreading on settlements beneath a fill. Canadian geotechnical journal 31, pp 145 - 150
- Cuevas JA (1936) The floating foundation of the new building for the National Lottery of Mexico: an actual size study of the deformations of flocculent structural deep soil. Proc. 1st ICSMFE, Harvard, Massachusetts
- Dames and Moore (1975) Atlantic generating station, engineering properties of foundation soils. AGS-PSAR Amendment 19
- Das BM (1983) Advanced soil mechanics. Hemisphere Publishing corporation, 2nd edn
- Das BM (1987) Theoretical foundation engineering. Elsevier, Amsterdam
- Das BM (1997) Advanced soil mechanics. Vol. 2, Taylor and Francis
- Day PW (1994) Factors influencing the movement of retaining structures. Proc. 8th ICSMFE, New Delhi, pp 109 - 114
- Davis EH, Poulos HG (1972) Rate of settlement under three-dimensional conditions. Géotechnique 22-2, pp 95 – 114
- De Beer E (1963) Scale effect in the transposition of the results of deep sounding tests on ultimate bearing capacity of piles and caisson foundations. Geotechnique 13, p 39

- De Beer E (1971-1972) Méthodes de déduction de la capacité portante d'un pieu à partir des résultats des essais de pénétration. Annales des Travaux Publics de Belgique. Brussels. No. 4 (pp 191 -268). 5 (pp 321 - 353). 6 (pp 351 - 405)
- De Beer E (1986) Verstärkung von Stahlpfählen. Beiträge zum Symposium Pfahlgründungen. Institut für Grundbau. Boden- und Felsmechanik der TH Darmstadt, pp 51 - 58
- Décourt L, Niyama S (1994) Predicted and measured behaviour of displacement piles in residual soils. XIII ICSMFE. New Delhi. India, pp 477 - 486
- DeLory FA, Lai HW (1971) Variation in undrained shearing strength by semiconfined tests. Canadian Geotechnical Journal 8, pp 538 - 545
- Desai CS (1978) Effects of driving and subsequent consolidation on behaviour of driven piles. International Journal for Numerical and Analytical Methods in Geomechanics. Vol. 2, pp 283 - 301
- DGGT Working group 2.1 (1998) Recommendations for static and dynamic pile load tests
- DGGT Deutsche Gesellschaft für Geotechnik e.V. (2002) Merkblatt für die Herstellung, Bemessung und Qualitätssicherung von Stabilisierungssäulen zur Untergrundverbesserung, Teil I – CSV - Verfahren
- DiBt-DGGT-DAfStB (2002) Guidelines for the design; dimensioning and construction of combined pile-raft-foundations (CPR-guideline). Berlin: Ernst & Sohn
- DiMaggio JA (1978) Stone columns for highway construction. U.S. Department of Transport, Federal Highway Administration, Technical Report No. FHWA-DP-46-1
- Döbbelin J, Rizkallah V (1996) Schadensvermeidung bei Baugrubensicherungen. Institut für Bauschadensforschung e.V.. Hannover. Heft 13
- Drucker DC, Gibson EE, Henkel DJ (1957) Soil mechanics and work hardening theories of plasticity. Trans. ASCE 122, pp 338 - 346
- Drucker DC (1964) Concepts of path independence and material stability for soils. Brown University
- Dubrovsky MP, Poizner MB, Yakovlev PI, Taran VM, Omelchenko YuM, Bibichkov AG, Shtoda AN (1997) Determination of soil lateral pressure loads on retaining wall taking into consideration its displacements and deformation. Proc. 14th ICSMFE, Hamburg, pp 795 - 798
- Dulácska E (1992) The structures, soil settlement effects on buildings, developments in geotechnical engineering. Elsevier, Amsterdam
- Duncan JM, Seed HB (1966) Anisotropy and stress reorientation in clay. Journal of Soil Mechanics and Foundation Division, ASCE 92-SM5, pp 21 - 50
- Duncan JM, Chang CY (1970) Non-linear analysis of stress and strain in soils. Journal of the Soil Mechanics and Foundation Division, ASCE 96-SM5, pp 1629 - 1653
- Duncan JM (1993) Limitations of conventional analysis of consolidation settlement. Journal of Geotechnical Engineering 119-9, pp 1333 – 1359
- Duncan JM, Bentler DJ (1998) Evolution of deep excavation technology. International Conference on Soil-Structure Interaction in Urban Civil Engineering, Darmstadt Geotechnics, Darmstadt, pp 139 – 150
- EAB (1994) Empfehlungen des Arbeitskreis „Baugruben“ der Deutschen Gesellschaft für Geotechnik. 3rd edn, Ernst & Sohn, Berlin
- Eden WJ (1970) Panel discussion on sampling of sensitive clays. ASTM, STP 483, pp 192 - 193
- Eden WJ (1971) Sample trial in overconsolidated sensitive clay. In Sampling of soil and rock, American Society for Testing and Materials, Special Technical Publication 483, pp 132 - 142
- Eden WJ, Law KT (1980) Comparison of undrained shear strength results obtained by different test methods in soft clays. Canadian Geotechnical Journal 17, pp 369 - 381

- Egorov KE, Konovalov PA, Kitaykina OV, Salnikov LF, Zinov'yev AV (1977) Soil deformation under circular footing. Proc. 9th ICSMFE, Tokyo, pp 489 – 492
- Eigenbrod KD (1998) Capacity of steel piles in silty soils under repeated loading. Proc. 51st Canadian Geotechnical Conference. Vol.2. Ed-monton, pp 359 - 365
- Eigenbrod KD, Hanke R, Basheer MAJ (2001) Interaction between end bearing and shaft-resistance of piles. Proceeding of 54th Canadian Geotechnical Conference. Session 9. Calgary
- Ellstein A (1980) El pilote penetrante o P3. Memoria de la reunión Consunta Consulores-Constructores Cimentaciones pronfundas. Sociedad Mexicana de Mecánica de suelos, Mexico
- El-Mossallamy Y (1996) Ein Berechnungsmodell zum Tragverhalten der Kombinierten Pfahl-Plattengründung. Mitteilungen des Institutes und der Versuchsanstalt für Geotechnik der Technischen Hochschule Darmstadt, Heft 36
- Endo M et al. (1969) Negative skin friction acting on steel pipe piles in clay. Proceedings of the 7th International Conference on Soil Mechanics and Foundation Engineering. Vol. 2, pp 85-92
- EVB (1993) Empfehlungen "Verformungen des Baugrundes bei baulichen Anlagen"—EVB: Arbeitskreis "Berechnungsverfahren" der Deutschen Gesellschaft für Erd- und Grundbau e.V., Ernst & Sohn, Berlin
- Evgin, Eisenstein (1985) Performance of an elastoplastic model. Canadian Geotechnical Journal 22, pp 177 - 185
- Fang H-Y (1991) Foundation engineering handbook. 2nd edn., Chapman & Hall, New York
- Feda J, Havlicek J, Seycek J, Skopek J (1977) Active zone beneath foundations. Proceeding of the 9th ICSMFE, Tokyo, pp 505 - 510
- Fellenius J (1927) Erdstatische Berechnungen. Ernst & Sohn, Berlin
- Fellenius BH (1971) Negative skin friction on long piles driven in clay. Swedish Geotechnical Institute. Proceedings No. 25
- Fellenius BH (1972) Down-drag on piles in clay due to negative skin friction. Canadian Geo-technical Journal, pp 323 - 337
- Fellenius BH (1975) Test loading of piles and new proof testing procedure. Journal Geot. Eng. Div.. ASCE (101). GT 9, p 855
- Fellenius BH, Altaee A, Kulesza R, Hayes J (1999) O-cell testing and FE analyses of a 28 m deep barrette in Manila. Phillipines. American Society of Civil Engineers. ASCE Journal of Geotechnical and Environmental Engineering. Vol.125. No.7. pp.566-575
- Fellenius BH (2001) The O-Cell – an innovative engineering Tool. Geotechnical News 12, pp 55 - 59
- Fensterbusch C (1964) Vitruv, Zehn Bücher über Architektur. Wissenschaftliche Buchgesellschaft, Darmstadt
- FGSV (Forschungsgesellschaft f. Straßen- und Verkehrswesen) (1979) Merkblatt für die Untergrundverbesserung durch Tiefenrüttler. FGSV, Köln
- FGSV (Forschungsgesellschaft f. Straßen- und Verkehrswesen) (1988) AG Erd- und Grundbau. Merkblatt über Straßen auf wenig tragfähigem Untergrund, Eigenverlag, Köln,
- FGSV (Forschungsgesellschaft f. Straßen- und Verkehrswesen) (1994) Merkblatt über den Einfluss der Hinterfüllung auf Bauwerke
- FHWA-RD-99-138 (2000) An introduction to the deep soil mixing methods as used in geotechnical applications. Prepared by Geosystems (D.A. Bruce) for US Department of Transportation, Federal Highway Administration, p 143
- Findlay JD, Brooks NJ, Mure JN, Heron W (1997) Design of axially loaded piles – United Kingdom practice; design of axially loaded piles – European practice. De Cock, Le grand (eds). Balkema, Rotterdam, pp 353 - 376

- Fischer D (2006) Interaktion zwischen Baugrund und Gebäude – Zulässige Setzungsdifferenzen und Beanspruchungen der Gründung. Schriftenreihe Geotechnik, Universität Kassel Heft 20 (to be published)
- Fjeld S (1963) Settlement damage to a concrete framed structure. Proc. 3rd European Conf. On SMFE, Wiesbaden, pp 391 – 399
- Fleming WGK, Weltman AJ, Randolph MF, Elson WK (1992) Piling engineering; 2nd edition. Halsted Press. New York
- Flores G (1948) Level control in buildings by means of adjustable piling. Proc. 2nd Int. Conf. on Soil Mech. and Foundation Eng., Rotterdam, Vol. IV, p 152
- Franke E (1980) Überlegungen zu Bewertungskriterien für zulässige Setzungsdifferenzen. Deutsche Gesellschaft für Erd- und Grundbau. Geotechnik 3, Heft 2
- Franke E (1980) Anwendbarkeit der undränierten Scherfestigkeit im Vergleich zur Anwendbarkeit der effektiven Scherparameter. Baugrundtagung, DGQT, pp 297 - 319
- Freiseder MG (1998) Ein Beitrag zur numerischen Berechnungen von tiefen Baugruben in weichen Böden. Gruppe Geotechnik Graz, Institute für Bodenmechanik und Grundbau, Heft 3
- Fröhlich OK (1934) Druckverteilung im Baugrund. Julius Springer, Wien
- Fujita K (1994) Soft ground tunnelling and buried structures. Proc. 8th ICSMFE, New Delhi, pp 89 – 107
- Gant EV (1959) Measurement of forces produced in piles by settlement of adjacent soil. Highway Research Board. Bulletin 173. Analysis of Soil Foundation Studies, pp 20-37
- Garlanger JE (1972) The consolidation of soils exhibiting creep under constant effective stress. Géotechnique 22-1 , pp 71 – 78
- Garlanger JE (1974) Measurement of pile downdrag beneath bridge abutment. Highway Research Board. Transportation Research Record. No. 517. pp. 61-69
- GCO (1982) Guide to retaining wall design. Geoguide 1, Geotechnical control Office, Engineering Development Department, Hong Kong
- Gebreselassie B (2003) Experimental, analytical and numerical investigations of excavations in normally consolidated soft soils. P.hD. thesis, University of Kassel.
- Gebreselassie B, Kempfert H-G, Raithel M (2003) Correlation of cone resistance with undrained strength of some very soft to hard cohesive clays. Proc. of the 6th Int. Symposium on Field Measurements in Geomechanics. Oslo, Norway
- Gens A, Carol I, Alonso EE (1989) An interface element formulation for the analysis of soil-reinforcement interaction. Computers and Geotechnics. Elsevier Science Publishers Ltd, England, pp 133 - 151
- Ghionna V, Jamiolkowski M (1981) Colonne di ghiaia, X Ciclo di conferenze dedicate ai problemi di meccanica dei terreni e ingegneria delle fondazioni metodi di miglioramento dei terreni. Politecnico di Torino Ingegneria, atti dell'istituto di scienza delle costruzioni, n°507
- Girault P (1964) A new type of pile foundation. Proc. Conference On Deep Foundations, Mexican Society of soil Mechanics, Vol. I, Mexico
- Goldscheider M (1986) Bodenmechanische Untersuchungen der historischen Gründungen am Salmansweilerhof in Konstanz. In: Erhaltung historischer bedeutsamer Bauwerke, Sonderforschungsbericht 315, Ernst & Sohn, Berlin, pp 331 - 352
- Goldscheider M, Scherzinger T (1991) Laboratory tests on the soft clayed soil of an old city. Deformation of Soils & Displacement of Structures, VI, Italy
- Goldscheider M (1993) Historische Gründungen: Bauweisen, Beurteilung, Erhaltung und Instandsetzung. Geotechnik 16,pp 178 - 192
- Goughnour RR, Bayuk AA (1979) Analysis of stone column-soil matrix interaction under vertical load. Colloque Int. sur le Renforcement des Sols, Vol.1, Paris, pp 271 - 277

- Gourvenec SM, Powrie W (1999) Three-dimensional finite element analysis of diaphragm wall installation. *Geotechnique* 49-6, pp 801 - 823
- Graham J, Noonan ML, Lew KV (1983) Yield states and stress strain relationships in natural plastic clay. *Canadian Geotechnical Journal* 20, pp 502 - 516
- Graham J, Kwok CK, Ambrosie RW (1987) Stress release, undrained storage and reconsolidation in simulated underwater clay. *Can. Geotech. J.* pp 279 - 288
- Grant K (1974) Laterites, ferricretes, bauxites and silcretes. Proceedings of the 2nd Int. Congress of the Int. Association of Engineering Geology, Sao Paulo, Brazil, Vol. 1
- Grant R, Christian JT, Vanmarcke EH (1974) Differential settlement of buildings. *Journal of the Geotechnical Engineering Division GT9*, pp 973 - 991
- Graßhoff H (1954) Der Einfluss der Schichtstärke auf die Sohldruckverteilung und die Biegemomente einer kreisförmigen Gründungsplatte. *Bautechnik* 31, Heft 10
- Graßhoff H (1955) Setzungsberechnungen starrer Fundamente. *Der Bauingenieur* 30-2, pp 53 - 54
- Graßhoff H (1978) Einflusslinien für Flächengründungen. Ernst & Sohn, Berlin
- Graßhoff H, Kany M (1982) Berechnung von Flächengründungen. In: Smolczyk U (eds) *Grundbau-Taschenbuch*, Vol. 2, 3rd edn, Wilhelm Ernst & Sohn, pp 47-155
- Graßhoff H, Siedek, Floss (1982) *Handbuch Erd- und Grundbau*. Vol. 1, Werner, Düsseldorf
- Grigorian AA et al. (1975) Effect of negative skin friction on the behaviour of piles in macroporous and weak soils. Proc. of the 1st Baltic Conf. on Soil Mechanics and Foundation Engineering. Gdansk. Vol. 3, pp 61-71
- Gruber FJ (1995) Verhalten einer Stopfverdichtung unter einem Straßendamm. Bundesministerium für wirtschaftliche Angelegenheiten, Straßenforschung Heft 448, Wien
- Gudehus G (1980) Materialverhalten von Sand. *Bauingenieur* 55, p 351
- Gudehus G (1981) Bodenmechanik. Ferdinand Enke, Stuttgart
- Gudehus G (1985) Requirement to constitutive relations for soils. In: Bazant Z (eds) *Mechanics of Geomaterials*, John Wiley & Sons Ltd., pp 47 - 64
- Gudehus G, Meißner H, Orth W, Schwarz W (1987) Geotechnische Probleme bei der Gründung des Postamtes Konstanz. *Geotechnik* 3, pp 105 - 122
- Gudehus G, Weißenbach A (1995) Limit state design of structural parts at and in the ground. *Ground Engineering*, September 1996, pp 42 - 45
- Gudehus G (2001) Standsicherheit und Gebrauchstauglichkeit bei muddeartigem Baugrund. (Manuskript)
- Gudehus G (2002) Constitutive laws for soils from a physical viewpoint. Earth pressure determination. In: Smolczyk (ed), *Geotechnical Engineering Handbook. Fundamentals*, Vol. 1, Ernst & Sohn, Berlin, pp 207 - 258, 407 - 436
- Gunn MJA, Clayton CRI (1992) Installation effects and their importance in the design of earth-retaining structures. *Geotechnique* 42-1, pp 137 - 141
- Gunn MJ, Satkunanathan A, Clayton CRI (1993) Finite element modelling of installation effects. *Retaining Structures*, Thomas Telford, London, pp 46 - 55
- Gwizdala K (1997) Polish design methods for single axially loaded piles; Design of Axially Loaded Piles – European Practice. De Cock & Legrand (eds). Balkema; Rotterdam, pp 291 - 306
- Hanisch J, Katzenbach R, König G (2002) Kombinierte Pfahl-Plattengründungen
- Hansbo S (1957) A new approach to the determination of the shear strength of clay by the fall - cone test. Royal Swedish Geotechnical Institute 4
- Hansbo S (1984) Foundation on friction creep piles in soft soils. International Conference on Case Histories in Geotechnical Engineering. St. Louis, Mi. USA, pp 913 - 922

- Hartung M (1993) Qualitätssicherung bei der Pfahlherstellung. Pfahl-Symposium. Institut für Grundbau und Bodenmechanik TU Braunschweig. Heft 41, pp 261 - 279
- Hayashi S, Yamanouchi T (1986) Plasticity modelling and its application to geomechanics. Balasubramaniam et al (eds) Proc. Intl. Symposium on Recent Developments in Laboratory and Field Testing and Analysis of Geotechnical Problems, A.A. Balkema, pp 435 - 450
- Head KH (1986) Manual of soil laboratory testing. ELE International Limited, Pentech Press, London
- Heijnen WJ (1985) Design of foundations and earthworks. The Netherlands Commemorative Volume. 11th International Conference on Soil Mechanics and Foundation Engineering. San Francisco, pp 53 - 70
- Heil HM, Huder J, Amann P (1997) Determination of shear strength of soft lacustrine clays. Proc. 9th ICSMFE, pp 507 - 510
- Henkel DJ (1971) The relevance of laboratory measured parameters in field studies. Proceedings of Rosco Memorial Symposium, Foulis, pp 669 - 675
- Herle I (1997) Hypoplastizität und Granulometrie einfacher Korngüste. Veröffentlichung des Inst. f. Bodenmechanik und Felsmechanik der Universität Karlsruhe, Heft 142
- Herrero O (1983) Universal compression index equation. ASCE Journal of Geotechnical Division 109-GT 10, pp 1349 - 1354
- Hettler A (1990) Der Duktilpfahl. Bauingenieur 65, pp 319 - 324
- Hettler A, Leibnitz S, Biehl F (2002) Zur Kurzzeitstandsicherheit bei Baugrubenverbaukonstruktionen in weichen Böden. Bautechnik, Heft 9, pp 612 - 619
- Hettler A, Stoll C (2004) Nachweis des Aufbruchs der Baugrubensohle nach der neuen DIN 1054:2003-01. Bautechnik 81, Heft 7, pp 562 - 568
- Hilmer K (1991) Schäden im Gründungsbereich. Ernst & Sohn, Berlin
- Holeyman A (1997) Design of axially loaded piles – Belgian practice; design of axially loaded piles – European practice. De Cock & Legrand (eds); Balkema. Rotterdam, pp 57 - 82
- Holloway DM, Clough GW, Vesic AS (1978) The effect of residual driving stresses on pile performance under axial loads. Proc. Of the 10th annual Offshore Technology Conference. OTC 3306. Houston, pp 2225 - 2236
- Holm G (2001) Deep mixing. Soft Ground Technology, Geotechnical Special Publication Number 112. JL Hanson, RJ Termaat (eds), ASCE, pp 105 - 122
- Holm G (2002) Deep mixing – research in Europe. Deep Mixing Work Shop 2002 in Tokyo
- Horpibulsuk S, Miura N, Nagaraj TS, Koga H (2002) Improvement of soft marine clays by deep mixing technique. Proc. 12th Int. Offshore and Polar Eng. Conf., Kitakyushu, Japan, pp 584 - 591
- Hough BK (1957) Basic soil engineering. Ronald Press Company, New York, pp 112 - 115
- Hu YF (2000) Zum Verformungsverhalten von wassergesättigten bindigen Böden unter zyklischer Belastung. Schriftenreihe Geotechnik, Universität Kassel, Heft 8
- Hvorslev MJ (1937) Über die Festigkeits-Eigenschaften gestörter bindiger Böden. Ingenvorvidenshadelige Skrifter, No. 45, Danmarks Naturvidenshabelige Samfund, Kobenhavn, p 159
- Hvorslev MJ (1949) Subsurface exploration and sampling of soils for civil engineering purposes. Waterways Experiment Station, Vicksburg, Mississippi, p 521
- Imai G (1995) Analytical examinations of the foundations to formulate consolidation phenomena with inherent time-dependence. Proc. Intl. Symposium on Compression and Consolidation of Clayey Solis, Hiroshima, pp 891 - 935
- Indraratna B et al. (1992) Development of negative skin friction on driven piles in soft Bangkok clay. Canadian Geotechnical Journal 29, pp 393 - 404

- ISSMFE Subcommittee on Field an Laboratory Testing (1985) Axial pile loading test – part 1: static loading. Geotechnical Testing Journal, pp 79 - 90
- Jaki J (1944) The coefficient of earth pressure at rest. Journal of Society of Hungarian Architects and Engineers, Budapest, Hungary, pp 355 - 358
- James RG, Brandsby PL (1971) A velocity field for some passive earth pressure problems. Geotechnique 21-1, pp 61 - 83
- Jamiolkowski M, Ladd CC, Germaine JT, Lancellotta R (1985) New developments in field and laboratory testing of soils. Proc. 11th ICSMFE, San Francisco, pp 57 - 153
- Janbu N (1957) Earth pressure and bearing capacity calculations by generalised procedure of slices. Proc. 9th ICSMFE, pp 207 - 212
- Janbu N (1977) Slopes and excavations in normally and lightly overconsolidated clays. Proc. 9th ICSMFE, Tokyo, pp 549 - 566
- Janbu N, Tokheim O, Sennwset K (1981) Consolidation tests with continuous loading. Proc. of the 10th ICSMFE, Stockholm, Vol. 1, pp 645 - 654
- Jardine JR, Chow FC (1996) New design methods for offshore piles. MTD Publication 96/103. Marine Technology Directorate, London
- Johannessen IJ, Bjerrum L (1965) Measurement of the compression of a steel pile due to settlement of the surrounding clay. Proc. of the 6th International Conference on Soil Mechanics and Foundation Engineering. 1965. Vol. 2, pp 261 - 264
- Jörß O (1998) Erfahrungen bei der Ermittlung von c_u -Werten mit der Hilfe von Drucksondierungen in bindigen Böden. Geotechnik 21-1, pp 26 - 27
- Joyce MD (1982) Site investigation practice. E & FN Spon, London
- Kany M (1974) Berechnungen von Flächengründungen. 2nd edn, Ernst & Sohn, Berlin
- Katzenbach R, Floss R, Schwarz W (1992) Neues Baukonzept zur verformungsarmen Herstellung tiefer Baugruben in weichem Seeton. Vorträge zur Baugrundtagung 1992 in Dresden. Deutsche Gesellschaft für Geotechnik e.V., pp 13 - 31
- Katzenbach R, Arslan U (1999) Vorträge zum Darmstädter Fortbildungsseminar „Kombinierte Pfahl-Plattengründungen (KPP)“, 3. Dezember 1999. Mitteilungen des Institutes und der Versuchsanstalt für Geotechnik der TU Darmstadt, Heft 47
- Kempfert H-G (1986) Gründung auf Verpresspfählen in weichen Sedimenten. Geotechnik, (2), pp 73 - 78
- Kempfert + Partner (1991-1993) Geotechnische Berichte und Aktenvermerk für das Bauvorhaben Wohnanlage Markgrafenstrasse in Konstanz. nicht veröffentlicht.
- Kempfert + Partner (1994-1998) Geotechnische Berichte und Meßprotokolle für das Wohn- und Geschäftshaus Sigismundstrasse 9 in Konstanz. nicht veröffentlicht.
- Kempfert H-G, Stadel M (1994) Verfahren zur Berechnung und messtechnischen Überwachung von Baugruben in normalkonsolidierten weichen tonigen Böden. Bericht zum F + E- Projekt. Manuscript
- Kempfert H-G (1997) Berechnung und Ausführung von Baugruben im Seeton. 3 Stuttgarter Geotechnik-Symposium, Baugruben in Locker- und Festgestein, pp 209 - 225
- Kempfert H-G, Stadel M (1997) Berechnungsgrundlagen für Baugruben in normalkonsolidierten weichen bindigen Böden. Bauingenieur 72, Springer-VDI, pp 207 - 214
- Kempfert H-G, Gebreselassie B (1999) Effect of anchor installation on settlement of nearby structures in soft soils. Proc. Int'l. Symposium on Geotechnical Aspects of Underground Construction in Soft Ground - IS-Tokyo'99, Tokyo, pp 665 - 670
- Kempfert H-G, Gebreselassie B (2000) Ergebnisse einer numerischen Vergleichsberechnungen von Mitgliedern des DGGT - Arbeitskreises „Baugruben“ an einer zweifach ausgesteiften Baugrube. In: Schweiger HF (eds) Verformungsprognose für tiefe Baugruben, AK 1.6 „Numerik in der Geotechnik“, pp 68 - 84

- Kempfert H-G (2001) Abschnitt 3.2 (1-7) „Pfahlgründungen“; Grundbautaschenbuch. 6th edn. Vol. 3. Ernst & Sohn, Berlin
- Kempfert H-G, Böhm F, Soumaya B, Hardt TH (2001) Verformungsanalysen von Flachgründungen in normalkonsolidierten bindigen Böden und Wirksamkeit von Stabilisierungsmaßnahmen mit schwimmenden Verpresspfählen auf der Grundlage von vorliegenden Setzungsmessungen. Zwischenbericht zur DFG. Manuskript
- Kempfert H-G, Gebreselassie B (2002) Zur Diskussion von dränierten oder undränierten Randbedingungen bei Baugruben in weichen Böden, Bautechnik 9, pp 603 – 611
- Kempfert H-G (2003) Ground improvement methods with spezial emphasis on column-type techniques. Int. Workshop on Geotechnics of Soft Soils-Theory and Practice. Vermeer, Schweiger, Karstunen & Cudny (eds). Noordwijkerhout, Netherlands, pp 101 - 112
- Kempfert H-G, Böhm F (2003) Experience with friction-micropiled-raft foundation on soft soils. Proc. of the European Conference on Soil Mech. and Geot. Engineering
- Kempfert H-G, Eigenbrod KD, Smolczyk U (2003) Chapter 3.2 “ Pile foundations”. In: Geotechnical Engineering Handbook. Vol. 3. Ernst & Sohn (Wiley Comp.), pp 83 - 227
- Kempfert H-G, Göbel C, Alexiew D, Heitz C (2004) German recommendations for reinforced embankments on pile similar elements. 3rd European Geosynthetic Conference, DGQT (German Geotechnical Society), Vol. 1, pp 279 - 285
- Kempfert H-G (2005) Kommentar zum Abschnitt Pfahlgründungen. In: Kommentar zur DIN 1054:2005-01 (under preparation)
- Kempfert H-G, Raithel M (2005) Foundation systems with encased columns and reinforced bearing layers. Indraratna, Jian Chu (eds), Ground improvement, Vol. 3
- Kézdi A (1964) Bodenmechanik, Vol. 2. Verlag für Bauwesen, Berlin
- Kézdi A (1969) Handbuch der Bodenmechanik. Bodenphysik, Vol. 1. VEB, Berlin
- Kézdi A (1970) Handbuch der Bodenmechanik. Bodenmechanik im Erd-, Grund- und Strassenbau, Vol.2. VEB, Berlin
- Kirkgard MN, Lade PV (1993) Anisotropic three - dimensional behaviour of a normally consolidated clay. Canadian Geotechnical Journal 30, pp 848 - 858
- Kishida H et al. (1976) Protusion of piles out of ground surface due to ground subsidence. Proc. of the 5th Int. Conference on Soil Mechanics and Foundation Engineering. Budapest, pp 337 - 352
- Klob B (1992) Eindimensionale Kompression und Konsolidation und darauf basierende Verfahren zur Setzungsprognose. Institut für Bodenmechanik und Felsmechanik der Universität Fridericiana in Karlsruhe, Heft 128
- Kolymbas D (1988) A generalized hypoplastic constitutive equation. Proc. 11th Int. Conf. on Soil Mechanics and Foundation Engineering, San Francisco 1985, Vol. 5, 2626, published by Balkema, 1988
- Kolymbas D (1989) Pfahlgründungen. Springer, Berlin
- Kolymbas D, Herle I, v. Wolffersdorff P-A (1995) Hypoplastic constitutive equation with back stress. Int. J. f. Analytical and Numerical Methods in Geomechanics, 19, pp 415 - 436
- Kolymbas D (2000) Introduction to Hypoplasticity. Advances in Geotechnical Engineering and Tunneling. Balkema, Rotterdam
- Kondner RL (1963) Hyperbolic stress - strain response cohesive soils. ASCE Journal of Soil Mechanics and Foundation Division 89-SM1, pp 115 - 143
- Kondner RL, Zelasko JS (1963) A hyperbolic stress-strain formulation for sands. Proc. 2nd Pan-American Conference on Soil Mechanics and Foundations Engineering, Brazil, Vol. I, pp 289 - 324

- Koppula SD (1981) Stastical estimation of compression index. ASTM Geotechnical Testing Journal 4-2, pp 68 – 73
- Koreck HW (1986) Zyklische Axialbelastung. Beiträge zum Symposium Pfahlgründungen. Institut für Grundbau. Boden- und Felsmechanik der TH Darmstadt, pp 139 - 144
- Kraft LM (1990) Computing axial pile capacity in sands for offshore conditions. Marine Technology. Vol. 9, pp 61 - 92
- Krieg S (2000) Viskoses Bodenverhalten von Mudden, Seeton und Klei. Veröffentlichungen des Institutes für Bodenmechanik und Felsmechanik der Universität Karlsruhe, Heft 150
- Kulhawy FH, Mayne PH (1990) Manuel on estimating soil properties for foundation design. Electric Power Research Institute, EPRI
- Ladd CC (1964) Stress - strain modulus of clay in undrained shear. ASCE Journal of Soil Mechanics and Foundation Division 90-SM5, pp 103 - 132
- Ladd CC, Bovee RB, Edgers L, Rixner JJ (1971) Consolidated-undrained plane strain shear tests on Boston blue clay. Research Report R71 - 13, No. 273, No. 284, Department of Civil Engineering, Massachusetts Institute of Technology, Cambridge
- Ladd CC, Edgers L (1972) Consolidated-undrained direct-simple shear tests on saturated clays. Res. Report R72-82, No. 284, Dept. of Civil Eng., Mass. Inst. of Technology, Cambridge, p 354
- Ladd CC, Foott R, Ishihara K, Schlosser F, Poulos HG (1977) Stress - deformation and strength characteristics. Proc. IX ICSMFE, Tokyo, pp 421 - 494
- Ladd CC, Assouz AS (1983) Stress history and strength of stiff offshore clays. Proc. of the Conference on Geotechnical Practice in Offshore Eng., Austin, Texas, pp 65 - 80
- Ladd PV, Duncan J-M (1976) Stress - path dependant behaviour of cohesionless soil. ASCE Journal of Geotechnical Engineering Division 102-GT1, pp 51 - 68
- Ladd PV (1977) Elasto-plastic stress - strain theory for cohesionless soil with curved yield surfaces. International Journal of Solids and structures 13, pp 1019 - 1035
- Ladd RS (1974) Specimen preparation and liquefaction of sand. JGED, ASCE, Vol. 100, No. SM10, pp 1180 - 1184
- Lafleur J, Silvestri V, Asselin R, Soulle M (1988) Behaviour of test excavation in soft Champlain sea clay. Canadian Geotechnical Journal 25, pp 705 - 715
- Lambe TW (1967) Stress - path method. ASCE Journal of Soil Mechanics and Foundation Engineering Division 93, pp 309 - 331
- Lambe TW, Whitman RV (1969) Soil mechanics. John Wiley & Sons, New York
- Lambe TW (1970) Braced excavation. Proc. of the 1970 Speciality Conference on Lateral Stresses in the Ground and Design of Earth-Retaining Structures, ASCE, Cornell University, June, pp 149 - 218
- Lambe TW (1973) Predictions in soil engineering. Geotechnique, Vol. 23, pp 151 - 202
- Lambe TW (1979) Braced excavations. Proc. of the 1970 Speciality Conference on Lateral Stresses, ASCE, Cornell University, pp 149 - 218
- Lambe TW, Mass WA (1979) Stress-path method. ASCE Journal of Geotechnical Engineering Division 105, pp 727 - 738
- La Rochelle P, Lefebvre G (1971) Sampling disturbance in Champlain clays. ASTM, STP 483, pp 143 - 163
- La Rochelle P, Sarraillh J, Tavenas F, Roy M, Leroueil S (1981) Causes of sampling disturbance and design of a new sampler for sensitive soils. Can. Geotech. Journal, Vol. 18, pp 52 - 66
- Larsson R (1977) Basic behaviour of Scandinavian soft clays. Swedish Geotechnical Institute, Linköping, Report No. 4
- Larsson R (1980) Undrained shear strength in stability calculation of embankments on soft clays. Canadian Geotechnical Journal 17, pp 591 – 602

- Lebegue MY (1964) Etude experimental des efforts d'arrachage et de frottement négatif sur les pieux en milieu pulvérant. Annales de l'Institut Technique du Batiment et des Travaux Publics Sols et Foundations (42)
- Lee YN, Jin BI (1979) Measurement and prediction of K_0 . Journal of Korean Society of Civil Engineering, pp 226 – 233
- Lefebvre G, Poulin C (1979) A new method of sampling in sensitive clay. Can. Geotech. Journal, Vol. 16, pp 226 – 233
- Lefebvre G, Langlois P, Lupien C (1984) Laboratory testing and in situ behaviour of peat as embankment foundation. Can. Geotech. Journal, Vol. 21, pp 322 - 337
- Lehane BM (1997) Design of axially loaded piles – Irish practice; Design of Axially Loaded Piles – European Practice. De Cock & Legrand (eds). Balkema; Rotterdam, pp 203-218
- Lehr H, Mattle B, Jaeger J (1993) Nichtlineare Setzungsanalyse einer tiefen Baugruben mit anstehendem Grundwasser im Salzburger Seeton. Technische Universität Graz, Heft 10, pp 78 - 93
- Leinenkugel HJ (1976) Deformations- und Festigkeitsverhalten bindiger Erdstoff. Experimentelle Ergebnisse und ihre physikalische Deutung, Veröffentlichungen des Institutes für Bodenmechanik und Felsmechanik der Universität Karlsruhe, Heft 66
- Leonards G A (1962) Foundation engineering. McGraw-Hill Book co., New York
- Leroueil S, Tavenas F (1981) Pitfalls of back-analyses. Proc. X ICSMFE, Stockholm, Vol.1
- Leroueil S, Tavenas F, Le Bihan JP (1983) Propriétés caractéristiques des argiles de l'est du Canada Canadian Geotechnical Journal 20 , pp 681 - 705
- Leroueil S, Kabbaj M, Tavenas F, Bouchard R (1985) Stress-strain-rate relation for the compressibility of sensitive natural clays. Géotechnique 35-2, pp 159 - 180
- Leroueil S, Tavenas F, Locat J (1985) Discussion of correlation between index tests and the properties of remolded clays. ed. by WD Carrier III and JF Beckman, Géotechnique 35-2, pp 223 - 226
- Leroueil S (1988) Recent development in consolidation of natural clay. Canadian Geotechnical Journal 25, pp 85 - 107
- Leroueil S, Vaughan P R (1990) The general and congruent effects of structure in natural soils and weak rocks. Géotechnique 40-3, pp 467 - 488
- Leroueil S (1996) Compressibility of clay fundamental and practical aspects. Journal of the Geotechnical Engineering Division 122, pp 534 - 543
- Leussink H (1954) Die Genauigkeit von Setzungsberechnungen. Vorträge der Baugrundtagung 1953 in Hannover. Berlin 1954
- Leussink H (1963, 1967) Ergebnisse von Setzungsmessungen an Hochbauten. Veröffentlichung des Institutes für Bodenmechanik und Grundbau der Technischen Universität Karlsruhe, Heft 13 und 25
- Lim K, Hosoi T, Ishii T (1989) Behaviour of diaphragm walls and settlements in marine clay. Proc. 9th Asian regional Conference on Soil Mechanics and Foundation Engineering, Bangkok, pp 331 – 334
- Linder WR (1977) Zum Eindring- und Tragverhalten von Pfählen in Sand. Diss. TU Berlin. Berlin
- Little JA et al. (1989) The development of shaft adhesion with onset of negative skin friction for a fixed base model pile. Proc. of the 2nd Int. Conference on Foundations and Tunnels. Vol. 1, pp 111 - 117
- Little JA (1994) Downdrag on piles: Review and recent experimentation. Vertical and horizontal deformations of foundations and embankments. Proc. of Settlement 94', pp 1805 - 1825
- Lo KY (1965) Stability of slopes in anisotropic soils. ASCE Journal of Soil Mechanics and Foundation Division91-SM4

- Lo KY, Milligan V (1967) Shear strength properties of two stratified clays. ASCE Journal of Soil Mechanics and Foundation Division 93-SM1, pp 1 - 15
- Lo KY, Morin JP (1972) Strength anisotropy and time effects of two sensitive clays. Canadian Geotechnical Journal 9, pp 261 - 277
- Lord JA (1967) Stresses and strains in an earth pressure problem. Ph.D. Thesis, Cambridge University
- Lunne T, Myrvoll F, Kiekstad O (1982) Observed settlements of five North Sea gravity platforms. Norwegian Geotechnical Institute 139
- Lunne T, Robertson PK, Powell JJM (1997) Cone penetration testing. Blackie Academic & Professional, London
- MacLeod IA, Abu-El-Magd SA (1980) The behaviour of brick walls under conditions of settlement. Structural Engineer 58-9, pp 279 - 286
- Manai AI (1978) Finite element analysis of deep excavation behaviour. Thesis, presented in partial fulfilment of the Ph.D. Degree, Stanford University, Stanford, California
- Mandolini A (1997) Design of axially loaded piles – Italian practice; Design of axially loaded piles – European practice. De Cock & Legrand (eds). Balkema; Rotterdam, pp 219 - 242
- Magnan P, Felix B, Mieussens C, Costaz J, Florentin P (1979) Comparaison de quelques méthodes d'étude des tassements des ouvrages sur sols compressibles. Proc. of the 7th ICSMFE, Brighton, England, pp 31 - 41
- Maslov NN, Le Ba Lyong (1986) Some problems of the computation of clay soil consolidation. Soil Mechanics and Foundation Engineering 23, pp 251 - 258
- Mayer H, Rüsch H (1967) Bauschäden als Folge der Durchbiegung von Stahlbetonbauteilen. Deutscher Ausschuss für Stahlbeton, Ernst & Sohn, Berlin, Heft 19
- Mazurkiewicz (1975) Research works on pile behavior. Proc. 1st Baltic CSMFE. Gdansk
- McCarron WO, Chen WF (1987) A capped plasticity model applied to Boston blue clay. Canadian Geotechnical Journal 24-4, pp 630 – 644
- McClelland B (1972) Design of deep penetrating piles for ocean structures. Journal of the Geotechnical Engineering Division. ASCE (100). GT7, pp 705 -747
- McRostii GC, Burn KN, Mitchell RJ (1972) The performance of tied - back sheet piling in clay. Canadian Geotechnical Journal 9, pp 206 - 218
- Meißner H (2002) Baugruben Empfehlungen des Arbeitskreises 1.6 “Numerik in der Geotechnik“. Abschnitt 3, Geotechnik 25, pp 44 - 56
- Mesri G (1973) Coefficient of secondary compression. Journal of the Soil Mechanics and Foundations Division, ASCE, Vol. 99, No. SM1, pp 123 - 237
- Mesri G, Rokshar A (1974) Theory of consolidation for clay. Journal of the Geotechnical Engineering Division 100, pp 889 - 904
- Mesri G (1975) Discussion on new design procedure for stability of soft clays. ASCE, Journal fo the geotechnical Eingineering Division 101-GT4, pp 409 - 412
- Mesri G, Godlewski PM (1977) Time- and stress- compressibility interrelationship. ASCE, Journal of Geotechnical Engineering 103-GT 5, pp 417 - 430
- Mesri G, Choi YK (1985) Settlement analysis of embankments on soft clay. Journal of the Geotechnical Engineering Division 111-4, pp 441 - 464
- Mesri G, Choi YK (1985) The uniqueness of the end-of-primary (EOP) void ratio- effective stress relationship. Proceeding of the 11th ICSMFE, San Francisco, pp 587 - 590
- Mesri G, Castro A (1987) C_a/C_c concept and K_0 during secondary compression. Journal of the Geotechnical Engineering Division 113-3, pp 230 - 247
- Mesri G, Shahien M, Feng TW (1995) Compressibility parameters during primary consolidations. Proc. of the intl. Symposium on Compression and Consolidation of Clayey Soils, -IS-Hiroshima, ed. by Yoshikuni H., Kusakabe , pp 1021 - 1037.

- Mets M (1997) The bearing capacity of a single pile – experience in Estonia. Design of axially loaded piles – European practice. De Cock & Legrand (eds). Balkema; Rotterdam, pp 115 - 132
- Meyerhof GG (1953) Some recent foundation research and its application to design. The Structural Engineer 6, pp 151 – 167
- Meyerhof GG, Murdock LJ (1953) An investigation of the bearing capacity of some bored an driven piles in London clay. Geotechnique. Vol. 3. No. 7, pp 267 - 282
- Meyerhof GG (1959) Compaction of sands and bearing capacity of piles. Journ. Geot. Eng. Div.. ASCE (85). SM 6, p 1
- Meyerhof GG (1970) Safety factors in soil mechanics. Canadian Geotechnical Journal 7, pp 349 – 355
- Meyerhof GG (1976) Bearing capacity and settlement of pile foundations. Journal of the Geotechnical Engineering Division. ASCE (102). GT 3, pp 197-228
- Meyerhof GG (1982) Limit states design in geotechnical engineering. Structural Safety 1, pp 67 - 71
- Meyerhof GG (1984) Safety factors and limit states analysis in geotechnical engineering. Canadian Geotechnical Journal 21, pp 1 - 7
- Mitchell JK (1993) Fundamentals of soil behaviour. 2nd ed., John Wiley & Sons, Inc
- Mizuno E, Chen WF (1986) Plasticity modelling and its application to geomechanics. Proc. of the Int. Symposium on Recent Developments in Laboratory and Field Testing and Analysis of Geotechnical Problems - Bangkok, edited by Balasubramaniam et al., Balkema, Rotterdam, pp 391 – 426
- Mohan D et al. (1981) Negative drag on an instrumented pile – a field study. Proc. of the 8th Int. Conference on Soil Mechanics and Foundation Engineering. Vol. 2, pp 787 - 791
- Moormann C, Katzenbach R, Arslan U (2000) Numerische Untersuchungen zum räumlichen Trag- und Verformungsverhalten von tiefen Baugruben. In: Schweiger HF (eds) Verformungsprognose für tiefe Baugruben: AK 1.6 „Numerik in der Geotechnik“, pp 89 – 109
- Moormann C (2002) Trag- und Verformungsverhalten tiefer Baugruben in bindigen Böden unter besonderer Berücksichtigung der Baugrund – Tragwerk - und der Baugrund – Grundwasser – Interaktion. Mitteilungen des Institutes und der Versuchsanstalt für Geotechnik der TU Darmstadt, Heft 59
- Morgenstern NR, Tchalenko JS (1967b) Microscopic structures in kaolin subjected to direct shear. Geotechnique, Vol. 17, No. 4, pp 309 - 328
- Nagaraj TS (1983) Prediction of soil behaviour. Recent development in laboratory and field tests and analysis of geotechnical problems, ed. by Balasubramaniam A.S., Chandra S, Bergado DT, Bangkok, pp 337 - 360
- Nagaraj TS, Miura N (2001) Soft clay behaviour, analysis and assessment. Balkema, Rotterdam
- Nendza H (1982) Gründungen in Bergbaugebieten. In: Smoltczyk U (eds) Grundbau-Taschenbuch. Ernst & Sohn, Berlin
- Naylor DJ, Pande GN (1981) Finite elements in geotechnical engineering. Pineridge Press, Swansea
- Newson TA (1997) Modelling the yielding behaviour of natural soft clay. Proc. 14th ICSMFE, Hamburg, pp 381 - 386
- Ng CWW, Lings ML, Simpson B, Nash DFT (1995) An approximate analysis o fthe three dimensional effects of diaphragm wall installation. Geotechnique, Vol. 45, No. 3, pp 497 - 507
- Ng CWW, Rigby DB, Ng WL (1999) Observed performance of a short diaphragm wall panel. Geotechnique 49-5 , pp 681 - 694

- Ng CWW, Yan RWW (1999) Three - dimensional modelling of a diaphragm wall construction sequence. *Geotechnique* 49-6, pp 825 - 834
- Ng RMC, Lo KY (1985) The measurements of soil parameters relevant to tunneling in clays. *Canadian Geotechnical Journal*, 22, pp 375 - 391
- Niemunis A (1996) A visco-plastic model for clay and its FE-implementation. XI Colloque Franco-Polonais en Mecanique des Sols et des Roches Appliquee. E Dembicki, W Cichy, L Balachowski (eds), University of Gdansk
- Niemunis A, Herle I (1997) Hypoplastic model for cohesionless soils with elastic strain range. *Mechanics of Frictional and Cohesive Materials*, 2, pp 279 - 299
- Nishida Y (1956) A brief note on compression index of soil. *ASCE Journal of Soil Mechanics and Foundation Engineering Division* 82-SM 3, pp 1027-1 to 1027-14
- Norman LEJ (1958) A comparison of values of liquid limit determined with apparatus having basis of different hardness. *Geotechnique* 8, pp 79 - 83
- Oexle J (1986) Die Grabung am Fischmarkt zu Konstanz. In: Erhaltung historischer bedeutsamer Bauwerke, Sonderforschungsbericht 315, Ernst & Sohn, Berlin, pp 305 - 330
- Ohde J (1939) Zur Theorie der Druckverteilung im Baugrund. *Der Bauingenieur* 20
- Ohde J (1942) Die Berechnung der Sohldruckverteilung unter Gründungskörpern. *Der Bauingenieur* 23, pp 99 - 107 and 122 - 127
- Olson R.E (1974) Shearing strength of kaolinite, illite, and montmorillonite. *ASCE Journal of Soil Mechanics and Foundation Engineering* 100-GT 11, pp 1215 - 1229
- Olson R.E (1977) Consolidation under time dependent loading. *Journal of the Geotechnical Engineering Division* 103, pp 55 - 60
- Olson R.E (1986) State of the art: Consolidation testing. *Consolidation of soils, testing and evaluation*, ASTM, STP 892, pp 7 - 70
- Omine K, Ohno S (1997) Deformation analysis of composite ground by homogenisation method. *Proc. Of ICSMFE*, Hamburg, pp 719 - 722
- O'Neill MW, Reese LC (1972) Behaviour of bored piles in Beaumont clay. *Journ. Geot. Eng. Div.. ASCE* (98), p 195
- Osterberg JO (1994) Recent advances in loading testing driven piles and drilled shafts using the Osterberg load cell method. *Proc. of the Geotechnical Lectures Series. Geotechnical Devision. Illinois Section. American Society of Civil Engineers. Chicago*
- Osterberg JO (1998) The Osterberg load test method for bored and driven piles. The first ten years. *Proc. of the 7th Int. Conference and Exibition on Piling and Deep Foundations. Vienna. Austria. Deep Foundation Institute. Englewood Cliff. New Jersey*, pp 1281 - 12811
- Ostermayer H, Gollub P (1996) Baugruben Karstadt in Rosenheim. Vorträge der Baugrundtagung 1996 in Berlin. Deutsche Gesellschaft für Erd- und Grundbau, pp 341 - 360
- Otero CS, Sagaseta C, Sainz JA, Ballester F (1979) Determination of consolidation parameters of clay from a large scale load test: Design parameters for soft clay. *Proc. of the 7th ECSMFE*, Brighton, England, pp 121 - 127
- Palmer JHL, Kenny TC (1972) Analytical study of a braced excavation in week clay. *Canadian Geotechnical Journal* 9, pp 145 - 164
- Parry RHG (1956) Strength and deformation of clay. Ph.D Thesis , London University
- Parry RHG (1960) Triaxial compression and extension tests on remoulded saturated clay. *Geotechnique* 10-4, pp 166 - 180
- Parry, Nadarajah (1974a) Observations on laboratory prepared lightly overconsolidated kaoli. *Geotechnique* 24, pp 345 - 357
- Parry, Nadarajah (1975b) Anisotropy in a natural soft clayey silt. *Engineering Geology* 8-3, pp 287 - 309

- Parry RHG, Wroth (1981) Shear properties of soft clay. Soft clay engineering, edited by EW Brand and RP Brenner), Elsevier, Amsterdam, pp 311 - 364
- Parry RHG (1995) Mohr circles, stress paths and geotechnics. E & FN Spon, London
- Peck RB (1969) Deep excavations and tunnelling in soft ground. State-of-the-Art Report, Proc. 7th ICSMFE, Mexico, pp 225 - 290
- Peck RB, Hansen WE, Thorburn TH (1974) Foundation engineering. 2nd ed., John Wiley and Sons, New York
- Pfefferkorn W (1994) Risschäden im Mauerwerk – Ursachen erkennen, Risschäden vermeiden, Reihe Schadenfreies Bauen. Band 7. IRB, Stuttgart
- Pieper K (1983) Sicherung historischer Bauten. Ernst & Sohn
- Placzek D (1982) Untersuchungen über das Schwindverhalten bindiger Böden bei der Trocknung unter natürlichen Randbedingungen. Mitteilungen aus dem Fachgebiet Grundbau und Bodenmechanik, Universität Essen, Heft 3
- Poh TY, Wong IH (1998) Effects of construction of diaphragm wall panels on adjacent ground field trial. ASCE Journal of Geotechnical and Geoenvironmental Engineering 124-8, pp 749 – 756
- Polshin DE, Tokar RA (1957) Maximum allowable non-uniform settlements of structures. Proc. 4th ICSMFE, London, pp 402 - 405
- Potyondy JG (1961) Skin friction between various soils and construction materials. Geotechnique 11, pp 339 - 352
- Potts DM, Fourie AB (1985) The effect of wall stiffness on the behaviour of a propped retaining wall. Geotechnique 35-3, pp 347 - 352
- Potts DM, Addenbrooke TI, Day RA (1993) The use of soil berms for temporary support of retaining walls. Proc. Int. Conf. Retaining Structures, Cambridge
- Potts DM, Addenbrooke TI, Day RA (1993) The use of soil berms for temporary support of retaining walls. In: Retaining Structures, Thomas Telford, London, pp 440 - 447
- Potts DM, Bond AJ (1994) Calculation of structural forces for propped retaining walls. XIII ICSMFE, New Delhi, India, pp 823 – 826
- Poulos HG, Davis EH (1980) Pile foundation analysis and design. J. Wiley & Sons
- Poulos HG (1987) Analysis of residual stress effects in piles; Journal of Geotechnical Engineering. ASCE 113. p. 216-229
- Poulos HG (1989) Pile behaviour - theory and application. Géotechnique 39. p. 365-415
- Poulos H (2002) Spannungen und Setzungen im Boden. In: Smoltczyk U (eds) Grundbau-Taschenbuch, Vol. 1, 6th edn, Ernst & Sohn, pp 255 - 305
- Powrie W (1997) Soil mechanics concept and applications. E & FN Spon, London
- Powrie W, Pantelidou H, Stallebrass SE (1998) Soil stiffness in stress paths relevant to diaphragm walls in clay. Geotechnique 48-4, pp 483 - 494
- Pradel D (1994) Active earth pressure distribution in cohesive soils. Proc. of the XIII ICSMFE, New Delhi, India, pp 795 – 798
- Prakash S, Sharma HD (1989) Pile foundations in engineering practice; J. Wiley & Sons
- Priebe H (1976) Abschätzung des Setzungsverhaltens eines durch Stopfverdichtung verbesserten Baugrundes. Die Bautechnik 53, Heft 5, pp 160 - 162
- Priebe HJ (1995) Die Bemessung von Rüttelstopfverdichtungen. Bautechnik 72, Heft 3, Ernst & Sohn, pp 183 - 191
- Puri VK et al. (1991) Negative skin friction on coated and uncoated model piles. Proc. of the Int. Conference on Piling and Deep Foundations Stresa / Italy 7-12.4.1991. Balkema, Rotterdam, pp 627 - 632
- Raithel M (1999) Zum Trag- und Verformungsverhalten von geokunststoffummantelten Sandsäulen. Schriftenreihe Geotechnik Universität Gh Kassel, Heft 6

- Raithel M, Kempfert H-G (2000) Calculation models for dam foundations with geotextile coated sand columns. Proc. International Conference on Geotechnical & Geological Engineering GeoEng 2000, Melbourne
- Raithel M, Küster V, Lindmark A (2004) Geotextile encased columns – a foundation system for earth structures. Illustrated by a dyke project for a works extension in Hamburg. Nordic Geotechnical Meeting 2004, Sweden
- Raithel M, Kempfert H-G, Kirchner A (2005) Geokunststoffe; Berechnungsverfahren und Bemessung von ummantelten Säulen – Entwicklung und aktueller Stand. *Geotechnik* 28, No. 1, pp 20 - 31
- Raju VR (1997) The behaviour of very soft soils improved by vibro replacement. Ground Improvement Conference, London
- Randolph MF, Carter JP, Wroth CP (1979) Driven piles in clay – the effects of installation and subsequent consolidation; *Géotechnique* 29, No.4, pp 361 - 393
- Rankine WJM (1857) On the stability of loose earth. *Trans. Royal Society, London*
- Rausch E (1955) Das Verhalten von Wohnhauswänden bei Bergschäden. *Fortschritte und Forschungen im Bauwesen*, Reihe D, Heft 22
- Raymond GP, Townsend DL, Lojkacek MJ (1971) The effect of sampling on the undrained soil properties of the Ieda soil. *Canadian Geotechnical Journal*, Vol. 8, No. 4, pp 546 - 557
- Rendulic L (1936) Porenziffer und Porenwasserdruck in Tonen. *Der Bauingenieur* 17, pp 559 - 564
- Reséndiz D (1964) On a type of point bearing pile through sinking subsoil. Proc. Conference on deep Foundations, Vol. I, Mexican Society of Soil Mechanics, Mexiko, pp 385 - 403
- Reséndiz D, Auvinet G, Silva C (1968) Conception et comportement des fondations du Palais des Sports de la ville de Mexico en présence de frottement négatif. Proc. Specialty Session on negative skin friction and settlements of piled structures, 7th Int. Conf. on Soil Mech. and Foundation Engineering, Mexico DF
- Reul O (2000) In-situ-Messungen und numerische Studien zum Tragverhalten der Kombinierten Pfahl-Plattengründung. Mitteilungen des Institutes und der Versuchsanstalt für Geotechnik der TU Darmstadt, Heft 53
- Richards DJ, Powrie W (1998) Centrifuge model test on doubly propped embedded retaining walls in overconsolidated kaolin clay. *Géotechnique* 48-6, pp 833 - 846
- Richards DJ, Powrie W, Page JRT (1998) Investigation of retaining wall installation and performance using centrifuge modelling techniques. Proc. of the Institute of Civil Engineers, *Geotechnical Engineering* 131, pp 163 - 170
- Richwien W (1976) Zum Einfluss der Konsolidierungsdauer auf die wirksame Spannungen und Scherfestigkeit von aufbereitetem Klei. Mitteilungen des Instituts für Grundbau und Bodenmechanik der TU Hannover, Heft 11
- Rollberg D (1976) Bestimmung des Verhaltens von Pfählen aus Sondier- und Rammergebnissen. *Forschungsberichte aus Bodenmechanik und Grundbau (FBG)*. TH Aachen. Heft 4
- Rosco KH, Burland JB (1968) On the generalised stress - strain behaviour of 'wet clay'. In *Engineering Plasticity*, edited by Heyman/Leckie, Cambridge University Press, Cambridge, England, pp 535 - 609
- Rowe PW (1952) Anchored sheet pile walls. Proc. of the Institute of Civil Engineers, *Geotechnical Engineering* 1-1, pp 27 - 70
- Rowe PW (1957) Sheet pile walls in clay. Proc. of the Institute of Civil Engineers, *Geotechnical Engineering* 7, pp 629 - 654

- Ruppert F-R (1980) Bodenmechanische Eigenschaften der Lauenberger Serie - Ein Beispiel für Statistik in der Bodenmechanik. Mitteilung des Lehrstuhls für Grundbau und Bodenmechanik, TU - Braunschweig, Heft 80 - 4
- Russel ER, Mickle JL (1970) Liquid limit values of soil moisture tension. ASCE Journal of the Soil Mechanics and Foundation Division 96, pp 967 - 987
- Rybicky R (1978) Bauschäden an Tragwerken: Analyse und Sanierung. Werner, Düsseldorf
- Santoyo E, Ovando-Shelley E (2002) Underexcavation at the Tower of Pisa and at Mexico City's Metropolitan Cathedral. International Workshop ISSMGE-Technical Committee TC36, Foundation Engineering in difficult soft soils conditions, Mexico city, pp 1 - 19
- Schäfer R, Triantafyllidis T (2004) Auswirkung der Herstellungsmethode auf den Gebrauchszustand von Schlitzwänden in weichen bindigen Böden. Bautechnik 81, Heft 11, pp 880 - 889
- Scheller PO, Reitmeier W (2001) Combined soil stabilization with vertical columns (CSV): A new method to improve soft soils. Soft Ground Technology, Geotechnical Special Publication Number 112. JL Hanson, RJ Termaat (eds), ASCE, pp 123 - 135
- Scherzinger T (1991) Materialverhalten von Seetonen - Ergebnisse von Laboruntersuchungen und ihre Bedeutung für das Bauen in weichem Baugrund. P.hD. thesis, Institut für Bodenmechanik und Felsmechanik der Universität Fridericiana in Karlsruhe, Heft 122
- Schmertmann JS (1975) Measurement of in-situ shear strength. State-of-the-Art Report, Proc. ASCE speciality on in-situ measurement of soil properties, Raleigh, Vol. II, pp 57 - 138
- Schmidt B (1966) Discussion of "Earth pressure at rest related to stress history". Canadian Geotechnical Journal 3-4, pp 239 – 242
- Schmidt HG (1996) Großbohrpfähle mit Mantelverpressung. Bautechnik 73, pp 169 - 174
- Schmidt HG, Seitz J (1998) Grundbau. Beton-Kalender. Vol. 3. Ernst & Sohn, Berlin
- Schofield AN, Wroth CP (1968) Critical state soil mechanics. McGraw-Hill, New York, NY
- Schram Simonsen A, Athanasiu C (1997) Design of axially loaded piles – Norwegian practice; design of axially loaded piles – European practice. De Cock & Legrand (eds). Balkema; Rotterdam, pp 267 - 289
- Schröder E (1996) S-Verfahren: Zur Abschätzung der äußeren Tragfähigkeit (Grenzlast) von gerammten Betonfertigpfählen in nichtbindigen Böden. Hamburg. nicht veröffentlicht
- Schultze E (1961) Distribution of stress beneath a rigid foundation. Proc. 5th ICSMFE, Paris, pp 807 - 813
- Schultze E, Muhs H (1967) Bodenuntersuchungen für Ingenieurbauten. 2nd edn. Springer, Berlin
- Schultze E (1974) Bericht über „Conference on settlement of structures“ in Cambridge. Baugrundtagung in Frankfurt, pp 215 – 248
- Schultze E, Horn A (1990) Spannungsberechnung. In: Smoltczyk U (eds) Grundbau-Taschenbuch, 4th edn, Vol. 1, Ernst & Sohn, Berlin
- Schweiger HF, Breymann H (1994) Baugrubenverformung zufolge Wasserhaltung Messung und rechnerische Betrachtung. Beiträge zum 9. Christian Veder Kolloquium, Technische Universität Graz, Institut für Bodenmechanik und Grundbau, Heft 11, pp 158 - 176
- Schweiger HF, Freiseder M, Breymann H (1997) Deep excavation in soft ground in-situ measurements and numerical predictions. Proc. 14th ICSMFE, Hamburg, pp 589 - 594
- Schweiger HF (2000) Ergebnisse des Berechnungsbeispiels Nr. 3 "3 - fach verankerte Baugrube": Gegenüberstellung der eingesandten Berechnungsergebnisse. In: Schwei-

- ger HF (eds) Verformungsprognose für tiefe Baugruben: AK 1.6 "Numerik in der Geotechnik", pp 7 - 67
- Schweiger HF (2002) Some remarks on pore pressure parameters A and B in undrained analyses with the hardening soil model. PLAXIS Bulletin 12, pp 6 - 9
- Scott RF (1963) Principles of soil mechanics. Addison-Wesley Publishing Company Inc.
- Semple RM, Rigden WJ (1984) Shaft capacity of driven piles in clay; analysis and design of pile foundations. American Society of civil engineers. New York, pp 59 - 79
- Semple RM, Rigden WJ (1986) Shaft capacity of driven pipe piles in clay. Ground Engineering, pp 11 - 19
- Seycek J (1991) Settlement calculation limited to actual deformation zone. Proc. of the 9th ECSMFE, Balkema, Amsterdam, pp 543 - 548
- SGF Report 4:95E (1997) Lime and lime cement columns - guide for project planning, construction and inspection. Swedish Geotechnical Society
- Sheng D, Westerberg B, Mattsson H, Axelsson K (1997) Numerical analysis of stress-strain inhomogeneities in a triaxial test specimen. Proc. of 14th ICSMFE, Hamburg, pp 403 - 407
- Sherif MA, Koch DE (1970) Coefficient of earth pressure at rest as related to soil recompression ratio and liquid limit Highway Research Record, Washington, No. 323, pp 39 - 48
- Sherif G (1973) Setzungsmessungen an Industrie- und Hochbauten und ihre Auswertung. Mitteilungen aus dem Institut für Grundbau und Bodenmechanik der TU Hannover, Heft 7
- Sherif G, Schultze E (1973) Setzungsmessungen an Industrie- und Hochbauten und ihre Auswertung. Mitteilung aus dem Institut für Verkehrswasserbau, Grundbau und Bodenmechanik, Technische Hochschule Aachen, Heft 57
- Shibata T et al. (1982) Model test and analysis of negative friction acting on piles. Soils and Foundations Vol. 22. No. 2, pp 29 - 39
- Simpson B (1992a) Retaining structures displacement and design. Geotechnique 42-4, pp 541 - 576
- Simpson B (1992b) Partial safety factors for design of retaining structures. Geotechnique 42-1, pp 131 - 136
- Skempton AW (1944) Notes on the compressibility of clays. Quarterly Journal of Geotechnical Society, London, pp 119 - 135
- Skempton AW (1953) Earth pressure, retaining walls, tunnels and struttied excavations. Proc 3rd ICSMFE, pp 353 - 361
- Skempton AW, Northey RD (1953) The sensitivity of clays. Geotechnique, 3, pp 30 - 53
- Skempton AW (1954) Discussion of the structure of inorganic soil. ASCE Proc. 80, separate No. 478, pp 19 - 22
- Skempton AW, Bishop AW (1954) Soils in "Building materials, their elasticity and inelasticity". MReiner ed, North Holland Publishing Co., Amsterdam, pp 417 - 482
- Skempton AW, McDonald DH (1956) The allowable settlements of buildings. Proc. of the Institute of Civil Engineers 5, pp 727 - 768
- Skempton AW (1957) Discussion on the planning and design of the new Hong Kong airport. Proc. of the Institute of Civil Engineers 7, pp 305 - 307
- Skempton AW, Bjerrum L (1957) A contribution to settlement analysis of foundations in clay. Géotechnique 7 , pp 168 – 178
- Skempton AW (1959) Cast-in-situ bored piles in London clay. Géotechnique. Vol.9. No. 4, pp 158 - 173
- Skopek J, TerStephanian G (1975) Comparison of liquid limit values determined according to Casagrande and Vasilev. Geotechnique 25-1, pp 135 - 136

- Skov R (1997) Pile foundation – Danish design methods and piling practice; design of axially loaded piles – European practice. De Cock & Legrand (eds); Balkema. Rotterdam, pp 101 - 113
- Smith (1968) Determining the settlement of soft clay. Highways and Public Works, London
- Smolczyk U (1983) Deep compaction. Proc. of the 8th European Conference on Soil Mechanics and Foundation Engineering, Helsinki, pp 1105 - 1116
- Smolczyk U (1985) Axial pile loading test. Suggested method. ISSMFE Subcommittee on Field and Laboratory Testing. ASTM Geotechnical Testing Journal, pp 19 - 90
- Smolczyk U (1996) Grundbau-Taschenbuch. Vol. I and II, 5th ed, Ernst & Sohn, Berlin
- Sokolovski VV (1960) Static of soil media. Butterworth, London
- Soumaya B (2005) Setzungsvorverhalten von Flachgründungen in normalkonsolidierten bindigen Böden. P.hD. Thesis, University of Kassel, Institute of Geotechnics, Heft 16
- Soumaya B, Kempfert H-G (2006) Auswertungen von Setzungsmessungen flachgegründeter Gebäude in weichen Böden. Bauingenieur (submitted)
- Sowers GF (1957) Proc. 4th ICSMFE, pp 157 - 175
- Soyez B (1987) Bemessung von Stopfverdichtungen. Ins Deutsche übertragen von H Priebe. BMT, pp 170 - 185
- Steinbrenner W (1934) Tafeln zur Setzungsberechnung. Die Strasse 1, pp 121 - 124
- Steinmann B (1985) Zum Verhalten bindiger Böden bei monotoner einaxialer Beanspruchung. Baugrund Institut Stuttgart, Heft 26
- Stocker M (1986) Schneckenbohrpfahl. kurz SOB-Pfahl. Beiträge zum Symposium Pfahlgründungen. Institut für Grundbau. Boden- und Felsmechanik TH Darmstadt, pp 1 - 6
- Stroh D (1974) Berechnung verankerter Baugruben nach der Finite - Element - Methode. Mitteilungen der Versuchsanstalt für Bodenmechanik und Grundbau der TH Darmstadt, Heft 13
- Tait RE, Taylor HT (1974) Design, construction, and performance of rigid and flexible bracing systems for deep excavation in San Francisco bay mud. Paper Presented at ASCE National Meeting, Los Angeles
- Takashi K et al (1974) Experiment and study on negative skin friction on piles. Rep. Port. a. Harbour Research Institut. Ministry of Transportation. Vol. 13. No. 1, pp 65 - 86
- Taylor DW, Merchant W (1940) A theory of clay consolidation accounting for secondary compression. Journal of Mathematics and Physics 19, pp 167 - 185
- Teferra A, Schultze E (1988) Formulas, charts and tables. Soil Mechanics and Foundation Engineering. Stresses in Soils. AA Balkema, Rotterdam
- Teng WC (1962) Foundation design. Prentice-Hall, New Jersey
- Terashi M, Tanaka H, Kitazume M (1983) Extrusion failure of ground improved by the deep mixing method. Proc. 7th Asian Regional Conf. Soil Mech. Found. Eng., Vol. 1, pp 313 - 318
- Terzaghi K (1943) Theoretical soil mechanics. John Wiley and Sons, New York
- Terzaghi K (1948) Theoretical soil mechanics. 5. Aufl. John Wiley and Sons, New York
- Terzaghi K, Peck RB (1948, 1961, 1967) Soil mechanics in engineering practice. 2nd edn, John Wiley and Sons, New York
- Tomlinson MJ (1970) Adhesion of piles in stiff clays. Construction Indian Research Inf. Association CIRIA. report No. 26
- Tomlinson MJ (1986) Foundation design and construction. 5th edn. Longman Scientific & Technical, Singapore
- Tomlinson MJ (1994) Pile design and construction practice, 4th edition. E & FN Spon. Chapman & Hall. London

- Topolnicki M (2003a) Ground improvement with in-situ wet soil mixing. Int. Workshop on Geotechnics of Soft Soils-Theory and Practice. Vermeer, Schweiger, Karstunen & Cudny (eds). Noordwijkerhout, Netherlands, pp 113 - 130
- Topolnicki M (2003b) Wglebne mieszanie mechaniczne gruntu na sucho. Inzynieria Morska Geotechnika, p 387
- Tschebotarioff GP (1973) Foundations, retaining and earth structures. McGraw-Hill, New York
- Tsukada Y, Yasuhara K (1995) Scale effects in one-dimensional consolidation of clay. Proc. of the Int. Symposium on Compression and Consolidation of Clayey Soils, ed by Yoshikuni H, Kusakabe O, Hiroshima, pp 211 - 216
- Ulrich G (1980) Verschiebungs- und kraftgesteuerte Plattendruckversuche auf konsolidierten Böden. Mitteilung 11. Baugrundinstitut Stuttgart, pp 4 - 92
- Vaid YP, Campanella RG (1974) Triaxial and plain strain behaviour of natural clay. JGED, ASCE, Vol. 100, No. GT3, pp 207 - 224
- Valsangkar AJ, Schriwer AB (1991) Partial and total factors in anchored sheet pile design. Canadian Geotechnical Journal 28, pp 812 – 817
- Van Impe W, De Beer E (1983) Improvement of settlement behaviour of soft layers by means of stone columns. Proceedings of the VIII. ECSMFE, Helsinki Vol. 1
- Van Oudenallen T (1999) Die Herstellung und Verwendung von Spannbetonrammpfählen in den Niederlanden. Pfahl-Symposium. Institut für Grundbau und Bodenmechanik TU Braunschweig, Heft 60, pp 13 - 27
- Van Weele AF, Schellingerhout AJ (1994) Effiziente Rammung von Fertigbetonpfählen. Geotechnik 17, pp 130 - 140
- Van Weele AF (2003) Chapter 2.7 "Driving and extraction". In: Geotechnical Engineering Handbook. Volume 2. Ernst & Sohn (Wiley Comp.). pp 255-300
- Vautrain J (1980) Comportement et dimensionnement des colonnes ballastées. Rev. française de Géotechnique, No. 11, pp 59 - 73
- Vaziri HH, Troughton VM (1992) An efficient three - dimensional soil - structure interaction model for analysis of earth retaining structures. Canadian Geotechnical Journal 29, pp 529 - 538
- Vermeer PA, Brinkgreve RBJ (1995) Hand book of the finite element code for soil and rock analysis "PLAXIS" Balkema Publisher
- Vermeer PA, Meier C-P (1998) Stability and deformations in deep excavations in cohesive soils. Intl. Conf. on Soil-Structure Interaction in Urban Civil Engineering, Darmstadt Geotechnics 1-4, pp 177 - 192
- Vermeer PA (1998) Column Vermeer. PLAXIS Bulletin 5, pp 2 – 3
- Vermeer PA, Meier C-P (1998) Standsicherheit und Verformungen bei tiefen Baugruben in bindigen Böden. Baugrundtagung, Stuttgart, pp 133 - 148
- Vesic AS (1963) Bearing capacity of deep foundations in sand. Highway Research Record (39), p 112
- Vesic AS, Clough GW (1968) Behaviour of granular materials under high stresses. JSMFD, ASCE, Vol. 94, No. SM3, pp 661 - 688
- Vesic AS (1975) Principles of pile foundation design. Duke University Durham N.C.. School of Engineering. Soil Mechanics series Nr. 38
- Vesic AS (1977b) On significance of residual loads for load response of piles. Proc. of the 8th Int. Conference on Soil Mechanic and Foundation Engineering. ICSMFE. Vol. 3. Tokyo, pp 374 - 379
- Von Wolffersdorff P-A (1996) A hypoplastic relation for granular materials with a pre-defined limit state surface. Mechanics of Cohesive-Frictional Materials, 1, pp 251 - 271

- Von Wolffersdorff P-A (1997) Verformungsprognosen für Stützkonstruktionen. Veröffentlichungen des Institutes für Boden- und Felsmechanik der Universität in Karlsruhe. Gudehus, Natau (eds), Heft 141
- Walker AF (1965) Stress-strain relationships for clay. Ph.D. Thesis, Cambridge University
- Walker LK, Morgan JR (1977) Field performance of a firm silty clay. Proc. of the 9th ICSMFE, Tokyo, pp 341 – 346
- Weiß K (1974) Pfahlversuche zur Ermittlung der Größe der negativen Mantelreibung in organischen Böden. Mitteilungen der Deutschen Forschungsgesellschaft für Bodenmechanik an der Technischen Universität Berlin. No. 30, pp 34 - 40
- Weißenbach A (1977) Baugruben. Teil I, II und III, Ernst & Sohn, Berlin
- Weißenbach A, Kempfert H-G (1994) German national report on braced excavation in soft ground. Proc. for the Intl. Symposium on Underground Construction in Soft Ground, New Delhi, India, pp 9 - 12
- Weißenbach A, Kempfert H-G (1995) German national report on braced excavation in soft ground. In: Fujita K, Kusakabe O (eds) Proc. Intl. Symposium on Underground Construction in Soft Ground, New Delhi, A. A. Balkema, pp 33 - 36
- Weißenbach A (1997) Kapitel „Baugrubensicherung“. Grundbau-Taschenbuch, 5th edn, Vol. 3. Ernst & Sohn, Berlin, pp 397 - 511
- Weißenbach A (2002) Empfehlungen des Arbeitskreises „Baugruben“ der DGQT zu Baugruben in weichen Böden. Bautechnik, Heft 9, pp 569 – 588
- Whitaker T, Cooke RW (1961) A new approach to pile testing. Proc. 5th ICSMFE. Vol. 2. Paris, pp 171 - 176
- Whitaker T, Cooke RW (1966) An investigation of the shaft and base resistance of large bored piles in London clay. Proc. of the Symposium on Large Bored Piles. London, pp 7 - 49
- Whyte IL (1982) Soil plasticity and strength a new approach using extrusion. Ground Engineering 15-1, pp 16 - 24
- Wichert H-W (1988) Einfluss der Alterung auf die Tragfähigkeit von historischen Spick-Pfahl-Gründungen. Mitteilung des Instituts für Grundbau und Bodenmechanik, TU Braunschweig, Heft 27
- Windisch ÉJ, Yong RN (1990) A statistical evaluation of some engineering properties of eastern Canadian clays. Canadian Geotechnical Journal, pp 373 – 386
- Winkler E (1867) Die Lehre von Elastizität und Festigkeit. Prag, Dominicus
- Witzel M (2004) Zur Tragfähigkeit und Gebrauchstauglichkeit von vorgefertigten Verdrängungspfählen in bindigen und nichtbindigen Böden. Schriftenreihe Geotechnik. Universität Kassel. Heft 15
- Wong IH (1971) Analysis of braced excavations. P.hD. thesis, Massachusetts Institute of Technology
- Wong PKK, Mitchell RJ (1975) Yielding and plastic flow of sensitive cemented clay. Geotechnique 25, pp 763 - 782
- Wong S, Broms B (1994) Analysis of retaining walls using the hyperbolic model. In: Bull JW (eds) Soil Structure Interaction, Numerical Analysis and Modelling, E & FN SPON, pp 605 - 645
- Wood DM (1983) Index properties and critical state soil mechanics. In: Balasubramaniam AS, Chandra S, Bergado DT (eds) Recent development in laboratory and field tests and analysis of geotechnical problems, Bangkok, pp 309 - 331
- Wroth CP, Wood DM (1978) The correlation of index properties with some basic engineering properties of soils. Canadian Geotechnical Journal 15,pp 137 – 145
- Wroth CP, Houldby GT (1985) Soil mechanics - property and analysis procedures. Proc. 11th ICSMFE, San Francisco, pp 1 – 55

- Wu W (1992) Hypoplastizität als mathematisches Modell zum mechanischen Verhalten granularer Stoffe. Veröffentlichung des Inst. f. Bodenmechanik und Felsmechanik der Universität Fridericiana in Karlsruhe, Heft 129
- Wu W, Bauer E, Niemann A, Herle I (1993) A visco-hypoplastic model for cohesive soils. Proc. of the Int. Workshop on Modern Approaches to Plasticity for Granular Materials, Horton, Greece, Ed. D. Kolymbas, Elsevier, pp 365 - 383
- Yin JH, Graham J (1989) Viscous-elastic-plastic modelling of one-dimensional time dependent behaviour of clays. Canadian Geotechnical Journal 26, pp 199 - 209
- Yong RN, Townsend FC (1982) Application of plasticity and generalised stress - strain in geotechnical engineering. ASCE
- York DL et al. (1974) Long term load transfer in end bearing pipe piles. Transportation Research Record. No. 517, pp 48 - 60
- Youssef MS, El - Ramle AH, El-Demery M (1965) Relationship between shear strength, consolidation, liquid limit and plastic limit for remoulded clays. Proc. ICSMFE, pp 126 - 129
- Zaeske D (2001) Zur Wirkungsweise von unbewehrten und bewehrten mineralischen Tragschichten über pfahlartigen Gründungselementen. Schriftenreihe Geotechnik, Universität Kassel, Heft 10
- Zaeske D, Kempfert H-G (2002) Berechnung und Wirkungsweise von unbewehrten und bewehrten mineralischen Tragschichten auf punkt- und linienförmigen Traggliedern. Bauingenieur Band 77
- Zdravkovic L, Potts DM (1999) Advances in modelling soil anisotropy. Constitutive modelling of granular materials, ed by Kolymbas, Springer, Berlin, pp 491 - 521
- Zeevaert L (1985) Consolidation in the intergranular viscosity of highly compressible soil. A Symposium on Consolidation of Soil: Testing and Evaluation, ASTM Special Technical Publication 892, pp 257 - 281
- Zeng GX, Pan QY, Hu YF (1986) Behaviour of excavation with sheet piling in soft clay. The international conference of deep excavation, Bejing, pp 3.1 - 3.6
- Zhu B, Liu G (1994) Elasto - plastic analysis of deep excavation in soft clay. Proc. 13th ICSMFE, New Delhi, pp 905 - 908
- Zweck H (1980) Tragfähigkeit von Pfählen aufgrund von Sondierergebnissen; Seminar 11090 "Pfahlgründungen". Technische Akademie e.V. Wuppertal

Index

- a
abutment 422, 424
action 406, 410, 411 *see also characteristic*
 destabilising 6
 dynamic 355
 effect of 410
 stabilising 6
active earth pressure *see pressure*
activity 16, 17
adhesion 87
adhesion coefficient *see coefficient*
adjustment factor 189, 190
ageing 48, 401
aggregate 348, 353, 362
analysis 36, 58, 116, 126, 129, 138,
 148, 157, 177, 186, 209, 219, 223,
 334, 457
 analytical 144
 back 3, 143, 159, 160, 199, 208, 213,
 231, 268, 274, 298, 299, 302, 309,
 310, 311, 314, 318, 320
 consolidation 3, 144, 176, 177, 178,
 211-215, 223, 224, 225, 233-242,
 275, 465
 deformation 56
 drained 74, 93, 139, 157, 162, 166,
 171, 172, 176, 177, 185, 213, 215,
 223, 225, 233, 235-240, 242
 effective stress 35, 142, 149, 399
finite element 157, 158, 208, 318,
 320, 494
groundwater flow 219
long-term 54
numerical 139, 317, 501
one-dimensional 279
plane strain 158, 208
preliminary 213, 216, 235
settlement 274, 278, 298
stability 141, 143, 461, 495
static 399
statistical 294
three dimensional 158
total stress 3, 35, 142, 394, 399, 407
undrained 3, 98, 139, 157, 171, 177,
 178, 185, 211, 213, 233
update mesh 3
anchor 108, 110, 115, 118, 119, 122,
 152, 158, 162, 195, 198, 228
 system 3, 123
 tendon 126, 285
 force 230, 238, 242
 free length 197
 ground anchor 9, 109, 113, 152, 228,
 251, 252, 256, 257
 grout body 197
 installation 229, 236, 240, 241
 pre-stressing 159, 229, 240, 241
 tie back 109, 110, 493
anchorage system 405
angle of internal friction 20, 30, 36, 46,
 55, 139, 370, 395, 408, 457, 462, 473,
 478
angle of overall shear strength *see shear strength*
angular distortion 285, 291, 297
angular rotation 481
angular strain 285
anisotropy 42, 44, 45, 47, 54, 117, 140,
 148, 189, 196
arch 451, 452
arching 136
arching effect 113, 118, 295, 449, 451
Asaoka's method 300, 315, 317
Atterberg limits 16
auger 360, 364, 483, 488, 497
 flight 356, 360, 470
 helical 355
 blade 356, 360, 364
boring 462
displacement 469
drilling 441

- twin rotary head method 360
 auger flight 481
 stem 356, 360
b
 back analysis *see analysis*
 backfill 507
 ballast 497-501
 barotropy 65, 66
 barrelling 66
 basal failure *see failure*
 basal stability 114, 116
 base expansion 348, 365
 base plate 347, 353, 355
 base resistance *see pile, resistance*
 base slab 134, 194, 195, 198, 474
 basement 109, 200, 202, 207, 250, 255,
 256, 266, 268, 300, 302, 303, 306,
 308, 315
 basement floor 233, 239, 244, 256
 compensated 255
 basement slab 205
 bearing capacity 5, 44, 114, 130, 137,
 316, 324, 334, 335, 341, 343, 344,
 356, 363, 366, 382, 389, 394, 401,
 417, 421, 449, 455, 458, 464, 474,
 478, 479, 485, 488, 490, 496, 499,
 506, 507 *see also pile*
 verification 412
 factor 394, 395
 bearing failure *see failuer*
 bearing layer 113, 195, 196, 198, 274,
 392, 416, 417, 449, 462, 465, 471,
 479, 490
 bearing strata 375, 451
 behaviour 96, 97, 143
 bearing 4, 462, 472
 compressibility 277
 compression 312, 313, 317
 consolidation 495
 contact 86, 208
 creep 377
 deformation 56, 72, 162, 223, 268,
 283, 299, 324, 458, 456, 459, 462,
 495
 drained 37, 57
 elastic 162, 220, 324, 460
 foundation-soil interaction 472
 frictional 370
 ideal-plastic 324
 interface 58
 linear 67
 linear-elastic 98, 162, 465, 466
 load-settlement 379, 472, 474
 material 220
 non-linear 58, 59
 plastic 220, 399
 reloading 103
 soil-structure-interaction 199
 strength 57, 72
 stress-strain 3, 13, 29, 183
 time-dependent 3, 57, 116
 time-settlement 275, 277, 335
 undrained 37, 57, 141, 171, 211, 213
 unloading 103
 viscose 284
 belling 361
 bending 114, 238, 285, 295
 bending moment 5, 115, 120, 122, 158,
 159, 160, 161, 166, 167, 168, 169,
 170, 220, 327, 328, 331, 353, 414
 bentonite 12, 13, 14, 109, 125, 347,
 356, 360-363, 498
 berm 107, 109, 129, 135, 158, 160, 162,
 173, 174, 175, 199, 214
 binder 469, 471, 473, 475, 476, 478,
 481, 484, 487, 489, 507
 binder factor 487
 mix 475
 binder-sand mix 470
 Bishop 141
 bitumen 412
 blade 483, 484
 bond 346, 489
 bore log 204
 bore profile 244
 bored pile *see pile*
 bored pile wall 124, 127 *see also wall*
 contiguous bored pile 108
 intermittent pile 112
 primary pile 112
 secant bored pile wall 108
 secant pile 112
 secondary pile 112
 tangent pile 108, 112
 bored tangent pile *see pile*
 borehole 13, 112, 204, 309, 315, 323,
 356, 360, 361, 362, 363, 364, 367,
 432, 439, 441, 451
 boring 112, 125, 126, 204, 302, 303,
 306, 308, 363, 488
 borrow pit 492

- bottom slab 158, 162, 190-192, 200, 220-222, 225, 234, 236, 237
 bottom support 134, 135, 175, 176, 189, 194, 214, 222, 245, 250, 252, 253, 257
 boulder clay 50, 165, 204, 211, 227, 233, 303, 306, 308, 311, 497
 boundary 157, 210, 222
 boundary condition 19, 29, 193, 279, 330, 334, 399, 421, 422, 458, 465, 491
 Boundary Element Method 398
 boundary surface 399
 Boussinesq 326, 268
 brick wall *see wall*
 bridge 422, 424, 506
 building 158, 188, 204, 205, 210, 218, 220, 225, 227, 228, 233, 239, 243, 250-252, 255, 256, 288-290, 297, 299-306, 309, 310, 314, 315, 321-325, 341, 343, 351, 354, 360, 417, 426, 430, 432, 437, 439, 440, 444, 445, 448-450, 453, 454, 449, 463, 469, 503, 509
 building damage 291
 Buisman faktor 284
 bulk density 125
 bulk modulus *see modulus*
 buoyancy 196
 c
 calcit 15
 calculation 158, 210, 385, 387, 399
 analytical 494
 back 444
 earth pressure 149, 193
 passive pressure 149, 198
 phase 171, 213, 215, 216, 223, 241
 plastic 3
 drained 3
 undrained 3
 step 225, 240
 calibration 382
 cam-clay model *see constitutive model*
 cap 472
 cap model 57, 67, 58
 carrying capacity 267, 476
 Casagrande 64, 334
 case history 2, 4, 199, 250, 255, 297-320, 420, 421
 casing 112, 340, 343, 347, 348, 351, 354, 355, 356, 360-363, 462, 464, 470, 494
 cast iron 343
 cavity 355, 361, 470, 482
 cavity expansion 400, 458
 cement 134, 361, 362, 365, 469, 476, 478, 481, 489, 497, 498, 507
 mortel 420
 suspension 420, 432, 441
 grout 367
 mortar 366, 367
 characteristic 5, 506
 actions 5, 6, 412
 earth reaction 190
 effects of actions 5, 6
 force 190
 geotechnical parameters 5
 load 5, 506
 passive resistance 189
 resistance 5, 6, 473, 474
 resultant force 190
 section force 140
 soil parameter 138
 weight 196
 characteristic point 270, 272, 299, 300
 chlorite 15
 clay 14, 16, 26, 28, 45, 76, 105, 117, 142, 157, 250, 353, 388, 399, 462, 464, 478, 481
 aged 11
 anisotropically consolidated 76
 cemented 11
 clay stone 50, 352
 delayed consolidation 11
 deposit 15
 fraction 15, 16
 heavily consolidated 126
 heavily overconsolidated 43
 inorganic 16, 283, 311
 lightly overconsolidated 43, 67, 68
 marine young 50
 medium 128
 mineral 15, 17
 mixed-layer 15
 normally consolidated 11, 37, 38, 43, 47, 51, 52, 58, 60, 64, 67, 68, 70, 109, 126, 131, 139, 140, 149, 154, 283, 311, 393, 397
 organic 16, 283, 503
 overconsolidated 11, 60, 57, 70, 152

- quaternary 50
 remoulded 26
 saturated 28, 37, 57, 141
 sensitive 28, 43, 149, 283
 slightly overconsolidated 50, 64
 soft 20, 48, 117, 118, 126, 128, 276,
 311
 stiff 115, 120, 341, 352
 tertiary 50
 undrained strength 44 *see also shear strength*
 strength
 very soft 126
 young 11
 cluster 222
 coating 342
 coefficient
 creep coefficient 283
 of adhesion 391, 392, 394
 of base resistance 394
 of active earth pressure 116, 189,
 465,
 of earth pressure at rest 19, 20, 116,
 187, 408
 of passive earth pressure 116, 186,
 457
 of viscosity 49
 of consolidation 275, 276
 of earth pressure 122
 of compressibility 143
 of consolidation 299, 302, 309, 311,
 313, 315, 320, 335
 of horizontal consolidation 404
 of permeability 320
 of pore pressure 146
 of secondary consolidation 24, 27,
 300, 302, 311
 of secondary settlement 309
 of uniformity 15
 of viscosity 283
 shear coefficient 296
 cofferdam 251
 cohesion 30, 36, 72, 74, 75, 87, 99, 116,
 138, 461, 474, 507, 509
 cohesionless soil *see soil*
 cohesive soil *see soil*
 column 449, 451, 456, 457, 466, 467,
 471, 477, 478, 482, 489, 505
 base resistance 458 *see also pile, resistance*
 cemented stone 500
 concrete 362, 363
 CSV-column 469, 470, 472 474, 476,
 506, 509
 design 458
 deep mixing (DM) *see deep mixing*
 encased 462, 469, 491, 496
 expansion 467
 floating 472, 479, 481
 geotextile encased sand/gravel
 column (GEC) 462, 464, 493, 494,
 495
 gravel 456, 458, 460, 461, 462, 464,
 475, 489
 group 479, 481, 485, 488
 grouted stone 449, 489, 490, 499,
 501, 502
 homogeneity 484
 incompressible 459
 installation 457, 459, 463, 470, 475,
 498
 MIP-column *see deep mixing*
 raster 456
 ready-mixed mortar 490
 resistance 458, 474
 sand 461, 462, 464, 474
 sand compaction 464
 secant 485
 settlement 475, 480, 488
 single 252, 456, 472, 473, 476, 478,
 479, 485, 487, 488, 504, 505, 506,
 507, 509
 spacing 458, 472, 478, 503
 stabilising 500
 stiffness 458, 471
 stone 455, 462, 465, 474, 489, 491,
 500
 strength 484, 487, 504, 505
 tangent 485
 unreinforced concrete 490, 491
 wall 485
 combination 8
 compaction 68, 57, 346, 348, 349, 350,
 471, 474, 476, 478
 comparison 216, 224, 376
 composition 30
 compressed air 13, 476
 compressibility 16, 275, 278, 299, 308,
 370, 449
 compressibility modulus *see modulus*
 compressible 258, 312, 316, 410, 458

- compression 19, 32, 33, 42, 45, 47, 48, 54, 61, 72, 75, 76, 86, 90, 156, 268, 284, 311, 334, 335, 374, 399, 505
 anisotropic 64
 creep 282, 284
 elasto-viscous 282
 irrecoverable 281
 irrecoverable viscous 281
 isotropic 64
 normal compression line 23, 24, 29
 one-dimensional 29
 recoverable elastic 281
 secondary 19, 27, 282
 time-dependant 281
 viscous 285
- compression hardening 68
 compression index 15, 24, 25, 27, 59, 277, 283, 300, 302, 309-313, 320, 328, 475
 overestimation 311, 312
- compression model 280, 283
 compression modulus *see modulus*
 compression path 283
 compression test 277
 compressive strength *see strength*
 computation 213, 220, 235
 concave 333
 concrete 87, 106, 109, 112, 113, 125, 134, 139, 175, 234, 252, 257, 346-349, 351, 353, 355, 360, 362-364, 367, 441
 dry compacted 351
 fast hardening 201, 202, 214, 222
 frame 288
 fresh 348, 356, 360, 362
 lean 47, 361
 mixing 362
 necking 348
 placement 361, 362, 364, 365
 plastic 348
 reinforced 202, 422
 slab 132, 134, 162, 207, 235, 236, 245, 246
 wall 288
- cone 457, 479, 498
 cone factor 50
 cone penetration test (CPT) 21, 44, 49, 204, 222, 385, 387, 389, 399, 428
 cone resistance 21, 50, 386, 387
 confined water pressure *see pressure*
 confining stress *see stress*
- consistency 16, 63, 227, 243, 251, 299, 348, 362, 451, 490, 493, 497
 consistency index 113, 258, 448
 consistency limit 51, 423
 consolidation 18, 19, 29, 58, 76, 213, 276, 278, 281, 311, 324, 334, 404, 413, 458, 449, 459
 creep 278, 280
 degree of 143, 275, 313, 394, 414
 end of primary 277, 311, 312
 end of 76
 isotropic 64
 normal consolidation 64
 normal consolidation line 22, 29, 59
 one-dimensional swelling 23
 phase 177
 primary 18, 27, 59, 275, 277, 280, 283, 284, 300, 304, 309, 311, 449
 rate 299
 secondary 28, 278, 281, 283, 311
 step 235, 236, 237
 swelling line 22, 24, 30, 59, 64
 three-dimensional 29
 time 176, 284, 302, 309, 493
 time factor 275
 virgin compression line 61, 272, 300
 consolidation analysis *see analysis*
 consolidation pressure *see pressure*
 consolidation test 298, 312, 313, 314
 consolidation theory 143, 279, 282
 constitutive model 2, 3, 57, 58, 59, 65, 68, 116, 157, 199, 233, 278, 279
 Drucker-Prager yield 60, 67
 elastic 2, 158
 elastic-perfect plastic model 58, 68
 elasto-plastic 2, 60, 57, 59, 60, 63, 64, 66, 68, 57, 157, 220
 elasto-visco-plastic 57
 hardening soil model (HSM) 33, 35, 59, 68, 81, 90-92, 94, 98, 101, 162, 177, 180, 208, 211, 233
 hyperelasticity 57, 58
 hypoelasticity 57, 58
 hypoplasticity 57, 65, 67
 Lade-Duncan model 60
 linear-elastic-plastic model 370
 Mohr-Coulomb model (MCM) 31, 32, 63, 68, 94, 95, 162, 180, 208
 soft soil creep model (SSCM) 68, 318, 320, 328
 soft soil model (SSM) 59, 68

- Tresca yield criteria 60
 viscous-elastic 283
 viscous-elastic-plastic 283
 visco-hypoplasticity 66
 visco-plastic 64
 Von-Mises yield criteria 60
 constrained modulus *see modulus*
 construction 141, 144, 145, 205, 216,
 252, 255, 318, 324, 335, 353, 360,
 361, 392, 429, 432, 439, 441, 449,
 454, 474, 490, 491, 494, 497, 500-
 502, 504, 509
 capacity 246
 daily output basis 201, 202, 222
 detail 216, 246, 341
 measure 194, 341, 412, 421, 454,
 456
 method 250, 337, 347, 356, 373, 493,
 494
 option 497
 phase 194, 201, 213, 225, 237, 244
 procedure 216, 236
 sequence 157, 231, 236
 stage 156, 166, 175, 194, 201, 213,
 222, 223, 230, 235-238, 242, 246,
 369, 434, 457, 495, 498
 step 171, 173, 474
 technique 157
 time 117, 225, 355, 491, 494
 top-down construction 110
 work 227, 246, 256, 491
 contact element 87, 171, 173
 contact pressure 337, 366
 contact surface 90, 166, 233
 correction factor 47, 48, 183, 274, 279,
 322
 correlation 25, 51, 384
 corrosion 342, 343, 346, 348, 366, 401
 crack 256, 287, 289, 346
 crack propagation 287, 289
 creep 19, 29, 48, 66, 284, 328, 334, 379,
 478, 501 *see also behaviour,*
deformation, settlement,
consolidation, compression
 critical friction angle 66
 critical soil mechanic 26, 29, 32, 45
 critical state 66, 399
 critical state line 319
 CSV-column *see column*
 curing 481, 490
 curvature 285, 288, 332
 radius of 285, 291
 cutter 353, 354
 d
 damage 216, 252, 255, 256, 287, 289,
 335, 348, 349, 355, 363, 364, 481
 limiting criteria 291
 limiting value 291, 294, 297
 deep mixing (DM) 476, 481, 485, 506
 dry deep mixing 470, 475, 477, 488
 Mixed-in-Place Method (MIP) 496-
 498
 wet deep mixing 475, 481, 483, 486,
 487, 488, 496, 505, 506
 deflection 57, 115, 123, 128, 134, 295,
 453, 499
 measured 238, 239, 240
 predicted 199
 deformation 1, 5, 7-11, 14, 18, 22, 56-
 60, 65-68, 86, 87, 90, 95, 111-118,
 122, 123, 126, 132, 136, 137, 140,
 159, 160, 175, 219, 245, 252, 253,
 257, 259, 285, 291, 295, 319, 371-
 374, 377, 379, 412-414, 456, 457,
 449, 463, 466, 467, 480, 500, 506
 behaviour 2
 calculated 218
 creep 19, 378, 413
 drained 81
 elastic 280
 elasto-plastic 280
 parameter 2
 permanent 362
 plastic 128, 316, 317, 319, 324
 radial 460
 rate of 300
 shear 296, 413, 457, 481
 time-dependent 19
 undrained 81
 undrained shear 28
 viscous 280
 deformation modulus *see modulus*
 deformation path 280
 densification 341, 351, 355, 356, 469
 density 15, 65, 87, 113, 117, 458
 density function 58
 deposit 1, 4, 45, 87
 deposition 21
 depth of embedment 137, 143 *see also*
embedment depth
 depth of excavation *see excavation*

-
- depth of penetration 115, 118, 120, 130,
 139, 143, 144, 159
 design 334, 337, 353, 362, 373, 392,
 473, 503, 506, 507
 action 6, 7, 473
 bearing resistance 196
 criterion 504
 effects of actions 6
 design approach 8
 load 229, 377, 378, 505
 passive resistance force 189
 preliminary 244
 reaction force 189
 resistance 6, 7, 196, 473, 474
 ultimate 120
 determinacy 289
 deviation 216
 deviatoric loading 11
 deviatoric stress 29, 31, 33, 35, 56, 66,
 74, 7681, 82, 92, 93, 100, 101, 103,
 183, 324
 dewatering 126, 469, 471, 476
 diagram
 load-deformation 380
 resistance-settlement 380
 dial gauge 377
 diaphragm wall *see wall*
 differential equation 451, 452, 453
 differential solution 295
 dike 462, 491, 493, 494, 495, 496
 dilatancy 59, 57, 58, 101, 473
 dilation 68
 dimensionless 143, 181
 direct shear 31, 87, 185
 displacement 6, 7, 40, 64, 58, 90, 114,
 115, 128, 134, 136, 139, 140, 162,
 169, 181, 194, 210, 213, 222, 231,
 259, 348, 353, 355, 356, 378, 398,
 410, 421, 456, 455, 475, 491, 492,
 497 *see also wall, pile*
 computed 215, 216, 217, 221, 224,
 225, 238
 gauge 377
 measured 215, 216, 221, 224, 225
 observed 225
 prescribed 180, 181
 distortion 114, 289, 291
 drain 199, 449, 464, 494
 drainage 29, 31, 36, 57, 58, 64, 71, 106,
 117, 133, 141, 143, 177, 185, 199,
 219, 277, 315, 335, 455, 496
 boundary 279
 gravity 199
 horizontal 277
 ring 199
 path 18, 143, 275, 302
 drained 85, 86, 99, 101, 225, 465
 drained analysis *see analysis*
 drained condition 139, 143, 144, 148,
 149, 151, 172, 173, 175, 211, 216,
 411
 dredging 492
 drill 353
 bit 354, 355
 casing 356
 hole 161, 356, 360, 365, 367
 pit 112
 rig 355, 360
 drillhole 362
 drilling 122, 353, 356, 360, 363, 364,
 367, 370, 482
 rate 360
 tool 355, 363
 driving 111, 112, 122, 125, 342, 346,
 347, 348, 349, 350, 352, 354, 367,
 370, 384, 389
 efficiency of 382
 energy 382
 vibratory 351
 energy 350
 tube 353
 drop hammer 343, 346, 347, 350, 382
 Drucker-Prager yield criteria *see*
 constitutive model
 dynamic hammer 350
 dynamic pile test *see pile*
 e
 EAB 1, 120, 122, 149, 157, 158
 earth pressure *see pressure*
 earth pressure at rest *see pressure*
 earth reaction 188, 252
 efficiency 160, 162, 173, 174, 175, 176,
 218, 456, 481, 484, 487
 elastic 45, 60, 58, 65, 68, 157, 180
 elastic model *see constitutive model*
 elastic-perfect plastic model *see*
 constitutive model
 elastic rebound 19
 elastic strain 63, 64
 elastic-half-space 269, 275, 325- 329,
 335
 elastic-isotropic-half-space 268

- elasticity 56, 282
 elasticity theory 60
elasto-plastic *see constitutive model*
elasto-visco-plastic *see constitutive mode*
 embankment 48, 141, 152, 277, 319, 320, 321, 335, 449-452, 462, 469, 485, 491, 496-503
 embedment 344, 365, 375, 394
 embedment depth 122, 146, 162, 185, 193-195, 198, 352, 390, 392, 395
 empirical 50, 474
 empirical correction 268
 empirical correlation 15, 390
 empirical equation 20, 24, 51, 53, 187
 empirical factor 401
 empirical formula 371
 empirical method 119, 126, 385
 empoldering 494
 enclosure 491
 end resistance *see pile, resistance*
 end bearing 369-371, 373, 375 *see also resistance*
 energy 16, 19, 58, 484
 equilibrium 8, 137, 138, 189, 197, 362, 382
 equipment 140, 251, 343, 350, 351, 353, 470, 476, 482
 equivalent angle 186
 equivalent diameter 432, 458
 equivalent time 283
 equivalent total angle 146, 147, 149, 151
 erosion 21, 57, 106
 Eurocode 4, 7, 9, 340, 371, 373
 excavation 1-3, 3, 35, 40, 47, 55, 57, 65, 68, 81, 90, 105-174, 185-237, 243-257, 271, 274, 300, 308, 356, 360, 421, 422, 444, 485, 497, 500, 509
 asymmetrical 412
 behaviour 160
 bottom 119, 122, 129-135, 140, 143, 155, 159, 161-165, 168-175, 178, 188, 190-198, 221, 228, 233, 236-239, 245, 252, 257
 braced 14, 108, 118, 119, 125, 126, 129, 130, 198, 252
 deep 105, 108, 109, 125, 135, 141, 143, 243, 250, 256, 257, 261
 depth 117, 123, 124, 128, 130, 134, 145, 148, 159, 160, 244, 355
 end of 207, 222, 226, 238, 255, 261
 final 175
 hand-over-hand 123
 level 195
 open 37, 141, 142
 overexcavation 122, 126
 performance 3, 105, 128, 136, 159, 160
 phase 195, 201, 207, 222
 preliminary 252
 procedure 222
 sequence 208, 209
 site 227, 250
 stability 159
 stage 134, 207, 215, 242, 497
 tied back 197, 198
 excess pore pressure *see pore pressure*
 expanded base 348, 350, 355, 361, 367
 exploration 244, 250, 303
 exponent 58
 extension 5, 32, 33, 42, 45, 47, 54, 75
 extensometer 247
 f
 fabric 45, 54
 failure 45, 48, 66, 72, 137, 168, 173, 195, 325, 369, 370, 378, 379, 390, 399, 400, 413, 416, 456, 457, 473, 474
 basal 112, 120, 129, 130, 131, 136, 195, 196, 252
 bearing 6, 130, 421
 bottom heave 453
 bulging 456
 column 464, 478, 487
 criteria 68, 66, 69, 74, 81, 82, 95
 deep rupture 197
 deep seated 197, 252
 global 6, 7, 9
 global bearing 421
 hydraulic 112, 136, 140, 195, 197, 348, 363
 internal 473
 line 32, 141, 324
 local 316
 mechanism 474, 495
 mode 488
 overall 246, 507, 509
 overturning 140
 passive 139, 145
 piping 133
 plane 38

-
- plastic 116, 317, 459
 progressive 317
 punching 456, 458
 rotational 140
 shear 114, 316, 456, 478, 479
 slope 6, 7, 9, 114
 stress 67, 72, 76, 77, 93
 stability 129
 state of 370
 surface 67, 370, 462
 undrained 143
 uplift 140
 zone 130
- fast hardening concrete *see concrete*
 finite element 33, 57, 63, 68, 58, 90, 154, 155
analysis see analysis
 calculation 166, 398, 240
 computation 154, 162, 213, 215, 216, 240, 241
 result 216
 mesh 163, 210, 231, 501
 method 2, 120, 126, 128, 157, 158, 161, 199, 318, 398, 399
 model 162, 165, 209, 213, 235, 238, 413
 program 157
 simulation 211
- field 20, 31, 41, 44, 48, 57, 58, 61, 67, 72, 106, 117, 119, 125, 128, 141, 144, 154, 211, 221, 235, 240, 244, 275, 300, 302, 309, 311-314, 320, 385, 400, 478, 483, 487, 500, 501
 field observation 298, 299
 field vane shear 117, 244, 258, 428, 451
 fill 194, 204, 211, 218, 219, 243, 250, 355, 410, 415, 427, 441, 451, 494, 497
 filter 64, 106, 219
 Finite Element Method *see finite element*
 first loading 60
 fissure 346
 fixed end *see wall*
 flexibility 108, 122, 130, 221, 470
 flexible 120, 288, 343
 flexural 122
 flexural stiffness 123
 flight auger *see auger*
 flood control 493
 flood protection 493, 494, 495
- flow 108, 111, 114, 143, 326
 flow net 193
 flow rule 65
 associated flow rule 60, 64
 non associated flow rule 60
 footing 228, 234, 505
 isolated 266, 267, 285, 297
 strip 267
 strip wooden 266
 force 5, 109, 137, 220, 434, 451, 453, 485
 active 137, 138, 149
 anchor 189
 centrifugal 346, 351
 cyclic 5
 damping 382, 384
 downdrag 405, 411
 dynamic 5
 hoop 466, 495
 impact 384
 inertia 382
 measured 444
 normal 197
 passive 138, 148, 151, 181
 pre-stressing 242
 reaction 195, 205, 207, 253, 365
 resisting 197
 section 5, 9, 185, 192, 193, 194, 195, 199, 335
 seepage 193
 shear 5, 295
 strut 189
 tensile 454, 466
 tension 346
 foundation 28, 48, 65, 113, 152, 194, 239, 255, 263, 266, 269-274, 285, 287, 288, 291, 318, 325, 326, 330, 341, 353, 416, 422, 429, 432, 439, 440, 449, 450, 458, 462, 464, 465, 469, 472, 480, 496, 507, 509
analysis 465
 box type 255, 291, 334
 building 266, 268
 caisson 337
 column type 337
 combined pile-mat 472
 combined pile-raft 4, 337
 combined sleeper-floating timber pile 263
 combined timbered floating pile
 sleeper 263

- compensated box type 267, 416, 419
 compensated raft 266
 deep 337
 design 465
 element 263, 289
 flexible raft 299
 floating pile 2, 4
 floating piled raft 416, 422, 457
 floating timber pile 263, 264
 historical 263
 improvement 462, 473
 isolated 285
 layout 437, 450
 masonry 264, 265
 mat 423, 509
 micropile 373 *see also pile*
 off-shore 373
 overcompensated raft 266
 pad 456, 505
 partially compensated raft 266
 pile 2, 4, 5, 285, 337, 338, 373, 404,
 406, 413, 416, 417, 418, 434, 491
 see also pile
 piled raft 417, 418
 raft 2, 4, 227, 267, 285, 298- 308,
 311, 314, 315, 317, 319, 323-326,
 328, 330-332, 334, 335, 416, 419,
 434, 437, 440, 448, 458, 475
 raft on floating injection piles (RFIP)
 4, 418-426, 432-437, 440-443, 457
 rigid monolithic 291
 rigid raft 266, 299
 shallow 2, 4, 5, 56, 111, 132, 218,
 263-268, 270, 274, 324, 334, 370,
 373, 394, 418, 421, 426, 444, 449,
 450, 457, 481, 485, 505, 509
 slab 503
 sleeper 263, 266
 spread 297, 334
 stability 461, 474, 485
 strip 285, 505
 tower 287
 fractured zone 367
 free end support *see wall* 134
 friction 74, 75, 86, 87, 99, 116, 130,
 138, 498
 Froehlich 268
 function 158, 160, 179, 181, 240, 381,
 392, 494, 499
- g
- Geotextile encased sand/gravel column (GEC) *see column*
 geocomposite 495
 geodetic 498
 geogrid 449, 450, 496, 497, 498, 499,
 500, 501, 502, 503
 geological 371
 geological history 15
 geomembrane 133
 geometry 161, 163, 165, 180, 181, 209,
 213, 216
 geophone 503
 geosynthetic 449, 450, 451, 453, 454,
 500
 geotechnical report 208, 211, 216, 219,
 233, 235, 238, 448, 451
 geotextile 9, 106, 449, 462, 464, 465,
 466, 491, 494, 495
 geotextile filter 132
 German Code 4, 373, 380
 German Geotechnical Society 1, 185,
 473
 girder 437
 girder beam 295
 glacial 28, 45
 glacial till 342
 global failure *see failure*
 global stability *see stability*
 gradient 41
 grain
 distribution 15
 size 15, 251, 346, 348, 427
 texture 15
 Graßhof 328
 gravel 68, 106, 165, 204, 227, 244, 250,
 251, 252, 255-258, 320, 342, 347,
 348, 351, 353, 361, 366, 370, 441,
 451, 462, 490, 501
 gravity 486, 488
 grid 419, 421, 432, 453, 449, 456, 458,
 464, 469, 485, 497, 500, 507, 509
 ground 193, 355, 363, 412
 ground anchor *see anchor*
 ground improvement *see improvement*
 ground movement 105, 109, 115, 122,
 123, 125, 126, 127, 139, 157, 158,
 159, 161, 412
 ground surface 140, 160, 195, 205, 219,
 220, 222, 225, 227, 238, 241, 243-

- 245, 251-253, 255, 257, 397, 440, 444, 448, 451
- groundwater 51, 108, 112, 122, 126, 132-139, 148, 162, 186, 192, 193, 197, 204, 205, 213, 216, 219, 223, 227, 235, 244, 251, 258, 308, 320, 338, 346, 348, 356, 361-364, 367, 400, 423, 429, 440, 444, 448, 451, 471, 499, 501, 505
- artesian condition 356
- confined 199, 205, 219, 244, 251
- dewatering 199
- fluctuation 199, 205, 219, 404, 429
- lowering 122, 193, 199
- grout 113, 135, 365, 366, 367
- grout pipe 365
- grout suspension 458
- grout tube 367
- grouting 109, 122, 343, 364-367, 420
- guide wall 113
- gunnite 108, 110
- gypsum 477
- h
- halloysite 15
- hardening 3, 65, 93, 201, 366, 509
- compression hardening 3, 94
 - function 59
 - law 64
 - model 68
 - parameter 59, 63, 67, 93
 - rule 63
 - shear hardening 3, 94
- hardening soil model (HSM) *see constitutive model*
- heave 18, 128, 136, 165, 170-172, 195, 241, 259, 261, 353, 405, 421
- highway 1, 114, 506
- historical building 285
- hogging 124, 263, 287, 288
- limiting values 295
- hollow stem 360
- homogeneous *see soil*
- Hook's law 57, 63, 98, 211, 295
- hydration 469, 471, 476
- hydraulic 470
- hydraulic binder 472
- hydraulic failure *see failure*
- hydraulic filling 491, 492, 493
- hydraulic gradient 8, 193
- hydraulic heave 6
- hydraulic jack 377
- hydrolysis 498
- hydrostatic 141, 193, 213, 219, 235
- hyperbolic 58, 78, 81, 82, 93, 385
- transformed 80, 81
- hyperbolic function 76, 182, 183
- hyperelastic 58
- hyperelasticity *see constitutive model*
- hypoelastic 58
- hypoelasticity *see constitutive model*
- hypoplasticity *see constitutive model*
- hypothesis 401
- i
- illite 15, 17
- impact energy 111
- impedance 383
- impermeable 193, 211, 219, 233
- improvement 365, 366, 421, 456, 458, 475, 476, 483, 484, 488
- ground 264, 449, 475, 484, 491
 - soil 449, 456, 459, 460, 462, 485, 506, 509
- soil improvement factor 456, 460
- stability 485
- technique 450, 462
- inclinometer 205, 207, 216, 224, 229, 231, 247, 248, 253, 259, 456, 495, 503
- increment tensor 63
- incremental plasticity 60
- induced anisotropy 52
- inelastic 59
- inequality 189, 473
- infinitesimal 58
- inflection point 124, 285
- influence area 441
- influence factor 271, 272, 386, 457
- influence zone 398, 432, 458, 464
- inherent anisotropy 41, 45, 54, 131
- initial anisotropy 54
- initial hydraulic gradient 278
- injection 347, 458, 484, 487, 489, 507
- injection horizon 419, 453, 457
- injection pile 250, 252 *see also pile installation* 457
- injection pressure *see pressure*
- inorganic 26, 47 *see also clay, soil*
- in-situ 41, 45, 47, 50, 64, 122, 125, 252, 275, 313, 314, 400
- installation 207, 347, 370, 470, 475, 476, 489, 490, 491, 509 *see also anchor, base slab, column, pile, wall*

- anchor 113, 114, 126
 base slab 134, 199
 bottom slab 114, 191
 bottom support 132, 175
 column 485, 507
 diaphragm wall 125
 lateral support 123
 prop 123
 sheet pile wall 201
 tie back anchor 110
 wall 113, 114, 123, 126
- instrumentation 205, 227, 247, 374
integrity test *see pile*
 interface 58, 86, 87, 88, 90, 116, 161, 218 *see also property*
 interface element 162, 166, 180, 212
 interpolation 162
 interpretation 207, 216, 224, 384
 invariant 58, 59
 investigation 139, 158, 194, 204, 223, 227, 302, 317, 385, 487, 500
 geotechnical 4
 numerical 501
 isotropic compression 29, 30
 isotropic hardening 63, 68
 isotropic stress line 33
 j
 jacking 350, 370
 Jaki 187
 jet 481, 487
 jet pile 162, 191
 jetting 337, 352, 489
 high-pressure 352
 k
 kaolinite 15, 17
 kinematic 63
 kinematic hardening 63
 kinetic energy 58
 l
 laboratory 20, 57, 117, 128, 144, 154, 157, 185, 211, 218, 244, 276, 277, 298, 300, 311-314, 334, 385, 390, 478, 487, 498
 lacustrine clay 1, 15, 17, 20, 27, 28, 47, 52, 57, 298, 299-311, 315, 317, 323, 335, 427, 432, 451
 lacustrine deposit 204, 257, 507
 lacustrine layer 220, 222, 241, 245, 252
 lacustrine sediments 1
 lacustrine soil 3, 4, 13, 16, 47, 50, 51, 58, 60, 65, 87, 126, 143, 165, 177, 199, 205, 211, 219, 222, 223, 227, 233, 238, 243, 249, 250, 251, 256, 258, 261, 274, 277, 308, 314, 334, 418, 424, 428, 439, 441
- Lade-Duncan failure criteria 60
 Lade-Duncan model *see constitutive model*
 lateral support 122
 layered underground 197, 273
 lean concrete *see concrete*
 lime 469, 476, 478
 limestone 352
 limit state 5, 6, 139, 160, 171, 179, 181, 183, 189, 190, 457, 473
 active 6, 117, 122
 passive 6, 117, 118, 148
 serviceability 5-7, 139, 140, 189, 190, 271, 286, 289, 324, 373, 406, 411, 421
 ultimate 5, 6, 9, 120, 140, 139, 189, 319, 324, 369, 370, 373, 390, 394, 399, 406, 412
 limit stress 93
 limiting depth 271, 274, 278, 311, 444
 linear 78, 157, 174, 348, 460
 linear elastic 57, 220
 linear elasticity 68
 linear elasticity theory 275
 linear-elastic-plastic model *see constitutive model*
 liquefaction 476
 liquid limit 15, 16, 20, 25, 27, 44, 87, 187, 244, 251, 319, 478
 liquidity index 15
 load 58, 59, 71, 134, 138, 140, 159, 161, 188, 189, 194, 266, 271, 304, 305, 306, 308, 314-316, 324, 337, 343, 422, 434, 439, 444, 458, 478, 481, 490, 498, 499
 asymmetrical surface 412
 building 162, 267, 308, 312, 337, 369, 434, 440, 443, 449
 change 375, 469
 combination 213
 concentration 469, 471, 476
 cylinder 71
 cyclical 347
 dead 196
 distributed 220
 distribution 194, 480
 dynamic impact 382

- dynamic 135
failure 417
flexible uniform surface 269
history 57, 59
increment 298, 312, 313, 334, 369,
 377, 379, 467
incremental 373, 377
lateral 413, 414
line 332
live 196, 503
modification factor 138
O-cell 376
point 268, 269
redistribution 449, 455, 461
rigid uniform surface 270
sharing factor 458
stage 379
structural 191, 406, 472, 473
surcharge 196, 210, 220, 233, 308,
 414, 416, 451
surface 269, 274, 300, 337, 404, 449
tension 347
traffic 162, 220, 233, 452
transducer 247, 253
transfer 366, 367, 373, 420, 449, 450
transfer mechanism 264
ultimate 324, 380
uniform surface 271
uniformly distributed 272
working 382
load test *see pile*
load-deformation curve 61, 376
loading 18, 22, 42, 58, 57, 68, 69, 70,
 85, 92, 93, 141, 167, 168, 169, 190,
 213, 216, 261, 280, 324, 353, 370,
 374, 377, 384
compression 375, 399
constant rate 313
cyclic 378
fast 317
history 393
incremental 311
primary 141
quick 289
rate 298, 313, 314, 317, 319, 334,
 378, 390
slow incremental 289
stage 320, 321
tensile 348
tension 375, 399
undrained 176
load-settlement 272, 312, 314, 381, 506
local shear 317
long term 37, 108, 115, 390
m
marine sediment 319
marl 352
marshy 491
masonry wall *see wall*
mass flow 107
material constant 58
material matrix 65
measurement 195, 207, 224, 229, 231,
 235, 238, 240, 259, 261, 313, 376,
 384, 422, 434, 440, 443, 449, 456,
 495, 496, 498
membrane 66, 185, 454
membrane correction 66
membrane effect 449, 451
method 350
 α -Method 394
analytical 229, 317, 328, 330
construction 297
conventional 317, 319, 320
deep mixing 475
design 456
displacement 462, 463, 465
installation 455, 462, 465
monitoring 250
numerical 229, 317, 330
replacement 462, 463, 465, 466
statistical 297
top-down construction 256
micropile *see pile*
Mindlin-equation 370
mineral layer 501
mineralogical composition 15
mineralogy 55
mix design 362
mixed hardening 63
mixer 484
mixing 481, 484, 487
mixing blade 482, 484
mixing plant 482
mixing shaft 482, 484
mixing tool 482, 484, 487
mixture 498
mobilisation 108, 171, 179
 curve 182
earth resistance 181, 189
function 179, 180, 183, 407
passive pressure 189, 466

- passive resistance 179, 180, 184
 safety 196
 shaft resistance 406
 soil strength 139
 model 157, 163, 165, 179, 180, 181,
 209, 216, 231, 233, 487 *see also*
finite element
 analytical 465
 model geometry 208
 model test 363, 453
 model theory 275
 modulus 171, 501
 bulk 56-58, 98, 211
 drained, undrained 57, 98
 compressibility 50, 268, 271, 426,
 444, 480
 compression 66, 478
 constrained 60-63, 85, 143, 168, 190,
 233, 268, 271, 274, 320, 326, 327,
 328, 467, 468, 475
 deformation 56, 218, 268, 326
 dynamic elasticity 383
 elasticity 56-60, 65, 76, 77, 81-86,
 98, 128, 141, 169, 233, 234, 268,
 374, 457, 459, 460
 number 58, 62, 77
 reloading 76
 secant 56, 76, 77, 81, 85, 86, 92, 93,
 170, 211, 233, 268
 shear 56, 57, 58, 87, 98, 399, 481
 subgrade 326, 327, 328, 330, 331,
 332, 333, 334, 335, 509
 subgrade reaction 190, 192
 tangent 56, 58, 77, 78, 86, 92, 93
 undrained 58, 103
 unloading 76
 variable 57, 59
 Young's 56, 399
 modulus of elasticity *see modulus*
 Mohr-Coulomb model *see constitutive soil model*
 Mohr-Coulomb yield criteria 60, 67
 moisture content 16, 24, 25, 27
 monitoring 136, 199, 200, 205, 247,
 259, 379, 503
 monolithic 474
 montmorillonite 15, 17
 moraine 165, 177, 204, 219, 227, 228,
 233, 244, 308, 427
 mortar 490
 mortar sheet 419, 458
 movement 2, 29, 58, 109, 114, 115,
 118, 122, 124, 128, 129, 136, 158,
 159, 173, 198, 205, 221, 224, 247,
 252, 253, 261, 355, 371, 376, 383,
 406, 470 *see also soil, wall*
 mud 491, 496, 497
 Muehlenberger Loch 491
 n
 Navier 295
 necking 363, 364
 negative skin friction *see skin friction*
 neutral line 296
 neutral plane 410
 neutral point 406, 410, 411, 416
 nomogram 271
 non-cohesive 68, 473
 non-linear 57, 58, 61, 67, 78, 81, 88,
 157, 174, 282, 370
 non-linear elastic 57
 non-linearity 57, 84
 normalised undrained strength 51, 52,
 normally consolidated soil *see soil*
 numerical
 analysis 57, 86, 106, 399
 calculation 399
 instability 211
 integration 162
 investigation 394
 method 2, 157, 370, 385, 398
 model 58, 401
 modelling 2
 simulation 398, 401, 502
 study 171, 177, 181
 o
 observation 195, 205, 241, 366, 501
 field 311
 long-term 311, 314
 time 311
 obstruction 352
 O-cell 376, 377
 oedometer 13, 19, 22, 58, 64, 85, 90-92,
 96, 168, 279, 312, 334
 one-dimensional 3, 59, 162, 311
 anisotropic compression 3
 compression 3, 19, 22, 23, 29, 30, 45,
 59, 60, 64, 65, 90, 92, 93, 94, 95,
 162, 268, 274, 275, 276, 277, 279,
 281, 311, 323, 509
 consolidation 58, 59, 275, 311
 isotropic compression 3
 loading 28

-
- theory 275
 open cut 485
 operation 424, 497
 optimisation 492
 organic 15, 26, 28, 82 *see also soil*
 organic content 428
 oscillatory speed 112
 Osterberg-cell 376 *see also O-cell*
 overall stability *see stability*
 overburden weight 410
 overconsolidation 281
 ratio 21, 22, 393
 overstress 114
 overturning 6, 114, 488
 p
 parabolic 124, 174, 369, 371
 parameter 31, 33, 165, 172, 173, 177,
 220, 223, 459, 461, 487
 characteristic 411
 compressibility 298
 compression 13, 15, 24, 29, 60, 313,
 314, 334
 deformation 13, 58, 65, 76, 81, 82,
 84, 85, 166, 268, 274, 299, 487
 design 397
 determination 65
 dimensionless 182
 drained 81
 effective 35, 37, 39-42, 67, 74, 75,
 98, 101, 115, 137, 141, 144, 402
 fluidity 64
 geometrical 278
 hardening soil model 165, 172
 identification 157
 index 15, 24, 51
 input 86, 155, 157, 318, 320, 328,
 330, 332, 387, 399
 material 67, 238
 model 3, 33, 95, 161, 167, 181
 physical 182
 pore pressure 39, 41, 42, 43, 141
 reference 155, 166, 167, 171, 216
 shear 7, 9, 32, 66, 93, 117, 138, 162,
 166, 171, 185, 186, 217, 316, 456,
 495
 stiffness 95, 98, 99, 167, 171, 183,
 211, 212, 218, 234, 238, 268, 271
 strength 13, 15, 58, 65, 69, 70, 72,
 75, 81, 101, 137, 138, 171, 185,
 487
 undrained strength 37, 39, 40
- variation 218
 study 3, 57, 68, 97, 98, 138, 146,
 154, 155, 158-162, 165, 173, 175,
 181, 185, 210, 216, 223, 231, 326,
 327, 328
- passive earth pressure *see pressure*
 peat 388, 462, 464, 481, 496, 497, 503
 penetration 211, 353, 354, 364, 417,
 463, 484, 497, 498
 rate 50, 378, 386, 487
- permeability 18, 29, 275, 276, 478, 487
- piers 424
- piezometer 204, 205, 247, 495
- pile 4, 228, 234, 246, 259, 337, 338,
 346, 371, 373, 383, 385, 389, 394,
 399, 457, 449, 454, 476, 491, 503,
 505, 506, 507 *see also foundation*
 adhesion bond 348
 Atlas 353
 base 341, 344, 346, 351, 352, 355,
 356, 360, 361, 363, 364, 365, 370,
 374, 376, 382, 383
 base expansion 342
 base resistance 9, 386, 390, 394, 396,
 397, 399, 401, 406 *see also*
 resistance
 batter 415
 bearing behaviour 4, 384
 bearing capacity 352, 366, 385, 390,
 398, 401, 404, 412, 417
 bending 412, 415
 bored 125, 244, 256, 398, 401, 416,
 418, 491
 cap 382, 416
 capacity 356, 370, 371, 373, 378
 cast iron pipe 343
 cast-in-place 343, 347, 351, 353,
 355, 363-365, 367, 399
 closed end 397
 collar 415
 compacto-Pile 347
 composite 367
 compression 361, 371, 380
 concrete 362, 376
 conical 346
 control 417
 creep 416
 cylindrical 346
 density 432, 437

- displacement 340, 341, 350, 366, 374, 375, 385, 386, 389, 397, 400, 401, 404, 407, 416
 displacement floating 422
 drilled 355, 356, 360, 361, 362, 363, 366, 374, 377
 drilled concrete 362
 drilling 356
 driven 340, 376
 driven cast-in-place concrete 348
 driven steel pipe 342
 driver 346, 351
 driving 351, 383, 394, 398, 400
 driving tension 401
 dynamic pile load test 384
 dynamic resistance 383
 dynamic testing 350, 373, 382
 end bearing 411
 floating driven 449, 450
 floating injection 457
 floating precast concrete driven 448
 Franki-type 348
 Franki-type method 347
 friction 411, 417
 full-displacement bored 355
 Fundex 354, 355
 GEWI 367, 432, 439, 441, 457
 GEWI- injection 420
 grid system 245
 group 6, 337, 412, 414, 475
 grouted 343
 grouted micropile 420
 injection 4, 419, 420, 421, 424, 432, 434, 437, 439-441, 443, 453, 456, 457, 458
 installation 340, 343, 346, 350-356, 360, 371, 395, 398, 400, 401, 404, 417, 432, 441, 456
 integrity testing 382
 load tension test 401
 load test 347, 350, 373, 374, 377, 378, 380, 382, 388-390, 401, 457, 487, 507
 deformation-controlled 379
 load-controlled 379
 micropile 4, 340, 366, 367, 419
 movement 382, 383
 non-destructive testing 382
 one-bar 366
 open end steel pipe 397
 overlapping 417
 partial displacement drilled 360
 penetrating 370
 pile-soil-interface 396
 pipe 366
 precast reinforced concrete 344, 346, 347, 351, 457, 364, 368
 prefabricated displacement 374
 pressure grouted 367, 374
 pressure grouted displacement 347
 pressure grouted drilled 366
 prestressed concrete 346
 prestressing 365
 raking 493
 reaction 374
 reinforced concrete 401
 resistance 365, 370, 373, 394, 401, 405, 411
 ultimate 377, 380
 resistance-settlement behaviour 398, 399, 400
 resistance-settlement line 385
 sand compaction 455, 462, 465
 screw 353
 settlement 356, 405, 406, 407, 411, 412
 shaft 341, 346, 348, 351, 353, 354, 355, 361, 362, 363, 364, 366, 367, 371, 375, 376, 382
 shaft resistance 9, 352, 354, 369, 387, 391, 393, 396, 399, 401, 402, 403, 405, 410
 shaft surface area 419
 simplex-type method 347
 single 6, 112, 134, 337, 414, 432, 509
 single compression 369
 skin friction *see skin friction*
 spacing 350, 414, 416, 432
 steel 338, 341, 342, 401, 404
 steel pipe 343, 393, 404
 steel tube 366
 stiffness 383
 structural 373, 415
 surface 346, 348
 system 337
 tangent bored 228
 tension 9, 257, 343, 362, 371, 405
 test pile 374
 timber 338, 341, 401
 ttop-down-load-testing 376, 377
 ultimate capacity 385

- vibrated concrete 337
 vibrating 351
 vibro-injection 347
 wall *see also wall*
 pipeline 492
 piping 8
 piping failure *see failure*
 piston 482
 placement 195, 201, 202, 207, 214, 225,
 235, 236, 244, 246, 346, 348, 362,
 367, 415, 492
 plane strain *see strain*
 plastic 45, 47, 57, 65, 62, 68, 251
 plastic anisotropy 63
 plastic deformation *see deformation*
 plastic failure *see failure*
 plastic flow 28, 63
 plastic limit 16, 44
 plastic strain 59, 64
 plastic straining 59, 68
 plastic yield 63
 plastic zone 119
 plasticity 15, 21, 26, 35, 55, 57, 108,
 112, 132, 220, 227, 319
 plasticity chart 16
 plasticity index 15, 16, 20, 21, 25, 27,
 48, 50, 52, 87, 187, 251, 258, 319
 plasticity theory 59
 plate 220, 221, 234, 296, 326, 328, 329,
 335, 449, 458
 flexible 456
 rigid 456
 PLAXIS 3, 57, 68, 62, 77, 86, 90, 92,
 103, 161, 171, 208, 211, 231, 318,
 320, 328
 pneumatic cylinder 71, 72
 Poisson's ratio 22, 56, 57, 59, 60, 68,
 85, 92, 166, 212, 399, 457, 459, 467
 drained Poisson's ratio 98
 undrained Poisson's ratio 98
 polder 491, 493
 pore pressure 1, 12, 13, 18, 74, 141,
 142, 148, 156, 205, 247, 457
 at failure 39
 dissipation 3, 143
 distribution 213
 drop 248
 excess 1, 18, 20, 29, 31, 35, 37, 45,
 54, 69, 71, 72, 74, 81, 98-103, 141-
 145, 147, 162, 172, 176, 186, 194,
 207, 211, 226, 235, 258, 275, 277,
 312, 319, 341, 400, 463, 471, 495
 measurement 320
 negative excess 238, 363
 parameter 148
 steady state 141
 transducer 247, 312, 495
 porosity 15, 98, 211
 postglacial 1, 199, 258, 277, 298, 319
 postgrouting 432, 441, 458
 potential function 59, 183
 potential surface 60
 power law 77, 93
 pre-consolidation 64, 277
 prediction 67, 58, 126, 141, 157, 370,
 386, 506 *see also displacement,*
 settlement
 predrilling 352
 prefabricated 346
 prefabricated concrete *see pile*
 preglacial 298
 preloading 365, 415
 pressure 61, 72, 188, 268, 269, 360,
 362, 364, 415, 420, 441, 453, 458,
 459, 464, 468, 478, 505
 active earth 113, 117, 118, 137, 144,
 169, 179, 188, 190, 191, 198, 413,
 488
 active earth reaction 191
 atmospheric 58
 cell 29, 74
 confined water 204
 confining 81, 96
 consolidation 61, 117
 contact 114, 272, 325, 326, 329, 444,
 509
 diagram 137
 distribution 195
 earth 17, 52, 57, 86, 115-117, 119,
 122, 130, 138, 144, 146, 149, 151,
 158, 159, 161, 166-168, 170, 185,
 193, 198, 413, 415, 465, 466, 495
 earth pressure at rest 181, 188, 190
 effective active earth 140
 effective consolidation 278, 280
 effective passive earth 140
 flow 413
 grouting 420, 421
 hydraulic 356, 361
 hydrostatic 367, 460

- injection 418, 419, 421, 432, 456,
 457, 458
 internal 459
 lateral 412, 414, 415
 net 315, 316
 nominal earth 138
 O-cell 376
 overburden 21, 187, 266, 267, 271,
 274, 278, 300, 312
 passive earth 117, 118, 119, 137,
 138, 169, 179, 189, 190, 353, 413,
 488
 pre-consolidation 63, 64, 266, 280,
 300, 308, 312
 reaction 207
 redistribution 195
 reference 58, 61, 79, 82, 84, 91, 92,
 284, 469
 relief 271
 resultant 120
 surcharge 196
 suspension 113
 total active earth 145, 148
 total passive 145, 148
 transducer 207
 undrained active earth 140
 undrained passive earth 140
 uplift 266, 272, 440
 water 8, 112, 113, 138, 139, 141,
 185, 188, 190-194, 363, 366
 pressure cell 13, 277, 377
 pressure grouting 364, 365, 366, 367
 pressuremeter 44, 457
 prestressing 341, 344, 421, 456
 prestressing bar 346
 primary loading 3, 63, 95, 104, 128,
 271, 272
 primary unloading 21
 project 143, 218, 229, 233, 238, 255,
 425, 426, 428, 444, 445, 448, 454,
 457, 505
 prop 108, 109
 property 2
 compression 11
 deformation 11, 14, 65, 369
 elastic 57, 459
 elastic material 295
 geotechnical 308
 index 11
 interface 216, 217, 218
 material 56, 86, 162, 175, 233, 234,
 235, 238
 mechanical 45, 65, 471, 481, 487
 physical 15
 strength 11, 14, 65, 139, 369
 proportionality factor 383
 propped I-steel beam 200, 207
 propped wooden 200-202
 pump 199, 482
 pumping 199, 362, 364, 365
 pycnotropy 65, 66
 r
 radius
 equivalent 432
 influence area 448
 raft foundation *see foundation*
 raft foundation on floating injection
 piles (RFIP) *see foundation*
 rail 497-503
 railway 1, 422, 424, 485, 491, 496-499
 raker 109, 119, 135
 ramming 394, 455
 Rankin 457
 raster 456
 reclamation 462, 491, 492, 493, 494
 recommendation 146, 185, 195, 197,
 209, 231, 233, 337, 362, 381
 recompression 300
 reconstruction 502
 reduction factor 119, 122, 386, 388
 reinforced concrete wall *see wall*
 reinforced slopes 9
 reinforcement 343, 344, 346, 348, 349,
 353, 361, 362, 365, 367, 449, 450,
 453, 454, 475, 497, 500
 relaxation 66, 284
 reloading 3, 22, 24, 60, 58, 57, 60, 62,
 63, 68, 69, 70, 77, 85, 92, 94, 95, 102,
 103, 104, 128, 141, 166, 169, 271,
 272, 378
 reloading modulus *see modulus* 76
 remolding 478
 replacement 364, 491, 492
 replacement ratio 459
 requirement 185, 252, 344, 484, 506,
 507
 residual 66, 123
 residual stress *see stress*
 resistance 384
 base 369, 371, 374, 377, 383, 479,
 see also pile

- bearing 9, 472
 creep 381
 driving 341, 382
 dynamic 384
 dynamic pile 382
 earth 179, 180, 189, 190
 end 472, 479
 end-bearing 374
 friction 185
 limit 385
 mobilised 182
 modification factor 138
 net 181
 passive 9, 115, 138, 171, 181, 183,
 198, 473
 penetration 383
 pile 381, 382, 384
 pressing 112
 shaft 342, 348, 365, 369, 371, 373,
 374, 375, 376, 383 *see also pile*
 shear 30, 197, 509
 skin 479
 slide 9, 198
 static 384
 total pile 374
 ultimate 381
 ultimate pile 379
 ultimate shaft 374
 resistance-settlement curve 369
 restoration 506
 retaining structure 3, 17, 40, 108, 110,
 114, 115, 116, 137, 138, 146, 152,
 162, 195, 200, 259, 476, 507
 retaining wall 58, 86, 115, 119, 135,
 137, 139, 141, 194, 199, 247, 257
 rheological model 279
 rigidity 108, 109, 159, 326, 382
 road 485, 491, 506
 rock anchors 9
 rotary 353
 drill 424
 method 363, 476
 mixing 475
 rotation 6, 152, 156, 196, 364, 497
 rupture 197, 457
 s
 safety 108, 112, 113, 124, 135, 137,
 140, 194, 199, 246, 271, 338, 453,
 473, 474, 506, 509
 against basal heave 129, 131
 verification 195, 196, 198, 406
 safety factor 108, 115, 116, 120, 130,
 137, 138, 139, 141, 142, 143, 319,
 324, 325
 partial 4-7, 138, 316, 318, 324, 196,
 338, 373, 406, 407, 473, 474, 504,
 506 507
 total 5, 14, 129, 137
 sagging 124, 263, 287, 288, 329
 limiting value 295
 sample 13, 47, 68, 84, 85, 90, 390, 478
 block 13, 14
 disturbance 11, 14, 66, 279
 horizontal oriented 79
 orientation 54, 59, 75
 remoulded 12
 undisturbed 11, 20, 73, 75, 85, 211,
 276, 277
 vertical oriented 79
 sampling 11
 block sampling 14
 disturbance 11, 185
 mechanical disturbance 12, 13, 276
 piston 12, 13
 technique 12, 13, 14
 thin tube 12, 13
 tube 11, 12, 14
 sand 68, 115, 117, 119, 122, 157, 165,
 177, 179, 194, 199, 204, 243, 244,
 323, 348, 351, 353, 355, 356, 363,
 364, 366, 370, 375, 397, 399, 401,
 462, 469, 481, 491-494, 497, 499,
 500, 503
 sandstone 352
 scale factor 386
 screw feeding 477
 screwing 350, 355
 seasonal 199
 secant method 64
 secant modulus *see modulus*
 sedimentation 57, 196
 seem
 sand 1, 108, 111, 132, 135, 199, 258,
 277, 427, 428
 silt 1, 108, 111, 135, 194, 199, 258,
 277, 427, 428
 seepage 485
 seepage force *see force*
 self weight 355
 semi-empirical method 389
 sensitive 55, 82, 97, 101, 112, 135, 258,
 354, 377

- sensitivity 2, 96, 101, 161, 172, 249, 478, 491
 sensitivity study 165
 serviceability *see limit state*
 settlement 1, 5, 6, 14, 22, 23, 68, 57, 109-113, 122-128, 132, 136, 143, 160, 165, 169-177, 199, 205, 206, 219, 220, 228-231, 241, 247, 255, 261, 263, 266-268, 270-276, 285, 306, 308, 309, 315, 323, 326, 363, 364, 370, 377, 378, 381, 404, 406, 407, 410, 411, 415-417, 424, 426, 439, 455, 456, 461, 464-467, 480, 491, 496, 498-501, 503, 505-507
 allowable 263, 286, 287, 294
 behind the wall 195
 calculated 284, 298, 300, 310, 311, 314, 316, 317, 320, 327, 333, 434, 444, 450
 calculation 271, 275, 278, 322, 324, 326, 465, 480, 491
 component 481
 computed 225, 240, 241, 321
 consolidation 274, 277, 411, 416
 contour 300
 creep 274, 285, 412
 curve 240, 241
 delayed 280
 differential 263, 285, 287, 289-291, 297, 321, 322, 323, 451, 481, 485
 elastic 300
 end 330, 334, 440
 entrainment 263
 excessive 240, 315-317, 322, 369, 449, 509
 extrapolated 334
 final 299, 300, 309, 315, 317, 332, 443
 hogging 294
 immediate 274, 280, 300
 improvement 457
 increment 378
 initial 434, 443
 isoline 299
 measured 225, 240, 241, 268, 284, 298-302, 311, 314-321, 332-334, 425, 434, 437, 440, 443, 449, 457, 495, 503
 measurement 291, 294, 297, 299, 300, 320, 322, 330, 334, 434, 444, 456, 498
 monitoring 229
 observation 276, 277, 299, 335
 predicted 276, 298, 315, 317, 320, 425, 449, 506
 prediction 263, 271, 277, 279, 298, 334
 primary 274, 280, 299, 300, 309
 rate 279, 322, 478
 reduction 418, 420, 421, 458, 476, 494, 496
 reduction factor 422, 457, 456, 459, 460
 sagging 295
 secondary 274, 279, 280, 284, 299, 300, 304, 309, 311, 440, 458
 surface 158, 159, 166, 168, 170, 178, 205, 206, 238, 459
 trough 288, 291, 325, 329, 332, 334
 ultimate 381
 uniform 256, 285
 unrecoverable 335
 velocity 379
 shaft 355, 462, 481, 482, 484
 shaft friction 365, 402
 shaft resistance *see pile, resistance*
 positive 406
 shallow foundation *see foundation*
 shear box 58
 shear failure *see failure*
 shear modulus *see modulus*
 shear parameter *see parameter*
 shear stiffness 57, 88, 90
 shear strength 1, 9, 35, 44, 66, 160, 233, 258, 316, 379, 393, 449, 478, 479, 480, 487
 angle of overall shear strength 33, 36, 42, 74, 99, 186,
 cohesive component 48
 drained 3, 54
 frictional component 48
 mobilisation 49
 normalised undrained 392, 394
 ultimate 324
 undrained 2, 3, 14-16, 33, 37, 41, 44-51, 53, 54, 58, 108, 113, 116, 117, 130, 131, 139, 140, 146, 151, 185, 186, 196, 244, 251, 299, 302, 305, 351, 389, 390, 394, 402, 407, 423, 428, 451, 455, 457, 473, 474, 478, 479, 491, 493, 509
 shear stress *see stress*

- sheet pile 112, 122, 124, 125 *see also wall*
 sheet pile wall *see wall*
 shell 451
 short term 37, 44, 115, 141, 143, 144, 195, 316, 390, 402, 421, 498, 500
 shotcrete 110
 shrinkage 17, 297, 323
 shrinkage limit 323
 significant 156, 217, 241, 248
 silt 45, 244, 250, 356, 388, 462, 464, 481, 503
 simple shear 31
 Simpson's rule 300
 simulation 221, 399 *see also finite element*
 site investigation 227
 Skempton 141
 skin friction 369, 371, 387, 397, 405, 407, 408, 457, 458, 472, 478
 negative 8, 404, 405, 406, 407, 410, 412, 417
 positive 410, 417
 slab 108, 135, 175, 215, 221, 222
 slice 134, 158, 162, 189, 190, 194, 198, 201, 214, 222, 225, 235, 236, 237, 257, 261
 slide failure *see failure*
 sliding 113, 114, 119, 156, 476, 485, 488
 rotational 488
 sliding surface 119, 198
 slip surface 116
 slit 489
 slope 24, 32, 45, 49, 56, 59, 61, 64, 73, 76, 103, 106, 108, 110, 129, 134, 135, 143, 157, 182, 235, 236, 324, 361, 413, 415, 494, 497
 slope doweling 9
 slope failure *see failure*
 slope protection 106
 slope stability *see stability*
 sloughing 348, 360, 362
 sludge 50, 462, 464, 481, 491, 492, 493
 sluice 490
 sluicing 493
 slumping 361, 363, 364
 slurry 113, 125, 337, 356, 360, 362, 363, 364, 365, 476, 481, 484, 487, 497, 498 *see also bentonite*
- soft soil creep model *see constitutive model*
 soft soil model *see constitutive model*
 softening 65, 112, 113
 soil 1, 14, 131, 136, 137, 138, 139, 158, 159, 171, 198, 263
 behaviour 3, 16, 23, 36, 57, 67, 128, 141, 157, 162, 211, 233, 481, 484
 block 198
 classification 2, 15, 16
 cohesionless 60, 352, 397
 cohesive 1, 106, 116, 120, 126, 179, 259, 275, 280, 341, 351, 355, 356, 360, 361, 367, 388, 389, 394, 396, 404, 407, 408, 414, 469, 489
 composition 16
 compressibility 101, 397
 compressible 404, 407
 compression 278
 condition 195, 350, 495, 498, 499
 deep soft 268, 278
 deformation 298, 356, 415
 dense 352, 370
 difficult 299
 displacement 350, 353, 354, 355, 366, 397
 exchange 267, 415
 expansive 17
 exploration 200, 204, 334
 failure 168
 fine grained 1, 348, 362
 flow 135, 413, 415
 granular 341, 344, 351, 355, 356, 361, 367, 469
 hardening 199
 heavily overconsolidated cohesive 68
 heterogeneous 503
 homogeneous 112, 162, 165, 180, 188, 192, 195, 196, 461
 improvement 2, 415, 420, 458
 interaction 285
 light overconsolidated 1
 liquefied 356
 mass 237
 movement 160, 162, 166, 167, 169, 177, 199
 natural 26, 28, 57, 283
 non-cohesive 57, 385, 394, 396, 401, 408
 normally consolidated 1, 19-22, 26, 39, 44, 45, 47, 48, 54-58, 66, 81,

- 85, 116, 117, 128, 137, 149, 167,
179, 185, 251, 258, 280, 291, 300,
302, 457, 480
organic 455, 469, 478, 481, 489, 496,
499, 501
overconsolidated 21, 22, 30, 352
parameter 2, 8, 31, 57, 60, 68, 58, 90,
91, 98, 137, 162, 180, 211, 216,
233, 238, 240, 318, 320, 448, 451,
459
partially consolidated 316
particle 19, 60
permeability 143
physical property 16, 116
poorly graded granular 360
profile 177, 208, 223, 231, 238, 279,
323, 423, 448, 451, 493, 509
property 45, 173, 238, 279, 306, 398,
459
replacement 416
resistance 278, 382, 460
saturated 2, 18, 24, 39, 77, 194, 196,
275, 341
sensitive 11, 26, 149, 455
skeleton 19, 57, 60
soft 1, 3, 4, 11, 13, 14, 27, 36, 111,
114, 132, 135, 141, 146, 165, 185,
187, 189, 199, 264, 267, 268, 299,
312, 313, 316, 319, 320, 324, 325,
328, 330, 334, 335, 353, 356, 363,
414, 416, 418, 419, 420, 422, 423,
458, 449, 451, 452, 454, 455, 459,
462, 464, 466, 468, 481, 489, 491,
493, 495, 499, 501
softening 356
stabilisation *see stabilisation*
stabilised 478, 481, 487, 488
stiff 342
stiffness 3, 160, 162, 166, 179, 183,
211, 216, 453, 456-459, 472
strength 453, 456, 458
stress-strain behaviour 3
structure 18, 276, 449
treated 484
uncemented 26
underconsolidated 1, 258
undisturbed 125, 390
unsaturated 341
unstabilised 478, 480, 481, 486
untreated 479, 480, 488, 509
weak 503
well-graded 351
soil exchange *see soil*
soil exploration *see soil*
soil mechanic 268, 396
soil model 2, 57, 59, 68, 157
soil nails 9
soil parameter *see soil*
soilcrete 109, 162, 188, 191, 198, 250,
252, 257, 261, 489, 503
installation 255, 261
soldier pile *see wall*
sounding 211, 302, 371, 509
spacing 346, 350, 362
specific gravity 24, 27
specific volume 24
specification 185, 364, 487
specimen 31, 32, 35, 64-66, 70, 74, 78-
80, 83, 87, 92, 94, 96, 99, 101, 103,
152, 165, 185, 277, 311-314, 323,
456
horizontal oriented 74, 75, 82
reconstituted 75, 84
vertical oriented 74, 75, 85
speed 482, 496, 497, 498, 499, 500, 501
penetration 482
rotation 487
rotational 484, 487
splice 341, 346
split gravel 132
stabilisation 135, 416, 420, 421, 422,
449, 453, 454, 457, 496
cement 498
column 475, 480
method 418
slope 199, 469
soil 449, 469, 481, 498
stabilising 235, 236, 342, 360, 413, 422,
484
column 509
foundation 509
stability 5, 44, 48, 106, 113-116, 120,
129, 132, 137, 142, 221, 449, 476,
491, 495, 497, 503, 506
calculation 5
external 488
number 119, 160
overall 7, 9, 114, 139, 474, 507
slope 197, 474, 480, 495
verification 193
stability failure *see failure* 129
stagnation gradient 258

- standard deviation 505
 standard penetration test (SPT) 50, 400
 standpipe 204, 205
state of stress *see stress*
 state variable 65
static analysis *see analysis*
 steady seepage 142
 steel 87, 90, 108, 134, 139, 234, 341,
 348, 352, 362, 366, 367, 422, 424,
 445, 462
 steel pile *see also pile*
 H-pile 341
 pipe pile 341
 square shaped pile 341
 steel pipe 367
 Steinbrenner 269
 stiffness 3, 58, 61-63, 72, 77, 78, 82-87,
 90, 92-94, 122-124, 128, 130, 157,
 159, 175, 180, 181, 213, 218, 220,
 222, 233, 234, 238, 239, 274, 276,
 288, 326, 327, 334, 421, 451, 454,
 455, 466, 472, 475, 476, 494, 503
 stiffness matrix 63
 stirrup 344, 346, 362
 strain 2, 19, 29, 31, 33, 48, 56-60, 63,
 64, 66-69, 72-76, 86, 87, 92, 93, 96,
 99, 100-102, 111, 268, 384, 466, 501
 at failure 66
 at rupture 295, 297
 elastic 68
 increment 58
 limiting 66
 plane 47, 68, 152, 158
 plastic volumetric 141
 rate 31, 48, 49, 65, 87, 117, 284, 509
 shear 295, 320
 tensor 58
 tensile 322
 strength 8, 105, 114, 128, 131, 139,
 140, 173, 189, 213, 299, 308, 337,
 342, 396, 471, 476, 487, 490, 491,
 500
 bending 341
 compression 343
 compressive 77, 341, 348, 455, 472,
 487, 489, 504, 505, 506
 envelope 74, 75
 factor 138
 field vane 509
 tensile 341, 462, 495, 498, 501
 tension 343
 unconfined 473, 474, 487, 503
 stress 2, 12, 19, 22, 24, 30-32, 36, 37,
 40, 45, 56-69, 71, 72, 88, 95, 109,
 114-116, 122, 141-144, 148, 155,
 156, 268-272, 284, 288-290, 317,
 326, 356, 365, 395, 398, 401, 416,
 417, 458, 466, 469
 3-dimensional state 152
 active stress 40
 anisotropic stress 58
 at failure 72, 79, 95, 101
 bending 5
 change 211, 274, 285
 compression 5, 504, 505
 compressive 152, 474, 506
 concentration 464, 495
 concentration factor 459
 confining 81
 consolidation 59, 187
 contact 266
 decrements 72
 difference 272, 466, 467
 distribution 268, 275, 295, 343, 452
 equivalent 36
 flexural 326, 334
 history 15, 30, 44, 45, 128, 271
 hoop 464, 465
 horizontal 20, 24, 40, 72, 73, 124,
 125, 145, 147, 140, 152, 156
 hydrostatic 458
 increment 72, 152, 155, 279
 incremental stress tensor 58
 initial 37, 54, 125, 141, 158, 160,
 418
 initial state of 42, 95, 167
 in-situ 12, 13, 158, 161, 277, 356
 lateral 32, 152, 340, 355, 371, 375
 level 31, 91, 92, 93, 271, 281, 457,
 468
 maximum previous 23
 mean principal 24
 minor principal 24
 normal 30, 87, 88, 90, 462
 orientation 54, 55
 overburden 370, 371
 passive 40
 principal 31, 37, 41, 42, 43, 66, 69,
 128, 141, 152, 190, 196
 principal stress orientation 181
 principal total 156
 radial 451

- rate 72
 ratio 152
 readjustment 142
 recovery 281
 redistribution 285
 reference 90
 relief 261, 274, 283, 308, 444, 451
 relieve 449
 residual 399
 shear 5, 32, 87, 88, 457, 462, 474,
 481
 state of 19, 59, 152, 213, 272
 system 55
 tensor 65
 trajectory 64
 tensile 5, 246, 474
 vertical 20-24, 32, 50, 63, 70-74, 91,
 116, 122, 145, 147, 152, 156, 272
 vertical distribution 271
 stress history *see stress*
 stress induced anisotropy 45
 stress path 3, 31-33, 35, 38, 40, 42, 54,
 57-59, 65, 67-75, 83, 85, 99, 101,
 103, 117, 128, 145, 147, 154, 155,
 156, 157, 177, 186, 375
 drained 68
 effective 33, 70, 74, 141, 146, 155,
 156, 319
 idealized 155, 156
 total 33, 41, 72, 73, 74, 84, 85, 86,
 145, 146, 148, 155
 stress-displacement 88
 stress-strain 22, 56-61, 66, 67, 71-73,
 76, 78, 80-83, 88, 91-94, 96, 116, 162
 transformed stress-strain 78, 81-83
 stress-strain behaviour *see behaviour*
 stretch 499, 501
 structural element 208, 209, 212, 231
 structure 31, 199, 216, 249, 255, 291,
 314, 317, 324, 338, 341, 350, 354,
 420, 422, 440, 445, 449, 472, 481,
 485, 486, 488, 500, 503, 509
 statically determinant 289
 stiffness 288
 geotechnical 7
 strut 108-122, 134, 138, 158, 161, 162,
 188, 189, 195, 220, 245, 252, 253
 force 247, 253
 pre-stressing 159
 steel tube 252
 wooden 200, 201
- subbase 497, 499, 501
 subgrade reaction 325, 326, 328, 329,
 330, 331, 332, 335, 454, 509
 suction 12, 13, 112, 360
 sufficient 194, 198, 199, 351, 353
 superstructure 268, 285, 335, 434
 support 161, 195
 installation 159, 162
 surface level 205
 surface water 199
 surveying 205, 241, 247
 suspension 113, 489
 swell potential 17
 swelling 17, 128, 141, 268
 swelling capacity 17
 swelling index 24, 25, 27, 59, 60, 63,
 328
 t
 tangent method 64
 tangent modulus *see modulus*
 Taylor's method 334
 temperature 31, 253, 297, 355, 377
 tension crack 116
 tensor 65
 Terzaghi's theory 275, 278, 280
 test pit 303, 493
 theory of elasticity 271, 370
 theory of plasticity 116
 thick wall 459
 thixotropy 2, 48, 111
 three-dimensional consolidation 275
 three-dimensional loading 28
 tilt 268, 285
 tilting 255, 263, 291
 timber sheeting 228, 233
 time 44, 48, 143, 281
 time dependent 64 *see also behaviour*
 time factor 143, 401, 404
 time-settlement 275, 300, 308, 318, 319
 torque 354, 355
 track 424, 497, 498, 499, 500, 501
 traffic 210, 497
 train 498
 transformed line 183
 treatment 481, 482, 485
 tremie-pipe 362
 trench 112, 113, 125, 134, 135, 161,
 194, 195, 201, 202, 214, 215, 222,
 337
- Tresca yield criteria *see constitutive model*

- triaxial 3, 29, 31, 35, 37, 38, 41, 47, 48, 52, 54, 55, 65-76, 85, 90-92, 96, 99, 152, 167, 168, 185, 186, 233, 456
 anisotropic consolidation 3, 65, 85
 anisotropically consolidated 38, 72, 74, 80, 82, 83, 146, 148
 cell pressure 64, 70, 72, 73
 confining pressure 31, 33, 77, 78, 79, 81, 83, 84, 91, 92, 93, 99, 101
 consolidated 147
 consolidated undrained 44, 47, 146
 drained 65-69, 71, 74, 75, 80, 85, 86, 96, 98, 103, 104
 isotropic consolidation 3, 33, 35, 65, 85
 isotropically consolidated 38, 67, 146
 compression 31
 standard 3
 tension 31
 unconsolidated undrained 44, 77
 undrained 40-42, 65-67, 71-75, 81, 83, 85, 86, 98, 104, 141
 stress path dependent tests 3
 trickling 493
 twisting 355
 u
 ultimate pile resistance *see pile*
 ultimate resistance *see resistance*
 unconfined compression 13, 44, 487
 underground 198, 201, 210, 243, 244, 250, 255, 258, 337, 419, 434, 443, 445
 underpinning 257, 417
 undrained 85, 86, 101, 102, 119, 157
see also triaxial, shear strength, stress path
 undrained analysis *see analysis*
 undrained condition 139, 141, 143, 148, 149, 151, 171, 174, 175, 186, 399, 402
 undrained loading 99
 undrained modulus *see modulus*
 undrained shear strength *see shear strength*
 unit cell 456, 457, 458, 464
 unit weight 27, 116, 130, 143, 193, 196, 459, 461, 504
 unloading 3, 18, 22, 24, 58-60, 62, 63, 68-70, 77, 79, 85, 92, 94, 95, 102-104, 128, 141, 166, 169, 271, 281, 283, 377, 378
 unloading modulus *see modulus*
 update mesh analysis *see analysis*
 upgrading 497, 499, 500, 501
 uplift 6, 8, 199, 356
 v
 vacuum 106, 135
 vacuum filter 199
 vacuum lance 199
 vane shear 41, 44, 47, 48
 vane test 52, 509
 variable modulus *see modulus*
 variation 163, 222, 348, 491
 velocity 363, 364, 383, 384, 481, 484, 489
 verification 6, 7, 9, 108, 113, 189, 194, 197, 271, 473, 474, 484, 503 *see also safety*
 vibration 111, 114, 125, 126, 251, 343, 347, 354, 355, 366, 462, 463, 469, 476, 497
 vibratory 111, 367
 vibro displacement 462, 494
 vibro-compaction 416, 455
 vibro-composer 455
 vibro-displacement 463, 491
 vibroflot 489, 490
 vibro-replacement 455
 virgin consolidation line *see consolidation*
 virtual thickness 217, 218
 virtual work 130, 295
 visco-hypoplasticity *see constitutive model*
 visco-plastic *see constitutive model*
 viscosity 65, 281, 282
 viscosity exponent 391
 viscosity index 284
 void 363, 364, 366
 void ratio 18, 22, 24, 27, 30, 44, 65, 67, 59, 278, 280, 283, 285, 300, 475
 critical void ratio 67
 volume 175, 370, 400, 413, 482, 487
 volume change 16, 17, 64, 67, 72, 91, 96, 97, 99, 162, 323
 volume decrease 297
 volumetric change 67
 volumetric strain 37, 41, 42, 57, 67, 68, 64, 67, 72, 97, 98
 Von-Mises yield criteria *see constitutive model*

- w
wale 134, 252
wall 40, 47, 55, 68, 58, 86, 87, 108-110, 115, 116, 120-124, 130, 134, 135, 138-141, 154, 156, 158-163, 166-173, 180-183, 188, 197-200, 205, 210, 213-217, 221, 228, 229, 231, 233, 237, 239, 247, 440, 441, 443, 507
active side 138, 152, 156, 161, 170, 188-192, 196
bored pile 108, 109, 110, 131, 161
brick 288
continuous pile 360
deflection 117, 158-161, 163, 165, 166, 168, 170, 175, 179, 194, 205, 207, 216, 229, 231, 238, 240, 253
deformation 166-168, 173, 175, 177, 195
diaphragm 108-110, 123-127, 134, 161, 252, 253, 256
displacement 158, 161, 165, 170, 171, 173, 178-190, 215-217, 219-224, 238, 239, 261
element 3
equivalent thickness 233
fixed end 134, 159, 198, 221, 222, 238
fixed end cantilever 118
flexible 160, 191
free end 134, 159, 195
friction 189, 198, 362
head 225, 238
infilled wall 295
installation 161, 205, 225, 238, 244, 251
Kingpost and planking wall 108
lateral translation 117, 119, 179
masonry 295, 506
movement 117, 152, 155, 156, 162, 169, 171, 175, 179, 182, 183, 188, 189, 205, 206, 248
movement pattern 179
panel 495
parallel translation 179, 181, 184
passive side 138, 152, 155, 170, 189, 191, 192, 196
penetration 139
pile 113, 257, 259, 261
reaction 189
reinforced concrete 295
replacement type 125
rotation 117, 118
rotation about head 181, 184
rotation about toe 117, 179, 181, 184
rotation about top 117, 179
secant bored pile 110
sheet pile 109, 118, 134, 137, 157, 159, 162, 200, 201, 205, 207, 209, 219, 220, 222, 244, 245, 248-253, 491, 493, 494, 497, 500
soldier pile 108, 110, 123, 228, 233, 234
stiffness 158, 160
tangent bored pile 110
toe 144, 156, 188, 189, 190, 195, 198, 219, 222, 224
wash boring 367, 424
water content 15, 17, 44, 82, 87, 204, 244, 258, 277, 299, 302, 305, 319, 323, 351, 423, 427, 448, 458, 476, 497
water level 204, 205, 423, 440, 444, 493
water pressure *see pressure*
water table 193, 219
water-cement mix 347
water-cement ratio 366
wave 383
impact 383
propagation theory 382
propagation velocity 382, 383
weathered rock 353
wedge 197
weight 145, 146, 213, 233, 261
well 135, 199
Winkler 326
wood lagging 124
work 497, 499, 500, 502
work hardening 67
working stress method 137
workmanship 105
y
yield function 59-66
yield surface 59-64, 68
yielding 326
Young's modulus *see modulus*